IDŐJÁRÁS

QUARTERLY JOURNAL
OF THE HUNGARIAN METEOROLOGICAL SERVICE

CONTENTS

****

http://www.met.hu/Journal-Idojaras.php

VOL. 118 * NO. 1 * JANUAR – MARCH 2014

IDŐJÁRÁS

Quarterly Journal of the Hungarian Meteorological Service

Editorial Office: Kitaibel P.u. 1, H-1024 Budapest, Hungary
P.O. Box 38, H-1525 Budapest, Hungary
E-mail: journal.idojaras@met.hu
Fax: (36-1) 346-4669

Indexed and abstracted in Science Citation Index Expanded™ and Journal Citation Reports/Science Edition
Covered in the abstract and citation database SCOPUS®

Subscription by mail:
IDŐJÁRÁS, P.O. Box 38, H-1525 Budapest, Hungary
E-mail: journal.idojaras@met.hu

IDŐJÁRÁS

Quarterly Journal of the Hungarian Meteorological Service
Vol. 118, No. 1, January – March, 2014, pp. 1–17

Risk analysis of the first and last frost occurrences during growing season of vegetables in the Elbe River lowland

Vera Potop[1]*, **Pavel Zahraniček**[2], **Luboš Türkott**[1], **Petr Štěpánek**[2], and **Josef Soukup**[1]

[1]*Czech University of Life Sciences Prague, Faculty of Agrobiology, Food and Natural Resources, Department of Agroecology and Biometeorology, Kamycka 129, 165 21 Prague 6 – Suchdol, Czech Republic*

[2]*Global Change Research Centre AS CR, Bědila 986/4a, 603 00 Brno, Czech Republic*

**Corresponding author E-mail: potop@af.czu.cz*

(Manuscript received in final form May 17, 2013)

Abstract–This study has, for the first time, analyzed in detail the risk occurrences of the last spring frost, first fall frost, and the length of the frost-free period during the growing season of vegetable crops at a high horizontal resolution of 10 km (CZGRIDS, ALADIN-Climate/CZ) in the Elbe River lowland. The daily minimum air temperature from 116 grid points throughout the studied area for the period 1961–2011 was used. The daily values of minimum air temperature ranges of 0 °C to −1.1 °C, −1.2°C to −2.2 °C, and below −2.2 °C were considered to constitute mild, moderate, and severe frosts intensities, respectively. Firstly, comprehensive analysis of the spatio-temporal variability of the date of the last spring frost, the date of the first fall frost, and the length of the frost-free period in the Elbe River lowland were provided. Secondly, a catalogue of the mean dates of the spring and fall frosts for the three frost severities (mild, moderate, and severe) and degrees of earliness (early, mean, and late ending/beginning), as well as the length of the frost-free period over the Elbe River lowland, was developed. Thirdly, to identify the areas with high-risk occurrences of damaging last spring frosts during the sowing/planting period of vegetables in the Elbe River Lowland.

According to the regional catalogue of frosts, an earlier ending of spring and a later beginning of fall frosts, simultaneous with the latest ending of the frost-free period, were recorded during the 1990s, 2000s, and 2010s. The severe spring frosts in the period of 1981–2011 ended earlier than in the period of 1961–1980; consequently, the end of the 20th and the beginning of the 21st century are suitable periods for the growth extension of species and varieties of vegetables with longer growing seasons and higher demands on temperature. Whereas the latest spring frost has ended on an earlier date across the Elbe lowland, the first frost date in the fall has generally been delayed to a later date.

Key-words: thermophilic, cold-resistant, frost-resistant vegetables, late spring frost, early fall frost, frost-free period

1. Introduction

Most of Europe experienced increases in the surface air temperature from 1901 to 2005, which amounts to a 0.9 °C increase in annual mean temperature over the entire continent (*Alcamo et al.*, 2007). In the mean temperature series for the Czech Republic determined for the period 1848–2000, the significant linear trend for the increase reached 0.69°C/100 years (*Brazdil et al.*, 2009). In context of global warming, *Karl et al.* (1993) noted an asymmetrical rise in temperature extremes that manifests as a swifter rise in minimum temperatures than in maxima, which resulted in a decrease in the diurnal temperature range. For example, in Australia and New Zealand, the frequency of days below 0 °C decreased with warming in daily minimum temperatures (*Plummer et al.*, 1999). *Easterling et al.* (2000) concluded that the number of frost days has decreased in every country (Australia, China, central and northern Europe, New Zealand, USA) where it has been examined.

For central Europe, *Menzel et al.* (2003) found a greater change in the frost-free period, most likely also due to the greater increase in daily minimum temperatures. Consequently, trees may not take advantage of the frost-free period as before but may profit from a reduced risk of damage by late spring frosts. *Scheifinger et al.* (2003) indicated that the occurrence date of the last spring frost in central Europe has been increasingly early during the last few decades.

Numerous studies have evaluated the variability in the frost events and associated statistics (e.g., *Thom,* 1959; *Easterling et al., 2000; Robeson,* 2002; *Tait* and *Zheng*, 2003; *Menzel et al., 2003; Scheifinger et al.*, 2003; *Rahimi et al.,* 2007; *Didari* et al., 2012). Nearly all of the studies in the previous decades have reported increases of the frost-free period. For example, *Bootsma* (1994) and *Shen et al.*, (2005) noticed an increased frost-free period, a later growing season end, and an increase in growing degree days for most of Canada. *Robeson* (2002) determined a trend toward earlier spring frosts in Illinois but no consistent trends in autumn frosts.

Variations in the frost-free period length and the timing of frost events can also be an important indicator of climatic change that may not be represented in mean conditions (*Robeson,* 2002; *Easterling et al.,* 2000). There are a large variety of extreme events, and their impacts can be highly variable. Our research examines the variations in the last spring frost, the first fall frost, and the frost-free period length for the Elbe River lowland in the Czech Republic as an indicator of climate variations in this region. Vegetable crops are the most sensitive to the timing of extreme cold events at the beginning and end of the growing season. Damage caused by late frosts in spring (or early frosts during fall) is a limiting factor, particularly in the case of fruits and vegetables in central Europe.

In the Czech Republic, research focusing on the risks of late spring and early autumn frosts and their impacts on agricultural production gained considerable attention during the 1960s and 1970s (*Stibral*, 1966; *Forgáč* and *Molnar*, 1967; *Pejml*, 1955, 1973). This subject has remained in the background of interest to climatologists, although frost is one of the most devastating weather events that diminishes agriculture productivity in the Czech Republic.

Therefore, there were three main objectives in this study: (i) comprehensive analysis of the spatio-temporal variability of the date of the last spring frost (LSF), the date of the first fall frost (FFF), and the length of the frost-free period (FFP) in the Elbe River lowland; (ii) estimation of the tendency of the last spring frost, the first fall frost, and the length of the frost-free period; and (iii) the evaluation of the risk occurrences of damaging last spring frosts during sowing/planting for thermophilic, cold-resistant, and frost-resistant vegetables.

2. *Methods and materials*

2.1. Quality control and homogenization of gridded datasets

Monthly and daily series of temperatures (mean, minimum, and maximum), rainfall and sunshine duration for period 1961–2011 were analyzed. A regular gridded network with a high horizontal resolution of 10 km (CZGRIDS, ALADIN-Climate/CZ) from the Czech Hydrometeorological Institute (CHMI) was applied (*Fig. 1a*). High-density gridded datasets allow very precise and detailed delimitation of the area in which frosts occur in comparison with the station network datasets. The station network in the Elbe River lowland has significantly fewer units located primarily in non-agricultural areas, and their data series are not complete. The gridded network was created using the technical series from 268 climatological and 784 rain-gauge stations of the CHMI network. From these technical series, new values for the regular 10×10 km grid network (ALADIN-Climate/CZ RCM outputs) were interpolated (*Štěpánek et al.* 2011a, 2011b). The spatial interpolation of the agroclimatological characteristics ranges between longitudes 13.7°E and 16.5°E and latitudes 49.6°N and 50.8°N. The lowest and highest altitudes of the gridded dataset were 169 m and 573 m above sea level, respectively.

In our approach, data quality control is carried out by combining several methods: (i) by analyzing difference series between candidate and neighbouring stations, i.e., pairwise comparisons (ii) by applying limits derived from interquartile ranges (this can be applied either to individual series, i.e., absolutely or to difference series between candidate and reference series, i.e., relatively), and (iii) by comparing the series values tested with "expected" (theoretical) values – technical series created by means of statistical methods for spatial data (e.g., IDW, kriging).

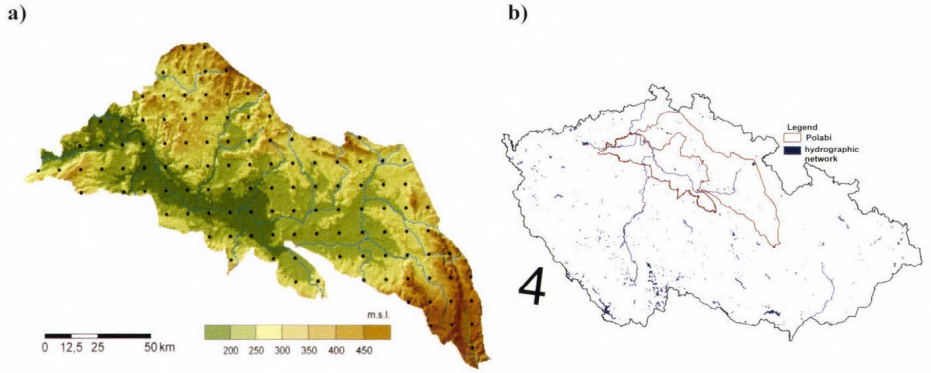

Fig. 1. (a) Location of the 116 grid points and their elevation (m a.s.l.) situated in the Elbe River lowland and (b) geographic boundaries of the Elbe River lowland.

The relative homogeneity tests applied were: the standard normal homogeneity test (SNHT) developed by *Alexandersson* (1986, 1995), the Maronna and Yohai bivariate test (*Potter*, 1981), and the *Easterling* and *Peterson* test (1995). The reference series were calculated as a weighted average from five nearest stations (with the same period of observations as the candidate series) with statistically significant correlation. The power of weights (inverse distance) for temperature was taken as 1 and for precipitation as 3. All the procedures for quality control and homogenization have been carried out with the ProClimDB and AnClim softwares (*Štěpánek,* 2010). More details on quality control and homogenization procedures are provided in *Štěpánek et al.* (2011a, 2011b).

2.2. Study region

The Elbe River lowland is the traditional and informal name for a lowlands region located in the Central Bohemian Region of the Czech Republic (*Fig. 1a-b*). The gridded data of the annual and growing season temperatures (mean, minimum, and maximum), rainfall, and sunshine duration were spatially averaged using ArcGIS Spatial Analyst extension over the Elbe River lowland. The results are presented in *Table 1*. In the Elbe River lowland, the mean long-term annual precipitation total was 591.6 mm compared with the 674 mm average for the entire territory of the Czech Republic. This precipitation primarily falls in the summer (40% of annual totals). In the growing season, the mean precipitation totals are 365 mm (*Table 1*). A significant excess of precipitation during some periods can result in catastrophic flooding (e.g., as in the year 2002), whereas a long-term lack of precipitation can contribute to extreme drought incidences (*Tolasz* et *al.*, 2007; *Potop,* 2010, *Potop et al.*, 2011).

Table 1. Areal averages of the basic agroclimatological characteristics determined using ArcGIS Spatial Analyst extension over the Elbe River lowland for the period 1961–2000. These averages are over all 116 grids (λ=13.7°E – 16.5°E; φ=49.6°N – 50.8°N, h=169 to 573 m a.s.l.)

	T_{mean} °C	T_{max} °C	T_{min} °C	Rainfall mm	Sunshine hours
Growing season					
Mean	14.5	20.5	8.9	365.0	1160.0
Minimum	12.7	17.8	7.4	304.7	1002.0
Maximum	15.6	21.4	10.0	461.1	1257.6
Range	2.9	3.6	2.6	156.4	255.6
Annual					
Mean	8.4	13.1	3.9	591.6	1574.2
Minimum	6.6	10.6	2.6	460.5	1327.2
Maximum	9.4	14.0	4.9	849.7	1730.3
Range	2.8	3.4	2.3	389.2	403.1

The annual mean temperature (T_{mean}) at the Elbe River lowland and in the country is 8.4 °C and 7.5 °C, respectively. The mean temperature during the growing season is 14.5 °C. The mean annual maximum (T_{max}) and minimum (T_{min}) temperatures are 13.1 °C and 3.9 °C, respectively. The average T_{max} and T_{min} during the growing season are 20.5 °C and 8.9 °C, respectively. The mean annual sunshine totals reach 1574.2 hours, whereas, in the growing season, the total is 1160 hours (*Table 1*).

The T_{mean} during the growing season ranges between 12.7 °C and 15.6 °C. The majority of the Elbe River lowland area had T_{mean} values from 14.5 °C to 15.0 °C. In terms of the mean T_{min}, the lowest values (less than 7.5 °C) were centered in the northern part of the Elbe River lowland, which has an altitude higher than 450 m (*Fig. 2a*). The mean T_{min} varies from 7.4 °C to 10.0°C over the Elbe River lowland territory. The mean T_{max} during the growing season ranged between 17.6 °C and 21.4 °C, while a small area had T_{max} values less than 18.5 °C (*Fig. 2b*). The mean precipitation total in the growing season fluctuates between 304 and 461 mm, but in a large portion of the Elbe River lowland, total precipitation is less than 350 mm. The mean sunshine duration total ranges from 1000 to 1257 hours, but the maximum value is received in the central portion of the Elbe River lowland. The warmest and longest duration of sunshine and the lowest precipitation totals during the growing season occur in the middle to lower reaches of the Elbe River, between Poděbrady and Litoměřice. As a practical recommendation, the authors suggest that this region may be suitable for cultivation of thermophile vegetable crops in combination with an irrigation system that would assure the qualitative yields (*Potop et al.*, 2012; *Potop et al.*, 2013).

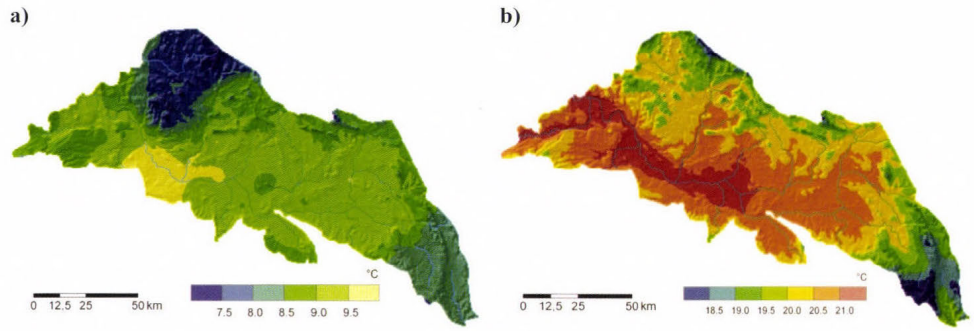

Fig. 2. Spatial distribution of the minimum (a) and maximum (b) temperatures during the growing season (April-September) for the period 1961–2000 over the Elbe River lowland.

2.3. *Determining the dates of the last spring first fall frosts, and the length of the frost-free period*

The daily minimum air temperature from 116 grid points throughout the studied area for the period 1961–2011 was used (*Fig. 1a*). For each grid point and for each year, the first and the last frost day and the frost-free period (i.e., the number of consecutive days from the date of the last frost with minimum air temperature greater than 0 °C) were identified. The LSF day is defined as the last date in a year on or before July 15 on which the daily minimum temperature $T_{min} \leq 0°C$. The FFF day is defined as the first date in a year after July 16 on which $T_{min} \leq 0°C$. The FFP is the number of days between the LSF and FFF.

The three degrees of frost severity were defined with regard to the physiological requirements of the vegetable types. The daily values of minimum air temperature ranges of 0 °C to −1. 1°C, −1.2 °C to −2.2 °C, and below −2.2 °C were considered to constitute mild, moderate, and severe frosts intensities, respectively (*WMO*, 1963). Using these definitions, the last three spring and first three fall frosts were specified for the spring and fall of each year. After determining the frost dates, it was necessary to transform them into a form that we could analyse statistically. For this purpose, Julian days (calendar days of the year) were used. These values were statistically processed, and we identified the mean, standard deviation, latest occurrence, earliest occurrence, and the length of the frost-free period. The extreme values were the latest beginning/ending, the earliest beginning/ending of spring and fall frosts and the shortest/longest FFP. The ending of the spring frost and beginning of the fall frost were classified into three categories: early, mean, and late. In this study, percentiles of date of spring and fall frosts for the fitted Gaussian distribution from 25 to 75% correspond to mean date of beginning/ending of frosts,

percentiles less than 25% are qualified as early date, and percentiles above 75% correspond to late date (*Table 2*).

*Table 2.*Classification of the timing of ending of the spring frost and beginning of the fall frost. The units used are Julian days

Categories	Percentile %	Last mild spring frost	Last moderate spring frost	Last severe spring frost	First mild fall frost	First moderate fall frost	First severe fall frost
early	< 25	< 102	< 92	< 86	< 284	< 290	< 294
mean	25–75	102–121	92–113	86–111	284–303	290–313	294–317
late	>75	>121	>113	>111	>303	>313	>317

3. Results and discussion

3.1. Statistical characteristics of the variability of frost series from 116 grid points

The mean, standard deviation, latest and earliest occurrence of the LSF and FFF, and length of the FFP are given in *Table 3*. The mean date of occurrence of the last mild spring frosts in the Elbe River lowland is on day 112 (April 22). The mean dates of the last spring frost with moderate and severe intensity were April 13 and April 8, respectively. The earliest last mild spring frost occurred on day 74 (March 15) in the period 1961–2011. The latest mild frosts occurred on day 164 (June 13). According to these results, the highest risk for field vegetables is a late spring frost.

Table 3. Statistical characteristics of the average frost series (at 116 grid points) of the studied area. The units used are dates and Julian days

	Last mild spring frost	Last moderate spring frost	Last severe spring frost	First mild fall frost	First moderate fall frost	First severe fall frost	Frost-free period
mean	112 (Apr 22)	103 (Apr 13)	98 (Apr 8)	293 (Oct 20)	302 (Oct 29)	305 (Nov 1)	180
STDev	15	16	14	15	17	16	25
earliest	74 (Mar 15)	59 (Feb 28)	65 (Mar 6)	260 (Sep 17)	270 (Sep 27)	276 (Oct 3)	93
latest	164 (Jun 13)	135 (May 15)	125 (May 5)	329 (Nov 25)	344 (Dec 10)	345 (Dec 11)	284

The earliest first mild fall frosts occurred on September 17, and the latest onset was November 25. Frosts with higher intensity occurred later, and the earliest beginnings of the moderate and severe frosts were on September 27 and October 3, respectively, whereas the latest onsets of moderate and severe frosts fell in the winter period on December 10 and 11, respectively. In the studied region, there were years with a possible extension of the growing season for frost-resistant vegetables, allowing distribution of the harvest. From the climatological point of view, this phenomenon indicates a delay in the onset of winter. The average length of the frost-free period was 180 days, almost half of the year.

3.2. Temporal evaluation of the frosts characteristic

3.2.1. Date of the last spring frost

Catalogues of the spring and fall frost dates of the three severities (mild, moderate, and severe), degrees of earliness (early, mean, and late ending/beginning), and the lengths of the frost-free periods were developed (*Table 4*). According to the timing (*Table 2*), the ending of the LSF and the beginning of the FFF, we can divide the earliness into three categories: early, mean, and late ending (beginning) to evaluate the impact of frost on the production of vegetables, where the highest risk is a late spring ending and early fall beginning of frosts. The mean dates of spring and fall frosts for three frost severities (mild, moderate, and severe) and earliness (early, mean, and late ending/beginning) and the length of the frost-free period was averaged over the Elbe River lowland for the period 1961–2011 (*Table 4*). As shown in *Table 4*, in the last two decades, the last mild spring frosts were concentrated into categories of early and mean ending, whereas in May they did not occur. Conversely, in the period from 1961 to 1980, the majority of cases were recorded in the mean and late ending categories of LSF. We observed that in the coolest decade of the 1970s (the lowest negative deviation of mean temperature since 1961), the majority of LSF and FFF events were concentrated in the late ending category. In this respect, the regional average of the late ending of mild spring frosts occurred in the first half of May in five consecutive years (1976, 1977, 1978, 1979, and 1980). At the same time, the years of 1977, 1979, and 1980 had shorter frost-free periods of 143, 152, and 156 days, respectively. Moreover, an extreme year in terms of the termination of the spring frost was 1976 with the latest end of the mild (May 4), moderate (April 25), and severe (April 30) frosts. This year, however, had an average length of the frost-free period (177 days), which was caused by the delayed onset of mild (October 30), moderate (November 17), and severe (November 26) fall frosts. The exceptionality of this year was also confirmed by a persistent extreme summer drought, and as a result, the yield was reduced for all vegetable types as well as for cereals in the

Czech Republic and central Europe (*Potop et al.*, 2011; *Potop et al.*, 2012; *Potop*, 2013).

Table 4. Mean dates of spring and fall frosts for three frost severities (mild, moderate, and severe) and earliness (early, mean, and late ending/beginning) and the length of frost-free period over the Elbe River lowland (1961–2011)

Year	Mild spring frost			Moderate spring frost			Severe spring frost			Frost-free period, days	Mild autumn frost			Moderate autumn frost			Severe autumn frost		
	Early	Mean	Late	Early	Mean	Late	Early	Mean	Late		Early	Mean	Late	Early	Mean	Late	Early	Mean	Late
1961	1 Apr			28 Mar			18 Mar			217			5 Nov			21 Nov			20 Nov
1962		28 Apr			22 Apr			9 Apr		173		19 Oct			25 Oct			26 Oct	
1963		28 Apr			17 Apr			8 Apr		169		14 Oct			23 Oct			9 Nov	
1964		23 Apr			2 Apr			27 Mar		167	8 Oct				25 Oct			1 Nov	
1965		28 Apr			3 Apr			29 Mar		166		12 Oct		15 Oct			18 Oct		
1966	11 Apr			2 Apr				28 Mar		202			30 Oct		3 Nov			31 Oct	
1967		28 Apr			19 Apr			4 Apr		177		23 Oct			4 Nov				14 Nov
1968		17 Apr			10 Apr			14 Apr		194		28 Oct			24 Oct			2 Nov	
1969		18 Apr			17 Apr			21 Apr		178		15 Oct				12 Nov		7 Nov	
1970		1 May			18 Apr			7 Apr		147	26 Sep			15 Oct				8 Nov	
1971		29 Apr			20 Apr			13 Apr		149	26 Sep			9 Oct			7 Oct		
1972	10 Apr				10 Apr				26 Apr	180	8 Oct			11 Oct			7 Oct		
1973			6 May		20 Apr			9 Apr		161		15 Oct			24 Oct		13 Oct		
1974		22 Apr		2 Apr				18 Apr		171	11 Oct				26 Oct			5 Nov	
1975		25 Apr			8 Apr			30 Mar		172		15 Oct			29 Oct			28 Oct	
1976			4 May			25 Apr			30 Apr	177			30 Oct			17 Nov			26 Nov
1977			12 May			24 Apr		19 Apr		143	3 Oct				25 Oct				24 Nov
1978			4 May			3 May		13 Apr		176		28 Oct			5 Nov				13 Nov
1979			7 May			6 May		3 Apr		152	7 Oct			15 Oct			18 Oct		
1980			12 May			7 May			26 Apr	156		15 Oct			23 Oct			28 Oct	
1981		30 Apr				24 Apr		20 Apr		176		24 Oct			3 Nov			9 Nov	
1982		30 Apr				26 Apr		20 Apr		182		30 Oct			8 Nov			6 Nov	
1983	9 Apr			2 Apr				28 Mar		190		17 Oct			28 Oct			28 Oct	
1984		26 Apr			20 Apr			19 Apr		184		28 Oct				13 Nov			29 Nov
1985		25 Apr			11 Apr			16 Apr		179		22 Oct			21 Oct			24 Oct	
1986	3 Apr				4 Apr			14 Apr		190	11 Oct				31 Oct				18 Nov
1987		24 Apr			8 Apr			27 Mar		184		26 Oct			4 Nov			3 Nov	
1988		22 Apr			15 Apr				25 Apr	190			29 Oct		30 Oct			27 Oct	
1989	10 Apr			30 Mar			23 Mar			190		18 Oct			7 Nov				16 Nov
1990		26 Apr			5 Apr			11 Apr		183		27 Oct			31 Oct			26 Oct	
1991			6 May		21 Apr			13 Apr		167		21 Oct			27 Oct			23 Oct	
1992		16 Apr			14 Apr			13 Apr		179		13 Oct		16 Oct			12 Oct		
1993	11 Apr				8 Apr			10 Apr		187		16 Oct			18 Oct			27 Oct	
1994		22 Apr			11 Apr			4 Apr		167	8 Oct			12 Oct			7 Oct		
1995		28 Apr			9 Apr			1 Apr		180		26 Oct			25 Oct			30 Oct	
1996		18 Apr			16 Apr			11 Apr		200			4 Nov		5 Nov				20 Nov
1997		24 Apr			20 Apr				23 Apr	170		12 Oct			21 Oct		20 Oct		
1998	11 Apr				2 Apr			6 Apr		199		28 Oct			6 Nov			12 Nov	
1999		15 Apr			14 Apr			28 Mar		186		19 Oct			26 Oct			21 Oct	
2000	4 Apr				3 Apr		16 Mar			210			31 Oct			28 Nov			18 Nov
2001		16 Apr			14 Apr			2 Apr		208			10 Nov			11 Nov		7 Nov	
2002	8 Apr				6 Apr			10 Apr		194		21 Oct			3 Nov			4 Nov	
2003		14 Apr			5 Apr			12 Apr		180		12 Oct			19 Oct		17 Oct		
2004		18 Apr			9 Apr		19 Mar			187		23 Oct			20 Oct			24 Oct	
2005		28 Apr			10 Apr				22 Apr	190			5 Nov			11 Nov		22 Oct	
2006	11 Apr				4 Apr			6 Apr		197		27 Oct			31 Oct			30 Oct	
2007		28 Apr			17 Apr			9 Apr		176		22 Oct		15 Oct				6 Nov	
2008		13 Apr			12 Apr			30 Mar		192		23 Oct			4 Nov			7 Nov	
2009	2 Apr			27 Mar			26 Mar			205		25 Oct			2 Nov				20 Nov
2010		18 Apr			10 Apr			28 Mar		175	11 Oct			15 Oct				23 Oct	
2011		29 Apr				28 Apr		5 Apr		171		19 Oct		17 Oct			20 Oct		

As we approach summer, the risk of the last spring frosts occurring after May 15 decreases. Extremely late occurrences of moderate spring frosts, reaching up to the month of June, were observed in 1975 and 1977 (June 6) and 1962 (June 3) (not shown). Severe frosts in June with intensities greater than –2.2 °C did not occur in any of the grid points during the entire study period.

3.2.2. Date of the first fall frost and the length of the frost-free period

The late onset of fall frosts extends the growing season of field vegetables. The longest lasting FFPs occurred in 1961 (217 days), 2000 (210 days), and 2009 (205 days) (*Table 4*). The shortest lasting FFPs occurred in 1977 (143), 1970 (147), and 1971 (149) (*Table 4*). In these years, the early beginnings of the mild fall frosts were on September 26. From 1970–1980, there were 6 years recorded with early beginnings of mild fall frosts, 4 years with early beginnings of moderate and severe frosts, and 9 years where the length of FFP was below average (180 days). According to the timing of frosts in 1980–1990, a mean fall frost beginning prevailed for all intensities, except for 1986, when mild frosts occurred on October 11 (early category) (*Table 4*). However, the severe fall frosts in 1986 had a late onset 38 days later (November 18). Usually, the first severe and moderate fall frosts occur closer to winter, after the mild ones. The period of the 1990s had a large number of years in which the severe fall frosts began earlier than mild frosts. In 1994, the FFP ended earlier due to the early beginning of the severe fall frosts (October 7), which occurred the day before the first mild frost. Similarly, in 1992, the severe fall frosts began on October 12, and the mild frosts began on October 13 (*Table 4*). In the first decade of the 21st century, such a situation occurred in 2001, when the severe fall frosts began approximately three days earlier than the mild frosts. This year also had the latest ending of the FFP (208 consecutive days, from April 10 to November 10) for the entire study period. The years with sudden commencement of the severe fall frosts are associated with the occurrence of an uncharacteristic synoptic situation for the fall season. The years 2010 and 2011 had an early beginning of fall frosts that occurred during the harvest period of root vegetables (*Table 4*).

An early ending of spring, together with the late onset of fall frosts in, e.g., 1961 (November 5) and 2000 (October 31), provides suitable conditions for sowing/planting of field vegetables, as well as their ripening and harvesting. However, our regional average frost date series suggests that the FFP exhibits a large amount of interannual variability, and it is also apparent that the region's average FFP has lengthened over the preceding two decades.

3.3. *Trends of changes in the last spring frost, first fall frost, and length of the frost-free period*

The change trends in the dates of the last and first frosts of the three severities, as well as the length of the frost-free period from 1961 to 2011 and their statistical significance according to a t-test (α=0.05) were evaluated. To study the mean tendency in the lowlands region, the results of individual grid points were averaged. For all thresholds, the linear trends of the start, end, and length of the frost-free period are plotted in *Fig. 3*. Overall, the last spring frosts display a decreasing trend, whereas the first fall frosts display an increasing tendency. The early start of the FFP and the consequent lengthening of the FFP also suggest an early ending of the spring frost for the last 51 years. This conclusion is confirmed by the results in *Fig. 3*, which indicate that, for the entire study region, the last mild spring frosts have shifted to an earlier date, and there is a trend of a 2-day earlier shift per decade on average. The last moderate and severe spring frosts have also shifted to an earlier date with a decadal trend of 1.5 days per 10 years. An early ending of spring frost is consistent with the increase of the region's daily minimum temperatures in the recent decades (*Potop et al.*, 2013).

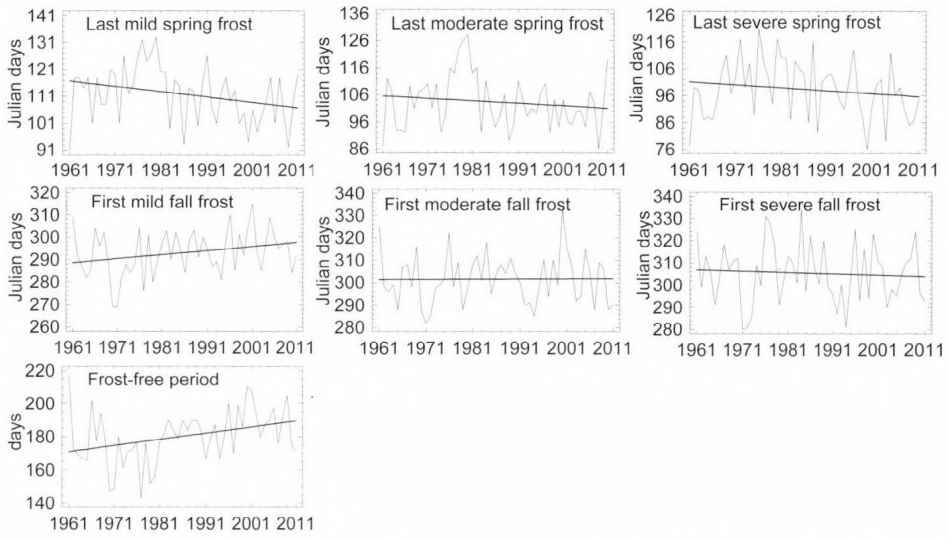

Fig. 3. Date change trends for the last spring frost and first fall frost of the three frost severities and length of frost-free period over the Elbe River lowland for the period 1961–2011.

The increases in the mean minimum temperatures have been demonstrated to have affected the length of the frost-free period (*Easterling et al.*, 1997; *Easterling et al.*, 2000). A pronounced trend towards higher daily minimum

temperatures can be observed, often coincidently with a decrease of the number of frost days over central Europe (*Scheifinger et al.*, 2003; *Menzel et al.* 2003), Australia, and New Zealand (*Plummer et al.,* 1999), the US (*Feng* and *Hu*, 2004) and large portions of the Earth's continents (*Easterling et al.,* 1997).

Whereas the latest spring frost has ended on an earlier date across the Elbe lowland, the first frost date in the fall has generally been delayed to a later date (*Fig. 3*). The delay of the first fall frost date exhibits a trend of 1.8 days per 10 years. There has been a general increase in the length of the frost-free period. The FFP is lengthening by up to 3.7 days per 10 years on average. The trend for the frost-free season displays two distinct periods: a shortening of the FFP in the 1960s and an intensified lengthening of the FFP since the 1980s. These changes are consistent with the global, European, and national temperature changes. For the first period, including the 1960s–1970s, the temperatures do not exhibit conspicuous changes, whereas in the second, beginning with the 1980s, significant warming is evident (*Brazdil et al.*, 2009).

The lengthening FFP in lowlands was primarily a result of an earlier start of the growing season. The consequences to agriculture from these changes include a reduced risk of spring and fall frost damage to crops and a lengthened growing season for vegetable crops. The earlier LSF implies that consecutive warm days in the spring occur earlier and, hence, allow spring melts to occur earlier too. These conditions raise soil temperature earlier for seed germination and, thus, reduce the frost risk for spring crops. The delay of consecutive cold days in the fall improves the chances for crops to mature to a higher-quality yield (*Shen et al.,* 2005).

These changes in the last spring and the first fall frosts are also in general agreement with those in *Feng* and *Hu* (2004), *Menzel et al.* (2003), and *Shen et al.*, (2005). For example, in Germany (1951–2000), the dates of the last spring frost have advanced by 0.24 days per year on average. The respective fall dates are delayed up to 0.25 days per year, whereas the frost-free period is lengthening by up to 0.49 days per year (*Menzel et al.,* 2003).

3.4. Risk occurrences of damaging last spring frosts during sowing/planting for thermophilic, cold-resistan,t and frost-resistant vegetables

The aim here is to identify the areas with high-risk occurrences of damaging LSF during the sowing/planting period of vegetables in the Elbe River lowland. A wide assortment of vegetables grown in the studied region has been divided into three basic types according to their sensitivity to low temperatures: *thermophilic vegetables* (heavy damage to plants in all development stages), *cold-resistant vegetables* (can tolerate a short period of decreasing temperature slightly below 0°C), and *frost-resistant vegetable* (can tolerate a frost less than –2.2°C depending on development stage) (*WMO*, 1997). The per cent risk values of LSF occurrence during the sowing/planting of thermophilic (*Fig. 4a*), cold-

resistant (*Fig. 4b*), and frost-resistant vegetables (*Fig. 4c*) in the Elbe River lowland for the period 1961–2011 are given in *Table 5* and *Fig. 4*. According to the per cent values for frost occurrences, four types of frost risk areas were defined: low, moderate, high, and critical (*Fig. 4*).

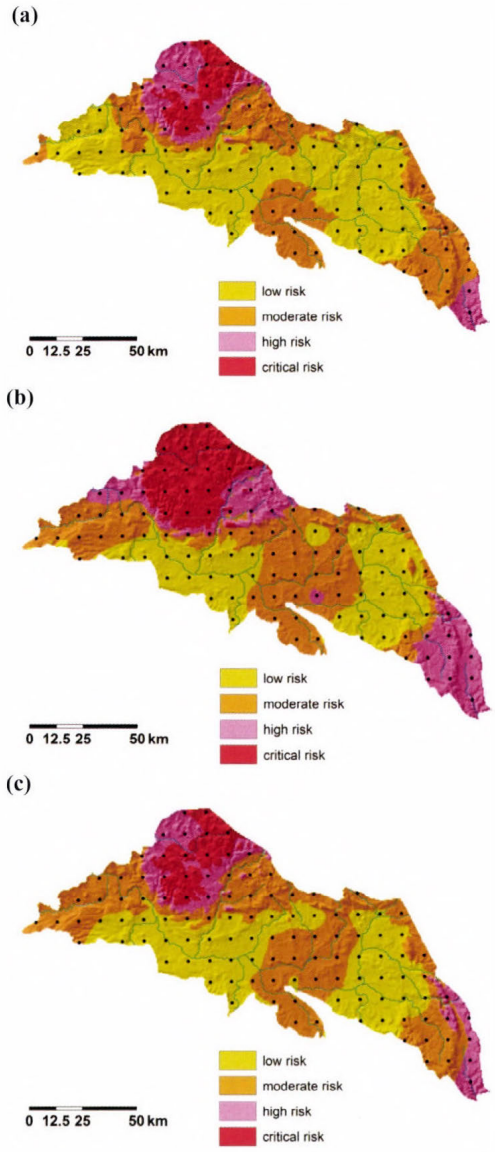

Fig. 4. Frost risk maps for last spring frosts during sowing/planting of thermophilic (a), cold-resistant (b), and frost-resistant (c) vegetables over the Elbe River lowland (1961–2011). Red indicates critical-risk areas, pink indicates high-risk areas, orange indicates moderate-risk areas and yellow indicates low-risk areas.

Table 5. Risk occurrences (%) of the last spring frosts during sowing/planting of thermophilic, cold-resistant, and frost-resistant vegetables in the Elbe River lowland (1961–2011)

Altitude m a.s.l.	Thermophilic t_{min} <–0.1 after May 15			Cold-resistant t_{min} <–2.2 after April 15			Frost-resistant t_{min} <–2.2 after April 1		
	mean	min	max	mean	min	max	mean	min	max
below 250	4.5	0	15.4	30.6	19.2	48.1	56.9	38.5	73.1
251–300	11.3	0	38.5	41	15.4	82.7	67.4	40.4	94.2
above 300	15.4	1.9	34.6	46.2	32.7	67.3	74.3	61.5	90.4

Thermophilic vegetables (e.g., tomato, pepper, pumpkins, and cucumber) from an agronomic point of view should be planted before May 15, considering risk (*Maly et al.*, 1998). The critical temperature after May 15 for thermophilic vegetables is Tmin $\leq$–0.1°C (*Table 5*). In areas with an altitude below 250 m, the risk of critical temperature occurrence is as high as 4.5%; at altitudes from 251 to 300 m, the risk is as high as 11.3%; and at altitudes above 300 m, the risk is as high as 15.4% (*Table 5*). The risk level of frost after May 15 in the traditional grown vegetable regions (up to 250 m) is low (*Fig. 4a*). At higher altitudes (251–300 m), areas with zero incidences of negative temperatures were found, which may allow for the possible expansion of thermophilic vegetable growth. The critical and high risks after May 15 are related to high altitudes in the region (higher than 300 m) and frost hollows, whereas low frost risk is observed in the lower areas (lower than 250 m) (*Fig. 4a*).

During the sowing/planting of *cold-resistant vegetables* (e.g., early kohlrabi, summer savoy cabbage, late cauliflower, late cabbage, late carrots, and celeriac), a severe LSF after April 15 has occurred every second year at higher altitudes. The risk levels for severe LSF occurrence (up to 250 m) are moderate (30.6%) at lower altitudes and high (46.2%) at higher altitudes (*Table 5*). Most vegetable growing areas fall within the low and moderate risk categories for severe spring frosts (*Fig. 4b*). It will be possible to extend the areas suitable for the growing of cold-resistant vegetables (i.e., mostly Brassicas) towards the north-east in the middle Elbe lowland.

Typically, the date of planting/sowing of *frost-resistant vegetables* (e.g., onion, root parsley) in the Czech Republic corresponds with the end of March, and a gradual shift occurs from the hottest regions of south Moravia towards the Elbe region. *Fig. 4c* defines two main areas with a low risk of severe frosts after April 1. The occurrence of severe frosts during the planting of frost-resistant vegetables in the growing area of the Elbe lowland is, on average, 56.9% (*Table 5*). It follows that, despite the considerable resistance of these vegetables to low temperatures, it is necessary to choose lands with southern exposure (or cover plants with non-woven textile). Utilizing resistant varieties and hardening seedlings before planting are advisable.

4. Summary and conclusions

This study has, for the first time, analyzed in detail the risk occurrences of the last spring frost, first fall frost, and the length of the frost-free period during the growing season of vegetable crops at a high horizontal resolution of 10 km in the Elbe River lowland. The main results for the period of 1961–2011 can be summarized as follows:

(i) The most frosts occurring during the vegetable growing season are the spring frosts in the last third of April. According to the frost series averaged over the Elbe River lowland region, the earliest and latest dates of the spring frost range have been March 15 and May 27, respectively. The earliest and latest dates of the fall frost range have been September 17 and November 25, respectively. The latest endings of the spring frost were recorded in 1973 (May 6), 1976 (May 4), 1977 (May 12), 1978 (May 4), 1979 (May 7), 1980 (May 12) and 1991 (May 6). Conversely, the earliest beginnings of the first frost were in 1970 and 1971 (September 26).

(ii) A catalogue of the mean dates of the spring and fall frosts for the three frost severities (mild, moderate, and severe) and degrees of earliness (early, mean, and late ending/beginning), as well as the length of the frost-free period over the Elbe River lowland, was developed. According to the regional catalogue of frosts, an earlier ending of spring and a later beginning of fall frosts, simultaneously with the latest ending of the frost-free period, were recorded during the 1990s, 2000s, and 2010s. The shortest frost-free periods were recorded in 1961–1970 and 1971–1980. The severe spring frosts in the period of 1981–2011 ended earlier than in the period, of 1961–1980; consequently, the end of the 20th and the beginning of the 21st century are suitable periods for the growth extension of species and varieties of vegetables with longer growing seasons and higher demands on temperature. These results agree with other studies conducted at a European scale (*Menzel et al.,* 2003, *Scheifinger et al.*, 2003).

(iii) The real risk of late frost damage for vegetable crops have been lower during the last three decades (1990s, 2000s, and 2010s) than estimated in the previous decades (1970s and 1980s). These results corroborate other research, indicating that spring frost is a critical period for detecting recent climatic changes and their impacts (*Robeson*, 2002; *Easterling et al.*, 2000; *Scheifinger et al.*, 2003).

Acknowledgements: This research was supported by S grant of MSMT CR and projects 6046070901 and CZ.1.07/2.3.00/20.0248.

References

Alcamo, J., Moreno, J.M., Nováky, B., Bindi, M., Corobov, R., Devoy, R.J.N., Giannakopoulos, C., Martin, E., Olesen, J.E. and *Shvidenko, A.*, 2007: Europe. In: Parry, M.L., Canziani, O.F., Palutikof, J.P., van der Linden, P.J., Hanson, C.E. (Eds.), *Climate Change 2007: Impacts, Adaptation and Vulnerability*. Contribution of Working Group II to the Fourth Assessment Report of the Intergovernmental Panel on Climate Change. Cambridge University Press, Cambridge, UK, 541–580.

Alexandersson, A., 1986: A homogeneity test applied to precipitation data. *J. Climatol. 6*, 661–675.

Alexandersson, A., 1995: Homogenity testing, multiple breaks and trends. In: *Proc. 6th Int. Meeting on Stat. Climatology*, Galway, Ireland. 439–441.

Brazdil, R., Chroma, K., Dobrovolny, P. and *Tolasz, R.*, 2009: Climate fluctuations in the Czech Republic during the period 1961-2005. *Int. J. Climatol. 29*, 223–242.

Bootsma, A., 1994: Long term (100yr) climatic trends for agriculture at selected locations in Canada. *Climatic Change 26*, 65–88.

Didari, S., Zand-Parsa, S., Sepaskhah A.R., Kamgar-Haghighi, A.A. and *Khalili, D.*, 2012: Preparition of frost atlas using different interpolation methods in a semiarid region of south of Iran. *Theor. Appl. Climatol. 108*,159–171.

Easterling, D.R. and *Peterson, T.C.*, 1995: A new method for detecting undocumented discontinuities in climatological time series. *Int. J. Climatol. 15*, 369–377.

Easterling, D.R., Horton, B., Jones P.D., Peterson, T.C., Karl, R.R., Parker, D.E., Salinger, M.J., Razuvayev, V., Plummer N., Jamason, P. and *Folland C.K.*, 1997: Maximum and minimum temperature trends for the globe. *Science 277*, 364–367.

Easterling, D.R., Evans, J.L., Groisman, P.Y.A., Karl, T.R., Kunkel, K.E. and *Ambenje, P.*, 2000: Observed variability and trends in extreme climate events: a brief review. *B. Am. Meteorol. Soc. 81*, 417–425.

Forgač, P. and *Molnar, F.*, 1967: Spring frost in Western Slovakia region. In: *Proccedings of HMÚ*, Bratislava: SHMU, 9, 31–86.

Feng, S. and *Hu, Q.*, 2004: Changes in agro-meteorlogoical indicators in the contiguous United States: 1950-2000. *Theor. Appl. Climatol. 78*, 247–264.

Karl T.R., Knight R.W., Gallo, K.P. and *Peterson T.C.* 1993: A New Perspective on Recent Global Warming: Asymmetric Trends of Daily Maximum and Minimum Temperature. *B. Am. Meteorol. Soc. 74*, 1007–1023.

Maly, I., Bartos, J., Hlusek, J., Kopec, K., Petrikova, K., Rod, J. and *Spistitz, P.*, 1998: Field Vegetable Growing. Prague, Czech Republic. *Agrospoj* 64. (in Czech)

Menzel, A., Gert, J., Rein, A., Helfried, S. and *Nicole, E.* 2003: Variations of the climatological growing season (1951–2000) in Germany compared with other countries. *Int. J. Climatol. 23*, 793–812.

Pejml, K., 1955: Development and current status of predictions night frosts during the growing season. *Meteorol. B. 8*, 8–42. (in Czech)

Pejml, K., 1973: Secular evolution of frequency and intensity of spring frosts. In*: Proceedings of HMÚ. 19*, 8–42. (in Czech)

Plummer, N., Salinger, M.J., Nicholls, N., Suppiah, R., Hennessy, K.H., Leighton, R.M., Trewin, B., Page, Ch.M. and *Lough, J.M.*, 1999: Changes in climates extremes over the Australian region and New Zealand during the Twentieth Century. *Climatic Change 42*, 183–202.

Potter, K.W., 1981: Illustration of a New Test for Detecting a Shift in Mean in Precipitation Series. *Mon. Weather Rev. 109*, 2040–2045.

Potop, V., 2010: Temporal variability of daily climate extremes of temperature and precipitation in the middle Polabí (Elbeland) lowland region. *Scientia Agriculturae Bohemica. 41*, 140–148.

Potop, V., Koudela, M. and *Možný, M.*, 2011: The impact of dry, wet and heat episodes on the production of vegetable crops in Polabí (River Basin). *Scientia Agriculturae Bohemica. 42*, 93–101.

Potop, V., Možný, M. and *Soukup, J.*, 2012: Drought evolution at various time scales in the lowland regions and their impact on vegetable crops in the Czech Republic. *Agr. Forest Meteorol. 156*, 121–133.

Potop, V., 2013: The evolution of the assortment and yield of vegetable crops in relation to climate in Polabí. In *Proceedings of influence of abiotic and biotic stresses on properties of plants 2013*. Praha 13.–14.2.2013, 198–201. (in Czech)

Potop, V., Türkott, L., Zahradníček, P. and *Štěpánek, P.*, 2013: Evaluation of agro-climatic potential of Bohemian plateau (České tabule) for growing vegetables. *Meteorol. B.. 66*, 42–48. (in Czech)

Rahimi, M., Hajjam, S., Khalili, A., Kamalid, G.A. and *Stigter, C.J.*, 2007: Risk analysis of first and last frost occurrences in the Central Alborz Region, Iran. *Int. J.f Climatol. 27*, 349–356.

Robeson, S.M., 2002: Increasing growing-season length in Illinois during the 20th century. *Climatic Change 52*, 219–238.

Shen, S. S. P., Yin, H., Cannon, K., Howard A., Chetner S. and *Karl, T.R.*, 2005: Temporal and Spatial Changes of the Agroclimate in Alberta, Canada, from 1901 to 2002. *J. Appl. Meteorol. 44*, 1090–1105.

Scheifinger, H., Menzel, A., Koch, E. and Peter, Ch., 2003: Trends of spring time frost events and phenological dates in Central Europe. *Theor. Appl. Climatol. 74*, 41–51.

Stibral, J., 1966. Frequency of frosts during flowering apple trees. *Meteorol. B. 19*, 177–179. (in Czech)

Štěpánek, P. 2010: ProClimDB – software for processing climatological datasets. CHMI, regional office Brno. http://www.climahom.eu/ProcData.html

Štěpánek, P., Zahradníček, P., Brazdil, R. and *Tolasz, R.*, 2011a: Methodology of data quality control and homogenization of time series in climatology. Praha. 118.

Štěpánek, P., Zahradníček, P. and *Huth, R.*, 2011b: Interpolation techniques used for data quality control and calculation of technical series. An example of Central European daily time series. *Időjárás 115*, 87–98.

Tait, A. and *Zheng, X.* 2003: Mapping frost occurrence using satellite data. *J. Appl. Meteorol. 42*, 193–203.

Tolasz, R., Brazdil, R., Bulir, O., Dobrovolny, P., Dubrovsky, M., Hajkova, L., Halasova, O., Hostynek, J., Janouch, M., Kohut, M., Krska, K., Krivancova, S., Kveton, V., Lepka, Z., Lipina, P., Mackova, J., Metelka, L., Mikova, T., Mrkvica, Z., Mozny, M., Nekovar, J., Nemec, L., Pokorny, J., Reitschlager, J.D., Richterova, D., Roznovsky, J., Repka, M., Semeradova, D., Sosna, V., Striz, M., Serlc, P., Skachova, H., Stepanek, P., Stepankova, P., Trnka, M., Valerianova, A., Valter, J., Vanicek, K., Vavruska, F., Vozenilek, V., Vrabik, T., Vysoudil, M., Zahradnicek, J., Zuskova, I., Zak, M. and *Zalud, Z.*, 2007: Atlas podnebí Česka. *Climate Atlas of Czechia*. ČHMÚ Praha, Univerzita Palackého v Olomouci, Praha-Olomouc, 254.

Thom, H.C.S., 1959: The distribution of freeze-date and freeze-free period for climatological series with freeze less years. *Mon. Weather Rev. 87*, 136–144.

WMO, 1963. Protection Against Frost Damage, WMO-No. 133. WMO, Geneva, Switzerland.

WMO, 1997. Definition of agrometeorological information required for vegetable crops. WMO-No. 866. WMO, Geneva, Switzerland. 110.

IDŐJÁRÁS

Quarterly Journal of the Hungarian Meteorological Service
Vol. 118, No. 1, January – March, 2014, pp. 19–40

Seasonality and geographical occurrence of West Nile fever and distribution of Asian tiger mosquito

Attila Trájer*[1,2], Ákos Bede-Fazekas[3], János Bobvos[4], and Anna Páldy[4]

[1] *Department of Limnology, University of Pannonia*
Egyetem u. 10, Veszprém 8200, Hungary

[2] *MTA-PE Limnoecology Research Group*
Egyetem u. 10, Veszprém 8200, Hungary

[3] *Corvinus University of Budapest, Faculty of Landscape Architecture*
Department of Garden and Open Space Design
Villányi út 29-43, H-1118 Budapest, Hungary

[4] *National Institute of Environmental Health*
Gyáli u. 2-6, Budapest 1097, Hungary

**Corresponding author E-mail: atrajer@gmail.com*

(Manuscript received in final form April 16, 2013)

Abstract—The importance and risk of emerging mosquito borne diseases is going to increase in the European temperate areas due to climate change. The present and upcoming climates of Transdanubia seem to be suitable for the main vector of Chikungunya virus, the Asian tiger mosquito, *Aedes albopictus* Skuse (syn. *Stegomyia albopicta*). West Nile fever is recently endemic in Hungary. We used climate envelope modeling to predict the recent and future potential distribution/occurrence areas of the vector and the disease. We found that climate can be sufficient to explain the recently observed area of *A. albopictus*, while in the case of West Nile fever, the migration routes of reservoir birds, the run of the floodplains, and the position of lakes are also important determinants of the observed occurrence.

Key-words: climate change, climate envelope model, vector-borne diseases, *Culex*, mosquitoes, *Aedes albopictus*, West Nile fever, Chikungunya disease

1. Introduction

1.1. Climate change and emerging mosquito-borne diseases

Within the class Insecta, the order Diptera has the greatest vectorial potential (e.g., flies, sand flies, mosquitoes) as vectors of important human infectious diseases. The most important family is Culicidae with such important genera as *Aedes* and *Culex*. Vector-borne diseases are sensitive to climatic conditions (*Githeko et al.*, 2000; *Harwell et al.*, 2002; *Hunter*, 2003; *Rogers* and *Randolph*, 2006). While the length of every development stages varies among species, it is common that it is greatly affected by the ambient temperature (*Rueda et al.*, 1990; *Bayoh* and *Lindsay*, 2003, 2004; *Teng* and *Apperson*, 2000). Global warming can cause the expansion and the increasing abundance of insect populations (e.g., pests of plants) by changing the length of vegetation period and moderation of the winter colds throughout Europe (*Cannon*, 2004; *Dukes* and *Mooney*, 1999; *Ladányi* and *Horváth*, 2010). Climate change can facilitate the migration of these arthropod vectors to north (*De la Roque et al.*, 2008). The projected warmer conditions are favored by mosquitoes and their parasites (*Epstein et al.*, 1998; *Reiter*, 2001). Since the adult mosquitoes have good flying ability, their expansion can be rapid. They are vectors of many serious viral infection, such as West Nile fever (hence: WNF) and Chikungunya disease which are re-emerging or emerging diseases in the Northern Hemisphere (*Meckenzie et al.*, 2004; *Reiter et al.*, 2006). The transmitters and main sources of the disease are *Culex* species.

While the potential mosquito vectors of West Nile virus (hence: WNV) live in the entire holarctic ecozone, theoretically West Nile virus may be endemic in every part of Eurasia and North America. In contrast to the theoretical investigations, the historical presence of WNF was less abundant. From this reason we aimed to study the climatic requirements of the disease itself and not those of the potential vectors. According to *Spielman* (2001), *Culex* mosquito populations begin to proliferate when the water temperature exceeds 15 °C during June, so the first stable week, when the ambient temperature reaches the 15 °C, can be used as the start of the WNF season.

Many of the potential vectors of WNV are native in Europe. As it is expected, the climate in the Carpathian Basin will be warmer, more arid, and will have extreme rainfalls more frequently in the colder half-year (*Bartholy et al.*, 2007). The increased frequency of heavy rainfall events, with consequential floodings may increase the incidence of mosquitoe-borne diseases and water-borne diseases (*Hunter*, 2003).

Chikungunya virus belongs to the family Togaviridae and is usually transmitted to humans by *Aedes* mosquitoes (e.g., the Asian tiger mosquito, *Aedes albopictus* Skuse (1894). Before 2006, Chikungunya disease and the *Aedes* mosquitoes were mainly reported from the sub-saharan Africa, the

Hindustan Peninsula, and Southeast Asia, but now the vector, *Ae. albopictus*, is presents widely in the Mediterranean Basin (in Spain, France, Italy, Slovenia, Croatia, Serbia, Bosnia and Herzegovina, Albania, and Greece).

Our aim was to study the influence of the ambient temperature and floods on WNF case number and to create a model to take into consideration the potential future distribution of West Nile virus and *Ae. albopictus* mosquito.

1.2. Climate envelope modeling

Ecological modeling methods are utilized in ecology to predict how species, diseases, or ecological structures will response to global warming or other changes of the ecological environment. To project the possible impact of climate change on the distribution of the selected vector, *Ae. albopictus*, and the occurrence of the disease WNF we used climate envelope modeling (CEM) method (*Hijmans* and *Graham*, 2006). *Fischer et al.* (2001) also used CEM to model the future expansion of *Ae. albopictus*. CEM is based on statistical correlations between the observed distributions of species (e.g., *Aedes albopictus* mosquito) or occurrences of diseases (e.g., WNF) and environmental variables to define the tolerance, the limiting ecological factors (e.g., minimum/maximum of temperature, precipitation, length of the vegetation season) of the species or the disease (*Guisan* and *Zimmermann*, 2000; *Elith* and *Leathwick*, 2009). Based on this bioclimatic envelope, using a selected climate scenario, one can predict the probable future range of the species/disease. The hidden and sometimes arguable idea of the CEM is assuming that climate plays primary role on the present and future distribution of the species (*Czúcz,* 2010). For example, in the case of a vector-borne infectious disease, the long-distance transport, the migrating workers and traveling can play a very important role as the determinant of the real geographical occurrence (*Walther et al.,* 2009; *Neghina et al.,* 2009).

1.3. Migrating birds, rivers, wetlands, and West Nile virus

Not only climatic factors determine the distribution of WNF. The principal vectors of the West Nile virus are *Culex pipiens* complex and *Culex modestus* (in Europe, *Culex* species and ticks in Russia also ticks, while migrating birds are the most important reservoirs and propagators of WNV) (*McLean et al.,* 2001; *Reed et al.,* 2003). Mosquitoes transmit the virus to birds, and then the next generation of the virus will infect the biting mosquitoes.

The mean water level and the changes of the water level of the rivers may have an important influence on the mosquito season.

WNV (a member of Flaviviridae) originally was autochthonous in Africa before the 1990's and it was first isolated in 1937, in the Sub-Saharan West Nile territory of Uganda. Then the virus was isolated from humans, birds, and mosquitoes in Egypt (Nile delta) in the early 1950s (*Hubálek* and *Halouzka*,

1999). In Europe it appeared at first, in Albania, 1958 (*Bárdos et al.,* 1959) and many of the early larger outbreaks were reported from the river deltas: from the Rhone delta in 1963 (*Hannoun et al.,* 1964), the Rumanian Danube delta in 1971 (*Topciu et al.,* 1971), and the Volga Delta in 1964 (*Chumakov et al.*, 1964).

Bird migration is the most important way of WNF/WNV introduction to the temperature areas (*Malkinson et al.,* 2002; *Reed et al.,* 2003). It is clear that rivers and riverbanks, coastal plains and deltas are the gathering and feeding places of migrating birds (*Malkinson et al.,* 2002). In Hungary also most of the cases occurred near to riversides, mainly between the riverbank of Tisza, Zagyva, and Rába, as it was seen in 2008. (*Krisztalovics et al.*, 2008).There are 3 main migration routes between Africa and Eurasia (via Gibraltar, via Sicily, via Sinai) (*Fig. 1A*), and one of them (*Fig. 1B*, red lines) makes connection between Eurasia and the eastern sub-saharan part of Africa, e.g., the West Nile territory (*Fig. 1B*), which is the most important migration route of white stork (*Ciconia ciconia* Linnaeus (1758) (*Berthold*, 2004), which bird species itself an important introducer of WNF (*Malkinson et al.,* 2002). It seems that migratory birds are the most important introductory hosts for the virus (*Rappole* and *Hubálek*, 2003). According to *Jourdain et al.* (2007), the risk for introduction of African pathogens, such as WNF into Mediterranean wetlands may be the highest from March to July, which is in accordance with the spring migration and breeding for birds.

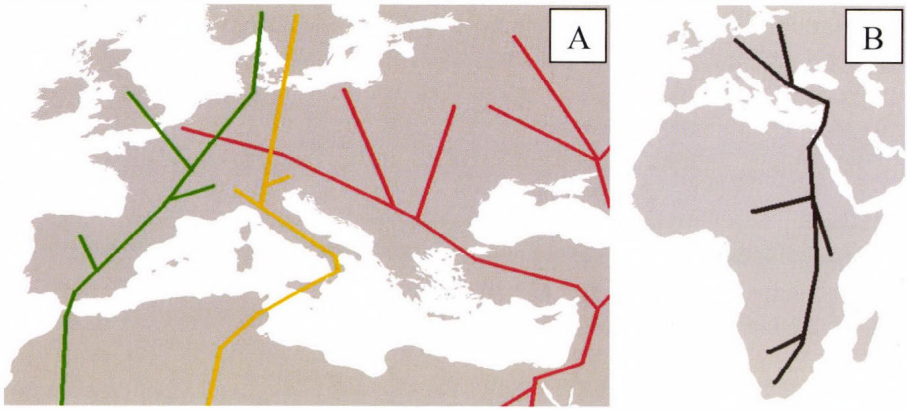

*Fig. 1.***A**: The simplified scheme of the main migration routes of birds between Africa and Europe. Red: Via Sinai per the Middle East from East Africa to Central and Eastern Europe, Yellow: Via Sicily per the Apennine Peninsula, Green: Via Gibraltar per the Hispanic Peninsula. The composite figure mainly was based on the migration routes of different birds of the homepage Global Register of Migratory Species. **B**: The right picture shows the eastern migration scheme route of white stark (Global Register of Migratory Species, *Ciconia ciconia*). Note, that the West Nile territory is an important part of their migration route.

1.4. The threshold minimum temperature of West Nile season

Since according to *Kilpatrick et al.* (2008), *Reisen et al.* (2006), and *Spielman* (2001) the temperature derived transmission of WNV from *Culex* mosquitoes to humans may be between 14–15 °C, we handle the 15 °C as the minimum temperature limit of the WNF season.

2. Materials and methods

2.1. Data sources

2.1.1. West Nile data of Hungary for the period of 2004–2010

The Hungarian WNF data was derived from the Hungarian Epidemiological and Surveillance System and Epinfo (2010A), Epinfo (2010B), and *Krisztalovics et al.* (2008). We could gain the geographical distribution data of the years 2008, 2010, 2011, and 2012.

2.1.2. The hydrological data of the river Tisza

The hydrological data of the river Tisza in the period of 2007–2012 were retrieved from the National Water Warning Network of Hungary (Hydroinfo). We averaged the monthly water levels of May to September. To depict the annual amplitude of the water regime, we used the difference between the annual maximum and minimum water levels.

2.1.3. Climate data

We used the REMO climate model (ENSEMBLES, 2013), which is nested into the ECHAM5 global climate model *(Roeckner et al.*, 2003, 2004) and is based on the IPCC SRES A1B scenario. The A1 scenarios suppose rapid economic and population growth, and rapid global transfer of technologies and knowledge (*Nakicenovic et al.*, 2000).

1961–1990 is the reference period of the REMO model, and the periods of 2011–2040 and 2041–2070 are the selected prediction periods. REMO has 25 km horizontal resolution and the entire Europe is within its domain. In our model we used about the 80% of the points of REMO.

2.1.4. Distribution and occurrence data

Since the model studied the climate requirements only of the European populations – the North African distribution segments were excluded –, it was able to project the shift of this part only. The distribution data of *A. albopictus* was derived from the VBORNET database of the European Centre for Disease

Prevention and Control according to stage in September 2012 (*Medlock et al.*, 2012).

The occurrence of WNF was also derived from European Centre for Disease Prevention and Control homepage and from the European Disease and European Centre for Disease Prevention and Control (ECDC) homepage (ECDC West Nile Fever Maps 2012 and 2011). Furthermore, we also used a publication of the Eurosurveillance journal (*Krisztalovics et al.*, 2008).

The Chironomidae (family Chironomidae) mosquito geographical presence data was derived from *Móra* and *Dévai* (2004). The original checklist and map was based on the review of the faunistical data in the period of 1990–2004. In these 104 years long period, 228 species were observed in Hungary and 98 species are expected to occur (*Móra* and *Dévai*, 2004).

We did not use weighting process, the distribution/occurrence maps of the mosquito and WNF was reduced to simple presence-absence maps. The regions entitled as 'indigenous' and 'recently present' of *Aedes albopictus* while in the case of WNF, the 'area reporting cases in 2012', 'area reporting cases in 2011', 'area reporting cases in 2010' were selected to be digitized. All the data were based on the NUTS3 regions, which are the third level public administration territories of the European Union. After a georeferencing process with third order polynomial transformation, the digitization of the bitmap-format distribution maps were realized with the assistance of the digital NUTS3 polygon borders (GISCO, 2013).

2.1.5. Population of the Hungarian regions

While we studied the regional WNF incidence rate of 2008, 2010, 2011, and 2012 (5-year-long short interval), we could use the population numbers of the year 2012. We retrieved the statistical data from the Central Statistical Office of Hungary (KSH, 2012).

2.2. Statistics

We applied descriptive statistics using SPSS 10.0 and Excel 2010 softwares.

2.3. Modeling method

According to *Thuiller et al.* (2004), climate has the greatest influence on forming the geographical distribution of the species in Europe. We used three physical (climate) factors averaged in the 30-year periods: the monthly mean temperature (T_{mean}, °C), the monthly minimum temperature (T_{min}, °C), and the monthly precipitation (P, mm) of the 12 months. This means 3×12 factors in the model.

Cumulative distribution functions were calculated by PAST statistic analyzer (*Hammer et al.*, 2001) for the selected 3×12 climatic parameters (T_{mean},

T_{min}, P). 10–10% from the extrema in the case of *Ae. albopictus* and 5–5% from the extrema in the case of WNF were neglected from the climatic values found within the observed distribution/occurrence. The selection of the amount of percentiles to be left from the climatic values was based on our former studies. The aim was to restrict the false positive error of the model result in a reasonably degree. We refined the climatic data by the inverse distance weighted interpolation method of ESRI ArcGIS 10 software. The modeling steps were the follows: first, the grid points within the distribution were quoted; second, the percentile points of the climatic parameters were calculated; third, the suitable percentiles of the climatic parameters were chosen; fourth, modeling phrases (3 strings) were created by string functions of Microsoft Excel 2007 for the three modeling periods; fifth, the ranges were selected where all the climatic values of the certain period were between the extrema selected in step 3.

3. Results

3.1. West Nile fever in the period of 2004–2012 in Hungary

3.1.1. Statistics

In Hungary, West Nile fever is recently endemic; 34 cases were reported in the period of 2004–2009 (*Krisztalovics et al.,* 2011; Epinfo, 2010A), 11 cases in 2010 (Epinfo, 2010B), 4 cases in 2011 and 12 cases in 2012 (ECDC, West Nile fever maps 2012). In the period of 2004–2012 WNF showed an increasing trend, but the annual incidence was low and highly variable (0–19/10 million) from year to year (*Fig. 2*), so the trend was not significant at 5% significance level.

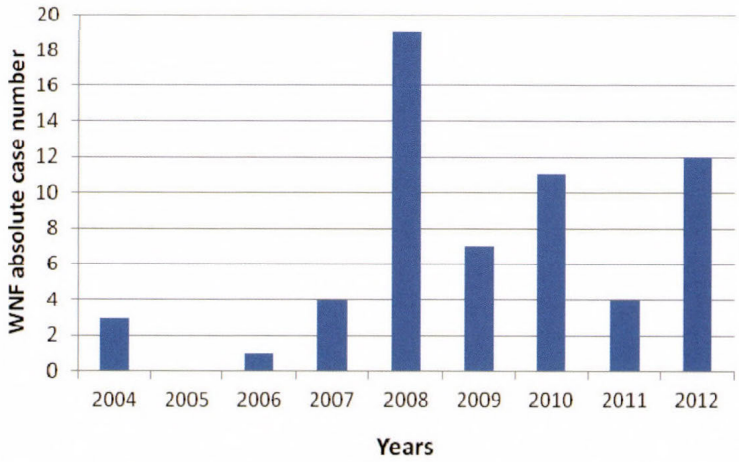

Fig. 2. The absolute annual WNF case number in the period of 2004–2012 in Hungary.

3.1.2. Regional distribution of the WNF incidences

The Hungarian regions correspond to the NUTS 2 statistical regions of the European Union. In 2008 and 2010–2012 (the geographical data of 2009 is missing), the highest WN incidence rates were observed in northern Great Plain (NGP; $6.6*10^{-6}$), southern Great Plain (SGP; $5.24*10^{-6}$), southern Transdanubia (STD; $5.2*10^{-6}$), and western Transdanubia (WTD; $5.01*10^{-6}$). In central Transdanubia (CTD; $3.62*10^{-6}$), northern Hungary (NH; $2.48*10^{-6}$), and central Hungary (CH; $2.41*10^{-6}$), the WNF average incidence of this 3 regions were about the half of the average incidence rate of NGP, SGP, STD, and WTD. The changing WNF incidence rate did not show any significant trends, and the geographic distribution of the cases showed that the focuses of occurrence changed from year to year (*Fig. 3*).

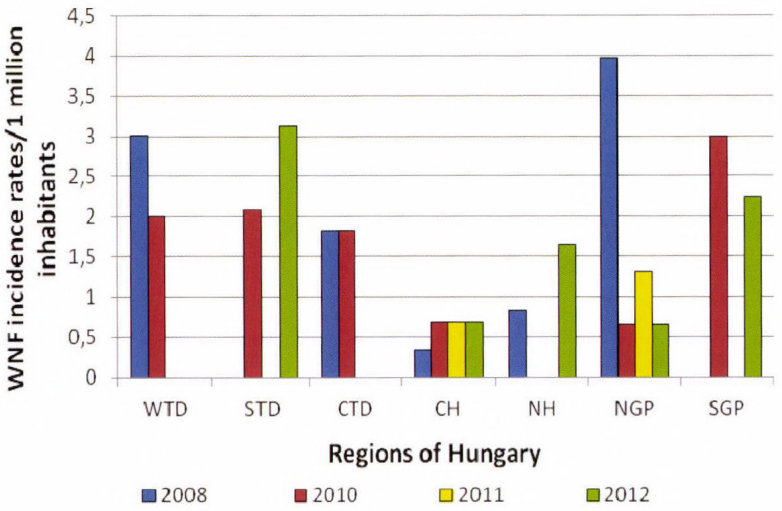

Fig. 3. WNF incidence rates per 1 million inhabitants in the different Hungarian regions in 2008 and 2010–2012 according to the population numbers of 2012. WTD=western Transdanubia, STD=southern Transdanubia, CTD=central Transdanubia, CH=central Hungary, NH=northern Hungary, NGP=northern Great Plain, SGP=southern Great Plain.

3.1.3. Seasonality

WNF showed a clear seasonality (*Fig. 4*). About the ¾ of the cases occurred in August and September. In most of the years the season started in late July (e.g.,

in the 30th week in 2010) or August (e.g., in 2007, 2008). No cases were recorded between December and March and in June.

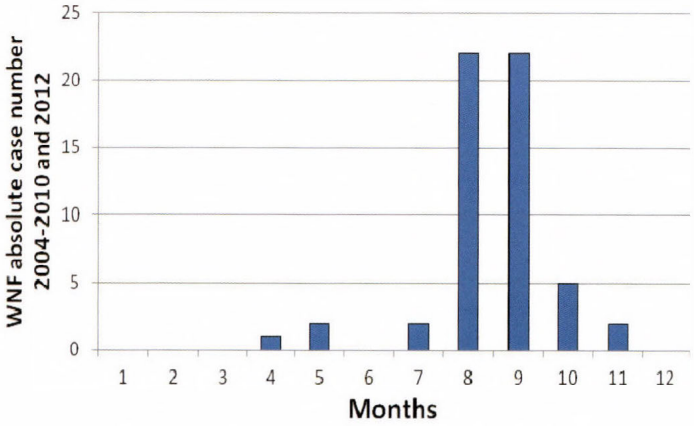

Fig. 4. The seasonal distribution of the WNF cases in Hungary in the period of 2004–2010 and 2012.

3.1.4. Ambient mean weekly temperature and WNF

In 2004–2010 and 2012, the 66.66% of the first symptoms of the disease cases occurred above 19 °C and 84,84% above 16 °C. The highest case numbers were observed between 21–21.9 °C weekly mean ambient temperatures (*Fig. 5*). No cases were observed under 10 °C. Note, that the incubation period of the infection with WNV is thought to range from 3 to 14 days (CDC), but the probability distribution of the latency interval is not known.

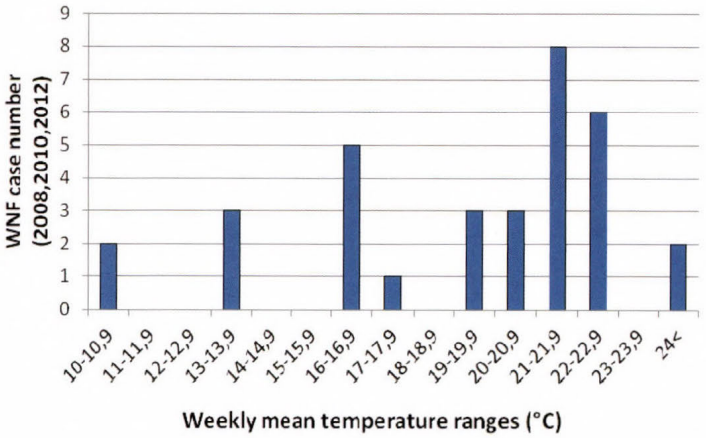

Fig. 5. The frequency histogram of weekly ambient temperatures of 2008, 2010, and 2012, and the number of the WNF cases.

3.1.5. West Nile season

The averaged ambient weekly temperature of the 4 previous weeks before the first WNF case was 21.6 °C in 2008 (*Fig. 4*), 23.82 °C in 2010 (*Fig. 5*), and 23.65 °C in 2012 (*Fig. 6*). 78.6% of the cases in the period of 2004–2010 and 2012 (the weekly data of 2011 is missing) occurred in August and September. In 2008 and 2010 the WNF cases terminated, when the weekly mean temperature dropped below 14.3–13.7 °C. In 2012 after the penultimate case, the ambient temperature dropped below 13.7 °C and the last case occurred, when the mean temperature was 7.5 °C. 19 weeks passed from the first stable week with 15 °C or more ambient temperature to the first WNF case 2008, 14 in 2010, and 13 in 2012.

As we mentioned in Section 2, we selected the weeks of the mean ambient temperature more than 15 °C as the season of *Culex* mosquitoes. According to these observations, we practically handled the period of May to September as the main time of the *Culex* season.

The *Culex* season started in the 18th week of the year (in mid-April) in 2008 and terminated in the 37th week in the first quarter of September. In 2008 the observed WNF season exceeded the theoretical *Culex* season by 2 weeks (*Fig. 6*).

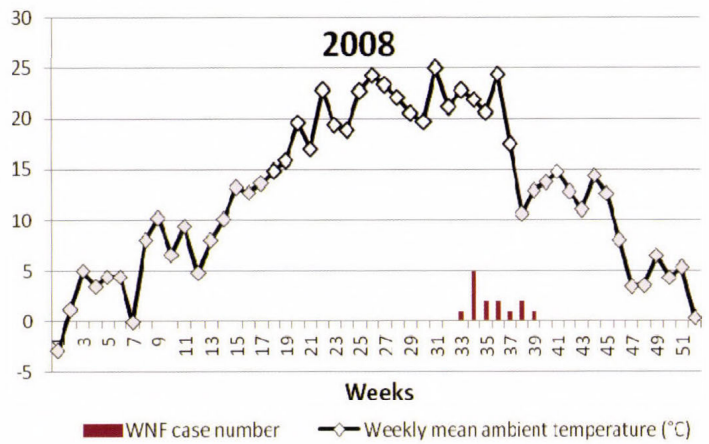

Fig. 6. The weekly ambient temperatures in 2008 and the absolute number of WNF cases. Light gray points mark the weeks, when the ambient temperature was less than 5 °C.

In 2010, the *Culex* season started in the 20th week in the start of May and terminated in the 35th week in late August. In 2009, the last case occurred in the last week of the theoretical season (*Fig. 7*).

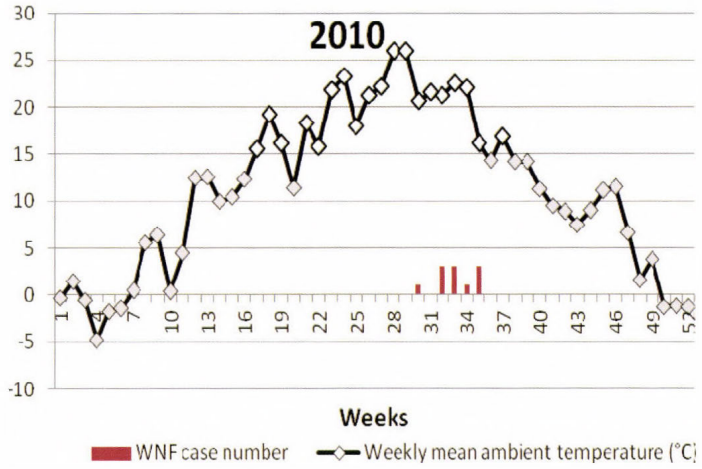

Fig. 7. The weekly ambient temperatures in 2010 and the absolute number of WNF cases. Light gray points mark the weeks, when the ambient temperature was less than 5 °C.

In 2012, the season started in the 16th week and terminated in the 43rd week in late October. In 2012, the last observed case exceeded the theoretical season by 4 weeks, the previous case occurred 1 week before the theoretical end of the mosquito season (*Fig. 8*).

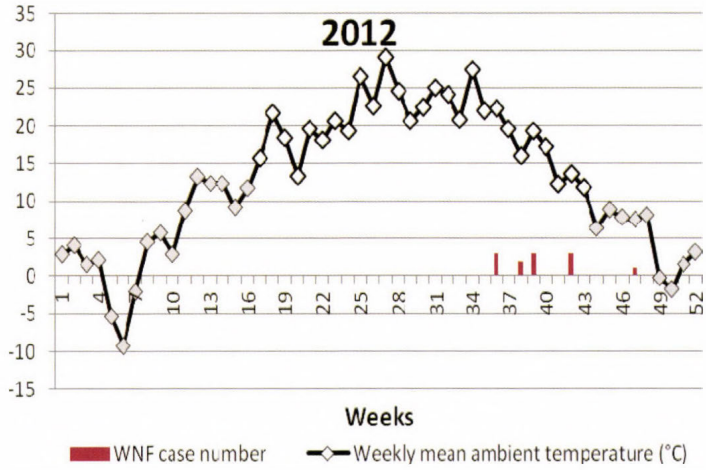

Fig. 8. The weekly ambient temperatures in 2012 and the absolute number of WNF cases. Light gray points mark the weeks, when the ambient temperature was less than 15 °C.

3.2. Floods and WNF in Hungary

3.2.1. Presence of Chironomidae mosquitoes as wetland indicators and WNF

From the first observed human WNF in Hungary in 2004 most of the cases were tied to the rivers Tisza, Raba, Drava, Zagyva, Körös, and Hernád channels (e.g., East Main Channel), and lake Balaton. The river Danube had a less importance. For example from January 2008 to September 2008, 8 WNF cases occurred in the Tisza valley and only 2 cases were observed in the Danube valley. Only 1–2 cases per year were matched to the river Danube. Since before 2007 the WNF level were very low (in the period 2004–2006 only 4 cases were observed), we used the period 2007–2012.

Despite the fact, that Chironomidae (non-biting) mosquitoes are not the vectors of WNF, this species are tied to wetlands, rivers in Hungary since the larvae live in aquatic or semi-aquatic habitats (*Móra* and *Dévai*, 2004). They are good water quality indicators as well, while the larvae can live in polluted waters (*Lindegaard*, 1995). The larvae of *Culex* mosquitoes are also live in aquatic habitats. In 2008, most of the WNF cases between May and September were linked to similar habitats (rivers, lakes, channels) as non-biting mosquitoes (*Fig. 9*).

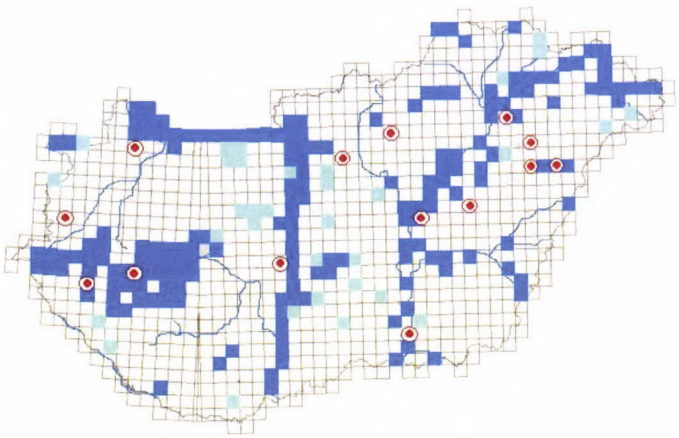

Fig. 9. The confirmed presence of Chironomidae mosquitoes (dark blue), the non-confirmed, but expected presence of Chironomidae mosquitoes (light blue) (according to *Móra* and *Dévai*, 2004), and the occurrence of WNF in 2008 between May and September (n=14) in 2008, Hungary (red circles within red spots; according to *Krisztalovics et al.*, 2008).

3.2.2. Amplitude of the water level changes of the rivers Tisza and Danube

The mean of the annual maximum and minimum water levels of river Danube was Δ=556 cm, since in the case of river Tisza it was 1.6 times higher: Δ=899 cm. (*Fig. 10*).

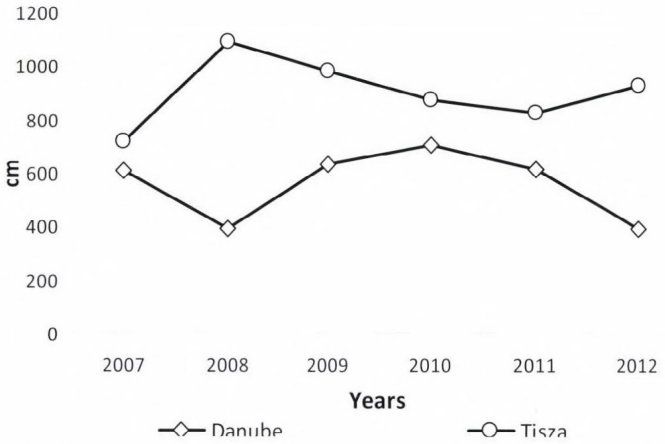

Fig. 10. Differences between the annual maximum and minimum water levels of the rivers Danube and Tisza in the period of 2007–2010.

3.2.3. Water level of the river Tisza at Szolnok (2007–2012)

Since over the Danube the number of the observed WNF cases was negligible under the studied period, we selected the river Tisza as a typical representative of the rivers in the Carpathian Basin, while the entire drainage basin of Tisza is within the Carpathian Basin, and the water regime of the Tisza is the consequence of the previous and the same year's precipitation patterns of the Carpathian Basin.

The average water level of Tisza between May and September in Szolnok (according to the long-time average, *l*) was the following: –71 cm in, 118.6 cm in 2008, –108 cm in 2009, 454.6 cm in 2010, –40.2 cm in 2011, and –99.6 cm in 2012. We calculated the own mean of the 6-year-long period, which was 42.4 cm. Thereafter, we calculated the water level differences from the mean: –113.4 cm in 2007, 76.2 cm in 2008, –150.4 cm in 2009, 412.2 cm in 2010, –82.6 cm in 2011, and –142 cm in 2012. After this process we calculated the percent values according to the absolute range –150.4 cm in 2009, 412.2 cm in 2010, absolute range 562.6 cm as 100%: –20.16% in 2007, 13.54% in 2008, –26.73% in 2009, 73.26% 2010, –14,68% in 2011, and –25.28% in 2012.

3.2.4. Changes in the WNF case number (2007-2012)

The case numbers of the years were the following: n=4 in 2007, n=19 in 2008, n=7 in 2009, n=11 in 2010, n=4 in 2011 and n=12 in 2012. The mean of the WNF case numbers was 9.5 cases per year in the period. We calculated the differences of the cases from the mean: –5.5 in 2007, 9.5 in 2008, –2.5 in 2009, 1.5 in 2010, –5.5 in 2011 and 2.5 in 2012. After this process we calculated the percent values of the differences according to the absolute range of the maxima and the minima of the WNF cases (–5.5 [2007, 2011]; 9.5 [2008]; absolute range)=15 as 100%): 36.6% in 2007, 63.3% in 2008, –16.6% in 2009, 10% in 2010, –36% in 2011 and 16.6% in 2012.

The comparison of the changes of the water level of the Tisza in Szolnok and the WNF cases- showed that five years from the six the sign (less or more than the mean, 0%) of this percent values changed simultaneously except the year 2012 (*Fig. 11*). The relative risk to the above-average number of WNF cases was 4 times higher when the mean level of the river Tisza was higher than the mean of the studied six years (WNF>mean and water level>mean: 2 years, WNF<mean and water level>mean: 0 year, WNF>mean and water level<mean: 1 year, WNF<mean and water level<mean: 3 years).

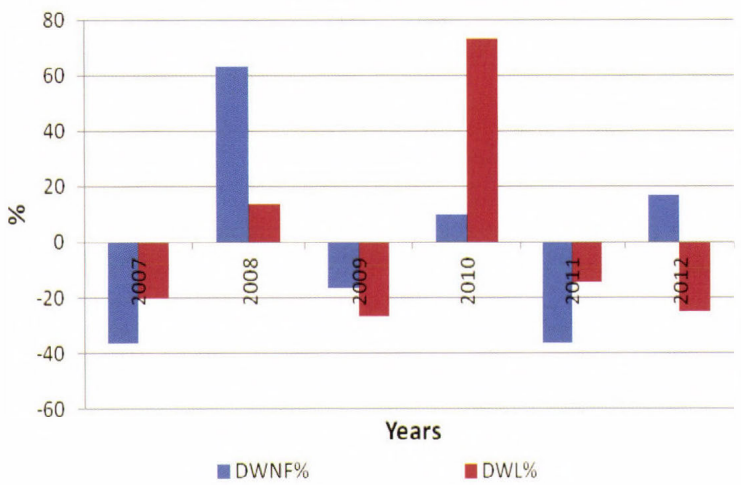

Fig. 11. The percent difference of the May-September mean water level of the period 2007–2012 within the absolute water level range of the river Tisza at Szolnok (DWL%) and the percent difference of the annual WNF case number in Hungary within the absolute water level range of the maxima and minima of the case inerval (DWNF%) in the period of 2007–2012.

3.3. Model results

3.3.1. The predicted occurrence of West Nile fever

The observed and predicted potential distributions of the WNF are shown in *Fig. 12*. The recent occurrence of visceral WNF is mostly restricted to the eastern Mediterranean areas and Eastern Europe. The model predicted the potential occurrence of WNF with the sporadic cases in the reference period to be greater than the observed current occurrence. The major difference can be seen in Spain. Future expansion is expected principally in Asia Minor, the Carpathian Basin, and the Balkan Peninsula, but the set of the affected countries is much larger: Spain, France and Hungary (mainly in the far future period), Serbia, Macedonia, Bulgaria, Romania, Ukraine, and Turkey. Considering the current occurrence and the model result, east-southeast Europe and the Carpathian Basin are highly vulnerable areas. In the western parts of Europe, the primary limiting value is the minimum temperature in July (T_{min} of July more than 20.9 °C). It seems that the continental climate with warm summers and September are favor of West Nile disease (T_{mean} from June to September should be more than about 22 °C). WNF need for moderate summer precipitation (P in July is less than about 80 mm).

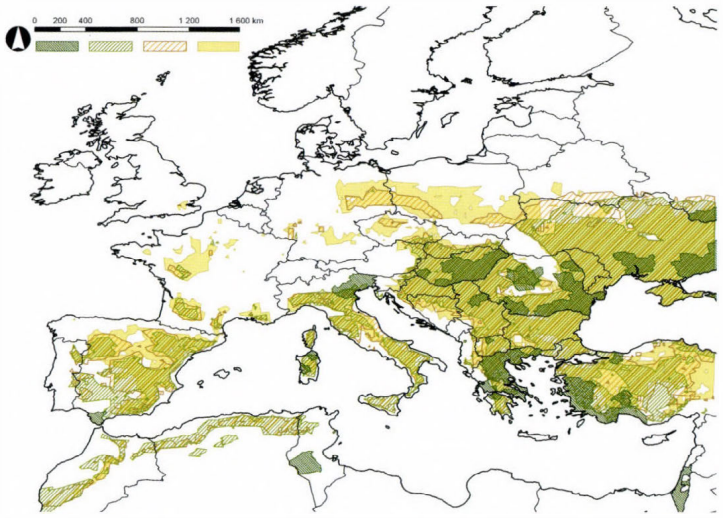

Fig. 12. The recent (2010–2012) distribution of WNF (dark green according to the VBORNET database), the potential distribution area for the reference period (1961–1990, light green), and the projected future distribution for the periods of 2011–2040 (orange) and 2041–2070 (yellow)

3.3.2. Predicted distribution of the Ae. albopictus mosquito

Observed and predicted potential distribution of the aggregation of the Asian tiger mosquito species are shown in *Fig. 13*. The Mediterranean, most of the territories of Italy, and some regions of the Balkan and Spain with Mediterranean climate are included in the observed distribution. The modeled potential distribution seems to be greater in Western Europe and in the north Balkan, and some parts of the Carpathian Basin. In the near future period expansion is predicted mainly in France, Spain, Croatia, Serbia, and Hungary. In the period of 2041–2070, significant expansion is projected in the northern parts of France. The primary limiting value is the minimum temperature in January (T_{min} should be more than about –2 °C), *Ae. albopictus* prefers the relatively dry summers (P in July is less than about 6 mm).

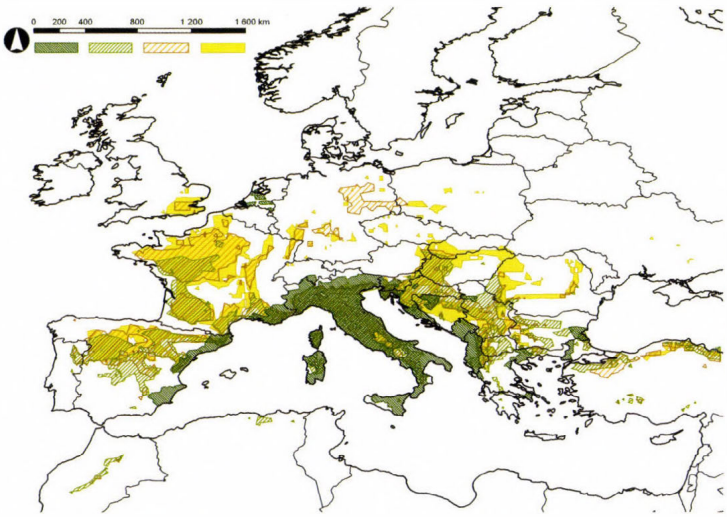

Fig. 13. The recent (2012) distribution of *A. albopictus* mosquito (dark green according to the VBORNET database), the potential distribution area for the reference period (1961–1990, light green), and the projected future distribution for the periods of 2011–2040 (orange) and 2041–2070 (yellow).

4. Discussion

The comparison of the recent and predicted future distributions of a vector and a vector-borne diseases, at first aspect, may seem to be problematic, but the recent geographical range of WNF is cannot be explained without the climate factors. The most important determinants of the spatial range of *Ae. albopictus* are climate factors according to our model.

The recent distribution of WNF suggests that climate, topographically the run of the rivers, floods, the migrating routes of birds, and the annual ontogeny of *Culex* mosquitoes together determine the occurrence of the disease.

The annual features of the epidemics suggest brief exposures in multiple focuses. In contrast to the Lyme disease occurrence in Hungary (Lyme disease is also an emerging vector-borne disease) WNF did not show constant occurrence pattern in 2008 and 2010–2012. It may explained by the fact, that in the case of Lyme disease, the parasite permanently persists in the local tick and host animal populations, while it is plausible, that birds recurring from Africa and the Mediterranean wetlands are re-introduce WNV into Hungary every year. It also explains the very low incidence of WNF in Hungary.

Our findings showed that floods have an important influence on annual WNF case number. There are differences between the major rivers, since over the larger Danube less WNF cases were observed in every year than between the smaller, but more natural rivers as Tisza and its tributaries, which have backwaters, wreaths and high amplitude water level changes. The high water level fluctuation can play an important role to create the appropriate conditions for mosquito populations (as this phenomenon is known in the case of *Anopheles darlingi* Anopheles Meigen (1818) malaria mosquitoe; *Rozendaal*, 1992) and consequently for the presence of WNF. The water level of Tisza as a characteristic representative of the rivers of the Carpathian Basin and the annual WNF case number simultaneously changed between 2007 and 2011. We studied separately the year of 2012 and we found, that the contradiction was apparent, since most of the cases occurred in Transdanubia and not in the Tisza valley thanks to the extraordinary low water level of the Tisza in this year.

According to *Epstein* (2010), the epidemic of WNF is ecologically similar to that of the St. Louis encephalitis, since these two vector-borne diseases are connected to long, hot, and dry (continental) summers with occasionally wet summers, when the case number generally is the highest. Extreme summer rainfalls are favored by WNF, and the increasing amount of extreme meteorological events are one of the consequences of climate change (*Fay et al.*, 2008; *Meehl et al.*, 2000). It may explain the observations, since the year of 2010 in Hungary was unusually wet; the total annual rainfall was two times higher than the average of the last 100 years, the 25% of the cases occurred in this year. Naturally, we cannot make conclusions based on the observations of a single year.

In the case of the *Aedes* mosquito, the connection between the climate and the geographical distribution is the clearest. The main determinants of the European distribution of *Ae. albopictus* are climatic conditions, mainly the mean temperature in July, the minimum temperature in January, and the low precipitation of the summer months (Mediterranean summers). Climatically the geographical occurrence of WNF is partly determined by the warm ambient

temperature of July and August with wet summers. According to the VBORNET (2012) database, the recent occurrence of WNF in Europe is mainly similar to the migration route of white stork from the east sub-saharan Africa (e.g., Uganda, by via Sinai) to central and eastern Europe. Although climatic factors alone cannot explain the observed occurrence of West Nile virus, they indicate that dry and warm summers, and heavy rainfalls can enhance the population density of *Culex* mosquitoes (*Reeves et al.*, 1994; *Reiter*, 2001). According to *Sellers* and *Maarouf* (1990), warm winds may carry infected mosquitoes from the dry riverbanks to northern areas. The above described extreme weather events are specific to continental climate conditions, where the disease recently occurred.

The seasonality of WNF is regular as far as it can be judged from the low case number of the last decade, it starts in late July, has a peak from August to mid-September and declines, when the weekly mean ambient temperature drops below 13–14 °C. Climate change may cause a shift in the WNF season elongating the hottest period of summer and enhancing the warmer period of the autumn season. This seasonality may correspond to the spring early summer migration of birds (*Jourdain et al.*, 2007), in the sense that time needs to ensure a sufficient number of mosquito contaminate with the virus for the chance of human transmission.

In contrast to, e.g., *Culex pipiens* or *Culex modestus, Ae. albopictus* mosquito prefers the more balanced conditions and milder winters of subtropical coasts of the Mediterranean basin. Higher summer precipitation seems to be a major limiting factor in the model for *Ae. albopictus*, which is in accordance with the study of *Alto* and *Juliano* (2001) who found that Asian tiger mosquito populations occurring in warmer regions are likely to produce more adults as long as water bodies (e.g., containers, little ponds) do not dry completely. We found, that *Ae. albopictus* does not prefer the wetter climate of the oceanic areas of Western Europe, which also matches with *Alto* and *Juliano* (2001) who found that the populations of the mosquito in cooler regions produce less amount of adults with the variability of precipitation. In the case of *Aedes* mosquito, wetlands and floodplains do not seem to be primary determinants of the distribution. Our model findings are highly in accordance with the findings of *Fischer et al.* (2011) who projected the future expansion of *Ae.albopictus* mosquito to the end of the 2060's to France, the western part of the Carpathian Basin.

The major benefit of our model is that the observed temperature requirement of the WNF peak season in Hungary is similar to the modeled temperature needs (T_{mean} of the summer months and September is more than 20 °C). Since 3 days to two weeks latency is plausible (CDC), the mosquito bites may occur at higher weekly mean temperatures.

5. Conclusions

Our study indicates that in creating a climate envelope model for a vector-borne disease or a vector, the primary concern is to consider the behavior, and the requirements of every elements of the vectorial chain. Climate can be the main determinant of the distribution, but in other cases climate itself is not sufficient to explain the observed distribution or occurrence. The predicted future warmer and dryer summer seasonal climate of the Carpathian Basin is likely to extend the northern distribution of *Ae. albopictus* and may modify the seasonality of West Nile fever. Floods has a very important role in modifying the mosquito abundance rivers which have a major water running as the river Tisza and have more or less preserved floodplains offering better conditions for mosquitos than the highly regulated rivers. Recently it is plausible, that birds re-introduce WNF into Hungary from year to year.

Acknowledgements—The authors would like to thank *Arnold Móra* MSc, the research assistant of the Balaton Limnological Research Institute of the Hungarian Academy of Sciences for the summary distribution map of Chironomidae mosquitos in Hungary. The research was supported by Project TÁMOP-4.2.1/B-09/1/KMR-2010-0005 and TÁMOP (4.2.2. A-11/1/KONV-2012-0064, 1.1). The ENSEMBLES data used in this work was funded by the EU FP6 Integrated Project ENSEMBLES (Contract number 505539) whose support is gratefully acknowledged.

References

Alto, B.W. and *Juliano, S.A.*, 2001: Precipitation and temperature effects on populations of Aedes albopictus (Diptera: Culicidae): implications for range expansion. *J. med. entomol. 38*, 646.

Bardos, V., Adamcová, J., Dedei, S., Gjini, N., Rosicky, B., and *Simkova, A.*, 1959: Neutralizing antibodies against some neurotropic viruses determined in human sera in Albania. *J. hyg. epid. microbial. immunol. 3*, 277.

Bartholy, J., Pongrácz, R.,and *Gelybó, Gy.*, 2007: A 21. század végén várható éghajlatváltozás Magyarországon. *Földrajzi Értesítő 56*, 147–168. (In Hungarian)

Bayoh, M.N. and *Lindsay, S.W.*, 2003: Effect of temperature on the development of the aquatic stages of Anopheles gambiae sensu stricto (Diptera: Culicidae). *B. entomol. res. 93*, 375–382.

Bayoh, M.N. and *Lindsay, S.W.*, 2004: Temperature-related duration of aquatic stages of the Afrotropical malaria vector mosquito Anopheles gambiae in the laboratory. *Med. veterinary entomol., 18*, 174–179.

Berthold, P., Kaatz, M., and *Querner, U.*, 2004: Long-term satellite tracking of white stork (Ciconia ciconia) migration: constancy versus variability. *J. Ornithol. 145*, 356–359.

Cannon, R.J., 2004: The implications of predicted climate change for insect pests in the UK, with emphasis on non-indigenous species. *Glob. Change Biol. 4*, 785–796.

Czúcz, B., 2010: Az éghajlatváltozás hazai természetközeli élőhelyekre gyakorolt hatásainak modellezése. PhD dissertation. Corvinus University of Budapest, Faculty of Horticultural Sciences. Budapest. (In Hungarian)

CDC: West Nile Virus (WNV) Infection: Information for Clinicians. Clinical features. http://www.cdc.gov/ncidod/dvbid/westnile/resources/fact_sheet_clinician.htm. Last accessed: 27 March 2013.

Chumakov, M.P., Belyaeva, A.P., and *Butenko, A.M.,* 1964: Isolation and study of an original virus from Hyalomma plumbeum plumbeum ticks and from the blood of a febrile patient in the Astrakhan region. *Materialy XI Nauchnoi Sessii Instituta Poliomielita i Virusnykh Encefalitov* (Moskva), 5–7.

De la Roque, S., Rioux, J.A., and *Slingenbergh, J.,* 2008: Climate change: Effects on animal disease systems and implications for surveillance and control. *Rev. Sci.t Tech. Int. Epizooties 27,* 339–354.

Dukes, J.S. and *Mooney, H.A.* (1999): Does global change increase the success of biological invaders? *Trends Ecol. Evolut. 14,* 135–139.

ECDC, West Nile fever maps 2012: Reported cases of WNF for the EU and the neighbouring countries. www.ecdc.europa.eu/en/healthtopics/west_nile_fever/West-Nile-fever-maps/Pages/index.aspx. Last accessed: 27 March 2013.

ECDC, West Nile fever maps 2011: Reported cases of WNF for the EU and the neighbouring countries. ecdc.europa.eu/en/healthtopics/west_nile_fever/West-Nile-fever-maps/Pages/index.aspx. Last accessed: 27 March 2013.

Elith, J., Leathwick, J.R., 2009: Species Distribution Models: Ecological Explanation and Prediction Across Space and Time. *An. Rev. Ecol. Evolut. Systematics 40,* 677–697.

ENSEMBLES, 2013: ENSEMBLES data archive. ensemblesrt3.dmi.dk. Last accessed: 27 March 2013.

Epinfo, 2010A: Nyugat-nílus láz megbetegedések Magyarországon és Európában. *Epinfo 17/34,* 449–452. (In Hungarian)

Epinfo, 2010B: Nyugat-nílus láz megbetegedések, Magyarországon, 2010. *Epinfo 17/36,* 417–424. (In Hungarian)

Epstein, P.R., Diaz, H.F., Elias, S., Grabherr, G., Graham, N.E., Martens, W.J., and *Susskind, J.,* 1998: Biological and physical signs of climate change: focus on mosquito-borne diseases. *B. Am. Meteorol. Soc. 79,* 409–417.

Fay, P.A., Kaufman, D.M., Nippert, J.B., Carlisle, J.D., and *Harper, C.W.,* 2008: Changes in grassland ecosystem function due to extreme rainfall events: implications for responses to climate change. *Glob. Change Biol. 14,* 1600–1608.

Fischer, D., Thomas, S.M., Niemitz, F., Reineking, B., and *Beierkuhnlein, C.,* 2011: Projection of climatic suitability for Aedes albopictus Skuse (Culicidae) in Europe under climate change conditions. *Glob. Planet. Change, 78,* 54–64.

Githeko, A.K., Lindsay, S.W., Confalonieri, U.E., and *Patz, J.A.,* 2000: Climate change and vector-borne diseases: a regional analysis. *B. WHO 78,* 1136–1147.

GISCO, 2013: GISCO - Eurostat (European Commission). epp.eurostat.ec.europa.eu/portal/page/-portal/gisco_Geographical_information_maps/popups/references/administrative_units_statistical_units_1. Last accessed: 2013.01.01

Global Register of Migratory Species. www.groms.de. Last accessed: 27 March 2013.

Global Register of Migratory Species. Ciconia ciconia. www.groms.de/groms/Ciconia_Info.html. Last accessed: 27 March 2013.

Goldblum, N., Sterk, V., and *Paderski, B.,* 1954: WNF, The clinical features op tue disease and the Isolation of West Nile Virus from the blood of nine human cases. *Am. J. Epidemiol. 59,* 89–103.

Guisan, A. and *Zimmermann, N.E.,* 2000: Predictive habitat distribution models in ecology. *Ecolog. Model. 135,* 147–186.

Hammer R.O., Harper D.A.T. and *Ryan P.D..,* 2001: PAST: Paleontological statistics software package for education and data analysis. *Paleontol Electron, 4,* 1-9.

Hannoun C, Panthier R, Mouchet J., and Eouzan Jp., 1964: Isolement En France Du Virus West-Nile 'A Partir De Malades Et Du Vecteur Culex Modestus Ficalbi. *C. R. Hebd. Seances Acad. Sci. 30,* 4170–4172.

Harvell, C.D., Mitchell, C.E., Ward, J.R., Altizer, S., Dobson, A.P., Ostfeld, R.S., and *Samuel, M.D.,* 2002: Climate warming and disease risks for terrestrial and marine biota. *Science 296,* 2158–2162.

Hijmans, R.J. and *Graham, C.H.,* 2006: The ability of climate envelope models to predict the effect of climate change on species distributions. *Glob. Change Biol. 12,* 2272–2281.

Hubálek, Z. and *Halouzka, J.,* 1999: WNF–a reemerging mosquito-borne viral disease in Europe. *Emerg. infect.dis. 5,* 643.

Hunter, P.R., 2003: Climate change and waterborne and vector-borne disease. *J. Appl.Microbiol. 94(s1)*, 37–46.

Hydroinfo. Országos vízjelző szolgálat. Archívum. Éves vízállástáblázatok. http://www.hydroinfo.hu–/Html/archivum/archiv_tabla.html. Last accessed: Last accessed: 27 March 2013.(In Hungarian)

Jourdain, E., Gauthier-Clerc, M., Bicout, D., and *Sabatier, P.*, 2007: Bird migration routes and risk for pathogen dispersion into western Mediterranean wetlands. *Emerg. Infect. Dis. 13*, 365.

Kilpatrick, A.M., Meola, M.A., Moudy, R.M., and *Kramer, L.D.*, 2008: Temperature, viral genetics, and the transmission of West Nile virus by Culex pipiens mosquitoes. *PLoS pathogens 4*, e1000092.

Krisztalovics, K., .Bán, E., Ferenczi, E., Zöldi, V., Bakonyi, T., Erdélyi, K., Szalkai, T., Csohán, Á., and *Szomor, K.*, 2011: Nyugat-nílus láz Magyarországon 2010. Epinfo, 18/9-10(6): 89–94. (In Hungarian)

Krisztalovics, K., Ferenczi, E., Molnár, Z.S., Csohán, Á., Bán, E., Zöldi, V., Kaszás, K,. 2008: West Nile virus infections in Hungary, August-September 2008. *Euro surveillance: bulletin européen sur les maladies transmissibles= European communicable disease bulletin, 13*(45), pii-19030.

KSH, 2012: Magyarország térképek. Lakónépesség 2012. január 1. http://www.ksh.hu/interaktiv/terkepek/mo/nepesseg.html. Last accessed: 27 March 2013. (In Hungarian)

Ladányi, M. and *Horváth, L.*, 2010: A review of the potential climate change impact on insect populations – general and agricultural aspects. *Appl. Ecol. Environ.Res. 8*, 143–152.

Lindegaard, C., 1995: Classification of water-bodies and pollution. The Chironomidae. 385-404. Springer, Netherlands.

Mackenzie, J.S., Gubler, D.J., and *Petersen, L.R.*, 2004: Emerging flaviviruses: the spread and resurgence of Japanese encephalitis, West Nile and dengue viruses. *Nature med. 10*, S98–S109.

Malkinson, M., Banet, C., Weisman, Y., Pokamunski, S., and *King, R.*, 2002: Introduction of West Nile virus in the Middle East by migrating white storks. *Emerg. Infect. Dis. 8*, 392.

McLean, R.G., Ubico, S.R., Docherty, D.E., Hansen, W.R., Sileo, L., and *McNamara, T.S.*, 2001: West Nile virus transmission and ecology in birds. *Ann. N Y Acad. Sci. 951*, 54-57.

Medlock, J.M., Hansford, K.M., Schaffner, F., Versteirt, V., Hendrickx, G., Zeller, H,. and *Bortel, W.V.*, 2012: A review of the invasive mosquitoes in Europe: ecology, public health risks, and control options. *Vector-Borne Zoonotic Dis. 12*, 435–447.

Meehl, G.A., Zwiers, F., Evans, J., Knutson, T., Mearns, L., and *Whetton, P.*, 2000: Trends in Extreme Weather and Climate Events: Issues Related to Modeling Extremes in Projections of Future Climate Change. *B. Am. Meteorol. Soc. 81*, 427–436.

Móra, A. and *Dévai, Gy.*, 2004: Magyarország árvaszúnyog-faunájának (Diptera: Chironomidae) jegyzéke az előfordulási adatok és sajátosságok feltüntetésével. *Acta Biol. Debr. Oecol. Hung 12*: 39.207. (In Hungarian)

Nakicenovic, N., Alcamo, J., Davis, G., de Vries, B., Fenhann, J., Gaffin, S., and *Dadi, Z.*, 2000: Special report on emissions scenarios: a special report of Working Group III of the Intergovernmental Panel on Climate Change (No. PNNL-SA-39650). Pacific Northwest National Laboratory, Richland, WA (US), Environmental Molecular Sciences Laboratory (US).

Neghina, R., Neghina, A.M., Merkler, C., Marincu, I., Moldovan R., and *Iacobiciu. I.*, 2009: Importation of visceral leishmaniasis in returning Romanian workers from Spain. *Travel Med Infect Dis. 7*, 35–39.

Rappole, J.H. and *Hubalek, Z.*, 2003: Migratory birds and West Nile virus. *J. Appl. Microbiol. 94*(s1), 47–58.

Reed, K.D., Meece, J.K., Henkel, J.S., and Shukla, S.K., 2003: Birds, migration and emerging zoonoses: West Nile virus, Lyme disease, influenza A and enteropathogens. *Clinic. Med. Res. 1*, 5–12.

Reeves, W.C., Hardy, J.L., Reisen, W.K., and *Milby, M.M.*, 1994: Potential effect of global warming on mosquito-borne arboviruses. *J. Med. Entomol. 31*, 323–332.

Reisen, W.K., Fang, Y., and *Martinez, V.M.*, 2006: Effects of temperature on the transmission of West Nile virus by Culex tarsalis (Diptera: Culicidae). *J. med. entomol. 43*, 309–317.

Reiter, P., Fontenille, D., and *Paupy, C.*, 2006: Aedes albopictus as an epidemic vector of chikungunya virus: another emerging problem? *Lancet infect. dis. 6*, 463–464.

Reiter, P., 2001: Climate change and mosquito-borne disease. *Environ. Health Perspect. 109*(S1), 141-161

Roeckner, E., Bäuml, G., Bonaventura, L., Brokopf, R., Esch, M., Giorgetta, M., Hagemann, S., Kirchner, I., Kornblueh, L., Manzini, E., Rhodin, A., Schlese, U., Schulzweida, U., and *Tompkins, A.*, 2003: The atmospheric general circulation model ECHAM 5. Part I: Model description. Max-Planck-Institut für Meteorologie, Hamburg.

Roeckner E., Brokopf, R., Esch, M., Giorgetta, M., Hagemann, S., Kornblueh, L., Manzini, E., Schlese, U., and *Schulzweida, U.*, 2004: The atmospheric general circulation model ECHAM 5. PART II: Sensitivity of Simulated Climate to Horizontal and Vertical Resolution. Max-Planck-Institut für Meteorologie, Hamburg.

Rogers, D.J. and *Randolph, S.E.*, 2006: Climate Change and Vector-Borne Diseases. *Adv. Parasitol. 62*. 345–381.

Rozendaal, J.A., 1992: Relations between Anopheles darlingi breeding habitats, rainfall, river level and malaria transmission rates in the rain forest of Suriname. *Med. veteran. entomol. 6*, 16–22.

Rueda, L.M., Patel, K.J., Axtell, R.C., and *Stinner, R.E.*, 1990: Temperature-dependent development and survival rates of Culex quinquefasciatus and Aedes aegypti (Diptera: Culicidae). *J. Med. Entomol. 27*, 892–898.

Sellers, R.F. and *Maarouf, A.R.*, 1989: Trajectory analysis and bluetongue virus serotype 2 in Florida 1982. *Can. J. Veterinar. Res. 53*, 100.

Spielman, A., 2001: Structure and seasonality of nearctic Culex pipiens populations. *Ann.N.Y. Acad. Sci. 951*, 220–234.

Teng, H.J. and *Apperson, C.S.*, 2000: Development and survival of immature Aedes albopictus and Aedes triseriatus (Diptera: Culicidae) in the laboratory: effects of density, food, and competition on response to temperature. *J. Med. Entomol. 37*, 40–52.

Thuiller, W., Araújo, M.B., and *Lavorel, S.*, 2004: Do we need land-cover data to model species distributions in Europe? *J. Biogeograph. 31*, 353–361.

Topciu, V., Roşiu, N., Arcan, P., Fufezan, V., and *Bran, B.*, 1971: The existence of arbovirus group B (Casals) disclosed by serological analysis of various animal species in the province of Banat (Rumania)]. *Arch. roumain. pathol. exp. microbial. 30*, 231.

The migration routes and staging areas of the storks. www.groms.de/groms/Ciconia_Info.html. Last accessed: 27 March 2013.

VBORNET, 2013: VBORNET maps-Mosquitoes. The current distribution of Aedes albopictus.ecdc.europa.eu/en/activities/diseaseprogrammes/emerging_and_vector_borne_diseases/Pages/VBORNET_maps.aspx. Last accessed: 27 March 2013.

Walther, G.R., Roques, A., Hulme, P.E., Sykes, M.T., Pyšek, P., Kühn, I., and *Settele, J,.* 2009: Alien species in a warmer world: risks and opportunities. *Trends Ecol. Evol. 24*, 686–693.

West Nile fever map 2012. Reported cases of the West Nile fever for the EU and the neighbouring countries. ecdc.europa.eu/en/healthtopics/west_nile_fever/West-Nile-fever-maps/Pages/index.aspx. Last accessed: 27 March 2013.

IDŐJÁRÁS

Quarterly Journal of the Hungarian Meteorological Service
Vol. 118, No. 1, January – March 2014, pp. 41–52

Impact of climate change on the potential distribution of Mediterranean pines

Ákos Bede-Fazekas[1]*, Levente Horváth[2], Márton Kocsis[3]

[1]*Corvinus University of Budapest, Faculty of Landscape Architecture, Department of Garden and Open Space Design*
Villányi út 29-43, H-1118 Budapest, Hungary
bfakos@gmail.com

[2]*Corvinus University of Budapest, Faculty of Horticultural Science, Department of Mathematics and Informatics;*
"Adaptation to Climate Change" Research Group
Villányi út 29-43, H-1118 Budapest, Hungary
levente.horvath@uni-corvinus.hu

[3]*Corvinus University of Budapest, Faculty of Horticultural Science, Department of Farm Management and Marketing*
Villányi út 29-43, H-1118 Budapest, Hungary
marton.kocsis@uni-corvinus.hu

* *Corresponding author*

(Manuscript received in final form March 27, 2013)

Abstract—The impact of climate change on the potential distribution of four Mediterranean pine species – *Pinus brutia* Ten., *Pinus halepensis* Mill., *Pinus pinaster* Aiton, and *Pinus pinea* L. – was studied by the Climate Envelope Model (CEM) to examine whether these species are suitable for the use as ornamental plants without frost protection in the Carpathian Basin. The model was supported by EUFORGEN digital area database (distribution maps), ESRI ArcGIS 10 software's Spatial Analyst module (modeling environment), PAST (calibration of the model with statistical method), and REMO regional climate model (climatic data). The climate data were available in a 25 km resolution grid for the reference period (1961–1990) and two future periods (2011–2040, 2041–2070). The regional climate model was based on the IPCC SRES A1B scenario. While the potential distribution of *P. brutia* was not predicted to expand remarkably, an explicit shift of the distribution of the other three species was shown. Northwestern African distribution segments seem to become abandoned in the future. Current distribution of *P. brutia* may be highly endangered by the climate change. *P. halepensis* in the southern part and *P. pinaster* in the western part of the Carpathian Basin may find suitable climatic conditions in the period of 2041–2070.

Key-words: Mediterranean pines, climate envelope model, CEM, potential distribution, climate change, distribution modeling, *Pinus brutia*, *Pinus halepensis*, *Pinus pinaster*, *Pinus pinea*

1. Introduction

According to the predictions for the period of 2011–2040, spatially analogue territories of Hungary – the territories with present climate similar to the future climate of Hungary – can be found in Southern Romania, Northern Bulgaria, Serbia, Macedonia, and Northern Greece (*Horváth*, 2008). Therefore, the ornamental plant assortment of Hungary – as the assortment of other central and eastern European countries – should be reconsidered (*Szabó* and *Bede-Fazekas*, 2012; *Schmidt*, 2006). This realization inspired some previous studies (*Bede-Fazekas*, 2012a,b) on whether some warm-demanding ligneous plants are able to be adapted in Hungary in the future.

By this time, regional climate models have good horizontal and temporal resolution and are reliable enough for creating some climate envelope models (CEMs) based on the current distribution of tree species. Our previous works of research were about modeling the future area of introduction of several Mediterranean ligneous plant species that can have significance in the future ornamental plant usage. Based on these former studies, it was aimed to run a new and more accurate model on four of the previously studied species. The improvement of the modeling method was achieved by statistical calibration based on an iterative error evaluation. Hence, the improved model is able to study not the future area of introduction but the future potential distribution.

We aimed to create multi-layered distribution maps with a GIS (Geographic Information System) software, displaying the predicted shift of the potential distributions. These maps can have importance not only in forestry, landscape architecture, and botany, but in visualization of the effects of climate change also for non-professionals (*Czinkóczky* and *Bede-Fazekas*, 2012). The studied species were Brutia pine (*Pinus brutia* Ten. syn. *Pinus halepensis* var. *brutia* (Ten.) A. Henry), Aleppo pine (*Pinus halepensis* Mill.), maritime pine (*Pinus pinaster* Aiton syn. *Pinus maritima* Lam.), and Italian stone pine (*Pinus pinea* L.), which are very close relatives (classified in section *Pinus*, subsection *Pinaster*) according to phylogenetic studies (*Wang et al.*, 1999; *Gernandt et al.*, 2005; *Eckert* and *Hall*, 2006).

2. Materials and methods

2.1. Climate data and distribution maps

The current (latest update was achieved in 2008) continuous distribution map of the species was derived from the EUFORGEN digital area database (*Euforgen*, 2008), while the discrete (fragmented) observations were ignored. Therefore 28 (*P. brutia*), 233 (*P. halepensis*), 23 (*P. pinaster*), and 109 (*P. pinea*) observed data were disregarded by the model. The distributions from 2008 were bound to

the reference period. This difference may not cause any problem since the pines have long life cycle and can slowly adapt to the changing climate.

The climatic data were gained from the REMO regional climate model (RCM); the grid had a 25 km horizontal resolution. The model REMO is based on the ECHAM5 global climate model (*Roeckner et al.*, 2003, 2004) and uses the IPCC SRES scenario called A1B. This scenario supposes a future world characterized by a very rapid economic growth, a global population that peaks in the mid-century, and rapid introduction of new and more efficient technologies (*Nakicenovic* and *Swart*, 2000). The reference period was 1961–1990, the two future periods of modeling were 2011–2040 and 2041–2070. The entire European continent is within the domain of REMO, we used, however, only a part of the grid (25724 of the 32300 points; *Fig. 1*).

36 climatic variables were used for the distribution modeling: monthly mean temperature (T, °C), monthly minimum temperature (M, °C), and monthly precipitation (P, mm). All climatic data were averaged in the three periods.

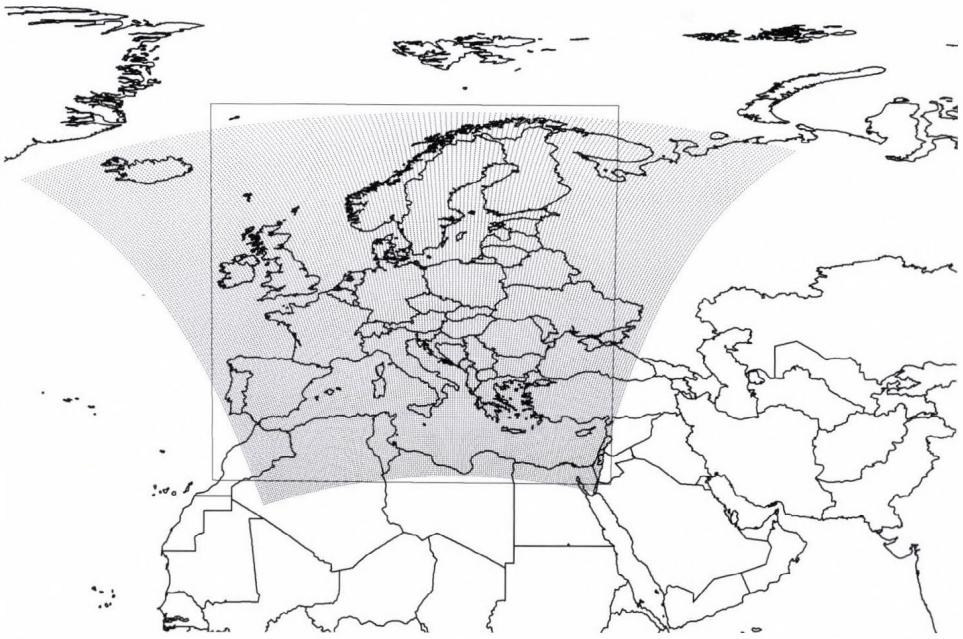

Fig. 1. The domain of climate model REMO and its part used in the study.

2.2. Climate envelope modeling

2.2.1. Modeling approach and software

ESRI ArcGIS 10 software was used for preparing climatic data, running the model, and displaying the model results. Climatic data were managed and the expressions for modeling were prepared with the assistance of Microsoft Excel 2010 program. PAST statistic analyzer software (*Hammer et al.*, 2001) was used for creating the cumulative distribution function of the climatic parameters, and getting the percentile values of the parameters (model calibration).

The impact of climate change on the distribution of selected species was modeled with climate envelope modeling (CEM; also known as niche-based modeling, correlative modeling) (*Hijmans* and *Graham*, 2006). This method is about predicting responses of species to climate change by drawing an envelope around the domain of climatic variables where the given species has been recently found, and then identifying areas predicted to fall within that domain under future scenarios (*Ibáñez et al.*, 2006). It hypothesizes that (both present and future) distributions are dependent mostly on the climatic variables (*Czúcz*, 2010) which is somewhat dubious (*Skov* and *Svenning*, 2004). Compared to mechanistic models, CEM tries to find statistical correlations between climate and distribution of species (*Guisan* and *Zimmermann*, 2000; *Elith* and *Leathwick*, 2009), and models the future temporal correspondence based on the present spatial correspondence between the variables (*Pickett*, 1989).

2.2.2. Calibration by iterative modeling

The calibration of the model has been conducted by iterative error evaluation. The model was run iteratively to determine the optimal amount of percentiles to be left from the climatic values. Cumulative distribution functions were calculated by PAST for all climatic parameters. Then 0 to 14 percentiles have been left from the lower values of a certain type of climate parameters (e.g., 12 monthly precipitations), while the maximum values were fixed and also the other 24 climatic parameters were fixed at the extreme values. In case of a certain species, 90 error evaluations were done. Two types of error values were calculated: internal (the ratio of the current distribution segment not determined by the model), and external (the ratio of area outside the current distribution, determined falsely by the model). Then the errors were summarized. The increasing accumulated error function determined the appropriate number of percentiles to left: the greatest number of percentiles was chosen which produces no more than 100% summarized error. Cohen's kappa values (*Cohen*, 1960) were estimated in two cases: without and with percentile leaving to evaluate the improvement achieved by the model calibration.

This iterative calibration technique shows several similarities with "area under the receiver operating characteristic (ROC) curve" (AUC; *Hanley* and *Mcneil*, 1982). The comments of *Lobo et al.* (2008) on AUC may also refer to the calibration method used in this research. For further error-based model calibration procedures see *Fielding* and *Bell* (1997).

2.2.3. Modeling method

First, climatic data were refined by Inverse Distance Weighted interpolation method. Then the modeling steps were as follows:

1. The grid points within the distribution were queried (a few hundred × 36 data; ArcGIS).
2. The percentile points of the 36 climatic parameters (101×36 data, PAST) were calculated.
3. The appropriate percentiles of the climatic parameters determined by the calibration were selected (2×36 data, Excel).
4. Modeling phrases (3 strings, Excel) were created by string functions for the three modeling periods.
5. Those territories were selected where all the climatic values of the certain period were between the extremes selected in step 3. (ArcGIS – Raster Calculator function).

Positive raster results were transformed to ESRI shapefile format (polygons). The order of the four layers (one observed and three modeled distributions) determines whether the result maps are able to display the northward expansion, not the retreat from the southern parts (trailing edge) of the current distribution. Therefore, two types of layer order were applied and are shown herein.

3. Results

3.1. Result of iterative modeling

Based on the iterative modeling, the optimal number of percentiles to be left was determined in case of the four species, and two extremes of the three types of climate variables (*Table 1*). The improvement of the model can be estimated by comparing the two different Cohen's kappa values. The most significant improvement can be seen in case of *P. pinaster*, while the Cohen's kappa value shows inessential increase in case of *P. pinea*.

Table 1. The result of model calibration: the number of percentiles to be left over, the Cohen's kappa value before (Ck 1) and after (Ck 2) percentile omission

Species	min(*T*)	max(*T*)	min(*M*)	max(*M*)	min(*P*)	max(*P*)	Ck 1	Ck 2
P. brutia	3	2	3	3	5	3	0.1157	0.2056
P. halepensis	9	2	9	3	3	2	0.1103	0.2474
P. pinaster	6	3	6	3	2	4	0.0862	0.2848
P. pinea	6	1	5	2	2	1	0.0805	0.1484

3.2. Modeled potential distributions

3.2.1. Brutia pine (Pinus brutia)

The current distribution of *P. brutia* (*Fig. 2a; Fig. 3a*) is focused on the eastern Mediterranean region (Turkey, Cyprus, and Malta), while the model results in a much larger potential distribution for the reference period that includes southern Portugal, southern Spain, northern Morocco, northern Algeria, Sardinia, southern Italy, and Greece. The Cyprian and Cretan distribution segments were however, not redrawn by the model. Significant northern expansion is not predicted, and Hungary is not affected by the model. Maritime distribution in Turkey seems to become partly viable for the species in the periods of 2011–2040 (near Adana) and 2041–2070 (near Denizli). The Turkish discrete distributions seem to remain climatically viable.

3.2.2. Aleppo pine (Pinus halepensis)

Segments of the observed distribution of *P. halepensis* (*Fig. 2b; Fig. 3b*) can be found in eastern Spain, southern France, Italy, southern Greece, northern Morocco, Algeria, Tunisia, and Libya. The model cannot redraw the Libyan distribution fragment. The potential distribution for the reference period seems to be larger than the observed area: southern Portugal and Spain, Italy, Corsica and Sardinia, the coast of the Aegean Sea, and greater North African territories are modeled to be suitable for the species. Future expansion is predicted in Spain, France, Italy, Croatia, Bosnia and Herzegovina, Serbia, Bulgaria, and the Crimea. The western territories seem to become suitable for living sooner, while the Balkan Peninsula and the Crimea are predicted to be affected only in the far future period. Although most of the discrete distributions in the western Mediterranean were redrawn by the model, discrete observations near Croatia, Lebanon, and Jordan were not. A large part of the distribution in North Africa seems to become abandoned in the period of 2011–2040. Also the Italian and Greek coastline may be negatively affected. Interestingly, some of the Spanish and French distribution segments are predicted to find more suitable climatic environment in the future than in the reference period.

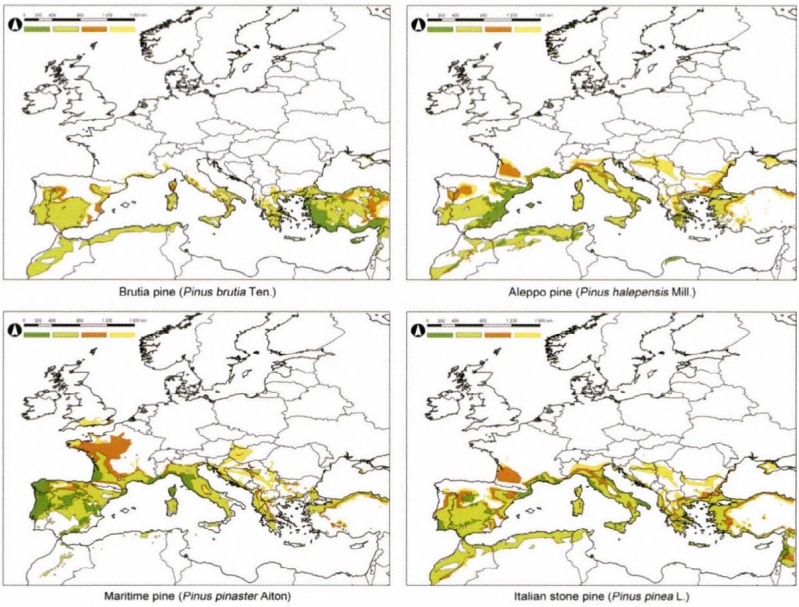

Fig. 2. Expansion: current distribution (dark green), modeled potential distribution in the reference period (light green), and modeled potential distribution in the periods of 2011–2040 (orange) and 2041–2070 (yellow) of the four studied *Pinus* species.

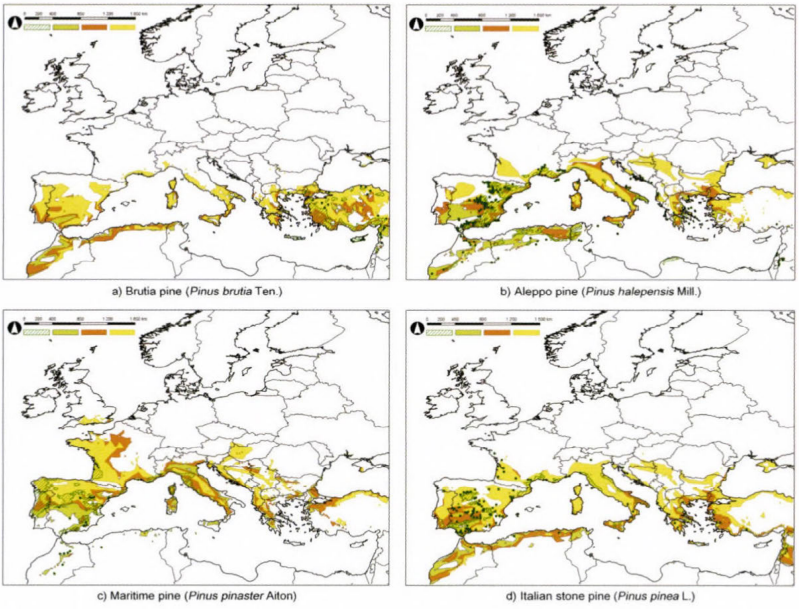

Fig. 3. Retraction: current distribution (dark green hatch and points), modeled potential distribution in the reference period (light green), and modeled potential distribution in the periods of 2011–2040 (orange) and 2041–2070 (yellow) of the four studied *Pinus* species.

3.2.3. Maritime pine (Pinus pinaster)

The current distribution of *P. pinaster* (*Fig. 2c; Fig. 3c*) is focused on the western Mediterranean (Portugal, Spain, southern France, Corsica, and northern Italy), which is well expressed by the model. The African (continuous and discrete) distribution segments are, however, not redrawn by the model. Significant northern expansion is predicted to occur in western France, southern England, the Balkans, and the western part of the Carpathian Basin. The latter areas may become suitable for the species in the far future period, while the expansion to western France seems to occur between 2011 and 2040. Maritime and southern Iberian distributions may become abandoned in the period of 2011–2040. By the end of the studied future periods the climate seems to remain suitable for the species in northern Spain and France.

3.2.4. Italian stone pine (Pinus pinea)

Apart from central Spain, *P. pinea* (*Fig. 2d; Fig. 3d*) is clearly a coastal pine: its current distribution includes maritime parts of Portugal, Spain, France, Italy, Turkey, Syria, and Lebanon. The potential distribution for the reference period is modeled to include North African coastal territories, southern Portugal and Spain, Italy, and the coastline of the eastern Mediterranean. Future northern expansion can be seen in France, Italy, and the Balkans. Only the Syrian, southern Spanish, and eastern Italian distribution segments are somewhat endangered (the latter one only in the far future period). Most of the distributions in Italy, France, and Spain seem to remain viable by the end of the studied period. Similarly to *P. halepensis*, some continuous and discrete Spanish and French distribution segments are predicted to find more suitable climatic conditions in the future than in the reference period. Discrete distributions in North Africa, Italy, Greece, and Turkey seem to remain viable at least by the period of 2011–2040.

4. Discussion

4.1. Model evaluation

Although the aforementioned predictions are obviously valuable and spectacular, there are some questions and disadvantages concerning the model applied. Opinions differ if climatic variables are by themselves sufficient or even the most important factors for explaining the real distribution of species (*Dormann*, 2007). In case of determining the potential distribution of plant species, edaphic characteristics found within their current distribution area seem to be the only parameters that may be as important as climatic factors are. The studied conifers are, however, tolerant to the alkalinity/lime content of the soil in an extent that they are able to be planted as ornamentals in their predicted future potential distribution

area. Nevertheless, it must be noted that the previously presented model results should, in botanical point of view, not to be acknowledged without considering edaphic characteristics. It should also be noted that extremes and absolute climatic values (rather than averages) may better explain the limits of distribution (*Kovács-Láng et al.*, 2008). The input climate data were obtained from RCM, which differ from the observed meteorological data. No bias correction was applied on the modeled climate data, since the bias correction should have been used in the same way in case of the reference and future periods and, therefore, no remarkable difference could have been evolved. The applied model calibration technique seems to result in a realistic and supportable model, since

1. the differences between the potential and observed distributions are not unacceptably large;
2. iterative model calibration resulted in doubled Cohen's kappa values in case of three of the four studied species; and
3. ornamental plantings of these pines in central and western Europe have proven that the predictions are not overestimations.

Various other ways can be found to determine the climate envelope, including simple regression, distance-based methods, genetic algorithms for rule-set prediction, and neural nets (*Ibáñez et al.*, 2006). Our subsequent aim is to develop a program module for ArcGIS that implements the artificial intelligence algorithm artificial neural network (ANN) for modeling the future distribution of Mediterranean tree species.

The model results for the reference period show the least difference to the observed distribution in case of *P. halepensis* and *P. pinaster*, while the model performed worst in case of *P. pinea* (*Table 2*).

Table 2. The points of grid are within the observed distribution; the ratio of modeled and observed points in the reference period; the expansion from the reference period to the near future period; and the expansion from the reference period to the far future period in case of the four studied species

Species	Observed points	Model/observation (%)	Expansion 2011–2040 (%)	Expansion 2041–2070 (%)
P. brutia	236	591.10	14.41	30.04
P. halepensis	326	380.06	22.28	56.98
P. pinaster	352	351.14	31.55	48.95
P. pinea	176	849.43	23.88	53.98

4.2. Shift of distributions

Our former research found that the extent of future shift of area of introduction is much larger. That model was, however, inaccurate. The results of this improved model show clearly and spectacularly the impacts of the predicted

climate change on the distribution of Mediterranean pines. The most affected territories may be France and the Balkans. By comparing the model results of the reference period to the results of the future periods (*Table 2*) it can be concluded that the greatest absolute expansion is predicted to occur in case of *P. pinaster*, the greatest relative expansion may occur in case of *P. halepensis* and *P. pinea*, while the distribution of *P. brutia* seems to be nearly unchanged. Although the current distribution of *P. halepensis* and *P. pinea* differs remarkably, the predictions are almost the same, which originates from the similar climatic demand and tolerance of the two species. The northwestern African coastline was predicted to be suitable for *P. brutia*, *P. halepensis*, and *P. pinea*. By 2070, the climate of western and southern Hungary seems to become suitable for *P. pinaster*. In the far future period, *P. halepensis* is predicted to occur in the southern part of the Carpathian Basin, while *P. pinea* and *P. brutia* seem to stay out of the basin. Nevertheless, it must be noted that *P. halepensis* is better adapted to drought but less adapted to cold than *P. brutia* (*Fady et al.*, 2003). Hence, the latter species is able to serve as ornamental plant in the near future period (when frost is limiting factor) and in moist (irrigated) plots in the far future period.

Some plant species originating from a certain part of the Mediterranean Basin and introduced to other parts of it seem to become particularly invasive (*Groves*, 1991), and are better to be treated as potentially invasive species in the territories predicted to become climatically suitable for them. *P. halepensis* is known to be invasive (*Acherar et al.*, 1984; *Trabaud et al.*, 1985; *Lepart* and *Debussche*, 1991). Other species, such as *P. brutia* in southern Anatolia (*Quézel et al.*, 1990), can effectively be established where they had been introduced and even expand in some extent but without becoming really invasive (*Le Floc'h*, 1991). The phenomena of plant invasion is now under revision in ecology, since some of the species treated to be invasive may become important elements of the natural vegetation due to climate change (*Walther et al.*, 2009).

It must be mentioned that the original distribution area of *P. pinea* is obscure, since it was extensively planted around the Mediterranean throughout historical times by Etruscans, Greeks, Romans, and Arabs because of its edible seeds. (*Groves*, 1991; *Barbéro et al.*, 1998; *Fady et al.*, 2004). The differentiation of autochthonous and non-autochthonous stands is, as also in the case of *P. pinaster*, controversial (*Alía* and *Martín*, 2003).

5. Conclusion

Mediterranean pines are potentially able to expand the ornamental plant assortment of the Carpathian Basin. Although some specimens of the four studied conifers can be found in arboreta of Hungary, they are susceptible to frost and, therefore, not widely introduced. In this research we aimed to examine whether these pines will be able to be planted without frost protection in the

future by modeling the future potential distributions. The result of CEM shows that *P. halepensis* in the southern part and *P. pinaster* in the western part of the Carpathian Basin may find similar climatic conditions in the period of 2041–2070 than the observed distributions of these species were living within in the reference period. Therefore, landscape architecture, dendrology, forestry, and botany should think of these pines as potential ornamental plants or even as potential plants of natural vegetation in the future in Hungary.

Acknowledgements—Special thanks to *Levente Hufnagel* (Corvinus University of Budapest, Department of Mathematics and Informatics) for his assistance. The research was supported by Project TÁMOP-4.2.1/B-09/1/KMR-2010-0005. The ENSEMBLES data used in this work was funded by the EU FP6 Integrated Project ENSEMBLES (Contract number 505539), whose support is gratefully acknowledged.

References

Acherar, M., Lepart, J., Debussche, M., 1984: La colonisation des friches par le pin d' Alep (Pinus halepensis, Miller) en Languedoc mediterraneen. *Acta Oecol. 5*, 179–189. (in French)

Alía, R., Martín, S., 2003: *EUFORGEN* Technical Guidelines for genetic conservation and use for *Maritime pine (Pinus pinaster)*. International Plant Genetic Resources Institute, Rome, Italy.

Barbéro, M., Loisel, R.,Quézel, P.,Richardson, D.,Romane, F., 1998: Pines of the mediterranean basin. In (Ed. *Richardson, D.M.*): Ecology and Biogeography of Pinus. Cambridge University Press, Cambridge, UK.

Bede-Fazekas, Á., 2012a: Melegigényes díszfák telepíthetőségi területének előrejelzése a 21. századra. Thesis, Corvinus University of Budapest, Faculty of Landscape Architecture, Budapest, Hungary. (in Hungarian)

Bede-Fazekas, Á., 2012b: Methods of modeling the future shift of the so called Moesz-line. *Appl. Ecol. Environ. Res. 10*, 141–156.

Cohen, J., 1960: A coefficient of agreement for nominal scales. *Edu. Psychol. Meas. 20*, 37–46.

Czinkóczky, A. and *Bede-Fazekas, Á.,* 2012: Visualization of the climate change with the shift of the so called Moesz-line. In (Eds. *Buhmann, E., Ervin, S., Pietsch, M.*): Peer Reviewed Proceedings of Digital Landscape Architecture 2012 at Anhalt University of Applied Sciences. Herbert Wichmann Verlag, Berlin, Germany.

Czúcz, B., 2010: Az éghajlatváltozás hazai természetközeli élőhelyekre gyakorolt hatásainak modellezése. PhD dissertation. Corvinus University of Budapest, Faculty of Horticultural Sciences, Hungary. (in Hungarian)

Dormann, C.F., 2007: Promising the future? Global change projections of species distributions. *Basic Appl. Ecology 8*, 387–397.

Eckert, A.J. and *Hall, G.D.,* 2006: Phylogeny, historical biogeography, and patterns of diversification for Pinus (*Pinaceae*): Phylogenetic tests of fossil-based hypotheses. *Mol. Phylogenet. Evol. 40,*, 166–182.

Elith, J., Leathwick, J.R., 2009: Species Distribution Models: Ecological Explanation and Prediction Across Space and Time. *Ann. Rev. Ecol. Evol. Systemat. 40*, 677–697.

EUFORGEN, 2008: Distribution maps. Bioversity International, Rome, Italy. Online: www.euforgen.org/distribution_maps.html. Last accessed: 2013.01.01.

Fady, B., Semerci, H., and *Vendramin, G.G.,* 2003: EUFORGEN Technical Guidelines for genetic conservation and use for Aleppo pine *(Pinus halepensis)* and Brutia pine *(Pinus brutia)*. International Plant Genetic Resources Institute, Rome, Italy.

Fady, B., Fineschi, S., and *Vendramin, G.G.,* 2004: EUFORGEN Technical Guidelines for genetic conservation and use for Italian stone pine *(Pinus pinea)*. Int. Plant Genetic Res.Institute, Rome, Italy

Fielding, A.H. and *Bell, J.F.,* 1997: A review of methods for the assessment of prediction errors in conservation presence/absence models. *Environ. Conservat. 24,* 38–49.

Gernandt, D.S., Geada López, G., Garcia, S.O., and *Liston, A.,* 2005: Phylogeny and classification of Pinus. *Taxon 54,* 29–42.

Groves, R.H., 1991: The biogeography of mediterranean plant invasions. In (Eds. *Groves, R.H., Di Castri, F.*) Biogeography of Mediterranean Invasions. Cambridge University Press, Cambridge, UK.

Guisan, A. and *Zimmermann, N.E.*, 2000: Predictive habitat distribution models in ecology. *Ecolog. Model. 135*, 147–186.

Hammer, Ř., Harper, D.A.T., and *Ryan, P.D.*, 2001: PAST: Paleontological statistics software package for education and data analysis. *Palaeontologia Electronica. 4*, 9.

Hanley, J.A. and *McNeil, B.J.*, 1982: The meaning and use of area under a receiver operating characteristics (ROC) curve. *Radiology 143*, 29–36.

Hijmans, R.J. and *Graham, C.H.*, 2006: The ability of climate envelope models to predict the effect of climate change on species distributions. *Glob. Change Biology 12*, 2272–2281.

Horváth, L., 2008: Földrajzi analógia alkalmazása klímaszcenáriók elemzésében és értékelésében. PhD dissertation, Corvinus University of Budapest, Budapest, Hungary. (in Hungarian)

Ibáñez, I., Clark, J.S., Dietze, M.C., Feeley, K., Hersh, M., Ladeau, S., Mcbride, A., Welch, N.E., and *Wolosin, M.S.*, 2006: Predicting Biodiversity Change: Outside the Climate Envelope, beyond the Species-Area Curve. *Ecology. 87*, 1896–1906.

Kovács-Láng, E., Kröel-Dulay, Gy., and *Czúcz, B.*, 2008: Az éghajlatváltozás hatásai a természetes élővilágra és teendőink a megőrzés és kutatás területén. *Term. Közl. 14*, 5–39. (in Hungarian)

Le Floc'h, E., 1991: Invasive plants of the Mediterranean Basin. In (Eds. *Groves, R.H., Di Castri, F.*): Biogeography of Mediterranean Invasions. Cambridge University Press, Cambridge, UK.

Lepart, J. and *Debussche, M.*, 1991:. Invasion processes as related to succession and disturbance. In (Eds. *Groves, R.H., Di Castri, F.*): Biogeography of Mediterranean Invasions. Cambridge University Press, Cambridge, UK.

Lobo, J.M., Jimenez-Valverde, A., and *Real, R.*, 2008: AUC: a misleading measure of the performance of predictive distribution models. *Glob. Ecol. Biogeogr. 17*, 145–151.

Nakicenovic, N. and *Swart, R. (eds.)*, 2000: Emissions Scenarios. Cambridge University Press, Cambridge, UK.

Pickett, S.T.A., 1989: Space-for-time substitution as an alternative to long-term studies. In (Ed. *Likens, G.E.*): Long-Term Studies in Ecology: Approaches and Alternatives. Springer, New York, USA.

Quézel, P., Barbéro, M., Bonin, G., and *Loisel, R.*, 1990: Recent plant invasions in the Circum-Mediterranean region. In (Eds. *Di Castri, F., Hansen, A.J., Debussche, M.*) Biological Invasions in Europe and the Mediterranean Basin. *Monographiae Biologicae 65.*

Roeckner, E., Bäuml, G., Bonaventura, L., Brokopf, R., Esch, M., Giorgetta, M., Hagemann, S., Kirchner, I., Kornblueh, L., Manzini, E., Rhodin, A., Schlese, U., Schulzweida, U., and *Tompkins, A.*, 2003: The atmospheric general circulation model ECHAM 5. Part I: Model description. Max-Planck-Institut für Meteorologie, Hamburg, Germany.

Roeckner E., Brokopf, R., Esch, M., Giorgetta, M., Hagemann, S., Kornblueh, L., Manzini, E., Schlese, U., and *Schulzweida, U.*, 2004: The atmospheric general circulation model ECHAM 5. PART II: Sensitivity of Simulated Climate to Horizontal and Vertical Resolution. Max-Planck-Institut für Meteorologie, Hamburg, Germany.

Schmidt, G., 2006: Klíma- és időjárás-változás és a fás szárú dísznövények. In: (Eds. Csete, Nyéki) Klímaváltozás és a magyarországi kertgazdaság. „AGRO-21" Kutatási Pr.iroda, Bp. (in Hungarian)

Skov, F. and *Svenning, J.C.*, 2004: Potential impact of climatic change on the distribution of forest herbs in Europe. *Ecography. 27*, 366–380.

Szabó, K. and *Bede-Fazekas, Á.*, 2012: A forgalomban lévő fásszárú dísznövénytaxonok szárazságtűrésének értékelése a klímaváltozás tükrében. *Kertgazdaság 44*, 62–73. (in Hungarian)

Trabaud, L., Michels, C., and *Grosman, J.*, 1985: Recovery of burnt Pinus halepensis mill. forests. II. Pine reconstruction after wildfire. *Forest Ecol. Manage. 13*, 167–179.

Walther, G-R., Roques, A., Hulme, P.E., Sykes, M.T., Pyšek, P., Kühn, I., Zobel, M., Bacher, S., Botta-Dukát, Z., Bugmann, H., Czúcz, B., Dauber, J., Hickle, T., Jarošik, V., Kenis, M., Klotz, S., Minchin, D., Moora, M., Nentwig, W., Ott, J., Panov, V.E., Reineking, B., Robinet, C., Semenchenko, V., Solarz, W., Thuiller, W., Vila, M., Vohland, K., and *Settele, J.*, 2009: Alien species in a warmer world: risks and opportunities. *Trends in Ecol. Evolut. 24*, 686–693.

Wang, X.-R., Tsumura, Y., Yoshimaru, H., Nagasaka, K., and *Szmidt, A.E.*, 1999: Phylogenetic relationships of Eurasian pines (*Pinus, Pinaceae*) based on chloroplast rbcL, matK, rpl20-rps18 spacer, and trnV intron sequences. *Amer. J. Bot. 86*, 1742–1753.

IDŐJÁRÁS

Quarterly Journal of the Hungarian Meteorological Service
Vol. 118, No. 1, January – March, 2014, pp. 53–77

Sensitivity analysis of microscale obstacle resolving models for an idealized Central European city center, Michel-Stadt

Anikó Rákai[1*], **Gergely Kristóf**[1], and **Jörg Franke**[2,3]

[1]*Department of Fluid Dynamics, Budapest University of Technology and Economics, Bertalan L. u. 4-6, H-1111 Budapest, Hungary*
E-mails: rakai@ara.bme.hu, kristof@ara.bme.hu

[2]*University of Siegen, Institute of Fluid- and Thermodynamics, 56068 Siegen, Germany*

[3]*Vietnamese-German University (VGU), Binh Duong New City, Vietnam, joerg.franke@vgu.edu.vn*

**Corresponding author*

(Manuscript received in final form March 8, 2013)

Abstract—Microscale meteorological models with obstacle resolving grids are an important part of air quality and emergency response models in urban areas providing the flow field for the dispersion model. The buildings as bluff bodies are challenging from the discretization point of view and have an effect on the quality of the results. In engineering communities the same topic has emerged, called computational wind engineering (CWE), using the methods of computational fluid dynamics (CFD) calculating wind load on buildings, wind comfort in the urban canopy, and pollutant dispersion. The goal of this paper is to investigate the sensitivity of this method to the discretization procedure used to resolve the urban canopy with meshes which are of operational size, i.e., which can be run on a single powerful computer of a design office as well. To assess the quality of the results, the computed mean and rms (root mean square) velocity components are compared to detailed wind tunnel results of an idealized Central European city center, Michel-Stadt. A numerical experiment is carried out where the numerical sensitivity of the solution is tested by additional solutions on different grid resolutions (at least 3 stages of grid refinement), unrelated grid types (tetrahedral, polyhedral, Cartesian hexahedral, and body fitted hexahedral, all automatically generated), and different discretization schemes. For an objective qualitative judgment two metrics are investigated, the well know hit rate and another metric that does not depend on threshold values. The quality of the meshes is investigated with correspondence to the numerical stability, CPU-time need, and grid quality metric. It is shown that the solution with the best resulting metric is not necessarily the most suitable for operational purposes and almost 20% difference in the hit rate metric can result from different discretization approaches.

Key-words: microscale air quality models, obstacle resolving, urban flow, polyhedral mesh, snappyHexMesh, OpenFOAM®

1. Introduction

Prognostic microscale obstacle resolving meteorological models and computational wind engineering (CWE) models deal with the common fields of wind and pollutant dispersion modeling inside the urban canopy. *Baklanov* and *Nuterman* (2009) show that these models with increasing computational capacity can be the final scale in a nested multi-scale meteorological and dispersion model. *Mészáros et al.* (2010) have also shown a coupled transport and numerical weather prediction system for accidental pollutant releases. They say that a microscale resolved model is also needed and investigated resolving obstacles at the smallest scale with a computational fluid dynamics (CFD) model in *Leelőssy et al.* (2012).

Stull (1988) defines microscale in meteorology being a few kilometers or less where the typical phenomena include mechanical turbulence caused by the buildings. *Britter* and *Hanna* (2003) suggest the following length-scales: regional (up to 100 or 200 km), city scale (up to 10 or 20 km), neighborhood scale (up to 1 or 2 km), and street scale (less than 100 to 200 m). The two last correspond to the microscale definition of *Stull* and are used in this paper.

Baklanov (2000) showed the possibilities and weaknesses of using CFD for air quality modeling and concluded that they have a good potential. *Balczó et al.* (2011) showed a real life test case of dispersion studies of motorway planning around Budapest, carried out with the code MISKAM®, compared to wind tunnel measurements. That was an extensive example of using microscale meteorological and dispersion models for operational purposes and also showed its difficulties. To be able to use these models with confidence for operational purposes in air quality forecasting or emergency response tools, without using additional experiments, a detailed knowledge on their quality is necessary.

There are several research groups dealing with this field who have issued best practice guidelines, mainly based on validation studies compared with wind tunnel measurements of fairly simple cases. Wind tunnel models are used because of the well defined boundary conditions and the relative ease of high resolution measurement points compared to full scale field models. In these microscale validation studies usually steady state flow models are used, assuming neutral stability and neglecting the Coriolis forces. The two most thorough guidelines are from the Architectural Institute of Japan (*Tominaga et al.*, 2008), and from a COST project, Quality assurance of microscale meteorological models (*Franke et al.*, 2011). The German Engineering Community has also a standard on validation of microscale meteorological models for urban flows with a database of simple building configurations (*VDI*, 2005).

Several studies have dealt with the problem of defining inflow conditions for the atmospheric boundary layer, the most influential being *Richards* and *Hoxey* (1993). There was a considerable effort on defining inflow conditions

which are maintained throughout the computational domain if no buildings are inside, i.e., aiming for lateral homogeneity, see *Blocken et al.* (2007a), *Yang et al.* (2007), *Parente et al.* (2010), *O'Sullivan et al.* (2011), and *Balogh et al.* (2012).

Another huge effort was made for developing turbulence models which are the best for the purpose of Computational Wind Engineering. Since buildings are bluff bodies, the stagnation point anomaly revealed by *Durbin* (1996) gives a challenge for the turbulence models. There were attempts to improve the linear approach of the Boussinesq assumption and choose the best model; a wide comparison of the possibilities is shown in *Tominaga et al.* (2004) and *Yoshie et al.* (2005). Nonlinear turbulence models were also considered for flow around a single cube obstacle by *Erhard et al.* (2000) and *Wright* and *Eason* (2003), and for topographical features by *Lun et al.* (2003).

The numerical discretization procedure has less focus but it can also have a significant effect on the quality of computations. In engineering communities, dealing with computational fluid dynamics (CFD), quality assurance, verification and validation, and numerical uncertainty analysis are becoming more and more important; see e.g., *Roache* (1997) , *Oberkampf* and *Trucano* (2002), and *Franke* (2010).

This paper shows different numerical discretization possibilities for a test case called Michel-Stadt. This is an idealized Central European city center investigated in a wind tunnel with detailed measurement results publicly available. When meshing a complex urban geometry, several approaches are possible, with different quality in performance and results, and with different cost in the meshing and computing procedure. *Franke et al.* (2012a) and *Hefny* and *Ooka* (2009) are the only ones to the knowledge of the authors who compared different mesh types when investigating microscale meteorological or air quality models. *Franke et al.* (2012a) compared a block-structured hexahedral meshing approach to an unstructured hexahedral and an unstructured hybrid mesh which consists of tetrahedral and prism elements, the latter comprising of 3 layers around the geometries. They investigated simple block geometries and rows of blocks, thus simpler urban arrangements than the one presented in this paper. Their findings about the quality of the results of mean velocity components compared to experiments showed that the unstructured meshes yield often better metrics which they attributed to the higher resolution of those meshes. In this paper different resolution is used for each mesh to enable to compare similar resolutions. For the geometry of rows of blocks, *Franke et al.* (2012a) found that second order simulations with unstructured meshes are unstable, which is similar to the findings of this paper. *Hefny* and *Ooka* (2009) compared hexahedral and tetrahedral elements only for a simple block geometry, and they compared the results of dispersion to each other. In their findings the hexahedral mesh had the best performance regarding estimated numerical error, but they did not compare the results to

experimental values. There is no comparison for the flow field in their paper either, which determines the results of the dispersion essentially. The study presented here gives important additional information to these two papers in several points. The geometry used is more complex, information about the computational cost is given qualitatively for the mean and turbulent velocity components as well (dispersion studies will be carried out in the next stage of the research), and the stability of the numerical solution is also addressed in a systematic way. Apart from the hexahedral and tetrahedral meshes, here a polyhedral mesh type is also used.

In the present paper, four mesh types are compared from the points of view mentioned above, a tetrahedral, a polyhedral, a Cartesian hexahedral, and a body fitted hexahedral mesh. At least 3 spatial resolutions and 3 discretization approaches of the convective term are considered for each mesh. For the calculations the open source CFD code, OpenFOAM® was used. It was already validated by *Franke et al.* (2012a) for simple obstacle geometries and by *Rakai* and *Kristof* (2010) for the Mock Urban Setting Test used in the COST Action 732. The test-case used in this study was also already calculated and compared to results of ANSYS® Fluent by *Rakai* and *Franke* (2012), which is a widely used industrial CFD code for CWE, and the results were similar with the two different codes.

The goal of the paper is to show the change in computational cost and quality of the results via statistical metrics of the mean and rms (root mean square) velocity components measured inside the urban canopy.

In Section 2, the numerical experiment is described with a detailed description of the case study, the numerical discretization methods, and the metrics used for comparison. In Section 3, results are shown from different viewpoints and conclusions are drawn in Section 4 with an outlook to future work.

2. *Numerical experiment*

2.1. Case study

The chosen case study is an idealized Central European city centre, Michel-Stadt. It was chosen as it is a complex geometry with detailed measurement results available (*Fischer et al.*, 2010). In the COST Action 732 (*Schatzmann et al.*, 2009) on the Quality assurance of microscale meteorological models, a more simple (Mock Urban Setting Test, simple rows of identical obstacles) and a more complex (a part of Oklahoma city) test-case was used, and it was found that an in-between complexity would be beneficial. In the COST Action ES 1006 on the Evaluation, improvement and guidance for the use of local-scale emergency prediction and response tools for airborne hazards in built environments (http://www.elizas.eu/), the Michel-Stadt case is used for the first evaluations.

Two component LDV (laser doppler velocimeter) measurements were carried out in the Environmental Wind Tunnel Laboratory of the University of Hamburg. They are part of the CEDVAL-LES database (http://www.mi.uni-hamburg.de/Data-Sets.6339.0.html), which consists of different complexity datasets for validation purposes. This case, Michel-Stadt, is the most complex case of the dataset. There are two versions of it, one with flat roofs and another with slanted roofs. In this paper the flat-roof case is used. 2158 measurement points are available for the flow field; they can be seen in *Fig. 1*. They consist of 40 vertical profiles (10–18 points depending on location for each), 2 horizontal planes (height 27 m and 30 m, 225 measurement points for each), and 3 so-called street canyon planes (height 2 m, 9 m and 1 m, 383 measurement points for each), which are located inside the urban canopy.

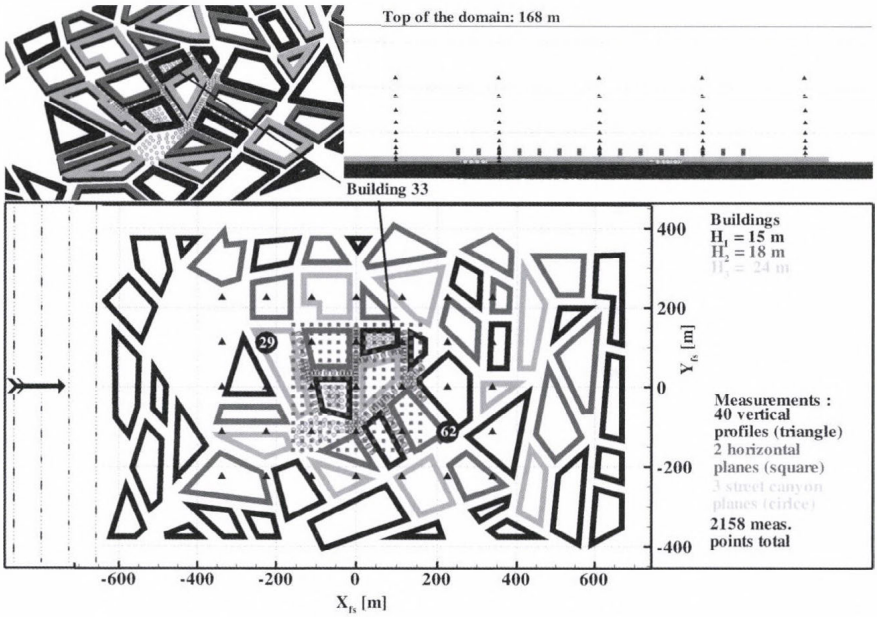

Fig. 1. Michel-Stadt with measurement points, Building 33 highlighted, the location of the roughness elements is just illustration, not exact.

The two available components are the streamwise and lateral velocity components, and time series are available for each of them. The dataset also contains the statistically evaluated mean (U_{mean}-streamwise, V_{mean}-lateral), rms (U_{rms}-streamwise, V_{rms}-lateral), and correlation values for comparison with steady state computations.

Approach flow data are provided from 3 component velocity measurements. The approach flow is modeled as an atmospheric boundary layer in the wind tunnel with the help of spires and roughness elements.

2.2. Computational model and boundary conditions

The computational domain was defined to correspond with the COST 732 Best Practice Guideline (*Franke et al.*, 2007) (*Fig. 1*), which resulted in a 1575 m × 900 m × 168 m domain, with a distance of the buildings of 11 H_3 from the inflow, 9.4 H_3 from the outflow, and at least 6 H_3 from the top boundaries, where H_3=24 m is the highest building's height. The computations were done in full scale, while the experiment was done at a scale of 1 : 225. The dependence of the results on this scale change was investigated by *Franke et al.* (2012b) using both full scale and wind tunnel scale simulations, and only a small difference in the statistical validation metrics was observed.

As *Roache* (1997) explains, the governing partial differential equations (PDE) and their numerical solution both add up to the total error of the simulation. To have a better view of the effect of the numerical discretization (and the resulting numerical error), the governing PDEs were kept the same during all the numerical experiments.

As inflow boundary condition, a power law profile (exponent 0.27, with a reference velocity U_{ref}=6.11 m/s defined at z_{ref}=100 m) fitted to the measured velocity values was given. This corresponds to a surface roughness length z_0=1.53 m. *Britter* and *Hanna* (2003) define this as a very rough or skimming approach flow. The turbulent kinetic energy and its dissipation profiles were calculated from the measured approach flow values by their definition and equilibrium assumption. At the top of the domain the measurement values corresponding to that height were fixed. The lateral boundaries were treated as smooth solid walls, as the computational domain's extension is the same as the wind tunnel width. The floor, roughness elements, and buildings were also defined as smooth walls. Standard wall functions were used. As the roughness elements are included in the domain, there is no need to use rough wall functions for the approach flow, and also the problem of maintaining a horizontally homogeneous ABL (atmospheric boundary layer) profile, which is reported (*Blocken et al.*, 2007b) to be problematic for this kind of modeling, is avoided. *Franke et al.* (2012b) have shown in a further investigation that this is not necessary as the flow is governed by interacting with the first buildings. They compared the modeling of the roughness elements explicitly and implicitly and found little influence on the results.

The Reynolds Averaged Navier-Stokes Equations were solved with standard k-ε turbulence model and the SIMPLE (semi-implicit method for pressure linked equations) method was used for pressure-velocity coupling (*Jasak,* 1996).

2.3. Discretization of the governing PDFs

As was stated before, numerical discretization has an effect on the results of the solution due to numerical error. In complex geometries its exact quantification is difficult as no analytical solution of the governing equations exists, but with a numerical experiment the effect can be investigated. In the following the mesh type, spatial resolution and the convective term discretization used for Michel-Stadt is explained. All the meshes were generated automatically which is a necessity for using this model for operational purposes and general building configurations.

2.3.1. Spatial discretization

Four mesh types are compared; their visual appearance is illustrated always for Building 33, highlighted in *Fig. 1*:

- *Unstructured full tetrahedral Delauney mesh generated with ANSYS® Icem.*

For the creation of the Delauney volume cells, first an Octree mesh was created and kept only at the surfaces, the Delauney mesh was grown from that surface mesh (*Fig. 2a*). The coarsening of the meshes was carried out by scaling the defined minimum length scales in ANSYS® Icem by 1.6. Resolution of buildings was given by the minimum face and edge size on each building. The maximum allowed expansion ratio was given for the Delauney algorithm.

- *Unstructured full polyhedral mesh created by ANSYS® Fluent from the tetra mesh.*

The polyhedral meshes were converted from the original tetrahedral meshes by ANSYS® Fluent. Each non-hexahedral cell is decomposed into sub-volumes called duals which are then collected around the nodes they belong to in order to form a polyhedral cell (see *Ansys*, (2009) for more details). The refinement ratio is thus kept very similar to the one in case of the tetra meshes(*Fig. 2b*).

- *Cartesian hexahedral mesh created with snappyHexMesh of OpenFOAM®.*

As the main research tool for these investigations is OpenFOAM®, its open source meshing tool is also used for mesh generation. This is done first by creating a Cartesian castellated mesh by refining around a given file in STL format and deleting cells inside the geometry. This mesh was also investigated in the studies (Fig. 2c), as the generation process for this one in much faster than for any of the other meshes mentioned. Building resolution cannot be given explicitly, only the resolution of the starting domain and the number of refinement iteration cycles can be defined.

- *Body fitted hybrid mesh with mostly hexahedral elements meshed with snappyHexMesh of OpenFOAM®.*

The Cartesian mesh is snapped to the edges of the geometry (*Fig. 2d*) as a next step, which takes approximately 10 times more time as the creation of the Cartesian mesh.

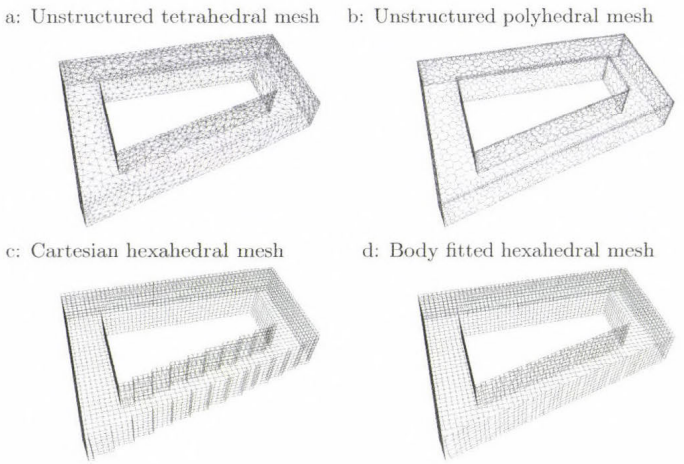

Fig. 2. Coarsest surface meshes on Building 33.

The grid convergence performance of the meshes was also investigated; at least 3 different resolutions were used for each mesh type. This makes it possible to use them for numerical uncertainty estimation at a later stage of the study.

The cell numbers of the investigated meshes can be found in *Table 1*. To have a better idea of the resolution of urban area and the buildings, in *Table 2* the number of faces on Building 33 is shown. This building was chosen as it is in the measured area close to other buildings, thus it is an indicator of street canyon resolution. The entire surface area of this building is approximately 12 000 m^2.

As it can be seen, the resolution on the building for different mesh types is not in linear relation with the total cell numbers of that mesh. See, e.g., in *Table 1* that the coarsest polyhedral mesh has 1.7 million cells and 4038 faces on the building, while the coarsest tetrahedral mesh has 6.65 million cells and 4317 faces on the building.

Table 1. Cell numbers (million cells) of the investigated meshes

	coarsest				**finest**
polyhedral	1.73	–	3.21	–	6.17
tetrahedral	6.65	–	13.17	–	26.79
Cartesian hexahedral	2.39	3.97	8.04	14.23	27.52
body fitted hexahedral	2.40	3.97	8.04	14.23	27.52

Table 2. Face numbers on Building 33

	coarsest				**finest**
polyhedral	4038	–	7455	–	12293
tetrahedral	4317	–	8934	–	15987
Cartesian hexahedral	3600	5486	11780	19879	36525
body fitted hexahedral	3416	5217	11180	18854	34660

2.3.2. Mesh quality

If we would like to resolve complex geometries properly, a compromise in mesh quality is unavoidable. This can cause a decrease both in numerical accuracy and stability of the computations, for more detail see *Jasak* (1996).

Some general measures on mesh quality to keep in mind when creating a mesh are the following:

- *Cell aspect ratio*

  Ratio of longest to shortest edge length is best to keep close to 1.

- *Expansion ratio/cell volume change*

Ratio of the size of two neighboring cells is best to keep under 1.3 in regions of high gradients (*Franke et al.*, 2007).

- *Non-orthogonality*

Angle α between the face normal $\underline{S}$ and PN vector connecting cell centers P and N is best to keep as low as possible, see in *Fig. 3.*

- *Skewness*

Distance between face centroid and face integration point is best to keep as low as possible, see $\underline{m}$ in *Fig. 3.* In OpenFOAM® this value is normalized by the magnitude of the face area vector $\underline{S}$.

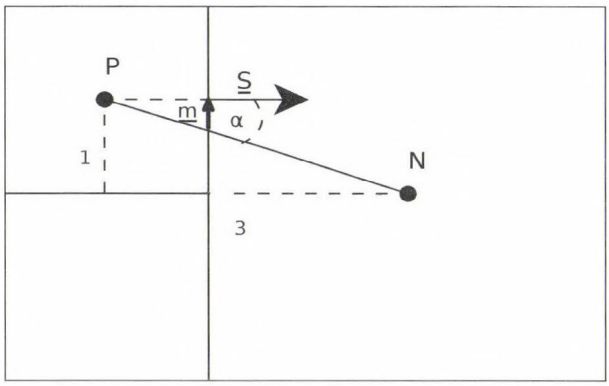

Fig. 3. Non-orthogonality and skewness.

2.3.3. Discretization of the convective/advective term

The discretization of the convective/advective terms of the transport equations solved is an important source of numerical discretization error. Upwind schemes use the values of the upwind cell as face value for the flux calculation (*Jasak*, 1996).

Central differencing uses a linear interpolation of the upwind and downwind cell value for the face value, which is of higher accuracy but may be unstable. Other schemes are defined as combination of the two for an optimal compromise between accuracy and stability (*Jasak,* 1996), like linearUpwind (a first/second order, bounded scheme) in OpenFOAM® (*OpenCFD Limited*, 2011) or second order upwind in ANSYS® Fluent (*Ansys*, 2009).

Different schemes can be used for the different variables, and to reach convergence, the following was found to be useful in OpenFOAM®:

- Initialize the solution domain with a potential flow solution.
- Use full upwind schemes for all convective terms.
- Use linearUpwind for momentum equation convective terms, upwind for the turbulence equations.
- Use linearUpwind for all convective terms.

The discretization of the pressure equation used to enforce mass conservation and all other gradients was approximated with the linear Gauss scheme. This can also add up to the instability of the solution.

It is important to note here that using higher order schemes of the convective/advective terms for meteorological models is not straightforward. E.g., in the MISKAM® model, which is a microscale operational model for urban air pollution dispersion problems, only upwind-differences are used for the discretization of the advection terms in the momentum equations (*Eichhorn,* 2008). *Janssen et al.* (2012) also shows that for certain meshes the use of higher order terms can cause convergence problems, so users may be forced to use lower order discretization. They suggest a not automatically generated hexahedral mesh to avoid this problem.

2.4. Validation metrics

With all the modeling and numerical errors inherent in the simulations, it is of vital importance to compare the simulation results to measurements. This way one can gain more information on the performance of the model. In case of wind engineering, the simulations are usually compared to wind-tunnel experiments as they are more controllable than field experiments with regard to boundary/meteorological conditions and have smaller measurement uncertainties, see *Schatzmann* and *Leitl* (2011) and *Franke et al.* (2007).

The most straightforward and inevitable part of the comparison is visual comparison with the aid of vertical profiles, contour and streamline plots, scatter plots, etc. It is also important, however, to quantify the differences in the models, for which reason validation metrics are used.

- *HR*

The most widespread metric in CWE (see, e.g., *VDI* (2005), *Schatzmann et al.* (2009), and *Parente et al.* (2010)) for wind velocity data is hit rate, which can be defined as in Eq. (1), where S_i is the prediction of the simulation at measurement point *i*, E_i is the observed experimental value, and W is an allowed absolute deviation, based on experimental uncertainty. N is the total number of measurement locations.

$$HR = \frac{1}{N}\sum_{i=1}^{N}\delta_i \,, \tag{1}$$

$$\delta_i \begin{cases} 1 for \left|\frac{S_i - E_i}{E_i}\right| \leq 0.25 \vee |S_i - E_i| \leq W \\ 0 for else \end{cases} .$$

The allowed relative deviation in Eq. (1) was used as 25% first in the VDI guideline (*VDI*, 2005), and from thereon this value is used by the CWE community. A disadvantage of the hit rate metric is that it takes into

consideration only the experimental uncertainty and it is sensitive to the used allowed experimental uncertainty (W) value. More detail on this can be found in the Background and Justification Document of the COST ES1006 Action (*COST ES1006,* 2012). When comparing different simulations with the same allowed threshold values, differences can equally be seen.

For the investigated Michel-Stadt case, the allowed absolute uncertainty was defined by *Efthimiou et al.* (2011) only for the streamwise and lateral normalized velocity components (0.033 for U_{mean}/U_{ref} and 0.0576 for V_{mean}/U_{ref}), so the calculation of the metric would only be possible for those variables. However, as time dependent measurement series are available and statistical results are also provided by the *EWTL*, it is beneficial to compare also the Reynolds stress components. Here the normalized diagonal components are shown as they are used to calculate turbulent kinetic energy, which will be of vital importance for the dispersion simulations.

For the allowed absolute uncertainty in the hit rate metric, different values were tested. It was found that the relation of metrics to each other is independent of the chosen value, so 0.003 are used for both U_{rms}/U_{ref} and V_{rms}/U_{ref}, which were found to be appropriate to have sensible values between 0 and 1 for the hit rate metric.

- *L2 norm*

Using matrix norms for comparison is also possible. With *L2* norm, the negative values of velocity components are not problematic. This metric can be seen as a normalized relative error of the whole investigated dataset.

$$L2 = \frac{\sqrt{\sum_{i=1}^{N}(E_i - S_i)^2}}{\sqrt{\sum_{i=1}^{N} E_i^2}}. \tag{2}$$

Finally, it is important to note that the most recent papers dealing with numerical uncertainty suggest metrics incorporating both experimental and numerical uncertainties in validation metrics as validation uncertainty, see, e.g., *Eca* and *Hoekstra* (2008). It is an important part of the quality assurance process and will be regarded in a separate publication.

3. Results and discussion

3.1. Mesh quality evaluation

The grid quality measures explained in Section 2 are investigated first for the mesh types used for the computations. The values of the quality metrics are shown in *Fig. 4* as a function of the number of cells. They were computed by the checkMesh utility of OpenFOAM®.

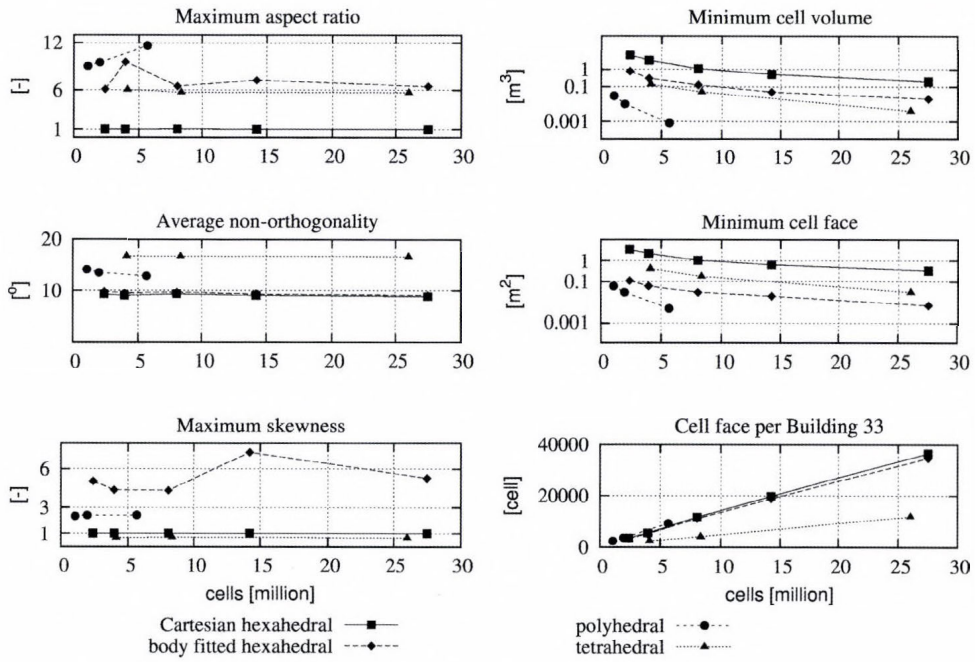

Fig. 4. Mesh quality as a function of cell number, in view of metrics explained in Section 2.3.2.

Maximum aspect ratio is highest for the polyhedral mesh, the tetrahedral and body fitted hexahedral ones are approximately half of it, while the Cartesian hexahedral mesh has an average aspect ratio of 1 as it can be expected.

The non-orthogonality is highest for the tetrahedral meshes, followed by the polyhedral ones, while all hexahedral based meshes have a constant value of 10°. Although these meshes are mainly Cartesian where 0° value is expected, by halving the cells this rule is broken for different sized neighbors. In *Fig. 3* it can be observed, how this affects the non-orthogonality. The angle for a transition of this kind in 2D can be computed as the ratio of the edges, 1 : 3 as can be seen in *Fig. 3* (angle α). This is an angle of approximately 20° which is averaged with the rest 0° values resulting in this 10° average.

Maximum skewness is the highest for the body fitted hexahedral mesh. For this metric no average value is given by the utility, it shows only the values of the worst quality cells. In that mesh, cells with skewness vector 3 times greater than the face area vector occur.

Minimum cell volume and face area decrease vary rapidly with the increase of resolution. The creation of polyhedral mesh is done by splitting the tetrahedral first, so smaller volumes and face areas occur in case of the polyhedral meshes. This can also be seen in *Fig. 2*.

About the expansion ratio it can be said, that it was set to maximum 1.3 in case of the tetrahedral meshes. For the snappyHexMesh meshes, neighboring cells can differ by a factor of 2 in edge length due to halving cells when refining locally. For unstructured meshes, the cell volume change in neighboring cells is a more useful indicator of the smoothness of transition between smaller and larger cells than expansion ratio. In case of the tetrahedral meshes, the majority of this cell volume change is below 2, while for the polyhedral meshes 6–8% of the neighbors have a cell volume change more than 10. For the hexahedral meshes, the cell volume change is below 2 in 90% of the neighbors and a jump appears around 7–8 due to the refinement method of cell halving which is expected in 3D.

3.2. Convergence

Reaching convergence in complicated geometries and low quality meshes is not always trivial, and in case of this test case, the first computations were often not successful. The best way to reach convergence for all of the cases was explained before. In cases of tetra- and polyhedral meshes, the simulations were unstable also with the described method with default relaxation factors (0.3 for p and 0.7 for the other variables). The cases had to be drastically underrelaxed to reach convergence (0.1 for p and 0.3 for the other variables). In the Best Practice Guideline for ERCOFTAC (European Research Community On Flow, Turbulence and Combustion) special interest group "Quality and Trust in Industrial CFD" (*ERCOFTAC*, 2000) it is suggested to increase the relaxation factors at the end of the solution to check if the solution holds, thus we checked it for one of the converged underrelaxed simulations. It is important also because *Ferziger* and *Peric* (2002) has shown that the optimum relation between the underrelaxation factors for velocities (uf_u) and pressure (uf_p) is $uf_p = 1 - uf_u$. With raising the relaxation factors each time by 0.1, the combination of 0.2 for p and 0.6 for the other variables were reached, but with the default combination the computation crashed again. For this reason, results with the low underrelaxation factors were investigated in the paper.

The difference between the convergence behavior of the hexahedral and polyhedral based meshes is not only their stability. Residual history is smoother for the hexahedral meshes, which makes them a more suitable tool for regulatory purpose simulations, where robustness is a big advantage and can save a lot of time for the operator.

It is an important question what may cause the instability of the tetrahedral and in one case also the polyhedral simulations. Looking at the quality metrics of the meshes, one similar behavior was found for the non-orthogality of the meshes, which can be seen in *Fig. 4*. It is clear that the tetrahedral meshes have the highest non-orthogonality followed by the polyhedral meshes, what can cause the instabilities. This indicates that gradient discretization is also

problematic. *Ferziger* and *Peric* (2002) show that in the discretization of non-orthogonal grids of the general transport equation mixed derivatives arise for the diffusive term. They say that if the angle between gridlines is small and aspect ratio is large, the coefficients of these mixed derivatives may be larger than the diagonal coefficients, which can lead to numerical problems. The checkMesh utility of OpenFOAM® reports the number of cells above the non-orthogonality threshold, which is given as 70° as a default. Although the tetrahedral meshes have higher averages of non-orthogonality, their maximum values never reached this threshold. For the polyhedral ones on the other hand, there were around 10 highly non-orthogonal cells in each mesh.

The convergence behavior of the meshes in general is explained in *Table 3*, where the necessary number of iterations is shown for each mesh, separately for the first order initialization (full upwind-11)/linearUpwind for momentum, first order for turbulence variables (mixed-21)/all higher order (full linearUpwind-22) variations. Convergence is considered when a plateau is reached in the residuals for all variables, see *Fig. 5*. For the meshes where the residuals were not smooth, other variables were also checked to stay stable.

Table 3. Necessary iterations for convergence (full upwind-11/mixed-21/full linearUpwind-22)

	coarsest				**finest**
polyhedral-11	500	–	5000	–	3000
polyhedral-21	+2500	–	+2500	–	+2500
polyhedral-22	+2500	–	+3000	–	+3000
tetrahedral-11	2000	–	2000	–	3000
tetrahedral-21	+1500	–	+1500	–	+2500
tetrahedral-22	+3500	–	+4500	–	+2500
Cartesian hexahedral-11	500	2500	2000	2500	3000
Cartesian hexahedral-21	+1000	+1000	+1000	+1000	+1500
Cartesian hexahedral-22	+500	+2000	+1000	+1000	+1500
body fitted hexahedral-11	1000	1500	1500	2000	2000
body fitted hexahedral-21	+500	+500	+1000	+1000	+1000
body fitted hexahedral-22	+1000	+1000	+1000	+1000	+1000

It can be observed that more iteration is necessary for more cells to reach the first converged state than the expected iterations for linear solvers. The outstanding value of 5000 for the medium polyhedral mesh can be explained by the instability of the computation which made heavy underrelaxation necessary.

In general, the iteration numbers are of the same order of magnitude for all of the meshes. The most orderly results are given by the snapped hexahedral meshes, which underlines again their robustness for operational simulations.

No big difference can be seen between the snapped and Cartesian hexahedral meshes, but in some cases periodic oscillation occurred using a Cartesian mesh. This reduced for the higher order computations, see *Fig. 5*.

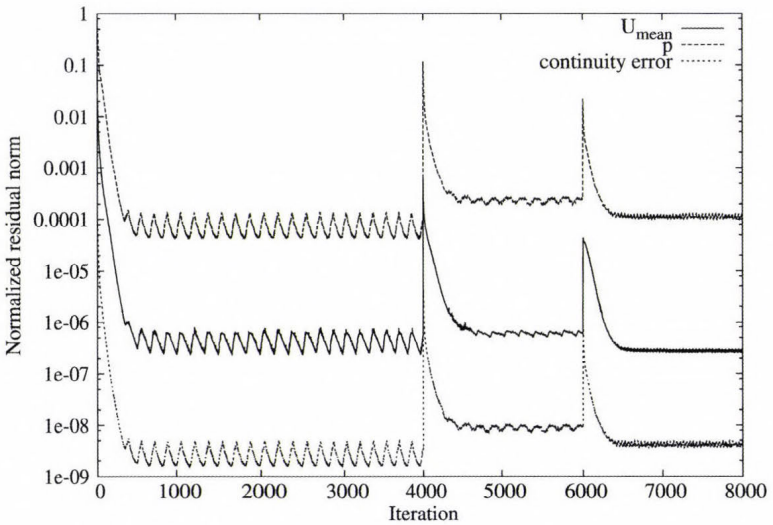

Fig. 5. Residual behavior of a Cartesian mesh.

Turning to the value of the residual norm and its drop from the beginning of the computation we observed, that this case is too complex and values do not reach the machine accuracy in single precision mode. The lowest drop is found in each case for the Poisson equation for the pressure, followed by the lateral and vertical mean velocity components. Another general observation is that all values drop below 10^{-5} for the first order calculations except for the pressure, while for the linearUpwind, only for the momentum equation this drop is usually smaller, followed by a drop below 10^{-5} again for the full linearUpwind computations. The continuity error had a similar behavior, but the first drop was usually below 10^{-8} (see *Fig. 5* for graphical explanation).

This behavior can be explained by the categorization of *Menter* (2012), who states that the classical example of a globally unstable flow is the flow past bluff bodies (like the buildings). Because of this unsteadiness, periodical changes in the residuals are appearing even if the boundary conditions are steady, like in our case.

3.3. Computational cost analysis

One of the main goals of the paper is to compare the models from a regulatory purpose point of view. When carrying out simulations for, e.g., a government, it is usually not possible to wait several days until the simulation is finished on a cluster, and stability is of high importance. For this reason, the computational costs are also evaluated.

The results of this analysis for all of the meshes can be seen in *Fig. 6*. It is apparent, that the memory usage scales linearly for all of the meshes, and the difference in the mesh types can be explained by the relative number of cell faces, i.e., the polyhedral mesh uses more memory for a given number of cells, while the tetrahedral mesh uses less. There is no significant difference between the two kinds of hexahedral meshes, but it is important to note that the solver itself takes no benefit from the fact that one of them is Cartesian.

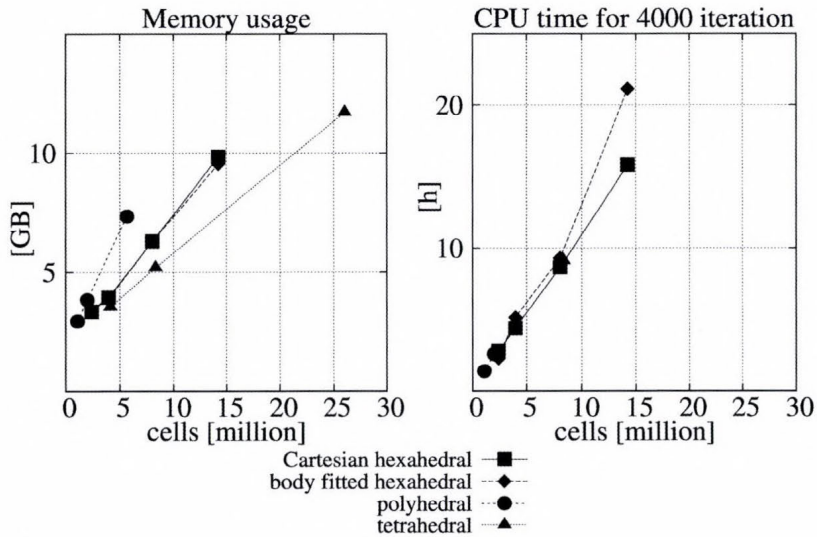

Fig. 6. Computational cost of the simulations for the full upwind simulations, 4000 iterations.

For the comparison of the CPU time, only the relative values are interesting, and it can be seen that the CPU time demand scales linearly with the number of cells, and there is no significant difference in the mesh types. These comparative simulations were carried out on the new cluster of the University of Siegen (http://www.uni-siegen.de/cluster/index.html?lang=en), run for 4000 iterations with first order upwinding for all variables on 24 cores. As a rule of thumb for this setup it can be said, that a simulation result can be obtained in

1 hour/1 million cells. Those meshes which were unstable with the default relaxation factors are omitted from the CPU-time graph.

3.4. Sensitivity to discretization in view of different metrics

Metrics are unavoidable when comparing a lot of different variations, but it is better to check with different metrics to reveal if one of them is biased. The metrics described in Section 2 are used to compare the performance of 4 mesh types, 3–5 spatial resolutions, and 3 discretization scheme combinations for the convective term of the transport equations. Hit rate results for all the cases investigated are shown in *Fig. 7* as a function of the number of cells. The metric based on *L2* normalization can be seen in *Fig. 8* also as a function of the number of cells.

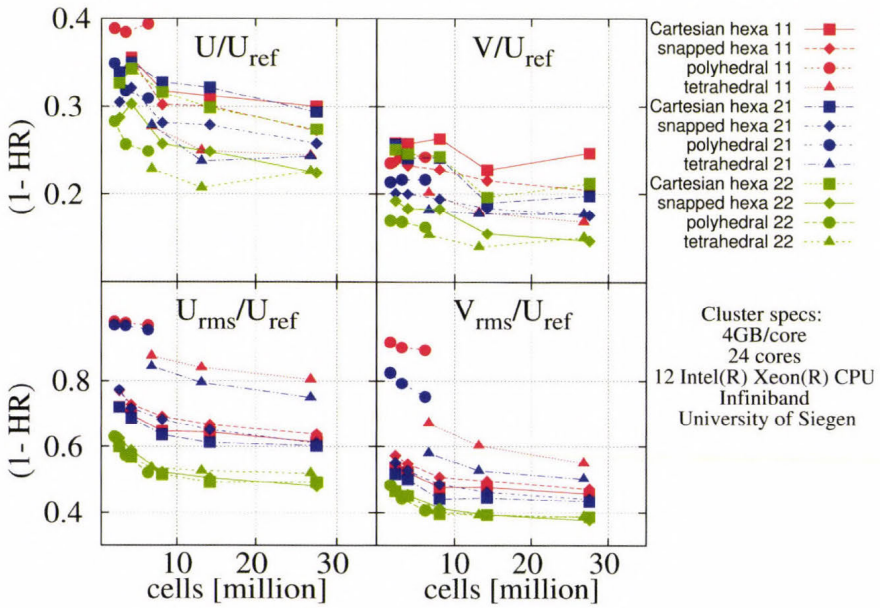

Fig. 7. Sensitivity to discretization, hit rate metric (full upwind-11/mixed-21/full linearUpwind-22).

Comparing the hit rate metric results in *Fig. 7* and the *L2* norm metric results in *Fig. 8* it is important to note, that in case of the hit rates, an "1 – *HR*" is shown to make them visually similar. Thus, on both figures the smaller is the better. However, the interpretation is very different. In case of the hit rate figure, a smaller value means that more points became "hits", the difference between simulation and experiment getting to the acceptable range. Once a point is in this

range, the hit rate will not improve even if the results get closer to each other. On the other hand, for the *L2* norm metric, a smaller value means that the difference between simulation and experiment got smaller.

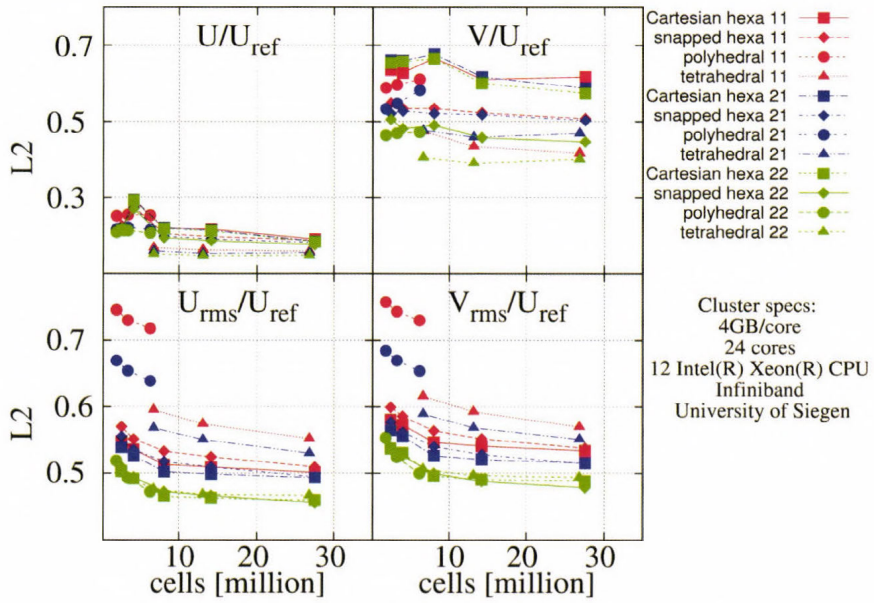

Fig. 8. Sensitivity to discretization, *L2* metric (full upwind-11/mixed-21/full linearUpwind-22).

For the absolute value of the hit rate metric for the mean velocity values it can be said, that these high hit rates are good results for this complex case. Similar values were found by *Efthimiou et al.* (2011) for two other codes, Andrea® and Star-CD®, and by *Franke et al.* (2012b) and *Rakai* and *Franke* (2012) for the ANSYS® Fluent code for the mean velocities. No further exact comments can be made for the turbulent quantities, as the threshold value was chosen arbitrarily and not based on measurement uncertainties. In the VDI guideline (*VDI*, 2005) an acceptable HR value is given for certain test cases, thresholds, and measurement points, but it is not easily transferable to a totally different case.

The absolute value of the *L2* norm metrics can be interpreted as a kind of relative error, showing that for the streamwise velocity results, where the values are essentially higher, the metric is smaller than for all the other variables. For the conclusions drawn later, the absolute value of this metric is not considered.

The conclusions which can be drawn from *Fig. 8* of the *L2* metric norm are the following:

1. For streamwise velocities, tetrahedral meshes perform outstandingly better.

From theoretical point of view, the smallest numerical error is expected from the hexahedral meshes. The reason for this is shown by *Juretic* and *Gosman* (2010): because the hexahedral mesh is aligned with the flow, the errors in fluxes cancel. Explanation for the superior performance of the same mesh size for the tetrahedral meshes in this case can be that those were made with the Delauney algorithm, so they are not "wasting" so many cells in the middle of the domain where there is no geometric feature to disturb the flow, so the gradients are small and do not make high mesh resolution necessary. In case of the hexahedral meshes, the underlying original mesh block has a quite high density. This can be seen in the two coarse meshes compared in *Fig 9*. It is also seen that the transition of tetrahedral cells is smoother from the fine to the coarse cells, and above the canopy where there are still strong gradients, the hexahedral meshes are not resolved enough. See *Fig. 10* for the visualization of these gradients above the urban canopy. A line is shown in *Fig. 9* below which high gradients occur in the solution.

Franke et al. (2012b) used also a block-structured hexahedral mesh for their investigations with ANSYS® Fluent and had better performance also in the mean velocities. That mesh is not automatically generated and has very different mesh quality metrics than the automatic snappyHexMesh meshes (average non-orthogonality 2.64, maximum skewness 1.47, and smooth cell volume transition). The worse results of the automatic hexahedral meshes can be explained by their larger and lower quality cells in the most important regions shown in *Fig. 9*.

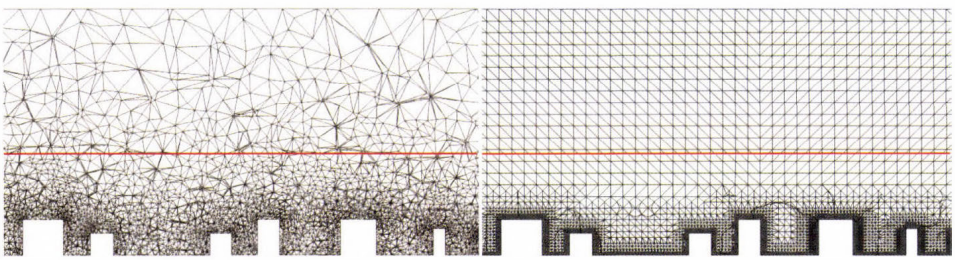

Fig. 9. Tetrahedral (6.65 $\times 10^6$ cells) and hexahedral (8.0 $\times 10^6$ cells) mesh cross sections (diagonal lines are just visualization tool specific features in the hexahedral mesh).

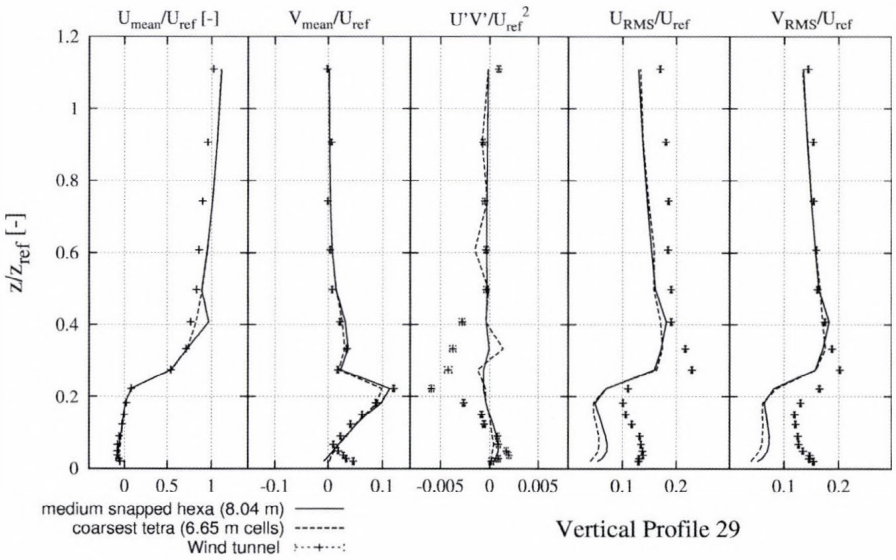

Fig. 10. Profile 29 of one tetrahedral (6.65 $\times 10^6$) and one hexahedral (8.0 $\times 10^6$) mesh (full linearUpwind solution).

2. Better performance of the tetrahedral meshes is not so apparent for lateral velocity, and disappears for the rms values.

To better understand this phenomenon, *Fig. 10* shows the profiles compared at location 29 (see *Fig. 1*) which is in the yard of an 18 m high building. In the non-dimensional scale 0.18 is the top of the building and it can be observed that changes in streamwise mean velocity reach 0.4, while for the other values the maximum is 0.3. So the smoother transition of the tetra mesh can help to better resolve the streamwise velocity, but for the other values it is not so important. The oscillations on the profiles for the tetra meshes can be found on other profiles computed with OpenFOAM® as well. They may be a consequence of the instability of the simulations, however, for the ANSYS® Fluent results they do not appear. This phenomenon needs further investigation.

3. Full second order solutions perform better already for the mean values, but that difference competes with the CPU-time cost of the results. For the turbulent quantities, however, full second order solutions are outstanding.

Theoretically this is obvious as higher order terms are more accurate, but on the other hand, this can amplify the errors in the modeling assumptions. In the Michel-Stadt case the higher order results for the simulation always compare better to the experimental values. It must be kept in mind that not all

micrometeorological models use higher order advective terms. As the turbulent quantities are used for the dispersion calculations, it can have a significant effect and higher order terms are suggested.

4. Polyhedral meshes have very low performance compared to all the other cases if not full second order discretization is used.

This can be a result of the larger volumes in those meshes and the large cell volume changes explained, strengthening the numerical errors. It is suggested to use polyhedral meshes only with higher order convective/advective terms, as those metrics are comparable with the other mesh types.

5. The Cartesian hexahedral meshes have lower performance in the mean velocities, but this disappears for the turbulent statistics.

More comparable results for rms value prediction need further investigation. This can be caused by the generally wrong rms predictions for all mesh types and by the numerical errors canceling the modeling errors.

6. There is a jump of low performance for the second coarsest hexahedral meshes which is visible both in the hit rate metric and *L2* norm metric.

This is a sign that mesh refinement does not always lead to improved solutions because of the error cancellation explained above. Also the importance of investigation of mesh dependency on more meshes must be noted.

4. Conclusions and outlook

Sensitivity of four different metrics to compare experimental and simulation results was investigated for a test case of an idealized Central European city center, Michel-Stadt. The numerical discretization approaches were compared with four different mesh types, at least 3 resolutions for each of them, and different discretization procedures of the convective/advective term in a numerical experiment.

It was found that snappyHexMesh meshes are more stable computationally. so they are more appropriate for operational purposes, although their metric performance is not as good as that of the tetrahedral meshes. The lower validation metric performance is not true in general for all hexahedral meshes, more time consuming block-structured meshes with higher mesh quality metrics can be generated which are both stable and more accurate.

For diagonal components of the Reynolds stresses, i.e., the rms values in experimental results, discretization schemes of the convective terms have a striking but expectable effect which must be kept in mind for dispersion studies where their value effects turbulent diffusion. Numerical discretization differences can cause almost 20 % change in the hit rate metric.

There are still many open questions to be further investigated, e.g., the oscillation in the tetrahedral profiles, correspondence between stability and mesh quality of the different mesh types, and the generation of the polyhedral mesh to explain their low upwind validation metrics. This will be carried out through further more detailed analyses of the datasets.

The work with Michel-Stadt continues in the framework of COST Action ES 1006 with numerical uncertainty estimation and dispersion studies for continuous and puff passive scalar sources. The Action involves several research groups who use different codes, including prognostic microscale obstacle resolving meteorological models, diagnostic flow models, and operational Gaussian type plume models. After investigations of the setup shown in this paper, a blind test will be carried out to evaluate the use of local-scale emergency prediction and response tools for airborne hazards in built environments.

Acknowledgement–This research was financed by a scholarship of the Hungarian Government and the project Talent Care and Cultivation in the Scientific Workshops of BME. The project is supported by the grant TAMOP-4.2.2/B-10/1-2010-0009. It is also related to the scientific programme of the project Development of Quality-Oriented and Harmonized R+D+I Strategy and the Functional Model at BME, the New Hungary Development Plan (Project ID: TAMOP-4.2.1/B-09/1/KMR-2010-0002), and the K 108936 ID project of the Hungarian Scientific Research Fund. Collaboration of the authors was possible thanks to two DAAD (German Academic Exchange Service) research grants, number A/10/82525 and A/11/83345.

References

Ansys®, 2009: Ansys Fluent 14.0 Theory Guide. Canonsburg, Pennsylvania.

Baklanov, A. and *Nuterman, R.B.*, 2009: Multi-scale atmospheric environment modelling for urban areas. *Adv. Sci. Res. 3,* 53–57.

Baklanov, A., 2000: Application of CFD methods for modelling in air pollution problems: possibilities and gaps. *Environ. Monit. Assess. 65,* 181–189.

Balczó, M., Balogh, M., Goricsan, I., Nagel, T., Suda, J., and *Lajos, T.*, 2011: Air quality around motorway tunnels in complex terrain – computational fluid dynamics modeling and comparison to wind tunnel data. *Időjárás 115,* 179–204.

Balogh, M., Parente, A., and *Benocci, C.*, 2012: RANS simulation of ABL flow over complex terrains applying an Enhanced k-ε model and wall function formulation: Implementation and comparison for fluent and OpenFOAM®. *J. Wind Eng. Ind. Aerod. 104–106,* 360–368.

Blocken, B., Stathopoulos, T., and *Carmeliet, J.*, 2007a: CFD evaluation of wind speed conditions in passages between parallel buildings – effect of wall-function roughness modifications for the atmospheric boundary layer flow. *J. Wind Eng. Ind. Aerod. 95,* 941–962.

Blocken, B., Stathopoulos, T., and *Carmeliet, J.*, 2007b: CFD simulation of the atmospheric boundary layer: wall function problems. *Atmos. Environ. 41,* 238–252.

Britter, R.E. and *Hanna, S.R.*, 2003: Flow and dispersion in urban areas. *Annu. Rev. Fluid Mech. 35,* 469–96.

COST ES1006, 2012: COST ES1006 Background and Justification Document. *COST. Action ES 1006: Evaluation, improvement and guidance for the use of local-scale emergency prediction and response tools for airborne hazards in built environments.*

Durbin, P.A., 1996: On the k- ε stagnation point anomaly. *Int. J. Heat Fluid Flow 17,* 89–90.

Eca, L. and *Hoekstra, M.*, 2008: Testing Uncertainty Estimation and Validation Procedures in the Flow Around a Backward Facing Step. In *Proceedings of the 3rd Workshop on CFD Uncertainty Analysis.*

Efthimiou, G.C., Hertwig, D., Fischer, R., Harms, F., Bastigkeit, I., Koutsourakis, N., Theodoridis, A., Bartzis, J.G., and *Leitl, B.*, 2011: Wind flow validation for individual exposure studies. In *Proceedings of the 13th International Conference on Wind Engineering (ICWE13)*, Amsterdam, The Netherlands.

Ehrhard, J., Kunz, R., and *Moussiopoulos, N.*, 2000: On the performance and applicability of nonlinear two equation turbulence models for urban air quality modelling. *Environ. Monit. Assess. 65*, 201–209.

Eichhorn, Dr. J., 2008: MISKAM manual for version 5. Spielplatz 2 55263 Wackernheim.

ERCOFTAC, 2000: Best Practice Guidelines. *ERCOFTAC Special Interest Group on "Quality and Trust in Industrial CFD".*

Ferziger, J.H. and *Peric, M.*, 2002: Computational Methods for Fluid Dynamics. Springer, Berlin Heidelberg New-York

Fischer, R., Bastigkeit, I., Leitl, B., and *Schatzmann, M.*, 2010: Generation of spatio-temporally high resolved datasets for the validation of LES- models simulating flow and dispersion phenomena within the lower atmospheric boundary layer. In *Proceedings of The Fifth International Symposium on Computational Wind Engineering (CWE2010)*, Chapel Hill, North Carolina, USA.

Franke, J., Hellsten, A., Schlünzen, H., and *Carissimo, B.*, 2007: Best Practice Guideline for the CFD Simulation of Flows in the Urban Environment. *COST Action 732: Quality Assurance and Improvement of Microscale Meteorological Models.*

Franke, J., 2010: A review of verification and validation in relation to CWE. In *Proceedings of the Fifth International Symposium on Computational Wind Engineering (CWE2010)* Chapel Hill, North Carolina, USA, May 23–27, 2010.

Franke, J., Hellsten, A., Schlunzen, K.H., and Carissimo, B. 2011. 2011 The COST 732 Best Practice Guideline for CFD simulation of flows in the urban environment: a summary. *International Journal of Environment and Pollution, 44(1–4), 419–427.*

Franke, J., Sturm, M., and *Kalmbach, C.*, 2012a: Validation of OpenFOAM® 1.6.x with the German VDI guideline for obstacle resolving microscale models. *J. Wind Eng. Ind. Aerod. 104–106*, 350–359.

Franke, J., Laaser, A., Bieker, B., and *Kempfer, T.* 2012b: Sensitivity analysis of RANS simulations for flow and dispersion in the generic European City Centre Michel-Stadt. In *Proceedings of Conference on Modelling Fluid Flow.* Budapest, Hungary, Sept 4–7 2012.

Hefny, M.M. and *Ooka, R.*, 2009: CFD analysis of pollutant dispersion around buildings: Effect of cell geometry. *J. Build. Environ. 44*, 1699–1706.

Janssen, W.D, Blocken, B., and *van Hoof, T.* 2012: Pedestrian wind comfort around buildings: comparison of wind comfort criteria based on whole-flow field data for a complex case study. *J. Build. Environ. accepted for publication.*

Jasak, H., 1996: Error Analysis and Estimation for the Finite Volume Method with Application to Fluid Flows. *PhD. Thesis, Imperial College of Science, Technology and Medicine.*

Juretic, F. and *Gosman, A.D.*, 2010: Error Analysis of the Finite-Volume Method with respect to Mesh Type. *Num. Heat Transfer 57*, 414–439.

Leelőssy, Á., 2012: Baleseti kibocsátásból származó szennyezőanyagok lokális skálájú terjedésének modellezése. *M.Sc. thesis, Eötvös Lóránd Univ. Dep. Meteorology.* (In Hungarian)

Lun, Y.F., Mochida, A., Murakami, S., Yoshino, H., and *Shirasawa, T.*, 2003: Numerical simulation of flow over topographic features by revised k – ε models. *J. Wind Eng. Ind. Aerod. 91*, 231–245.

Menter, F.R., 2012: Best Practice: Scale-Resolving Simulations in ANSYS® *CFD. ANSYS®*, Germany.

Mészáros, R., Vincze, Cs., and *Lagzi, I.*, 2010: Simulation of accidental release using a coupled transport (TREX) and numerical weather prediction (ALADIN) model. *Időjárás 114*, 101–120.

Oberkampf, W.L., and *Trucano, T.G.*, 2002: Verification and validation in computational fluid dynamics. *Prog. Aerospace Sci, 38.* 209–272.

OpenCFD Limited, 2011: OpenFOAM® User Guide – Version 2.0.0. OpenCFD Limited.

O'Sullivan, J.P., Archer, R.A., and *Flay, G.J.,* 2011: Consistent boundary conditions for flows within the atmospheric boundary layer. *J. Wind Eng. Ind. Aerod. 99,* 65–77.

Parente, A., Gorlé, C., van Beeck, J., and *Benocci, C.* 2010: A Comprehensive Modelling Approach for the Neutral Atmospheric Boundary Layer: Consistent Inflow Conditions, Wall Function and Turbulence Model. *Bound-Lay. Meteorol. 140,* 411–428.

Rakai, A. and *Franke, J.,* 2012: Validation of two RANS solvers with flow data of the flat roof Michel-Stadt case. In *Proc. 8th International Conference on Air Quality – Science and Application,* Athens, Greece.

Rakai, A., and *Kristóf, G.,* 2010: CFD Simulation of Flow over a Mock Urban Setting Using OpenFOAM®. In Gépészet 2010: *Proceedings of the Seventh Conference on Mechanical Engineering.* Budapest, Hungary.

Richards, P.J. and *Hoxey, R.,* 1993: Appropriate boundary conditions for computational wind engineering models using the k – turbulence model. *J. Wind Eng. Ind. Aerod. 47,* 145–153.

Roache, P.J., 1997: Quantification of Uncertainty in Computational Fluid Dynamics. *Annu. Rev. Fluid Mech. 29,* 123–60.

Schatzmann, M., Olesen, H., and *Franke, J.* 2009: COST 732 Model Evaluation Case Studies: Approach and Results. *COST Action 732: Quality Assurance and Improvement of Microscale Meteorological Models.*

Schatzmann, M. and *Leitl, B.,* 2011: Issues with validation of urban flow and dispersion CFD models. *J. Wind Eng. Ind. Aerod. 99,* 169–186.

Stull, R.B., 1988: An Introduction to Boundary Layer Meteorology. Kluwer Academic Pub.

Tominaga, Y., Mochida, A., Yoshie, R., Kataoka, H., Nozu, T,, Kazuyoshi, Y,, M., and *Shirasawa, T.,* 2008: AIJ guidelines for practical applications of CFD to pedestrian wind environment around buildings . *J. Wind Eng. Ind. Aerod. 96,* 1749–1761.

Tominaga, Y., Mochida, A., Shirasawa, T., Yoshie, R., Kataoka, H., Harimoto, K., and Nozu, T., 2004: Cross Comparison of CFD Results of Wind Environment at Pedestrian Level around a High-rise Building and within a Building Complex. *J. Asian Arch. Build. Engin., 3.*

VDI., 2005: Environmental Meteorology – Prognostic microscale wind field models – Evaluation for flow around buildings and obstacles, *VDI guideline 3783, Part 9.*

Wright, N.G., and *Easom, G.J.,* 2003: Non-linear k – turbulence model results for flow over a building at full scale. *Appl. Math. model. 27,* 1013–1033.

Yang, Y., Gu, M., Chen, S., and *Jin, X.,* 2007: New inflow boundary conditions for modeling the neutral equilibrium atmospheric boundary layer in computational wind engineering. *J. Wind Eng. Ind. Aerod. 97,* 88–95.

Yoshie, R., Mochida, A., Tominaga, Y., Kataoka, H., and *Yoshikawa, M.,* 2005: Cross Comparison of CFD Prediction for Wind Environment at Pedestrian Level around Buildings Part 1-2. In *Proceedings of the 6th Asia-Pacific Conference on Wind Engineering (APCWE-VI).*Seoul, Korea, September 12–14, 2005.

IDŐJÁRÁS

Quarterly Journal of the Hungarian Meteorological Service
Vol. 118, No. 1, January – March, 2014, pp. 79–92

Facts about the use of agrometeorological information in Hungary and suggestions for making that more efficient

Zoltán Varga

Department of Agrometeorology, Faculty of Agricultural and Food Sciences,
University of West Hungary,
Vár 2, H-9200 Mosonmagyaróvár, Hungary
e-mail: varzol@mtk.nyme.hu

(Manuscript received in final form February 15, 2013)

Abstract–Demands on use of information upon relationship between meteorological conditions and agricultural production were from the beginning of meteorology and from the beginning of human civilization. The sudden development of natural sciences during the 19th and 20th centuries opened up a new prospect in producing meteorological information which was of use to food processing. On the other hand, contemporary agricultural development needed supply of more detailed and more practical agrometeorological information. Increasing importance of ecological agriculture at the expense of intensive farming systems and uncertain effects of climate change did not reduce the want for agrometeorological information; in fact, they extended the needs for those in the last decades. But positive tendencies of domestic agrometeorological research and information service in the second half of the 20th century declined till the 1990s, and there is no reason to be optimistic on the grounds of current situation.

This work attempts to review not only possibilities and results of agrometeorological information supply, but also interdisciplinary factors, such as factors of economical development and regulation, education, agricultural-advisory system, etc., which set back the development of this area. The base of our investigations is a SWOT analysis which is a strategic planning method of economical sciences used to evaluate strengths, weaknesses, opportunities, and threats involved in a project. This way we try to answer the following questions:

- Why is agrometeorology no longer an important economical factor in Hungary?
- How could we make agrometeorological research and information service become a productive economical factor again?

Key-words: agrometeorological information, agrometeorological research, SWOT analysis, climate change, decision-making

1. Introduction

The agrometeorological use of information started after the cold event called as Younger Dryas. The climate shock – a drastic warming - following that event caused a significant rise in sea level, and it changed the coastlines and topography of continents. But after that neither the sea level (topography), nor the climatic conditions changed enormously, so it helped the mankind to develop from hunter-gatherer to agricultural societies in the early Holocene (*Behringer,* 2010). According to *Bernal* (1963), it is important to make a distinction between prescientific stage of cognition and stages of history of science. Those early attempts to come to know and to influence the environmental (meteorological) effects on agricultural production belonged to the previous one of course. The ancient ploughmen awaked to their dependence on their environment and especially on weather and climate. Namely, they discovered that more sunshine and higher temperature accelerated development of plants and more rainfall caused higher yields. Results of observations about relationship between meteorological conditions and development, growth, and yields of crops came down from father to son, but this kind of knowledge could not have been quantified. People tried to influence natural forces, but it happened in a superstitious and mystificated way as they were not able to discover causal relationships. Anyhow, these efforts were the first – although not scientific – attempts to use agrometeorological information (*Varga*, 2010).

A new approach, which supposed that the world around us could have been discovered and which focused on understanding the causal relationships between phenomena of that world, rose in the first millennia BC and it helped scientific thinking to improve. It was a beneficial method also for meteorological and applied (agro)meteorological studies. Several findings and ideas – including some erroneous ones – of that era were undisputed and unsurpassable knowledge of the given area of science for the following two thousand years. The only way for gathering information was the theoretical (speculative) one, as instrumental measurements still were not possible. It obstructed to define numerically the processes and attributes of atmosphere and relationships of climate-agriculture-soil system, respectively. Consequently, use of agrometeorological information was not able to develop for further centuries.

The sudden development of natural sciences during the 19th and 20th centuries opened up a new prospect in producing meteorological information which was of use to food processing. On the other hand, contemporary agricultural development needed supply of more detailed and more practical agrometeorological information. The science of agrometeorology developed parallel with agriculture, and it worked as a prerequisite of agricultural production in those decades.

That period can be considered as the days of glory for using agrometeorological information. The well-organized agrometeorological

information supply system met the demand of intensive crop production better and better. To make the first move for this a network of phenological stations for observing the development of field crops was organized – under the direction of Zoltan Varga-Haszonits – by the Hungarian Meteorological Institute (now: Hungarian Meteorological Service). To help this work, a monograph (manual) was published (*Varga-Haszonits,* 1967), then observers working in collective farm systems were drawn into the phenological network. That study used also the database collected by the National Institute for Agricultural Quality Control (now: Central Agricultural Office). The most comprehensive Hungarian phenological database – especially for the period 1955–2000 – can be built up by unification of those two databases organized by the National Institute for Agricultural Quality Control and Hungarian Meteorological Service, respectively. The phenological data for field crops collected by the observational network of Hungarian Meteorological Service were stored at and used by the Department of Agricultural Information Supply and later by the Department of Agrometeorological Forecasting. The agrometeorological information service using those data worked under the direction of Zoltan Varga-Haszonits, after that it was organized by Sándor Dunay. Agroclimatological model-based crop yield forecasts were done for decades on behalf of the agricultural ministry.

Increasing importance of ecological agriculture at the expense of intensive farming systems and uncertain effects of climate change did not reduce the want for agrometeorological information; in fact, they extended the needs for those in the last decades. But positive tendencies of domestic agrometeorological research and information supply in the second half of the 20th century declined till the 1990s and there is no reason to be optimistic on the grounds of current situation.

This way we try to answer the following questions:

- Why – and what kind of - agrometeorological information is important for agricultural production?
- Why is agrometeorology no longer an important economical factor in Hungary?
- How could we make agrometeorological research and information service become a productive economical factor again?

2. The SWOT analysis of agrometeorological information service

Position, possibilities, and problems of agrometeorological information service were surveyed by the help of SWOT (sometimes SLOT) analysis. This method is a strategic planning used to evaluate strengths, weaknesses (or limitations), opportunities, and threats involved in a project. The internal and external factors which are favorable or unfavorable to achieve the objective can be determined (*Székely,* 2000). Identification of SWOTs is important, because they can inform

later steps in planning to achieve the objective. The usefulness of this method is not limited to profit-seeking organizations. SWOT analysis may be used in any decision-making situation when a desired objective has been defined (URL[1]). The objective of our examined area is to help agricultural decisions and to raise food production a higher level. So it seemed to be reasonable to estimate the internal advantageous and disadvantageous characteristics of agrometeorological research and information supply, as well as the external opportunities and threats of those by means of this generally accepted method.

Table 1 summarizes the SWOTs of agrometeorological information service.

Table 1. The SWOTs of agrometeorological information service

	Helpful (+)	**Harmful (-)**
Internal origin	***Strengths:***	***Weaknesses/Limitations:***
	– the agricultural production's need for agrometeorological information	– stochastic relationships of soil-atmosphere-agriculture system
	– domestic agrometeorological research includes all important approaches of that science	– over-emphasizing the importance of individual factors
	– information supply can be based on results of former agrometeorological research	– sometimes meteorological effects are treated as background noise by farmers
	– interdisciplinary nature of agrometeorology	– inexact data and information supply
		– the biological respects are usually in the rough in climate scenarios
External origin	***Opportunities:***	***Threats:***
	– growing need for interdisciplinary research	– current academic structures do not foster interactions between biological and physical scientists
	– more attention should be payed to investigation of agricultural impacts of global warming	– problems of educational and agricultural-advisory systems
	– former favorable experiences suggest that agrometeorological information supply can work in Hungary	– financial problems
	– the potential to handle data and information by computers and exchange them globally is growing	– legal and economical regulation of agricultural production does not always inspire use of agrometeorological information
	– high-level food production and food security need adequate information supply	– problems of observational networks
		– tendency for senescence of agrometeorological experts

2.1. Strengths

It can be stated that a permanently high level agriculture which always tries to make the best of its environmental potential can not be realized without using agrometeorological information. The must for agricultural information supply is

explained by multiple influences of atmosphere on agricultural production. In support of this, let us have a short review of relationship between meteorological factors and crop production.

The atmosphere can be considered as a system of terms and conditions for plant production. The climate fundamentally determines:

- which plants can not be grown in a given area (see the failed attempts for growing orange or cotton in Hungary in the 1950s),
- which species and varieties can be planted there, and
- in which period of the year are those plants able to grow (it could be basically decided if we compared the length of actual growing season of crops to beginning and end of potentially available growing season (in weather and climate respect)).

The atmosphere means also system of resources for agriculture. Plants are not able to produce organic matter without climatic resources (energy and substances) which come from – or through – the surrounding atmosphere. Amounts of factors which are required for both photosynthesis and respiration, such as water (precipitation), carbon dioxide, oxygene, carbohydrates, temperature, and photosyntheticallay active radiation, are significantly influenced by weather and climate.

The atmospheric factors work as a system of affecting factors for plants. Crops are constantly influenced by (meteorological) factors of their environment during the whole growing season. Intensity of life processes continually changes as a result of favorable or unfavorable, development accelerating or delaying, yield increasing or yield decreasing effects. More unfavorable values of meteorological elements cause more serious anomalies of life processes. Influences of meteorological elements below the lower or above the upper threshold values can be considered as damaging effects. The frequency of those marks production risk of varieties and hybrids. That is why the atmospheric relations are risk factors for farming as well (*Varga-Haszonits* and *Varga,* 1999).

There is a continuous must for decision-making in agricultural practice. The quality of decision-making determines the level of farming.

Decisions can be divided into two groups on the base of term of their implication. Strategic decisions are fundamental, directional, and over-arching. They affect long term goals. Tactical (or operational) decisions affect the day-to-day implementation of strategic decisions and are for short term. Strategy defines the "what" is to be done and tactics define the "how". Decision-making always needs information, but information requirements depend on kind of decision. Both tactical and strategic decisions of farming demand agrometeorological information. Tactical decisions need information about weather and short term forecast, however, strategic planning needs climatic information and long term forecast.

Farming success basically depends on the base of decision-making. Effectiveness of planning is influenced by thoroughness of the decision-maker. In this respect, decisions can be divided into the following groups: intuition-based decisions, past experience-based decisions, and decision based on professionally collected and processed data and scientific information. Intuition means instinctive and unconscious knowing without deduction or reasoning. This first group also includes decisions based on information of doubtful origin. Effectiveness of these decisions is low, but it is not zero. So we can make even good intuition-based decisions, but in this case we can not know why it works. All farming decisions without agrometeorological information belong to this group.

For the most part of past experience-based decisions, recent experiences are used. It is because of the fact that memory of bygone days fades from our minds. However there is no guarantee for similar meteorological conditions or effects of consecutive years. Sometimes climatic features of distant time periods are analogous. That is why this kind of decision is also a hazardous one. A further problem is that individual experiences are not able to give enough information for a complex approach of agrometeorological problems.

That complex approach is assured only by decisions based on professionally collected and processed data and scientific information. Scientific information supply developed from individual experiences by making those more objective, integrated, and verifiable (*Varga*, 2010). In the case of those decisions we also know probability of effectiveness for different alternatives. Effectiveness of these decisions is in general high, but it is not 100 %. So we can make even inexact scientific information-based decisions, but in this case we can search the source of the problem and it helps to make better decisions in the future.

For this reason, good agrometeorological decisions require exact data and information supply. The appropriate data come from professional agrometeorological observation networks or from laboratory or field experiments. The other two principal elements of agrometeorological information service are theoretical and methodical research and information service itself. These three elements have to be in close connection with each other, and all of them must depend largely on the agricultural requirements (*Varga-Haszonits,* 1983, 1997). Some typical characteristics of a functional agrometeorological information service are described in the following.

The basic element of the system is data collection. The efforts in various countries led to the recognition of a need for combining and coordinating phenological and meteorological observations. Data of professional network of meteorological observations combined with data from additional measurements of soil properties (temperature, moisture etc.) and with data from phenological and other agricultural observations provide an integrated database for research of atmosphere-soil-plant system. Agrometeorological information service can use all available observed or measeured data of controlled origin.

The data must be elaborated and analyzed. The detected false data have to be corrected or excluded from the database. Data analysis is a process of cleaning and transforming data. Afterwards, the analyzed data should be transformed into agricultural research or directly into agricultural information service. The goal of this process is highlighting useful agrometeorological information, suggesting conclusions, and supporting decision-making. It is important to send not data, but helpful information for users. This is the task – and strength – of agrometeorological service.

The objective of agrometeorological research is to study and numerically determine the influence of meteorological elements on plant development and yield of crops. The investigations in this field consist of the following research areas: agroclimatological studies, agromicrometeorological model research, elaboration of new agrometeorological forecasting methods, and verification of new results. The investigations include analysis of databases, field experiments, and laboratory experiments (*Varga-Haszonits,* 1983).

The data measured in these experiments are much more detailed than that of observational network, because those are measured by special instruments. Therefore, on the basis of these data, the atmosphere-(soil)-crop basic relationships can be elaborated and can be used as fundamental knowledge for agroclimatological modeling. The obtained relationships between meteorological factors and life processes of crops are fundamental knowledge for agrometeorological information service. The results have to be expressed in objective, mathematically exact terms which do not depend on the person giving information.

We can change mainly characteristics of plants and agricultural production technologies – as input parameters - in the case of field experiments, however, also modified weather conditions can be studied in laboratory experiments (in plastic tunnels or houses, greenhouses, climate chambers, or phytotrones). Therefore, field experiments allow examining the current agricultural production and laboratory experiments are suitable for also simulating and giving information about the future conditions of plant production.

The analysis of agroclimatological databases is based on long-term data series. These studies include investigations of climatic conditions of crop production and relationship between climate and agricultural production, as well as determination of regions or zones with different agroclimatologic characteristics and conditons. These surveys can use much longer but less detailed dataseries than that of agroclimatological experiments. In the case of building an agroclimatological database, it is very important to check the reliability of data sets of different origin.

Methodological investigations – including models for forecasting soil moisture, actual evapotranspiration, plant development, crop yield, etc. - allow detailed analysis of climate-agriculture relationship and help decision-making on the base of verified information.

The verification of methods means that we compare the values obtained by elaborated methods with the actual measured or observed values. The accuracy of results is measured by error of estimation – that is the difference between calculated and measured value – and then by studying the frequency of these errors. Verification is needed for determining the effectiveness of methods and effectiveness of decisions based on these proceedings. The practical objective of verification process is to improve the information quality and to reduce the probability of false decisions.

The practical importance of agrometeorology depends on quantity and quality of information presented for agricultural producers. But agrometeorological information service could not be qualified as not satisfactory if its results are not used in practical decisions. It is because the use of information devolves on producers. To supply information to agriculture, it is necessary to analyze the biological and meteorological data and transform them into agricultural information. In the process of analysis, numerical characteristics of meteorological and phenological elements are calculated, tables and figures are prepared. In the process of preparation of information, the knowledge obtained from data analysis is drafted into answers concerning the meteorological effects on agricultural operations and on crop life (*Dmitrenko*, 1971). Information service can include information about past, present, and expected future meteorological effects on agricultural production. The answers can be published in rather different forms: orally or in writing, in television, in radio, on internet, in newspapers, in agrometeorological bulletins etc.

There are some criteria for servicing directly applicable information. The most important ones are the following:

- An information is more valuable than others if it has not only more accuracy, but also longer time interval between the date of issue and the beginning of practical use of information.
- The information must be drafted in agricultural terms as it is used by agricultural producers.
- The probability of decision alternatives should be known.

If we suppose that:

- a given problem of agricultural production depends on weather conditions, and
- required information is provided by agrometeorological information service, and
- we have methods for problem solving,

then we could choose one of the three possibilities:

- adapting agricultural production to meteorological conditions, or
- mitigating the unfavorable meteorological effects, or
- modification of meteorological factors.

Adaptation is the type of decision when we try to avoid plant damages. Several examples can be mentioned for this. Agricultural production can be adapted to climatic conditions by cautious choosing of:

– plant species, varieties, hybrids,

– cultivation area,

– date of sowing or planting, and

– agrotechnical processes

of agricultural production.

Mitigation means reducing unfavorable effects of environmental factors. If we are not able to prevent susceptible crop from meeting extreme meteorological effects (by the help of adaptation techniques), then we should try to minimize the damages suffered. Two kinds of mitigation can be mentioned from agrometeorological point of view: prevention of direct and indirect effects of meteorological elements. Damages can be caused by single meteorological elements (e.g., frost) and by combined meteorological effects (e.g., drought). They exert a harmful influence on plants directly, therefore, they are called damaging factors with direct effect. There are cases when the meteorological factors cause loss to the agricultural production indirectly, that is when meteorological conditions are favorable for those factors (e.g., plant diseases) which reduce productivity (*Varga-Haszonits*, 1983). Both types of mitigation can be applied only based on agrometeorological information.

Modification means effectively influencing meteorological factors to make those more favorable for cultivated crops. Theoretically, modification of meteorological conditions can be achieved in three levels: macro-, meso-, and microscale meteorological elements can be changed. But because of lack of energy and lack of exact information about feedbacks of the system, it is impossible to modify macroclimate. Opportunities for successful mesoclimatic modifications are also limited, but use of shelterbelt planting or preventing hail can be mentioned in this field. Methods for modification of micrometeorological environment, such as using various reflective materials, changing orientation and width of the crop rows, companion planting system, etc., are commonly used in agricultural practice. Using all kinds of controlled-environment facilities, such as greenhouses, phytotrones, etc., means an effective form of modification. These plant-growth chambers would provide the most ideal conditions also for commercial production, but these facilities function primarily as research tools.

It should be emphasized that all the environmental factors are interrelated; therefore, any attempt to modify one parameter may influence the others as well; for example the higher air humidity conditions of irrigated fields are favorable for plant diseases. This is the reason why quality of information should be important in decision-making. Without decisions based on professionally collected and processed data and scientific

information, only schematic farming with higher risk can be realized which ignores actual variability of weather conditions and effects.

Advances in weather forecasting and computer technology have improved the potential of farmers to prepare and adjust farming operations in response to climatic variations. For this potential to be realized, the complexity of decision-making in agricultural systems needs to be acknowledged, and the challenges facing farmers in accessing and learning to apply agrometeorological information need to be addressed (*Mavi* and *Tupper,* 2004).

Hungarian agrometeorological research includes all important approaches of this science: agroclimatology, agromicrometeorology approached in an inductive way, and agromicrometeorology approached in an analytic and deductive way (*Szász,* 1997). In addition, research activity of different agrometeorological departments concerns different ecological conditions of our country. This complexity of domestic agrometeorological research can be considered as strength.

2.2. Weaknesses, limitations

Sometimes it is quite difficult to give the required agrometeorological information for producers because of the stochastic relationships of soil-atmosphere-agriculture system. The farming is exposed to random effects among which the meteorological factors have an important role. In the agricultural production it can not be foreseen, whether we can achieve the wanted purpose or not, and if we can, with what kind of accuracy. Weather factors can cause a wide fluctuation in the yield, so that the role of random effects is very important in every case. The yield fluctuations of improved varieties or hybrids are greater than that of traditional varieties. The year-to-year differences in yield of improved varieties are sometimes greater than the total yield value of old varieties (*Varga-Haszonits* and *Varga*, 1999).

The further specific feature of the soil-atmosphere-agriculture system is its exposure to synchronous effect of different external and internal factors. The productivity of plants is influenced by biological, genetical properties, applied agrotechnical methods, soil and weather conditions. These complex synchronical effects are realized by direct and indirect processes. Therefore, it is difficult to separate the effect of a single factor. Another special biological feature, the so-called seasonality makes agrometeorological information supply more difficult. It means that crops respond differently to meteorological effects during various phenological stages (*Varga-Haszonits,* 1983).

Over-emphasizing the importance of individual factors of production levels defined by de Wit (*de Wit* and *van Keulen*, 1987; *Goudrian* and *van Laar*, 1994) and leaving the stochastic relationships of soil-atmosphere-agricultural production system out of consideration also may cause problems. This way, agrometeorological information could be considered unnecessary.

According to *Cousens* and *Mortimer* (1995), many farmers regard meteorological conditions as unpredictable and beyond their control. Yearly variations are usually treated as background noise and are ignored.

As we mentioned before, the good agrometeorological decisions require professionally gathered data and data-based information supply. It suggests that if:

– used data or information are of unchecked source, or

– farmers use their own (agro)meteorological data schematically (to reduce costs of production), or

– information supply is independent from the agricultural requirements, or

– data are not transformed into agricultural information,

then agricultural decisions would not be able to use agrometeorological information actually.

The biological respects are usually in the rough in climate scenarios, which are the main tools for the assessment of future developments in the complex climate-agriculture system. It is often ignored that not only the atmospheric conditions but also the agricultural ones could be dynamically changing systems when analyzing hypothetical relationships between climate and agriculture. Therefore, yield responds on climatic changes should be interpreted circumspectly (*Kocsis* and *Anda,* 2010). It also emphasizes that an agrometeorologist have to be fluent in both the biological and physical sciences and have to look at the world from a different and wider perspective than the physical and biological scientist does (*Mavi* and *Tupper*, 2004). That is why we can state that the interdisciplinary nature of agrometeorology – and agrometeorological information supply – is both its greatest strength and its greatest weakness (*Hollinger*, 1994).

2.3. Opportunities

As we could see earlier, agrometeorological research and agrometeorological information supply are in strong relationship with each other. Information supply about effects of a dynamically changing atmospheric system on a constantly developing farming system can be done only on the base of continuous agrometeorological research activities. It is the reason why it is practical to review the opportunities of agrometeorological research and information service jointly.

In recent decades, interdisciplinar research became more and more important, because problems may cut right across the borders of any discipline *(Popper,* 1963). The interdisciplinar approach of agrometeorology is well-known, and it can be advantageous in this respect.

The study of climate change can be identified as research priority because of its global impacts. It is like enough that more attention should pay to investigation of agricultural impacts of global warming in the future.

Moreover, favorable experiences of agrometeorological information service during 1967–1990 suggest that it can work again in Hungary.

The potential to handle data and information by computers and exchange them globally via the internet is growing continuously.

Progressing food production supported rise and development of human civilization. High-level food production and food security need adequate information supply – especially when environmental conditions are changing, resources are limited, and human population growth is increasing.

2.4. Threats

Agrometeorological information supply has to face several problems which originate from its external relations.

- There is no need for B.Sc. or M.Sc. degree in agricultural science for farming in Hungary. It can cause problems in the quality of decision-making.
- Most of domestic agricultural BSc and MSc courses do not contain agrometeorological studies. Therefore, not even a qualified agronomist can realize the importance of using agrometeorological information.
- Neither Hungarian agricultural-advisory system includes agrometeorological information supply.
- Legal and economical regulation of agricultural production does not always inspire use of agrometeorological information.
- Hungarian farmers are not interested in agrometeorological information service because of their financial problems.
- Current academic structures do not foster interactions between biological and physical scientists.
- Both the Hungarian Meteorological Service and the agricultural faculties including agrometeorological departments or groups have financial problems.
- Financial problems influence also observational (meteorological and phenological) networks.
- There is not any gradual or postgradual course in agrometeorology in Hungary.

All the above threats originate in financial and organizational problems.

Average age of Hungarian agrometeorologists is about 54.5 years, two-third of them are over 50, one-third of them are over 60 years according to a

study written by Anda for the Agrometeorological Committee of Hungarian Academy of Sciences (URL[2]). This tendency for senescence is also a threat of agrometeorological research and information supply. It could be compensated by agrometeorological training programs, but it is far from a solution yet.

3. Summary

Agricultural production and human civilization developed in parallel in the Holocene. The intense farming activities of our early agrarian ancestors improved food supply, and thus, opened up a new prospect for social processes (*Behringer*, 2010). *Ruddiman* (2003) – modifying Crutzen`s "anthropocene" theory (*Crutzen et al.,* 2000 cit. *Behringer,* 2010; *Crutzen* and *Steffen,* 2003) – thinks that human-induced changes in greenhouse gases did not begin in the eighteenth century with advent of coal-burning factories and power plants of the industrial era, but date back to 8,000 years ago, triggered by increasing agricultural production. These theories suggest that the relationships between climate, agriculture, and society are more complex than we supposed it before. Agriculture needs meteorological information not only for increasing productivity, but also for reducing environmental damages.

The global warming tendency means both opportunity and threat for us. *Behringer* (2010) distinguishes between warm and cold periods of the Holocene and highlights the ability of agricultural production to adapt to climatic changes. He rates warm periods positively and cold periods negatively. On the other hand, climate change forces adaptation of farming for it. It is expected that modern farming systems should produce big amount and high quality yields under changing climatic conditions – in an economically reasonable and sustainable way. Adaptation strategies require professionally gathered meteorological and phenological data and data-based information supply.

In this study, advantageous and disadvantageous internal features and external relations of agrometeorological information service were analyzed by means of a SWOT analysis. It was found that several and significant strengths and opportunities enable agrometeorological research and information supply to help agricultural decision-making effectively.

Weaknesses originate in complex and stochastic nature of the atmosphere-soil-plant system, that makes difficult to give the required agrometeorological information, and in inadequate working of agrometeorological information supply. Threats include educational, organizational, and financial problems.

Acknowledgement–The author would like to thank for the support of TÁMOP-4.2.2A-11/1/KONV-2012-0003 project.

References

Behringer, W., 2010: A klíma kultúrtörténete. Corvina Kiadó, Budapest. (in Hungarian)

Bernal, J.D., 1963: Tudomány és történelem. Gondolat Kiadó, Budapest. (in Hungarian)

Cousens, R. and *Mortimer, M.*: 1995: Dynamics of weed populations. Cambridge University Press, Cambridge.

Crutzen, P.J. and *Steffen, W.*, 2003: How long have we been in the Anthropocene Era? *Climatic Change 61*, 251–257.

de Wit, C.T. and *van Keulen, H.*, 1987: Modelling production of field crops and its requirements. *Geoderma 40*, 253–265.

Dmitrenko, V.P., 1971: Features of agrometeorological service (in Russian). *Trudi UNIGMI. 109*, 37–49.

Goudrian, J. and *van Laar, H.H.*, 1994: Modelling potential crop growth processes. Textbook with exercises. Kluwer Academic Publishers, Dordrecht.

Hollinger, S.E., 1994: Future directions and needs in agricultural meteorology/climatology and modeling. *Agr. Forest Meteorol. 69*, 1–7.

Kocsis, T. and *Anda, A.*, 2010: A légköri nyomgázok hatása: az üvegházhatás és fokozódásának következményei. In (eds.: *Anda, A., Kocsis, T.*): Agrometeorológiai és klimatológiai alapismeretek. Mezőgazda Kiadó, Budapest. 36–74. (in Hungarian)

Mavi, H.S. and *Tupper, G.J.*, 2004: Agrometeorology: principles and applications of climate studies in agriculture. Food Products Press, London.

Ministry of Agriculture and Food Administration, Hungarian Meteorological Service 1974: Agroclimatology and plant production. Budapest.

Popper, K.R., 1963: Conjectures and refutations: the growth of scientific knowledge. Routledge and Kegan Paul, New York.

Ruddiman, W.F., 2003: The Anthropogenic Greenhouse Era began thousands of years ago. *Climatic Change 61*, 261–293.

Szász, G., 1997: A mikroklíma fogalma. In (eds: *Szász, G., Tőkei, L.*) Meteorológia mezőgazdáknak, kertészeknek, erdészeknek, Mezőgazda Kiadó, Budapest, 264–342. (in Hungarian)

Székely, Cs., 2000: Stratégia és tervezés. In: (eds.: *Buzás, Gy., Nemessályi, Zs., Székely, Cs.*) Mezőgazdasági üzemtan I., Mezőgazdasági Szaktudás Kiadó, Budapest. 237–271. (in Hungarian)

Varga, Z. 2010: Az agrometeorológiai információk hasznosításának alapjai. In (eds.: *Anda, A., Kocsis, T.*): Agrometeorológiai és klimatológiai alapismeretek. Mezőgazda Kiadó, Budapest, 291–314. (in Hungarian)

Varga-Haszonits, Z., 1967: Útmutatás kulturnövényfenológiai megfigyeléskre. OMI. Budapest.(In Hungarian)

Varga-Haszonits, Z., 1983: Agroclimatology and agrometeorological forecasting. Lecture notes. Budapest.

Varga-Haszonits, Z., 1997: Agrometeorológiai információk és hasznosításuk. In (eds: *Szász, G., Tőkei, L.*) Meteorológia mezőgazdáknak, kertészeknek, erdészeknek, Mezőgazda Kiadó, Budapest. 651–679.

Varga-Haszonits, Z. and *Varga, Z.*, 1999: Agroklimatológia (Climate and crop production). Lecture notes. Mosonmagyaróvár. (in Hungarian)

URL[1]: http://en.wikipedia.org/wiki/SWOT_analysis

URL[2]: http://www.mettars.hu/wp-content/uploads/2010/09/Anda100831.pdf

INSTRUCTIONS TO AUTHORS OF *IDŐJÁRÁS*

The purpose of the journal is to publish papers in any field of meteorology and atmosphere related scientific areas. These may be

- research papers on new results of scientific investigations,
- critical review articles summarizing the current state of art of a certain topic,
- short contributions dealing with a particular question.

Some issues contain "News" and "Book review", therefore, such contributions are also welcome. The papers must be in American English and should be checked by a native speaker if necessary.

Authors are requested to send their manuscripts to

Editor-in Chief of IDŐJÁRÁS
P.O. Box 38, H-1525 Budapest, Hungary
E-mail: journal.idojaras@met.hu

including all illustrations. MS Word format is preferred in electronic submission. Papers will then be reviewed normally by two independent referees, who remain unidentified for the author(s). The Editor-in-Chief will inform the author(s) whether or not the paper is acceptable for publication, and what modifications, if any, are necessary.

Please, follow the order given below when typing manuscripts.

Title page: should consist of the title, the name(s) of the author(s), their affiliation(s) including full postal and e-mail address(es). In case of more than one author, the corresponding author must be identified.

Abstract: should contain the purpose, the applied data and methods as well as the basic conclusion(s) of the paper.

Key-words: must be included (from 5 to 10) to help to classify the topic.

Text: has to be typed in single spacing on an A4 size paper using 14 pt Times New Roman font if possible. Use of S.I. units are expected, and the use of negative exponent is preferred to fractional sign. Mathematical formulae are expected to be as simple as possible and numbered in parentheses at the right margin.

All publications cited in the text should be presented in the *list of references*, arranged in alphabetical order. For an article: name(s) of author(s) in Italics, year, title of article, name of journal, volume, number (the latter two in Italics) and pages. E.g., *Nathan, K.K.,* 1986: A note on the relationship between photo-synthetically active radiation and cloud amount. *Időjárás 90,* 10-13. For a book: name(s) of author(s), year, title of the book (all in Italics except the year), publisher and place of publication. E.g., *Junge, C.E.,* 1963: *Air Chemistry and Radioactivity.* Academic Press, New York and London. Reference in the text should contain the name(s) of the author(s) in Italics and year of publication. E.g., in the case of one author: *Miller* (1989); in the case of two authors: *Gamov* and *Cleveland* (1973); and if there are more than two authors: *Smith et al.* (1990). If the name of the author cannot be fitted into the text: *(Miller,* 1989); etc. When referring papers published in the same year by the same author, letters a, b, c, etc. should follow the year of publication.

Tables should be marked by Arabic numbers and printed in separate sheets with their numbers and legends given below them. Avoid too lengthy or complicated tables, or tables duplicating results given in other form in the manuscript (e.g., graphs).

Figures should also be marked with Arabic numbers and printed in black and white or color (under special arrangement) in separate sheets with their numbers and captions given below them. JPG, TIF, GIF, BMP or PNG formats should be used for electronic artwork submission.

Reprints: authors receive 30 reprints free of charge. Additional reprints may be ordered at the authors' expense when sending back the proofs to the Editorial Office.

More information for authors is available: journal.idojaras@met.hu

Published by the Hungarian Meteorological Service

Budapest, Hungary

INDEX 26 361

HU ISSN 0324-6329

IDŐJÁRÁS

QUARTERLY JOURNAL
OF THE HUNGARIAN METEOROLOGICAL SERVICE

CONTENTS

****

http://www.met.hu/Journal-Idojaras.php

VOL. 118 * NO. 2 * APRIL – JUNE 2014

IDŐJÁRÁS

Quarterly Journal of the Hungarian Meteorological Service

Editorial Office: Kitaibel P.u. 1, H-1024 Budapest, Hungary
P.O. Box 38, H-1525 Budapest, Hungary
E-mail: journal.idojaras@met.hu
Fax: (36-1) 346-4669

Indexed and abstracted in Science Citation Index Expanded™ and Journal Citation Reports/Science Edition
Covered in the abstract and citation database SCOPUS®

Subscription by mail:
IDŐJÁRÁS, P.O. Box 38, H-1525 Budapest, Hungary
E-mail: journal.idojaras@met.hu

IDŐJÁRÁS

Quarterly Journal of the Hungarian Meteorological Service
Vol. 118, No. 2, April – June, 2014, pp. 93–118

Modeling dry flux of ammonia and nitric acid between the atmosphere and Lake Balaton

Szilvia Kugler[1,2], **László Horváth***[3,4], and **Tamás Weidinger**[1]

[1]*Department of Meteorology, Eötvös Loránd University, Pázmány Péter sétány 1/A, 1117 Budapest, Hungary*

[2]*Institute for Solid State Physics and Optics, Wigner Research Centre for Physics, Hungarian Academy of Sciences, Konkoly-Thege Miklós út 29-33, 1121 Budapest, Hungary*

[3]*Hungarian Meteorological Service, Gilice tér 39, 1181 Budapest, Hungary*

[4]*MTA-SZIE Plant Ecology Research Group, Szent István University, Páter K. u. 1, 2103 Gödöllő, Hungary*

**Corresponding author E-mail:* horvath.l@met.hu

(Manuscript received in final form January 30, 2014)

Abstract—N-deposition from atmosphere contributes to the eutrophication of Lake Balaton (Hungary). To estimate the share of N-input compared to the effect of other sources, measurements have started in the 70's of the last century. However, in previous calculations the flux of N-gases (NH_3 and HNO_3) was estimated using deposition velocity parameters determined for terrestrial ecosystems. These simplifications were accompanied by an overestimation of the role of these compounds. According to our results for years 2001–2004, ammonia has a mean net emission flux from the lake (32.7 t N $year^{-1}$), while nitric acid deposition takes –21.8 t N $year^{-1}$ that are one order of magnitude lower than sum of other deposition forms (esp. wet N-deposition). The pH range in lake water (pH = 8.3–8.9) allows the bi-directional flux for ammonia. Ammonia exchange can act as a buffering system, i.e., in case of a high N-load to the lake from other sources (rivers, waste water, run-off, etc.) N-accumulations can be buffered through nitrogen emission in form of NH_3 as a consequence of the elevated compensation-point concentration. From this reason, eutrophication of Lake Balaton is phosphorus limited. Comparing the measured ammonia flux with the fluxes calculated by compensation-point models based on single Henry's law theory and by Hales-Drewes theory, it can be concluded that in our case latter theory describes better the exchange processes, suggesting that effect of carbon dioxide on the solubility of ammonia can not be excluded. However, in contrast with Hales and Drewes who suggested a decreased solubility of ammonia in presence of CO_2, we find an opposite effect, i.e., CO_2 favors the solubility of ammonia in the slight alkaline pH-range representative to the lake.

Key-words: eutrophication, FLake model, Monin-Obukhov theory, resistance model, compensation-point model, ammonia flux, nitric acid flux

1. Introduction

Atmospheric load of trace materials is one of the most important nutrient sources for freshwater ecosystems. Nutrient enrichment causes change of ecosystem structure and function; this process is termed eutrophication (*Durand et al.*, 2011). Generally, the two limiting elements in eutrophication are the nitrogen and the phosphorus. According to an international survey (*ICLF*, 2010), Lake Balaton nowadays is co-limited; i.e., both N and P are limiting factors for eutrophication.

The mean surface of Lake Balaton is 598 km^2 with a contributing area of 5775 km^2. Being a shallow lake (mean depth of water is 3 m), Balaton is especially sensitive to nutrient loading (*Jordan et al.*, 2005). The first serious extinction of fish caused by algal bloom as a consequence of nutrient enrichment was observed in 1975 (*Herodek*, 1977).

Since then, intensive investigations have been started to estimate the source and strength of nutrient loading to the lake for mitigation purposes. *Jolánkai* and *Bíró* (2005) compiled the load of N and P into the lake from different sources for a three-decade period between 1975 and 2004. According to this work, the atmospheric nitrogen deposition has varied within a wide range between 300 and 1,800 t N $year^{-1}$. The reason of this large variation is the lack of direct measurement of dry deposition of nitrogen compounds to the surface of the lake. In all of previous studies, dry deposition of nitrate and ammonium particles and nitric acid vapor was estimated by the inferential method taking into account deposition velocities determined for terrestrial surfaces (*Horváth et al.*, 1981; *Horváth*, 1990). It led to an overestimation of nitrogen load, especially as the consequence of different surface characteristics (e.g., roughness) between terrestrial and water systems. To eliminate these discrepancies, a field campaign has started in 2002 to measure the dry deposition of nitrogen compounds also providing direct measurement data for validation of modeled fluxes. In a previous study (*Kugler* and *Horváth*, 2004), it was pointed out that dry deposition rates of nitrate and ammonium particles over Lake Balaton are much lower than it was supposed before and takes a nearly negligible share in the total atmospheric N-load to the lake.

In another paper (*Kugler et al.*, 2008), results of a preliminary analysis concerning the atmospheric dry deposition of nitric acid and net flux of ammonia for a year period (March 2002–February 2003) was reported based on a simple compensation-point model. It was found that deposition rate for nitric acid is less by one order of magnitude compared to grass surfaces, and ammonia has bi-directional flux resulting in either monthly average net emission or net deposition as the function of physical and chemical conditions in air and water. As ammonia has bi-directional flux, it is a key component in the nitrogen balance between the atmosphere and the lake, since compensation-point concentration and emission rate of ammonia is increasing parallel with increase

of N-load from other sources (waste water, rivers, creeks, leaching of fertilizers, etc.). It means a negative feedback mechanism which probably emits the excess nitrogen in the form of ammonia into the atmosphere (*Kugler et al.*, 2008). Moreover, in other case, in the lack of nutrient-N the atmosphere may act as nitrogen (ammonia) source for this aquatic ecosystem.

The aim of the paper is to investigate in more details the dry fluxes of gaseous nitrogen compounds and to estimate their share in total atmospheric N-load. Our investigations are based on sophisticated models for a four-year period (2001–2004) validated by flux data measured by the gradient method.

2. *Methodology*

2.1. Measurements

Meteorological and chemical parameters have been measured at the Storm Warning Observatory of Hungarian Meteorological Service, at the shore of lake (46° 54' 48.88" N; 18° 2' 19.76" E) in the town Siófok.

Meteorological measurements as wind direction and velocity, air temperature, relative humidity, and air pressure were observed by standard meteorological instruments. The global radiation and long wave radiation components were calculated by different parameterization schemes (*Holtslag* and *van Ulden,* 1983; *Mészáros*, 2002; *Foken*, 2006).

Measurement protocol for ammonia and nitric acid concentrations are: i) for the compensation-point model calculations: March 2002–February 2003 by 24-h continuous sampling at the height of 12.3 m above lake surface; ii) for the gradient measurements: July 12, 2002–July 25, 2012, 3-hour samplings, 8 times a day at two levels above the lake surface (12.3 and 2.8 m); iii) for interpolation of concentration data to Siófok: K-puszta and Farkasfa background air pollution monitoring stations (46° 58' N, 19° 33' E and 46° 55' N, 16° 18' E) (2001–2004). Ammonia and nitric acid were sampled by a NILU EK-type three-stage bulk filter-pack sampler (*EMEP*, 1996). Concentrations of nitrate and ammonium ions in the extract of filters water were determined by ion-chromatography and spectrophotometry, respectively. Minimum detection limit (MDL) was 0.1 $\mu g\, N\, m^{-3}$ for both ions. The bulk relative error of sampling and measurements is 10%.

The NH_3+NH_4^+ concentration (by spectrophotometry) and pH in the lake water were sampled and measured on the basis of bi-weekly samplings by the Middle Transdanubian Inspectorate for Environmental Protection, Natural Protection, and Water Management and by the VITUKI, Research Centre for Environmental Protection and Water Management. Sampling points were selected at Balatonakali, Keszthely, Siófok, and Szigliget settlements.

For validation of models, dry fluxes of ammonia and nitric acid were measured by the gradient method as described in Section 2.3.

2.2. The compensation-point model

Net dry flux of a gas having bi-directional exchange can be estimated by a modified compensation-point model (first described by *Farquhar et al.*, 1980):

$$F = -\left(C(z_{ref}) - C(z_0)\right) \cdot \left(\frac{1}{R_a + R_b}\right), \tag{1}$$

where F is the flux of gases, $C(z_{ref})$ is the atmospheric concentration of gases measured at the level z_{ref} (in our case 12.3 m), $C(z_0)$ is the compensation-point concentration at z_0 (roughness length) level, R_a and R_b are the resistances of turbulent and laminar layers, respectively. In case of ammonia and nitric acid vapor above water surfaces, the canopy resistance (R_c) can be neglected according to *Erisman et al.* (1994) and *Shahin et al.* (2002).

The net dry flux of nitric acid vapor can be calculated by Eq. (1), taking into account that in the slightly alkaline water HNO_3 molecules are completely dissociated, i.e., $C(z_0) = 0$ (*Kugler et al.*, 2008).

During the measurement campaign, the compensation-point concentrations for ammonia were calculated by two different methods. First, the simple Henry's law was used to determine the compensation-point concentration:

$$C(z_0) = \frac{C_w}{\left[H^+\right]\frac{K}{K_w}H_1 + H_1}, \tag{2}$$

where C_w and $[H^+]$ are concentrations of sum of ammonia+ ammonium and hydrogen ion in water phase, respectively, H_1 is the Henry's law constant of ammonia, K, K_w are constants at a given temperature (*Horváth*, 1982).

According to *Hales* and *Drewes* (1979), the simple Henry's law cannot be applied to calculate the compensation-point concentration, since carbon dioxide decreases the solubility of ammonia in water phase that must be taken into account in compensation-point calculation by the following formula:

$$C(z_0) = \frac{C_w(H_1H_2[CO_2]Q + 1)}{H_1H_2P[CO_2] + \left[H^+\right]\frac{K}{K_w}H_1 + H_1}, \tag{3}$$

where, Q, P, K, K_w are constants at a given temperature, H_2 is the Henry's law constant of carbon dioxide, $[CO_2]$ is the concentration of carbon dioxide in the air (calculated from the average mixing ratio of 380 ppm, in 2002–2003).

Later on, laboratory experiments (*Ayers et al.*, 1985; *Dasgupta* and *Dong*, 1986) demonstrated by laboratory experiments that theory of *Hales* and *Drewes* (1979) is not suitable, and the classical Henry's law should be used to calculate the compensation-point concentration. Due to the obvious contradiction among different authors and results between field and laboratory measurements, we have calculated the compensation-point concentrations using single Henry's law and the modified solubility theory of Hales-Drewes as well.

2.3. The gradient method

The gradient method was applied for validation of compensation-point models and in case of ammonia to verify two different outputs of models based on different solubility theories. The net gradient flux of a gas can be determined by the following equation supposed the similarity in exchange of heat and trace gases (*Weidinger et al.*, 2000; *Foken*, 2006):

$$F = -\rho_m \overline{K}_H \frac{\Delta C}{\Delta z}, \tag{4}$$

where $\overline{K}_H$ is the turbulent diffusion coefficient of the heat flux in a certain layer, ΔC is the concentration difference between two heights above surface, Δz is the difference between the two heights, ρ_m is the average density of the moist air. Turbulent diffusion coefficient at dimensionless height ($\zeta = (z-d)/L$) can be calculated using the similarity theory by the following formula:

$$K_H(\zeta) = \frac{\kappa u_* (z-d)}{\varphi_H(\zeta)}, \tag{5}$$

where κ is the Kármán constant (usually set to 0.4), u_* is the friction velocity, z is the height, d is the displacement height, L is the Monin-Obukhov length, φ_H is the universal function of sensible heat flux. Above water surface the displacement height is zero. Parameterizations of *Businger et al.* (1971) and *Dyer* (1974) were used for determination of the universal functions in different stratifications. The calculations of the friction velocity are described in Section 2.4.

2.4. The micrometeorological input

Turbulent diffusion coefficient for the gradient method and different resistances for compensation-point model were calculated by two different micrometeorological methods. First, we used the Monin-Obukhov theory to determine the turbulent sensible heat fluxes, the Monin-Obukhov length, and the friction velocity. It is named as resistance model (RM), since it was applied to

calculate the resistances (*Weidinger et al.*, 2000; *Ács* and *Szász*, 2002; *Ács*, 2003). Another model, namely the 1D numerical FLake model (FM) was also used to determine the same characteristics (*Mironov*, 2008).

At first, both models calculate the net radiation (Q_S) by the following equation:

$$Q_S = Q_H + Q_E + Q_G, \tag{6}$$

where Q_H, Q_E are the sensible and latent heat fluxes, Q_G is the heat flux into the water.

Calculation of momentum flux (τ), sensible heat flux (Q_H), latent heat flux (Q_E), and trace gas fluxes (Q_C) can be described by the following equations (*Foken*, 2006):

$$\tau = \rho_m u_*^2 = \rho_m K_M \frac{\partial \bar{u}}{\partial z}, \tag{7}$$

$$Q_H = -c_{pm}\rho_m u_* T_* = -\rho_m c_{pm} K_H \frac{\partial \bar{\theta}}{\partial z}, \tag{8}$$

$$Q_E = -\lambda \rho_m u_* q_* = -\lambda \rho_m K_E \frac{\partial \bar{q}}{\partial z}, \tag{9}$$

$$Q_C = -\rho_m u_* c_* = -\rho_m K_C \frac{\partial \bar{c}}{\partial z}, \tag{10}$$

where c_{pm} is the specific heat at constant pressure, λ is the phase transition energy, z is the height, $\bar{\theta}$, $\bar{q}$, $\bar{c}$, $\bar{u}$ are average potential temperature, specific humidity, trace gas concentration, and wind velocity, respectively, u_*, T_*, q_*, c_* are dynamical parameters for wind velocity, air temperature, specific humidity, and trace gas concentration, respectively. K_s is the turbulent diffusion coefficient of a certain property $s \in (M, H, E, C)$ as momentum, sensible, latent heat, and trace gas. We assume that eddy diffusivity coefficients of sensible and latent heat and trace gases are similar $K_H = K_E = K_C$.

With the knowledge of the gradient of certain micrometeorological parameters (*Weidinger et al.*, 2000; *Mészáros*, 2002), the universal functions of momentum, heat, humidity, and trace gases can be calculated as:

$$\frac{\partial \bar{u}}{\partial z} = \frac{u_*}{\kappa(z-d)} \varphi_M(\zeta), \tag{11}$$

$$\frac{\partial \bar{\theta}}{\partial z} = \frac{T_*}{\kappa(z-d)} \varphi_H(\zeta), \tag{12}$$

$$\frac{\partial \bar{q}}{\partial z} = \frac{q_*}{\kappa(z-d)} \varphi_E(\zeta), \tag{13}$$

$$\frac{\partial \bar{c}}{\partial z} = \frac{c_*}{\kappa(z-d)} \varphi_C(\zeta), \tag{14}$$

where $\zeta = (z-d)/L$ is the dimensionless height and L is the so-called Monin-Obukhov length. Other parameters have been described previously. φ_S $s \in (M, H, E, C)$ is the universal function of a certain property as momentum, heat, humidity, and trace gas.

The Monin-Obukhov length is determined by this formula:

$$L = \frac{u_*^2}{\kappa \beta T_*}, \tag{15}$$

where $\beta = g/\bar{\theta}$ is the stability parameter, g is the acceleration of gravity.

The general forms of universal functions (*Arya*, 2001) of momentum and sensible heat are described as:

$$\varphi_M = (1-\gamma_1\zeta)^{-\frac{1}{4}}, \qquad \text{if } 0 > \zeta \quad \text{(unstable)}, \tag{16}$$

$$\varphi_M = 1+\beta_1\zeta, \qquad \text{if } 0 \le \zeta \quad \text{(stable)}, \tag{17}$$

$$\varphi_H = \alpha(1-\gamma_2\zeta)^{-\frac{1}{2}}, \qquad \text{if } 0 > \zeta \quad \text{(unstable)}, \tag{18}$$

$$\varphi_H = \alpha + \frac{\beta_2}{\alpha}\zeta = \alpha(1+\beta_2\zeta), \qquad \text{if } 0 \le \zeta \quad \text{(stable)}, \tag{19}$$

where $\alpha, \beta_1, \beta_1, \gamma_1, \gamma_2$ are constants derived from the micrometeorological experiments of *Businger et al.* (1971) and *Dyer* (1974).

By integration of the Eqs. (11–12), turbulent characteristics for a certain layer are described as follows:

$$u(z_2)-u(z_1)=\frac{u_*}{\kappa}\left[ln\frac{z_2}{z_1}-\int_{\zeta_1}^{\zeta_2}(\varphi_M-1)\mathrm{d}ln\zeta\right]=\frac{u_*}{\kappa}\left[ln\frac{z_2}{z_1}-(\Psi_M(\zeta_2)-\Psi_M(\zeta_1))\right], \quad (20)$$

$$\theta(z_2)-\theta(z_1)=\frac{T_*}{\kappa}\left[ln\frac{z_2}{z_1}-\int_{\zeta_1}^{\zeta_2}(\varphi_H-\alpha)\mathrm{d}ln\zeta\right]=\frac{T_*}{\kappa}\alpha\left[ln\frac{z_2}{z_1}-(\Psi_H(\zeta_2)-\Psi_H(\zeta_1))\right], \quad (21)$$

where Ψ_M, Ψ_H are integral forms of stability function of momentum and sensible heat.

Stability functions in cases of stable and unstable stratifications are:

$$\Psi_M(\zeta)=ln\left[\left(\frac{1+x_M{}^2}{2}\right)\left(\frac{1+x_M}{2}\right)^2\right]-2tan^{-1}x_M+\frac{\pi}{2}, \quad \text{if } 0>\zeta, \quad (22)$$

$$\Psi_H=2ln\left(\frac{1+x_H{}^2}{2}\right), \quad \text{if } 0>\zeta, \quad (23)$$

$$\Psi_M=-\beta_1, \ \Psi_H=-\frac{\beta_2}{\alpha}, \quad \text{if } 0\le\zeta, \quad (24)$$

where $x_M=(1-\gamma_1\zeta)^{1/4}$, $x_H=(1-\gamma_2\zeta)^{1/4}$.

RM model uses Eqs. (16-19) for calculation, where the constants used have been measured at the Kansas experiment of *Businger et al.* (1971):

$$\alpha=0,74;\ \beta_1=4,7;\ \beta_2=4,7/\alpha;\ \gamma_1=15;\ \gamma_2=9. \quad (25)$$

After calculation of radiation balance, RM is resolving the Eqs. (15, 20–21). We considered $z_1=z_0=0.0003$ m, and water temperature was applied at height z_1. Model uses iteration method to calculate friction velocity (u_*), dynamic temperature (T_*), and sensible heat flux using Eq. (8). Sensible heat flux was calculated using the assumption that $\varphi_E=\varphi_H$ based on the difference in specific humidity. At the end of calculations, heat flux into the water is determined as residual term in radiation balance.

Since RM uses measured water temperatures at depth of 1 m for calculations, we tried to find a lake model which is able to predict the surface

temperature of a shallow lake. The FLake model (FM) is able to predict a vertical temperature structure in lakes at various depths on time scales from a few hours to a year.

The change in water temperature is described by the following equation in FM:

$$h\frac{\partial T_S}{\partial t} = \frac{1}{\rho_w \cdot c_w}[Q_W + I_W - Q_M - I(h)], \tag{26}$$

where h is the depth of mixed layer, T_s is the surface temperature of water (the same as the temperature in the upper water layer), ρ_w is the density of water, c_w is the specific heat capacity of water, Q_w is the heat flux through air-ice-water or air-water interface, I_w is the radiation flux through air-ice-water or air-water interface, Q_M is the heat flux at the bottom of mixed layer, $I(h)$ is the radiation flux at the bottom of depth layer (h). Terms Q_w and I_w are defined as $Q_G = Q_w + I_w$ for Q_G referring to Eq. (6).

FM uses the following method for calculations. First, prognostic and diagnostic values of the model are set to their initial values. As next step, the albedo of water, ice, and snow and also optical characteristics of water are determined. It follows the calculation of long wave radiation from surface and shortwave heat balance. With the Monin-Obkuhov theory momentum, sensible, and latent heat fluxes plus the dynamic velocity are derived. At the parameterization of the universal functions Eqs. (16–19), FM uses constants of *Dyer* (1974):

$$\alpha = 1; \beta_1 = \beta_2 = 5; \gamma_1 = \gamma_2 = 16\,. \tag{27}$$

For further calculations FM uses the Euler explicit scheme. In all time steps all model variables are derived. As the next step, heat flux through air-ice-water or air-water interface, a heat flux utilized in calculations of the convective boundary-layer evolution in the lake water, then heat flux through water-bottom sediment interface are computed. Later on, it follows to determine change in thickness and temperature of ice and snow, mean temperature of water column, mixed-layer depth, mixed-layer temperature, bottom temperature, and shape factor with respect to temperature profile in thermocline. Depth of upper layer of bottom sediments penetrated by thermal wave and temperature at that depth are computed. At the end, lake surface temperature is updated. That is set equal to either temperature of the water-surface temperature, or to surface temperature of ice or snow. The model applies a 10-step iteration method. More details for the FLake model description refer to *Mironov* (2008) and *Mironov et al.* (2010).

Both models determine the turbulent fluxes dynamic velocity, and also stratification. Then, aerodynamic resistances can be derived to solve the following equation (*Ács et al.*, 2000) using Eq. (5):

$$R_a = \int_{z_0}^{z} \frac{1}{K_H(z)} dz \,, \tag{28}$$

where K_H is the turbulent diffusion coefficient of sensible heat flux in a certain layer.

The boundary layer resistance can be calculated by the following formula (*Kramm et al.*, 1996):

$$R_b = \frac{2}{\kappa u_*} \left(\frac{\mathrm{Sc}}{\mathrm{Pr}} \right)^P , \tag{29}$$

where Sc is the Schmidt-number, Pr is the Prandtl-number, and P is an empirical constant (2/3). The quotient of Schmidt- to Prandtl-numbers are 0.96 for ammonia and 1.44 for nitric acid (*Hicks et al.*, 1987).

3. *Results and discussions*

3.1. Calculation of resistances and turbulent diffusion coefficients

Turbulent heat and momentum fluxes and diffusion coefficient were parallel determined by resistance (RM) and Flake models (FM) (*Ács* and *Szász*, 2002; *Mironov*, 2008) between January 2001 and December 2004 on hourly base.

Input data for resistance model are: water and air temperature, wetness characteristics (e.g., specific humidity), wind velocity and direction, cloudiness, and global radiation. Output data are: hourly averages of momentum flux (τ), sensible (Q_H) and latent (Q_E) heat fluxes, turbulent diffusion coefficients (K_H), resistances (R_a, R_b), and Monin-Obukhov length (L) on the basis of methods described by *Ács et al.* (2000), *Weidinger et al.* (2000), and *Foken* (2006).

Input data for FLake model are: rate of snow accumulation, global radiation, longwave radiation, wind velocity, and temperature, humidity, and pressure of air. Initial conditions (*Table 1*) were determined by *Vörös et al.* (2010) based on measurements and sensitivity analysis. Initial mean water temperature was always set to the measured water temperature of the lake.

Table 1. Initial conditions and predicted variables in FLake model

Type	Symbol	Name	Setting/ initialization
Initial conditions	$Depth_{\_w}$	Depth of lake*	0.9 m
	Fetch	Wind fetch	3000 m
	T_{bs0}	Sediment temperature	283.15 K
	$Depth_{\_bs}$	Depth of sediment	3 m
	Latitude	Geographical situation	47°
	Albedo	Albedo	0.095
Prognostic variables	T_{snow}	Snow temperature	273.15 K
	T_{ice}	Ice temperature	273.15 K
	T_{mnw}	Mean water temperature	274.25 K
	T_{wML}	Temperature in boundary layer	274.25 K
	T_{bot}	Temperature at boundary of water/sediment	274.25 K
	T_{B1}	Temperature at the bottom of upper sediment	283.15 K
	C_θ	Shape factor	0.50
	h_{snow}	Snow depth	0 m
	h_{ice}	Ice depth	0 m
	h_{ML}	Thickness of mixing layer	0.9 m
	h_{B1}	Depth of upper layer of sediment	3 m
	T_{sfc}	Temperature in the previous time step	274.25 K

*Based on the sensitivity analysis of FLake model for Lake Balaton after *Vörös et al.* (2010)

Output data of FLake model are: turbulent fluxes over lake, turbulent diffusion coefficient of sensible heat flux, aerodynamic and boundary layer resistances, and Monin-Obukhov length.

Data of calculated hourly energy balance components by the two methods were governed mainly by the water temperature and input meteorological variables. Extreme figures caused by i) difference of measured (RM) and modeled (FM) water temperature, ii) high negative value of sensible heat flux during stable conditions at high wind velocity, and iii) by overestimation of latent heat flux during very unstable stratifications were filtered. Corrections were applied for cases with extreme large deviations between the figures calculated by the two methods caused by unreliable output data at least from one of the methods. Filtration criteria were as follows:

i) radiation balance must not be lower than -120 W m^{-2},
ii) latent heat flux must not reach 450 W m^{-2},
iii) lower and upper thresholds for sensible heat flux were -75 W m^{-2} and 175 W m^{-2}, respectively.

Application of these criteria is justified by, e.g., *Liu et al.* (2011) in calculation of direct fluxes for a water reservoir. Data over or below these limits

were replaced by the limit figure itself. Hourly energy balance was closed in these cases by change of heat flux into water.

Corrections were applied in cases when difference in heat fluxes into water was larger than 200 W m^{-2}. In these cases by proportional variation of sensible and latent heat fluxes – keeping the Bowen-ratio constant calculated by the two methods –, the difference between heat flux into water was kept below 200 W m^{-2}. According to the criteria above, corrections were applied in 3 to 6% of cases in the different years.

For validation of results we compared the monthly evaporation rates with that of calculated by Central-Transdanubian Water Directorate on the basis of Meyer-formula (*Anda* and *Varga*, 2010), for the period of 2001–2004. According to *Kovács* (2011) and *Szilágyi* and *Kovács* (2011), the Meyer-formula (MF) simulates well the real evaporation for Balaton. The monthly evaporation rates calculated by the different methods can be seen in *Fig. 1*. Correlations between model results (MF)–(FM) and (MF)–(RM) are r=0.93 and r=0.80, respectively, both are significant relations at p=0.01 probability level.

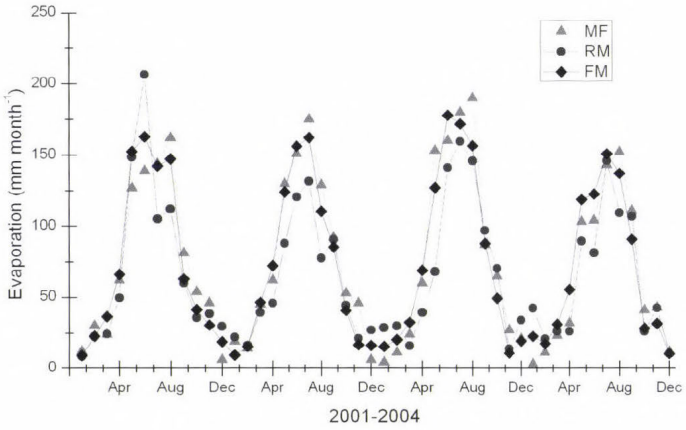

Fig. 1. Monthly evaporation rate calculated by three different ways for Lake Balaton (MF: Meyer-formula, FM: FLake model, RM: resistance model)

Yearly sum of evaporation calculated by the three different methods can be seen in *Table 2*. There is a good agreement between the mean values of MF an FM models, while RM underestimates the evaporation in comparison to others. The deviations among the mean values of three models are below 20%.

Table 2. Yearly evaporation (in mm) calculated by three different methods ((MF: Meyer-formula, FM: FLake model, RM: resistance model)

Year	MF	FM	RM
2001	887	892	841
2002	922	855	725
2003	982	938	843
2004	778	817	728
Mean	**892**	**876**	**784**

Mean monthly sensible heat fluxes were also determined by both FM and RM methods (*Fig. 2a*). It is generally a small value for lakes in comparison to radiation balance (*Fig. 2b*), because the stratifications over the lake are close to the neutral. The differences probably derive from differences between measured (RM) and calculated (FM) water surface temperatures.

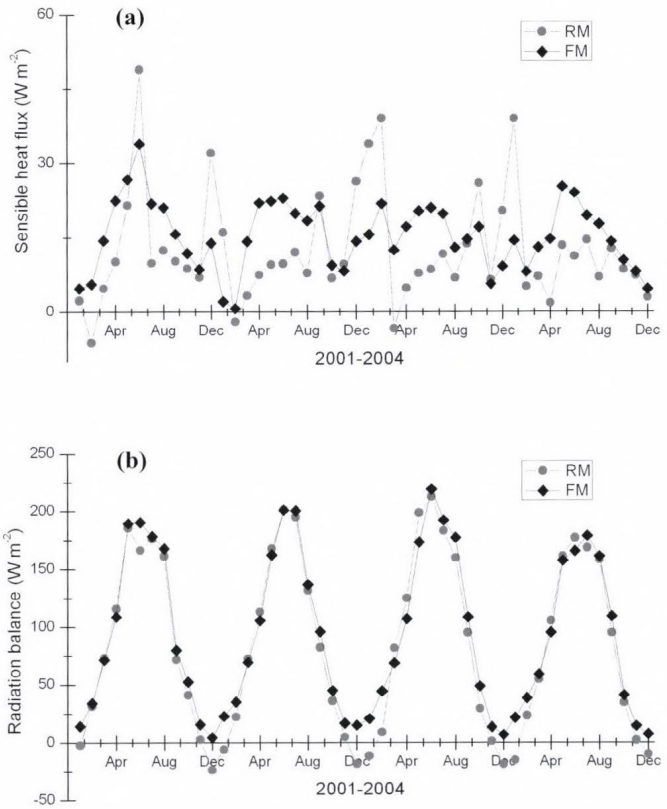

Fig. 2. Variation of monthly mean of sensible heat flux, Q_H (a) and radiation balance, Q_S (b) calculated by two different models (FM: FLake model, RM: resistance model)

Fig. 2b shows the course of monthly mean of radiation balance. Parameterization of surface energy budget components can be described by Eq. (6). The agreement between the two models is appropriate. Calculated turbulent diffusion coefficient of sensible heat between the heights of 12.3 and 2.8 meters using FM and RM methods for the period of experiment carried out in July 2002 gives also a good agreement as it can be seen in *Fig. 3a*. By the knowledge of K_H, we can estimate the exchange rate of gases by the gradient method supposing that exchange for heat and for trace gases are similar as mentioned above. Correlation between the diffusion coefficients determined by the two methods is $r=0.96$ ($p=0.01$).

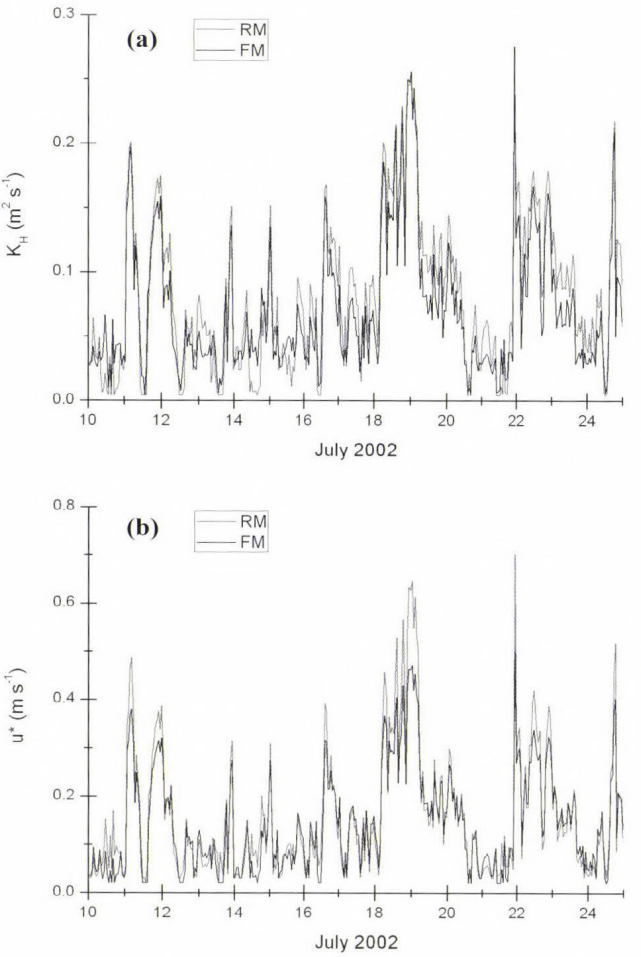

Fig. 3. Turbulent diffusion coefficients of sensible heat flux, K_H for the height between 12.3 and 2.8 meters (a) and friction velocity (b) calculated by the two different methods (July 10–25, 2002)

Finally, friction velocities (u_*) were also compared derived from RM and FM models (*Fig. 3b*). Agreement is good between results of the two models; systematic deviations can only be observed in case of higher values. Correlation is significant, $p=0.97$ ($p=0.01$).

In summary, it can be stated that the agreement between turbulent fluxes calculated by the two models is reasonable providing appropriate input data for determination of gas fluxes.

3.2. Modeling of fluxes

Ammonia and nitric acid fluxes were modeled at first for the period of July 12–25, 2002 for intercomparison (validation) of modeled fluxes by the results of gradient flux measurements conducted in the same period (*Figs. 4a,b*).

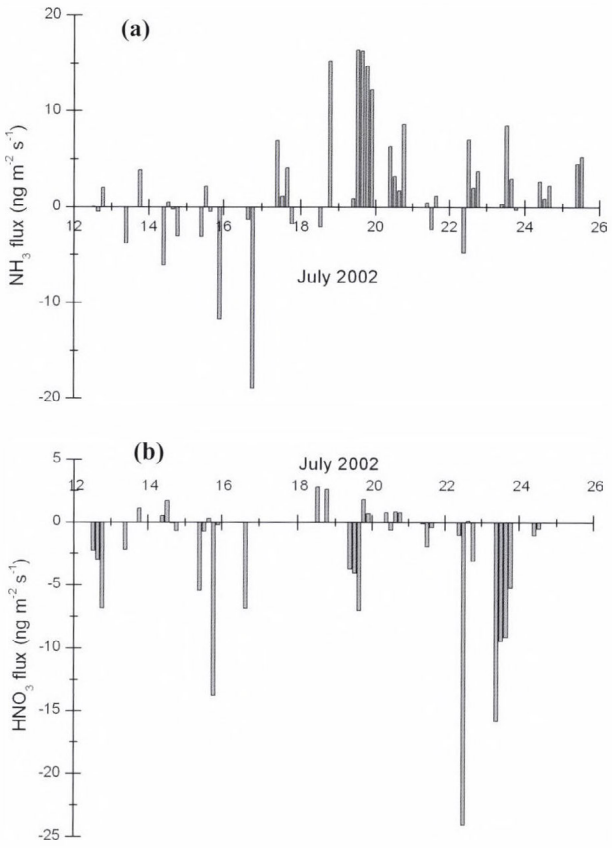

Fig. 4. Ammonia (a) and nitric acid (b) fluxes measured by the gradient method during a summer campaign at Siófok observatory

Ammonia exchange between the lake and the atmosphere was calculated on the basis of hourly micrometeorological parameters and 3-hour measured concentrations by means of the compensation-point model Eq. (1) using RM and FM methods for calculation of resistances. Only good fetch cases (wind from lake dominantly during duration of 3-hour samplings) were taken into consideration in evaluation. Compensation-point concentration of ammonia was calculated parallel by using the simple Henry's law equation and by the modified solubility theory of Hales-Drewes taking into account the effect of carbon dioxide on the solubility of ammonia in water at low concentrations. Ammonia concentration in air (at $h = 12.3$ m above water surface), ammonium+ammonia concentration and pH in water were measured as described in Section 2.1. Average of the 3-hour eddy diffusion coefficients for sensible heat was used in calculation.

The pH is a crucial parameter in controlling ratio the of ammonia to ammonium in diluted water solutions. It follows form Eqs. (2) and (3), that one unit decrease in pH results in one order decrease in compensation-point concentration. Ammonia in acidic solutions ($pH < 7$) – being a weak base – exists dominantly in protonated form (NH_4^+) prohibiting the escape of ammonia gas from the water. In the range of pH of the lake (pH=8.3–8.9), ammonia and ammonium exist together making the bi-directional change (either volatilization or absorption) of ammonia between the water and the atmosphere possible. Sign of the flux is determined by the difference in compensation-point and atmospheric concentration of ammonia according to the Eq. (1).

Other two input parameters of compensation-point model were the aerodynamic and boundary-layer resistances; they were calculated using both the resistance and FLake models as described in Section 2.4. Average resistances calculated by the two models were used (for details refer to 3.5).

Flux of nitric acid was modeled by the same way as of ammonia, the only difference is that HNO_3 does not exist in molecular form in diluted solutions, especially in the pH range of 8.3–8.9. It follows, that in Eq. (1) the compensation-point concentration of nitric acid equals to zero. Nitric acid concentrations in air were sampled by 3-hour sampling and analyzed as described in Section 2.1.

3.3. Measurement of fluxes of ammonia and nitric acid by the gradient method

For validation of models, dry fluxes of ammonia and nitric acid were measured during a summer campaign at the shore of the lake by the gradient method between July 12 and 25, 2002. Concentration gradients were determined by concentrations measured at 2.8 m and 12.3 m heights near/above the water surface by 3-hour samplings according to Eq. (4). Turbulent diffusion coefficient was derived from Eq. (5). Averages of 3-hour diffusion coefficient were used in calculation. Fluxes of ammonia and nitric acid by the gradient

method during expedition can be seen in *Figs. 4a,b*. The 3-hour mean fluxes were varied between -18.9 ng m^{-2} s^{-1} and 16.3 ng m^{-2} s^{-1} for ammonia and between 2.8 ng m^{-2} s^{-1} and -24.1 ng m^{-2} s^{-1} for nitric acid. (Positive figures derive from the 10% uncertainty of nitric acid concentration measurements.) Certainly, only good fetch cases (wind dominantly from lake during the duration of 3-hour samplings) were taken into consideration in the evaluation. Concentrations – especially for nitric acid – sometimes were below the detection limit; in these cases fluxes were not computed.

3.4. Validation, comparison of modeled and measured fluxes

The 3-hour mean of ammonia fluxes measured by the gradient method and modeled by the compensation-point model (using both resistance and FLake models for calculation of resistances) were compared for the period of summer campaign in 2002. The regression of the measured and modeled fluxes can be seen in *Figs. 5a,b*. Compensation-point concentrations for models were calculated both by simple Henry's law and Hales-Drewes solubility theory. Three-hour averages of calculated and modeled fluxes were plotted. Modeled fluxes are calculated as the mean of the results of the resistance and the FLake models. (The deviation between results of resistance and FLake models can be seen in *Table 2*.)

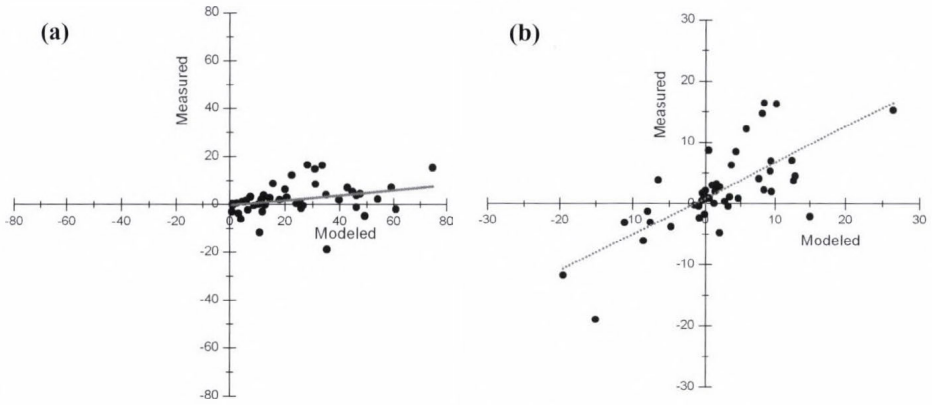

Fig. 5. Comparison of measured ammonia fluxes with results of compensation-point model used a) Henry's law; and b) Hales-Drewes theory for calculation of compensation-point concentration in ng m^{-2} s^{-1} for the period of July 12–25, 2002

The main parameters of comparison can be seen in *Table 3*. According to *Fig. 5* and *Table 3*, the difference between results of the two solubility theories

is significant. In contrast of finding of *Ayers et al.* (1985) and *Dasgupta* and *Dong* (1986), who demonstrated by laboratory measurement that classical Henry's law is applicable for solubility of ammonia, it seems that modeled fluxes by the theory of Hales and Drewes ranges much better with our gradient method measurements. Though, according to theory of *Hales* and *Drewes* (1979), carbon dioxide decreases the solubility of ammonia (increases the compensation-point concentration as a probable effect of carbamic acid), a reversed picture can be observed from our results. As *Fig. 5* and *Table 3* show, the fluxes are much lower calculated by Hales-Drewes theory suggesting that solubility of ammonia is rather increasing in the pH regime representative for the lake water. The supposed effect of carbon dioxide as the function of pH is illustrated in *Fig. 6* calculated at 20° C with the average $[NH_4^+]_w+[NH_3]_w$ concentrations measured in the modeled period ($1.61\ 10^{-6}$ M) by Eq. (3). As it can be seen, the effect of carbon dioxide strongly depends on the pH. At pH < 8.25, CO_2 enhances the volatilization of ammonia above that the influence turns to the inverse. This relationship explains our results, because during the summer experiment the pH of lake water was always above 8.65.

Table 3. Mean parameters in comparison of ammonia fluxes measured and modeled by the two solubility theories

	Hales-Drewes theory	**Henry's law**
Water temperature	22–29 °C	
pH	8.65–8.72	
C_w (ammonia + ammonium)	48–58 μM	
Mean flux	2.21 ng m^{-2} s^{-1}	24.4 ng m^{-2} s^{-1}
Degree of freedom	46	
Correlation	r = 0.72	r = 0.24
Significance (probability level)	p = 0.01	Non significant

Data in *Table 3* suggest the applicability of Hales-Drewes solubility theory instead of the classical Henry's law in calculation of compensation-point concentration in flux modeling, since correlation is significant, furthermore, the measured (2.11 ng m^{-2} s^{-1}) and modeled (2.21 ng m^{-2} s^{-1}) average fluxes were practically the same (SD=6.59 and 8.08, respectively). In contrast, modeled fluxes using the single Henry's law equilibrium constant only for ammonia (excluding CO_2) gives a mean flux higher by one order without significant relationship with the measured fluxes. Deviation from single Henry's law solubility theory was found in earlier investigations as well (*Lau* and *Charlson*, 1977; *Horváth*, 1982), underlying the disagreement among field and laboratory measurements in estimating the effect of CO_2 on the solubility of ammonia. To clarify the reason of this disagreement, further research is needed in this field.

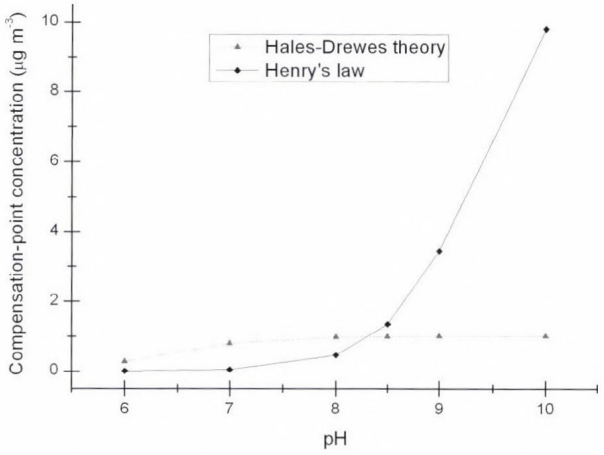

Fig. 6. Compensation-point concentration of ammonia in diluted water solution at 20 °C in the function of pH calculated by the Henry's law and the Hales-Drewes theory at $[NH_4^+]_w + [NH_3]_w = 1.61\ 10^{-6}$ M

Modeled fluxes of nitric acid were verified by fluxes measured by the gradient method similarly to ammonia. Samplings, gradient measurements, and gradient flux calculations were the same. Regression is illustrated by *Fig. 7*. The correlation between the calculated and modeled fluxes is $r=0.68$ ($p=0.01$).

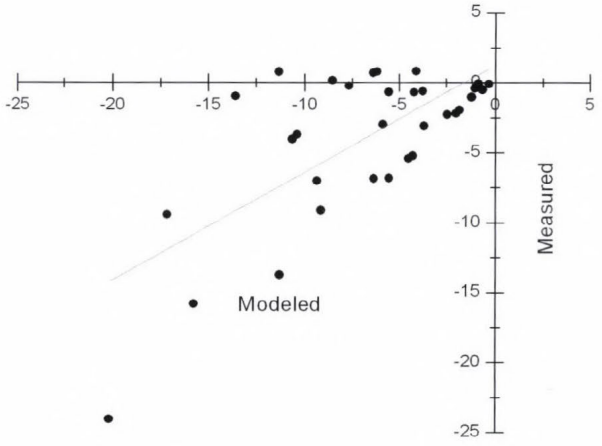

Fig. 7. Comparison of measured nitric acid fluxes with results of compensation-point model (ng m^{-2} s^{-1}) for the period of July 12–25, 2002

3.5. Flux calculation by the RM and FM models using new solubility theory

Ammonia exchange between the lake and the atmosphere was modeled on the basis of hourly micrometeorological parameters and daily concentration measurement of atmospheric ammonia between 2001 and 2004 by the compensation-point model Eq.(1) using the RM and FM models for calculation of resistances. Daily ammonia concentrations were measured near the lake between March 2002 and February 2003, while for the remaining period, interpolated data were used from two Hungarian background air pollution monitoring stations (*Farkasfa* and *K-puszta*). The agreement is relatively good (*Fig. 8a*), showing a uniform pattern of background ammonia concentration all over Hungary.

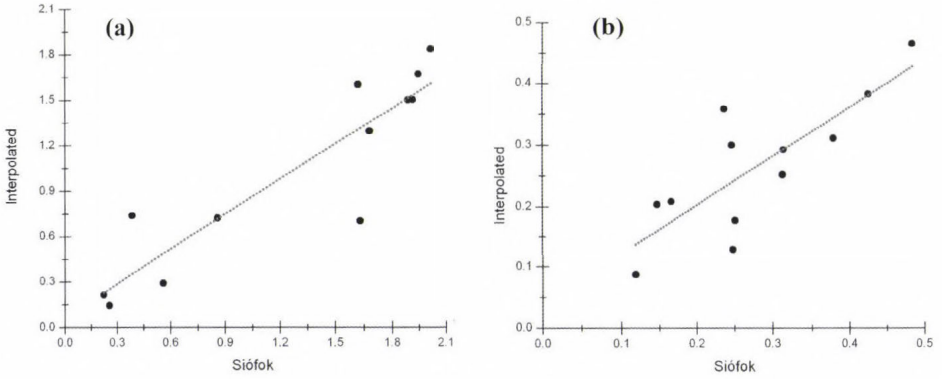

Fig. 8. Comparison of monthly mean ammonia (a) and nitric acid (b) concentrations in μg N m^{-3} measured near the lakeside (Siófok) and the average of two background air pollution monitoring stations (K-puszta, Farkasfa) in μg m^{-3}, between March 2002 and February 2003 (r = 0.90 and 0.78 for ammonia and nitric acid, respectively, and $p = 0.01$)

For calculation of the compensation-point concentration, the knowledge of pH, and sum of NH_3 and NH_4^+ concentrations in water were necessary. They were provided by the Middle Transdanubian Inspectorate for Environmental Protection, Natural Protection, and Water Management, measured on the basis of periodic measurement at five sampling points around the lake (*Figs. 9a,b*).

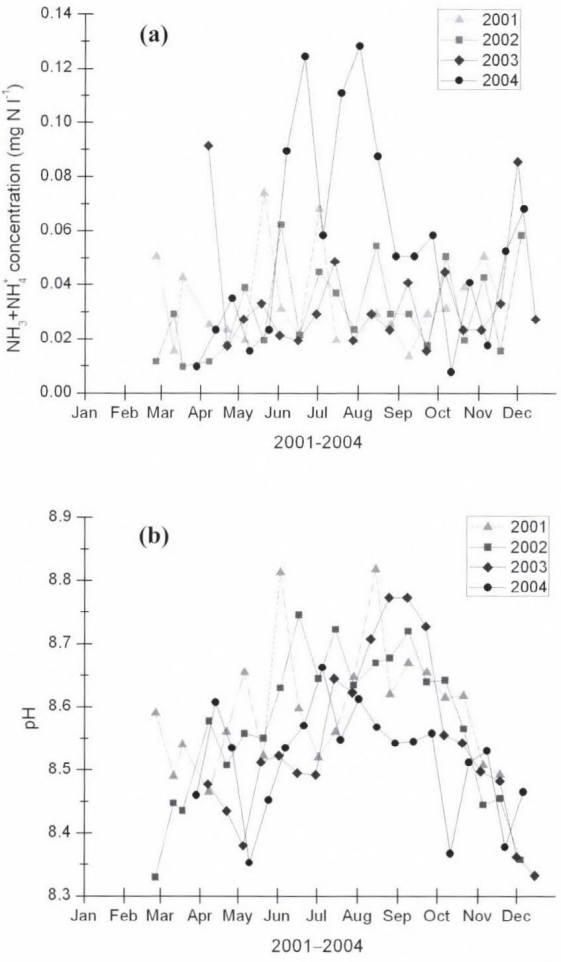

Fig. 9. Concentration of ammonia + ammonium (a) and pH (b) in the lake water, mean of 5 sampling points

Flux rates calculated by the two models had to be selected according to the wind direction. Determined by the location of the measurement point, the fetch criteria (homogeneous open water surface within at least 1 km) are fulfilled in the sector of 203 to 68 degrees clockwise. In the "wrong" sector, air temperature and wind velocity – both determining the exchange processes – are different from parameters measured in the "good fetch" sector.

Fluxes by the compensation-point model based on RM and FM were calculated on hourly base. Mean monthly fluxes can be seen in *Fig. 10a*. The compensation-point concentration of ammonia was generally higher in summer

half-year compared to the atmospheric concentrations resulting in emission peaks in this season. As a yearly average, net flux can be calculated in each year.

Deposition model of nitric acid is similar to the compensation-point model of ammonia. Only difference is that compensation-point concentration of nitric acid is zero in Eq. (1). Calculation method of nitric acid fluxes was the same as for ammonia using direct concentration measurements (March 2002–February 2003) and interpolated concentrations from the 2 background monitoring stations. The correlation between direct measurements and interpolated concentrations can be seen in *Fig. 8b*. *Fig. 10b* shows the mean monthly nitric acid fluxes for the four-year period.

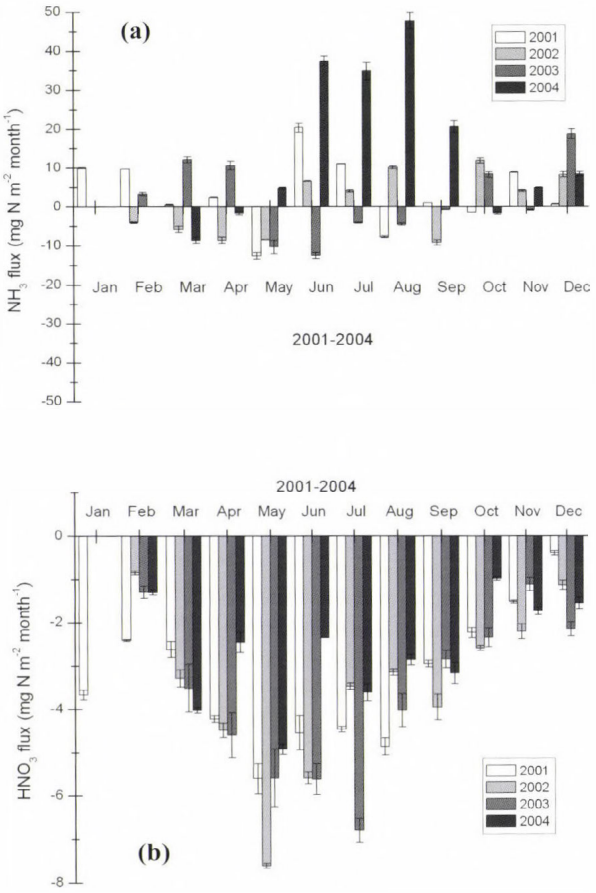

Fig. 10. Modeled mean monthly rates of ammonia (a) and nitric acid (b) fluxes (error bars denote the difference between two modeled fluxes by RM and FM)

In frozen periods (typically between the end of December to middle of February), fluxes were not computed since compensation-point concentration of ammonia is unambiguously zero, because the frozen surface prevents emission. Theoretically, deposition (adsorption) is possible onto ice surface probably followed by emission (desorption). Moreover, concentrations of ammonia and nitric acid in winter season are much lower since the equilibrium of $(NH_3)_{gas}+(HNO_3)_{gas}\leftrightarrow(NH_4NO_3)_{particle}$ process highly depends on air temperature and humidity (*Stelson* and *Seinfeld*, 1982). Low temperature and high humidity favor aerosol formation in frozen periods. For these reasons, deposition during frozen lake event was estimated to be negligible.

Yearly average of ammonia (by Hales-Drewes theory) and nitric acid dry fluxes calculated by FLake (FM) and resistance (RM) models are compiled in *Table 4*. For ammonia, upward (emission) fluxes were modeled in each year with large difference among years caused by extremely high ammonia+ammonium concentrations in lake water in different years (*Fig. 9a*). For nitric acid, the pattern is more even, there are no large differences among years.

Table 4. Yearly mean of ammonia and nitric acid fluxes over Lake Balaton (2001–2004) using the different turbulence models (FM: Flake model, RM: resistance model)

models	**2001**	**2002**	**2003**	**2004**	***mean***
			(mg N m^{-2} $year^{-1}$)		
FM NH_3	42.6	6.01	17.3	138	*51.0*
RM NH_3	43.8	12.5	23.4	156	*58.9*
mean	**43.2**	**9.27**	**20.4**	**147**	***54.9***
FM HNO_3	–38.3	–37.8	–39.7	–28.5	*–36.1*
RM HNO_3	–40.6	–38.9	–40.0	–29.4	*–37.2*
mean	**–39.5**	**–38.3**	**–39.9**	**–29.0**	***–36.7***

4. Conclusions

Dry flux of ammonia gas and nitric acid vapor were modeled both by a simple resistance model and by the more sophisticated FLake model.

Between the years of 2001 and 2004, net yearly ammonia emission and nitric acid deposition were observed at Lake Balaton. Calculated net NH_3 emission and HNO_3 deposition to the whole surface of lake between 2001 and 2004 were 32.7 t N $year^{-1}$ and –21.8 t N $year^{-1}$, respectively. The magnitude of these figures is less by one order of magnitude compared to nitrogen load from wet deposition and from dry deposition of aerosol particles that takes

–437 t N $year^{-1}$ in the same period (*Kugler* and *Horváth*, 2008). It means that dry fluxes of ammonia and nitric acid do not play important role in the N-budget and in the eutrophication of Lake Balaton in those years.

The pH range in the lake water allows bi-directional flux of ammonia. Direction of net flux (emission or deposition) depends mainly on concentrations in the water and air. Ammonia exchange can act as a buffering system, i.e., in case of a high N-load into the lake from other sources (rivers, waste water, run-off, etc.), the effect can be buffered through nitrogen emission in form of NH_3 as a consequence of the elevated compensation-point concentration. In contrast, in lack of enough nitrogen for living systems, ammonia can be absorbed (deposited) parallel with decrease of compensation-point concentration controlled by the water. The main consequence of this phenomenon can be that eutrophication of Lake Balaton (and probably of other lakes with similar pH) is probably phosphorus limited.

Comparing the measured ammonia flux with the fluxes calculated by compensation-point model based on the single Henry's law theory and by the modified solubility theory of Hales-Drewes, it can be concluded that in our case latter theory describes better the exchange processes, suggesting that effect of carbon dioxide on the solubility of ammonia can not be excluded. However, in contrast with Hales-Drewes, who suggested the decrease the solubility of ammonia in presence of CO_2, we find an opposite effect, i.e., CO_2 favors the solubility of ammonia in the pH-range of the lake. To eliminate the obvious contradiction among the different solubility theories, further researches are needed in the future.

Acknowledgements—Our research was supported by the OTKA K46824 project.

References

Ács, F., Hantel, M., and *Unegg, J.W.*, 2000: Climate Diagnostics with the Budapest-Vienna Land-Surface Model SURFMOD. Austrian Contributions to the Global Change Program Volume 3, Austrian Academy of Sciences, Vienna.

Ács, F. and *Szász, G.* 2002: Characteristics of microscale evapotranspiration: a comparative analysis. *Theor. Appl. Climatol. 73,* 189–205.

Ács, F. 2003: On the relationship between the spatial variability of soil properties and transpiration. *Időjárás 10*, 257–272.

Anda, A. and *Varga, B.*, 2010: Analysis of precipitation on Lake Balaton catchments from 1921 to 2007. *Időjárás 114,* 187–201.

Arya, S.P., 2001: Introduction to micrometeorology, 2nd edition. Academic Press, San Diego, London.

Ayers, G.P., Gillett, R.W., and *Caeser, E.R.*, 1985: Solubility of ammonia in water in the presence of atmospheric CO_2. *Tellus 37B*, 35–40.

Businger, J.A., Wyngaard, J.C., Izumi, Y., and *Bradley, E.F.*, 1971: Flux-Profile Relationships in the Atmospheric Surface Layer. *J. Atmos. Sci. 28*, 181–189.

Dasgupta, P.K. and *Dong, S.*, 1986: Solubility of Ammonia in Liquid Water and Generation of Trace Levels of Standard Gaseous Ammonia. *Atmos. Environ. 20*, 565–570.

Durand, P., Breuer, L., Johnes, P.J., Billen, G., Butturini, A., Pinay, G., van Grinsven, H., Garnier, J., Rivett, M., Reay, D.S., Curtis, C., Siemens, J., Maberly, S., Kaste, O., Humborg, C., Loeb, R., de Klein, J., Hejzlar, J., Skoulikidis, N., Kortelainen, P., Lepisto, A., and *Wright, R.*, 2011: Nitrogen processes in aquatic ecosystems. In (Eds. *Sutton, M. A., Howard, C. M., Erisman, J. W., Billen, G., Bleeker, A., Grennfelt, P., van Grinsven, H.,* and *Grizzetti, B.*) The European Nitrogen Assessment Cambridge University Press, Cambridge, U.K., 126–146.

Dyer, A.J., 1974: A review of flux-profile relationships. *Bound-Lay.Meteorol. 7*, 363–372.

EMEP, 1996: EMEP Manual for sampling and chemical analysis. EMEP/CCC-Report 1/95, NILU, Kjeller, Norway.

Erisman, J.W., van Pul, A. and *Wyers, P.*, 1994: Parameterization of dry deposition mechanisms for the quantification of atmospheric input to ecosystems. *Atmos. Environ. 28*, 2595–2607.

Farquhar, G.D., Firth, P.M., Wetselaar, R., and *Weir, B.*, 1980: On the Gaseous Exchange of Ammonia between Leaves and the Environment: Determination of the Ammonia Compensation Point. *Plant Physiol. 66*, 710–714.

Foken, Th., 2006: Angewandte Meteorologie. Springer-Verlag, Berlin, Heidelberg, New York.

Hales, J.M. and *Drewes, D.R.*, 1979: Solubility of ammonia at low concentrations. *Atmos. Environ.13*, 1133–1147.

Herodek S., 1977: A balatoni fitoplankton kutatás újabb eredményei. *Ann. Inst. Biol.(Tihany) Hun. Acad. Scient. 44*, 181–198.

Hicks, B.B., Baldocchi, D.D., Meyers, T.P., Hosker, R.P., and *Matt, D.R.*, 1987: A preliminary multiple resistance routine for deriving dry deposition velocities from measured quantities. *Water Air Soil Poll. 36*, 311–330.

Holtslag, A.A.M. and *van Ulden, A.P.*, 1983: A simple scheme for daytime estimates of the surface fluxes from routine weather data. *J. Climate Appl. Meteorol. 22*, 517–529.

Horváth, L., Mészáros, Á., Mészáros, E., and *Várhelyi, G.*, 1981: On the atmospheric deposition of nitrogen and phosphorus into Lake Balaton. *Időjárás 85*, 194–200.

Horváth, L., 1982: On the vertical flux of gaseous ammonia above water and soil surfaces. In (eds. Georgii, H-W. and Pankrath, J.) Deposition of Atmospheric Pollutants. D. Reidel Publishing Company, Dordrecht, Boston, London, 17–22.

Horváth L., 1990: Légköri szennyező anyagok töménysége és ülepedése a Balaton térségében. *Vízügyi Közlemények 77*, 204–208.

International Committee Lake Foundation, 2010: World Lakes Database, http://www.ilec.or.jp/.

Jolánkai G. and *Bíró I.*, 2005: A Balaton tápanyag terhelésének mérlege, mérése és modellezése, 2004. A munka második részének zárójelentése. Témaszám: 714/31/648601. VITUKI Kht. Vízminőség-védelmi Szakágazat, 77p. (In Hungarian)

Jordan, Gy., van Rompaey, A., Szilassi, P., Csillag, G., Mannaerts, C., and *Woldai, T.*, 2005: Historical land use changes and their impact on sediment fluxes in the Balaton basin (Hungary). *Agric. Ecosyst. Environ. 108*, 119–133.

Kovács, Á.D., 2011: Tó- és területi párolgás becslésének pontosítása és magyarországi alkalmazásai.PhD értekezés. BME, Budapest, 101p. (In Hungarian)

Kramm, B., Dlugi, R., Foken, Th., Mölders, N., Müller, H., and *Paw U.K.T.*, 1996: On the determination of the sublayer Stanton numbers of heat and matter for different types of surfaces. *Contrib. Atmos. Phys. 69*, 417–430.

Kugler, Sz. and *Horváth, L.*, 2004: Estimation of the nitrogen loading from the atmospheric dry deposition of ammonium and nitrate aerosol particles to Lake Balaton. *Időjárás 108*, 155–162.

Kugler, Sz., Horváth, L., and *Machon, A.*, 2008: Estimation of nitrogen balance between the atmosphere and Lake Balaton and a semi natural grassland in Hungary. *Environ. Poll. 154*, 498–503.

Lau, N.-Ch. and *Charlson, R.J.*, 1977: On the discrepancy between background atmospheric ammonia gas measurements and the existence of acid sulfates as a dominant atmospheric aerosol. *Atmospheric Environment 11*, 475–478.

Liu, H., Blanken, P.D., Weidinger, T., Nordbo, A., and *Vesala, T.*, 2011: Variability in cold front activities modulating cool-season evaporation from a southern inland water in the USA. *Environ. Res. Lett. 6*, 024022.

Mészáros R., 2002: A felszínközeli ózon száraz ülepedésének meghatározása különböző felszíntípusok felett. PhD értekezés, ELTE, Budapest, 113p. (In Hungarian)

Mironov D.V., 2006: Synopsis of FLake Routines, http://www.flake.igb-berlin.de/docs.shtml.

Mironov, D.V., 2008: Parameterization of lakes in numerical weather prediction. Description of a lake model. COSMO Technical Report, No. 11, Deutscher Wetterdienst, Offenbach am Main, Germany, 41 p.

Mironov, D., Heise, E., Kourzeneva, E., Ritter, B., Schneider, N., and *Terzhevik, A.*, 2010: Implementation of the lake parameterisation scheme FLake into the numerical weather prediction model COSMO. *Boreal Environ. Res. 15*, 218–230.

Shahin, U.M., Holsen, T.M., and *Odabasi, M.*, 2002: Dry deposition measured with a water surface sampler: a comparison to modeled results. *Atmos. Environ. 36*, 3267–3276.

Stelson, A.W. and *Seinfeld, J.H.*, 1982: Relative humidity and temperature dependence of the ammonium nitrate dissociation constant. *Atmos. Environ. 16*, 983–992.

Szilágyi, J. and *Kovács, Á.*, 2011: A calibration-free evapotranspiration mapping technique for spatially-distributed regional-scale hydrologic modeling. *J. Hydrol. Hydromech. 59*, 118–130.

Vörös, M., Istvánovics, V., and *Weidinger, T.*, 2010: Applicability of the FLake model to Lake Balaton. *Boreal Environ. Res. 15*, 245–254.

Weidinger, T., Pinto, J., and *Horváth, L.*, 2000: Effects of uncertainties in universal functions, roughness length, and displacement height on the calculation of surface layer fluxes. *Meteorol. Z. 9*, 139–154.

IDŐJÁRÁS

Quarterly Journal of the Hungarian Meteorological Service
Vol. 118, No. 2, April – June, 2014, pp. 119–132

Homogenization of Hungarian daily wind speed data series

Csilla Péliné Németh[1*], **Judit Bartholy**[2], and **Rita Pongrácz**[2]

[1]*Geoinformation Service of the Hungarian Defence Forces*
Szilágyi Erzsébet fasor 7–9., H-1024 Budapest, Hungary

[2]*Department of Meteorology, Eötvös Loránd University*
Pázmány Péter sétány 1/A, H-1117 Budapest, Hungary

**Corresponding author E-mail: pelinenemeth.csilla@mhtehi.gov.hu*

(Manuscript received in final form October 24, 2013)

Abstract—Reliable long time series have key role in climatological research. Long term observations involve inhomogeneities due to change of measuring methods, sensors, surroundings of stations, or moving into a new location. Therefore, homogenization is necessary in order to make reliable analysis of datasets. In this study, the MASH (Multiple Analysis of Series for Homogenization) procedure developed at the Hungarian Meteorological Service was applied to improve our wind time series. Daily wind datasets were homogenized at 19 Hungarian synoptic stations in the period from 1975 to 2012. This paper discusses the validation of the homogenization process and presents the quality control results.

Key words: wind speed, homogenization, MASH application, Hungarian wind climate, measurement automation

1. Introduction

The existence of long and reliable instrumental climate records is necessary both to assess climate variability and climate change and to validate climate model outputs (*Freitas et al.,* 2013). Analysis of appropriate and good quality datasets may help to mitigate possible negative effects of climate change. Furthermore, besides temperature and precipitation, wind is also a key meteorological element, therefore, it is essential to study average and extreme characteristics and tendencies of present and future wind climate.

Hungarian wind climate research at the Eötvös Loránd University in Budapest is based on the analysis of past, present, and modeled wind field data

sets. Projected wind fields are provided by the adapted and validated RegCM3 regional climate model (*Torma et al.,* 2008) experiments for future periods (2021–2050 and 2071–2100) for the Carpathian Basin.

We analyzed present wind climate using measurements of Hungarian synoptic stations, and gridded reanalysis data (*Péliné et al.,* 2011). Hungarian synoptic measurement network has been developed and installed by the Hungarian Meteorological Service taking into account suggestions of the World Meteorological Organisation (*WMO,* 2011). Because of the last decades' developments of measurement and communication technologies, the wind observing network has changed several times, which is unfortunately quite usual. The most significant change was automation – i.e., change traditional measuring instruments into automated measuring systems – during 1995–1996. This major change introduced large variations in the climate signal, and caused inhomogeneities in the data sets. In fact, long instrumental records are very rarely homogeneous because of the changing surroundings of measuring sites (new buildings, vegetation growth, etc.). To avoid misinterpretation due to this inhomogeneity, the available time series can be divided into subsets. For instance, we used two subsets in case of previous (*Péliné et al.,* 2011) wind climate analysis using wind data originating from traditional (1975–1994) and automated (1997–2012) measuring systems.

In addition to automation other causes may also lead to inhomogeneities such as substitution or relocation of weather stations, changing anemometer type or aging of the instruments, changes in measuring height, surroundings (e.g., urbanization), surface coverage, and roughness. Therefore, documentation of metadata is a crucial issue during any kind of meteorological measurement.

The above-mentioned changes could result in inhomogeneities, which cannot be explained by climatological reasons. Brake points in the data sets coincide with change in the probability distribution function of the measurements. These inhomogeneities must be detected and removed before further analyses. For this purpose mathematical methods are widely used, one of them is the Multiple Analysis of Series for Homogenization, MASH v3.03 (*Szentimrey,* 1999, 2011) developed in HMS. This technique is used here for homogenization of available daily wind speed time series between 1975 and 2012 for records of 19 Hungarian synoptic stations.

2. Homogenization with MASH application

A homogeneous climatological time series can be defined as time series where variability is only caused by changes in weather and climate (*Aguilar et al.,* 2003). To decide whether or not a long time series is homogeneous, there are different detection and correction methods available for possible use. These methods are all based on mathematical formulation and climatological

experience, however, their performances are different. Objective comparison of these existing methods was carried out in the framework of a scientific programme COST Action HOME ES0601: Advances in Homogenization Methods of Climate Series: an integrated approach (*HOME,* 2011; *Szentimrey,* 2013). The HOME tests concluded that MASH was one of the most successful methods (*Domonkos et al.*, 2012, *Domonkos* 2013, *Venema et al.,* 2012), that is why we used it in this study.

MASH application is a relative homogeneity test procedure (*Szentimrey,* 1999). This tool consists of mathematical formulation, climatological station information (metadata), and software development for automation. Application does not assume that the reference series are homogeneous. The candidate series is chosen from the available time series (for example daily wind speed data), and the remaining series are considered as reference series. As running the application, the role of series changes step by step during the procedure. Depending on the climatic element, additive (for temperature) or multiplicative (for precipitation or wind speed) models can be used.

It is possible to homogenize monthly, seasonal, or annual time series. The daily inhomogeneities can be derived from the monthly ones (*Szentimrey,* 2008). The application provides automatically the probable dates of break points for further usage, and the homogenized, completed and quality controlled time series. Although MASH is able to use metadata (for example the date of relocation) during the break point detection, it was not used during this work.

In this study, daily wind speed data sets for 19 stations (*Fig. 1*) were derived from at least 8 hourly wind speed data a day. Before calculating daily wind speed, hourly data was quality controlled and corrected. Metadata of stations is summarized in *Table 1*. Data are available from 1975 to 2012 at most stations. At station Paks (No. 15), measurements started only on May 1, 1979. Altogether more than one year is missing at Zalaegerszeg (No. 11) during 1993 and 1994. It is also important to note that 50 days are missing at Kecskemét (No. 17) in 2009.

A multiplicative model was applied for homogenization of daily wind speed data using the 0.05 significance level. Original series can be described as Eq. (1) affected by climate change, inhomogeneity, and noise effect (*Szentimrey,* 2011).

Original series for multiplicative model is

$$X^*_{O,j}(t) = C^*_j(t) \cdot IH^*_j(t) \cdot \varepsilon^*_j(t), \quad (j = 1,2,\dots,n), \tag{1}$$

where C^* is the climate change, IH^* is the inhomogeneity, ε^* is the noise.

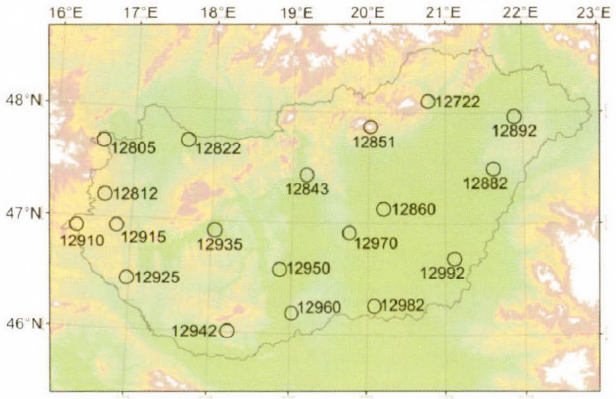

Fig. 1. Hungarian stations used at MASH application for homogenization.

Table 1. Metadata of Hungarian stations used at MASH application for homogenization (in 2012)

No.	WMO	Station name	Lon [° E]	Lat [° N]	Altitude [m]	Anemometer elevation [m]	Missing data [%]
1	12772	Miskolc	20.77	48.10	232.8	16.25	0.0
2	12805	Sopron	16.60	47.68	233.8	18.40	< 0.1
3	12812	Szombathely	16.65	47.20	201.1	10.56	< 0.1
4	12822	Győr	17.67	47.71	116.7	11.16	0.0
5	12843	Budapest Lőrinc	19.18	47.43	139.1	14.68	< 0.1
6	12851	Kékestető	20.02	47.87	1011.3	25.07	< 0.1
7	12860	Szolnok	20.13	47.17	108.1	10.40	< 0.1
8	12882	Debrecen	21.61	47.49	107.6	10.23	0.1
9	12892	Nyíregyháza	21.89	47.96	142.1	15.98	0.2
10	12910	Szentgotthárd	16.31	46.91	311.7	16.61	0.1
11	12915	Zalaegerszeg	16.81	46.93	240.1	10.40	3.3
12	12925	Nagykanizsa	16.97	46.46	139.8	13.69	0.1
13	12935	Siófok	18.04	46.91	108.2	15.10	0.0
14	12942	Pécs	18.23	46.01	202.8	10.55	0.0
15	12950	Paks	18.85	46.57	97.2	9.80	11.4
16	12960	Baja	19.02	46.18	113.0	10.30	0.1
17	12970	Kecskemét	19.75	46.91	114.0	10.40	0.4
18	12982	Szeged	20.09	46.26	81.8	12.25	< 0.1
19	12992	Békéscsaba	21.11	46.68	86.2	6.50	< 0.1

3. Results

MASH v3.03 procedure produces quality control results automatically (e.g., the number of days with error, total number of errors; their dates), identifies problematic series, and gives the estimated error values. First, our input data was

checked with partially automated self-developed computer codes including basic controlling rules and the detected errors were corrected manually before homogenization. As a result, only 2 errors (on two consecutive days) were detected at one of the stations, Szombathely (No. 3). Normally, file of MASH quality control results contains the detected maximal positive and the minimal negative errors and their dates; however minimal negative error was zero in this work (*Table 2*).

Table 2. Quality control results

Dates of the detected errors	Maximal positive error [m/s]
August 9, 1995	0.31
August 10, 1995	0.54

During verification of homogenization, the null hypothesis supposes that the examined series are homogeneous. The homogenization is acceptable if the following condition is true (*Lakatos et al.,* 2013): the test statistic after homogenization (TSA) has to be either near the critical value (20.57, significance level 0.05) or much less than the test statistic before homogenization (TSB). TSA and TSB values are summarized in *Table 3.* Since TSA values are much smaller compared to TSB values, it can be concluded that the homogenizations are acceptable and improve the qualities of the station time series considerably. The smallest TSB value – less than 100.0 – is found in case of station 3 (30.11) where the homogenization could not improve the data quality (station 3 is the only station with this feature among the 19 stations evaluated in this study). In fact, the TSA value of station 3 is larger than the TSB value. The small difference between them suggests that only a slight correction was made in the time series of station 3, since the original time series can be considered homogeneous. However, due to missing data of the original data set at this station, we used the homogenized time series in the analysis.

Table 3. Yearly test statistics for inhomogeneity of series

Station No.	TSA	TSB	Station No.	TSA	TSB
1	151.21	2590.78	11	42.39	953.13
2	26.69	137.10	12	100.19	218.26
3	39.76	30.11	13	69.66	395.84
4	29.49	113.96	14	16.70	492.12
5	23.93	285.97	15	50.67	574.81
6	147.45	229.40	16	47.14	512.55
7	53.85	1715.00	17	35.86	490.28
8	60.62	116.63	18	57.82	178.88
9	49.72	1680.52	19	84.57	359.90
10	36.61	578.96			
			Average	**59.17**	**613.38**

Table 4 lists annual relative estimated inhomogeneities (REI) and annual relative modification of wind speed data sets (RMS). They are proportional to standard fluctuation based on their definitions (*Szentimrey,* 2011).

Fluctuation of series is

$x(t)(>0)y(t)(>0)$ $(t = 1,2, \dots, n)$:

$$F(x) = \left(\prod_{t=1}^{n} max\left(\frac{x(t)}{y(t)}, \frac{y(t)}{x(t)}\right)\right)^{\frac{1}{n}}. \tag{2}$$

Standard fluctuation of series is

$x(t)(>0)$ $(t = 1,2, \dots, n)$:

$$SF(x) = \left(\prod_{t=1}^{n} max\left(\frac{x(t)}{\bar{x}_G}, \frac{\bar{x}_G}{x(t)}\right)\right)^{\frac{1}{n}}, \tag{3}$$

where G is the geometric mean.
Relative estimated inhomogeneity (REI) is

$$SF\left(I\widehat{H}^*\right) \approx SF(X_0^*)^{REI}. \tag{4}$$

Relative modification of series (RMS) is

$$F(X_0^*, X_H^*) \approx SF(X_0^*)^{RMS}. \tag{5}$$

Annual variability of wind speed is definitely smaller than other meteorological parameters such as maximum temperature or sunshine duration. Seasonal REI of daily wind speed time series shows an annual cycle with very small amplitude. Analysis of time dependence of REI suggests that averaged values for all stations are slightly larger in spring (0.46) and summer (0.55) than in winter (0.39) and autumn (0.44). Seasonal REI values vary from zero to 1.01 (*Fig. 2*), the smallest values appear in autumn and summer at stations 3 and 4, respectively, whereas the largest REI values can be found in summer at station 7 (in Szolnok). The maximum difference between the seasonal REI values is in Sopron (station 2), where REI is eight times larger in summer than in spring (the difference is 0.36). Considering the monthly RMS values (*Fig. 3*), the average adjustments were higher during those months when natural variability of wind speed is larger (due to higher thunderstorm frequency). *Fig. 3* illustrates the RMS analysis at three stations, i.e., Szombathely (station 3), Zalaegerszeg (station 11), and Kecskemét (station 17), where annual REI and RMS are minimum, maximum, and around the multi-station mean values, respectively.

Table 4. Annual relative estimated inhomogeneities (REI) and annual relative modification of series (RMS)

Station name	REI	Station name	RMS
Zalaegerszeg	0.90	Zalaegerszeg	1.57
Szolnok	0.90	Szolnok	1.30
Miskolc	0.88	Nyíregyháza	1.07
Nyíregyháza	0.80	Miskolc	1.06
Pécs	0.61	Pécs	0.90
Szentgotthárd	0.60	Siófok	0.77
Paks	0.53	Békéscsaba	0.70
Siófok	0.51	Szentgotthárd	0.67
Kecskemét	0.51	Paks	0.66
Baja	0.51	Kecskemét	0.63
Békéscsaba	0.50	Baja	0.61
Debrecen	0.36	Debrecen	0.58
Nagykanizsa	0.33	Nagykanizsa	0.45
Kékestető	0.23	Szeged	0.31
Szeged	0.19	Kékestető	0.27
Sopron	0.17	Sopron	0.18
Budapest Lőrinc	0.11	Budapest Lőrinc	0.13
Győr	0.06	Győr	0.08
Szombathely	0.06	Szombathely	0.07
Average	**0.46**	**Average**	**0.64**

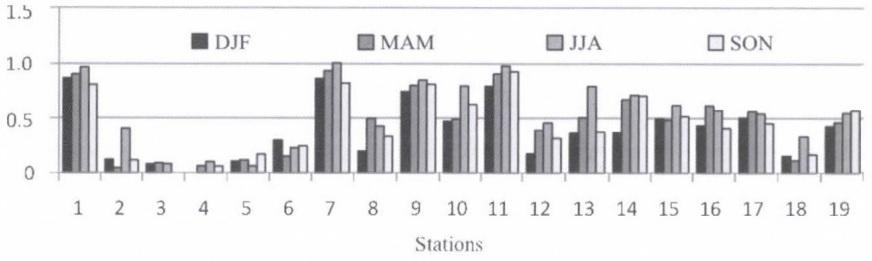

Fig. 2. Seasonal relative estimated inhomogeneity in different stations.

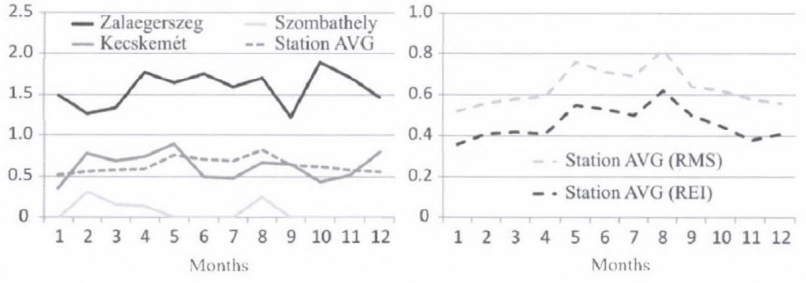

Fig. 3. Monthly RMS at three stations and station average (*left*), and average monthly RMS and average monthly REI calculated from values of the 19 stations (*right*).

During the homogenization process, time series can be modified in any year. Break points usually were found throughout the whole period, however, data series of some stations were corrected only in a shorter period. *Fig. 4* demonstrates annual number of stations where break points were detected.

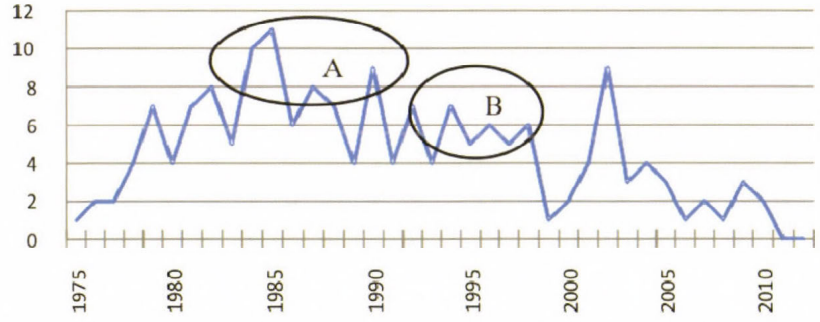

Fig. 4. Number of stations of annually detected break points. (Ellipse A: missing values during the 1980's. Ellipse B: inhomogeneity due to automation.)

In general, there is a decreasing trend towards fewer break points in recent times. Metadata may be valuable either during the homogenization or the validation procedure (*Auer et al.,* 2005). Based on documented metadata, missing values were found frequently mainly at night in most of the analyzed stations in the 1980's (ellipse A). Consequently, daily average wind speed was calculated from less number (at least eight) of measurement records. Automation process obviously caused inhomogeneity in data series at almost every station (ellipse B). Moreover, relocated stations and changed height of the measuring sensors also could cause break points (after 2000). In these latter cases, the modification factors suggest that the inhomogeneity is often more explicit than the effect of automation. Therefore, it is important to take into account these effects in planning and installation of measurement systems, moreover, it is essential to document any changes in meteorological measurement network.

After completing the homogenization process, the distribution of daily wind speed changed considerably. *Fig. 5* shows the relative frequencies of wind speed at three stations before and after homogenization. The REI and RMS at Zalaegerszeg (station 11) are the largest, while the minimum values can be found at Szombathely (station 3). Therefore, the largest difference between pre- and post-homogenized distributions is at Zalaegerszeg, where the distribution shifted to a higher wind speed regime.

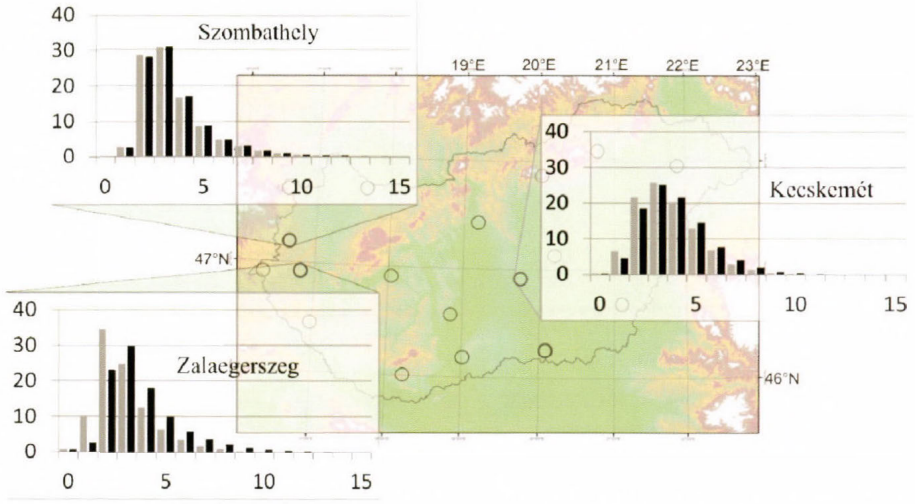

Fig. 5. Relative frequencies [%] of daily wind speed [m/s] at different stations before (grey) and after (black) homogenization (1975–2012).

The original and homogenized average yearly wind speed time series are shown in *Fig. 6* for all analyzed stations. Detected numbers of annual break points are indicated at the upper right corner of each diagram. Most of the break points can be identified from the documented metadata, however, the actual required adjustments cannot be quantified from metadata (*Menne et al.,* 2005).

In many cases (Miskolc, Szolnok, Siófok), time series were modified (see vertical lines in *Fig. 6*) in the first half of the entire period. Measuring station in Miskolc moved to another place in 1990, this change caused a significant increase in wind speed. Other documented changes include the automation, during which both the type of the anemometer (from Fuess to Vaisala) and the method of measurement have changed. Moreover, this modernization usually coincided with change of the sensor's height. For example, stations at Miskolc and Szolnok were automated in 1997, and at Siófok in 1995. At Miskolc, the sensor was installed from 10 meter (standard elevation of anemometers) to 16.25 meter. Station Siófok is located at the waterfront of Balaton (the biggest lake in Central Europe), the measurements were automated in 1995, when the height of the anemometer was lifted to 15.10 meters. After automation in 1997 at Szolnok, the type of the anemometer was changed twice, in 2004 and 2011.

However, there are some stations, such as Szombathely and Sopron, where smaller modifications were applied during the homogenization process. The automation in both stations was completed in 1995. Other effects also influenced the homogeneity, namely, (i) station of Szombathely was moved in 2002 with unchanged sensor's height, (ii) station of Sopron was reinstalled twice, in 2003 and 2005, when height of the anemometer was lifted from 15.64 to 18.40 meter.

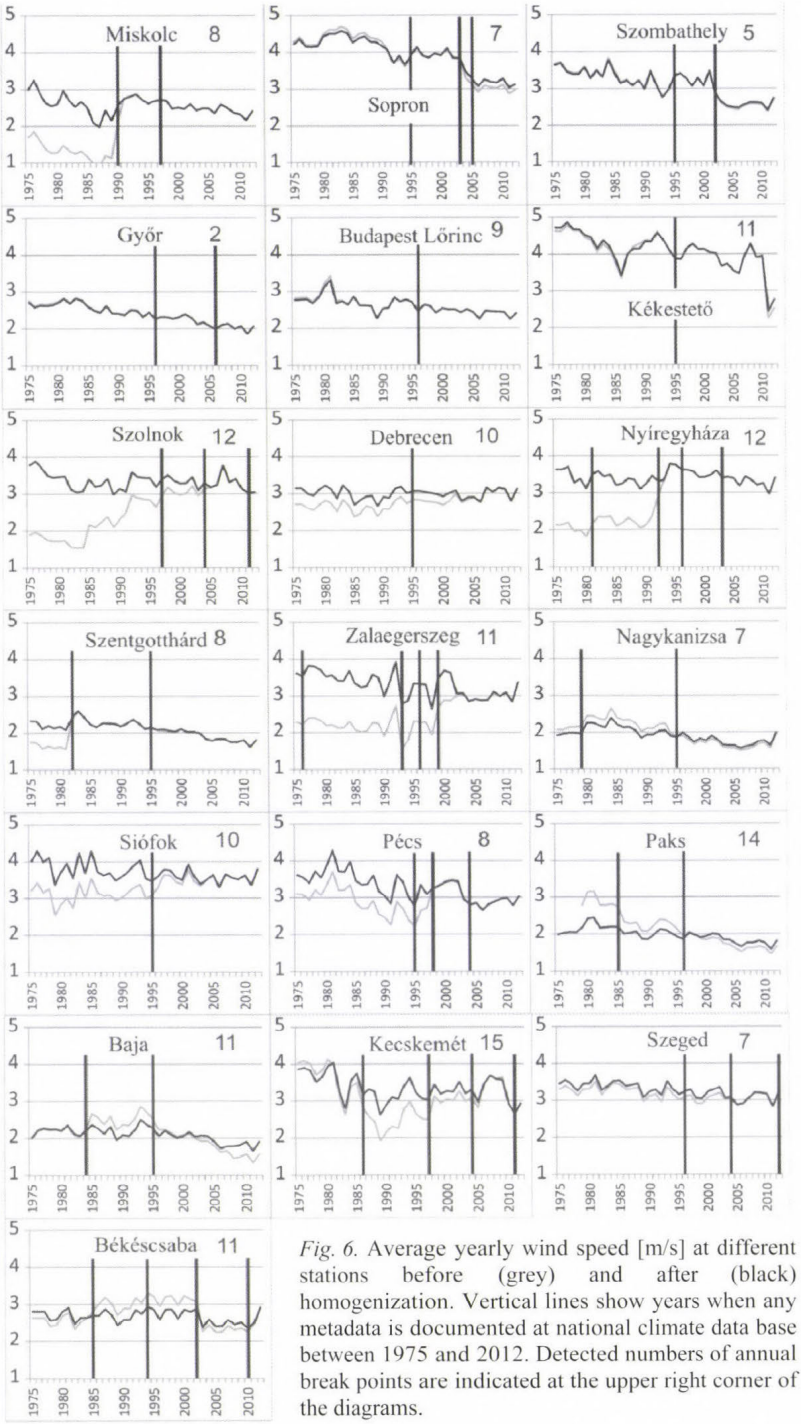

Fig. 6. Average yearly wind speed [m/s] at different stations before (grey) and after (black) homogenization. Vertical lines show years when any metadata is documented at national climate data base between 1975 and 2012. Detected numbers of annual break points are indicated at the upper right corner of the diagrams.

MASH procedure homogenizes monthly and daily time series and completes missing data for further analysis, e.g., extreme value evaluation or model output verification. In this study, different yearly and seasonal percentile values (median, 0.90 and 0.99) were calculated for 19 stations from 38-year-long time series (1975–2012) before and after homogenization. *Fig. 7* and *8* show that the largest difference was found at Zalaegerszeg. At this station the yearly homogenized percentile values (0.50, 0.90, and 0.99) were increased by 131%, 128% and 140%, respectively. The highest decreasing was at station 19 (Békéscsaba), where homogenized percentiles are 98%, 96%, and 95% compared to percentiles of original time series. Median decreased at six stations, 0.90 and 0.99 percentiles were decreased in eight cases each. The smallest correction was applied to station data at Szombathely, No. 3 (100.0%, 99.8% and 98.3%) and in Kékestető, No. 6 (100.0%, 100.4% and 104.5%). Moreover, some smaller differences are demonstrated in *Fig. 8* comparing seasonal percentile values.

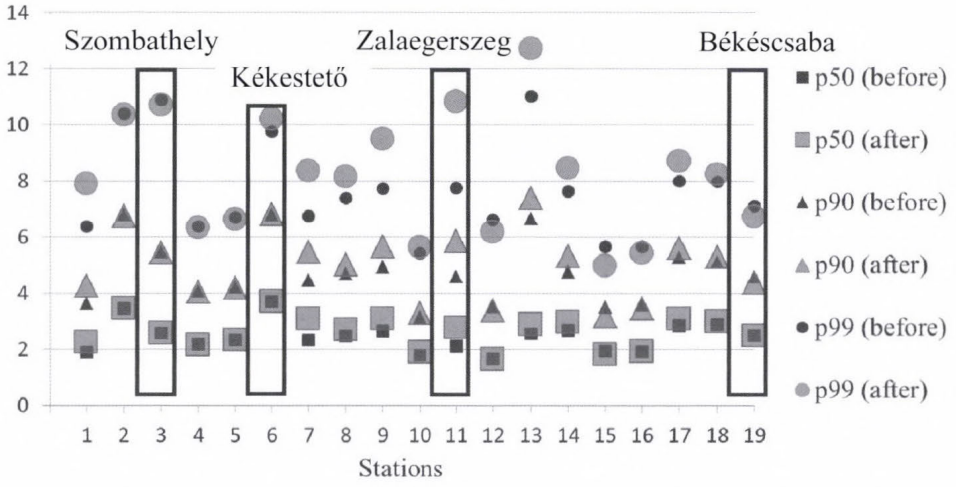

Fig. 7. Different yearly percentile values before and after homogenization for involved 19 stations calculated from 38-year time series (1975–2012).

Average yearly wind speed was modified significantly by homogenization procedure (*Fig. 6*). Consequently, the fitted linear trends of average and different percentile values also changed at many stations. In this paper, three stations (Szolnok, Zalaegerszeg, and Siófok) were chosen to demonstrate these differences emphasizing that inhomogeneities may lead to misinterpretations. *Fig. 9* shows monthly linear trend coefficients of 0.9 percentile values for two periods (1975–2012 and 1997–2012) calculated from daily wind speed data before (left) and after (right) homogenization for the three stations. Decreasing trends dominate in the homogenized datasets analyzing the whole period (1975–2012), and most of

the increasing trends of the non-homogenized data disappeared. Smaller differences were found between homogenized and original data after automation (1997–2012). For instance, in case of Siófok, both in November and December the detected trends are significant and similar for the homogized and non-homogenized times series.

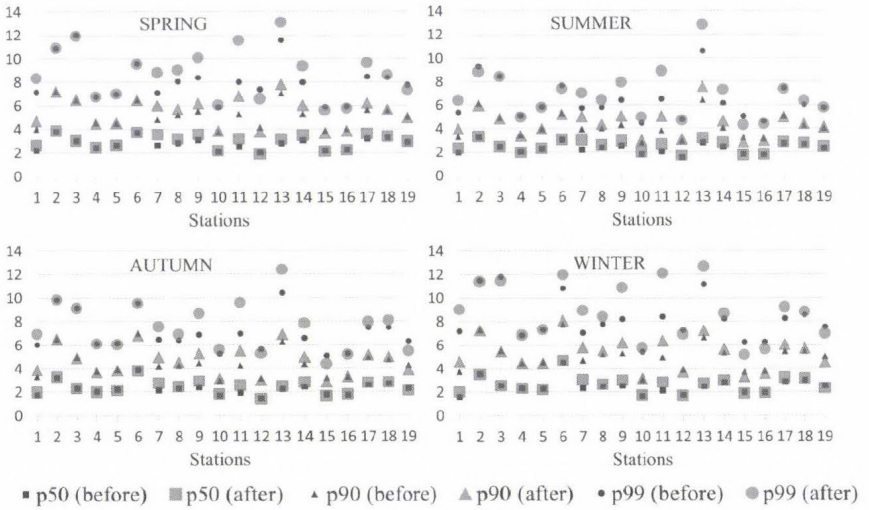

Fig. 8. Different seasonal percentile values [m/s] before and after homogenization for the 19 stations calculated from 38-year time series (1975–2012).

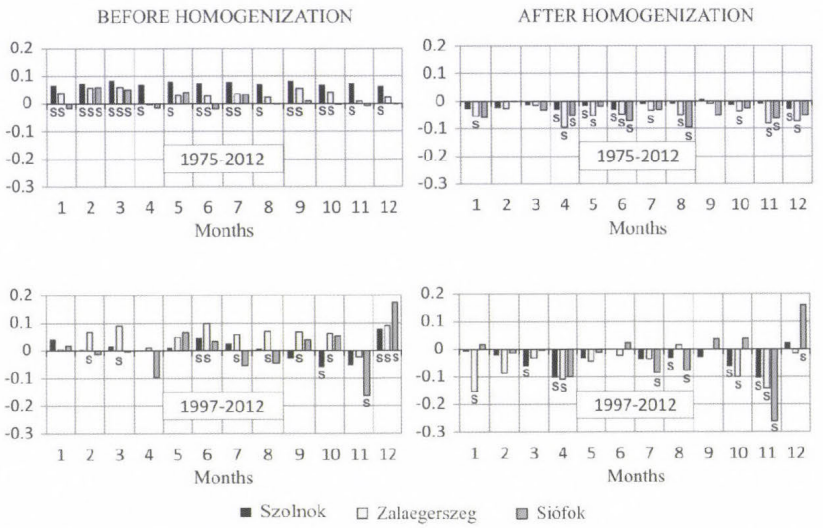

Fig. 9. Monthly linear trend coefficients of 0.9 percentile value for periods 1975–1912 and 1997–2012 calculated from daily wind speed data before (left) and after (right) homogenization for 3 stations. The significant changes are marked with letter "S".

4. Conclusions

Daily wind speed data sets of 19 Hungarian synoptic stations were homogenized for 1975–2012. Our preliminary results are summarized in this paper, based on them the following conclusions can be drawn. (1) Automation, relocated stations, and changed height of measurement sensors could cause break points in time series. Analyzing the modification factors, the inhomogeneity is often larger due to relocations than automation. Therefore, it is important to take into account these effects in planning and installation of measurement systems, moreover, it is essential to document any changes in meteorological measurement network. (2) Homogenization process determined the main break points of stations' time series. Most of the break points could be identified from documented metadata, however, it is not possible to deduce the number of break points from the metadata only. Consequently, non-climatic biases cannot be quantified solely from documented metadata. (3) Spatial variability of wind speed is high, but the temporal variability is small compared to other meteorological parameters (e.g., maximum temperature, sunshine duration). Seasonal relative estimated inhomogeneities of daily wind speed suggest very small changes within the year. (4) Values of RMS are higher when thunderstorm events occur more frequently, i.e., from spring to autumn.

Acknowledgement—We would like to express our very great appreciation to *Tamás Szentimrey* (Hungarian Meteorological Service) for providing MASH application, moreover, for his guidance and help in analyzing the results of homogenization. We are grateful to the Hungarian Meteorological Service and the Geoinformation Service of the Hungarian Defence Forces for the wind data of the Hungarian synoptic meteorological stations. This work was partially supported by the European Union and the European Social Fund through the project FuturICT.hu (grant no.: TÁMOP-4.2.2.C-11/1/KONV-2012-0013). Research leading to this paper has been supported by the Hungarian National Science Research Foundation under grant K-78125, and projects KMR_12-1-2012-0206 and GOP-1.1.1.-11-2012-0164.

References

Aguilar, E., Auer, I., Brunet, M., Peterson, T.C., and *Wieringa, J.,* 2003: Guidelines on climate metadata and homogenization. *WCDMP-No. 53, WMO-TD No. 1186.* World Meteorological Organization, Geneve.

Auer, I., Böhm, R., Jurković, A., Orlik, A., Potzmann, R., Schöner, W., Ungersböck, M., Brunetti, M., Nanni, T., Maugeri, M., Briffa, K., Jones, P., Efthymiadis, D., Mestre, O., Moisselin, J.- M., Begert, M., Brazdil, R., Bochnicek, O., Cegnar, T., Gajić-Čapka, M., Zaninović, K., Majstorović, Ž., Szalai, S., Szentimrey, T., and Mercalli, L., 2005: A new instrumental precipitation dataset for the greater Alpine region for the period 1800–2002. *Int. J. Climatol. 25,* 139–166.

Domonkos, P., Venema, V., and *Mestre, O.,* 2012: Efficiencies of homogenization methods: our present knowledge and its limitation. In *Proceedings of the 7th Seminar for Homogenization and Quality Control in Climatological Databases in press,* www.c3.urv.cat/publicacions/publicacions2012.html

Domonkos, P., 2013: Measuring performances of homogenization methods. *Időjárás 117,* 91–112

Freitas, L., Gonzalez Pereira, M., Caramelo, M., Mendes, M., and *Nunes, L.,* 2013: Homogeneity of monthly air temperature in Portugal with HOMER and MASH. *Időjárás 117*, 69–90

HOME, 2011: Homepage of the COST Action ES0601 - *Advances in Homogenisation Methods of Climate Series: an Integrated Approach* (HOME), http://www.homogenisation.org.

Lakatos, M., Szentimrey, T., Bihari, Z., and *Szalai, S.,* 2013: Creation of a homogenized climate database for the Carpathian region by applying the MASH procedure and the preliminary analysis of the data. *Időjárás 117,* 143–158.

Menne, M.J., and *Williams Jr. C.N.*, 2005: Detection of undocumented changepoints using multiple test statistics and composite reference series. *J. Climate 18*, 4271–4286.

Péliné, N. Cs., Radics, K., and *Bartholy, J.*, 2011: Seasonal Variability of Wind Climate in Hungary. *Acta Silv. Lign. Hung. 7*, 39–48.

Szentimrey, T., 1999: Multiple Analysis of Series for Homogenization (MASH). Proceedings of the Second Seminar for Homogenization of Surface Climatological Data, Budapest, Hungary; WMO, WCDMP-No. 41, 27–46.

Szentimrey, T., 2008: Development of MASH homogenization procedure for daily data, *Proceedings of the Fifth Seminar for Homogenization and Quality Control in Climatological Databases,* Budapest, Hungary, 2006; *WCDMP-No. 68, WMO-TD No. 1434*, 116–125.

Szentimrey, T., 2011: Manual of homogenization software MASHv3.03. *Hungarian Meteorological Service*, Budapest.

Szentimrey, T., 2013: Theoretical questions of daily data homogenization, Special Issue of the COST-ES0601 (HOME) ACTION, *Időjárás 117*, 113–122.

Torma, Cs., Bartholy, J., Pongrácz, R., Barcza, Z., Coppola, E., and *Giorgi, F.,* 2008: Adaptation and validation of the RegCM3 climate model for the Carpathian Basin. *Időjárás 112*, 233–247.

Venema, V., Mestre, O., Aguilar, E., Auer, I., Guijarro, J.A., Domonkos, P., Vertacnik, G., Szentimrey, T., Stepanek, P., Zahradnicek, P., Viarre, J., Müller-Westermeier, G. Lakatos, M., Williams, C.N., Menne, M., Lindau, R., Rasol, D., Rustemeier, E., Kolokythas, K., Marinova, T., Andresen, L., Acquaotta, F., Fratianni, S., Cheval, S., Klancar, M., Brunetti, M., Gruber, C., Duran, M.P., Likso, T., Esteban, P., and *Brandsma, T.,* 2012: Benchmarking monthly homogenization algorithms. *Climate of the Past 8*, 89–115.

World Meteorological Organization, 2011: Guide to Climatological Practices, WMO/No. 100, Geneva.

IDŐJÁRÁS

Quarterly Journal of the Hungarian Meteorological Service
Vol. 118, No. 2, April – June, 2014, pp. 133–145

Spatial modeling of the climatic water balance index using GIS methods

Agnieszka Wypych[1]* and **Ewelina Henek**[2]

[1]*Jagiellonian University, Department of Climatology*
7 Gronostajowa Str., 30-387 Krakow, Poland
agnieszka.wypych@uj.edu.pl

[2]*Institute of Meteorology and Water Management – National Research Institute*
14 Borowego Str., 30-215 Krakow, Poland
ewelina.henek@imgw.pl

**Corresponding author*

(Manuscript received in final form December 13, 2013)

Abstract—The aim of this study is to find the optimal spatialization method to model spatial differentiation of the climatic water balance (CWB). Monthly mean values from the period 1986–2010 for air temperature and precipitation as well as monthly solar radiation totals over Poland were considered in the study. Potential evapotranspiration data were calculated via the Turc formula.

Two simultaneous methods were used in the modeling: simple and multiple linear regression (with latitude, altitude, and distance from the coastline as variables) and the map algebra method. Map algebra was shown to be the better spatialization method; however, its optimization would require a reduction in the research scale and the use of more in-situ data. This would allow more local variables such as landform and land cover to be included in the analysis.

Key-words: spatial analysis, regression model, map algebra, climatic water balance, Poland

1. Introduction

Geographic information systems (GIS) provide a variety of methods for the modeling and presentation of data. GIS provides a powerful research tool for climatology and meteorology, where detailed analysis at different temporal and spatial scales is essential in order to understand processes prevailing in the

atmosphere. Although temperature and precipitation have received the most attention in GIS research, increasingly complex meteorological and climatological indices are also under examination, as they provide information useful in the environmental and social sciences (*Tveito et al.*, 2008).

One such index is the climatic water balance (*CWB*). It focuses on the difference between precipitation (*RR*) and evapotranspiration (*ETP*), presenting a basis for a climatic assessment of water resources in a given geographic area. An understanding of the spatial distribution of the climatic water balance appears to be very important to its comprehensive application in spatial management, agriculture, and hydroclimatological modeling.

Although the *CWB* index seems to be quite simple to compute, it is dependent on many different variables such as solar radiation, relief, land use, and urban development, among others. This creates certain difficulties. It is, first and foremost, a subject involving evapotranspiration, which varies considerably with changes in the natural environment. As data availability is poor, issues arise with proper index interpretation, mainly due to spatial differentiation.

GIS techniques enable the merging of different data processing and integration methods with complex analyses and modeling methods. However, given the complicated nature of the subject, it is no wonder that there exist many GIS methods that attempt to model the spatial differentiation of evapotranspiration (e.g., *Nováky*, 2002; *Xinfa et al.*, 2002; *Fernandes et al.*, 2007; *Vicente-Serrano et al.*, 2007). Remote sensing techniques are also becoming more commonly used to address this research issue and is often used to supplement ground-based observations (*Rosema*, 1990; *Kalma et al.*, 2008).

The purpose of this paper is to describe a new methodology for climatic water balance index implementation using geographic information systems (GIS) in cases when there is no appropriate spatial information given from in-situ observations.

The area under consideration is the territory of Poland, located in Central Europe. Poland was chosen because of its relatively diverse relief from the north (Baltic Sea coast) to the south (the Carpathians), which impacts weather and climate conditions. The lie of the land as well as the country's location suggest that an analysis based on the study area (Poland) seems to be representative of the greater region, e.g., Central and Eastern Europe.

2. *Data and methodology*

As mentioned before, evapotranspiration seems to be the crucial element of climatic water balance index calculations. Regrettably, the complexity of the process (caused by many factors) makes it very difficult to obtain exact values of *CWB* for current meteorological analyses. The alternative solution, the value of ETP, can be calculated to a high degree of precision with the use of simplified

models including meteorological elements that are typically observed by meteorological stations. Therefore, analyses of the climatic water balance (*CWB*) are usually developed for regions where the input data, mainly air temperature and precipitation, can be readily obtained.

The research described herein is based on mean monthly values of air temperature and precipitation totals obtained from 60 meteorological stations as well as monthly totals for solar radiation obtained from 21 actinometric stations. The data cover the periods 1951–2010 and 1986–2010, respectively.

Not all the actinometric stations considered collect the necessary meteorological data, therefore, detailed analyses of the climatic water balance use data obtained only from 16 stations covering the period from 1986 to 2010.

Meteorological data were compiled using topographic information from the SRTM DEM model (*EROS,* 2011).

Given the limited nature of the source data, Turc formula (1961) was used to obtain potential evapotranspiration values. This method was confirmed (*Kowanetz*, 2000) to be suitable for describing the relationship between evapotranspiration and relief. The resulting formula is as follows:

$$CWB = RR - 0.4\frac{t}{t+15}I + 50\,, \tag{1}$$

where *RR* is the monthly precipitation totals [mm], *t* is the monthly average air temperature [°C], and *I* is the monthly sum of total solar radiation [cal cm^{-2} day^{-1}].

Climatic water balance modeling was carried out using two approaches simultaneously. The first approach, examining correlations between environmental elements, used a linear regression method. Statistical relationships between *CWB* and geographic variables such as latitude, elevation, and distance from the coast line were taken into account. The second approach was based on data modeling implementing a map algebra procedure. The results of both approaches were validated using common error estimators.

The *CWB* values calculated for 16 stations were used as reference data (*Fig. 1*). In this study, climatic water balance modeling was conducted using the two methods simultaneously.

An analysis was conducted for the growing season, defined as the time period from May until October. This is consistent with what is frequently considered in agrometeorology.

2.1. Regression models: simple linear regression, multiple linear regression

As mentioned above, the first approach utilized regression models: simple linear regression (SLR) and multiple linear regression (MLR). Close relationships between climatic water balance and geographic factors became the basis for the

model (*Wypych* and *Henek*, 2012), with longitude, latitude, elevation, as well as distance from the coast as explanatory variables.

Fig. 1. Location of the climatic water balance data source stations.

Due to the limited number of samples and also the smallest correlation (from all the analyzed predictors) coefficient between *CWB* values and longitude, it was finally decided to exclude longitude as a variable from regression models, Eqs. (2–4), and not use it in further analyses:

$$Z(s) = \beta_0 + \beta_2 H(s) + \varepsilon(s), \tag{2}$$

$$Z(s) = \beta_0 + \beta_1 \varphi(s) + \beta_2 H(s) + \varepsilon(s)\,, \tag{3}$$

$$Z(s) = \beta_0 + \beta_1 \varphi(s) + \beta_2 H(s) + \beta_3 d(s) + \varepsilon(s)\,, \tag{4}$$

where $Z(s)$ is the dependent variable, $\varphi(s)$ is the latitude, $H(s)$ is the elevation [m a.s.l.], $d(s)$ is the distance from the coast [m], and $\varepsilon(s)$ is the regression residuals.

CWB values were calculated for points on a grid with a spatial resolution of 1 km on the basis of the described linear relationships and using the described regression method.

Data interpolation using radial basis functions (RBF) was used in the final step of creating the climatic water balance spatial differentiation map. RBF is an interpolation technique, which takes into account general tendencies as well as local variability. Research conducted hitherto (*Wypych* and *Ustrnul*, 2011) has confirmed the suitability of RBF as a method for CWB index spatialization.

2.2. Map algebra

The second approach was based on a map algebra application. This type of model requires a process of raster data transformation using GIS tools.

For this study, map algebra was used to create the final CWB spatial differentiation map. First, a series of maps showing the spatial distribution of climatic water balance index components such as air temperature, precipitation totals, and solar radiation, were created using in-situ data.

Component maps of the climatic water balance index were constructed according to a method developed by international research teams dealing with GIS implementation in meteorology and climatology (*Dobesch et al.*, 2007). The method most widely used and commonly considered most effective is kriging (*Dobesch et al.*, 2007).

Temperature spatial differentiation maps were created as the first CWB component using the residual kriging method (*Ustrnul* and *Czekierda*, 2005). Several geographic parameters including elevation, latitude, longitude, and distance to the Baltic coast (for stations located within 100 km), were used as predictor variables.

Precipitation totals were interpolated for the territory of Poland using the kriging method (*Łupikasza et al.*, 2007).

A solar radiation surface was obtained by the application of Solar Analyst ArcGIS. All necessary information such as sunshine duration, altitude at the given location, radiation parameters (diffuse factor and transmittivity), as well as topographic factors such as slope, aspect, and shaded relief based on the SRTM was implemented. Because of element sensitivity to local conditions (astronomical, geographic, meteorological), a variety of different settings in the Solar Analyst application were tested to achieve satisfactory final results. In most cases, the diffuse factor and transmittivity were adjusted. For Poland, the diffuse factor approaches 0.5, while a transmittivity value of 0.4 may also be assumed. In-situ data were used as the reference for parameter selection and model estimation.

All of the layers created were used as input parameters for the potential evapotranspiration model in the Turc formula (air temperature and solar radiation map) and used along with the precipitation map to calculate the climatic water balance for the territory of Poland using the map algebra method. Transformations affected entire layers; all cells of the raster were used as variables. Raster cell values were changed due to previously cited formulas for potential evapotranspiration and the CWB index.

2.3. Validation

The final step was to validate the proposed methods. Due to the limited number of reference points and the use of several different interpolation methods (which are not the typical methods of spatial data interpolation), only simple statistical evaluation measures could be used. The first and most basic measure of model adjustment was the value of the correlation coefficient between the real (from in-situ measurements) and modeled data (R). In addition, bias (RE), percentage error (PE), and absolute error (AE) were calculated and used. Because of the limited number of reference points, it became impossible to evaluate the models using the most common validation methods used for interpolation. Neither cross-validation nor the method of independent sampling could be properly used in this case. However, the suggested estimation factors used for analyzing the results of spatial analyses conducted using different interpolation methods (*ESRI,* 2001) were implemented to assess average real spatial interpolation errors. These include errors for points gained in the first validation step: RMSE (root-mean square error), MPE (mean percentage error), MAPE (mean absolute percentage error). All the model adjustment measures were implemented in relation to values obtained at field measurement sites.

3. Results

Research has shown that the spatial differentiation of the climatic water balance in Poland in the growing season (May – October) amounted to less than –200 mm in the central part of the country and hundreds of millimeters in the high mountain regions of the Carpathians Mountains and the Sudety Mountains (*Fig. 2*).

Most of the territory of Poland is characterized by a moisture shortage. Positive moisture values are typical only in the southern highlands, foothills, and mountain areas (*Fig. 2*). In addition, the spatial distribution of the climatic water balance varies seasonally.

Nevertheless, a detailed analysis of the climatic water balance index distribution shows regional and local differences attributable to the spatialization method implemented as described below.

The regression models used in this research study have shown to be most strongly affected by elevation in a significant correlation. The predominant role of this predictor has been to influence the spatial differentiation of the climatic water balance index in Poland. However, regardless of the regression method, the belt-like distribution of *CWB* index values is still discernible. This pattern holds true mainly in the spring and summer months, but it is less visible in the autumn. The Baltic Sea also affects seasonal differences by limiting evapotranspiration – higher *CWB* values noted between July and October. In May and June, it was not shown to have an important effect.

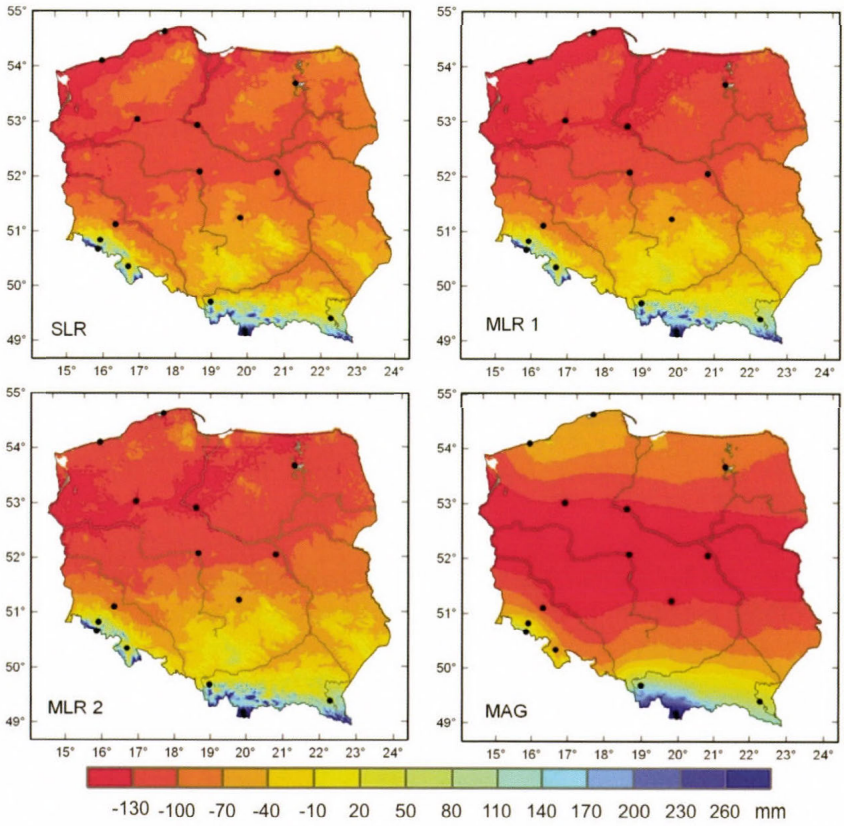

Fig. 2. Spatial differentiation of climatic water balance (*CWB* in mm) in Poland in the growing season (May–October) based on different methods.
SLR – simple regression: f (H), MLR 1 – multiple regression: f (φ, H), MLR 2 – multiple regression: f (φ, H, d), MAG – map algebra

With an understanding of the spatial differentiation of climate conditions in Poland, it can be stated that regression models can slightly deform *CWB* differentiation visualizations, especially in coastal areas, as mentioned previously.

When using the map algebra method (MAG), the belt-like distribution of the *CWB* shows that the index is dependent on geographic parameters such as elevation and latitude. The "distance from the Baltic coastline" variable is indirectly (i.e., by differentiation of temperature values and precipitation totals) implemented in the MAG model. The climatic water balance field shows a significant moisture deficit (the lowest *CWB* index values) in the lowlands of

Central Poland, whereas values estimated much higher than what other models produce can be observed along the coastline. This situation is characteristic of the entire growing season.

Fundamental evidence acknowledging and supporting the MAG approach can be used for a detailed analysis of *CWB* component spatial fields, which serve as the basis of this study. A MAG image is the effect of the spatialization of different elements such as precipitation and evapotranspiration, whereas the latter is a result of integrating solar radiation and temperature maps.

Research results produced using both methods were validated using universal statistical error estimators. *CWB* values calculated for the 16 weather stations considered in the study were used as reference data.

For all 16 weather stations considered, *CWB* values were calculated for the study period. For each point, the deviations of the modeled values were defined by subtracting the true values (*CWBmod – CWBcalc*) for the growing season (May–October) for each month separately. Positive error values (calculated differences) indicate model overestimation, whereas negative error values show undervaluation of predicted values.

Results for the growing period (May–October) clearly show that the map algebra (MAG) method gives the best fitting results in relation to the reference data. The highest (close to 1), correlation coefficient value confirms the best model adjustment. Absolute errors are also significantly smaller than those produced by other research methods (*Table 1*). The MAG model overestimates *CBW* values for northern and central Poland and produces the best predictions for the northeastern part of the country, and the least accurate predictions for the central part of Poland. For southern Poland, modeled values of the climatic water balance are lower than calculated values.

The differences reach an average in the tens of millimeters; however, in extreme cases, the model can give *CWB* index values different from true values by several hundred millimeters. This has been reported for the Kasprowy Wierch and Śnieżka mountain weather stations. Regression models not considering the distance from the Baltic coastline as a predictor (MLR 1) as well as simple regression (SLR) were shown to be the least accurate methods. The correlation coefficient is about 0.5 lower, and other estimators show minimally higher values in both cases (*Table 1*). It is worth noting that the spatial differentiation of the results produced by the methods used in this paper is readily observable. Simple linear regression (SLR) gives better results for areas near the Baltic coast and for the Sudety mountains in southern Poland. On the other hand, in the central Polish lowlands, differences between the methods used cannot be clearly distinguished. Finally, the MLR 1 method performs well in the Carpathian region.

Table 1. Climatic water balance values (*CWB*) with selected model errors at reference points in the growing season (May – October)

Reference stations	*CWB* [mm]	SLR		MLR_1		MLR_2		MAG	
		APE (%)	RE [mm]	APE (%)	RE [mm]	APE (%)	RE [mm]	APE (%)	RE [mm]
Kołobrzeg	–73.3	107.9	–79.2	17.5	12.8	146.1	–107.2	66.4	–48.7
Łeba	–69.4	122.0	–84.7	16.4	11.3	176.6	–122.6	88.9	–61.7
Piła	–155.4	19.5	30.4	14.2	22.0	12.4	19.3	12.4	19.3
Toruń	–160.9	21.7	35.0	13.3	21.4	14.5	23.3	14.5	23.4
Mikołajki	–97.6	1.4	–1.4	5.0	4.8	28.3	–27.6	28.3	–27.6
Koło	–181.8	38.6	70.2	9.5	17.3	39.3	71.5	39.3	71.5
Warszawa	–177.6	38.0	67.5	16.9	30.0	38.5	68.4	38.5	68.4
Legnica	–165.6	37.9	62.7	27.7	45.9	47.4	78.5	47.4	78.5
Sulejów	–157.9	52.8	83.4	13.3	21.0	60.5	95.5	60.5	95.5
Jelenia Góra	–16.1	117.2	18.9	46.7	–7.5	154.3	24.9	154.6	24.9
Śnieżka	271.1	40.7	110.2	55.3	–149.9	50.2	136.0	50.0	135.6
Kłodzko	–44.5	77.3	34.4	38.2	–17.0	139.0	61.8	138.9	61.8
Bielsko-Biała	165.2	88.4	–146.1	26.5	–43.8	75.8	–125.2	75.8	–125.3
Zakopane	378.5	39.7	–150.2	11.0	–41.7	37.0	–140.2	37.0	–140.2
Kasprowy Wierch	819.7	32.0	–262.4	35.7	–292.7	21.6	–177.1	21.5	–176.6
Lesko	86.5	87.5	–75.7	44.1	–38.2	56.0	–48.4	56.0	–48.5
MAE [mm]		82.0		83.0		75.5		48.6	
RMSE [mm]		102.5		95.3		88.3		86.1	
MAPE (%)		57.7		68.6		58.1		24.4	
R		0.940		0.937		0.950		0.988	

RE – bias, APE – absolute percentage error, MAE – mean absolute error, RMSE – root-mean-square error, MAPE – mean absolute percentage error, R – Pearson's correlation coefficient, MAG – map algebra, SLR – simple linear regression: f (H), MLR_1 – multiple linear regression: f (φ, H), MLR_2 – multiple linear regression: f (φ, H, d)

The least accurate results, regardless of method, were observed for Poland's mountain regions. All of the models predict values lower than real values for the Carpathians (*Table 1*). For the Sudety Mountains, significant positive differences were modeled only for Mount Śnieżka. Other weather stations are characterized by errors commonly found in the rest of the country. Coastal areas encountered the same difficulty as mountain areas when it came to the spatialization of the *CWB* index. Regression models significantly lower the

prediction and estimate values close to those recorded for Poland's lake districts and the central part of the country.

As previously mentioned, map algebra images are produced by the spatialization of climatic water balance index components. Therefore, it could be supposed that the final map additionally contains some errors such as precipitation errors, and above all, potential evapotranspiration interpolation errors, since the latter were obtained using map algebra, where the temperature field was integrated with solar radiation. Moreover, solar radiation was modeled using the Solar Analyst tool, and the potential solar radiation field was based primarily on elevation.

4. Discussion

The climatic water balance is a complex index influenced by many different factors. These factors affect both precipitation and evapotranspiration values including solar radiation, relief and slope aspect, land use, and degree of urbanization.

In the course of research and analysis, several problems were identified that could potentially affect further research in this area.

Climatic water balance components such as precipitation and potential evapotranspiration are characterized by considerable spatial and temporal differentiation as well as strong correlations between atmospheric circulation, meteorological conditions, and local factors. Therefore, *CWB* spatial variability is difficult to identify. Current understanding of mesoclimate differentiation, especially that of mountain areas, suggests that many geographic variables should be taken into consideration. In order to accurately describe the spatial distribution of *CWB*, it is necessary to take into account variables such as slope, aspect, land use, and soil type, all of which determine how much solar radiation is available to produce given air temperature values (*Ustrnul* and *Czekierda*, 2005). Both solar radiation and air temperature affect the degree of evapotranspiration. Furthermore, both parameters must be calculated independently for smaller regions – especially regions characterized by specific mesoclimate conditions such as those found in coastal or mountain areas.

In order to determine the value of the *CWB* index, the magnitude of evapotranspiration must be properly estimated. Although Turc formula used in this paper is strongly correlated with geographic factors (especially elevation), it seems insufficiently sophisticated to fully represent evapotranspiration conditions. The purpose of this study was to identify the best spatialization method in a situation with a shortage of data; therefore, Turc formula was chosen as the least demanding. Ultimately, the final results do contain errors.

At least 30 years of daily data are needed in order to analyze the climatology of an element; in this case, the spatial and temporal differentiation of the climatic water balance. The data must address all *CWB* components. As

mentioned before, no evapotranspiration data were available, and the available data required the use of complex formulas that are not completely suitable for long-term data. Furthermore, commonly used formulas providing potential evapotranspiration data only fulfill environmental requirements to a certain extent and tend to produce unreliable data (*Jaworski*, 2004).

The main objective of this research study was to depict *CWB* spatial differentiation using a limited quantity of homogenized data. Recent developments in GIS techniques have produced a wide range of powerful methods for capturing, modeling, and displaying of climate data. Using geospatial analysis seems to be the sensible response to the current research needs for this topic. Nevertheless, even the most advanced data processing methods we use contain failures and problems that need to be solved in order to perform detailed analysis of the climatic water balance index on different temporal and spatial scales.

Using only 16 reference points to create the regression models and validate the data, the results were error laden. The magnitude of the regression model errors cannot be accepted. The weather stations were not representative enough to build the final model. This is why, among other things, the land use factor was removed from the formula. In the regression methods, the most deficient were solar radiation data. It would be possible to use more reference points (however not so many as 60 stations as used for temperature and precipitation data), if modeled data were used instead of in-situ solar radiation data. There exist empirical formulas (*Podogrocki*, 1978) for which daily sums of total solar radiation are obtained using sunshine duration data.

It would also be possible to generate the missing data from, for instance, the Solar Analyst application. Nevertheless, the more generalized or simplified the data, the greater the possibility of error in the final model.

The data deficit problem also concerns the map algebra model and validation section. Model errors generated for "blank" areas (without measuring points) cumulate while being aggregated in the map algebra method. As far as estimating the models, weather stations located in the northeast and east of Poland, as well as in mountain areas are desirable.

The least accurate results were obtained for mountain areas. This is mainly because in the mountains weather systems are strongly affected by the topography, and the modeling of climate conditions requires representative points for different elevations, landforms, aspects, etc. The spatial resolution suggested for mountainous areas is at least one weather station per 1,300 km^2 for temperature, wind velocity, precipitation, and one weather station per 500 km^2 for snow data (*Barry*, 1992). The validation results for climatic water balance variability would be different (more positive) if the Kasprowy Wierch and Śnieżka weather stations were not taken into account. Model errors are also the effects of temporal/seasonal differentiation of particular climate elements included in the CWB index. Local factors are of great importance, especially in the spring and summer months, which is also reflected in the selected estimator values.

Regardless of the validation results, the obtained maps of climatic water balance spatial differentiation in Poland show certain problems with the methods used. Regression models are affected mainly by the lack of data used to create the formulas taking into account long-term and homogenous data series of necessary meteorological elements. The fundamental error source was the irregular location of the data gathering points and subsequently limited representativeness regarding various environmental conditions. This can be more clearly seen along the Baltic coast, but also in the northeastern part of Poland, and of course, in its mountains in the south. On the other hand, solar radiation field data seems to be the vulnerable point of the map algebra method. The limitations of the Solar Analyst application – mainly due to highly variable cloud cover – and the lack of a sufficiently dense network of weather stations failed to ensure good interpolation results.

5. Conclusions

The primary objective of this study was to find the optimal spatialization method to describe spatial differentiation of the climatic water balance (*CWB*) in Poland. Two different approaches employing five spatialization methods were used – regression models (simple linear regression, various multiple linear regression formulas) and map algebra. Climatic water balance values and their spatial distribution are dependent on both atmospheric circulation (i.e., weather conditions) and local environmental conditions. Hence, it was necessary to use many different geographic predictors including coordinates, elevation, and others.

The research confirmed that the application of GIS techniques is a useful and promising tool for constructing maps of different climate elements and indices. At the same time, through a detailed analysis of the research results, certain shortcomings of the proposed method can be reported. Aside from the nature of the method itself, the principal problem can be the lack of source data. As a consequence, there is the risk of performing extrapolation instead of interpolation.

The largest differences between model values and real values were noted for regions with a sparse weather station network. This means that the final results may be the effect of the particular method used in spatial analysis, especially for areas with few measuring points. Such cases warrant a very careful interpretation of the research results.

Regardless of the research method used, the obtained results confirm the role of local factors in CWB modification. Therefore, it is necessary to take into account not only the spatial scale, but also the time scale used for explanatory variables. This is because, depending on the area and the season, their impact on the predictand will vary.

No matter how accurate the results are, research experience and scientific intuition are the keys to the interpretation of research results. Careful and detailed analysis is required as well as thorough knowledge of pertinent physical processes and complexity of the geographic environment. Both types of factors need to be considered when choosing predictors and later in the course of model validation, where a complex series of explanatory variables is used.

References

Barry, R.G., 2008: Mountain weather and climate. Routledge, London-New York.

Dobesch, H., Dumolard, P., Dyras, I. (eds.), 2007: Spatial Interpolation for Climate Data: the Use of GIS in Climatology and Meteorology. ISTE, London.

EROS: Earth Resources Observation and Science Center, 2011: on-line at: http://earthexplorer.usgs.gov/, accessed: December 2011.

ESRI, 2001: ArcGIS Geostatistical Analyst: Statistical Tools for Data Exploration, Modeling and Advanced Surface Generation. ESRI White Paper, New York – Redlands.

Fernandes, R., Korolevych, V., Wang, S., 2007: Trends in land evapotranspiration over Canada for the period 1960–2000 based on in situ climate observations and a land surface model. *J. Hydrometeorol. 8*,1016–1030.

Kalma, J.D., McVicar, T.R., and *McCabe, M.F.*, 2008: Estimating land surface evaporation: A review of methods using remotely sensed surface temperature data. *Surv. Geophys. 29*, 421–469.

Jaworski, J., 2004: Evaporation in hydrological cycle of river basins. Polskie Towarzystwo Geofizyczne, Warszawa (in Polish).

Kowanetz, L., 2000: On the method of determining the climatic water balance in mountainous areas, with the example from Polish Carpathians. *Zeszyty Naukowe UJ, Prace Geograficzne* 105, 137–164.

Łupikasza, E., Ustrnul, Z., Czekierda, D., 2007: The role of explanatory variables in spatial interpolation of selected climate elements. *Roczniki Geomatyki* 5, 55–64.

Nováky, B., 2002: Mapping of mean annual actual evaporation on the example of Zagyva catchment area. *Időjárás 106*, 227–238.

Podogrocki, J., 1978: Spatial distribution of global solar radiation in Poland. *Publ. Inst. Geophys. Pol. Acad. Sc., D5-120*, 17–30.

Rosema, A., 1990: Comparison of Meteosat-based rainfall and evapotranspiration mapping in the Sahel region. *Int. J. Remote Sens. 11*, 2299–2309.

Turc, L., 1961: Evaluation des besoins en eau d'irrigation, évapotranspiration potentielle. *Ann. Agronomiq.12*, 13–49.

Tveito, O.E., Wegehenkel, M., Wel van der, F., and *Dobesch, H.* (eds.), 2008: The use of geographic information systems in climatology and meteorology. Final Report COST Action719, COST Office.

Ustrnul, Z. and *Czekierda, D.*, 2005: Application of GIS for the development of climatological air temperature maps: an example from Poland. *Meteorol. Appl. 12*, 43–50.

Vicente-Serrano, S.M., Lanjeri, S., and *López-Moreno, J.I.*, 2007: Comparison of different procedures to map reference evapotranspiration using geographical information systems and regression-based techniques. *Int. J. Climatol. 27*, 1103–1118.

Wypych, A. and *Ustrnul, Z.*, 2011: Spatial differentiation of the climatic water balance in Poland. *Időjárás 115*, 111–120.

Wypych, A. and *Henek, E.*, 2012: Using GIS in spatial differentiation of the climatic water balance research in Poland. *Przegląd Geofizyczny 57*, 233–244 (in Polish).

Xinfa, Q., Yan, Z., and *Changming, L.*, 2002: A general model for estimating actual evaporation from non-saturated surfaces. *J. Geograph. Sci. 12*, 479–484.

IDŐJÁRÁS

Quarterly Journal of the Hungarian Meteorological Service
Vol. 118, No. 2, April – June, 2014, pp. 147–166

Modification of the Tourism Climatic Index to Central European climatic conditions – examples

Attila Kovács* and **János Unger**

Department of Climatology and Landscape Ecology, University of Szeged
P.O. Box 653, H-6701 Szeged, Hungary

**Corresponding author E-mail: kovacsattila@geo.u-szeged.hu*

(Manuscript received in final form September 18, 2013)

Abstract—Climate is a decisive tourism resource and plays key role in the attractiveness of tourist destinations and the seasonality in tourism demand. The suitability of climate for general tourism purposes (i.e., sightseeing, shopping, and other light outdoor activities) is most frequently expressed by the Tourism Climatic Index (TCI), which combines several tourism-related climatic elements. In this study, the original TCI is modified in two ways. On the one hand, one of the most popular and widely used bioclimatic indices, Physiologically Equivalent Temperature (PET) is applied instead of effective temperature (ET) in the part of the index related to thermal comfort conditions. Furthermore, the TCI is adjusted to a ten-day scale since it is more relevant to tourism than the original monthly averages of the climatic parameters. Using the modified TCI we characterize and compare climatically suitable or even unfavorable places and periods of the year in case of some Hungarian and two other relatively close tourist destinations as examples. Analytical results indicate that the most optimal climatic conditions are in the shoulder seasons in all investigated places. The summer period is more unpleasant for sightseeing activities mainly due to the instense heat load. There are some remarkable differences between the cities in the time of occurence of different tourism climatic conditions and, therefore, in the seasonality conditions.

Key-words: climatic conditions, tourism, modified Tourism Climatic Index, Physiologically Equivalent Temperature, Central Europe

1. Introduction

Tourism is one of the key sectors in Hungarian economy. In 2011, more than 41 million foreign tourists contributed with 1200 billion HUF to the tourism sector. Tourism related industries generate about 5.9% of national gross domestic product (GDP) and employ 8.4% of all workers in Hungary (*KSH,* 2012).

The attractiveness of a tourist destination is influenced by several factors. Together with geographical location, topography, landscape, flora and fauna, climate constitutes the natural tourism resource of a place (*de Freitas,* 2003). Climate can directly affect tourism in many ways. Climate may be a decisive factor in the choice of a destination by determining the time of the year, when climatic conditions are at their optimum, or by designating the area that offers the most suitable climatic conditions (*Mieczkowski,* 1985). Ultimately, it affects tourists' satisfaction with the destination area, thermal comfort, and climatic well-being of visitors. Inter-annual climate variability influences the length and quality of tourism seasons, and thus, the tourism demand (*Scott* and *McBoyle,* 2001; *Scott et al.,* 2008).

Mainly due to the increasing competition between tourist destinations, considerable effort has been put into defining an easily applicable metric in order to investigate the suitability of different tourist activities in terms of climatic conditions. It is generally accepted that tourists respond to the integrated effects of the atmospheric environment, therefore, a comprehensive tourism climatic metric has to integrate all three tourism-relevant aspects of climate identified by *de Freitas* (2003): thermal, physical, and aesthetic (*Matzarakis,* 2006; *Scott et al.,* 2008; *Yu et al.,* 2009; *Perch-Nielsen et al.,* 2010). An overview of these three different facets of climate and their significance to tourists is provided in *Table 1*.

One of the most comprehensive and widely used metrics in tourism climatology is the Tourism Climatic Index (TCI) (*Mieczkowski,* 1985), which attempts to reflect the destination's climatic suitability for "average" tourists engaged in light physical outdoor activities (e.g., sightseeing, shopping). TCI is also capable to characterize global or regional effects of climate change to tourism according to projected scenarios of future climatic conditions. For example, *Scott et al.* (2004) used the TCI to assess its temporal and spatial distribution and seasonal variability in the future focusing on destinations in North America, while *Amelung* and *Viner* (2006) and *Perch-Nielsen et al.* (2010) in Europe. *Zaninović et al.* (2010) studied the influence of climate change on summer tourism potential in the Pannonian lowland (great parts of Hungary and Croatia) by analysing the differences between future and present bioclimatic and tourism climatic conditions based on climate simulations focusing on the changes in single climatic parameters and Physiologically Equivalent Temperature (PET, see in Section 2). The results indicate diverse

changes in summer tourism potential of the area due to the global warming. In addition, *Németh* (2013) analyzed the changes of the tourism climate potential in the Lake Balaton region of Hungary in detail during the last half-century based on the original TCI index. According to the results, the best climatic conditions for tourism purpose can be observed in the summer months. Between three climatological normal periods, significant changes in tourism climatic conditions cannot be detected in the last half-century.

Table 1. Various aspects of tourism climate, their impact, and significance (based on *de Freitas,* 2003)

Facets of climate	**Impact, significance**
Thermal	**Physiological impact**
integrated effects of air temperature, humidity, wind speed, short- and long-wave radiation, personal factors	heat sensation, thermal comfort, physiological stress climate therapy
Physical	**Physical impact**
wind	dust, sand, damage to property
rain	wetting, reduced visibility and enjoyment
snow	winter sports/activities
ice	personal injury, damage to property
air quality	health, allergies, well-being
ultraviolet radiation	health, suntan, sunburn
Aesthetic	**Psychological impact**
sunshine/cloudiness	enjoyment, attractiveness of site
visibility	enjoyment, attractiveness of site
day length	period of activities, convenience

The present study aims a modification of the original TCI in order to reduce its two current serious limitations and reflect a more current state of knowledge. We make an attempt to update the thermal comfort parts of the index and its original temporal scale to the Central European conditions. We present the behavior of the modified index while describing climatically suitable or even unfavorable periods of the year in case of some Hungarian and two relatively close tourist destinations as examples.

2. The Tourism Climatic Index

TCI was developed by *Mieczkowski* (1985) based on previous research related to climate classifications for tourism and human biometeorology. In TCI, monthly averages of seven climate variables relevant for tourism are integrated into five sub-indices, listed in *Table 2*: daytime comfort index (CId), daily comfort index

(CIa), precipitation (R), sunshine (S), and wind (W). All of them are rated on different scales from 0 (unfavorable) to 5 (optimal) values while the thermal comfort sub-indices (CId and CIa) are rated from –3 to 5. By distinct weightings and then combining all weighted sub-indices, the overall TCI is calculated as follows:

$$TCI = 2\times(4\times CId + CIa + 2\times R + 2\times S + W). \quad (1)$$

Table 2. Summary of the sub-indices, their impact, and weigthing in TCI (based on *Scott* and *McBoyle*, 2001)

Sub-index	Monthly averages	Influence on TCI	Weighting
daytime comfort index (CId)	daily maximum temperature (°C) and minimum relative humidity (%)	represents thermal comfort when maximum tourist activity occurs (usually between 12 a.m. and 4 p.m)	40%
daily comfort index (CIa)	daily mean temperature (°C) and mean relative humidity (%)	represents thermal comfort over the full 24-hour period	10%
precipitation (R)	total precipitation (mm)	negative impact on outdoor activities and climatic well-being	20%
sunshine (S)	sunshine duration (hour)	positive impact	20%
wind (W)	wind speed (ms^{-1})	variable impacts depending on its value and the maximum temperature	10%

As all sub-indices have a maximum score of 5, *Mieczkowski* (1985) proposed a rating system of TCI with an overall maximum score of 100, where acceptable scores are above 40, good climatic conditions are above 60, and excellent scores are above 80 (*Table 3*).

Table 3. Tourism Climatic Index rating system (*Mieczkowski*, 1985)

TCI scores	Descriptive categories
90 – 100	ideal
80 – 89	excellent
70 – 79	very good
60 – 69	good
50 – 59	acceptable
40 – 49	marginal
30 – 39	unfavorable
20 – 29	very unfavorable
10 – 19	extremely unfavorable
< 10	impossible

Scott and *McBoyle* (2001) presented a conceptual framework of six possible types of annual TCI distributions; the tourism resource of all destinations can be classified into one of them (*Fig. 1*). In our study, this framework is used to characterize the tourism climatic conditions in the selected cities.

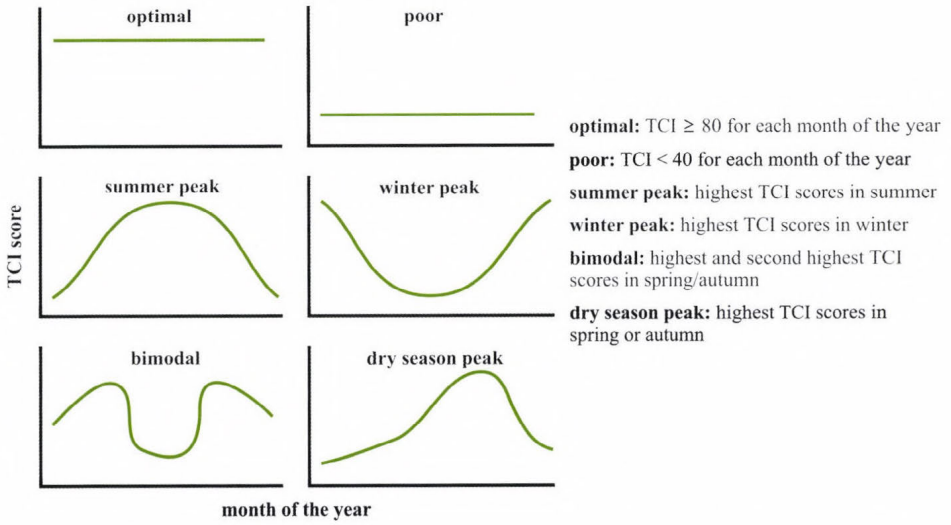

Fig. 1. Conceptual framework of annual tourism climate distributions (based on *Scott* and *McBoyle,* 2001).

The sub-indices of TCI expressing thermal comfort conditions (CId, CIa) are based on the effective temperature (ET), which is a simple empirical index of air temperature/relative humidity combinations (*Houghten* and *Yaglou,* 1923). The optimal comfort zone of ET is between 20 and 27 °C according to *ASHRAE* (1972) rated with maximum point 5. The rating scale then decreases on both sides of the optimal zone with 1 or 0.5 points. However, the rating points of the zones are based on the subjective opinion of the author, they are not empirically tested against the preferences of tourists (*de Freitas,* 2003; *de Freitas et al.,* 2008). A further important shortcoming of ET is that it does not include the effects of such thermal parameters as wind speed, short- and longwave radiation fluxes, in addition, it does not take into account such physiologically, and thus, bioclimatically relevant personal data as age, gender, height, weight, metabolic rate, and clothing. Therefore, it cannot evaluate the thermal conditions of the human body in a physiologically significant manner.

Instead of empirical indices, a full application of rationale indices based on the energy balance of the human body gives detailed information on the effect of thermal environment on humans (*VDI,* 1998). Such indices include all relevant

thermophysiological parameters: air temperature, relative humidity, wind speed, short- and longwave radiation fluxes. One of the most popular and widely used rationale bioclimate indices is the Physiologically Equivalent Temperature (PET), which was developed typically for outdoor applications (*Mayer* and *Höppe,* 1987; *Höppe,* 1999). The interpretation of the index refers to indoor standard reference conditions and the evaluation of the thermal comfort conditions concerns a standardized fictive person. PET is defined as the air temperature at which, in a typical indoor setting, the heat budget of the body is balanced with the same core and skin temperature as those under the prevailing complex outdoor conditions (*Höppe,* 1999). The PET value categories were initially defined according to thermal sensations and physiological stress levels of Western and Central European people, where the thermally neutral heat sensation and stress are indicated by PET value range of 18–23 °C (*Fig. 2*) (*Matzarakis* and *Mayer,* 1996).

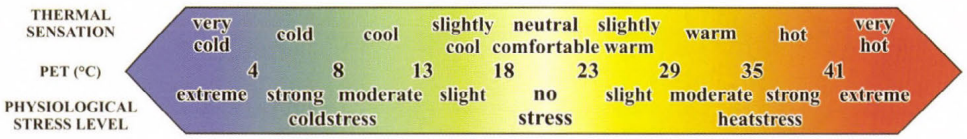

Fig. 2. Categories of the PET values (°C) for different grades of thermal sensation and physiological stress level of Western and Central European people (based on *Matzarakis* and *Mayer,* 1996).

3. Modification methods on Tourism Climatic Index

Despite the comprehensive nature and wide applications of TCI, a number of limitations were addressed and some modification possibilities were suggested by different studies (e.g., *de Freitas,* 2003; *Matzarakis,* 2006; *de Freitas et al.,* 2008; *Perch-Nielsen et al.,* 2010). The rating systems and the weightings of the sub-indices are partly based on human biometeorological literature, but also on the author's subjective opinions. A further important limitation is the application of ET, which was addressed by e.g., *Scott et al.* (2004), *Amelung* and *Viner* (2006) and *Perch-Nielsen et al.* (2010), therefore, they used apparent temperature (AT) (*Steadman,* 1979) instead of ET. However, AT is also based only on temperature/humidity combinations, and it is not really applied in recent human biometeorological research. A further important shortcoming of TCI is its temporal scale since monthly averages of the applied climatic parameters are considered, which are insufficient for tourism climatic purposes because tourists' length of stay during sightseeing is generally shorter (*de Freitas et al.,* 2008; *Scott et al.,* 2008; *Yu et al.,* 2009; *Perch-Nielsen et al.,* 2010).

Based on the above mentioned shortcomings, in the present study two modifications are performed in the structure of the original TCI, which means an initial step forward in the development of an updated index applicable at Central European climatic conditions. Firstly, in order to take into account human thermal comfort conditions more precisely in TCI, we attempted to integrate PET into the thermal sub-indices instead of ET, and for this purpose, a new rating system of PET has been developed, too. Secondly, the TCI is adjusted to a ten-day scale, i.e., ten-day averages of each climatic variables were rated, and then the values obtained in this way were taken at the index calculation.

The annual variations of the modified index and its sub-indices are presented and compared in case of four Hungarian and two other European cities: Szeged-Bajai út (46°15'N, 20°05'E), Siófok (46°54'N, 18°02'E), Debrecen (47°29'N, 21°36'E), Győr-Likócs (47°42'N, 17°40'E), Prague-Libus (50°0'N, 14°26'E), Thessaloniki-Airport (40°31'N, 22°58'E) (*Fig. 3*). The analysis concerns the periods of 1996–2010 and 2000–2010 in the first three and second three places, respectively.

Fig. 3. The investigated Hungarian and other European cities.

For the calculation of PET, hourly air temperature, relative humidity, wind speed, and cloudiness data of Hungarian Meteorological Service were used in the case of the Hungarien cities, while hourly and three-hourly synop report queries were utilized for Prague and Thessaloniki, respectively. PET was

calculated by means of the bioclimate model RayMan (*Matzarakis et al.*, 2007). The measured wind speed data were transformed to the bioclimatological reference height of 1.1 m. Ultimately, the daytime (CId) and daily comfort (CIa) sub-indices of the modified TCI consist of the calculated daily maximum and daily average PET values holding the basic concept of *Mieczkowski* (1985) (see in *Table 2*). In addition to the data necessary for PET, daily precipitation and sunshine duration data obtained from the above mentioned databases were utilized. Concerning the parameters used for the calculation of PET, it is often difficult to access appropriate data, especially the radiation component of PET due to the lack of long-term or fine temporal scale (i.e., hourly) data sets. For example, application of global radiation instead of cloudiness data would be more appropriate, but its availability is often limited due to the uncertain measurement program and the lack of long-term data. Nevertheless, we could select several tourist destinations with complete data sets in different climatic regions, and evaluation and comparison are possible using these datasets representing these regions.

The original rating systems of wind speed (W), precipitation (R), and sunshine duration (S), and the weightings of all TCI sub-indices remained unchanged. (Note: Mieczkowski rated monthly precipitation on a scale from 0 to 5. Because of the ten-day averages, this scheme was changed by simply dividing the monthly values by 3, and these categories were rated by the original scores).

However, for the evaluation of PET, a new rating scheme had to be developed keeping in mind that the rating categories and scores should be based on objective, international standards, and subjective factors should be eliminated. The rating scores of PET were derived based on the principle that the comfortable thermal conditions should get higher scores while in case of intesifying warm or cold thermal stress conditions the values should decrease progressively on both sides of the comfort zone in an objective way.

Therefore, in the derivation of rating scores of PET, we utilized the function relationship declared in *ASHARE* (2004) and *ISO* (2005) between two bioclimatic measures, predicted mean vote (PMV) and predicted percentage of dissatisfied (PPD) (*Fanger,* 1972). PMV derived from the comfort equation of *Fanger* (1972) predicts the mean values of the thermal votes of a large group of persons on a seven-point (later nine-point) thermal sensation scale (from –4 very cold to +4 very hot) based on the heat balance of the human body in an environment characterized by given thermal variables (air temperature, relative humidity, wind speed, mean radiant temperature) (*ASHRAE,* 2004; *ISO,* 2005). Individual votes are obviously scattered around this mean PMV value, i.e., thermal environment characterized by the same PET value does not necessarily evoke the same thermal sensation of all persons. However, the distribution of thermal votes as a function of PMV can be statistically predictable. PPD establishes a quantitative prediction of the ratio of thermally dissatisfied people

who feel too cold or too warm, i.e., do not vote –1, 0, or +1 on the seven-point scale (*ASHRAE,* 2004; *ISO,* 2005). For example, in case of 0, PMV such thermal votes belong to only 5% of the given population, while 95% of them can be considered thermally satisfied. The relationship between PPD and PMV can be given as follows (*ASHRAE,* 2004; *ISO,* 2005) (*Fig. 4*):

$$PPD = 100 - 95 \times \exp(-0.03353 \times PMV^4 - 0.2179 \times PMV^2). \quad (2)$$

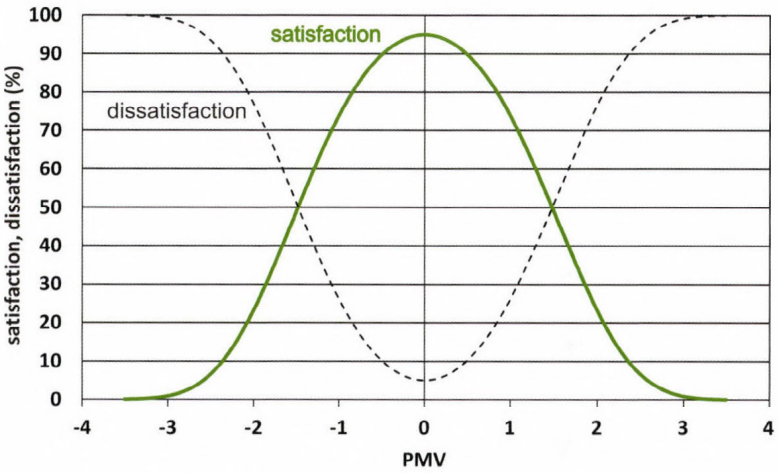

Fig. 4. Relationship between PMV and satisfaction-dissatisfaction with thermal conditions (based on *ASHRAE,* 2004; *ISO,* 2005).

In the derivation of the rating scores we utilized Eq. (2) and assumed that the TCI scores as a function of PET should decrease in the same way as the satisfaction with the thermal environment characterized by PMV declines. Our initial value was 0 PMV related to neutral thermal sensation, which was considered equivalent to the median value (20.6 °C) of the neutral PET category values (18.1–23.0 °C). Towards cold or warm discomfort conditions, decline of satisfaction associated with one-hundredth continuous PMV change was corresponded to decrease of TCI rating score associated with one-tenth PET change. Therefore, we obtained rating scores for all decimal PET values.

In this study, we utilized the widely used PET thermal sensation categories applicable in Western and Central European climatic conditions (*Fig. 2*), and these ranges were rated in case of the selected cities. All categories were characterized by an above derived rating score belonging to the median values of each PET categories. Thus, extreme cold conditions have lower rating scores

than those of the warm extremities, because PET covers a larger range towards cold direction (*Table 4; Fig. 5*).

The above rating system was applied in the rating of the ten-day averages of both thermal comfort sub-indices in TCI.

Table 4. Rating system of PET-based sub-indices (CId, CIa) in the modified TCI (neutral PET category is marked with green)

PET categories (°C)	Median of PET categories (°C)	Rating score
35.1 – 41.0	38.1	1.9
29.1 – 35.0	32.1	3.5
23.1 – 29.0	26.1	4.7
18.1 – 23.0	20.6	5.0
13.1 – 18.0	15.6	4.7
8.1 – 13.0	10.6	3.9
4.1 – 8.0	6.1	2.8
0.1 – 4.0	2.1	1.6
–10.0 – 0.0	–5.0	0.3

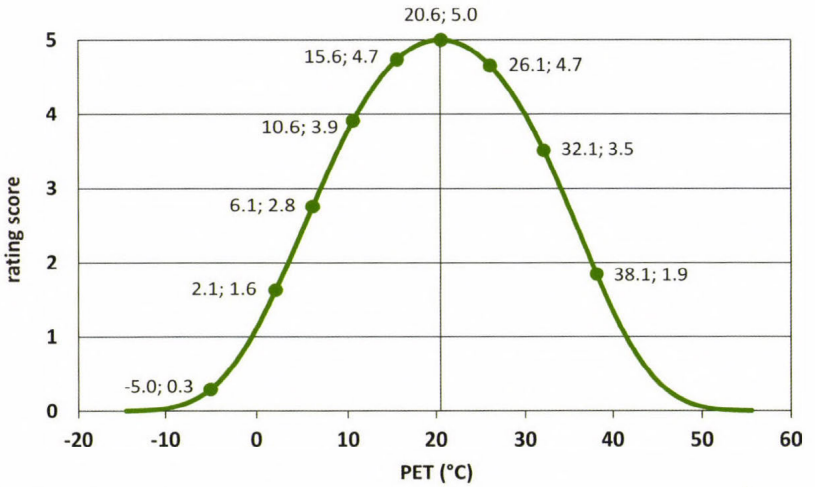

Fig. 5. Medians of PET thermal sensation categories (°C) and their obtained rating scores.

4. *Application of modified TCI in case of European examples*

4.1. Annual variation of ten-day TCI

In the following, the annual variations of the modified TCI and its sub-indices are analyzed in the selected cities. In *Fig. 6*, the annual cycle of the ten-day TCI is presented. In all cities, bimodal type of distribution (see *Fig. 1*) was obtained, that is the most pleasant climate in terms of sightseeing activities in spring and autumn, while in summer, the climatic conditions are rather unfavorable. There are excellent climatic conditions (TCI > 80) in several ten-day intervals of spring and autumn, while in summer more unpleasant but still very good (70 < TCI < 80) conditions prevail. However, in the last decade of July and in early August, TCI often falls below 70 (except Siófok) but it still refers to good conditions. In Thessaloniki, this can be observed as early as mid-June and it lasts till mid-August.

During the winter season, generally unfavorable and marginal conditions (30 < TCI < 50) occur. From the last ten days of February, the climatic conditions are getting acceptable (TCI > 50), which lasts until the end of November or early December. It is remarkable that the conditions of Thessaloniki are suitable for sightseeing almost all winter (TCI > 60) (*Fig. 6*).

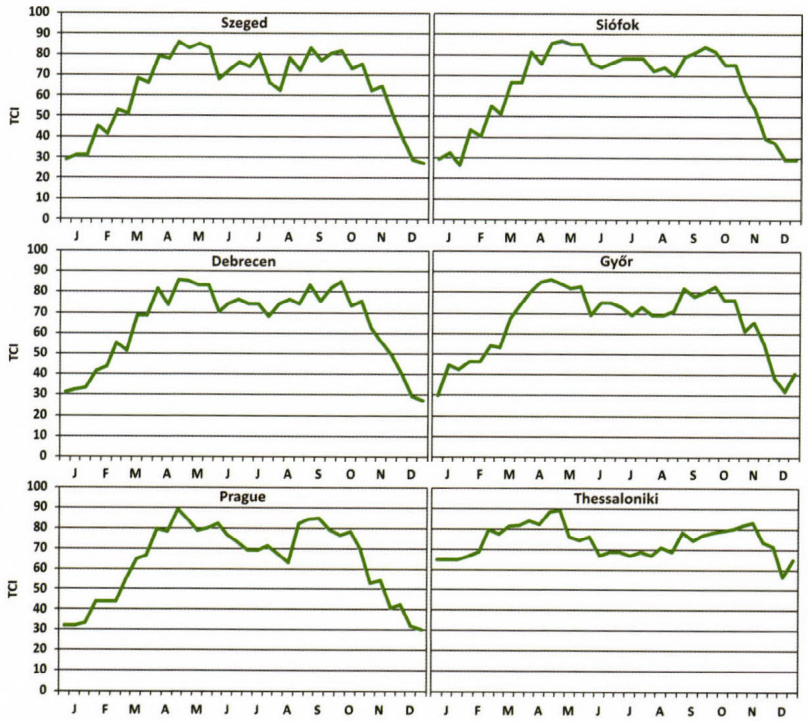

Fig. 6. Annual cycle of the modified ten-day TCI rating scores.

In order to analyze the differences between the cities and their possible causes in details, it is also necessary to examine the contribution of each sub-indices to the overall value of TCI (*Fig. 7*). It is obvious that the daily maximum PET sub-index (CId) is mainly responsible for the bimodal structure of TCI, because in the afternoon hours of summer ten-day intervals, when usually the maximum PET occurs, the prevailing heat stress (slight to strong stress conditions in *Fig. 2*) greatly reduces the rating scores in all cities, particularly in Thessaloniki. In summer and autumn, however, the average maximum values are closer to the comfort zone resulting higher rating scores. Furthermore, CId causes the plesant climate in winter in the Greek city (*Fig. 7*). In early August, a setback in CId in Szeged occurs, which is equal to the CId score of Thessaloniki. Therefore, overall TCI (62.2) barely indicates good climate in Szeged, and this warm load can particularly adversely affect the outdoor activities. It is interesting to note that the Greek city has somewhat higher TCI (66.6) in early August, which is caused by the higher average sunshine duration and lower precipitation conditions; however, the strong warm stress can reduce the comfort level of tourists to such an extent there, that this presumably cannot be fully compensated by the pleasant effects of sun and lack of rain.

The daily average PET (CIa) substantially contributes to TCI only from March to November in Hungary and Prague, while in the summer decades (in the Czech capital only in mid-summer) it falls into the comfort zone providing maximum score. In Thessaloniki, this is limited only to the second and third ten-day intervals of May, while in summer this sub-index indicates slight heat stress. However, CIa has significant effect also in the other periods, because it does not indicate such a level of cold stress conditions there as in the other cities (*Fig. 7*).

From May to August, relatively significant precipitation amount (R) is detected in terms of the ten-day averages in Hungary and Prague, which reduces tourism climatic conditions according to its rating system. Therefore, the contribution of precipitation is less in summer than in the other periods. Thus, in addition to CId, precipitation is also responsible for the bimodal structure shown in *Fig. 6*, even though it has smaller effect than CId because of its lower weight. Thessaloniki has very uneven distribution of rainfall, nevertheless, except in winter, less average precipitation can be detected compared to the other places, therefore it does not influence significantly the outdoor activities in most part of the year as shown in *Fig. 7*.

TCI score is increased the most obviously in summer and the least in winter by the sunshine (S). It should be noted that lower sunshine in Prague can affect adversely, while more hours of sunshine in the Greek city can influence favorably the attractiveness of the place. Significant differences cannot be explored in the averages of wind speed (W) during the year. Their rating scores are somewhat smaller in summer, but there are not any significant monthly or seasonal characteristics and differences between the cities (*Fig. 7*).

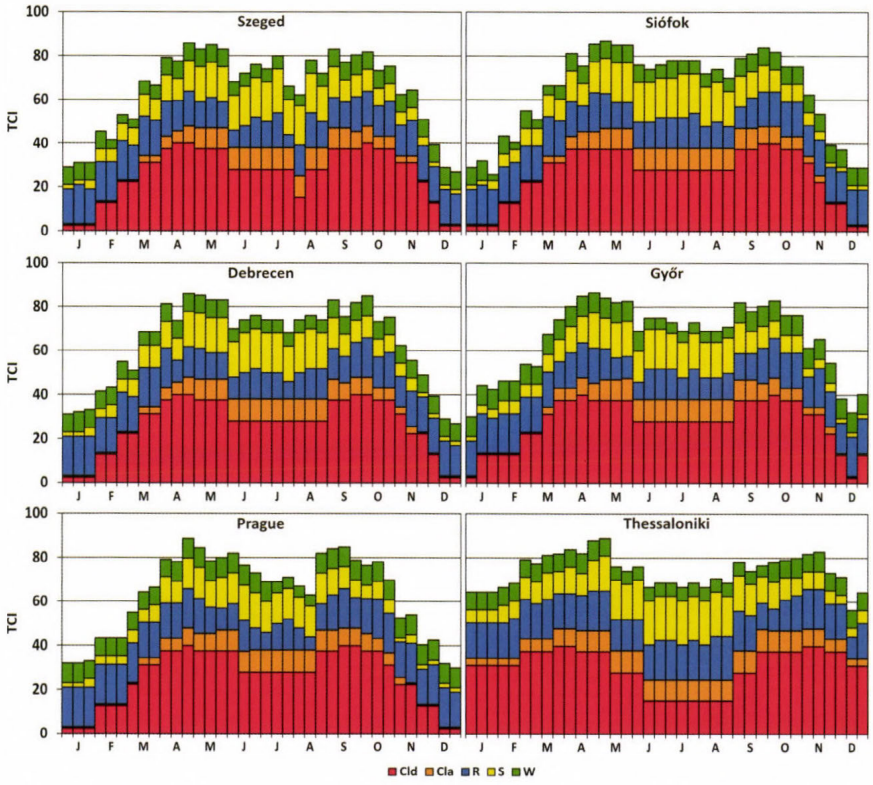

Fig. 7. Ten-day TCI sub-index rating scores (CId: daily maximum PET, CIa: daily mean PET, R: daily precipitation, S: daily sunshine duration, W: daily average wind speed).

4.2. Frequencies of TCI classes per ten-day intervals and seasonality

We have highlighted three distinctive threshold values of TCI (40, 60, 80), and the annual cycle of the average number of days (frequency) per ten-day interval above these thresholds was also investigated. As between the Hungarian cities there are not significant differences, the results are presented in case of Szeged, Prague, and Thessaloniki (*Fig. 8*). Climate is considered to be at least marginal/acceptable, good, and very good in terms of tourism above 40, 60, and 80, respectively.

In Szeged and Prague, all days are at least marginal (TCI > 40) from March to November, while this is valid for the whole year in Thessaloniki. In the distribution of the number of climatologically good days (TCI > 60), a bimodal structure can be recognized, particularly in Szeged. The Greek city has at least good days relatively uniformly throughout the whole year. The distribution of excellent days (TCI > 80) has some interesting characteristics, especially

regarding the time of occurence. Bimodal structure remains in all three places, but while excellent days also occur already from the end of winter until the end of autumn in the Greek city, this starts later and ends earlier in Szeged and Prague. It is remarkable that in the shoulder seasons, one more excellent days can be expected in Prague and Thessaloniki than in the Hungarian city. In the summer period, decline in the number of excellent days can be observed in all cities, but there are significant differences in their temporal occurences. For example, in Thessaloniki, it decreases quickly in spring and reappears only in early autumn, while in Szeged some excellent days occur also in summer. However, in Prague, these rather unpleasant conditions are limited to a very short period in summer: excellent days can be expected even in June and already at the end of summer (*Fig. 8*).

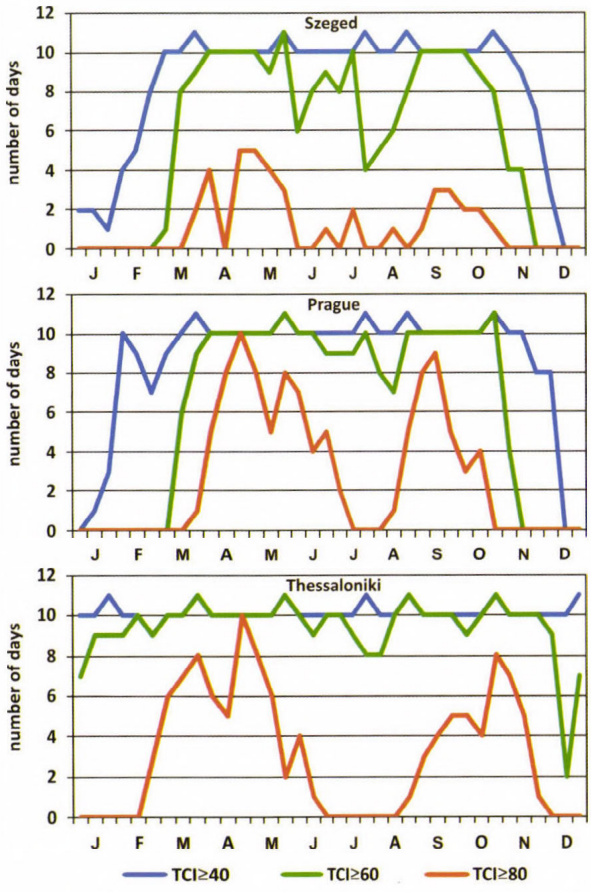

Fig. 8. Average number of days per ten-day interval above different TCI thresholds. At least marginal/acceptable, good, and excellent days are defined as having a TCI above 40, 60, and 80, respectively.

Fig. 9 illustrates the average relative frequencies of all TCI classes (see in *Table 3*) per ten-day interval resulted by the ratio of the average number of days belonging to a given class in a given ten-day interval and the number of days of that unit. According to *Fig. 9*, it can be definitely concluded that the best tourism climatic conditions in terms of the whole year can be observed in Thessaloniki, and the unpleasant climatic conditions occur most commonly in Szeged. In terms of ideal conditions, they appear the least frequently in Szeged and only in some periods of spring. In December and January, very and extremely unfavorable conditions can be often observed there. It should be noted that in summer acceptable and marginal conditions also appear in Szeged to a great extent besides the good categories, which indicates the frequent occurence of warm stress there. It can also be clearly detected that Thessaloniki has the most stable conditions in the whole year without significant diversities: there are almost only good, very good, and excellent days (*Fig. 9*).

The above findings and charts can be associated with the seasonality in tourism, which is one of the most worrisome yet least understood facets of the tourism industry (*Jang,* 2004). We used the "seasonality ratio" (SR), a simple indicator to measure the seasonality in tourism. SR expresses seasonality in a single value, therefore, it is easy to use in tourism climatology. It was initially defined in relation to the ratio of tourist flows (*Yacoumis,* 1980), and the concept was then applied in the context to climate resources characterized by TCI. It is calculated by simply dividing the mean number of good days (TCI > 60) per month by the number of good days in the month with maximum good days (the „best" month) (*Perch-Nielsen et al.,* 2010). The lower the value, the stronger the seasonality, while value 1 indicates equal distribution of good days across all months. We applied this concept in ten-day resolution. SR illustrated in *Fig. 9* indicates approximately moderate seasonality in Prague (SR=0.56) and a slightly higher seasonality in Szeged (SR=0.52) due to their winter and summer conditions. However, Thessaloniki is essentially free of seasonality (SR=0.85), therefore, its SR also confirms that this city offers relatively stable climatic conditions throughout the year.

5. Discussion and conclusions

The applied modifications of Tourism Climatic Index are an initial but significant step towards developing the index for use in Central European climatic conditions. By integrating the PET index into TCI, the thermal comfort sub-indices of TCI are based on more advanced knowledge of bioclimatology than in case of the original index. During the development of the rating system of PET, objective and international standards related to the evaluation of thermal environment were utilized. We assumed that the standardized relationship between the heat sensation of large number of persons evoked by thermal

environment, and their resulting satisfaction with the environment may be appropriate for the rating of the thermal environment of the tourists characterized by PET. The rating system of PET was derived based on this relationship, and the PET thermal sensation ranges used in Western and Central European climatic conditions were applied. By using ten-day averages instead of monthly ones, the climatic conditions can be described suiting better to tourists' length of stay during sightseeing.

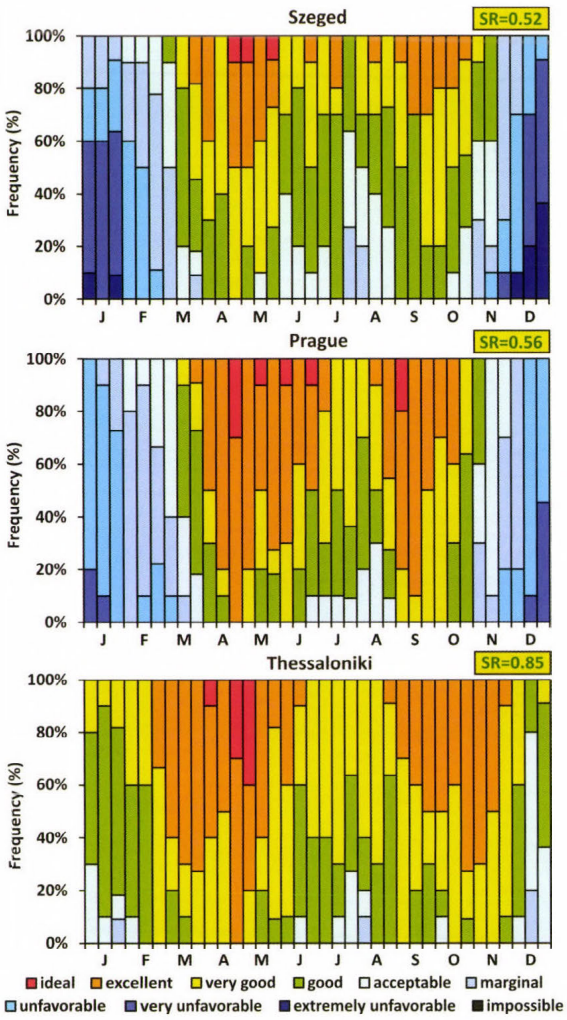

Fig. 9. Average relative frequencies of TCI categories per ten-day interval (see *Table 3* for details). SR indicates the "seasonality ratio".

Our results clearly show the optimal or even unfavorable periods for outdoor (sightseeing) tourism activities in a given place or the comparability of places in a given period. According to the bimodal structure of TCI, summer period has slightly less favorable climatic conditions in all six investigated cities mainly due to the heat load in the afternoon hours, therefore, the shoulder seasons may be the best times for sightseeing. Unlike the other places, in Thessaloniki, winter can also offer suitable climatic conditions. Between the four Hungarian cities only small differences are found, significant and characteristic differences can be detectable only in larger spatial scale. Considering the entire year, Thessaloniki is suitable for sightseeing activities throughout the year without significant seasonality, and it provides pleasant conditions most frequently. Szeged and Prague have higher seasonality and show unfavorable conditions more frequently, but except for winter, these cities are also appropriate for outdoor activities without any doubt, though in Szeged (moreover slightly in Prague, too) warm stress often can impair the level of thermal comfort and well-being of tourists in summer.

It should be noted that it is not sufficient to consider only the overall TCI itself, but it is desirable to analyze individually the contribution of all sub-indices. As an example, Thessaloniki has only a slightly less favorable conditions in summer according to its overall TCI, but if considering each sub-indices, PET sub-indices indicate worse thermal stress conditions by 1–2 categories compared to the other cities, which has a substantial negative impact on the comfort level and well-being of tourists. Presumably, these discomfort conditions cannot be fully compensated by the pleasant (physical-aesthetic) effects of more sunhine and less precipitation there.

During the analysis, basically three drawbacks of the index were identified which would, therefore, need to be changed in order to reflect more accurately and realistically the tourism climatic conditions. Firstly, the precipitation sub-index – particularly in case of convective rainfall – substantially distorts the value of TCI in some ten-day intervals in the calculation of the many-year and ten-day averages, therefore it has such a low rating score compared to other intervals that it rates too unfavorably and unrealistically the climatic conditions. Moreover, such heavy but short rainfalls usually do not have a great effect from a tourist perspective. Some annual differences in rating scores of precipitation can be noticed due to the definite maximum amount in summer and minimum in winter. Nevertheless, if possible, it would be worth changing the applied precipitation variable and its rating system.

Secondly, in the structure of the original TCI, wind speed is rated by means of different scales depending on the value of average maximum temperature and wind speed (as seen in *Table 2*). In case of very cold conditions and high wind speeds, a wind chill rating system has to be used but its rating scores downgrade significantly the relevant ten-day intervals compared to the others. We used this original rating system in this study, but it was developed mainly according to the

thermal effects of wind, which is already expressed by PET in our study, therefore, rather the physical (mechanical) effects of wind should be taken into account in a modified and simplified rating system.

Finally, it would be reasonable to exclude the night hours from the study currently covering the whole day due to the negligible tourist activities at night and to use only the daytime periods, for example the hours between the average sunrise and sunset. Nevertheless, as after sunset the tourist activities often remain significant for a few hours, particularly in summer, this period after sunset would worth being investigated separately.

Our further analysis will be directed to the application of new PET thermal sensation ranges according to an outdoor field survey revealing subjective estimations of thermal environment carried out in Szeged, south Hungary (*Kántor et al.*, 2012). As it is expected, it will provide information on the differences in bioclimatic and tourism climatic conditions of European places for travellers visiting these places but living in south Hungary, therefore accustomed to the thermal conditions prevailing there. By means of the ranges reflecting the thermal sensation of the south Hungarian people, we can compare the results based on the original and new ranges.

References

Amelung, B. and *Viner, D.*, 2006: Mediterranean tourism: exploring the future with the tourism climatic index. *J. Sustainable Tour. 14,* 349–366.

ASHRAE, 1972: Handbook of fundamentals. American Society of Heating, Refrigerating and Air-Conditioning Engineers, Inc., New York

ASHRAE, 2004: Thermal environmental conditions for human occupancy. ASHRAE Standard 55-2004. American Society of Heating, Refrigerating and Air-Conditioning Engineers, Inc., New York

De Freitas, C.R., 2003: Tourism climatology: evaluating environmental information for decision making and business planning in the recreation and tourism sector. *Int. J. Biometeorol. 48,* 45–54.

De Freitas, C.R., Scott, D. and *McBoyle, G.*, 2008: A second generation climate index for tourism (CIT): specification and verification. *Int. J. Biometeorol. 52,* 399–407.

Fanger, P.O., 1972: *Thermal Comfort*. McGraw Hill Book Co., New York

Houghten, F.C. and *Yaglou, C.P.*, 1923: Determining equal comfort lines. *J. Am. Soc. Heat. Vent. Eng. 29,* 165–176.

Höppe, P., 1999: The physiological equivalent temperature – an universal index for the biometeorological assessment of the thermal environment. *Int. J. Biometeorol. 43,* 71–75.

ISO, 2005: Ergonomics of the thermal environment – Analytical determination and interpretation of thermal comfort using calculation of the PMV and PPD indices and local thermal comfort criteria. ISO 7730:2005(E), ISO copyright office, Geneva

Jang, S., 2004: Mitigating tourism seasonality: A quantitative approach. *Ann. Tour. Res. 31,* 819–836.

Kántor, N., Égerházi, L. and *Unger J.*, 2012: Subjective estimation of thermal environment in recreational urban spaces – Part 1: investigations in Szeged, Hungary. *Int. J. Biometeorol. 56,* 1075–1088.

KSH, 2012: Magyarország számokban 2011. Központi Statisztikai Hivatal, Budapest. (In Hungarian)

Matzarakis, A. and *Mayer, H.,* 1996: Another kind of environmental stress: thermal stress. *WHO Newsletter 18,* 7–10.

Matzarakis, A., 2006: Weather- and climate-related information for tourism. *Tourism Hospit. Plann. Dev. 3,* 99–115.

Matzarakis, A., Rutz, F. and *Mayer, H.,* 2007: Modelling radiation fluxes in simple and complex environments – application of the RayMan model. *Int. J. Biometeorol. 51,* 323–334.

Mayer, H. and *Höppe, P.,* 1987: Thermal comfort of man in different urban environments. *Theor. Appl. Climatol. 38,* 43–49.

Mieczkowski, Z.T., 1985: The tourism climatic index: a method of evaluating world climates for tourism. *Can. Geogr. 29,* 220–233.

Németh, Á., 2013: Estimation of tourism climate in the Lake Balaton Region, Hungary. *J. Environ. Geography 6,* 49–55.

Perch-Nielsen, S.L., Amelung, B. and *Knutti, R.,* 2010: Future climate resources for tourism in Europe based on the daily Tourism Climatic Index. *Climatic Change 103,* 363–381.

Scott, D. and *McBoyle, G.,* 2001: Using a 'tourism climate index' to examine the implications of climate change for climate as a natural resource for tourism. In (*Matzarakis, A.* and *de Freitas, C.R* (Eds.)) Proceedings of the First International Workshop on Climate, Tourism and Recreation, International Society of Biometeorology, Commission on Climate, Tourism and Recreation, Halkidi, Greece, 5–10 October 2001, 69–88.

Scott, D., McBoyle, G. and *Schwartzentruber, M.,* 2004: Climate change and the distribution of climatic resources for tourism in North America. *Climate Res. 27,* 105–117.

Scott, D., Gössling, S. and *de Freitas, C.R.,* 2008: Preferred climates for tourism: case studies from Canada, New Zealand and Sweden. *Climate Res. 38,* 61–73.

Steadman, R.G., 1979: The assessment of sultriness. Part I: A temperature-humidity index based on human physiology and clothing Science. *J. Appl. Meteorol. 18,* 861–873.

VDI, 1998: Methods for the human-biometeorological assessment of climate and air hygiene for urban and regional planning. Part I: Climate. VDI 3787, Part 2. Beuth, Berlin

Yacoumis, J., 1980: Tackling seasonality: The case of Sri Lanka. *Int. J. Tourism Manag. 1,* 84–98.

Yu, G., Schwartz, Z. and *Walsh, J.E.,* 2009: A weather-resolving index for assessing the impact of climate change on tourism related climate resources. *Climatic Change 95,* 551–573.

Zaninović, K., Srnec, L., Patarčić, M., Perčec Tadić, M., Mika, J. and *Németh, Á.,* 2010: Influence of climate change on summer tourism potential in the Pannonian basin. In (*Matzarakis, A., Mayer, H.* and *Chmielewski, F-M.* (Eds.)) Proceedings of the 7th Conference on Biometeorology, 12–14 April 2010, Freiburg, Germany. *Berichte des Meteorologischen Instituts der Albert-Ludwigs-Universität Freiburg 20,* 336–341.

IDŐJÁRÁS

Quarterly Journal of the Hungarian Meteorological Service
Vol. 118, No. 2, April – June, 2014, pp. 167–191

Long-term trend of deposition of atmospheric sulfur and nitrogen compounds in Hungary

Andrea Móring*[1,2,3] and **László Horváth**[4]

[1]*University of Edinburgh*
The King's Buildings, Crew Building, West Mains Road,
Edinburgh, EH9 3JN, United Kingdom

[2]*Centre for Ecology and Hydrology, United Kingdom*
Bush Estate, Midlothian, Penicuik, EH26 0Q, United Kingdom

[3]*Hungarian Meteorological Service*
Kitaibel P. u. 1, H-1024 Budapest, Hungary

[4]*Hungarian Meteorological Service*
Gilice tér 39, H-1181 Budapest, Hungary

Corresponding author E-mail: a.moring@sms.ed.ac.uk

(Manuscript received in final form April 11, 2014)

Abstract—Acidification caused serious environmental problems over Europe in the 70's and 80's. The signs of the phenomenon were observed also in Hungary. However, a comprehensive assessment of acidic deposition on long term has not been carried out yet. Therefore, the purpose of this study is to assess the degree of this process and to investigate its long-term change in Hungary based on deposition time series for oxidized sulfur, oxidized nitrogen, and reduced nitrogen compounds. To achieve our goal, we used existing results of atmospheric chemistry transport models, and precipitation chemistry as well as background air pollution measurements at the Hungarian K-puszta site. Comparing the results with national emission datasets, we also made an attempt to interpret the changes in depositions. According to our time series (oxidized sulfur: 1880–2011, oxidized nitrogen: 1982–2012, reduced nitrogen: 1981–2012), the effect of acidification was most likely to intensify before 1980. Since then, the phenomenon presumably has been weakening gradually. In the case of oxidized sulfur and nitrogen compounds, transboundary transport has to be considered while comparing them to depositions. On the other hand, the impact of Hungarian industrial recession as well as the improvement of emission abatement techniques and national emission controlling measures can be observed not just on the emissions, but depositions as well. Moreover, we found that the atmospheric concentration and subsequent deposition of ammonia is strongly affected by the atmospheric concentration of sulfur dioxide, which highlights the need for further refinement of the estimation method for yearly dry deposition of ammonia.

Keywords: acidic deposition, long-term, oxidized nitrogen, oxidized sulfur, reduced nitrogen, ammonia, atmospheric concentration, emission, emission reduction.

1. Introduction

The problem of acidification got wider public and scientific attention at first in the beginning of the 70's, when the reason for the serious damage of Scandinavian lakes and German forests was identified: the decreasing pH of freshwaters and soil (*Almer et al.*, 1974; *Sakamoto et al.*, 1986). It was found that the phenomena had been caused by the excessive emission and subsequent deposition of oxidized sulfur (sulfur dioxide, SO_2 and sulfate, SO_4^{2-}) and oxidized nitrogen compounds (nitric acid, HNO_3, nitrogen oxides, NO_x and nitrate, NO_3^-) (see the quoted references in *Galloway*, 1989). Since then, the problem has been considerably mitigated over Europe, owing to a series of emission control measures (*Grennfelt* and *Hov*, 2005). However, it has been a more and more serious environmental issue in the developing countries of Asia, especially in China (*Duan et al.*, 2013).

The process that leads to acidification consists of three main steps: i) emission of acidifying components or their precursors, ii) their atmospheric transport, simultaneous chemical conversion, phase transition to particles, iii) deposition to the surface. The main source for oxidized sulfur as well as nitrogen compounds is anthropogenic. Most of the oxidized sulfur compounds are emitted during the combustion of fossil fuels (*Seinfeld* and *Pandis*, 2006). These usually contain a certain amount of sulfur, which is oxidized to SO_2 during burning. The primary emission sectors of the oxidized nitrogen compounds are transportation and energy industry (see the same reference). In both cases, nitrogen content of the air is oxidized mainly to nitric oxide (NO) and in smaller amount to nitrogen dioxide (NO_2) at the high burning temperature.

In addition, reduced nitrogen compounds (ammonia, NH_3, and ammonium, NH_4^+) are considered as additional exacerbating factors for acidification. In the soil during nitrification, NH_4^+ ions are oxidized while two equivalent hydrogen-ions (H^+) are produced (*Raven*, 1985). In freshwater ecosystems, algae and macrophyte species release equivalent H^+ when NH_4^+ is consumed (*Goldman* and *Brewer*, 1980). Therefore, further sources must be considered for acidifying components. The largest emission sector of reduced nitrogen compounds is agriculture, releasing gaseous NH_3 to the atmosphere. The primarily source of NH_3 is the breakdown of urea in livestock excreta, but a similar process takes place in the case of urea- and ammonium-based fertilizers as well.

There are two ways for an atmospheric compound to get back to the surface from the atmosphere: by wet or dry deposition. Wet deposition occurs when the compound is washed out from the atmosphere by being dissolved in precipitation, whilst during dry deposition, the substance is transported to the surface by the turbulent flux.

In the atmosphere, SO_2 and NO_x compounds are further oxidized to sulfurous acid (H_2SO_3) and sulfuric acid (H_2SO_4), as well as nitrous acid

(HONO) and nitric acid (HNO_3), respectively. The produced acidic components may be neutralized by dissolved NH_3, forming aerosol particles. These usually act as condensation nuclei; therefore, they can be easily washed out of the atmosphere by precipitation. In addition, during droplet growing as well as rainfall, acidic species and gaseous SO_2 and NH_3 may also dissolve to the droplets. Dry deposition of acidifying compounds is possible as gas molecules as well as in the form of aerosol particles. Deposition of NH_3 and SO_2 in this way is closely related and largely dependent on the pH of the surface wetness (*Flechard et al.*, 1999).

The distance, from the source the atmospheric trace compounds can be transported to, besides meteorological conditions, is basically determined by their atmospheric lifetime. Calculating with a lifetime of 2 days (172 800 s) for SO_2 (*Seinfeld* and *Pandis*, 2006) and an average wind speed of 3 m s^{-1} at 2 m height, the result is more than 500 km. The lifetime of NO_x as well as NO_3^-, SO_4^{2-}, and NH_4^+ aerosols usually ranges also from a few days to weeks, which raises the problem of transboundary air pollution. On the other hand, as a result of their high solubility and reactivity, NH_3 and HNO_3, depending on the surface characteristics and micrometeorological conditions, especially at higher air temperature and lower humidity when dissociation of ammonium nitrate particles into gases is dominant (*Stelson* and *Seinfeld*, 1982), can have a lifetime of a few hours, causing local rather than regional problems.

Beside the damage of surface water and forest ecosystems, high concentration of acidic components can have a severe impact also on human health through inhaling the respirable, fine fraction of formed aerosols (*Pope et al.*, 2002). In addition, in the 70's and 80's, erosion of buildings and statues by "acid rain" was reported (*Lipfert*, 1987). Despite serious acidification caused mainly by excessive emission of SO_2 (*Johnson* and *Reuss*, 1984) has been largely mitigated over Europe, the environmental effect of reactive nitrogen compounds (N_r), such as NH_3, HNO_3, and NO_x, has been still in the focus of scientific research projects (e.g., GRAMINAE, NitroEurope, ENA, ÉCLAIRE). *Sutton et al.* (2011) identified five key threats related to excessive N_r emissions: water quality, air quality, greenhouse balance due to the aerosol particles, ecosystems and biodiversity, and soil quality.

Signs of acidification occurred also in the country: yield reduction of crops, potential forest damage, especially in synergy with other biotic factors, corrosion of historic monuments, and deformation of building ornaments made of limestone were reported (*Várallyay et al.*, 1986; *OKTH/MTA*, 1987). Since then, the impact of acidic compounds, similarly to the whole European region, has been weakening in the country.

Although *Horváth et al.* (2009) published time series of measured atmospheric concentration and wet deposition of NH_3 and NH_4^+ for the period of 1981–2005 for a Hungarian site, for the country a comprehensive assessment of acidic deposition on long term has not been carried out yet. Therefore, the

purpose of this study is to assess the degree of this process and to investigate its long-term change in Hungary based on deposition time series for oxidized sulfur, oxidized nitrogen, and reduced nitrogen compounds. The data sets were compiled from existing atmospheric chemistry transport model results and air concentration as well as precipitation chemistry data measured at the Hungarian K-puszta site.

2. *Methods and data*

2.1. Oxidized sulfur compounds

The long-term deposition data set for oxidized sulfur compounds were compiled from existing results from different versions of the atmospheric chemistry transport model (ACTM) ran by the European Monitoring and Evaluation Programme (EMEP) under the Convention on Long-range Transboundary Air Pollution (CLRTAP). An ACTM calculates atmospheric concentration and deposition fields for a given time and grid from predefined emission fields. Driven by a meteorological model it is capable of simulating the horizontal and vertical transfer of atmospheric trace compounds, as well as the mixing of the different pollutants and the possible chemical reactions between them.

EMEP is a policy driven program for international co-operation to solve transboundary air pollution issues. The model results from their ACTM are used by policy makers Europe-wide. EMEP consists of five Centers and four Task Forces. Among them, the Meteorological Synthesizing Centre-West (MSC-W) is responsible for the modeling of acidifying and eutrophying air pollutants, photochemical oxidants, and particulate matter.

The first part of our deposition data set, for the period 1880–1980, originates from a model experiment (*Mylona*, 1992) for 1880–1991 with an early version of the EMEP model (*Sandnes* and *Styve*, 1992). *Mylona* determined the required SO_2 emission fields based on historical energy and industry statistics. The effect of meteorological variability was disregarded in the experiment, meteorological data for 1991 were used for every year. Depositions were simulated over the 150×150 km^2 EMEP grid, for every fifth year.

From the year 1980 we obtained model results, derived from later versions of the EMEP model, from the open database of MSC-W (*EMEP/MSC-W*, 2013). The main differences compared to the version used by *Mylona* are that these operate on a higher resolution grid (50×50 km^2), and in every year the meteorological data for the given year were fed to the model (for detailed description of the different model versions see the references at *EMEP/MSC-W*, 2013). The data to the second part of our deposition time series, for the period 1980–2011, are originating from the following model versions:

- version rv4.4: for the years 1990, 2000–2011,
- version rv2.5: for the years 1995–1999,
- version rv2.1: 1980, 1985.

During personal communication, Sophia Mylona provided us her model results for the four 150×150 km^2 grid cells in which the fraction of Hungarian area are the largest (the shaded cells in *Fig. 1*). To keep the consistency of the deposition data set for the whole period (1880–2011), we downloaded the gridded version of the model results from the MSC-W database, and then selected the 36 pieces of 50×50 km^2 grid cells covered by the four grid cells provided by Sophia Mylona. All the deposition data were given as flux; therefore, to get the total deposited sulfur over the grid cells, we multiplied the fluxes by the corresponding grid area. According to *Kugler et al.* (2014), the background air pollution in Hungary can be considered homogenous. Therefore, to get country scale depositions, we up-scaled the grid depositions (for 4×150×150=90,000 km^2) for the area of Hungary (93,036 km^2).

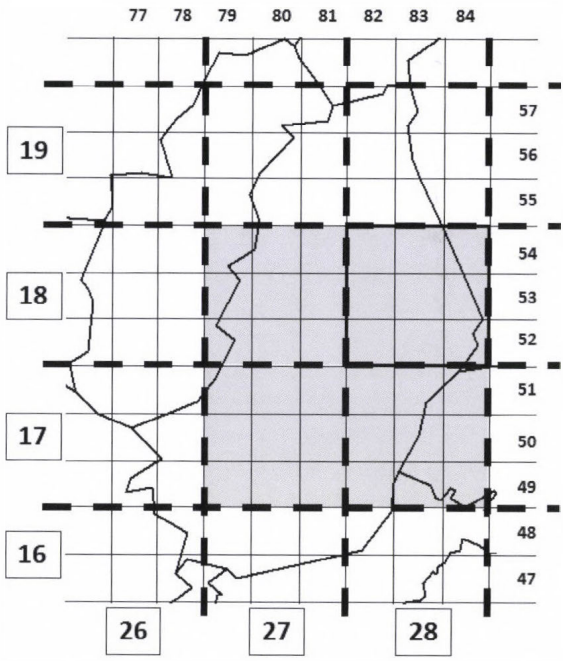

Fig. 1. Hungary on the new EMEP grid with 50×50 km^2 resolution (solid lines), and on the old EMEP grid with 150×150 km^2 resolution (dashed lines). Plain numbers and numbers in boxes indicate the EMEP coordinates for the new and the old grid, respectively. For our sulfur deposition calculations, the shaded grid cells were used from both grids.

2.2. *Oxidized and reduced nitrogen compounds*

The longest available Hungarian atmospheric chemistry data set for oxidized and reduced nitrogen compounds can be obtained from the measurement data base of the Hungarian precipitation chemistry and background air pollution monitoring network maintained by the Hungarian Meteorological Service (HMS). Among the stations of the network, K-puszta has the longest measurement time series; it has been operating since 1974. Therefore, we choose it as the base of our further investigations.

K-puszta (46°58' N, 19°33' E, 136 m a.s.l.) is situated on the Hungarian Great Plain, in the clearing of a mixed coniferous-deciduous forest, far from main anthropogenic emission sources. The site is a part of the network of the Global Atmospheric Watch (GAW) and the EMEP. The starting year of the available data sets for atmospheric concentration and rainwater chemistry (including also precipitation sums) can be seen in *Table 1.*

Table 1. Starting year of the measurements of concentration in air and in precipitation of the depositing nitrogen compounds at K-Puszta station

	Oxidized nitrogen compounds	**Reduced nitrogen compounds**
Atmospheric concentrations	NO_2 : 1974	NH_4^+: 1977
	NO_3^- : 1977	NH_3 : 1981
	HNO_3: 1982	
Concentration in the rain water	NO_3^- : 1974	NH_4^+: 1974

As we attempted to assess the country scale deposition of nitrogen compounds on the base of a single station's measurements, we kept the data in the form of fluxes, rather than calculating the total mass of deposited nitrogen over the country. For simplicity's sake, in the following we will refer to only deposition without 'flux'. We calculated the total deposition as a sum of dry and wet deposition. Calculation of dry deposition was carried out by the inferential method using Eq. (1) for both oxidized and reduced N-compounds:

$$F_{dry} = \sum_i F_{dry,i} = \sum_i c_{air,i} v_{d,i} f \,, \tag{1}$$

where

- F_{dry} – total yearly deposition flux of oxidized/reduced nitrogen compounds (g N m^{-2} $year^{-1}$),

- $F_{dry,i}$ – yearly dry deposition of the oxidized/reduced compound i (g N m^{-2} $year^{-1}$),
- $c_{air,i}$ – yearly average air concentrations of the oxidized/reduced nitrogen compound i (μg N m^{-3}),
- $v_{d,i}$ – yearly average dry deposition velocity of the oxidized/reduced nitrogen compound i (cm s^{-1}), and
- f – conversion factor between the different units (3.1536×10^{-1}).

According to its definition (Eq. (2), *Seinfeld* and *Pandis*, 2006), dry deposition velocity is the reciprocal of the sum of the resistances between the atmosphere and the surface. These are the aerodynamic resistance (R_a), the resistance of the quasi-laminar layer (R_b), and the bulk canopy resistance (R_c). Whilst R_a and R_b account for the atmospheric turbulence, R_c expresses for a given trace substance the absorbing or adsorbing capacity of the canopy that covers the surface. Therefore, v_d is a function of the actual micrometeorological conditions, and it strongly depends on the surface characteristics. For our yearly estimations, however, we used constant yearly average deposition velocities, collected from the literature for selected land-cover types.

$$v_d = \frac{1}{R_a + R_b + R_c}. \tag{2}$$

For both oxidized and reduced compounds we gave estimation for dry deposition on grass, and in the case of oxidized compounds, we calculated it also for mixed land-cover types (grass, forest, arable, urban), giving a closer approach for dry deposition on country level. The same could not been carried out for reduced nitrogen compounds due to the relatively rare occurrence of NH_3 and NH_4^+ dry deposition velocity values in the literature. All the applied dry deposition velocities can be seen in *Table 2*. Data for oxidized nitrogen compounds are originating from the deposition velocity inventory compiled by *Marner* (2003). To get the dry deposition velocities for mixed land coverage, we averaged the data for every oxidized compound using the land-cover fractions (*Table 3*) from the CORINE CLC-50 database over Hungary as weights.

The steps of calculation of yearly wet deposition are described in Eqs. (3), (4), and (5). Daily wet deposition of oxidized and reduced nitrogen compounds can be calculated as a product of the amount of daily precipitation (p_i, dm^3 m^{-2} day^{-1}) and the concentrations of NO_3^- and NH_4^+ ions measured in precipitation samples ($c_{aq,i}$, mg N dm^{-3}), respectively. Summed up these for a month (Eq. (3)), one can get the monthly wet deposition ($F_{wet,j}$, mg N m^{-2} $month^{-1}$).

Table 2. Applied yearly average dry deposition velocities for reduced and oxidized nitrogen compounds (latter from the inventory by *Marner* (2003)) for different surface types, their references and - where applicable – their weighted average, as used in our dry deposition calculations for mixed vegetation (for the weights see *Table 3*)

Compound	Deposition velocity (cm s^{-1})				
	Grass	Arable	Forest	Urban	Weighted average
NH_3	0.99 (*Horváth et al.*,2005)	–	–	–	–
NH_4^+	0.087 (*Gallagher et al.*,2002)				
NO_2	0.16 (*Nicholson et al.*, 2001)	0.16 (*Nicholson et al.*, 2001)	0.26 (*Puxbaum and Gregori*, 1998)	0.08 (*Nicholson et al.*, 2001)	0.17
HNO_3	1.39 (*Marner*, 2003)	2.06 (*Marner*, 2003)	7.33 (*Marner*, 2003)	7.33 (*Marner*, 2003)	3.81
NO_3^-	0.15 (*Slinn*, 1982)	0.26 (*Davidson et al.*, 1982)	1.78 (*Ruijgrok et al.*, 1997)	1.78 (*Ruijgrok et al.*, 1997)	0.77

Table 3. Area of the different land cover types over Hungary and their fraction in the total area of the country, used as weights in our dry deposition calculations

	Grasslands		Forest			Arable	Urban
	Semi-natural	Pasture	Deciduous	Mixed	Coniferous		
Area (10^{10} m^2)	0.58	0.39	1.55	0.08	0.16	5.12	1.42
Fraction	10.43%			19.25%		55.05%	15.27%

The variability of the time series derived in this way is influenced by that of the monthly precipitation amount. According to *Horváth* (1978), there is a positive, strong and significant relationship between the monthly amount of precipitation and the monthly wet deposition. Same was true for our datasets (*Fig. 2*). Based on this, we normalized the monthly wet deposition values applying Eq. (4), where a and b are the slope and the intercept of the regression line, respectively (*Fig. 2*), p_j is the monthly precipitation, and $F_{wet,ave}$ is the wet deposition with the long-term average monthly precipitation (for the values of a, b, and $F_{wet,ave}$ see *Table 4*). Finally, to get the yearly wet deposition (F_{wet}, mg N m^{-2} $year^{-1}$), we summed up the normalized monthly values ($F_{wet,j}^{norm}$ mg N m^{-2} $month^{-1}$) for a year (Eq. (5)).

$$F_{wet,j} = \sum_i c_{aq,i} p_i, \tag{3}$$

$$F^{norm}_{wet,j} = F_{wet,ave} \frac{F_{wet,j}}{ap_j + b}, \tag{4}$$

$$F_{wet} = \sum_{j=1}^{12} F^{norm}_{wet,j}. \tag{5}$$

After calculating the total deposition ($F_{total}=F_{wet}+F_{dry}$) for both the oxidized and reduced nitrogen compounds, to get the total nitrogen load we summed up the two total deposition values over grass. To characterize the change in all of the resulted nitrogen time series, we fitted trends to them. The trends with the best fit were determined by applying the Akaike information criterion (AIC, *Sakamoto et al.*, 1986), as a built-in function in the statistical programming language R.

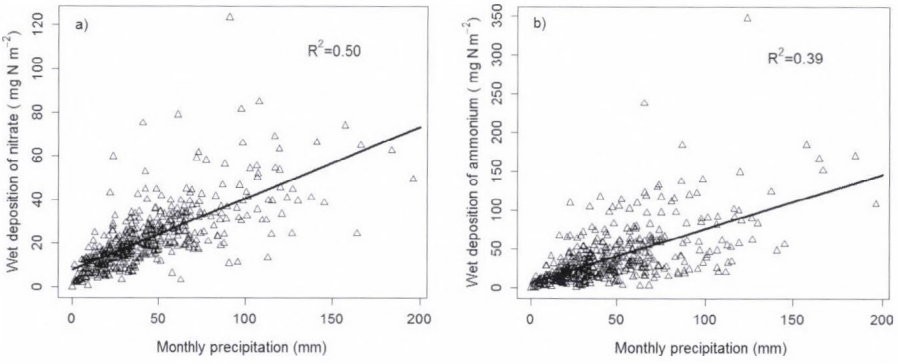

Fig. 2. Regression between monthly precipitation and wet deposition of nitrate (a) and ammonium (b) over the period 1974-2012 at K-puszta. R^2 indicates the square of correlations between the datasets.

Table 4. Parameters of the regression between the monthly precipitation and monthly wet deposition of nitrogen species, where p_{ave} (mm) is the long-term average of the monthly precipitation values, a (mg N dm^{-3} month^{-1}) is the slope, b is the intercept (mg N m^{-2} month^{-1}), and $F_{wet,ave}$ ($a \times p_{ave}+b$) is the wet deposition with the average monthly precipitation (mg N m^{-2} month^{-1})

Ions	p_{ave}	a	b	$F_{wet,ave}$
NH_4^+	44.3	0.70	5.92	36.9
NO_3^-		0.33	7.90	22.4

2.3. Further data sources

During the interpretation of our results, we used further data sources. In the case of oxidized sulfur compounds, we compared the deposition time series to a national emission time series compiled from the historical emission database of A.S.L. & Associates (*Lefohn et al.*, 1999) for the period 1880–1990 and from emissions reported to the EMEP (*CEIP*, 2013) for the period 1990–2011. The emission data obtained from the open database of A.S.L. & Associates (*A.S.L. & Associates*, 1999) are in a good agreement with the emissions published by *Mylona* (1992); however, for illustration purposes the A.S.L. data set is better, as it has a finer, yearly temporal resolution compared to the 5-year resolution of the data set by *Mylona*.

The deposition of oxidized nitrogen species were compared to the national NO_x emissions reported to EMEP that are available in the emission database of EMEP for the period of 1980–2011. In addition, we refined our comparison with data for the total number of cars in Hungary for 1974–2011, from the freely available database (*KSH*, 2013) of the Hungarian Central Statistical Office.

To interpret our results for NH_3 and NH_4^+ depositions, we compiled a national NH_3 emission dataset from *Horváth et al.* (2009) (for 1980–2005) and from the EMEP database (for 2006–2011). As deposition of SO_2 and NH_3 has a strong relationship, for further investigations we calculated also the average yearly SO_2 surface concentrations based on the daily HMS measurements at K-puszta.

3. Results

3.1. Time series of oxidized sulfur compounds

Between 1880 and 1950, deposition of oxidized sulfur compounds over Hungary showed a moderate increase (*Fig. 3*), which was interrupted only by World War II. Over this period, sulfur deposition was mainly under 100 Gg S $year^{-1}$, except in 1940, when it slightly exceeded this limit. From 1950, sulfur deposition was intensifying until it peaked at 381 Gg S $year^{-1}$ in 1980. In the last three decades deposition has been decreasing. Since 2005, the values has been under 100 Gg $year^{-1}$ again.

The emission time series (*Fig. 4*) is very similar to that of the deposition. However, also differences can be noticed between the two time series. In 1880–1950, the increase of emission was not as steady as that of the deposition. Despite it reached its maximum in 1940, there were several other substantial peaks and lows over this period, including a clear minimum after World War II. For this difference more explanations are feasible.

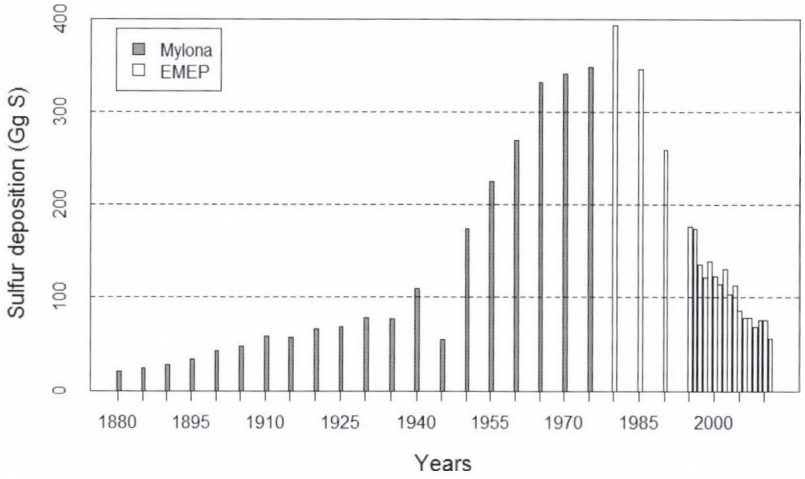

Fig. 3. Sulfur deposition over Hungary between 1880 and 2011 compiled from the two data source: *Mylona* (1992) and the EMEP database (*EMEP/MSC-W*, 2013).

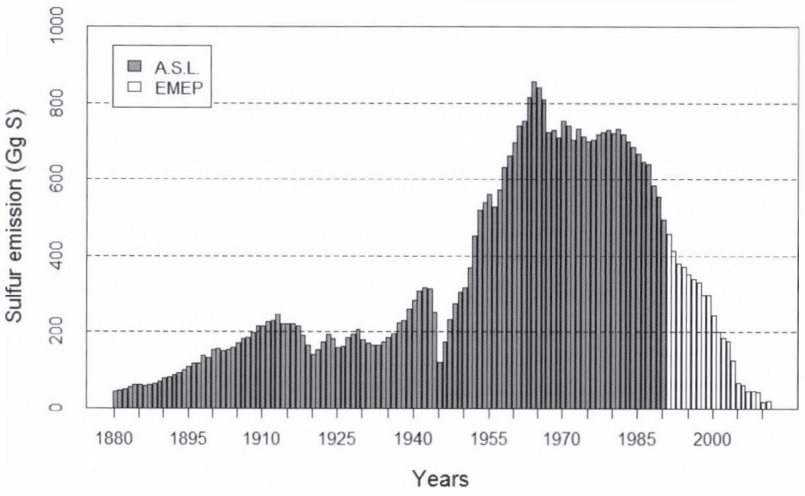

Fig. 4. Sulfur emission in Hungary between 1880 and 2011 compiled from the two data source: *A.S.L. & Associates* (1999) and the EMEP emission database (*CEIP*, 2013).

Firstly, over this period for deposition modeling another emission data set was used. On the other hand, the relationship between emission and deposition of oxidized sulfur compounds on country scale is not linear, as due to their long atmospheric lifetime, their atmospheric transport is transboundary. Consequently, not all of the sulfur emitted in Hungary deposits over the country, and similarly, a part of the deposited sulfur originates from the neighboring countries. As a consequence, even an intense increase in national emission can lead to a more moderate change in national depositions.

Emission reached its absolute maximum in 1964, 16 years earlier than deposition. Same is true for the emission dataset published and used in the model runs by *Mylona* (1992) (not presented here): the most sulfur was emitted in 1960. This could imply that the later maximum in deposition is a result of the imperfect match of the two deposition data sets. However, in the whole deposition time series derived by *Mylona* for 1880–1991, the highest value occurred also in 1980. The difference can be explained only by the above described phenomena of transboundary air-pollution, i.e., the emission tendencies on a larger scale in Europe suppressed the local emission trends. This is supported by the European total emission time series by *Mylona*, that shows an absolute maximum in 1980, at the same time with the highest deposition in Hungary.

It is difficult to qualify the strength of acidification, because it depends, among others, on the buffering capacity of the surface. However, based on the observations – the higher deposition, the stronger the effect of acidification – it can be concluded that during 1950–1980, Hungary was the most exposed to the harmful effects of acidification triggered by the deposition of oxidized sulfur compounds. In the last 3 decades, sulfur emissions has been reducing presumably due to the recession of Hungarian industry as well as the more conscious handling of European industrial emissions as a result of – among other international conventions on air pollution – the 1979 Geneva Convention on Long-range Transboundary Air Pollution. Consequently, the oxidized sulfur deposition has been also decreasing over the last 30 years, possibly leading to gradually weakening acidification.

3.2. Oxidized nitrogen compounds

The wet deposition of oxidized nitrogen compounds (*Fig. 5*) in the period of 1974–2012 ranged between 150 and 350 mg N m^{-2}, except in 1975, when it reached an extreme high value of 446 mg N m^{-2}. Two waves of the tendency can be distinguished: one in 1974–1998 with the highest values during the middle of the 80's, and another from 1998 to 2012 with the largest values in the middle of the last decade. However, the fitted 2nd order polynomial trend shows a steady decline over the whole period (for a summary of our results for nitrogen species see *Table 5*).

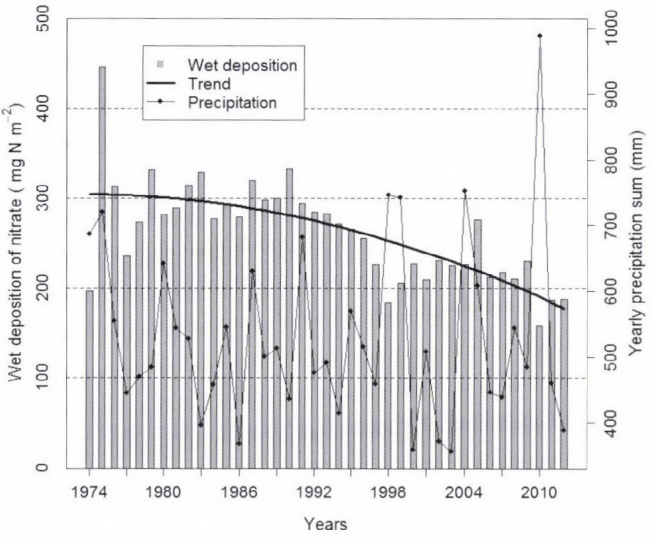

Fig. 5. Wet deposition of oxidized nitrogen compounds between 1974 and 2012 at K-puszta, the best fit line, and the yearly precipitation sum.

Table 5. Summary of our results for the deposition time series of the nitrogen compounds, with their starting year (the last year was 2012 in every case) and the order of the best fit trends

Compounds	**Deposition**	**Beginning of the time series**	**Order of the fitted trend**
Oxidized nitrogen compounds	Wet	1974	2
	Dry[g]	1982	4
	Dry[m]	1982	1
	Total[g]	1982	4
	Total[m]	1982	1
Reduced nitrogen compounds	Wet	1974	3
	Dry[g]	1981	4
	Total[g]	1981	1
Total nitrogen load[g]		1982	1

[g] calculated for grass, [m] calculated for mixed vegetation

For grass the dry deposition ranged from 200 to 500 mg N m^{-2}, whilst for mixed vegetation it varied mostly between 400 mg and 800 N m^{-2}, except in four years (1982, 1983, 1993, and 1994), when deposition was around or over 1,000 N m^{-2} (*Fig. 6*). Despite that the atmospheric concentration of NO_2 (*Fig. 7*) was the highest over the whole period, dry deposition of HNO_3 particles was predominant for both surface types. This is a result of the high reactivity and solubility of HNO_3 and consequently its deposition velocity, that is larger by one order of magnitude compared to those of the other two compounds. This led also to

the above mentioned four peak values in dry deposition for mixed vegetation, as HNO_3 concentrations were relatively high in these years. The higher dry deposition for mixed vegetation compared to grass was caused mostly by the almost three times larger average HNO_3 deposition velocity applied for this surface type.

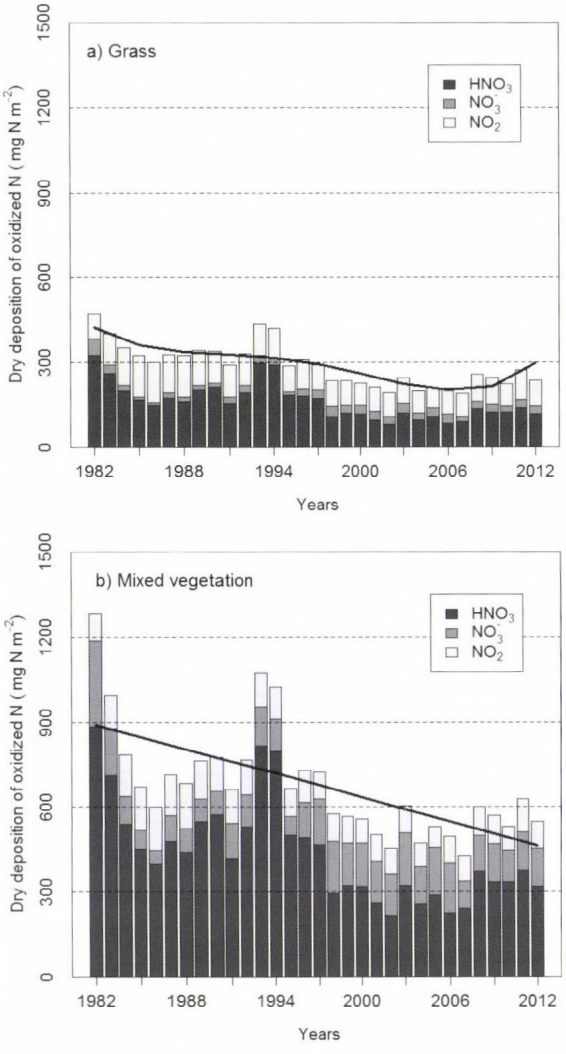

Fig. 6. Dry deposition of oxidized nitrogen compounds over grass (a) and mixed vegetation (b) between 1982 and 2012 at K-puszta, and the best fit lines to the total dry depositions.

In the case of grass, the year-to-year variability was smaller than for mixed vegetation. The fitted 4th order polynomial trend shows a moderate decrease

over most of the period with an increase over the last four years. However, the significance of this rise can be considered low, regarding that the length of the period is quite short and the depositions over the four year do not change consistently. For mixed vegetation the decreasing is much clearer, the best fit trend is linear with a slope of 14 mg N m^{-2} $year^{-1}$.

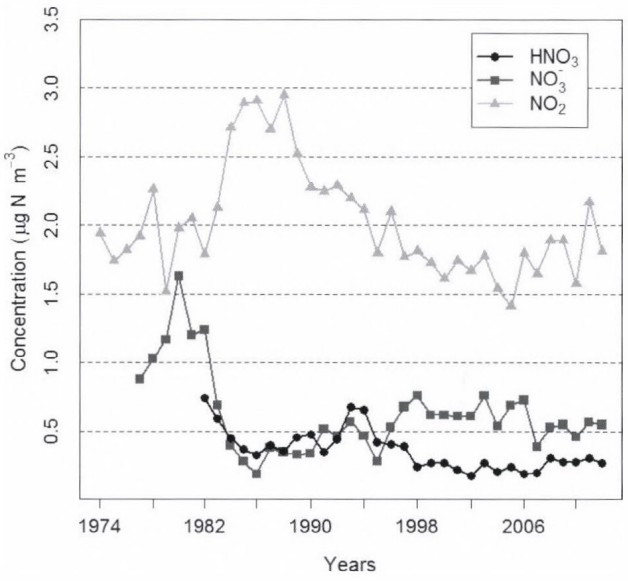

Fig. 7. Atmospheric concentration of oxidized nitrogen species between 1974 and 2012, measured at K-puszta.

Since the variability in wet deposition was smaller, the tendency of total deposition followed that of the dry deposition for both surface types (*Fig. 8*). The ranges of total deposition were 200 mg N m^{-2} higher than for dry deposition for both grass and mixed vegetations. The fitted trends are of the same order like the trends of dry depositions: 1st for mixed vegetation with a yearly reduction of 18 mg N m^{-2} $year^{-1}$, and 4th for grass with a slightly stronger decrease than in dry deposition.

Apparently, the relationship between national NO_x emissions (*Fig. 9*) and depositions is not as clear as in the case of oxidized sulfur compounds. A possible reason for that could be that we are comparing national emissions to depositions calculated from the data of a single station. On the other hand, due to the relatively long atmospheric lifetime of oxidized nitrogen compounds, transboundary transport of pollutants also has a strong influence on depositions. Finally, *Fowler et al.* (2007) suggested, that such non-linearity between emissions and depositions for oxidized nitrogen compounds grows with

distance from the main European source region of the highly populated northern Europe, stretching from the Czech Republic to South East England.

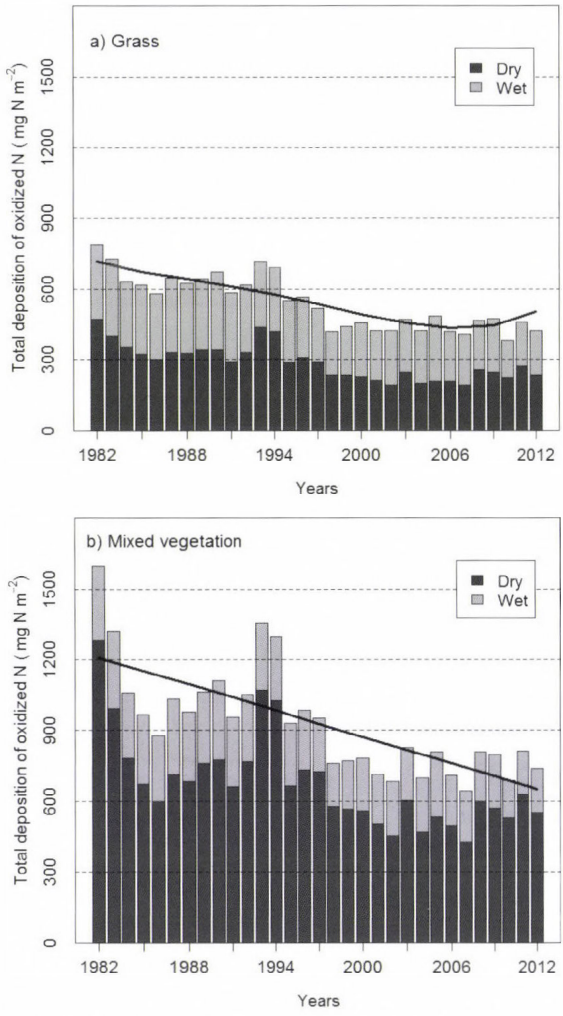

Fig. 8. Total deposition (dry + wet) of oxidized nitrogen species over grass (a) and mixed vegetation (b) between 1982 and 2012 at K-puszta, and the best fit lines to the total depositions.

The approximately 25% decrease in NO_x emission since the beginning of 90's is due to the breakdown of heavy industry after political changes. However, the steadily growing number of cars over the whole period (*Fig. 9*) comparing to the decreasing trend both of emission and total deposition may suggest the impact of technical improvements and national measures in abatement of oxidized

nitrogen emission and resulting deposition – from 1990 the usage of catalyst in cars is ordered by the Hungarian law for newly sold vehicles.

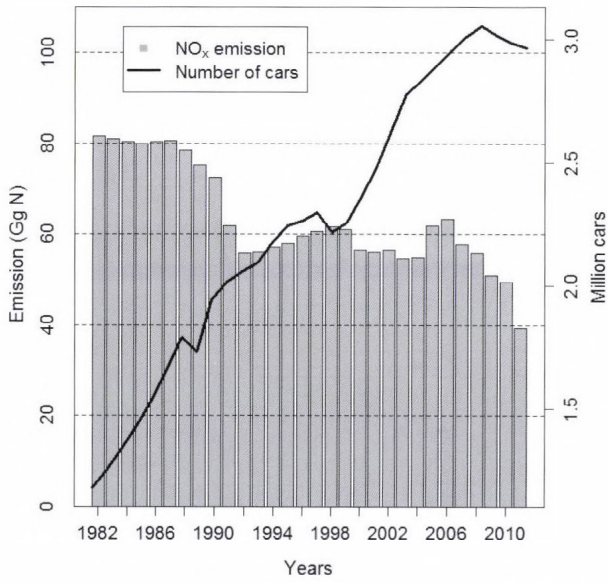

Fig. 9. National emission of NO_x and the number of cars in Hungary between 1982 and 2011.

3.3. Reduced nitrogen compounds

Yearly wet deposition of NH_4^+ ion between 1974 and 1982 (*Fig. 10*) varied from 800 to 1,600 mg N m^{-2}, then the values were under 800 mg N m^{-2}. The best fit trend was a 3rd order polynomial, showing a strong decrease in the first 20 years, and then a moderate further reduction until the end of the period.

Yearly dry deposition (*Fig. 11*) ranged mostly between the values of 200 and 400 mg N m^{-2} before 1996, then the great majority of deposition ranged between 300 and 500 mg N m^{-2}. The fitted 4th order polynomial trend shows a wave-like tendency, with a period of decrease before 1986, followed by a 20-year long increasing period and then a subsequent reduction until 2012. Despite that atmospheric concentration of NH_4^+ was higher in the first 20 years (*Fig. 12*), dry deposition was dominated by NH_3 deposition over the whole period. The cause of that is that NH_3 is highly soluble, resulting in a one order of magnitude higher dry deposition velocity than that of NH_4^+. Moreover, majority of ammonium are in the range of fine particles ($PM_{2.5}$) (*Horváth*, 2003), where deposition velocity has smaller rate than that of ammonia gas.

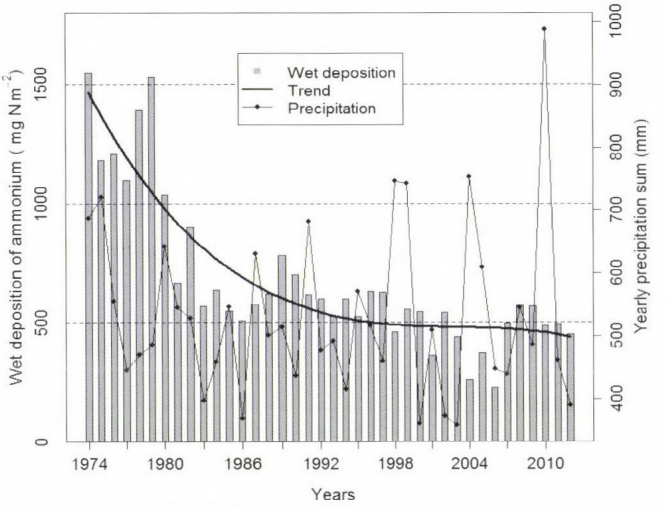

Fig. 10. Wet deposition of reduced nitrogen compounds between 1974 and 2012 at K-puszta, the best fit line, and the yearly precipitation sum.

Total deposition (*Fig. 13*) is mainly dominated by wet deposition, especially in the first half of the period. As the difference between wet and dry deposition is not too large, the opposite tendencies compensated each other, resulting in a balanced total deposition. The best fit, linear trend shows a weak decline of 1.7 mg N year^{-1}.

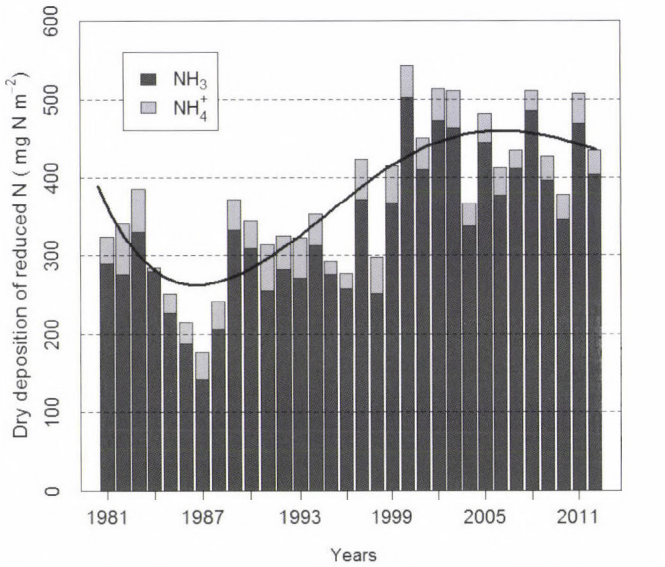

Fig. 11. Dry deposition of reduced nitrogen species between 1981 and 2012 at K-puszta, and the best fit line to the total dry deposition.

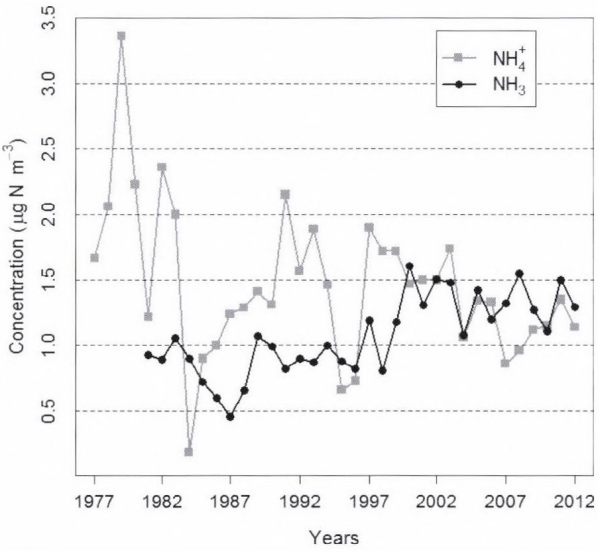

Fig. 12. Atmospheric concentration of reduced nitrogen species between 1974 and 2012, measured at K-puszta.

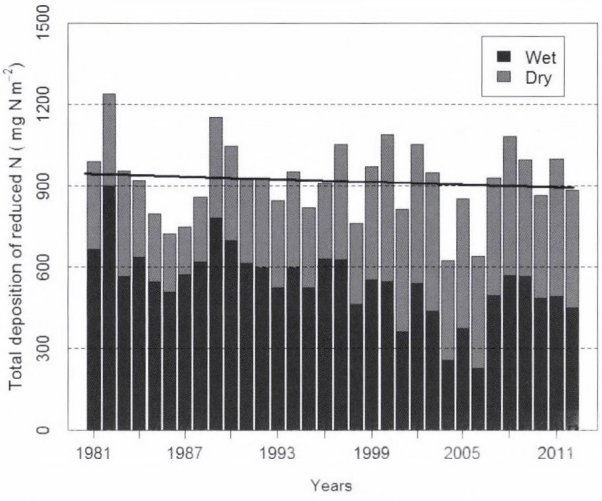

Fig. 13. Total deposition (dry + wet deposition) of reduced nitrogen species between 1981 and 2012 at K-puszta, and the best fit line to the total deposition.

In the national NH_3 emissions (*Fig. 14*), a rapid decrease can be seen between 1989 and 1994, with a close-to-constant emission before and after it. This is mainly parallel with the tendency of wet deposition, but apparently it is

the opposite of the trend in dry deposition. This raises the obvious question: how can the dry deposition grow if emission is reducing? Considering that in our approach the atmospheric concentration and deposition of NH_3 differ only in a constant multiplying factor, the question is the same for concentrations and emissions. Since gaseous NH_3 after emission dissolves quickly on the surface, in this case the influence of long-range transport is presumably weak.

As an alkaline compound, dry deposition of NH_3 is largely dependent on the acidity of the surface water (water film on the surface). Therefore, its deposition is influenced by the deposition of atmospheric acidic components (*Flechard et al.*, 1999). According to *Erisman et al.* (2001) and *Fowler et al.* (2001), the lower the ratio of atmospheric concentration of SO_2 to NH_3 (i.e., SO_2 concentration is relatively low or NH_3 concentration is relatively high), the higher the surface resistance to NH_3 deposition. Consequently, even if the atmospheric input of ammonia decreases with a decreasing SO_2 concentration, it cannot be removed from the atmosphere as the higher pH of the surface water film, caused by the less dissolved SO_2, hampers NH_3 dissolution. As a result, the emitted NH_3 remains in the atmosphere raising its atmospheric concentration, as it was observed earlier by *Horváth et al.* (2009).

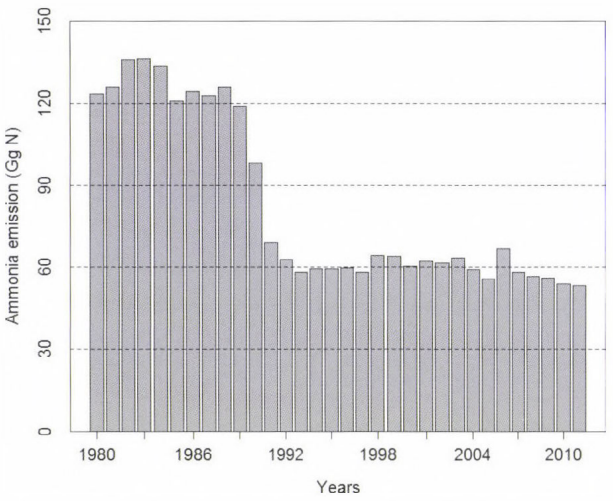

Fig. 14. National emission of ammonia in Hungary between 1980 and 2011.

According to *Fig. 15*, the above described process, referred as the co-deposition of NH_3 and SO_2, was most likely the key process in Hungary as well. On the other hand, this founding highlights the weakness of our simple estimation approach for dry deposition of NH_3, as the process, preventing NH_3

removal from the atmosphere, could lead to lower deposition than our calculations. Therefore, the estimation of NH_3 dry deposition requires further investigation.

In addition, the transfer of ammonia between atmosphere and surface is bi-directional, i.e., not just deposition but also emission can occur depending on the difference between the atmospheric NH_3 concentration and above the surface (*Farquhar et al.*, 1980). Further influencing factors on the magnitude of NH_3 exchange are, among others, temperature, wind speed, and relative humidity, which were all neglected during our approach.

However, considering bi-directional exchange would require a much complex estimation, which has not been applied either in operational ACTMs (*Sutton et al.*, 2013). ACTMs nowadays calculate dry depositions based on the same formula we used, that – even if the calculations are more detailed in an ACTM – supports the relevance of our simple approach.

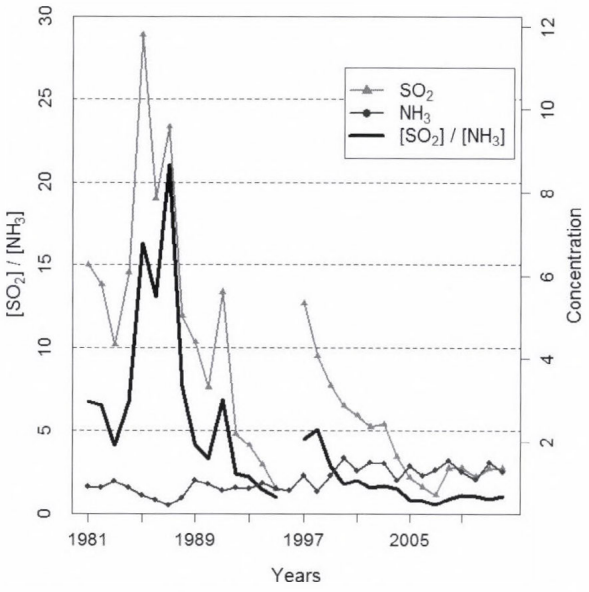

Fig. 15. Atmospheric concentration of SO_2 (μg S m^{-3}, triangles) and NH_3 (μg N m^{-3}, dots), and their ratio (thick line) between 1981 and 2012 at K-puszta.

3.4. Total nitrogen load

Summing up the total depositions of oxidized and reduced nitrogen compounds for grass, we got the total nitrogen load over grass-covered surface (*Fig. 16*). In the period of 1982 and 2012, it varied mainly between 1,000 and

1,600 mg N m^{-2}. According to the measurement practice of air concentration and dry deposition velocity, we estimated the uncertainty of the total nitrogen load ±10% shown as error bars in *Fig. 16*. This uncertainty covers much possibly the year-to-year variability of yearly dry deposition velocities. Compared to the oxidized compounds, deposition of reduced nitrogen compounds had a larger fraction in the total load. As we showed it, both of them had a slow decreasing trend, resulting in a moderate decrease in the total load as well. The fitted trend is linear, with a slope of 12 mg N m^{-2} $year^{-1}$.

Likewise in the case of oxidized sulfur compounds, it is difficult to quantify the acidifying effect of the nitrogen compounds examined above. In addition, in this case the neutralizing effect of dissolving gaseous NH_3 has to be also considered. However, even if dry deposition of reduced nitrogen compounds is highly dominated by NH_3 deposition, in the total load the other components overcame it. Overall, the declining trend of the total nitrogen load implies a mitigating tendency of acidification.

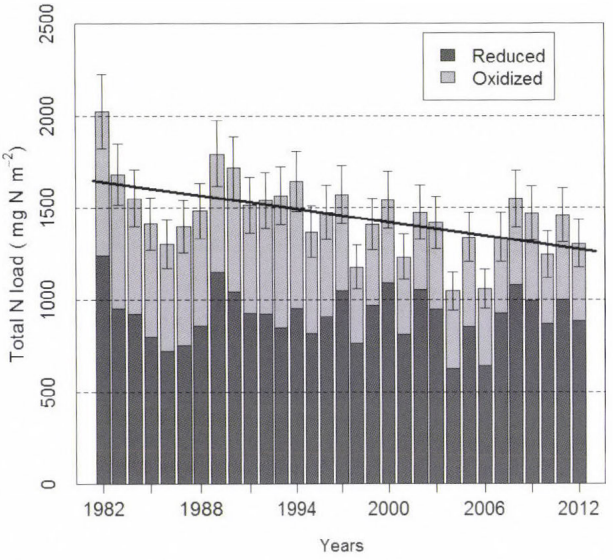

Fig. 16. Total nitrogen load (as a sum of the total deposition of reduced and oxidized nitrogen compounds) over grass between 1982 and 2012 at K-puszta.

4. Conclusions

The purpose of this work was to compile long-term deposition time series for Hungary for acidifying compounds, such as oxidized sulfur, as well as oxidized and reduced nitrogen compounds. To achieve our goal, we used existing results from ACTMs and precipitation chemistry as well as background air pollution

measurements. Comparing the results with national emission datasets, we also made an attempt to interpret the changes in depositions. Finally, we gave a qualitative estimation for the strength of acidification on long term.

In the case of oxidized sulfur compounds, according to the 132-year long deposition time series, 1980 was a changing point: until this year, deposition was steadily increasing, and since then it has been decreasing rapidly. For deposition of oxidized nitrogen compounds, we got declining trend between 1982 and 2012; however, in the case of grass, a non-significant increase occurred in the last four years of the period. We found that the deposition of reduced nitrogen compounds has been also decreasing since 1982. Consequently, our calculation showed that also the total nitrogen load followed a slowly declining tendency.

Despite that the transboundary transport of both oxidized sulfur and nitrogen compounds, influences the national depositions, in the case of the oxidized sulfur compounds the relationship between the emissions and depositions was clearer than for the oxidized nitrogen compounds. On the other hand, we found that the decrease of total deposition of oxidized nitrogen compounds is most likely a sign of the improvement of emission abatement techniques and national emission controlling measures. Same is true for the total deposition of oxidized sulfur species; however, in this case, also the Hungarian industrial recession could be a substantial influencing factor. The total deposition of reduced nitrogen compounds showed only a weak declining tendency in contrast with drastically weakening NH_3 emissions. Moreover, atmospheric NH_3 concentration is nearly constant in spite of emission reduction. We showed that this trend in atmospheric concentration and – in our approach – dry deposition of NH_3 is possibly a result of the declining surface concentration of SO_2. Considering this effect, estimation of dry deposition of NH_3 requires further investigation.

Based on our results, only qualitative conclusions can be drawn regarding the progress of acidification in Hungary: the effect of acidification was most likely to intensify before 1980, since then the phenomenon presumably has been weakening gradually. On the other hand, if atmospheric concentration of NH_3 continuously grows in Hungary, in spite of its potential neutralizing effect in the atmosphere, it may raise new environmental issues in the future due to its key role in the cycle of reactive nitrogen compounds (*Galloway et al.*, 2008).

Acknowledgement – The authors are grateful to Sophia Mylona for providing her model results and to László Haszpra, who contacted her. In addition, we would like to express our appreciation to Ben Marner for sending us his PhD thesis.

References

Almer, B., Dickson, W., Ekstrom, C., Hornstrom, E. and *Miller, U.*, 1974: Effects of acidification on Swedish lakes. *Ambio 3*, 30–36.

A.S.L. & Associates, 1999: Sulfur emissions by country and year. Available: http://www.asl-associates.com/sulfur.htm [Accessed: 15 Novemeber 2013].

CEIP, 2013: Officially reported emission data.

Davidson, C., Miller, J. and *Pleskow, M.*, 1982: The influence of surface structure on predicted particle dry deposition to natural grass canopies. *Water Air Soil Poll.18*, 25–43.

Duan, L., Liu, J., Xin, Y. and *Larssen, T.*, 2013: Air-pollution emission control in China: Impacts on soil acidification recovery and constraints due to drought. *Sci. Total Environ. 463–464*, 1031–1041.

EMEP/MSC-W, 2013: EMEP MSC-W modelled air concentrations and depositions. Available: http://emep.int/mscw/index_mscw.html [Accessed: 12 December 2013].

Erisman, J.W., Hensen, A., Fowler, D., Flechard, C.R., Grüner, A., Spindler, G., Duyzer, J.H., Weststrate, H., Römer, F., Vonk, A.W. and *Jaarsveld, H. v.*, 2001: Dry Deposition Monitoring in Europe. *Water Air Soil Poll. Focus 1*, 17–27.

Farquhar, G.D., Firth, P.M., Wetselaar, R. and *Weir,B.*, 1980: On the Gaseous Exchange of Ammonia between Leaves and the Environment: Determination of the Ammonia Compensation Point. *Plant Physiol. 66*, 710–714.

Flechard, C,R., Fowler, D., Sutton, M.A. and *Cape, J.N.*, 1999: A dynamic chemical model of bi-directional ammonia exchange between semi-natural vegetation and the atmosphere. *Q. J. Roy. Meteorol. Soc. 125*, 2611–2641.

Fowler, D., Smith, R., Muller, J., Cape, J., Sutton, M., Erisman, J. and *Fagerli, H.*, 2007: Long Term Trends in Sulphur and Nitrogen Deposition in Europe and the Cause of Non-linearities. *Water Air Soil Poll. Focus 7*, 41–47.

Fowler, D., Sutton, M.A., Flechard, C.R., Cape, J.N., Storeton-West, R., Coyle, M. and *Smith, R.I.*, 2001: The control of SO_2 dry deposition on to natural surfaces and its effects on regional deposition. *Water Air Soil Poll. Focus 1*, 39–48.

Gallagher, M.W., Nemitz, E., Dorsey, J.R., Fowler, D., Sutton, M.A., Flynn, M. and *Duyzer, J.*, 2002: Measurements and parameterizations of small aerosol deposition velocities to grassland, arable crops, and forest: Influence of surface roughness length on deposition. *J. Geophys. Res. Atmos.107*, AAC 8-1-AAC 8-10.

Galloway, J. N., 1989: Atmospheric Acidification: Projections for the Future. *Ambio 18*, 161–166.

Galloway, J.N., Townsend, A. R., Erisman, J.W., Bekunda, M., Cai, Z., Freney, J.R., Martinelli, L.A., Seitzinger, S.P. and *Sutton, M.A.*, 2008: Transformation of the Nitrogen Cycle: Recent Trends, Questions, and Potential Solutions. *Science 320*, 889–892.

Goldman, J.C. and *Brewer, P.G.*, 1980: Effect of Nitrogen Source and Growth Rate on Phytoplankton-Mediated Changes in Alkalinity. *Limnol Oceanog. 25*, 352–357.

Grennfelt, P. and *Hov, Ø.*, 2005: Regional Air Pollution at a Turning Point. *Ambio 34*, 2–10.

Horváth, L., 1978: A csapadékvíz kémiai összetétele és a légköri nyomanyagok depozíciója Budapesten. *Időjárás 82*, 211–224. (in Hungarian)

Horváth, L., 2003: Dry deposition velocity of PM2.5 ammonium sulfate particles to a Norway spruce forest on the basis of S- and N-balance estimations. *Atmos. Environ. 37*, 4419–4424.

Horváth, L., Asztalos, M., Führer, E., Mészáros, R. and *Weidinger, T.*, 2005: Measurement of ammonia exchange over grassland in the Hungarian Great Plain. *Agric. Forest Meteorol.* 130, 282–298.

Horváth, L., Fagerli, H. and *Sutton, M.A.*, 2009: Long-term record (1981–2005) of ammonia and ammonium concentrations at K-puszta Hungary and the effect of SO_2 emission change on measured and modelled concentrations. In (Eds.:*M.A., S., Reis, S.* and *Baker, S.M.H.), Atmospheric Ammonia – Detecting Emission Changes and Environmental Impacts. Results of an Expert Workshop Under the Convention on Long-range Transboundary Air Pollution.* Springer Science + Business Media B.V.

Johnson, D.W. and *Reuss, J.O.*, 1984: Soil-mediated effects of atmospherically deposited sulphur and nitrogen. *Philosop. Transac. Roy.Soc. London Series B-Biol. Sci.305*, 383–392.

KSH, 2013: *Szállítás (1960–)*. Available: http://www.ksh.hu/docs/hun/xstadat/xstadat_hosszu/h_odme001.html [Accessed: 15 August 2013].

Kugler, Sz., Horváth, L. and *Weidinger, T.*, 2014: Modeling dry flux of ammonia and nitric acid between the atmosphere and Lake Balaton. *Időjárás 118*, 93–118.

Lefohn, A.S., Husar, J.D. and *Husar, R.B.*, 1999: Estimating historical anthropogenic global sulfur emission patterns for the period 1850–1990. *Atmos. Environ. 33*, 3435–3444.

Lipfert, F.W., 1987: Effects of acidic deposition on the atmospheric deterioration of materials. *Materials Perform. 26*, 12–19.

Marner, B.B., 2003: Atmospheric nitrogen deposition to a nitrate vulnerable zone. Ph.D. Thesis. University of Birmingham, UK.

Mylona, S., 1992: Trends of sulphur dioxide emissions, air concentrations and depositions of sulphur in Europe since 1880. *EMEP/MSC-W Report 2/93.* EMEP/MSC-W, Oslo, Norway.

Nicholson, J.P., Weston, K.J. and Fowler, D., 2001: Modelling horizontal and vertical concentration profiles of ozone and oxides of nitrogen within high-latitude urban areas. *Atmos.Environ.*35, 2009–2022.

OKTH/MTA, 1987: A környezet erősödő savasodása. *Környezet és természetvédelmi kutatások 7.* OKTH, Budapest, Hungary.(In Hungarian)

Pope, C.A., III, Burnett, R.T., Thun, M.J., Calle, E.E., Krewski, D., Ito, K. and *Thurston, G.D.,* 2002: Lung cancer, cardiopulmonary mortality, and long-term exposure to fine particulate air pollution. *J. Am. Medic. Ass. 287*, 1132–1141.

Puxbaum, H. and *Gregori, M.,* 1998: Seasonal and annual deposition rates of sulphur, nitrogen and chloride species to an oak forest in north-eastern austria (wolkersdorf, 240 m a.s.l.). *Atmos. Environ. 32*, 3557–3568.

Raven, J.A., 1985: Regulation of pH and generation of osmolarity in vascular plants: a cost-benefit analysis in relation to efficiency of use of energy, nitrogen and water. *New Phytologist 101*, 25–77.

Ruijgrok, W., Tieben, H. and *Eisinga, P.,* 1997: The dry deposition of particles to a forest canopy: A comparison of model and experimental results. *Atmos. Environ. 31,* 399–415.

Sakamoto, Y., Ishiguro, M. and *Kitagawa, G.,* 1986: Akaike Information Criterion Statistics. D. Reidel Publishing Company, Dordrecht, Netherlands.

Sandnes, H. and *Styve, H.,* 1992: Calculated Budgets for Airborne Acidifying Components in Europe, 1985, 1987, 1988, 1989, 1990 and 1991. *EMEP/MSC-W Report 1/92.* EMEP/MSC-W, Oslo, Norway.

Seinfeld, J.H. and *Pandis, S.N.,* 2006: Atmospheric Chemistry and Physics: From Air Pollution to Climate Change. John Wiley & Sons, New York, USA.

Slinn, W.G.N., 1982: Predictions for particle deposition to vegetative canopies. *Atmos. Environ. 16*, 1785–1794.

Stelson, A.W. and *Seinfeld, J.H.,* 1982: Relative humidity and temperature dependence of the ammonium nitrate dissociation constant. *Atmos. Environ. 16*, 983–992.

Sutton, M.A., Howard, C.M., Erisman, J.W., Bealey, W.J., Billen, G., Bleeker, A., Bouwman, A.F., Grennfelt, P., van Grinsven, H. and *Grizzetti, B.,* 2011: The challenge to integrate nitrogen science and policies: the European Nitrogen Assessment approach. In (Eds.: *Sutton, M.A., Howard, C.M., Erisman, J.W., Billen, G., Bleeker, A., Grennfelt, P., Van Grinsven, H.* and *Grizzetti, B.*) The European Nitrogen Assessment: Sources, Effects and Policy Perspectives. Cambridge, UK.

Sutton, M.A., Reis, S., Riddick, S.N., Dragosits, U., Nemitz, E., Theobald, M.R., Tang, Y.S., Braban, C.F., Vieno, M., Dore, A.J., Mitchell, R.F., Wanless, S., Daunt, F., Fowler, D., Blackall, T.D., Milford, C., Flechard, C.R., Loubet, B., Massad, R., Cellier, P., Personne, E., Coheur, P.F., Clarisse, L., Van Damme, M., Ngadi, Y., Clerbaux, C., Skjøth, C. A., Geels, C., Hertel, O., Wichink Kruit, R.J., Pinder, R.W., Bash, J.O., Walker, J.T., Simpson, D., Horváth, L., Misselbrook, T.H., Bleeker, A., Dentener, F. and *de Vries, W.,* 2013: Towards a climate-dependent paradigm of ammonia emission and deposition. *Philosop. Transact. Roy. Soc. B: Biol.Sci. 368*, 20130166.

Várallyay, G., Rédly, L. and *Murányi, A.,* 1986: A savas ülepedés hatása a talajra Magyarországon. *Időjárás 90*, 169–190. (In Hungarian)

INSTRUCTIONS TO AUTHORS OF *IDŐJÁRÁS*

The purpose of the journal is to publish papers in any field of meteorology and atmosphere related scientific areas. These may be

- research papers on new results of scientific investigations,
- critical review articles summarizing the current state of art of a certain topic,
- short contributions dealing with a particular question.

Some issues contain "News" and "Book review", therefore, such contributions are also welcome. The papers must be in American English and should be checked by a native speaker if necessary.

Authors are requested to send their manuscripts to

Editor-in Chief of IDŐJÁRÁS
P.O. Box 38, H-1525 Budapest, Hungary
E-mail: journal.idojaras@met.hu

including all illustrations. MS Word format is preferred in electronic submission. Papers will then be reviewed normally by two independent referees, who remain unidentified for the author(s). The Editor-in-Chief will inform the author(s) whether or not the paper is acceptable for publication, and what modifications, if any, are necessary.

Please, follow the order given below when typing manuscripts.

Title page: should consist of the title, the name(s) of the author(s), their affiliation(s) including full postal and e-mail address(es). In case of more than one author, the corresponding author must be identified.

Abstract: should contain the purpose, the applied data and methods as well as the basic conclusion(s) of the paper.

Key-words: must be included (from 5 to 10) to help to classify the topic.

Text: has to be typed in single spacing on an A4 size paper using 14 pt Times New Roman font if possible. Use of S.I. units are expected, and the use of negative exponent is preferred to fractional sign. Mathematical formulae are expected to be as simple as possible and numbered in parentheses at the right margin.

All publications cited in the text should be presented in the *list of references*, arranged in alphabetical order. For an article: name(s) of author(s) in Italics, year, title of article, name of journal, volume, number (the latter two in Italics) and pages. E.g., *Nathan, K.K.,* 1986: A note on the relationship between photo-synthetically active radiation and cloud amount. *Időjárás 90,* 10-13. For a book: name(s) of author(s), year, title of the book (all in Italics except the year), publisher and place of publication. E.g., *Junge, C.E.,* 1963: *Air Chemistry and Radioactivity.* Academic Press, New York and London. Reference in the text should contain the name(s) of the author(s) in Italics and year of publication. E.g., in the case of one author: *Miller* (1989); in the case of two authors: *Gamov* and *Cleveland* (1973); and if there are more than two authors: *Smith et al.* (1990). If the name of the author cannot be fitted into the text: *(Miller,* 1989); etc. When referring papers published in the same year by the same author, letters a, b, c, etc. should follow the year of publication.

Tables should be marked by Arabic numbers and printed in separate sheets with their numbers and legends given below them. Avoid too lengthy or complicated tables, or tables duplicating results given in other form in the manuscript (e.g., graphs).

Figures should also be marked with Arabic numbers and printed in black and white or color (under special arrangement) in separate sheets with their numbers and captions given below them. JPG, TIF, GIF, BMP or PNG formats should be used for electronic artwork submission.

Reprints: authors receive 30 reprints free of charge. Additional reprints may be ordered at the authors' expense when sending back the proofs to the Editorial Office.

More information for authors is available: journal.idojaras@met.hu

Published by the Hungarian Meteorological Service

Budapest, Hungary

INDEX 26 361

HU ISSN 0324-6329

IDŐJÁRÁS

QUARTERLY JOURNAL
OF THE HUNGARIAN METEOROLOGICAL SERVICE

CONTENTS

****

http://www.met.hu/Journal-Idojaras.php

VOL. 118 * NO. 3 * JULY – SEPTEMBER 2014

IDŐJÁRÁS

Quarterly Journal of the Hungarian Meteorological Service

Editorial Office: Kitaibel P.u. 1, H-1024 Budapest, Hungary
P.O. Box 38, H-1525 Budapest, Hungary
E-mail: journal.idojaras@met.hu
Fax: (36-1) 346-4669

Indexed and abstracted in Science Citation Index Expanded™ and Journal Citation Reports/Science Edition
Covered in the abstract and citation database SCOPUS®

Subscription by mail:
IDŐJÁRÁS, P.O. Box 38, H-1525 Budapest, Hungary
E-mail: journal.idojaras@met.hu

IDŐJÁRÁS

Quarterly Journal of the Hungarian Meteorological Service
Vol. 118, No. 3, July – September, 2014, pp. 193–206

The effects of climate change on grape production in Hungary

Ildikó Mesterházy*, **Róbert Mészáros**, and **Rita Pongrácz**

Department of Meteorology, Eötvös Loránd University,
Pázmány P. sétány 1/A, H-1117 Budapest, Hungary

**Corresponding author; E-mail: mesildiko@caesar.elte.hu*

(Manuscript received in final form November 3, 2013)

Abstract—Spatial distribution of several indices characterizing wine production in Hungary are analyzed in this paper using the bias-corrected outputs of three different regional climate models: RegCM, ALADIN, and PRECIS. For this purpose, the daily minimum, maximum, and mean temperature, and daily precipitation time series were used. The indices include the active degree days, Huglin's heliothermal index, length of vegetation period according to thermal conditions, hydrothermal coefficient, and frequencies of extreme temperature events. In the study, first, the past changes of these indices are evaluated, and then, the main focus is on the projected changes until the end of the 21st century. Our results suggest that white wine grapes are very likely to lose their dominance over red wine grapes in Hungary in the next few decades. Furthermore, the ripening of late-ripening and very-late-ripening grape varieties will become more likely. Extreme high summer temperatures will become more frequent, while the risk of frost damage in the reproductive cycle is projected to decrease.

Key-words: Vitis vinifera, RegCM, ALADIN, PRECIS, regional climate change, Hungarian wine regions

1. Introduction

Wine grape production is a segment of major importance in Hungarian agriculture. The life cycle of the grape is influenced by climatic, edaphic, and biotic factors, from which climatic factors are the most dominant and dynamically changing ones (*Kozma*, 2002). As vineyards in Hungary produce grapes for 25–30 years, predicting these climatic factors for the next decades has a great importance.

In this work, we analyze the temporal trends of selected climatic factors, and use several indices to identify grape varieties in Hungary that are more

suitable for the projected climatic changes. Additionally, we predict the trend of change in the probability of desease development for the next decades. Although there has been a recent work studying the future changes of ecological factors affecting Hungarian grape fields (*Szenteleki*, 2012), our work is the first climatic study of the entire Hungarian region focusing specifically on grape and wine production.

2. Studied regions and applied methods

2.1. Studied regions

The wine subregions of Hungary belong to the northern territorries of grape production. Grape production is made possible primarily by the diverse microregions of the country and their specific meso- and microclimate. Based on microclimatic similarities, the 22 Hungarian wine subregions are categorized to 7 regions (127/2009. (IX. 29.) FVM regulation, appendix 1), covering Danube (Duna), Balaton, Eger, North-Transdanubia (Észak-Dunántúl), Pannon, Sopron, and Tokaj. On these wine regions, the wine grape production is dominated by white wine grapes, however, in some regions (e.g., in Sopron region), red grape production is also important. From the grape varieties, both early-, medium-, and late-ripening ones are produced in the different regions (*Hajdú*, 2003).

2.2. Applied regional climate models

Results provided by global climate models (GCMs) cannot be applied to small regions like the Carpathian Basin and Hungary. Therefore, in our analysis we applied regional climate models (RCMs) nested in GCMs. The RCMs have finer spatial resolution than GCMs, thus they can take into account local scale landscape features and topography.

We used the outputs of the following model simulations carried out in the framework of the European ENSEMBLES project (*van der Linden* and *Mitchell*, 2009): the RegCM (*Giorgi et al.*, 1993), the ALADIN (*Déqué et al.*, 1998) regional climate models, and the PRECIS regional climate model developed by the UK Met Office Hadley Centre for Climate Prediction and Research (*Wilson et al.*, 2007) applied specifically to the Carpathian Basin (*Pieczka*, 2012). The raw RCM outputs generally overestimate the temperature in summer and the precipitation throughout the entire year (*Pongrácz et al.*, 2011; *Pieczka et al.*, 2011). Therefore, they were corrected using a percentile-based bias correction technique (*Formayer* and *Haas*, 2009) consisting of correcting the simulated daily outputs on the basis of the monthly distributions of observed meteorological data. Observations are available from the gridded E-OBS database (*Haylock et al.*, 2008). The RCM simulations use the A1B emission scenario (*Nakicenovic* and *Swart*, 2000) for the 21st century. This scenario

assumes a slowly growing trend of atmospheric carbon-dioxide concentration, which is likely to exceed 700 ppm by the end of the century.

All RCMs applied a horizontal resolution of 25 kilometers. This resolution is still too coarse for detailed studies on the changing microclimatic conditions of vineyards, but it enables us to estimate some general tendencies. The simulated model datasets used in this study cover the geographic region between latitudes 44°–50° N and longitudes 14°–26° E, and contain the time interval 1951–2100 (except for the PRECIS simulation, where the time interval was 1951–2098). The applied RCM outputs include the daily minimum, maximum, and mean temperature, as well as the daily precipitation, which are used to calculate past and future time series of various indices described in Section 2.3, and derive conclusion on their effect on wine grape production in Hungary in the *middle of the 21st century* (for the period 2021–2050) and in the *end of the 21st century* (for the period 2071–2100; or between 2069–2098 for the PRECIS model due to shorter simulation time range). The years 1961–1990 is defined as the *reference period.*

2.3. The applied indices

The indices that we analyze in this paper are the following.

Active degree days (ADD). This can be easily calculated from the daily mean temperatures and can be used to determine the grape varieties that the given region is suitable for (see *Table 1*). The calculation is carried out by summing the residual above 10 °C of the daily mean temperatures throughout the growing season (*Davitaja*, 1959; *Kozma*, 2002). Note, that in all our calculations we defined the growing season as the period of a year when the daily mean temperature is above 10 °C for at least three consecutive days (*Kozma*, 2002). This practically corresponds to the time beginning with budburst and ending with leaf-fall, and thus, covers a longer interval of the year than the one discussed in *Table 1*.

Table 1. Grouping of grape varieties based on the active degree days (*Davitaja*, 1959; *Kozma*, 2002)

Ripening categories	**Active degree days**	**Number of days**
	(from budburst to full ripening of berries)	
very-early-ripening varieties	690–850 °C	110–120 days
early-ripening varieties	850–1150 °C	120–130 days
medium-ripening varieties	1150–1350 °C	130–145 days
late- & very-late-ripening varieties	>1350 °C	>145 days

Huglin's heliothermal index (HI) (*Huglin,* 1978). This gives a measure on the suitability of a region for different grape varieties based on the daily mean and maximum temperatures of the region, and on a factor denoted as d, which depends on the geographic latitude of the region (and thus the average length of the days during the growing season). Huglin's heliothermal index can be written as:

$$HI = d\sum \frac{[(T - 10°\mathrm{C}) + (T_x - 10°\mathrm{C})]}{2}, \quad (1)$$

where d is the latitude coefficient increasing monotonically from d_{40}=1.02 at latitude 40° N to d_{50}=1.06 at latitude 50° N; T is the daily mean temperature, and T_x is the daily maximum temperature, both given in °C. In Eq. (1), each term of the sum corresponds to one day in the growing season, and thus, the sum goes through all the days of the growing season. The optimal values of *HI* for selected grape varieties are shown in *Table 2.*

Table 2. The optimal values for Huglin's heliothermal index (HI) for selected white (normal fonts) and red (italic fonts) wine grape varieties. (*Huglin*, 1978; *Kozma*, 2002)

Huglin's Heliotermal Index (HI; in °C)	Grape varieties
2300	*Aramon*
2200	*Carignan, Zinfandel*
2100	*Cinsaut, Grenache, Syrah, Sangiovese*
2000	Ugni blanc
1900	Chenin blanc, Welschriesling, *Merlot, Cabernet Sauvignon*
1800	*Cabernet franc, Blaufränkisch*
1700	Chardonnay, Rhine Riesling, Silvaner, Sauvignon blanc, *Pinot noir*
1600	Pinot blanc, Gewürztraminer, *Gamay*
1500	Müller-Thurgau
1400	Irsai Olivér

Occurrences of extreme temperature episodes. Thermal susceptibility of wine grapes depends on many biotic and climatic factors, and it is variety and site specific according to different levels of risk severity at different extreme temperature values. Therefore, several thermal indices can be defined. To give examples, we used the following measures in studying the occurrences of extreme temperatures (*Dunkel* and *Kozma,* 1981; *Kozma*, 2002):

◇ daily minimum temperature is below −17 °C in the reproductive cycle,

◇ daily minimum temperature is below −21 °C in the reproductive cycle,

◇ daily maximum temperature is above 35 °C in the vegetative cycle.

Hydrothermal coefficient (HTC). We can characterize the combined effect of precipitation and temperature on grapes using the hydrothermal coefficient (*HTC*). This characteristic number, which measures the water supply of a vegetation, is calculated as:

$$HTC = 10P / T_0, \tag{2}$$

where P is the precipitation during the growing season in mm and T_0 is the effective degree days in °C (which is the sum of daily mean temperatures for days of the growing season when this temperature is above 10 °C). In areas, where the *HTC* is below 0.5 mm/°C, grape production is only possible if the humidity is high or if irrigation is applied. The maximum value of the *HTC* is in the range of 1.5–2.5 mm/°C, while its optimal value is around 1.0 mm/°C (*Szeljanyinov*, 1928; *Kozma*, 2002).

3. Results and discussion

According to the RCM simulations, the ADD values were in the range of 1200–1400 °C* in the Hungarian wine regions during the 1961–1990 reference period (*Fig. 1*). These results suggest that climatic conditions were in favor of early- and medium-ripening grape varieties at the end of the 20th century. However, there are certain regions where late-ripening varieties are also produced (*Hajdú*, 2003). The reason for this controversy is that RCMs do not take into account the extra heat the grapes are subjected to when they are grown on hill- and mountainsides and are being exposed to sunlight at lower incoming angles. Thus, maps of heat distribution are biased to lower-than-actual heat supply conditions at hilly terrains (such as the Sopron regions), and consequently, they falsely suggest that these regions are only suitable for low heat demanding grape varieties. As it can be seen in *Fig. 2*, based on *HI*, we could think that heat conditions in Sopron wine regions can only support less heat demanding varieties, and only the Danube regions are optimal for more heat demanding ones. In practice, the Sopron regions are known to be optimal for more heat demanding varieties, which can be explained by taking into account the extra heat the regions are obtaining from sunlight arriving at lower incoming angles.

* These values are only averages, i.e., in some years the *ADD* can be lower or higher. Negative deviations from these averages can lead to an insufficient amount of heat for the ripening of grape varieties that require a longer growing season.

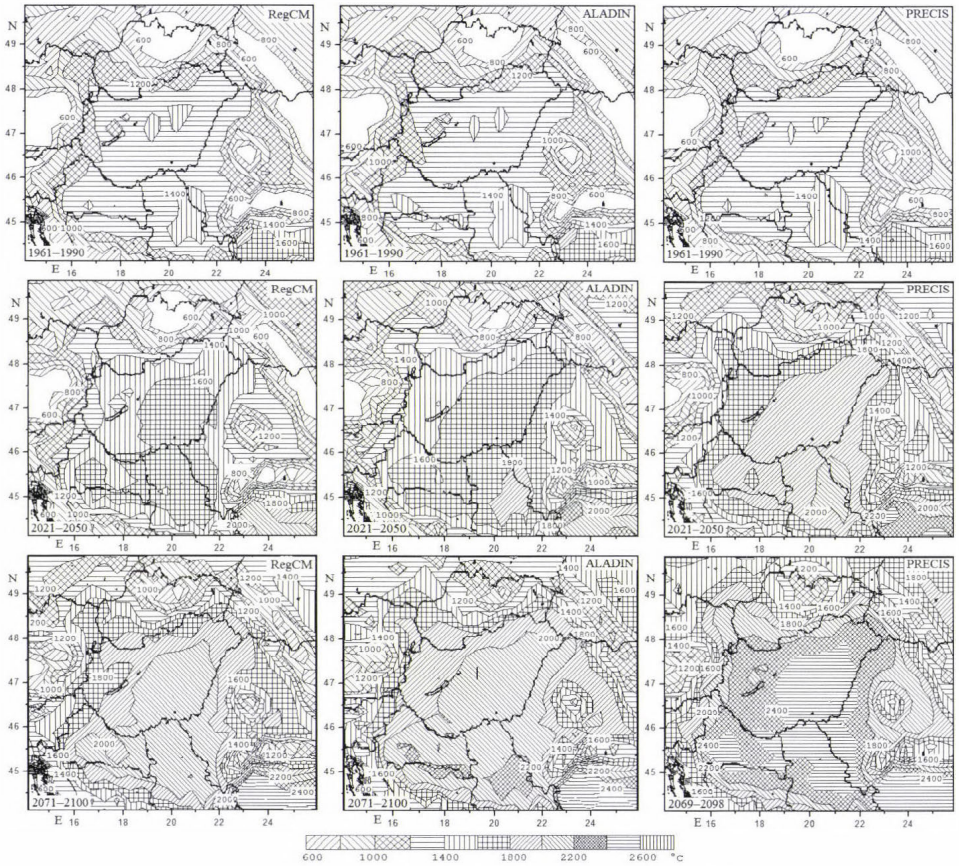

Fig. 1. The values of active degree days (*ADD*) in the Carpathian Basin. The upper row corresponds to the reference period, while the middle and lower rows correspond to the predicted middle and end of the 21st century, respectively. The three columns show our results using the RegCM (left), ALADIN (middle), and PRECIS (right) regional climate models' outputs.

The length of the growing season allowed by the thermal conditions in Hungary is between 160–190 days within the reference period of the RCM simulations. This is about 1 month longer than that is necessary for early- and medium-ripening varieties (see *Table 1* and *Fig. 3*). Thus, we can conclude that the projected thermal conditions by the end of the 21st century are optimal for late-ripening and very-late-ripening grape varieties.

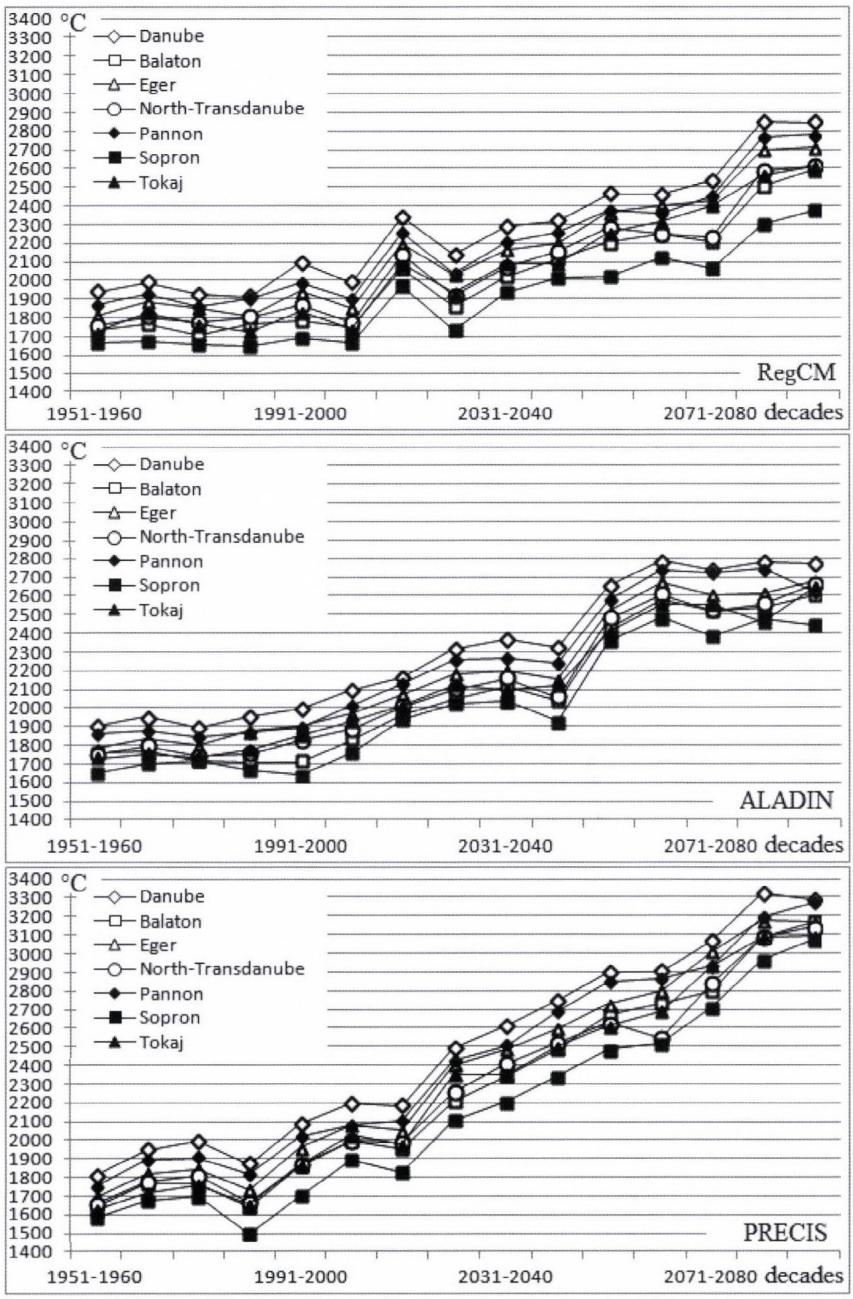

Fig. 2. The temporal evolution of Huglin's heliothermal index (*HI*) in the Carpathian Basin based on the RegCM (upper), ALADIN (middle), and PRECIS (lower) regional climate models' outputs.

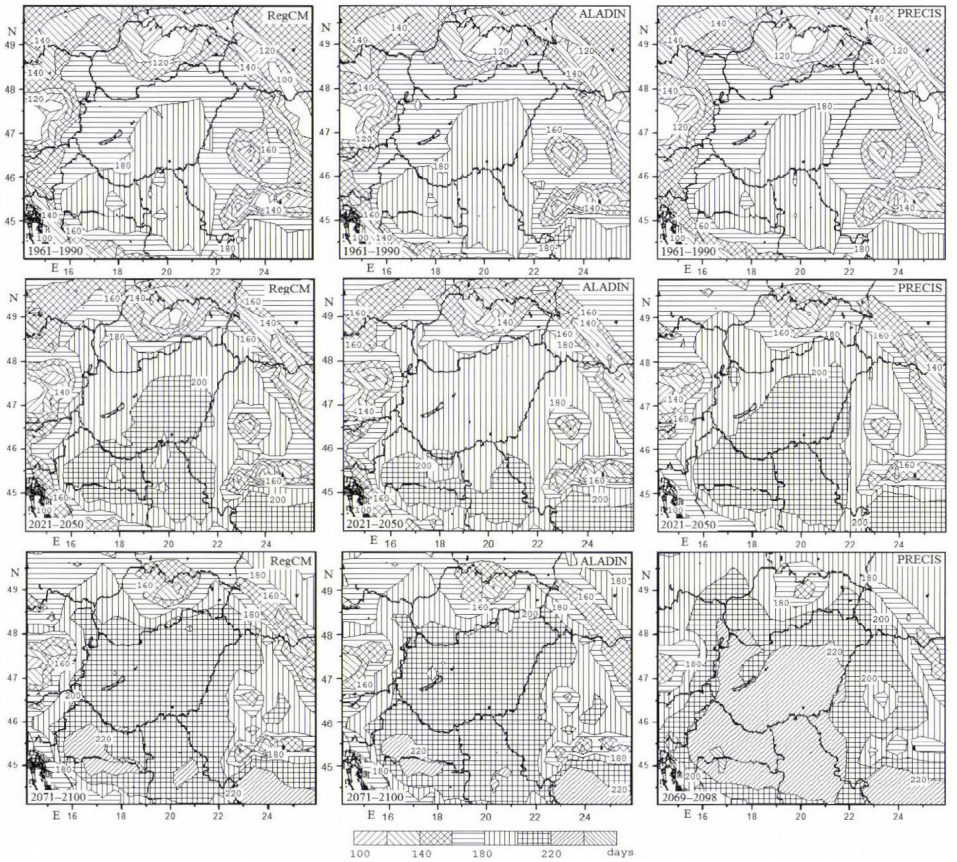

Fig. 3. The length of the growing season in days allowed by thermal conditions. The upper row corresponds to the reference period, while the middle and lower rows correspond to the predicted middle and end of the 21st century, respectively. The three columns show our results using the RegCM (left), ALADIN (middle), and PRECIS (right) regional climate models' outputs.

Results obtained from the ALADIN and RegCM data show a correlation with each other in the middle of the 21st century. Based on these, the *ADD* will increase up to 1400–1700 °C in this period. The value of *HI* is projected to increase to 1800 °C, however, in the Danube region values above 2300 °C will also be possible. The values of *HI* increase with an increased rate from the 1980s in every wine region, as shown in *Fig. 2*.

The PRECIS model simulation suggests a much more significant rise in the index values. The *ADD* can increase up to 1600–2000 °C in the middle of the 21st century. *HI* will reach 2300 °C in the whole country. In *Fig. 2*, curves corresponding to the PRECIS model increase with the highest rate, which shows that this model predicts the greatest change in the local climate by the middle of the 21st century.

All three models predict longer growing season in the immediate future (see *Fig. 3*) compared to the reference period. By the middle of the 21st century, the vegetation cycle length allowed by thermal conditions can be as long as 180–210 days, however, the change will be slightly smaller (180–200 days) according to the ALADIN model.

Similar tendencies are expected to occur in the end of the 21st century. Based on the ALADIN and RegCM models, the *ADD* can be as high as 1700–2200 °C. Similar to the results for the end of the 21st century, PRECIS predicts a more remarkable change: according to this model, *ADD* can be between 2000–2500 °C. In this period, all three models predict *HI* to be above 2300 °C throughout the whole country.

The vegetation cycle length allowed by thermal conditions can be even longer in the far future (see *Fig. 3*). Its duration can reach 200–220 days, or 210–230 days according to the PRECIS model.

All these suggest that certain regions will allow the ripening of late-ripening grape varieties by the middle of the 21st century. As the increased heat allows the development of color- and aroma essences, growing a higher ratio of red wine grapes will be feasible in several wine regions. According to results corresponding to the end of the 21st century, the thermal conditions of the Hungarian wine regions will allow the growing of Mediterranean red wine grapes.

In addition to the average conditions, the occurrences of extreme temperatures in the reproductive and vegetation cycles also have important roles. Since PRECIS simulation does not include any occurrence of daily minimum temperature below −17 °C, we only analyze the extremes based on the other two RCMs simulations.

The regional distribution of the number of days with minimum temperatures below −17 °C (as obtained from the RegCM and ALADIN simulations) is in a good agreement with the results presented in *Dunkel* and *Kozma* (1981) (see *Fig. 4*). However, note, that the time interval investigated in *Dunkel* and *Kozma* (1981) is slightly different from our reference period.

We found that less frost-tolerant grape varieties suffered frost damage in every 2–3 years within the reference period (see *Table 3*). This occurrence is projected to decrease by the middle of the 21st century to only one major frost damage in the winter season in every 4–10 years. The risk of frost damage will almost disappear in the end of the 21st century.

The RCM simulations underestimate the number of days with a minimum temperature below −21 °C compared to the findings of *Dunkel* and *Kozma* (1981). This difference can be related to the slightly different periods applied. Independently from this fact, the occurrence of extreme cold temperatures will decrease in the middle of the 21st century, and almost completely disappear in the end of the 21st century.

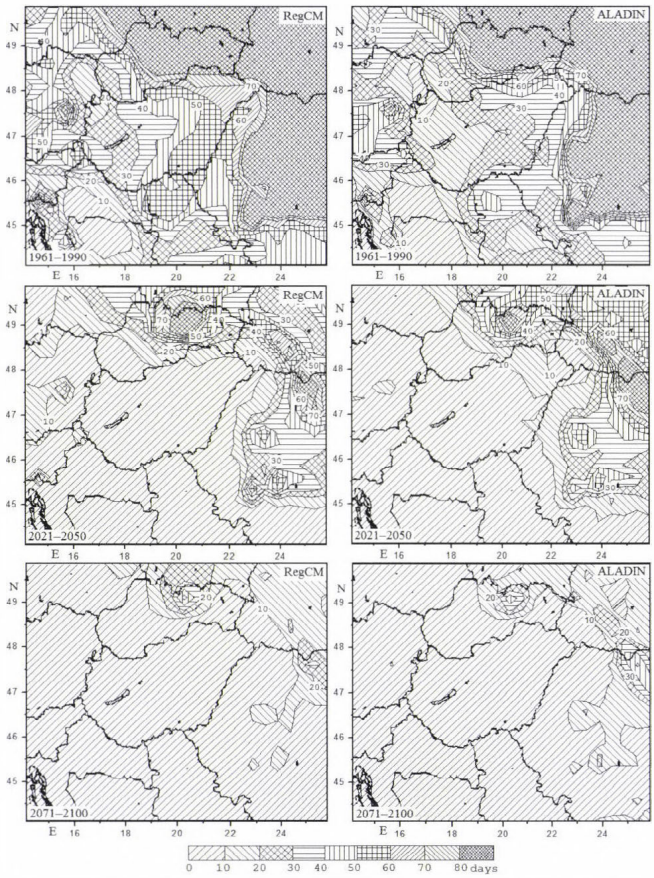

Fig. 4. The number of days in the reproductive cycle with minimum temperature below –17 °C. The two columns correspond to the RegCM (left) and ALADIN (right) simulations' results. The rows of the figure show the model results for the reference period (upper), and the predictions for the middle (middle) and the end (lower) of the 21st century.

The plants can be damaged due to extreme hot days in the growing season, too. In the reference period, the occurrence of days with maximum temperature above 35 °C was one per 2–10 years according to the RCM results (see *Fig. 5*). The most of such years are simulated by the RegCM model, and the least by the ALADIN model. On yearly average, about 1–4 days occurred when the maximum temperature exceeded 35 °C.

Table 3. The number of years having at least one day in the reproductive cycle with minimum temperature below –17 °C. The numbers are given for the different Hungarian wine regions, and using the RegCM (Re) and ALADIN (AL) simulations outputs.

	Danube		**Balaton**		**Eger**		**North-Transdanubia**		**Pannon**		**Sopron**		**Tokaj**	
	Re	AL	Re	AL	Re	AL	Re	AL	Re	AL	Re	AL	Re	AL
Reference period	19	17	14	15	21	19	16	16	15	12	11	10	21	18
Middle of the 21st cenrury	5	8	6	2	8	8	5	3	5	2	2	1	7	7
End of the 21st century	1	2	2	3	2	4	2	1	1	1	0	2	1	2

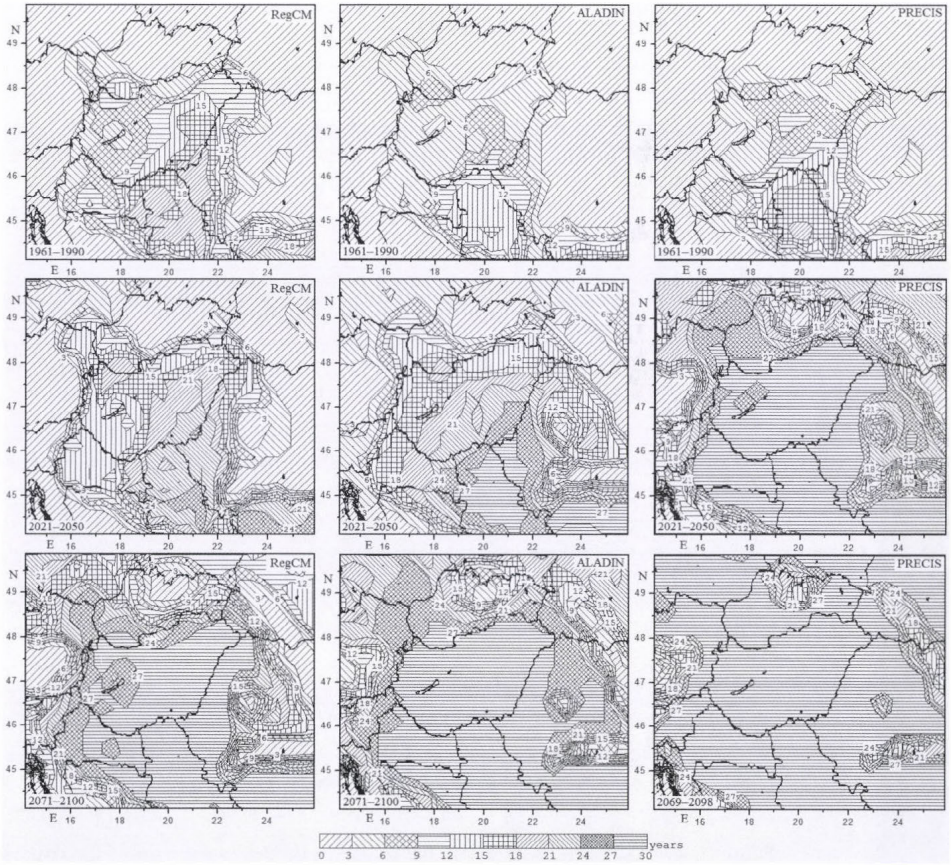

Fig. 5. The number of days in the vegetation cycle with maximum temperature above 35 °C. The two columns correspond to the RegCM (left), ALADIN (middle), and PRECIS (right) simulations' results. The rows of the figure show the model results for the reference period (upper), and the predictions for the middle (middle) and the end (lower) of the 21st century.

There will be a drastic rise in the number of years with extreme high temperature both in the middle and the end of the 21st century. All three models predict such days to occur in every two years in the middle of the 21st century, and in every year in the end of this century. In years, when there is at least one day with a maximum temperature above 35 °C, there will be a rise in the number of such days both in the middle and the end of the 21st century. The highest occurrence of such days is projected in Duna region. According to the RegCM predictions, there will be 2–4 days yearly with extreme hot temperatures in the middle of the 21st century, and can be as many as 5–13 such days per year in the end of this century. The rise in the number of extreme hot days is even greater when using the ALADIN and PRECIS simulations' outputs. Based on these models, we can expect 8–16 extreme hot days per year in the middle of the 21st century and 27–40 such days per year in the the end of this century.

Our results based on the three RCMs' simulations show (see *Table 4*) that the *HTC* will not reach the critical threshold value of 0.5 mm/°C neither in the immediate, nor in the far future. This means that the climatic conditions will be suitable for wine production in the Hungarian wine regions. It depends on the deviation of the *HTC* from 1 mm/°C whether these conditions move closer to or away from the optimum in particular regions.

Table 4. The values of the hydrothermal coefficient (*HTC*, in mm/°C) in the different Hungarian wine regions based on RegCM (Re), ALADIN (AL), and PRECIS (PR) model predictions.

	Danube			**Balaton**			**Eger**			**North-Transdanubia**		
	Re	AL	PR	Re	AL	PR	Re	AL	PR	Re	AL	PR
Reference period	0.90	0.92	0.89	1.12	1.21	1.15	1.05	1.07	1.03	0.99	1.03	1.00
Middle of the 21st cenrury	0.90	0.83	0.71	1.18	1.14	0.95	1.02	0.95	0.72	1.01	0.98	0.78
End of the 21st century	0.75	0.71	0.59	1.01	0.88	0.75	0.85	0.78	0.60	0.87	0.78	0.67

	Pannon			**Sopron**			**Tokaj**		
	Re	AL	PR	Re	AL	PR	Re	AL	PR
Reference period	0.92	0.98	0.94	1.24	1.32	1.32	1.15	1.19	1.14
Middle of the 21st cenrury	0.96	0.89	0.79	1.28	1.29	1.04	1.13	1.02	0.79
End of the 21st century	0.82	0.75	0.68	1.14	1.00	0.82	0.93	0.81	0.63

In the reference period, all three models showed excess heat in Danube and Pannon regions, and excess precipitation in Balaton, Eger, Sopron, and Tokaj regions. All three models resulted in North-Transdanubia region being climatic optimal.

The changes in the middle of the 21st century are not unambiguous. RegCM simulation does not show any change for Danube region, while for Balaton and Pannon regions it predicts an increase in excess precipitation. The climatic conditions are projected to become more suitable for grape production in Eger, Pannon, and Tokaj regions. ALADIN simulation predicts a decrease in excess precipitation or an increase in excess heat for all regions. This could lead to more favorable conditions in Balaton, Eger, Sopron, and Tokaj. Similarly to ALADIN, PRECIS simulation shows either a decrease in excess precipitation or an increase in excess heat for all wine regions, which results in an improvement in Balaton and Sopron regions.

All three models project similar conditions for the end of the 21st century, which means that we expect a decrease in excess precipitation or an increase in excess heat in all regions compared to the reference period. According to all three models, this again means better conditions for Sopron region and worse for Danube, Eger, North-Transdanubia, and Pannon regions compared to the conditions in the reference period. This change lead to more favorable conditions in Balaton (according to RegCM and ALADIN) and Tokaj (according to RegCM) regions.

4. Conclusions

Our investigations showed that in terms of modeled heat conditions, the 21st century will favor red wine grape and late-ripening varieties. We can derive this conclusion from the estimated increasing tendency of active degree days and of Huglin's heliothermal index. At the same time, we expect longer growing season allowed by the climatic conditions.

Frost-damages in the dormancy periods would become more rare due to the warming climate. However, the number of days with maximum temperature above 35 °C may increase, which could lead to serious heat damages. There should be more care spent on preventing and mitigating damages due to increased heat stress using adequate horticultural practices.

We expect a decrease in the hydrothermal coefficient in all regions by the end of the 21st century, which can lead to non-optimal climatic conditions, because heat as its denominator will likely be dominant.

Acknowledgments—Simulation of the PRECIS regional climate model was supported by grant OTKA K-78125. The authors are grateful for Ildikó Pieczka for providing bias-corrected model outputs. The RegCM and ALADIN simulations were developed within the ENSEMBLES project (505539) which was funded by the EU FP6 integrated program. The E-OBS database was provided by the

ENSEMBLES and ECA&D projects. This work has been supported by OTKA grants K81933 and K81975, also, by the projects KMR_12-1-2012-0206 and GOP-1.1.1.-11-2012-0164. The project was supported by the European Union and the European Social Fund (TÁMOP-4.2.1/B-09/1/KMR-2010-0003, FuturICT.hu grant no.: TÁMOP-4.2.2.C-11/1/KONV-2012-0013). We would also like to thank Peter Raffai for his valuable help with the English translation.

References

Davitaja, F.F. (*Давитая*, Ф.Ф.), 1959: Климатические показатели сырьевой базы виноградо-винодельческой промышленности. *Труды ВНИИВИВ „Магарач", 6(1)* 12–32. (in Russian)

Déqué, M., *Marquet*, P., and *Jones*, R.G., 1998: Simulation of climate change over Europe using a global variable resolution general circulation model. *Clim. Dynam. 14*, 173–189.

Dunkel, Z. and *Kozma*, F., 1981: A szőlő téli kritikus hőmérsékleti értékeinek területi eloszlása és gyakorisága Magyarországon. *Légkör 26. 2*, 13–15. (in Hungarian)

Formayer, H. and *Haas*, P., 2009: Correction of RegCM3 model output data using a rank matching approach applied on various meteorological parameters. Deliverable D3.2 RCM output localization methods (BOKU-contribution of the FP6 CECILIA project)

Giorgi, F., *Marinucci*, M.R., *Bates*, G.T., and *DeCanio*, G., 1993: Development of a second generation regional climate model (RegCM2). Part II: Convective processes and assimilation of lateral boundary conditions. *Mon. Weather Rev. 121*, 2814–2832.

Hajdú, E., 2003: Magyar szőlőfajták. Mezőgazda Kiadó, 11–223. (in Hungarian)

Haylock, M.R., *Hofstra*, N., *Klein Tank*, A.M.G., *Klok*, E.J., *Jones*, P.D., and *New*, M., 2008: A European daily highresolution gridded data set of surface temperature and precipitation for 1950-2006., *J. Geophys. Res. 113*, 1–12.

Huglin, P., 1978: Nouveau mode d'évaluluation des possibilites héliothermiques d'un milieo viticole. In: *Proceedings of the Symposium International sur l'ecologie de la Vigne. Ministére de l'Agriculture et de l'Industrie Alimentaire, Contanca,* 89–98. (in French)

Kozma, P., 2002: A szőlő és termesztése I. Akadémiai Kiadó, 13–19., 213–272. (in Hungarian)

van der Linden, P. and *Mitchell*, J.F.B., 2009: Summary of research and results from the ENSEMBLES project. Met Office Hadley Centre, Exeter, UK. 164.

Nakicenovic, N. and *Swart*, R.J., 2000: Emissions Scenarios 2000 – Special Report of the Intergovernmental Panel on Climate Change. Cambridge University Press, Cambridge. 570p.

Pieczka, I., *Pongrácz*, R., *Bartholy*, J., *Kis*, A., and *Miklós*, E., 2011: A szélsőségek várható alakulása a Kárpát-medence térségében az ENSEMBLES projekt eredményei alapján. In (Szerk.*: Lakatos M.)* 36. Meteorológiai Tudományos Napok - Változó éghajlat és következményei a Kárpát-medencében. Országos Meteorológiai Szolgálat, Budapest. 77–87. (in Hungarian)

Pieczka, I., 2012: A Kárpát-medence térségére vonatkozó éghajlati szcenáriók elemzése a PRECIS finom felbontású regionális klímamodell felhasználásával. PhD értekezés. ELTE Meteorológiai Tanszék, Budapest. 1–95. (in Hungarian)

Pongrácz, R., *Bartholy*, J., *Miklós*, E., 2011: Analysis of projected climate change for Hungary using ENSEMBLES simulations. *Appl. Ecol. Environ. Res. 9*, 387–398.

Szeljanyinov, G., T., 1928: On agricultural climate valuation. *Proc.of Agricul. Meteorol. 20,* 165–177.

Szenteleki, K., *Ladányi*, M., *Gaál*, M., *Zanathy*, G., and *Bisztray*, Gy. D., 2012: Climatic risk factors of Central Hungarian grape growing regions. *Appl. Ecol. Environ. Res 1*, 87–105.

Wilson, S., *Hassell*, D., *Hein*, D., *Jones*, R., and *Taylor*, R., 2007: Installing and using the Hadley Centre regional climate modelling system, PRECIS. Version 1.5.1. UK Met Office Hadley Centre, Exeter.

IDŐJÁRÁS

Quarterly Journal of the Hungarian Meteorological Service
Vol. 118, No. 3, July – September, 2014, pp. 207–216

Positive bias caused by residual water in reference PM_{10} measurements

Kornélia Imre[1]*, Ágnes Molnár[1], Viktor Dézsi[2], and András Gelencsér[3]

[1]*MTA-PE Air Chemistry Research Group, Egyetem u. 10, H-8200 Veszprém, Hungary*

[2]*Hungarian Meteorological Service, Air Quality Reference Centre, Gilice tér 39, H-1181 Budapest, Hungary*

[3]*Department of Earth and Environmental Sciences, University of Pannonia, Egyetem u. 10, H-8200 Veszprém, Hungary*

**Corresponding author: kornelia@almos.uni-pannon.hu*

(Manuscript received in final form March 4, 2014)

Abstract—Dry aerosol mass concentrations (PM_{10}, $PM_{2.5}$) are determined after conditioning of the filter at t=20±1 °C and RH=50±5% for 48 hours according to the standard protocol EN 12341. The main result of this work is that applying the standard pre-conditioning step, complete removal of adsorbed water cannot be attained. In our experiment, aerosol samples collected in Budapest between November 2008 and March 2010 using a CEN (European Committee for Standardization) gravimetric sampler (Digitel, DHA-80) were studied. Following PM_{10} mass concentration measurements according to the EN 12341 protocol, we repeated the gravimetric aerosol mass measurements in the laboratory using a glove box after in-situ pre-conditioning for 48 h at t=20±1 °C and RH<30%. We assumed that at this low relative humidity all the adsorbed residual water was removed, and the absolute dry mass concentrations of PM_{10} could be determined (referred in the following as dry PM_{10} concentration). The mass concentration of adsorbed residual water, defined as the difference between the results of the standard and dry PM_{10} measurements, varied greatly in the range of 0.05–16.9 $\mu g\ m^{-3}$. Expressed relative to the absolute dry PM_{10} mass concentrations, the residual water content in the standard measurement procedure amounted to 4.2±1.5% and 7.9±0.8% in summer and winter, respectively. In winter, relative contributions of adsorbed water as high as 33.2 m/m% was found. The significant seasonal differences as well as the large variations between individual samples may depend on various factors such as the chemical composition of the samples, particle load, and the RH history of the particles before and after sample collection. This last factor is expected to exert rather significant influence on the amount of adsorbed residual water, yet it is impossible to reconstruct. These findings have severe implications on reported dry PM_{10} mass concentrations using the EN 12341 protocol, especially in the winter period when most limit exceedances occur.

Key-words: urban PM_{10}, standard protocol, adsorbed residual water, dry mass concentration, low relative humidity

1. Introduction

Liquid water is a highly variable, but very often overlooked constituent of atmospheric particulate matter (PM_{10} or $PM_{2.5}$). The interaction between ambient aerosol particles and water vapor plays a crucial role in many fundamental atmospheric processes. Adsorbed water may significantly increase the size of the particles, which, in turn, enhances the extinction (mainly scattering) of visible light in the atmosphere. This is manifested in strongly reduced standard visibility at high relative humidity (RH) (*Cheng et al.,* 2011, *Deng et al.,* 2011). Liquid water on aerosol particles can serve as a medium for multiphase reactions (e.g., sulfur conversion in sea-salt aerosol particles, *Sievering et al.* (1991)), or secondary organic aerosol formation *Strollo* and *Ziemann* (2013); *Ervens* and *Volkamer* (2010). In supersaturated air, particles called cloud condensation nuclei can grow into cloud or fog droplets. The interaction between particles and water vapor depends on the relative humidity as well as the size, chemical composition, and wettability of the particles. Based on differences in their chemical compositions, particles of various origins can behave quite differently with changing humidity, from being purely hydrophobic to strongly hygroscopic. Hygroscopic particles take up water continuously with increasing RH, whereas deliquescent particles do not adsorb water up to a certain RH limit called the deliquescence point (DRH). At this point, however, a sudden phase change occurs with a steep increase in the mass of the particles. Increasing the RH further above the DRH, the liquid particle will continue to grow. However, once such a particle is turned into liquid, decreasing the RH will not make the particle recrystallize at the DRH. Below the DRH, the liquid particle becomes supersaturated resulting in a metastable state until the RH decreases below a critical value at which recrystallization occurs (*Hansson et al.,* 1998). This RH is called efflorescence relative humidity (ERH). For example, aqueous ammonium sulfate is saturated with respect to its crystalline phase at 82.6% RH at 260 K (*Clegg et al.,* 1998; *Onasch et al.,* 1999; *Cziczo* and *Abbatt,* 1999), whereas laboratory studies show that homogeneous crystallization of droplets does not occur before RH drops to 32.7% (*Onasch et al.,* 1999). Conversely, solid ammonium sulfate does not deliquesce at RH lower than 82.6%. Therefore, in the range 32.7% < RH < 82.6% the physical state of such a particle in the atmosphere depends on its RH history (*Colberg et al.,* 2003), the particles exist as a metastable droplet when the particles had not been exposed to relative humidity greater than their deliquescence RH.

There is often a discrepancy in chemical mass closures of atmospheric aerosol samples when they are normalized to gravimetrically measured mass of particulates. In other words, after all identified components are quantified, a part of PM mass remains unidentified. One possible source for the observed discrepancy between gravimetric PM mass and the total mass of all identified

components is particle-bound water. The amount of water in PM samples varies for different samples and measurement sites, depending on the particle composition and the ambient relative humidity and temperature (e.g., *Warneck,* 2000). According to *Kajino et al.* (2006), in winter when the relative humidity is high and the concentration of hygroscopic compounds is also high, approximately 70% of unidentified non-carbonaceous fraction of urban $PM_{2.5}$ (or about 10% of $PM_{2.5}$ mass) was assumed to be water. The authors also found that the aerosol water content in winter was 6–7 times higher in winter than in summer.

In spite the fact that *Saxena et al.* (1995) pointed out the importance of atmospheric water-soluble organic carbon (WSOC) for the observed hygroscopic behavior of atmospheric aerosols, the water uptake of aerosol particles has been largely associated with their inorganic constituents. Depending on the ambient conditions during and prior to sampling, particles can either adsorb or lose water under post-equilibration (*Tsyro,* 2005). The relationship among particle mass and composition and particle water content is rather complicated due to hysteresis in the behavior of particle-bound water. In many cases the atmospheric aerosol particles show strong RH-hysteresis behavior and retain substantial particle-bound water (*Santarpia et al.,* 2004; *Randriamiarisoa et al.,* 2006). This means that potentially a significant fraction of strongly hygroscopic particles exist as supersaturated droplets even at RH as low as 50%. One possible explanation for the significant amount of retained water is the acidity of the particles. This was observed in several places, e.g., in Pittsburgh, USA (*Khlystov et al.,* 2005) and in Switzerland (*Fisseha et al.,* 2006). According to *Tsyro* (2005), pure ammonium sulfate particles can still retain as much as 30% (m/m) of water at 50% relative humidity. *Ansari* and *Pandis* (1999) investigated the hysteresis of equimolar model aerosol mixtures (Na_2SO_4-NaCl and Na_2SO_4-NaCl-$NaNO_3$) and found that the residual mass of retained water at RH=50% was 83% and 71%, respectively. On the other hand, beside particle acidity, a number of organic components are shown to inhibit the aerosol deliquescence and efflorescence behavior (*Marcolli* and *Krieger,* 2006). *Zardini et al.* (2008) showed that the retained mass of water in the case of ammonium sulfate: adipic acid (2:1.1) model mixture was 30% at RH=50% following equilibrium dehumidification.

In recognition of the water-retaining characteristics of atmospheric particulate matter, standard off-line gravimetric measurement protocols all require the relative humidity to be set at a relatively low value and the filter samples be equilibrated before weighing. In Europe, the reference method developed by the European Committee for Standardization (CEN) prescribes that the filters should be equilibrated for 48 h prior to weighting at RH=50±5% and t=20±2 °C before and after sampling. This standard reference method is used to validate the readings of automatic beta-gauge

monitors (FH 62-IN, Thermo Andersen) that are in use in hourly PM concentration measurements.

Several studies indicated that there were deviations between automatic and standard off-line PM mass concentration measurements (*Shin et al.,* 2011, *Takahashi et al.,* 2008, *Salminen* and *Karlsson,* 2003), with higher differences at high ambient RHs (*Chang* and *Tsai,* 2003). These results also imply the significance of retained water of particles under the standard reference methods.

The objective of this study is to determine the residual water content of PM filter samples collected in winter and summer in the city of Budapest, Hungary, which are equilibrated according to the standard analysis protocol. This is done to determine the potential bias of standard gravimetric measurements due to the incomplete removal of particle-bound water upon equilibration.

2. Methodology

2.1. Aerosol sampling

The aerosol sampling was carried out in Budapest (Marczell György Observatory, Hungarian Meteorological Service) at a suburban sampling site. The aerosol sampling were carried out in 57 consecutive days in winter of 2008–2009, 22 days in summer of 2009, and further 75 days in winter of 2009–2010.

PM_{10} aerosol samples were collected on glass fiber filters (Munktell MG 160, d=150 mm) at a flow rate of 30 $m^3 h^{-1}$ by using a Digitel-DH 80 reference sampler (CEN, 1998) at a height of 2 m.

2.2. Gravimetric measurements

Before and after the sampling, glass fiber filters were placed for 48 hours into an isolated chamber at a temperature of 20±1 °C and RH of 50±5%, as required by the EN 12341 standard protocol (CEN, 1998). Then PM_{10} mass was determined by weighing with an electrical micro-balance (Sartorius, BP 211 D) of 10 μg accuracy.

Filter blanks were treated in the same way. The relative humidity was measured by a hygrograph, which was calibrated in the climate chamber of the Hungarian Meteorological Service. The detailed measurement conditions can be found in *Imre* and *Molnár* (2008). In order to determine the residual water content of aerosol mass measured according to the EN 12341 protocol, the filter sample was equilibrated for another 48 h at t=20±1 °C and RH<20% prior to the following gravimetric measurement. The relative humidity in the measurement chamber was set by DRIERIT (calcium sulfate, W.A. Hammond Drierite Co. Ltd.) heated at 230 °C for 2 hours.

3. Results and discussions

The PM_{10} dry mass concentrations measured from the collected filter samples according to EN 12341 standard protocol are shown *Fig. 1.* The 24-hour health threshold limit for PM_{10} concentration in Hungary (and EU) is 50 $\mu g\ m^{-3}$, while the air quality public warning "Information" and "Alert" threshold limits are 75 and 100 $\mu\ gm^{-3}$, respectively, as regulated by the Ministry of Rural Development (4/2011) are also indicated in the figure.

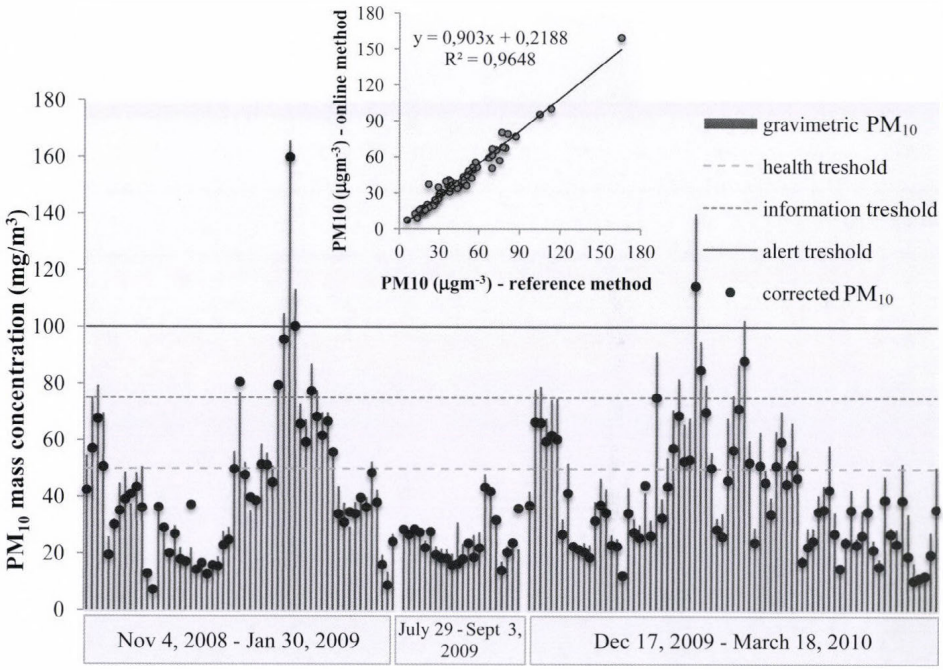

Fig. 1. Gravimetrically determined dry mass concentration at 50% RH according to EN 12341 (CEN 1998) and the relationship between the online and gravimetric PM_{10} concentrations (inserted picture).

According to the regulations, the evaluation of the limit exceedances should be based on the 24 h PM_{10} mass concentrations measured by an automatic beta-gauge monitor FH 62-IN (Thermo Andersen) and not on those measured by the reference method. For this reason these data are also shown in *Fig. 1.* (It should be noted that this instrument was located adjacent to the Digitel-DH 80 reference sampler and the data of beta-gauge monitor are averaged for the time period of sample collection.) Adding this constraint (to the

calculation) the measured PM_{10} reference dry mass concentrations exceeded the alert threshold for 34 days, for additional 14 days the information, threshold and for another 5 days the health limits.

In the following we considered that under the equilibrium conditions required by the reference method (20±1°C and RH of 50±5% for 48 h), residual water was retained in the particles. In order to determine the residual water content of the aerosol, further gravimetric measurements were necessary that is specified by equilibration at t=20±1 °C and RH<30% lasting for 48 h. The mass concentration of water retained under the conditions of the standard protocol was determined as a difference between the mass concentrations measured according the EN 12341 protocol and the dry mass concentration specified above. The mass fraction of residual water expressed in percentage of the PM_{10} mass concentrations measured by the reference method is shown in *Fig. 2*. It is interesting to note, that despite the fact, that the aerosol water content was higher in winter than in summer, no significant relationship between the ambient RH (during the sampling) and the measured water content was found.

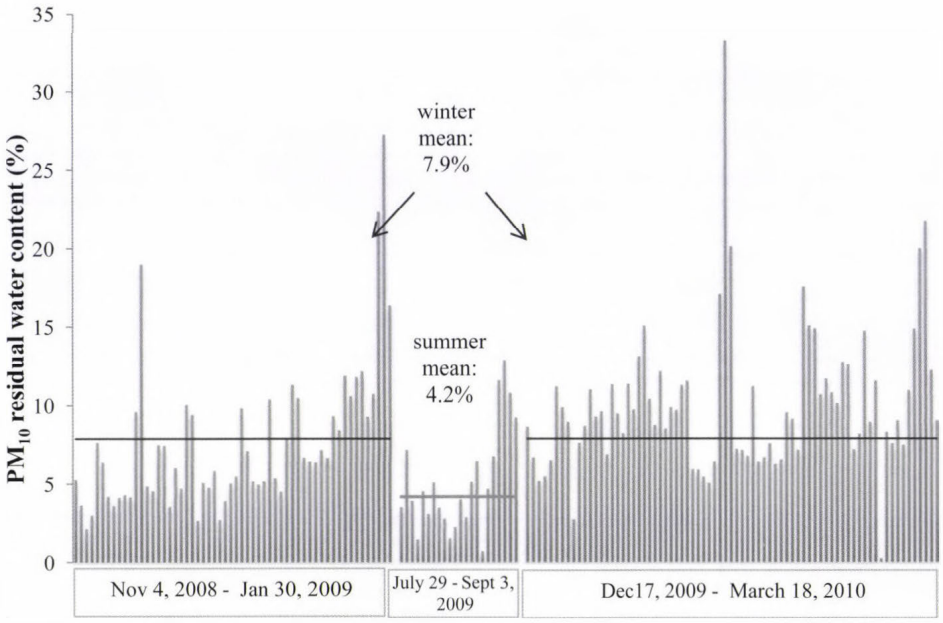

Fig. 2. Experimentally determined residual water content of PM_{10} under the conditions on EN 12341 protocol.

It follows that the mass fraction of residual water quantity reflects the share of particle-bound water to the mass of particles measured at 30% RH. The mass concentrations of residual water varied between 0.05 and 16.9 $\mu g\ m^{-3}$. The histograms of the relative contributions of residual water are depicted in *Fig. 3* both for summer and winter.

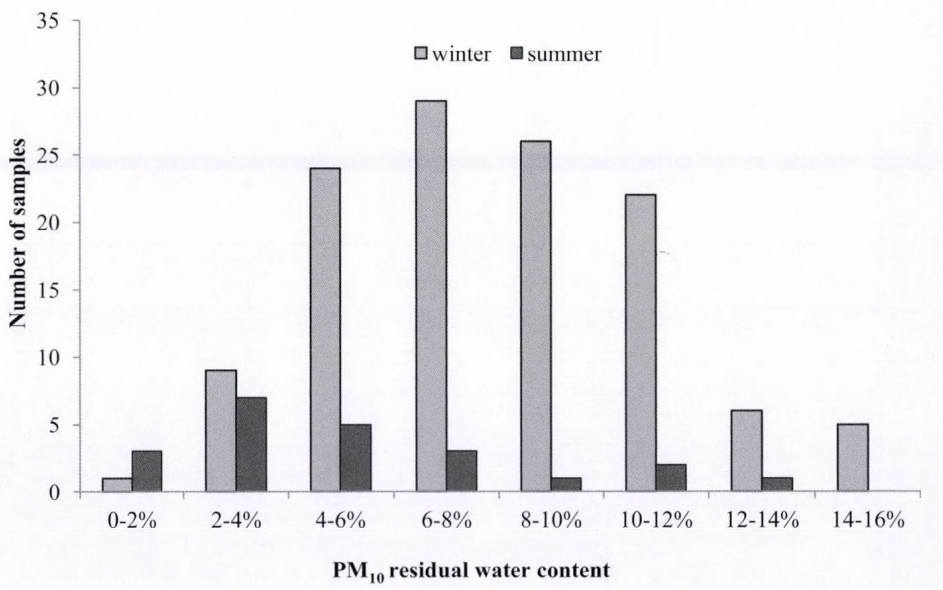

Fig. 3. Frequency distributions of residual water content of PM_{10} mass measured according to EN 12341 protocol.

The frequency of the contribution of residual water can be well described by a log-normal distribution in both seasons. In summer the mean water content is 4.2±1.5% (p=95% (Student-probe), while in winter the peaks are significantly shifted towards higher values (mean: 7.9±0.8%, p=95%) indicating that in winter the aerosol has lower DRH values and more hygroscopic than in summer.

After determination of the water content of the aerosol particles, the PM_{10} mass concentrations were corrected with these water content values. An important consequence of replacing the measured PM_{10} reference with the absolute dry mass concentrations is that the number of total exceedances of the health, information, and alert limits could be reduced by 9 (26%), 7 (50%), and 2 (40%) days, respectively (*Fig. 4*).

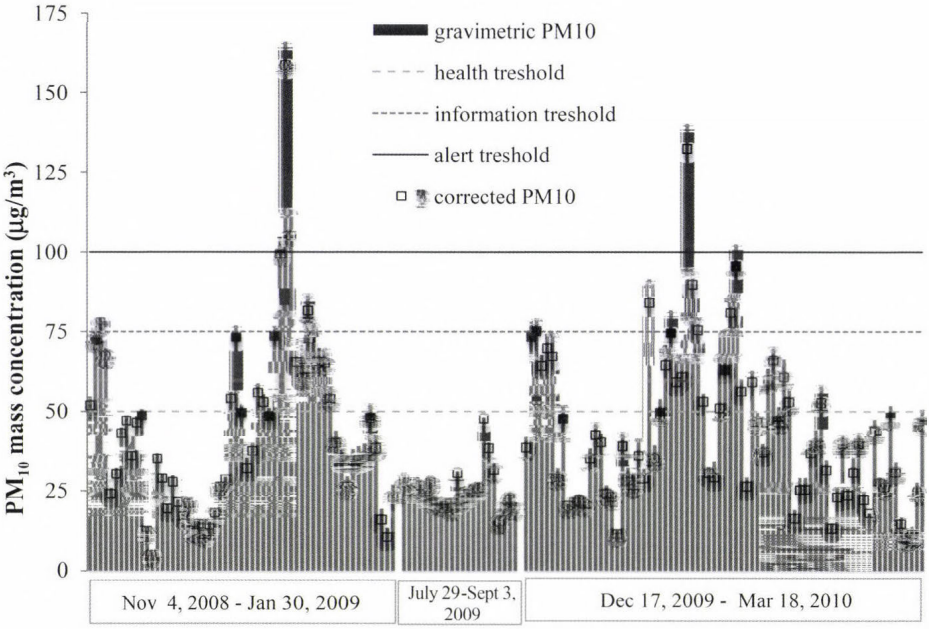

Fig. 4. Gravimetrically determined and calculated dry mass concentrations.
(Full squares indicate when the corrected PM_{10} concentration falls below the threshold limits.)

The results of our experiments suggest that PM_{10} filters measured gravimetrically according to the EN 12341 protocol do retain variable but sometimes significant amount of residual water at RH of 50±5% and at temperature of 20±1 °C after equilibration for 48 h. This finding questions that the reference measurements yield dry PM_{10} mass concentrations as intended to be according to the EN 12341 protocol. These results are not necessarily surprising based on previous laboratory and theoretical studies that showed that many abundant aerosol constituents exhibit hysteresis in their hygroscopic behavior and retain water down to their efflorescence RH well below 50% (*Weingartner et al.,* 1995; *Zhou et al.,* 2000; *Gao et al.,* 2008). Since adsorbed water does not pose any health risk but contributes quite significantly to measured PM_{10} mass concentration, the justification of environmental legislation based on EN 12341 protocol is questionable. Given the complexity of the issue and for lack of feasible methodological solutions, we suggest that the uncertainties of measured PM_{10} concentration values should be extended with a statistically derived seasonal factor that may account for the residual water content that causes positive bias in the reference measurements. Since the scope of our study is limited, extension of this research to biases caused by residual water in the readings of automatic beta-gauge monitors is clearly warranted.

Acknowledgements–Present article was published in the frame of the project TÁMOP-4.2.2.A-11/1/KONV-2012-0064: „Regional effects of weather extremes resulting from climate change and potential mitigation measures in the coming decades". The project is realized with the support of the European Union, with the co-funding of the European Social Fund.

References

Ansari, A.S. and *Pandis, S.N.*, 1999: Prediction of multicomponent inorganic atmospheric aerosol behaviour. *Atmos Environ 33,* 745–757.

CEN, 1998: Air Quality—Determination of the fraction of suspended particulate matter—Reference method and field test procedure to demonstrate reference equivalence of measurement methods. EN 12341.

Cheng, S., Yang, L., Zhou, X., Xue, L., Gao, X., Zhou, Y., and *Wang, W.*, 2011: Size-fractionated water-soluble ions, situ pH and water content in aerosol on hazy days and the influences on visibility impairment in Jinan, China. *Atmos Environ 45,* 4631–4640.

Chang, C.T. and *Tsai, C.J.*, 2003: A model for the relative humidity effect on the readings of the beta-gauge monitor. *Aerosol Sci 34,* 1685–1697.

Clegg, S.L., Brimblecombe, P., and *Wexler, A.S.*, 1998: A thermodynamic model of the system H^+-NH_4^+-SO_4^{2-}-NO_3^--H_2O at tropospheric temperatures. *J. Phys. Chem. A102*, 2137–2154.

Cziczo, D.J. and *Abbatt, J.P.D.*, 1999: Deliquescence, efflorescence, and supercooling of ammonium sulfate aerosols at low temperature: Implications for cirrus cloud formation and aerosol phase in the atmosphere. *J. Geophys. Res. 104,* 13781–13790.

Colberg, C.A., Luo, B.P., Wernli, H., Koop, T., and *Peter Th.*, 2003: A novel model to predict the physical state of atmospheric H2SO4/NH3/H2O aerosol particles. *Atmos. Chem. Phys. 3,* 909–924.

Deng, J., Wang, T., Jiang, Z., Xie, M., Zhang, R., Huang, X., and *Zhu, J.*, 2011: Characterization of visibility and its affecting factors over Nanjing, China. *Atmos. Res. 101,* 681–691.

Ervens, B. and *Volkamer, R.*, 2010: Glyoxal processing by aerosol multiphase chemistry: towards a kinetic modeling framework of secondary organic aerosol formation in aqueous particles, *Atmos. Chem. Phys. 10,* 8219–8244.

Fisseha, R., Dommen, J., Gaeggeler, K., Weingartner, E., Samburova, V., Kalberer, M., and *Baltensperger U.*, 2006: On line gas and aerosol measurement of water soluble carboxylicacids in Zurich. *J. Geophys. Res. 111,* 12316. doi:10.1029/2005JD006782.

Gao, Y., Yu, L.E., and *Chen, S.B.*, 2008: Effects of organics on efflorescence relative humidity of ammonium sulfate or sodium chloride particles. *Atmos. Environ. 42,* 4433–4445

Hansson, H.C., Rood, M.J., Koloutsou-Vakakis, S., Hämeri, K., Orisini, D., and *Wiedensohler A.*, 1998: NaCl aerosol particle hygroscopicity dependence on mixing with organic compounds. *J. Atmos. Chem. 31,* 312–346.

Imre, K. and *Molnár, A.*, 2008: Hygroscopic behavior of Central European atmospheric background aerosol particles in summer. *Időjárás 112,* 63–82.

Kajino M., Winiwarter W., and *Ueda H.*, 2006: Modeling retained water content in measured aerosol mass. *Atmos. Environ. 40,* 5202–5213.

Khlystov, A., Stanier, C.O., Takahama, S. and *Pandis, S.*, 2005: Water content of ambient aerosol during the Pittsburgh Air Quality Study. *J. Geophys. Res. 110,* D07S10, doi:10.1029/2004JD004651.

Marcolli, C. and *Krieger, U.K.*, 2006: Phase changes during hygroscopic cycles of mixed organic/inorganic model systems of tropospheric aerosols. *J. Phys. Chem. A110,* 1881–1893

Ministry of Rural Development 4/2011. (2011). (I.14.) VM rendelet a levegőterheltségi szint határértékeiről és a helyhez kötött légszennyező pontforrások kibocsátási határértékeiről. (in Hungarian)

Onasch, T.B., Siefert, R.L., Brooks, S.D., Prenni, A., Murray, B., Wilson, M., and *Tolbert, M.A.*, 1999: Infrared spectroscopic study of the deliquescence and efflorescence of ammonium sulfate aerosol as a function of temperature. *J. Geophys. Res.104,* 21317–21326.

Randriamiarisoa, H., Chazette, P., Couvert, P., Sanak, J., and *Megie, G.*, 2006: Relative humidity

impact on aerosol parameters in a Paris suburban area. *Atmos. Chem. Phys.6,* 1389–1407.

Salminen, K. and *Karlsson, V.,* 2003: Comparability of low-volume PM_{10} sampler with β-attenuation monitor in background air. *Atmos. Environ. 37,* 3707–3712.

Santarpia, J.L., Li, R., and *Collins, D.R.,* 2004: Direct measurement of the hydration state of ambient aerosol populations. *J. Geophys. Res. 109,* D18209, doi:10.1029/2004JD004653.

Saxena, P., Hildemann, L.M., McMurry, P.H. and *Seinfeld, J.H.,* 1995: Organics alter hygroscopic behavior of atmospheric particles, *J. Geophys. Res. 100,* D9, 18755–18770.

Shin, S., Jung, C., and *Kim, Y.,* 2011: Analysis of the Measurement Difference for the PM_{10} Concentrations between Beta-ray Absorption and Gravimetric Methods at Gosan. *Aeros. Air Qual. Res. 11,* 846–853.

Sievering H., Boatman J., Galloway J., Keene W., Kim Y., Luria M., Ray J., 1991: Heterogeneous sulfur conversion in sea-salt aerosol particles: the role of aerosol water content and size distribution *Atmos. Environ. Part A. General Topics 25,* 1479–1487.

Strollo, C. and *Ziemann, P.,* 2013: Products and mechanism of secondary organic aerosol formation from the reaction of 3-methylfuran with OH radicals in the presence of NOx. *Atmos. Environ. 77,* 534–543.

Takahashi, K., Minoura, H., and *Sakamoto, K.,* 2008: Examination of discrepancies between beta-attenuation and gravimetric methods for the monitoring of particulate matter. *Atmos. Environ. 42,* 5232–5240.

Tsyro, G., 2005: To what extent can aerosol water explain the discrepancy between model calculated and gravimetric and PM2.5? *Atmos. Chem. Phys. 5,* 515–532.

Warneck, P., 2000: Chemistry of the natural atmosphere, Academic Press, USA.

Weingartner E., Baltensperger, U., and *Burtscher, H.,* 1995: Growth and structural changes of combustion aerosols at high relative humidity. *J. Aeros.Sci. 26,* 667–668.

Zardini, A.A., Sjogren, S., Marcolli, C., Krieger, U.K., Gysel, M., Weingartner, E., Baltensperger, U., and *Peter, T.,* 2008: A combined particle trap/HTDMA hygroscopicity study of mixed inorganic/organic aerosol particles. *Atmos. Chem. Phys. 8,* 5589–5601.

Zhou, J., Swietlicki, E., Martinsson, B.G., Frank, G., and *Karlsson, M.N.A.,* 2000: Hygroscopic properties of aerosol particles during the Holme Moss hill cap cloud experiment. *J.f Aeros. Sci. 11,* 299–300.

IDŐJÁRÁS

Quarterly Journal of the Hungarian Meteorological Service
Vol. 118, No. 3, July – September, 2014, pp. 217–241

Comparison of the BMA and EMOS statistical methods in calibrating temperature and wind speed forecast ensembles

Sándor Baran[1]*, **András Horányi**[2], and **Dóra Nemoda**[1]

[1]*Faculty of Informatics, University of Debrecen*
Kassai út 26, H-4028 Debrecen, Hungary

[2]*Hungarian Meteorological Service*
Kitaibel pál u. 1, H-1024 Budapest, Hungary

**Corresponding author E-mail: baran.sandor@inf.unideb.hu*

(Manuscript received in final form June 6, 2014)

Abstract—The evolution of the weather can be described by deterministic numerical weather forecasting models. Multiple runs of these models with different initial conditions and/or model physics result in forecast ensembles which are used for estimating the distribution of future atmospheric states. However, these ensembles are usually under-dispersive and uncalibrated, so post-processing is required. In the present work we compare different versions of Bayesian model averaging (BMA) and ensemble model output statistics (EMOS) post-processing methods in order to calibrate 2m temperature and 10m wind speed forecasts of the operational ALADIN limited area model ensemble prediction system of the Hungarian Meteorological Service. We show that compared to the raw ensemble, both post-processing methods improve the calibration of probabilistic and accuracy of point forecasts. In case of temperature, the BMA method with linear bias correction slightly outperforms the corresponding EMOS technique, while the EMOS model shows the best performance for calibrating ensemble forecasts of wind speed.

Key-words: Bayesian model averaging, ensemble model output statistics, ensemble calibration

1. Introduction

The evolution of the weather can be described by numerical weather prediction (NWP) models, which are capable to simulate the atmospheric motions taking into account the physical governing laws of the atmosphere and the connected spheres (typically sea or land surface). Without any doubts, these models

provide primary support for weather forecasting and decision making. As a matter of fact, the NWP models and consequently the weather forecasts cannot be fully precise, and on top of that, their accuracy might change with the meteorological situation as well (due to the chaotic character of the atmosphere, which manifests in being very sensitive to its initial conditions). Therefore, it is a relevant request from the users to provide uncertainty estimations attached to the weather forecasts. The information related to the intrinsic uncertainty of the weather situation and the model itself is very valuable additional information, which is generally provided by the use of ensemble technique. The ensemble method is based on the accounting of all uncertainties exist in the NWP modeling process and its expression in terms of forecast probabilities. In this process first, all the uncertainties (possible error sources) of the NWP model are listed and then these error sources are quantified. The quantified errors are used to determine such perturbations, which are used for the creation of the forecast ensemble. In practice, the ensemble method is realized by the exploitation of an ensemble prediction system (EPS). An EPS exploits several NWP model runs (and these ensemble model members differ within the known uncertainties of the initial and boundary conditions, model formulation, etc.) and then evaluates the ensemble of forecasts statistically. Ensemble prediction systems are widely used by the meteorological community especially for medium-range weather forecasts (*Buizza et al.,* 2005), and this tool is becoming more and more popular for short range (*Iversen et al.,* 2011) and even ultra-short range (*Bouallègue et al.,* 2013) weather prediction.

One possible improvement area of the ensemble forecasts is the calibration of the ensemble in order to transform the original ensemble member-based probability density function (PDF) into a more reliable and realistic one. The main disadvantage of the method is that it is based on statistics of model outputs, and therefore unable to consider the physical aspects of the underlying processes. The latter issues should be addressed by the improvements of the reality of the model descriptions and particularly the better uncertainty descriptions used by the different model realizations.

From the various modern post-processing techniques (for an overview see, e.g., *Williams et al.,* 2014), probably the most widely used methods are the Bayesian model averaging (BMA, see, e.g., *Raftery et al.,* 2005; *Sloughter et al.,* 2007, 2010; *Soltanzadeh et al.,* 2011) and the ensemble model output statistics (EMOS, see, e.g., *Gneiting et al.,* 2005*; Wilks* and *Hamil,* 2007; *Thorarinsdottir* and *Gneiting,* 2010) which are implemented in ensembleBMA (*Fraley et al.,* 2009, 2011) and ensembleMOS packages of R. Both approaches provide estimates of the densities of the predictable weather quantities and once a predictive density is given, a point forecast can be easily determined (e.g., mean or median value).

The BMA method for calibrating forecast ensembles was introduced by *Raftery et al.* (2005). The BMA predictive PDF of a future weather quantity is

the weighted sum of individual PDFs corresponding to the ensemble members. An individual PDF can be interpreted as the conditional PDF of the future weather quantity, provided that the considered forecast is the best one and the weights are based on the relative performance of the ensemble members during a given training period.

The EMOS approach, proposed by *Gneiting et al. (*2005), uses a single parametric distribution as a predictive PDF with parameters depending on the ensemble members.

In both post-processing techniques, the unknown parameters are estimated using forecasts and validating observations from a rolling training period, which allows automatic adjustments of the statistical model to any changes of the EPS system (for instance seasonal variations or EPS model updates). EMOS method is usually more parsimonious and computationally more effective than BMA, but shows less flexibility. E.g., in case of a weather quantity following normal or truncated normal distribution the EMOS predictive PDF is by definition unimodal, while BMA approach allows multimodality.

The aim of the present paper is to compare the performance of BMA and EMOS calibration on the ensemble forecasts of temperature and wind speed produced by the operational limited area model ensemble prediction system of the Hungarian Meteorological Service (HMS) called ALADIN-HUNEPS (*Hágel*, 2010; *Horányi et al.,* 2011).

2. ALADIN-HUNEPS ensemble

The ALADIN-HUNEPS system of the HMS covers a large part of continental Europe with a horizontal resolution of 12 km, and it is obtained with dynamical downscaling (by the ALADIN limited area model) of the global ARPEGE based PEARP system of Météo France (*Horányi et al.*, 2006; *Descamps et al.,* 2009). The ensemble consists of 11 members, 10 initialized from perturbed initial conditions and one control member from the unperturbed analysis, implying that the ensemble contains groups of exchangeable forecasts.

The initial perturbations for PEARP are generated with the combination of singular vector-based and EDA-based perturbations (*Labadie et al.*, 2012). The singular vectors are optimized for 7 subdomains and then combined into perturbations. The EDA perturbations are computed as differences between the EDA members and the EDA mean (there is a 6-member EDA system running in France). These two sets of perturbations are combined into 17 perturbations, which are added to and subtracted from the control initial condition. Random sets of physical parameterizations (there are 10 sets of different physical parameterization packages) are attributed to the forecasts run from the differently perturbed initial conditions. All these combinations result in a 35-member (one control without perturbation and 34 perturbed members) global ensemble. The

ALADIN-HUNEPS system simply takes into account (and dynamically downscales) the control and the first 10 members of the PEARP system. These members contain the first 5 global perturbations added to and subtracted from the control.

The database contains 11 member ensembles of 42-hour forecasts for 2-meter temperature (given in K) and 10-meter wind speed (given in m/s) for 10 major cities in Hungary (Miskolc, Szombathely, Győr, Budapest, Debrecen, Nyíregyháza, Nagykanizsa, Pécs, Kecskemét, Szeged) produced by the ALADIN-HUNEPS system of the HMS, together with the corresponding validating observations for the one-year period between April 1, 2012 and March 31, 2013. The forecasts are initialized at 18 UTC. The data set is fairly complete, since there are only six days when no forecasts are available. These dates were excluded from the analysis.

Fig. 1 shows the verification rank histograms of the ensemble forecasts of temperature and wind speed. These are the histograms of ranks of validating observations with respect to the corresponding ensemble forecasts computed from the ranks at all locations and over the whole verification period (see, e.g., *Wilks*, 2011, Section 8.7.2). Both histograms are far from the desired uniform distribution, as in many cases the ensemble members either underestimate or overestimate the validating observations. The ensemble ranges contain the observed temperature and wind speed only in 60.61% and 68.52% of the cases, respectively (while their nominal values equal 10/12, i.e., 83.33%). Hence, both ensembles are under-dispersive and, in this way, they are uncalibrated. This supports the need of statistical post-processing in order to improve the forecasted probability density functions.

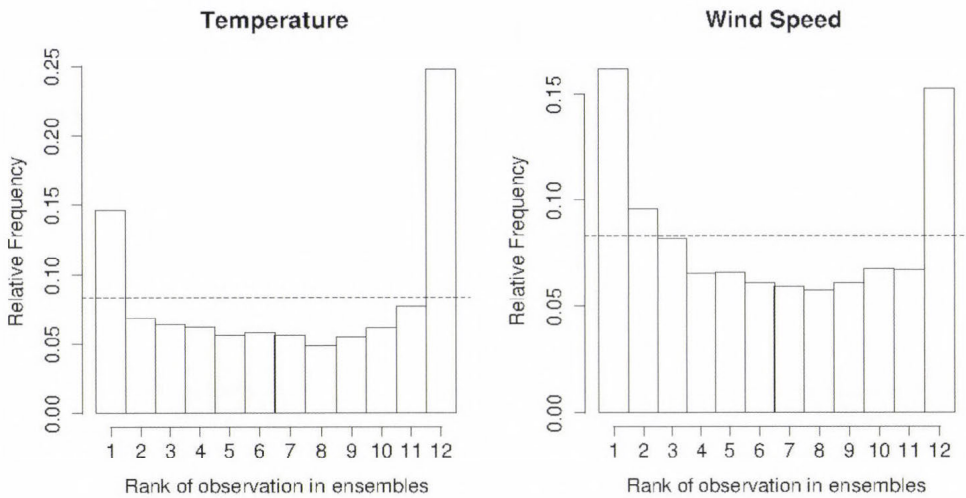

Fig. 1. Verification rank histograms of the 11-member ALADIN-HUNEPS ensemble forecasts of 2 m temperature and 10 m wind speed. Period: April 1, 2012 – March 31, 2013.

Note that BMA calibration of wind speed (*Baran et al.*, 2013; *Baran*, 2014) and temperature (*Baran et al.*, 2014) forecasts of the ALADIN-HUNEPS system have already been investigated by the authors using smaller data sets covering the period from October 1, 2010 to March 25, 2011. These investigations showed that significant improvements can be gained with the use of BMA post-processing. Nevertheless, it is interesting to see what enhancement can be obtained by BMA with respect to an improved raw EPS system and particularly in comparison to the EMOS calibration technique.

3. *Methods and verification scores*

As it has been mentioned in the Introduction, our study is concentrating on BMA and EMOS approaches. By $f_1, f_2, \ldots, f_M$ we denote the ensemble forecast of a certain weather quantity X for a given location and time. The ensemble members are either distinguishable (we can clearly identify each member or at least some of them) or indistinguishable (when the origin of the given member cannot be identified). Usually, the distinguishable EPS systems are the multi-model, multi-analyses ensemble systems, where each ensemble member can be identified and tracked. This property holds, e.g., for the University of Washington mesoscale ensemble (*Eckel* and *Mass,* 2005) or for the COSMO-DE ensemble of the German Meteorological Service (*Gebhardt et al.,* 2011).

However, most of the currently used ensemble prediction systems incorporate ensembles where at least some members are statistically indistinguishable. Such ensemble systems are usually producing initial conditions based on algorithms, which are able to find the fastest growing perturbations indicating the directions of the largest uncertainties (for instance, singular vector computations (*Buizza et al.*, 1993) or search for breeding vectors (*Toth* and *Kalnay*, 1997)). In most cases, these initial perturbations are further enriched by perturbations simulating model uncertainties as well. It is typically the case for the 51-member European Centre for Medium-Range Weather Forecasts ensemble (*Leutbecher* and *Palmer*, 2008) or for the PEARP and ALADIN-HUNEPS ensemble (*Hágel*, 2010; *Horányi et al.*, 2011) described in Section 2. In such cases, one usually has a control member (the one without any perturbation) and the remaining ensemble members are forming one or two exchangeable groups.

In what follows, if we have M ensemble members divided into m exchangeable groups, where the kth group contains $M_k > 1$ ensemble members ($\sum_{k=1}^{M} M_k = M$), notation $f_{k,\ell}$ is used for the ℓth member of the kth group.

3.1. Bayesian model averaging

In the BMA model proposed by *Raftery et al.* (2005), to each ensemble member f_k corresponds a component PDF $g_k(x|f_k, \theta_k)$, where θ_k is a parameter to be estimated. The BMA predictive PDF of X is

$$p(x|f_1, \dots, f_M) := \sum_{k=1}^{M} \omega_k g_k(x|f_k; \theta_k),$$

where the weight ω_k is connected to the relative performance of the ensemble member f_k during the training period. Obviously, these weights form a probability distribution, that is $\omega_k \geq 0, k = 1,2,..,M$, and $\sum_{k=1}^{M} \omega_k = 1$.

For the situation when M ensemble members are divided into m exchangeable groups, *Fraley et al.* (2010) suggested to use the following model

$$p(x|f_{1,1}, \dots, f_{1,M_1}, \dots, f_{m,1}, \dots, f_{m,M_m}) := \sum_{k=1}^{m} \sum_{\ell=1}^{M_k} \omega_k \, g_k(x|f_{k,\ell}; \theta_k), \quad (1)$$

where ensemble members within a given group have the same weights and parameters. Since this is the case for the ALADIN-HUNEPS ensemble (i.e., it consists of groups of exchangeable members), in what follows, we present only the weather variable specific versions of Eq. (1).

Temperature

For modeling temperature (and pressure) *Raftery et al.* (2005) and *Fraley et al.* (2010) use normal component PDFs, and Eq. (1) takes the form

$$p(x|f_{1,1}, \dots, f_{1,M_1}, \dots, f_{m,1}, \dots, f_{m,M_m}) := \sum_{k=1}^{m} \sum_{\ell=1}^{M_k} \omega_k \, g(x|f_{k,\ell}; \beta_{0,k}, \beta_{1,k}, \sigma^2), \quad (2)$$

where $g(x|f; \beta_0, \beta_1, \sigma^2)$ is a normal PDF with mean $\beta_0 + \beta_1 f$ (linear bias correction) and variance σ^2. Mean parameters $\beta_{0,k}$ and $\beta_{1,k}$ are usually estimated with linear regression of the validating observation on the corresponding ensemble members, while weights ω_k and variance σ^2, by maximum likelihood (ML) method using training data consisting of ensemble members and verifying observations from the preceding n days (training period). For example, taking $n = 30$, the predictive PDF, e.g., for 12 UTC March 31, 2013 at a given place can be obtained from the ensemble forecast for this particular day, time, and location (initialized at 18 UTC, March 29, 2013) with model parameters estimated from forecasts and verifying observations for all 10 locations from the period February 28 – March 29, 2013 (30 days, 300 forecast cases).

Another method for estimating model parameters is to minimize an appropriate verification score (see Section 3.3) using the same rolling training data as before.

As special cases of the model given by Eq. (2), one can also consider the situations when only additive bias correction present, that is $b_{1,k} = 1$, and when bias correction is not applied at all, i.e., $b_{0,k} = 0$ and $b_{1,k} = 1, k = 1,2, \dots, m$.

Wind speed

Since wind speed can take only non-negative values, for modeling this weather quantity a skewed distribution is required. A popular candidate is the Weibull distribution (see, e.g., *Justus et al.,* 1978), however, *Tuller* and *Brett* (1984) pointed out that the necessary conditions for fitting this distribution are not always met. *Sloughter et al.* (2010) proposes the BMA model

$$p(x|f_{1,1}, \dots, f_{1,M_1}, \dots, f_{m,1}, \dots, f_{m,M_m}) := \sum_{k=1}^{m} \sum_{\ell=1}^{M_k} \omega_k h(x|f_{k,\ell}; b_{0,k}, b_{1,k}, c_0, c_1), \quad (3)$$

for power transformations of the observed wind speed, where by $h(x|\mathrm{f}; b_0, b_1, c_0, c_1)$ we denote the PDF of gamma distribution with mean $b_0 + b_1 f$ and standard deviation $c_0 + c_1 f$. Parameters can be estimated in the same way as before, that is either mean parameters by regression and weights and standard deviation parameters by ML method or by minimizing a verification score. It is worth mentioning that in the ensembleBMA package of R, a more parsimonious model is implemented, where the mean parameters are constant across all ensemble members. In what follows, we will use this simplification, too. Further, preliminary studies (*Baran*, 2014) showed that for the ALADIN-HUNEPS ensemble, untransformed gamma BMA model gives the best fit, so no power transformations are needed.

As an alternative to the gamma BMA approach, *Baran* (2014) suggests to model wind speed with a mixture of truncated normal distributions with a cut-off at zero $\mathcal{N}^0(\mu, \sigma^2)$, where the location μ of a component PDF is an affine function of the corresponding ensemble member. The proposed BMA model is

$$p(x|f_{1,1}, \dots, f_{1,M_1}, \dots, f_{m,1}, \dots, f_{m,M_m}) := \sum_{k=1}^{m} \sum_{\ell=1}^{M_k} \omega_k q(x|f_{k,\ell}; \beta_{0,k}, \beta_{1,k}, \sigma^2), \quad (4)$$

where $q(x|\mathrm{f}; \beta_0, \beta_1, \sigma^2)$ is a truncated normal PDF with location $\beta_0 + \beta_1 f$ and scale σ^2, that is

$$q(x|\mathrm{f}; \beta_0, \beta_1, \sigma^2) := \frac{\frac{1}{\sigma}\varphi((x-\beta_0-\beta_1 f)/\sigma)}{\Phi((\beta_0+\beta_1 f)/\sigma)}, \text{ for } x \geq 0,$$

and 0, otherwise. Here φ and Φ denote the PDF and the cumulative distribution function (CDF) of the standard normal distribution, respectively.

For estimating parameters of the model specified by Eq. (4) *Baran* (2014) uses a full ML method, which means that all parameter estimates are obtained by maximizing the likelihood function corresponding to the training data.

3.2. Ensemble model output statistics

As noted, the EMOS predictive PDF is a single parametric density where the parameters are functions of the ensemble members.

Temperature

Similarly to the BMA approach, for modeling temperature (and pressure) normal distribution seems to be a reasonable choice. The EMOS predictive distribution suggested by *Gneiting et al.* (2005) is

$$\mathcal{N}(a_0 + a_1 f_1 + \cdots + a_M f_M, b_0 + b_1 S^2) \tag{5}$$

with $$S^2 := \frac{1}{M-1} \sum_{k=1}^{M} (f_k - \bar{f})^2,$$

where $\bar{f}$ denotes the ensemble mean. Location parameters $a_0 \in \mathbb{R}$, $a_1, \ldots, a_M \geq 0$ and scale parameters $b_0, b_1 \geq 0$ can be estimated from the training data by minimizing an appropriate verification score (see Section 3.3).

In the case when the ensemble can be divided into groups of exchangeable members, ensemble members within a given group get the same coefficient of the location parameter resulting in a predictive distribution of the form

$$\mathcal{N}(a_0 + a_1 \sum_{\ell_1=1}^{M_1} f_{1,\ell_1} + \cdots + a_m \sum_{\ell_m=1}^{M_m} f_{m,\ell_m}, b_0 + b_1 S^2), \tag{6}$$

where again, S^2 denotes the ensemble variance.

Wind speed

To take into account the non-negativity of the predictable quantity, in the EMOS model for wind speed proposed by *Thorarinsdottir and Gneiting* (2010), the normal predictive distribution of Eqs. (5) and (6) is replaced by a truncated normal distribution with cut-off at zero. This model is nearly as simple as the normal EMOS model for temperature, for exchangeable ensemble members the predictive distribution is

$$\mathcal{N}^0(a_0 + a_1 \sum_{\ell_1=1}^{M_1} f_{1,\ell_1} + \cdots + a_m \sum_{\ell_m=1}^{M_m} f_{m,\ell_m}, b_0 + b_1 S^2). \tag{7}$$

A summary of the above described models is given in *Table 1*, where the BMA component and EMOS predictive PDFs and their mean/location and

standard deviation/scale parameters are given as functions of the ensemble members f_ℓ and ensemble variance S^2.

Table 1. Summary of post-processing methods for temperature and wind speed forecasts. BMA component and EMOS predictive PDFs and their mean/location and standard deviation/scale parameters as functions of the ensemble members f_ℓ and ensemble variance S^2

		Predictive PDF	**Mean/location**	**Std. dev./scale**
Temperature	BMA	Normal mixture	$\beta_{0,k} + \beta_{1,k} f_k$	σ
	EMOS	Normal	$a_0 + \sum_{\ell=1}^{M} a_\ell f_\ell$	$\sqrt{b_0 + b_1 S^2}$
	BMA	Gamma mixture	$b_0 + b_1 f_k$	$c_0 + c_1 f_k$
Wind speed	BMA	Truncated normal mixture	$\beta_{0,k} + \beta_{1,k} f_k$	σ
	EMOS	Truncated normal	$a_0 + \sum_{\ell=1}^{M} a_\ell f_\ell$	$\sqrt{b_0 + b_1 S^2}$

3.3. Verification scores

In order to check the overall performance of the calibrated forecasts in terms of probability distribution function, the mean continuous ranked probability scores (CRPS; *Wilks*, 2011; *Gneiting* and *Raftery*, 2007) and the coverage and average width of 83.33% central prediction intervals are computed and compared for the calibrated and raw ensemble. Additionally, the ensemble mean and median are used to consider point forecasts, which are evaluated with the use of mean absolute errors (MAE) and root mean square errors (RMSE). We remark that for MAE and RMSE, the optimal point forecasts are the median and the mean, respectively (*Gneiting*, 2011; *Pinson* and *Hagedorn*, 2012). Further, given a CDF $F(y)$ and a real number x, the CRPS is defined as

$$crps(F, x) := \int_{-\infty}^{\infty} \left(F(y) - \chi_{\{y \geq x\}}\right)^2 dy,$$

where χ_H denotes the indicator of a set H. The mean CRPS of a probability forecast is the average of the CRPS values of the predictive CDFs and corresponding validating observations taken over all locations and time points considered resulting in a value in the units of the forecast variable. For the raw ensemble, the empirical CDF of the ensemble replaces the predictive CDF. Note that CRPS, MAE, and RMSE are negatively oriented scores, that is the smaller the better. Finally, the coverage of a $(1-\alpha)100\%$, $\alpha \in (0,1)$, central prediction interval is the proportion of validating observations located between the lower

and upper $\alpha/2$ quantiles of the predictive distribution. For a calibrated predictive PDF, this value should be around $(1-\alpha)100\%$.

4. *Results*

Using the ideas of *Baran et al.* (2013, 2014), we consider two different groupings of the members of the ALADIN-HUNEPS ensemble. In the first case we have two exchangeable groups ($m = 2$). One contains the control member denoted by f_c ($M_1 = 1$), while in the other are 10 ensemble members ($M_2 = 10$) corresponding to the differently perturbed initial conditions denoted by $f_{p,1}, \ldots, f_{p,10}$. Under these conditions, for temperature data we investigate the BMA model specified by Eq. (2) with three different bias correction methods (linear, additive, no bias correction) and the EMOS model given by Eq. (6), while for wind speed data the BMA models defined by Eqs. (3) and (4) and the EMOS model specified by Eq. (7) are studied. In this two-group situation we have only one independent BMA weight $\omega \in [0,1]$ corresponding, e.g., to the control, that is $\omega_1 = \omega$ and $\omega_2 = (1-\omega)/10$.

In the second case, the odd and even numbered exchangeable ensemble members form two separate groups $\{f_{p,1}, f_{p,3}, f_{p,5}, f_{p,7}, f_{p,9}\}$ and $\{f_{p,2}, f_{p,4}, f_{p,6}, f_{p,8}, f_{p,10}\}$, respectively ($m = 3$, $M_1 = 1$, $M_2 = M_3 = 5$), which idea is justified by the method their initial conditions are generated. For more details see Section 2, particularly the fact that only five perturbations are calculated and then they are added to (odd numbered members) and subtracted from (even numbered members) the unperturbed initial conditions. For calibrating ensemble forecasts of temperature and wind speed, we use the three-group versions of BMA and EMOS models considered earlier in the two-group case.

As typical example for illustrating the two different post-processing methods and groupings, we consider temperature data and forecasts for Debrecen valid on July 2, 2012. *Figs. 2a* and *2b* show the BMA predictive PDFs in the two- and three-group cases, the component PDFs corresponding to different groups, the median forecasts, the verifying observations, the first and last deciles, and the ensemble members. Besides the EMOS predictive PDFs the same quantities can be seen in *Figs. 2c* and *2d*, too. On the considered date the spread of the ensemble is reasonable (the ensemble range equals 2.368 K), but all ensemble members overestimate the validating observation (306.45 K). Obviously, the same holds for the ensemble median (308.927 K), while BMA median forecasts corresponding to the two- and three-group models (both equal to 306.524 K) are quite close to the true temperature. The point forecasts produced by the EMOS model are slightly worse (306.921 K for both groupings) but still outperform the ensemble median.

We start our data analysis by determining the optimal lengths of the training periods to be used for estimating the parameters of BMA and EMOS predictive distributions for 2m temperature and 10m wind speed. After finding them we compare the performances of BMA and EMOS post-processed forecasts using these optimal training period lengths. For EMOS models, the parameter estimates are obtained by minimizing the CRPS values of the predictive PDFs.

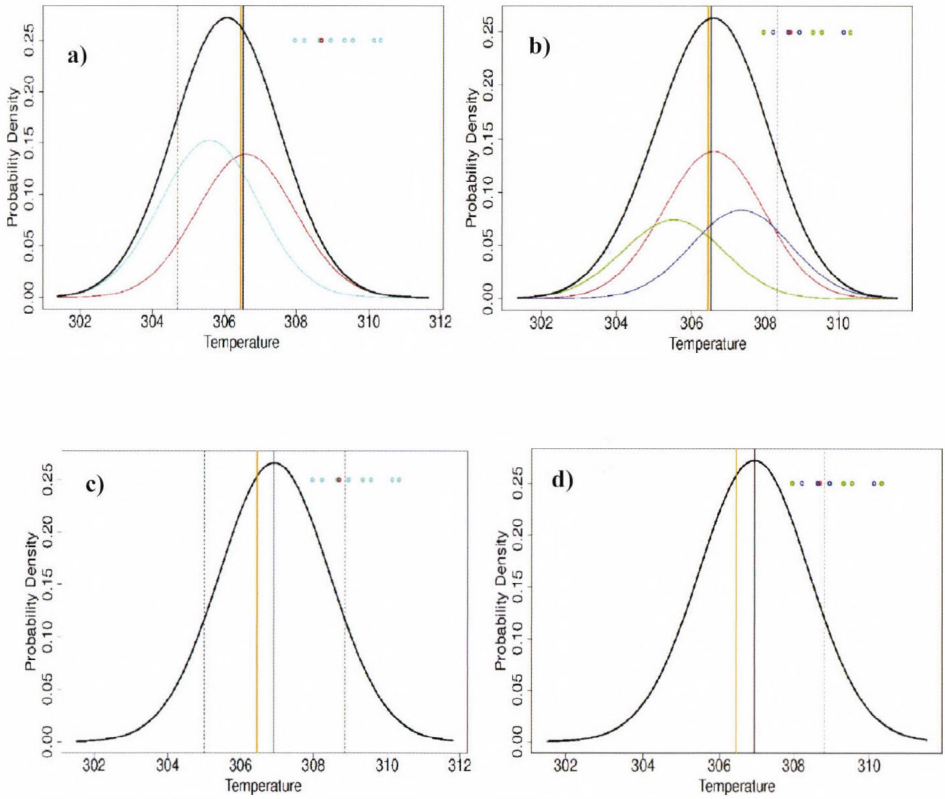

Fig. 2. (a) and *(b):* BMA; *(c)* and *(d):* EMOS density forecasts for 2m temperature (given in K) for Debrecen valid on July 2, 2012. BMA PDFs with linear bias correction in two- and three-group cases (overall: thick black line; control: red line; sum of exchangeable members on (a): light blue line; on (b): green (odd members) and blue (even members) lines), EMOS predictive PDFs in two- and three-group cases (thick black line), ensemble members (circles with the same colours as the corresponding BMA PDFs), BMA/EMOS median forecasts (vertical black line), verifying observations (vertical orange line) and the first and last deciles (vertical dashed lines).

4.1. Training period

Similarly to our previous studies (*Baran et al.*, 2013, 2014), we proceed in the same way as *Raftery et al.* (2005) and determine the length of training period to be used for BMA and EMOS calibrations by comparing MAE values of median forecasts, RMSE values of mean forecasts, CRPS values of predictive distributions, and coverages and average widths of 83.33% central prediction intervals calculated from the predictive PDFs using training periods of length of $10,11,\ldots,60$ calendar days. In order to ensure the comparability of the verification scores corresponding to different training period lengths, we issue calibrated forecasts of temperature and wind speed for the period from June 1, 2012 to March 31, 2013 (6 days with missing data are excluded). This means 298 calendar days following the first training period of maximal length of 60 days.

Temperature

For temperature data we consider BMA predictive PDF given by Eq. (2) with linear bias correction and EMOS model Eq. (6) with parameters minimizing the CRPS of probabilistic forecasts corresponding to the training data. In order to ensure a more direct comparison of the two models, we also investigated the performance of the BMA predictive PDF specified by Eq. (2) with parameter estimates minimizing the same verification score. It yielded sharper central prediction intervals and lower coverage for all training period lengths considered, but there were no significant differences in CRPS, MAE, and RMSE values corresponding to different parameter estimation methods.

Consider first the two-group situation. In *Fig. 3* the CRPS values of BMA and EMOS predictive distributions, MAE values of median, and RMSE values of mean forecasts are plotted against the length of the training period. Note that for normal EMOS model, mean and median forecasts are obviously coincide. First of all it is noticeable that the results are very consistent for all diagnostics, i.e., the curves are similar for all measures. EMOS produces better verification scores, and after 32 days there is no big difference among scores obtained with different training period lengths. In case of the BMA model, CRPS, MAE, and RMSE reach their minima at day 35, and this training period length gives the minima of CRPS and RMSE of the EMOS model, too (see *Table* 2). Although the minimum of MAE of the EMOS model is reached at day 42, the value at day 35 is very near to this minimum as well.

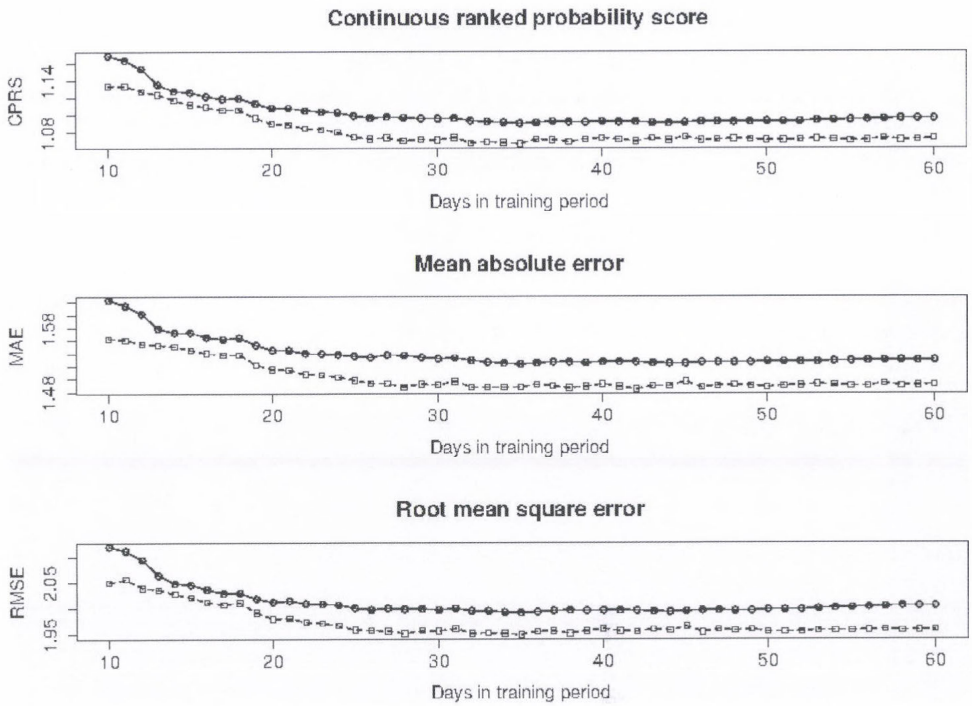

Fig. 3. Mean CRPS of predictive distributions, MAE of BMA/EMOS median, and RMSE of BMA/EMOS mean forecasts for temperature (given in K) corresponding to two-group models for various training period lengths (BMA: solid and ○; EMOS: dashed and □).

Table 2. Optimal training period lengths for temperature with respect to mean CRPS, MAE, and RMSE (given in K), the corresponding optimal scores, and scores at the chosen 35 days length.

		Mean CRPS			MAE			RMSE		
		opt. day	**opt. value**	**day 35 value**	**opt. day**	**opt. value**	**day 35 value**	**opt. day**	**opt. value**	**day 35 value**
Two groups	BMA	35	1.0901	1.0901	35	1.5230	1.5230	35	1.9914	1.9914
	EMOS	35	1.0671	1.0671	42	1.4843	1.4868	35	1.9494	1.9494
Three groups	BMA	35	1.0896	1.0896	35	1.5227	1.5227	36	1.9897	1.9899
	EMOS	26	1.0703	1.0718	26	1.4843	1.4895	28	1.9529	1.9570

Fig. 4 shows the average width and the coverage of the 83.33% central prediction interval for both models considered. Similarly to the previous diagnostics, after 32 days all curves are rather flat showing only a slightly increasing trend. EMOS model yields significantly sharper central prediction intervals for all training period lengths considered, but its coverage stays below the nominal value of 83.33% (dashed line). Unfortunately, the coverage of the BMA model also fails to reach the nominal value, but it is very close to 83.33% from day 35 onwards. The maximal coverage is attained at day 37. Comparing the average width and coverage, one can observe that they have opposite behavior, i.e., the average width values favor shorter training periods, while the coverage figures prefer longer ones. On the other hand, the trend of the average width values is rather flat after day 30 (or so). In any case, a reasonable compromise ought to be found, which is at the range of 30 – 40 days.

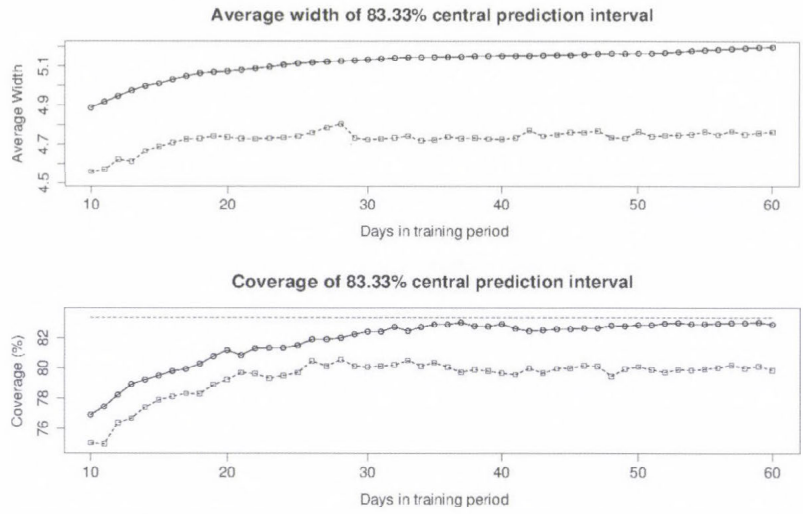

Fig. 4. Average width (given in K) and coverage of 83.33% BMA/EMOS central prediction intervals for temperature corresponding to two-group models for various training period lengths (BMA: solid and ○; EMOS: dashed and □).

As a summary, it can be said that a 35-day training period seems to be an acceptable choice both for the BMA and EMOS models (particularly see conclusions based on *Fig. 3*, which are not compromised by the other two diagnostics at *Fig. 4*).

Very similar conclusions can be drawn for the three-group models. The overall behaviors of the two post-processing methods for the various diagnostics (not shown) are very similar to those of their two-group counterparts. EMOS

model provides lower CRPS, MAE, and RMSE values and, moreover, the lower coverage combined with sharper central prediction interval all over the time periods. In terms of specific values, the minima of CRPS and MAE for the BMA model are reached again at day 35, while the RMSE takes its minimum at day 36 (the value at day 35 is very near to this minimum, see *Table 2*). For the EMOS model, CRPS, MAE, and RMSE reach their minima in the range of 26–28 days, and values at day 35 are again very close to these minima.

Regarding the average width, shorter training periods yield sharper central prediction intervals. The coverage for the EMOS model is always below the nominal value, while the maximal coverage of the BMA model is reached at day 59. However, as in general shorter training periods are preferred, a reasonable compromise is to consider the 35–38-day interval where the BMA coverage is also very high. Hence, the training period proposed for the two-group model can be kept for the three-group model as well, therefore, for temperature we suggest the use of a training period of length 35 days for all the investigated post-processing methods.

Wind speed

To calibrate ensemble forecasts of wind speed, we apply gamma and truncated normal BMA models given by Eqs. (3) and (4), respectively, and EMOS model specified by Eq. (7). In the latter case, similarly to EMOS calibration of temperature forecasts, estimation of parameters is done by minimizing the CRPS of probabilistic forecasts corresponding to the training data.

First, consider again the case when we have two groups of exchangeable ensemble members. Generally, the various scores have rather flat evolution with respect to the training lengths (see *Fig. 5* and *Fig. 6*). It is particularly true after day 25, which would suggest that basically any training length longer than 25 days might be an acceptable choice. Observe that the order of different methods with respect to a given score remains the same for all training period lengths. Truncated normal BMA produces the lowest CRPS values, while the best MAE and RMSE values correspond to EMOS post-processing. In any case if we wanted to pick up a single training period length as an optimal one, 43 days would be a reasonable choice. This is the value where the minima of CRPS of all three methods and the minimum of RMSE of gamma BMA are reached (see *Table 3*). The MAE values of the truncated normal BMA and EMOS models attain their minima at day 59, however, values corresponding to day 43 are practically the same. Finally, the minima of the MAE of the gamma BMA model and the RMSE of the truncated normal BMA and EMOS models are reached at days 47, 41, and 29, respectively, while in all three cases the values at day 43 are the second smallest ones.

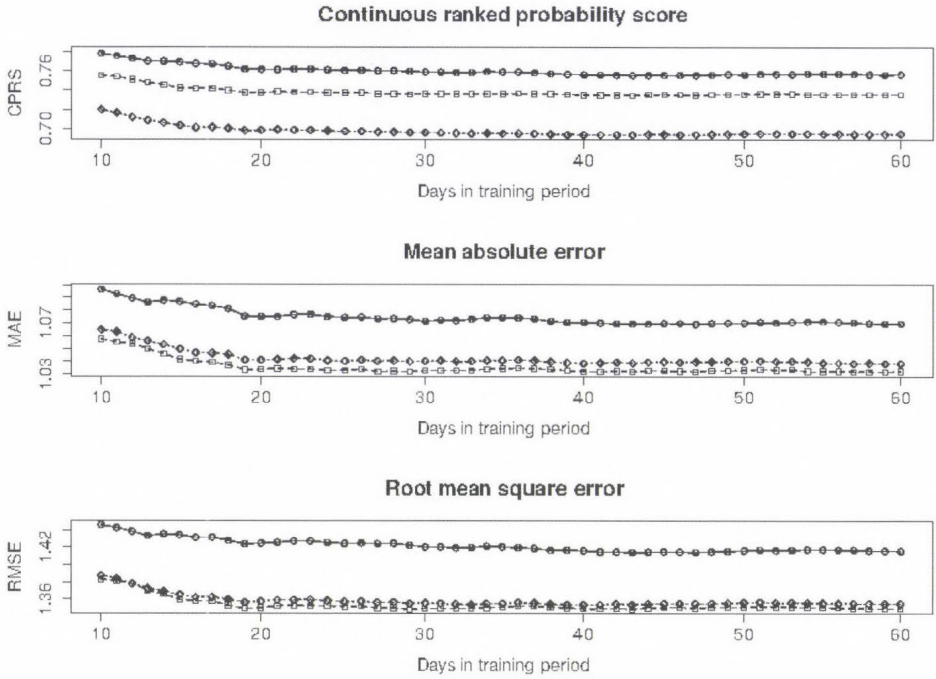

Fig. 5. Mean CRPS of predictive distributions, MAE of BMA/EMOS median and RMSE of BMA/EMOS mean forecasts for wind speed (given in m/s) corresponding to two-group models for various training period lengths (Gamma BMA: solid and ○; truncated normal BMA: dotted and ◊; EMOS: dashed and □).

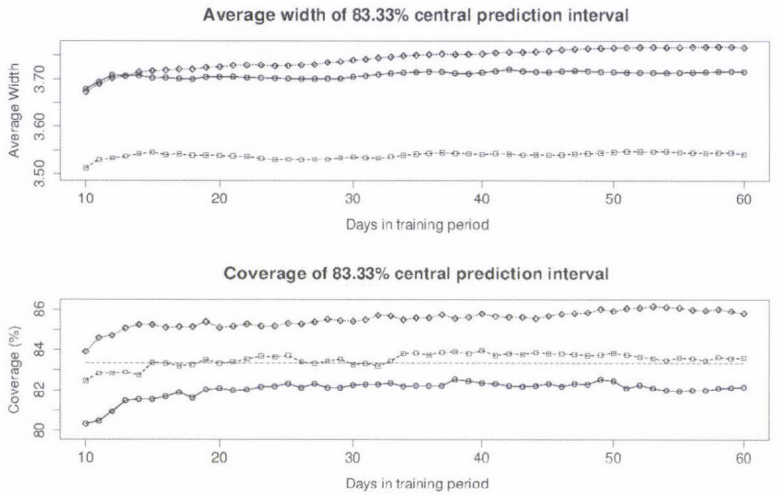

Fig. 6. Average width (given in m/s) and coverage of 83.33% BMA/EMOS central prediction intervals for wind speed corresponding to two-group models for various training period lengths (Gamma BMA: solid and ○; truncated normal BMA: dotted and ◊; EMOS: dashed and □).

EMOS post-processing yields the sharpest central prediction intervals and coverage values which are very close to the nominal level for all considered training period lengths (*Fig. 6*). The 83.33% central prediction intervals for the truncated normal BMA model are significantly wider than those of the EMOS together with a coverage varying between 83.89% and 86.14%. Gamma BMA results in narrower central prediction intervals, but its coverage never reaches the nominal level. The maximal coverage is attained at days 38 and 49. In this way, a 43-day training period length is also acceptable from the point of view of central prediction intervals.

The analysis of verification scores corresponding to the alternative grouping of ensemble members (not shown) leads again to very similar results. The most important difference between the two-group and three-group models is that forming three groups (especially for training periods longer than 20 days) improves MAE and RMSE values of the truncated normal BMA model, and they become very close to the corresponding values of EMOS. For the three-group EMOS model, CRPS and RMSE reach their minima at day 43, and this is the training period length where the minimal CRPS and the second smallest values of MAE and RMSE of the gamma BMA model are attained (see *Table 3*). For the latter model, the global minima of MAE and RMSE are at day 42. In case of truncated normal BMA, post-processing, CRPS, MAE, and RMSE have their minima at day 39, but since these curves are rather flat, values corresponding to a training period of length 43 days are very near. In this way, a 43-day training period seems to be acceptable for both groupings of ensemble members.

Table 3. Optimal training period lengths for wind speed with respect to mean CRPS, MAE and RMSE (given in m/s), the corresponding optimal scores, and scores at the chosen 43-day length.

		Mean CRPS			MAE			RMSE		
		opt. day	**opt. value**	**day 43 value**	**opt. day**	**opt. value**	**day 43 value**	**opt. day**	**opt. value**	**day 43 value**
Two	BMA, g.	43	0.7551	0.7551	47	1.0692	1.0694	43	1.4145	1.4145
groups	BMA, tr.	43	0.6933	0.6933	59	1.0385	1.0389	41	1.3536	1.3540
	EMOS	43	0.7346	0.7346	59	1.0320	1.0322	29	1.3488	1.3491
Three	BMA, g.	43	0.7559	0.7559	42	1.0690	1.0691	42	1.3940	1.3941
groups	BMA, tr.	39	0.6930	0.6930	39	1.0377	1.0382	39	1.3535	1.3543
	EMOS	43	0.7355	0.7355	28	1.0326	1.0328	43	1.3504	1.3504

4.2. Ensemble calibration using BMA and EMOS post-processing

According to the results of the previous section, to compare the performance of BMA and EMOS post-processing on the 11-member ALADIN-HUNEPS ensemble, we use rolling training periods of lengths 35 days for temperature and 43 days for wind speed.

Temperature

For post-processing ensemble forecasts of temperature, we consider the BMA model defined by Eq. (2) with all three bias correction methods introduced in Section 3.1 (linear, additive, none) and EMOS model minimizing the CRPS of probabilistic forecasts corresponding to the training data. The application of three different BMA bias correction methods is justified by a previous study dealing with statistical calibration of the ALADIN-HUNEPS temperature forecasts (*Baran et al.*, 2014), where the simplest BMA model without bias correction showed the best overall performance (although that study was using different ALADIN-HUNEPS dataset period, which preceded the one investigated in this article).

The use of a 35-day rolling training period implies that ensemble members, validating observations, and predictive PDFs are available for the period from May 7, 2012 to March 31, 2013 (having 323 calendar days just after the first 35-day training period). This time interval starts nearly 4 weeks earlier than the one used for determination of the optimal training period length.

The first step in checking the calibration of our post-processed forecasts is to have a look at their probability integral transform (PIT) histograms. The PIT is the value of the predictive CDF evaluated at the verifying observations (*Raftery et al.*, 2005), which provides a good and easily interpretable measure about the possible improvements of the under-dispersive character of the raw ensemble. The closer the histogram to the uniform distribution, the better the calibration. In *Fig. 7,* PIT histograms corresponding to all three versions of the BMA model and to the EMOS model are displayed both in the two- and three-group cases. A comparison to the verification rank histogram of the raw ensemble (see *Fig. 1*) shows that at every case, post-processing significantly improves the statistical calibration of the forecasts. However, the BMA model without bias correction now becomes over-dispersive and the PIT values of the EMOS are slightly better, while at the same time, for the BMA models with linear and additive bias correction, one can accept uniformity. This visual perception is confirmed by the p-values of Kolmogorov-Smirnov tests for uniformity of the PIT values (see *Table 4*). Therefore, the BMA model with additive bias correction produces the best PIT histograms (the linear bias correction case is just slightly worse), the performance of the EMOS model is also quite good, while the fit of the BMA model without bias correction is rather

poor. One can additionally observe that the three-group models systematically outperform the two-group ones.

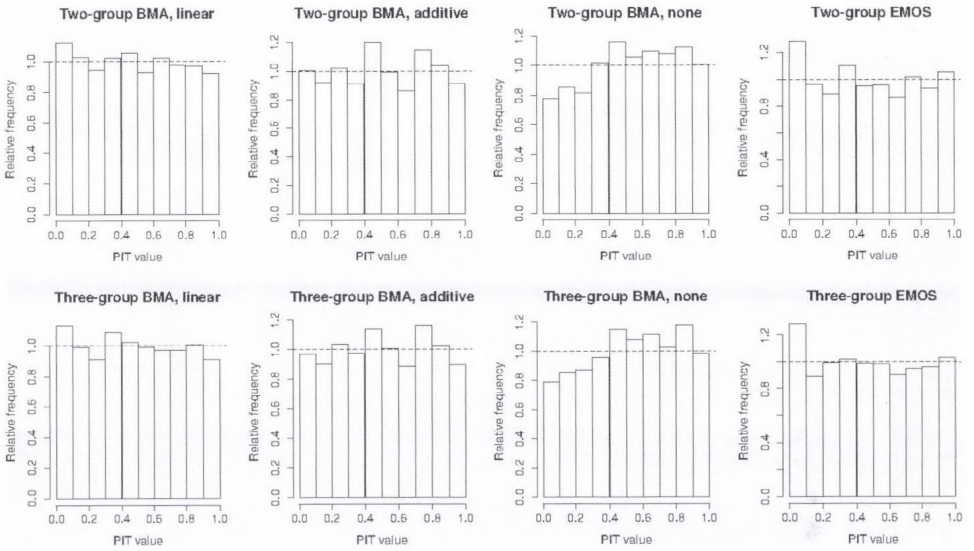

Fig. 7. PIT histograms for BMA and EMOS post-processed forecasts of temperature using two- and three-group models.

Table 4. p-values of Kolmogorov-Smirnov tests for uniformity of PIT values corresponding to predictive distributions of temperature

	BMA model with bias correction			EMOS model
	linear	additive	none	
Two groups	0.1393	0.2405	2.2×10^{-10}	0.0062
Three groups	0.2281	0.4617	4.1×10^{-9}	0.0093

In *Table 5*, verification measures of probabilistic and point forecasts calculated using BMA and EMOS models are given together with the corresponding scores of the raw ensemble. By examining these results, one can clearly observe again the obvious advantage of post-processing with respect to the raw ensemble. This is quantified in decrease of CRPS, MAE, and RMSE values and in a significant increase in the coverage of the 83.33% central

prediction intervals. On the other hand, the post-processed forecasts are less sharp (e.g., 83.33% central prediction intervals are around 30% – 40% wider than the raw ensemble range). This fact is coming from the small dispersion of the raw ensemble, as also seen in the verification rank histogram of *Fig. 1*. Furthermore, BMA and EMOS models distinguishing three exchangeable groups of ensemble members slightly outperform their two-group counterparts (in agreement with the interpretations based on the PIT histograms). Comparing the different post-processing methods, it is noticeable that on the one hand, EMOS produces the lowest CRPS, MAE, and RMSE values and sharpest central prediction intervals both in the two- and three-group cases, although with coverages far below the targeted 83.33%. On the other hand, in terms of CRPS, MAE, and RMSE, the behavior of the BMA model with linear bias correction is just slightly worse, and at the same time this method produces the best approximation of the nominal coverage. Taking also into account the fit of the PIT values to the uniform distribution (see *Fig. 7* and *Table 4* again), one can conclude that overall from the four competing post-processing methods, the BMA model with linear bias correction shows the best performance. These results are not in contradiction with the ones for a previous period (see *Baran et al.* (2014), where the no bias correction case proved to be the optimal), since the characteristics of the raw ALADIN-HUNEPS system had been slightly changed in between. The coverage of the system had been significantly improved (from 46% to 60%), although the latest system became slightly biased (as compared to the previously examined one). Therefore, due to the existence of the bias, it is not surprising that one of the versions with bias correction has the best behavior.

Table 5. Mean CRPS of probabilistic, MAE, and RMSE of median/mean forecasts, average width, and coverage of 83.33% central prediction intervals for temperature (given in K)

		Mean CRPS	MAE		RMSE		Average widths	Coverage (%)
			median	mean	median	mean		
Two groups	BMA, lin.	1.0815	1.5101	1.5097	1.9789	1.9765	5.1375	83.00
	BMA, add.	1.1029	1.5395	1.5329	2.0028	1.9871	5.5146	84.21
	BMA none	1.1131	1.5536	1.5444	2.0167	2.0014	5.7191	84.80
	EMOS	1.0586	1.4731	1.4731	1.9348	1.9348	4.7203	80.43
Three groups	BMA, lin.	1.0801	1.5082	1.5059	1.9767	1.9726	5.1369	83.28
	BMA, add.	1.0998	1.5346	1.5254	1.9962	1.9783	5.5096	84.12
	BMA none	1.1123	1.5509	1.5407	2.0156	1.9988	5.7095	85.11
	EMOS	1.0591	1.4689	1.4689	1.9308	1.9308	4.7523	80.53
Raw ensemble		1.2284	1.5674	1.5512	2.0434	2.0131	3.9822	60.53

Wind speed

According to results of Section 4.1, to compare the predictive performances of gamma BMA (Eq. (3)), truncated normal BMA (Eq. (4)) and EMOS (Eq. (7)) post-processing on the 11-member ALADIN-HUNEPS ensemble forecast of wind speed, we use a training period of length 43 calendar days. In this way, ensemble members, validating observations, and predictive distributions are available for the period from May 15, 2012 to March 31, 2013 (313 calendar days).

First, consider again the PIT histograms of various calibration methods, which are displayed in *Fig. 8*. Compared to the verification rank histogram of the wind speed ensemble (see *Fig. 1*), the statistical post-processing induced improvements are obvious, however, e.g., in case of truncated normal BMA, both corresponding PIT histograms are slightly over-dispersive. The p-values of Kolmogorov-Smirnov tests given in *Table 6* also show that truncated normal BMA models produce the poorest fit, while for gamma BMA and EMOS models one can accept uniformity. In case of BMA calibration, the three-group models again outperform the two-group ones, while for EMOS the situation is the reverse. A similar behavior can be observed in *Table 7*, where the verification scores of probabilistic and point forecasts calculated using BMA and EMOS post-processing and the corresponding measures of the raw ensemble are given. Considering first the probabilistic forecasts (in terms of CRPS, average width of central prediction interval, and coverage), one can observe that the calibrated forecasts are smaller in CRPS, wider in central prediction intervals, and higher in coverage compared to the raw ensemble. Equally, to the two- and in three-group cases the smallest CRPS values belong to the truncated normal BMA model, while EMOS post-processing produces the sharpest central prediction intervals and the best approximation of the nominal coverage of 83.33%. Regarding the point forecasts (median and mean) calculated from the truncated normal BMA and EMOS predictive PDFs, generally there are smaller MAE and RMSE values than those of the raw ensemble. However, there is an exception for the gamma BMA model, since these scores are higher indicating degradations. A possible explanation might be related to the fact that in the investigated period (May 15, 2012 – March 31, 2013) both the raw ensemble median and the ensemble mean slightly overestimate the validating observations (their average biases (standard errors) are 0.0907 (0.0249) and 0.0972 (0.0244), respectively). Therefore, the small bias should be removed by relevant bias corrections. On the other hand, we believe that the simplest bias correction procedure of the gamma BMA model cannot eliminate these inaccuracies, moreover, it might introduce some additional errors. It is a matter of fact that in the two-group case, the average biases of the median and mean of the gamma BMA predictive PDF are -0.1935 and -0.1318 with standard errors of 0.0250 and 0.0253, respectively, while for the EMOS model showing the lowest MAE and RMSE values, these biases are only -0.0735 and

−0.0293, both having a standard error of 0.0242. Therefore, the EMOS model is able to compensate for the existing biases, which is also the case for the truncated normal BMA case, but not for the gamma BMA calibration. The difference in behavior between the two BMA calibration methods is attributed to the more sophisticated bias correction algorithm, which is applied for the truncated normal BMA case.

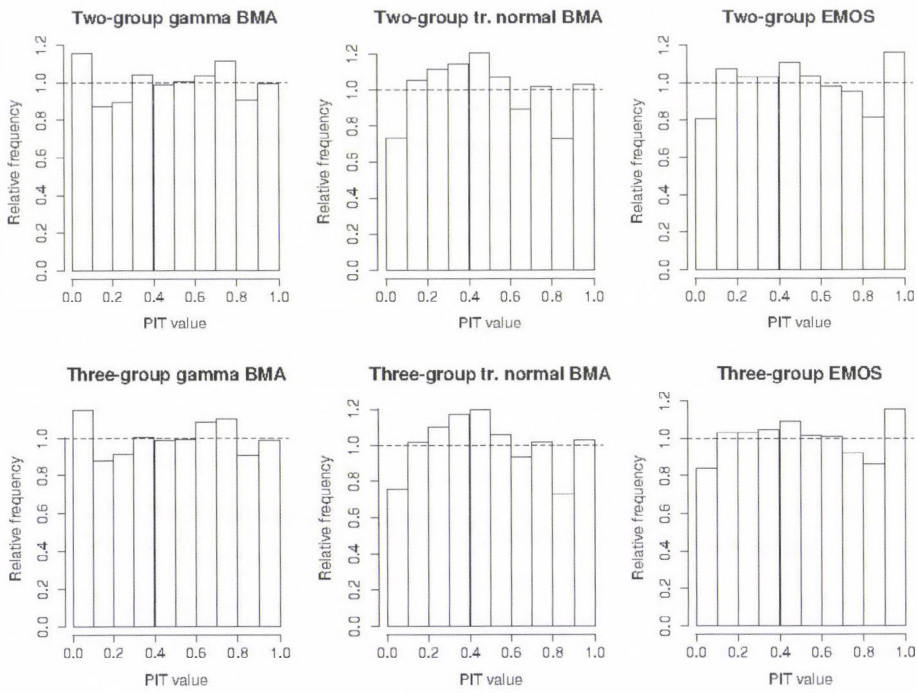

Fig. 8. PIT histograms for BMA and EMOS post-processed forecasts of wind speed using two- and three-group models.

Table 6. p-values of Kolmogorov-Smirnov tests for uniformity of PIT values corresponding to predictive distributions of wind speed.

	BMA model with bias correction		**EMOS model**
	gamma	**tr. normal**	
Two groups	0.1812	0.0023	0.1272
Three groups	0.2085	0.0043	0.0967

Table 7. Mean CRPS of probabilistic, MAE, and RMSE of median/mean forecasts, average width, and coverage of 83.33% central prediction intervals for wind speed (given in m/s).

		Mean CRPS	MAE		RMSE		Average widths	Coverage (%)
			median	mean	median	mean		
Two groups	BMA, gamma	0.7601	1.0747	1.0895	1.4176	1.4267	3.7151	81.87
	BMA, tr. n.	0.6982	1.0446	1.0471	1.3693	1.3632	3.7621	85.46
	EMOS	0.7381	1.0369	1.0375	1.3593	1.3572	3.5340	83.59
Three groups	BMA, gamma	0.7612	1.0754	1.0828	1.4192	1.4052	3.7064	82.03
	BMA tr. n.	0.6980	1.0437	1.0460	1.3696	1.3639	3.7498	85.08
	EMOS	0.7349	1.0381	1.0388	1.3620	1.3597	3.5219	83.11
Raw ensemble		0.8029	1.0688	1.0549	1.3980	1.3728	2.8842	68.22

To summarize, gamma BMA model outperforms the other two methods in terms of fit of PIT values, but it has the highest CRPS and very poor verification scores for the point forecasts. MAE and RMSE values corresponding to EMOS and truncated normal BMA are lower than those of the raw ensemble and rather similar to each other. From these two methods, truncated normal BMA produces much lower CRPS, while EMOS post-processing results in sharper central prediction intervals, better coverage, and better fit of PIT values to the uniform distribution, so we conclude that the overall performance of this method is the best for the calibration of the wind speed raw ensemble forecasts.

5. Discussion and conclusions

In this paper we have compared different versions of the BMA and EMOS statistical post-processing methods in order to improve the calibration of 2 m temperature and 10 m wind speed forecasts of the ALADIN-HUNEPS system. First, we have demonstrated the weaknesses of the ALADIN-HUNEPS raw ensemble system being under-dispersive and therefore uncalibrated. We have indicated that the under-dispersive character of the ALADIN-HUNEPS system had been improved compared to studies based on a former dataset, however, more enhancements are still needed. On the other hand, the latest dataset shows some features of bias of ALADIN-HUNEPS, which were not observed in the earlier studies. This fact has an influence on the optimal choice of statistical calibration, since the use of bias correction is getting more essential. Some standard measures were applied, which are related to the characteristics of the ensemble probability density functions and also the point forecasts as described by the mean/median of the ensemble. The various systems improve different aspects of the ensemble, however, overall both the BMA and the EMOS method

are capable to deliver significant improvements on the raw ALADIN-HUNEPS ensemble forecasts (for temperature and wind speed as well). In case of temperature, the best BMA method slightly outperforms the EMOS technique (although it should not be forgotten that, for instance, in terms of point forecasts, EMOS is better than BMA), while for calibrating ensemble forecasts of wind speed, the EMOS model shows the best performance.

Acknowledgments–Research was supported by the Hungarian Scientific Research Fund under Grant No. OTKA NK101680 and by the TÁMOP-4.2.2.C-11/1/KONV-2012-0001 project. The project has been supported by the European Union, co-financed by the European Social Fund. Essential part of this work was made during the visiting professorship of the first author at the Institute of Applied Mathematics of the University of Heidelberg. The authors are indebted to Tilmann Gneiting for his useful suggestions and remarks, to Thordis Thorarinsdottir for the R codes of EMOS for wind speed, and to *Mihály Szűcs* from the HMS for providing the data. Last but not least, the authors are very grateful to the Reviewers for their valuable comments.

References

Baran, S., 2014: Probabilistic wind speed forecasting using Bayesian model averaging with truncated normal components. *Comput. Stat. Data. Anal. 75*, 227–238.

Baran, S., Horányi, A. and *Nemoda, D.*, 2013: Statistical post-processing of probabilistic wind speed forecasting in Hungary. *Meteorol. Z. 22*, 273–282.

Baran, S., Horányi, A. and *Nemoda, D.*, 2014: Probabilistic temperature forecasting with statistical calibration in Hungary. *Meteorol. Atmos. Phys. 124*, 129–142.

Bouallégue, B.Z., Theis, S. and *Gebhardt, C.*, 2013: Enhancing COSMO-DE ensemble forecasts by inexpensive techniques. *Meteorol. Z. 22*, 49–59.

Buizza, R., Houtekamer, P.L., Toth, Z., Pellerin, G., Wei, M., and *Zhu, Y.*, 2005: A comparison of the ECMWF, MSC, and NCEP global ensemble prediction systems. *Mon. Wea. Rev. 133*, 1076–1097.

Buizza, R., Tribbia, J., Molteni, F. and Palmer, T., 1993: Computation of optimal unstable structures for a numerical weather prediction system. *Tellus A 45*, 388–407.

Descamps, L., Labadie, C., Joly, A., and *Nicolau, J.* (2009) Ensemble Prediction at Météo France (poster introduction by Olivier Riviere) *31st EWGLAM and 16th SRNWP meetings*, September 28 – October 1, 2009. Available at: http://srnwp.met.hu/Annual Meetings/2009/download/sept29/morning/posterpearp.pdf

Eckel, F.A. and *Mass, C.F.*, 2005: Effective mesoscale, short-range ensemble forecasting. *Wea. Forecasting 20*, 328–350.

Fraley, C., Raftery, A.E.. and *Gneiting, T.*, 2010: Calibrating multimodel forecast ensembles with exchangeable and missing members using Bayesian model averaging. *Mon. Wea. Rev. 138*, 190–202.

Fraley, C., Raftery, A.E., Gneiting, T., and *Sloughter, J.M.*, 2009: EnsembleBMA: An R package for probabilistic forecasting using ensembles and Bayesian model averaging. *Technical Report 516R*, Department of Statistics, University of Washington. Available at: www.stat.washington.edu/research/reports/2008/tr516.pdf

Fraley, C., Raftery, A.E., Gneiting, T., Sloughter, J.M. and Berrocal, V.J., 2011: Probabilistic weather forecasting in R. *The R Journal 3*, 55–63.

Gebhardt, C., Theis, S.E., Paulat, M., and *Bouallégue, Z.B.*, 2011: Uncertainties in COSMO-DE precipitation forecasts introduced by model perturbations and variation of lateral boundaries. *Atmos. Res. 100*, 168–177.

Gneiting, T., 2011: Making and evaluating point forecasts. *J. Amer. Statist. Assoc. 106*, 746–762.

Gneiting, T. and *Raftery, A.E.*, 2007: Strictly proper scoring rules, prediction and estimation. *J. Amer. Statist. Assoc. 102*, 359–378.

Gneiting, T., Raftery, A.E., Westveld, A.H., and *Goldman, T.,* 2005: Calibrated probabilistic forecasting using ensemble model output statistics and minimum CRPS estimation. *Mon. Wea. Rev. 133*, 1098–1118.

Hágel, E., 2010: The quasi-operational LAMEPS system of the Hungarian Meteorological Service. *Időjárás 114*, 121–133.

Horányi, A, Kertész, S., Kullmann, L., and *Radnóti, G.,* 2006: The ARPEGE/ALADIN mesoscale numerical modeling system and its application at the Hungarian Meteorological Service. *Időjárás 110*, 203–227.

Horányi, A., Mile, M., and *Szűcs, M.,* 2011: Latest developments around the ALADIN operational short-range ensemble prediction system in Hungary. *Tellus A 63*, 642–651.

Iversen, T., Deckmyn, A., Santos, C., Sattler, K., Bremnes, J.B., Feddersen, H., and *Frogner, I-L.,* 2011: Evaluation of 'GLAMEPS' - a proposed multimodel EPS for short range forecasting. *Tellus A 63*, 513–530.

Justus, C.G., Hargraves, W.R., Mikhail, A., and *Graber, D.*, 1978: Methods for estimating wind speed frequency distributions. *J. Appl. Meteor. 17*, 350–353.

Labadie, C., Descamps,L., Cebron, P., and *Michel, Y.,* 2012: PEARP initialization with Ensemble Data Asssimilation and Singular Vectors. International Conference on Ensemble Methods in Geophysical Sciences, Toulouse, France, November 12–16, 2012. Available at: http://www.meteo.fr/cic/meetings/2012/ensemble.conference/presentations/session07/2.pdf

Leutbecher, M. and *Palmer, T.N.*, 2008: Ensemble forecasting. *J. Comp. Phys. 227*, 3515–3539.

Pinson, P. and *Hagedorn, R.*, 2012: Verification of the ECMWF ensemble forecasts of wind speed against analyses and observations. *Meteorol. Appl. 19*, 484–500.

Raftery, A.E., Gneiting, T., Balabdaoui, F., and *Polakowski, M.,* 2005: Using Bayesian model averaging to calibrate forecast ensembles. *Mon. Wea. Rev. 133*, 1155–1174.

Sloughter, J.M., Gneiting, T., and *Raftery, A.E.,* 2010: Probabilistic wind speed forecasting using ensembles and Bayesian model averaging. *J. Amer. Stat. Assoc. 105*, 25–37.

Sloughter, J.M., Raftery, A.E., Gneiting, T., and *Fraley, C.,* 2007: Probabilistic quantitative precipitation forecasting using Bayesian model averaging. *Mon. Wea. Rev. 135*, 3209–3220.

Soltanzadeh, I., Azadi, M., and *Vakili, G.A.,* 2011: Using Bayesian Model Averaging (BMA) to calibrate probabilistic surface temperature forecasts over Iran. *Ann. Geophys. 29*, 1295–1303.

Thorarinsdottir, T.L. and *Gneiting, T.,* 2010: Probabilistic forecasts of wind speed: ensemble model output statistics by using heteroscedastic censored regression. *J. Roy. Statist. Soc. Ser. A 173*, 371–388.

Toth, Z. and *Kalnay, E.*, 1997: Ensemble forecasting at NCEP and the breeding method. *Mon. Wea. Rev. 125*, 3297–3319.

Tuller, S.E. and *Brett, A.C.*, 1984: The characteristics of wind velocity that favor the fitting of a Weibull distribution in wind speed analysis. *J. Appl. Meteorol. 23*, 124–134.

Wilks, D.S., 2011: Statistical Methods in the Atmospheric Sciences. 3rd ed., Elsevier, Amsterdam.

Wilks, D.S. and *Hamill, T.M.*, 2007: Comparison of ensemble-MOS methods using GFS reforecasts. *Mon. Wea. Rev. 135*, 2379–2390.

Williams, R.M., Ferro, C.A.T., and *Kwasniok, F.*, 2014: A comparison of ensemble post-processing methods for extreme events. *Q. J. R. Meteorol. Soc.140*, 1112–1120.

IDŐJÁRÁS

Quarterly Journal of the Hungarian Meteorological Service
Vol. 118, No. 3, July – September, 2014, pp. 243–256

Effects of leveling error on the measurement of global radiation

László Menyhárt[1*], **Angéla Anda**[1], and **Zoltán Nagy**[2]

[1]*Department of Meteorology and Water Management, University of Pannonia Georgikon Faculty, Festetics u. 7, H-8360 Keszthely, Hungary*

[2]*Hungarian Meteorological Service, Gilice tér 39, H-1181 Budapest, Hungary*

**Corresponding author E-mail: menyhart-l@georgikon.hu*

(Manuscript received in final form January 10, 2014)

Abstract—Pyranometers are fundamental instruments widely used for measuring global irradiance. When operating weather stations without continuous manning, pyranometer may tilt from horizontal position. Error caused by inclination of a few degrees was calculated for the annual, daily, and instantaneous global radiations. Global irradiance incident on both horizontal and tilted surfaces were calculated from the direct beam, diffuse and ground-reflected irradiances. These components were measured by accurately leveled and regularly supervised instruments. The second purpose of this paper was to determine the minimum tilt angle that is detectable by calculating certain quantities. To detect the east-west inclination, the sum of the global radiation before and after the solar noon was compared. To detect the north-south inclination, it was tested whether the global irradiance measured at a fixed solar elevation with a horizontal and a tilt pyranometer is stochastically equal. Our findings show that tilt angle of 1° in east-west direction is already detectable. Tilting to the direction at an angle of 15° from the north-south is the most difficult to detect. Here 3° is the smallest detectable tilt angle.

Key-words: global radiation, global irradiance, pyranometer, tilt error, detection of tilt, leveling of pyranometer

1. Introduction

The demand for high-precision global radiation measurement has risen steadily in recent decades. Global radiation data with high spatial and temporal resolution are required in different fields including meteorological and climate models, active and passive solar energy systems, agriculture, and the solar architecture. Consequently, the instruments measuring solar radiation have shown significant progress. The number of weather stations equipped with solar instruments continues to grow, and the use of pyranometers for industrial purposes became general. In spite of this, compared to other meteorological variables, the measurement of solar radiation is more prone to errors *(Moradi,* 2009*)*. *Younes et al.* (2005) classified the most general types of errors into two major categories: (1) equipment error and uncertainty, and (2) operational related problems and errors. The former includes the cosine response, azimuth response, temperature response, spectral selectivity, stability, non-linearity, and dark offset long-wave radiation error. The latter includes the incorrect sensor leveling, shading caused by objects above the horizon, electric fields in the vicinity of cables, mechanical loading of cables (piezoelectric effects), dust, snow, dew, bird -droppings, etc. A variety of useful procedures for post-measurement quality control have been published in the past years *(Geiger et al.,* 2002*;* *Muneer* and *Fairooz,* 2002*;*, *Younes et al.,* 2005*;* *Shi et al.,* 2008; *Moradi,* 2009*;*, *Tang et al.,* 2010; *Journée* and *Bertrand,* 2011*;* *Miras-Avalos et al.,* 2012*)*. These methods define an upper and a lower threshold and remove values being outside the acceptance range. So the extremely low or high values are eliminated, however, a value between the thresholds may also be erroneous. The correction of the equipment errors are dealt with in several papers as well *(Stoffel et al,* 2000*;* *Reda,* 1999*;*, *Bush et al.,* 2000*;* *Reda et al.,* 2005*;* *Lester* and *Myers,* 2006*;*, *Ji,* 2007*;* *Marquez et al.,* 2010*)*.

Our aim is to develop a method to detect the tilt of the pyranometer without additional measurements. This paper is the first step in the program. One purpose is to quantify the effects of the tilt. The second purpose is to estimate the minimum tilt angle which is detectable from the time series of global irradiance alone.

To help the accurate leveling of the pyranometer, the instrument is supplied with a spirit level. In case of careful mounting, the angle between the plane of the sensor and the horizontal is less than 1° or 0.1°, depending on the type of the pyranometer. In case of tilt, posterior correction is not possible, since neither the direction nor the extent of the tilt are known. Global radiation incident on a tilted surface is essential for different uses of solar energy, so numerous studies focus on its estimation. In such cases, the angle between the absorbing surface and the horizontal is considerably greater than in the case of pyranometer leveled incorrectly. If the latter is tilted over 5°, it is already visible to the naked eye. Therefore, the effects of tilt angle not greater than 10° were investigated.

Bacher et al. (2013) presented a method to correct systematical errors, including tilt error. The sensor output level under clear-sky conditions is estimated directly from the observation by means of quantile regression. This is compared to solar radiation calculated with a clear-sky model. The different types of systematical errors are not examined separately, all of them are corrected in the same step.

Tilt error is particularly common if solar irradiance is measured from ship, buoy, aircraft, or other moving platforms. Correction methods developed for moving platforms is presented in *Long et al.,* (2010) and *Boers et al.,* (1998). The error due to the rocking motion and preferential tilt were calculated using the assumption that the diffuse to direct ratio was constant (*Katsaros* and *DeVault,* 1986). The novelty of the present study is that instead of estimating this ratio, a full-year time series of direct, diffuse, and reflex irradiances are used.

2. *Material and methods*

The error caused by tilt depends basically on the solar position, direction and magnitude of the tilt, and the diffuse to direct ratio. Carrying out measurements with pyranometers tilted in different directions and to different degrees would be extremely lengthy and costly. Therefore, both the global irradiance incident on horizontal and that incident on inclined surface were calculated from diffuse horizontal irradiance, direct normal irradiance, and ground-reflected irradiance. The data used in this paper were measured in the György Marczell Main Observatory (47°25'45"N and 19°10'56"E) of the Hungarian Meteorological Service from January 1, 2011 to November 27, 2011 and from December 8, 2011 to December 31, 2011. Both the diffuse irradiance and the ground-reflected irradiance were measured with Kipp&Zonen CM11 pyranometers while the direct normal irradiance was measured by Kipp&Zonen CH1 pyrheliometer. All measurements were carried out with precisely leveled instruments with continuous supervision. Sampling took place in every two seconds and their means were recorded on ten minute basis. The solar coordinates were calculated for the middle of the ten-minute intervals by the algorithm proposed by *Reda* and *Andreas* (2004).

In case of horizontal pyranometers, the global irradiance was calculated as the sum of the diffuse sky irradiance and the vertical component of the direct solar irradiance.

$$G_H = B \cdot \sin\varphi + D, \tag{1}$$

where G_H is the global irradiance incident on horizontal surface, B is the direct normal irradiance, D is the diffuse sky irradiance, and φ is the solar elevation.

When the pyranometer is tilted, it loses irradiance from a portion of the sky and instead receives radiation from below the horizon. So, in such a case the global irradiance was calculated by

$$G_t = B_t + D_t + R_t, \tag{2}$$

where G_t is the global irradiance incident on tilted surface, B_t, D_t, and R_t are the components of direct normal, sky diffuse, and ground-reflected irradiances, respectively. These components are perpendicular to the plane of the pyranometer and calculated by

$$B_t = B \cdot [\sin\varphi \cdot \cos s + \cos\varphi \cdot \cos(\alpha - \gamma) \cdot \sin s], \tag{3}$$

$$D_t = D \cdot \frac{1 + \cos s}{2}, \tag{4}$$

$$R_t = R \cdot \frac{1 - \cos s}{2}, \tag{5}$$

where s is the tilt angle that the plane of the pyranometer makes with the horizontal surface (s is always positive and represents the slope in any direction), γ is the azimuth angle of the tilt, where γ=0 for slopes oriented to south and it increases in clockwise direction. α is the solar azimuth and R is the ground-reflected irradiance measured by a horizontal, downward facing pyranometer. Eqs. (3), (4), and (5) are detailed in *Iqbal* (1983). Both the sky diffuse and ground-reflected irradiances were considered as isotropic, since the investigated tilt angle was restricted below 10°. Eqs. (4) and (5) show that if s is small then $D_t \approx D$ and $R_t \approx 0$. Consequently, the direct component is mostly affected by the inclination.

If a measured value or the calculated B_t component was negative it was replaced with zero.

The relative error caused by the tilt was calculated by

$$E = \frac{G_t - G_H}{G_H}, \tag{6}$$

where γ was varied between 0° and 330° by 30°, as well as s was varied between 1° and 10° by 1°. Annual, diurnal, and instantaneous global radiations

were calculated for each case. The tilt of the pyranometer was assumed to be constant all year.

Quantities appropriate to detect the tilt of the pyranometer were looked for. Tilt towards the east or west causes diurnal asymmetries in the global radiation. Asymmetry may also be caused by diurnal variation of the atmospheric transmittance. Whereas the direction of the asymmetry caused by the tilt is the same on each day, that caused by the variation of the transmittance varies stochastically. To detect the inclination, those days shall be used when the direct to global ratio is high and the diurnal variation of the atmospheric transmittance is low. Three days where the diurnal global radiation was the highest were selected in each month. Sum of the global radiation measured before and after the solar noon were compared with paired samples t-test. The assumption underlying this test is that the difference of the two variables follows a normal distribution. Normality was tested with Shapiro-Wilk test. Statistical significance level was accepted to be $p<0.05$.

Tilt towards the north or south does not cause diurnal asymmetry. However, it causes distortion in the annual course of global irradiance corresponding to a given solar elevation. The lower the sun, the higher the angle of incidence and the greater the tilt error. At low solar elevation angles, around the winter solstice the sun is in the southern sky, and around the summer solstice it is in the northern sky. Consequently, the global irradiance measured by a pyranometer tilted towards the south is higher in winter and lower is summer compared with those measured by a horizontal pyranometer. This effect decreases with the increase of solar elevation in summer, because the sun moves away from the north. That is why the days around the winter solstice are the most suitable to detect the north-south tilt.

Sixty days before and after the winter solstice were used. These days were randomly divided into two groups of equal size. On the days being in the first and second group, the global irradiance measured with the horizontal and the tilted pyranometer was modeled, respectively. The highest 20 values corresponding to a given solar elevation were selected from both groups. Since these data did not follow the normal distribution, they were compared with the nonparametric Mann-Whitney U test. Statistical significance level was accepted to be $p<0.05$. Global irradiance corresponding to the solar elevation of 8°, 10°, 12°, 14°, 16°, 18°, 20°, and 22° were examined one by one. In order to eliminate the effect of randomness, the days when the pyranometer was assumed to be horizontal and tilted, respectively, were interchanged. The statistical test was repeated in this way. The difference was considered to be due to the tilt only if it was found significant in both cases.

If there is not a sufficient number of clear-sky measurements, the twenty highest values may include partially cloudy measurements too. It may reduce the power of the method. Therefore, the whole procedure was repeated with the highest 10 values corresponding to the given solar elevation.

The measurements were not carried out at the same solar elevation on each day. Therefore, the values of solar elevation expressed in degree were rounded to the nearest whole number. Hence, the global irradiance was corrected with linear interpolation as follows. When the solar elevation was rounded up before the solar noon or rounded down after the solar noon, then

$$G_t^{\text{int}} = G_t + \frac{G_{t+1} - G_t}{\varphi_{t+1} - \varphi_t}\left(\varphi_t^{\text{int}} - \varphi_t\right). \tag{7}$$

When the solar elevation was rounded down before the solar noon or rounded up after the solar noon, then

$$G_t^{\text{int}} = G_t + \frac{G_{t-1} - G_t}{\varphi_{t-1} - \varphi_t}\left(\varphi_t^{\text{int}} - \varphi_t\right), \tag{8}$$

where G_t^{int} is the global irradiance corresponding to the rounded solar elevation, G_t, G_{t+1}, and G_{t-1} are the global irradiance corresponding to the actual, 10 minutes later, and 10 minutes earlier measurements, respectively.

3. *Results*

3.1. Annual total global radiation

The relative error of the annual total global radiation was found to be directly proportional to the tilt angle in case of a fixed tilt direction (*Fig. 1*) in the examined range. It was found to be estimated by

$$E_{year} = s(-0.00054 + 0.0070\cos\gamma), \tag{9}$$

where E_{year} is the relative error of the annual total global radiation and s is expressed in degree. The goodness of fit of the model was excellent, R^2=0.99. Tilt towards the north and south results in a relative error of –0.0075 and 0.0065 per degree, respectively. The lowest error, 0.0005 per degree, was found in the case of tilt towards the east or west.

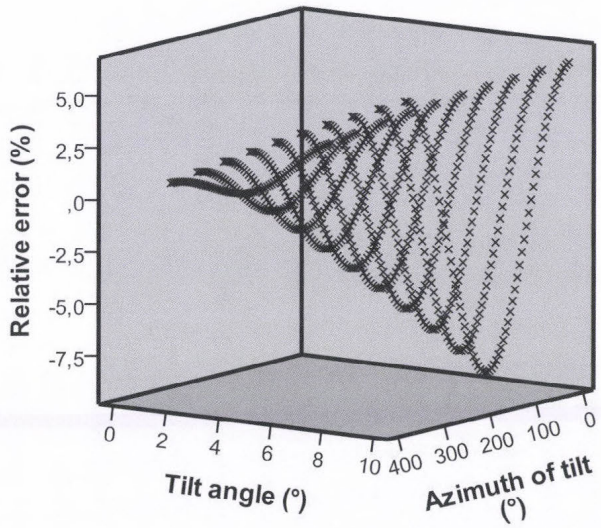

Fig. 1. Relative error of the annual total global radiation in 2011.

3.2. Daily total global radiation

The annual course of the error of the daily total global radiation has a typical pattern. The two most different cases are shown in *Fig. 2*. As it was expected, the lowest relative error was found on clear-sky day in winter with pyranometer tilted towards the north. In case of tilt angle of 1°, this error was lower than –4.5% (*Fig. 2a*). The same tilt caused an error about –0.3% around the summer solstice. The errors around zero were observed on the overcast days when the direct normal irradiance was zero or negligible. There were some days on summer, when the error was positive. It occurred on the days, when the direct normal irradiance was high in the morning and in the evening, and the sun was in the northern sky, and it was low around the solar noon when the sun was in the southern sky. The lower envelope of the scatter plot (*Fig. 2a*) shows the relative error corresponding to the clear-sky days.

In case of pyranometer tilted towards the east or west, the relative error was about zero both on the clear-sky and the overcast days (*Fig. 2b*). The relative error with the highest absolute value was found on the days when the morning was overcast and the afternoon was clear-sky or vice versa. On these days the absolute value of the relative error caused by tilt angle of 1°was about 1%, while on clear-sky days it was about 0.1%.

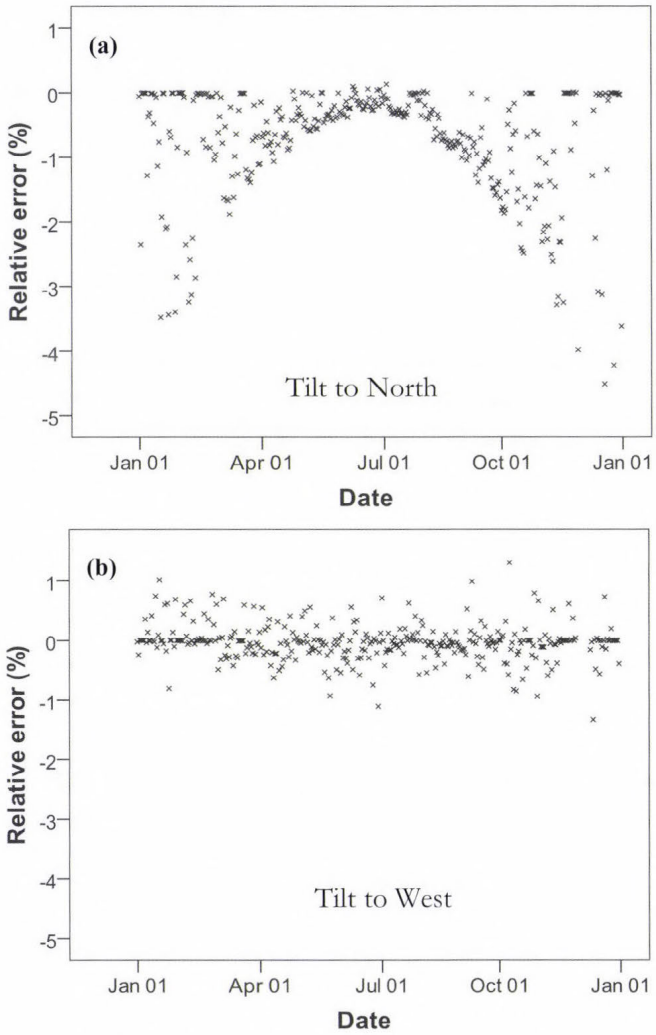

Fig. 2. Relative error of the daily total global radiation for tilt of 1° (a) to the north and (b) to the west, in 2011.

3.3. Global irradiance

The daily course of the relative error of the global irradiance depends strongly on the apparent daily path of the sun. To present the three most different cases, a clear-sky day was selected from around the summer solstice, autumn equinox, and winter solstice (*Fig. 3*). Compared to the annual or daily total, the relative

error of the 10-minute average, caused by the same tilt, was notably higher. Around the winter solstice at low solar elevation angles, the error caused by the tilt of 1° to the south exceeds 8%. At solar elevation angles higher than 30°, even if the pyranometer is tilted towards the sun, the error caused by the tilt of 1° is lower than 1% (*Fig. 3a*).

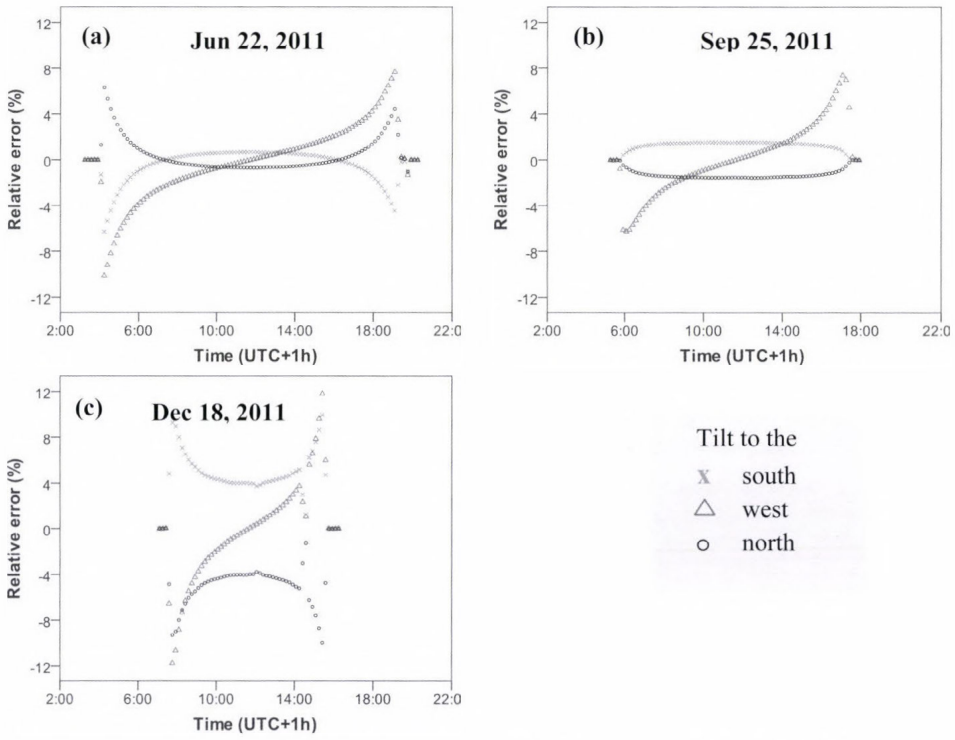

Fig. 3. Relative error of global irradiance, caused by the tilt of 1° around the (a) summer solstice, (b) autumnal equinox, and (c) winter solstice.

3.4. Comparison of the total global radiation measured before and after the solar noon

The tilt angles and the azimuth angles at which the comparison was carried out are shown in *Table 1* and *Table 2*. The difference of the two quantities followed normal distribution in each case. The results, as shown in *Table 1*, indicate that even tilt of 1° resulted in significant asymmetry if the azimuth of the tilt was within the range of 60° to 120° or 240° to 300°. For tilt angle of 1.5°, the asymmetry was significant when the azimuth of the tilt ranged from 30° to 150° or from 210° to 330°. The closer the tilt direction to the north or to the south, the less the asymmetry expected to be significant. If the direction, of the tilt makes

an angle of 15° with the south-north direction the tilt angle must be at least 3° to result in significant asymmetry (*Table 2*).

Table 1. Difference of the total global radiation measured before and after the solar noon (kJ/m^2) in case of tilt angles smaller than 2°

tilt angle	0°	30°	60°	90°	120°	150°	180°	210°	240°	270°	300°	330°
0.5°	27	92	139	157	139	91	12	–101	–149	–166*	–149	–52
1.0°	18	149	253**	287**	251**	155	11	–166*	–262**	–296**	–262**	–178*
1.5°	19	216*	366**	417**	364**	220**	10	–232**	–374**	–427**	–389**	–244**

(*:$p<0.05$; **:$p<0.01$)

Table 2. Difference of the total global radiation measured before and after the solar noon (kJ/m^2) in case of tilt angles of 2° and 3°

tilt angle	15°	165°	195°	345°
2°	155	144	–171*	–169*
3°	194*	209**	–238**	–242**

(*:$p<0.05$; **:$p<0.01$)

3.5. Global irradiance corresponding to a given solar elevation angle

This quantity has a typical annual course due to the annual variation of the Sun-Earth distance and the atmospheric transmittance. It was modified by the tilt of the pyranometer (*Fig. 4*). The closer the solar azimuth corresponding to the given solar elevation angle to the azimuth of the tilt, the higher the relative error. Consequently, the error with the highest absolute value was found around the winter solstice in case of tilt to north-south (*Fig. 5a*). In case of tilt to east-west, it was found sometimes after the spring equinox as well as sometimes before the autumn equinox (*Fig. 5b*). Obviously, the exact date depends on the solar elevation angle in question.

Global irradiance corresponding to a given solar elevation was expected to show the tilt to the south-north direction. That is why the global irradiance incident on the horizontal and the tilted surface was only compared when the azimuth of the tilt was within the ranges of 0°–30°, 150°–210° and 330–360°. Due to the high number of the comparisons, only the significance of the

difference is reported. Let a particular tilt be called detectable at a given solar elevation angle if the difference corresponding to the given solar elevation angle was found statistically significant regardless of which days were considered horizontal. These cases are highlighted with dark background in *Table 3*. The tilt of 1.5° to south was detectable at none of the solar elevation angles. Even the tilt of 2° to south was detectable at only two solar elevation angles. Tilt of 3° within the ±30° range around the south-north direction was already detectable at four different solar elevation angles. These results indicate that tilt to south-north is harder to detect than the tilt to east-west. The smallest detectable tilt angle in each tilt direction is presented in *Fig 6*.

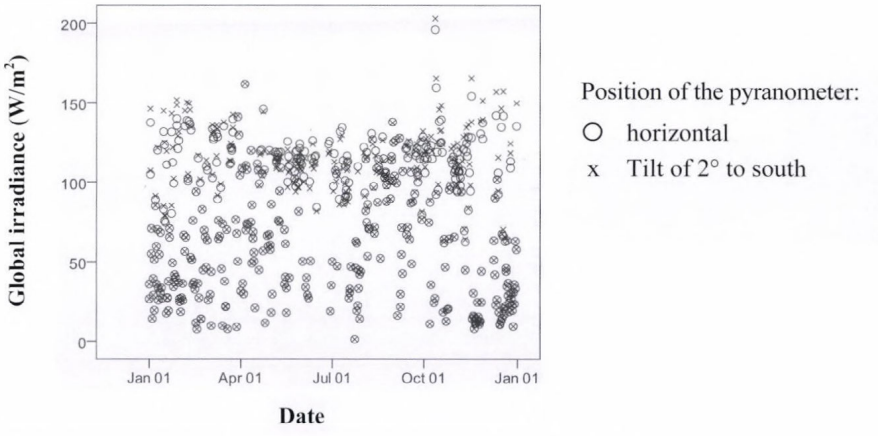

Fig. 4. Global irradiance corresponding to the solar elevation of 10°, in 2011.

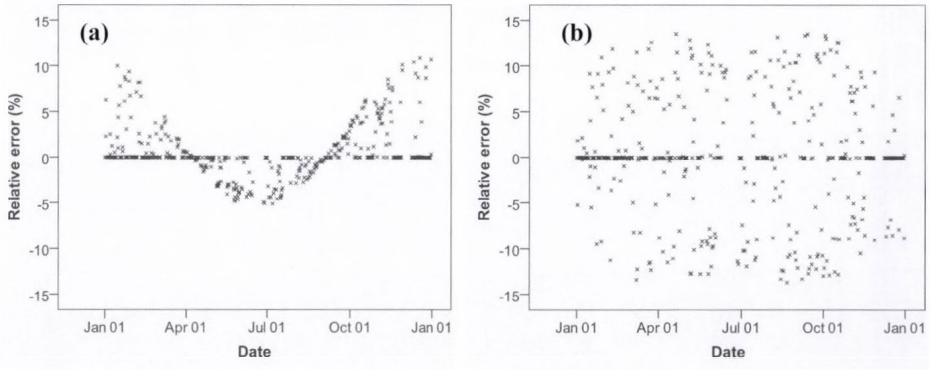

Fig. 5. Relative error of the global irradiance corresponding to the solar elevation of 10° in case of a 2° tilt (a) towards the south and (b) west, in 2011.

Table 3. Significance of the difference of global irradiance incident on the horizontal and the tilted surface. At tilt azimuth of 15°, 165°, 195°, 345°, the test was carried out at tilt angle of only 3°.

tilt angle	sol. elev.	0°	15°	30°	150°	165°	180°	195°	210°	330°	345°
1,5°	8°	* d		* d	* d		*dd		* d	* d	
	10°	* d		* d	* d		* d		* d	* d	
	12°	* d		* d	* d		* d		* d	* d	
	14°	* d		* d	*		*		*	* d	
	16°	* d		* d	*		*		*	*	
	18°	* d		* d	* d		* d		* d	* d	
	20°	*		* d	* d		* d		* d	* d	
	22°	*		* d	*		*		*	*	
2°	8°	* dd		* d	* d		*dd		*dd	*dd	
	10°	* d		*d	* d		*dd		* d	* d	
	12°	* d		*d	* d		* d		* d	* d	
	14°	* dd		*dd	* d		*dd		*	*dd	
	16°	* d		*d	*		**d		*	* d	
	18°	* d		*d	* d		* d		* d	* d	
	20°	*		*d	* d		* d		* d	*	
	22°	* d		d	*		*		*	*	
3°	8°	* dd	* d	* d	* d	**dd	**dd	**dd	**dd	*dd	*dd
	10°	* dd	*dd	* d	*dd	*dd	*dd	*dd	* d	* d	* d
	12°	* dd	*dd	* d	* d	*dd	* dd	*dd	* d	* d	*dd
	14°	* dd	*dd	*dd	**d	**dd	**dd	**dd	*dd	*dd	*dd
	16°	**dd	**dd	*dd	**d	*dd	**dd	* dd	**dd	*dd	**dd
	18°	**d	**d	**d	**d	**d	**d	**d	**d	**d	**d
	20°	* d	* d	* d	* d	* d	* d	* d	* d	* d	* d
	22°	**dd	** dd	** dd	**	*dd	**dd	** d	** d	**dd	**dd

*: p<0.05 with the 20 highest values; d: p<0.05 with the 10 highest values;
**: p<0.05 with the 20 highest values regardless of which days were considered horizontal; dd: p<0.05 with the 10 highest values regardless of which days were considered horizontal. ** and dd are denoted with grey background.

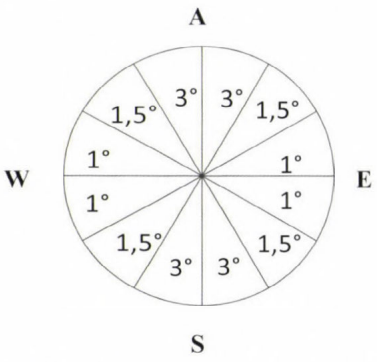

Fig. 6. The smallest detectable tilt angles in each tilt direction. Sectors represent ranges of 30°.

4. Discussion

The uncertainty of the daily total global radiation shall not exceed 2%, 5%, and 10% in cases of the secondary standard, first class, and second class pyranometers, respectively, according to the ISO standard (*ISO,* 1990). Our findings show that even a tilt of 1° can cause greater variation in the daily total values than the inherent uncertainty of a secondary standard pyranometer. The effect of a tilt of 2.5° can exceed the inherent uncertainty of even a second class pyranometer. It indicates that developing a method that assesses the data series of global irradiance with respect to the leveling would be very useful.

The aim of this paper was to find quantities that are calculated only from global radiation and suitable to assess the leveling of the pyranometer. The difference of the total global radiation measured before and after the solar noon has been shown to be very sensitive to the tilt to east-west. As small as tilt of 1° to east-west can be detected. The method is adaptable to any latitude, but the value of 1° refers only to the latitude of around 47°N. The selection of clear-sky days is a key element in the process. Refinement of the selection method is expected to shorten the length of the measurements necessary for the detection of a tilt.

The highest error in both the annual and the daily total global radiation is caused by the tilt to south-north, yet it is the most difficult to detect. Three degrees as the smallest detectable tilt seems like a lot. Assessing the global irradiance corresponding to a given solar elevation angle requires reference data that is considered as horizontal global irradiance. In the current study it was calculated from measurements of a few days. Future work will involve a multi-annual high accuracy measurement series. It will give the opportunity to analyze the annual course of the solar irradiance corresponding to a given solar elevation angle rather than the 10 or 20 highest values measured around the winter solstice. It is expected to allow smaller tilts to become detectable.

Overall, the power of the method using the twenty highest values is greater than that using the ten highest values. However, half of the cases showed by the twenty highest values were not showed by the ten highest values. It proves that both procedures were reasonable to use. The strength of investigating the solar irradiance corresponding to a given solar elevation angle is that it does not require clear-sky days, only shorter clear-sky periods of time. Its drawback is that the power to detect the tilt is not the same in each part of the year. Investigating the morning and afternoon solar irradiances separately can contribute to the detection of the tilt to east-west.

It has been shown that there is a good chance to detect a tilt as small as 1° to east-west, and we hope that as small as 2° will be detectable in any other directions by the refinement of the method. Future works will carry out measurements with tilted pyranometers to verify these findings.

Acknowledgements–The financial and infrastructural support of the State of Hungary and the European Union in the frame of the TÁMOP-4.2.2/B-10/1-2010-0025 project is gratefully acknowledged.

References

Bacher, P., Madsen, H., Perers, B., and *Nielsen, H. A.,* 2013: A non-parametric method for correction of global radiation observations. *Solar Energy 88*, 13–22.

Boers, R., Mitchell, R.M., and *Krummel, P.B.,* 1998: Correction of aircraft pyranometer measurements for diffuse radiance and alignment errors. *J. Geophys. Res. 103(D13)*, 16753–16758.

Bush, B.C., Valero, F.P.J., Simpson, A.S., and *Bignoneet, L.,* 2000: Characterization of thermal effects in pyranometers: a data correction algorithm for improved measurement of surface insolation. *J. Atmos. Ocean. Tech. 17*, 165–175.

Geiger, M., Diabate, L., Menard, L., Wald, L., 2002: A web service for controlling the quality of measurements of global solar irradiation. *Solar Energy 73*, 475–480.

ISO: International Organization for Standardization, 1990: Solar Energy – Specification and Classification of Instruments for Measuring Hemispherical Solar and Direct Solar Radiation. ISO 9060.

Iqbal, M., 1983: An introduction to solar radiation. Academic press, New York, Chap 11, 303–334.

Ji, Q., 2007: A method to correct the thermal dome effect of pyranometers in selected historical solar irradiance measurements. *J. Atmos. Ocean. Tech. 24*, 529–536.

Journée, M. and Bertrand, C., 2011: Quality control of solar radiation data within the RMIB solar measurements network. *Solar Energy 85*, 72-86.

Katsaros, K.B. and *DeVault, J.E.,* 1986: On irradiance measurement errors at sea due to tilt of pyranometers. *J. Atmos. Ocean. Tech. 3*, 740–745.

Long , C.N., Bucholtz, A., Jonsson, H., Schmid, B., Vogelmann, A., and *Wood, J.,* 2010: A Method of Correcting for Tilt from Horizontal on Downwelling Shortwave Irradiance Measurements on Moving Platforms. *Open Atmos. Sci. J. 4*, 78–87.

Lester, A. and *Myers, D.R.,* 2006: A method for improving global pyranometer measurements by modeling responsivity functions. *Solar Energy 80*, 322–331.

Marquez, J.M.A., Bohorquez, M.A.M., Garcia, J.M., and *Nieto, F.J.A.,* 2010: A new automatic system for angular measurement and calibration in radiometric instruments. *Sensors 10*, 3703–3717.

Miras-Avalos, J.M., Rodriguez-Gomez, B.A., Meizoso-Lopez, M.C., Sande-Fouz, P., Gonzalez-Garcia, M.A., and *Paz-Gonzalez, A.,* 2012: Data quality assesment and monthly stability of ground solar radiation in Galicia (NW Spain) *Solar Energy 86,* 3499–3511.

Moradi, I., 2009: Quality control of global solar radiation using sunshine duration hours. *Energy 34,* 1–6.

Muneer, T. and *Fairooz, F.,* 2002: Quality control of solar radiation and sunshine measurements–lessons learnt from processing worldwide databases. Building *Serv. Engin. Res. Tech. 23*, 151–66.

Reda, I., 1999: Improving the Accuracy of Using Pyranometers to Measure the Clear Sky Global Solar Irradiance. *9th ARM Science Team Meeting Proceedings,* San Antonio, Texas, March 22–26.

Reda, I. and *Andreas, A.,* 2004: Solar Position Algorithm for Solar Radiation Applications, *Solar Energy 76*, 577–589.

Reda, I., Hickley, J., Long, C., Myers, D., Stoffel, T., Wilcox, S., Michalsky, J.J., Dutton, E. G. and *Nelson, D.,* 2005: Using a blackbody to calculate net longwave responsivity of shortwave solar pyranometers to correct for their thermal offset error during outdoor calibration using the component sum method. *J. Atmos. Ocean. Tech. 22*, 1531–1540.

Shi, G.Y., Hayasaka, T., Ohmura, A., Chen, Z.H., Wang, B., Zhao, J.Q., Che, H.Z., and *Xu, L.,* 2008: Data quality assessment and the long-term trend of ground solar radiation in China. *J. Appl. Meteorol. Climatol. 47*, 1006–1016.

Stoffel T, Redo I, Myers D, Renne D, Wilcox S, and *Treadwell J.,* 2000: Current issues in terrestrial solar radiation instrumentation for energy, climate andspace applications. *Metrologia 37*, 399–402.

Tang, W., Yang, K., He, J., and *Qin, J.,* 2010: Quality control and estimation of global solar radiation in China. *Solar Energy 84,* 466–475.

Younes, S., Claywell, R., and *Muneer, T.,* 2005: Quality control of solar radiation data: present status and proposed new approaches. *Energy 30,* 1533–1549.

IDŐJÁRÁS

Quarterly Journal of the Hungarian Meteorological Service
Vol. 118, No. 3, July – September, 2014, pp. 257–281

Microclimate-vegetation relationships in natural habitat islands: species preservation and conservation perspectives

Zoltán Bátori[1]*, Attila Lengyel[2], Miklós Maróti[3], László Körmöczi[1], Csaba Tölgyesi[1], András Bíró[3], Miklós Tóth[3], Zoltán Kincses[4], Viktória Cseh[1], and László Erdős[1]

[1]*University of Szeged, Department of Ecology, H-6726 Szeged, Közép fasor 52, Hungary*

[2]*Hungarian Academy of Sciences, Institute of Ecology and Botany, H-2163 Vácrátót, Alkotmány u. 2-4, Hungary*

[3]*University of Szeged, Bolyai Institute, H-6720 Szeged, Aradi vértanúk tere 1, Hungary*

[4]*University of Szeged, Department of Technical Informatics, H-6720 Szeged, Árpád tér 2, Hungary*

**Corresponding author E-mail: zbatory@gmail.com*

(Manuscript received in final form February 10, 2014)

Abstract— Information about the relationship between the spatial and temporal patterns of different climatic parameters and the vegetation is especially important from a nature conservation perspective. We studied the influence of microclimatic parameters (air temperature and air humidity) on certain natural habitat islands (karst sinkhole and sand dune slack) and on their plant species composition and vegetation pattern in Hungary. Vegetation data together with topographic variables were collected along transects to reveal the vegetation patterns on the slopes. Microclimatic parameters were measured with wireless sensor motes equipped with air temperature and humidity sensors. Interactions were examined using distance-based redundancy analysis. We found that the species composition of natural habitat islands varied markedly within short distances, depending on the prevailing microclimatic conditions. Elements of microclimate (daily, daytime, and nighttime averages) have different effects on vegetation pattern and species composition. The observed patterns can be interpreted based on our knowledge on the structure of plant communities and on the role of geomorphology. Future temperature increase, droughts, and forestry activities are the main threats to the habitat diversity and hence to the species diversity of habitat islands in Hungary.

Key-words: air humidity, air temperature, climate change, habitat island, Hungary, refugium, vegetation inversion, wireless sensor

1. Introduction

Microclimate is a suite of climatic conditions measured usually directly on the ground or very close to it (*Geiger*, 1965). The effects of different microclimatic parameters (e.g., air temperature and air humidity) on animals and plants have been widely studied because they are essential to individual organisms for reproduction (e.g., germination) and ecological processes (e.g., evapotranspiration, microbial activity, nutrient cycling, photosynthesis, and regeneration) (*Bátori et al.*, 2012a; *Forseth* and *Teramura*, 1987; *Holl*, 1999; *Marlatt*, 1961; *Schimel* and *Parton*, 1986). The interactions between microclimate and vegetation have been studied both at local and regional scales. Local-scale studies have focused mainly on individuals and stands, providing important information about the local ecological processes and sometimes, based on the extension and generalization of the results, about larger-scale ecological processes (*Antonić et al.*, 1997; *Bátori et al.*, 2011; *Herrera*, 1995). The number of landscape studies examining microclimate and its relationship with flora, vegetation, and related ecological processes in the context of landscape is much lower (*Xu et al.*, 2004).

The interaction between topography and climate is complex and its details are not completely understood (*Dobrowski*, 2011). There is no doubt, however, that topography and related terrain effects strongly affect the local environmental and climatic conditions (*Bátori et al.*, 2009; *Geiger*, 1950; *Whiteman et al.*, 2004). The effect of geomorphology on temperature inversion strengths, diurnal temperature regimes, and vertical temperature gradients has a great impact on vegetation pattern and plant survival. However, vegetation cover usually has a mitigating effect on air and soil temperatures (*Allen* and *Burton*, 1993; *Fetcher et al.*, 1985; *Oliver et al.*, 1987); therefore, elements of microclimate are usually less extreme in forests than in grasslands. In addition, many studies suggest that not only the diurnal or monthly average temperature and humidity values but also the differences between the daytime and nighttime averages as well as their changes affect markedly species composition, vegetation pattern, and ecological processes (*Liu et al.*, 2006; *Mohammed* and *Tarpley*, 2009; *Shiu et al.*, 2009). It is important to note that management related variables often explain more variation in vegetation than any other variables together, indicating the importance of management as determining species composition (*Aude* and *Lawesson*, 1998). Therefore, the effects of microclimate must be interpreted differently under different disturbance regimes, various topographical features, and vegetation covers.

The spatial distribution of microclimate is an essential factor for habitat suitability for many species (*Mantilla-Contreras et al.*, 2011; *Rich* and *Weiss*, 1991). Since climate change apparently affects the occurrences of species and the phenology of animal and plant activity (*Molnár et al.*, 2012; *Rijnsdorp et al.*, 2009; *Thomas et al.*, 2004; *Walther et al.*, 2002) by shifting the overall

temperature distribution, changing the precipitation regime and increasing the frequency of extreme weather events (*Easterling et al.*, 2000; *Parmesan et al.*, 2000), the investigation of the habitats suitable for providing refugia for affected species is of crucial importance. One of the most important insights that scientists can offer for conservation biology is how species are expected to respond to changes in regional and local climate. Hence, an increasing number of species distribution models have recently been reported (*Rasztovits et al.*, 2012; *Schwartz et al.*, 2006). From the point of view of an ecologist, investigations of island-like habitats can offer many possibilities to answer the above question (*Bátori et al.*, 2012b; *Körmöczi et al.*, 1981). According to the well accepted theory, 'islands' should not necessarily be land masses in water but may be particular geological types, soil types, or vegetation types surrounded by dissimilar types of rock, soil or vegetation (*Begon et al.*, 2006). However, we must distinguish between (semi)natural habitat islands and artificially created habitat islands (e.g., agricultural fields, cities, secondary grasslands), because environmental conditions (e.g., microclimate, nutrient availability, water supply), ecological processes, and organism responses are fundamentally different in the two types (*Pinke et al.*, 2012; *Unger*, 1999).

Several previous studies focused on relatively small areas with special temperature and humidity properties that harbor many species that once occurred in larger and more continuous populations (*Müller et al.*, 2006; *Turlure et al.*, 2010). For example, the lowland fens of the Carpathian Basin serve as refuges for many boreal plants (e.g., *Menyanthes trifoliata* L., *Potentilla palustris* (L.) Scop., *Trollius europaeus* L.), and the karst sinkholes and deep ravines of hill and mountain ranges preserved high-mountain species (e.g., *Rubus saxatilis* L., *Stachys alpina* L., *Viola biflora* L.) (*Király*, 2009; *Simon*, 2000). Most of these plants are climatic relicts, whose populations persist in isolated enclaves of suitable climate space surrounded by areas where the climate is not suitable for them (*Hampe* and *Jump*, 2011). Therefore, these habitats can be used for vegetation history studies as well, because their flora reflects cooler climatic periods (*Bátori et al.*, 2012b). Not only climate relicts but also other groups of species may be good indicators for microclimatic conditions of different habitats. For example, *Erdős et al.* (2013) revealed that the vascular plants of the mosaic of lowland xeric grasslands and mesic forests indicate very different climatic conditions along an edge to interior gradient. They also pointed out that the species composition of these habitat complexes may be very diverse and may contain many rare and endangered mesic forest plants, which are more characteristic of the hill and mountain ranges of the Carpathian Basin. In these cases, the local climatic conditions allow many species to maintain their populations in places where the surrounding environmental conditions (e.g., warmer climate) are not suitable for them.

The objective of this study is to examine and compare the species composition and vegetation pattern of natural habitat islands in Hungary, and to

make an attempt to explain these phenomena with microclimatic variables including the daily, daytime and nighttime air temperature and air humidity regimes. We also discuss the potential role of these habitats in preserving different groups of plant species under future climate change.

2. Methods

2.1. Study sites and vegetation survey

Study sites were selected in two different parts of Hungary (*Fig. 1*), where the landscapes contain many natural habitat islands. The fieldwork was conducted between 2009 and 2012 in a large karst sinkhole of the Mecsek Mountains (46°7'17" N, 18°12'11" E; 498 m above sea level) and in a deep sand-dune slack of Bugac (46°41'46" N, 19°36'9" E; 111 m above sea level). All samples were taken in summer, when the influence of spatial microclimatic properties was expected to be the greatest on the habitat islands. Neither site showed signs of considerable human or animal disturbance.

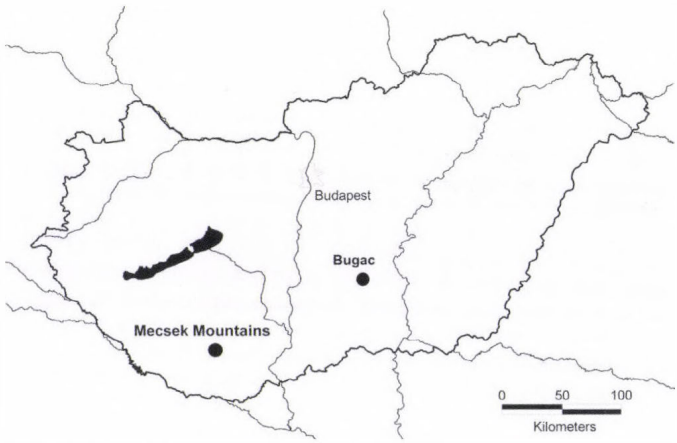

Fig. 1. Location of the study sites in Hungary.

Transect sampling was applied in both sites. Plot sizes were optimized according to our former studies and experiences (*Bátori et al.*, 2012b; *Tölgyesi* and *Körmöczi*, 2012).

In the Mecsek Mountains, a sub-Mediterranean type, middle-aged mesic oak-hornbeam (*Asperulo taurinae-Carpinetum*) and beech forests (*Helleboro odori-Fagetum*) covered the north-facing, east-facing, and west-facing slopes of the approximately 30 m deep sinkhole. A transition between a xeric turkey oak-sessile oak forest (*Potentillo micranthae-Quercetum dalechampii*) and an oak-

hornbeam forest occurred on the south-facing rim and an oak-hornbeam forest on the south-facing slope. The sinkhole bottom was covered by a ravine forest (*Scutellario altissimae-Aceretum*) (*Bátori et al.*, 2011). Herb layer was sampled along a 2 m wide and 243 m long transect consisting of 50 plots, 2 m × 1 m each. The transect was established in a north to south direction traversing the deepest point of the sinkhole.

At Bugac, a xeric grassland (*Festucetum vaginatae*) occupied the major part of the investigated sand dune (*Körmöczi* and *Balogh*, 1990), which is part of the Kiskunság Sand Ridge. The lower parts of the dune were covered by a remnant of a wet interdune vegetation patch (*Molinio-Salicetum rosmarinifoliae*). The vegetation was sampled along a 1 m wide and 14 m long transect consisting of 14 plots, 1 m × 0.25 m each. The transect was established in a northeast to southwest direction (following the orientation of the dune) traversing the deepest point of the dune slack. The elevation difference between the highest and deepest points was approximately 1.7 m.

Presence/absence of all vascular plant species (including tree saplings and low shrubs), mosses and lichens of the summer aspect was recorded in all plots (see *Appendix*). According to the topographic profiles of each transect, the plots were classified into two groups: plots of the upper slopes and plots of the bottoms. The different habitats (the bottom and upper transect sections) were compared based on vegetation and microclimatic parameters during subsequent analyses.

Plant community names are used according to *Borhidi et al.* (2012), the nomenclature of mosses and lichens follow *Simon* (1991), while the names of vascular plant taxa follow *Király* (2009).

2.2. Microclimate measurement

We used 50 IRIS (XM2110CA) wireless sensor motes from Crossbow, each of which was equipped with an MTS400 (SN21140CA) weather sensor board, which included air temperature and air humidity sensors. We measured air temperature (°C) and air humidity (%) for 24 hours 25 cm above the ground surface in the plots of the 2 transects. The signals from the sensors were recorded once every minute, therefore, 1440 temperature and 1440 humidity datapoints (24 × 60, respectively) were obtained from each mote. From these data, the daily minimum air temperature (DMinAT), daily maximum air temperature (DMaxAT), daily minimum air humidity (DMinAH), daily maximum air humidity (DMaxAH), mean daily air temperature (MDAT), mean daily air humidity (MDAH), mean daytime air temperature (MDtAT), mean daytime air humidity (MDtAH), mean nighttime air temperature (MNtAT), and mean nighttime air humidity (MNtAH) were calculated. 'Daytime' is defined as the time interval between 7 a.m. and 7 p.m., while 'nighttime' is the interval between 7 p.m. and 7 a.m. Microclimate measurements were carried out after a dry period, under clear weather conditions.

2.3. Analysis

Percentage frequencies for the species were determined with the JUICE 7.0.25 program (*Tichý*, 2002). After testing normality, one-way ANOVA and subsequent Tukey's HSD post hoc tests were applied in order to reveal the differences in species number between the different habitats, using the stats package of R 2.10.1 (*R Development Core Team*, 2009).

Detrended correspondence analysis (DCA) (*Hill* and *Gauch*, 1980) was used to detect the major gradients of floristic variation of the plots within the study sites. DCA is an ordination technique, which is able to identify gradients in community composition. Its advantage over other unconstrained ordination methods is that it is theoretically free from the so-called 'arch effect', thus, DCA axes correspond better to gradients with high turnover (*Legendre* and *Legendre*, 1998). The procedure was computed using Past 1.18 (*Hammer et al.*, 2001).

Variation of species presence/absence data was related to temperature and humidity measurements using distance-based redundancy analysis (db-RDA) (*Legendre* and *Anderson*, 1999). db-RDA is an ordination method, which arranges data objects in a space defined by the linear combinations of explanatory (environmental) variables and, at the same time, quantifies the variation in species composition explained by the environmental variables. The variation of species composition in db-RDA has to be expressed on the basis of a dissimilarity measure between pairs of community sample units. Here we applied the complement of Sörensen index as a dissimilarity measure, with the formula

$$D_{\text{Sörensen}}=1-2*a/(2*a+b+c),$$

where a is the number of species present in both members of the pair, b and c are the number of species present in one and the other plot (*Legendre* and *Legendre,* 1998). Considering our previous results (*Bátori et al.* 2011), the following measurements were used as explanatory variables: MDAT, MDtAT, MNtAT, MDAH, MDtAH, and MNtAH. For each study site, the gross effect of each climatic variable was calculated by constructing a db-RDA model with the tested variable as the only predictor and the compositional data as the dependent variables (hereafter called 'one-predictor model'). Effect strengths of each climatic variable were quantified by the percentage explained variance and F value of the respective db-RDA model, and their significance was assessed by a permutation test (see *Table 1*). Then, for each study site, the most effective temperature and humidity variables were selected based on the lowest P and the highest F values. With these two as background variables, a new db-RDA was performed ('two-predictor model') in order to assess the cumulative effect of the best climatic variables (see *Table 2*). There was high collinearity within temperature variables and humidity variables, thus, the other 2–2 variables of

these climatic factors were not involved in the model. 'Two-predictor models' were visualized on biplots. Ordinations were performed using the vegan R package (*Oksanen et al.*, 2009; *R Development Core Team*, 2009).

Moreover, we also used the coenological preferences of the plant species (*Soó*, 1980) to characterize each habitat.

Table 1. Summary statistics for the 'one-predictor' db-RDA models. MDAT: mean daily air temperature, MDtAT: mean daytime air temperature, MNtAT: mean nighttime air temperature, MDAH: mean daily air humidity, MDtAH: mean daytime air humidity, MNtAH: mean nighttime air humidity

Predictors	Var. %	F value	P value
	Mecsek Mountains: sinkhole		
MDAT	18.7	9.160	<0.001
MDtAT	17.5	8.478	<0.001
MNtAT	17.7	8.592	<0.001
MDAH	16.8	8.039	<0.001
MDtAH	14.9	7.028	<0.001
MNtAH	16.7	7.994	<0.001
	Bugac: sand-dune slack		
MDAT	32.5	5.071	<0.005
MDtAT	24.1	3.387	<0.05
MNtAT	30.2	4.560	<0.005
MDAH	34.8	5.578	<0.001
MDtAH	31.9	4.935	<0.001
MNtAH	29.0	4.328	<0.005

Table 2. Summary statistics for the 'two-predictor' db-RDA models. MDAT: mean daily air temperature, MDAH: mean daily air humidity

Predictors	Var. %	F value	P value
	Mecsek Mountains: sinkhole		
MDAT + MDAH	21.0	6.249	<0.001
	Bugac: sand-dune slack		
MDAT + MDAH	37.8	3.342	<0.005

3. *Results*

3.1. Microclimate and flora of the karst sinkhole

The MDAT changed from 19.9 to 17.6 °C along a microclimatic gradient in the sinkhole (*Fig. 2).*

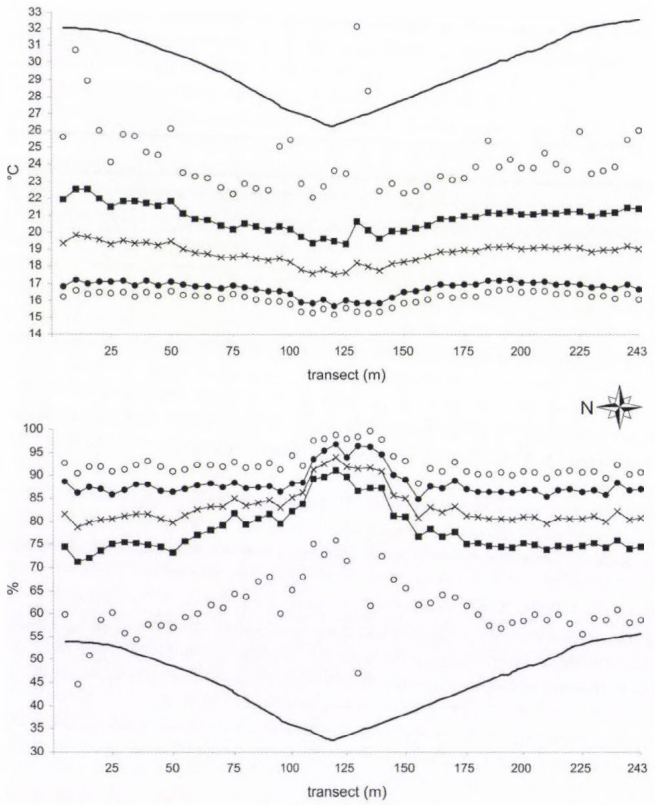

Fig. 2. Air temperature and air humidity values along the transect of the sinkhole of the Mecsek Mountains (August 9–10, 2010). Notations: ○: minimum and maximum air temperature (DMinAT, DMaxAT) and air humidity (DMinAH, DmaxAH) values; ■: mean daytime air temperature (MDtAT) and air humidity (MDtAH) values; ×: mean daily air temperature (MDAT) and air humidity (MDAH) values; ●: mean nighttime air temperature (MNtAT) and air humidity (MNtAH) values.

The maximum MDAT (19.9 °C) was detected in a plot of the south-facing rim where the transition between a turkey oak-sessile oak forest and an oak-hornbeam forest situated consisting of many dry oak forest and mesic oak forest species. The lowest MDAT (17.6 °C) and the DMinAT (15.1 °C) were recorded

on the bottom of the sinkhole, under the ravine forest. The MNtAT and MDtAT showed a very similar pattern, however, the DMaxAT (32.1 °C) was detected on the bottom of the sinkhole. Air humidity values also changed markedly along the transect with the lowest MDAH (79%) on the higher zone of the sinkhole slopes and with the highest MDAH (94%) in the sinkhole bottom (*Fig. 2*). The rest of the air humidity values followed a similar pattern. The 24-hour pattern of air temperature and air humidity also differed markedly between the upper sinkhole slopes and the sinkhole bottom (*Figs. 3–4*).

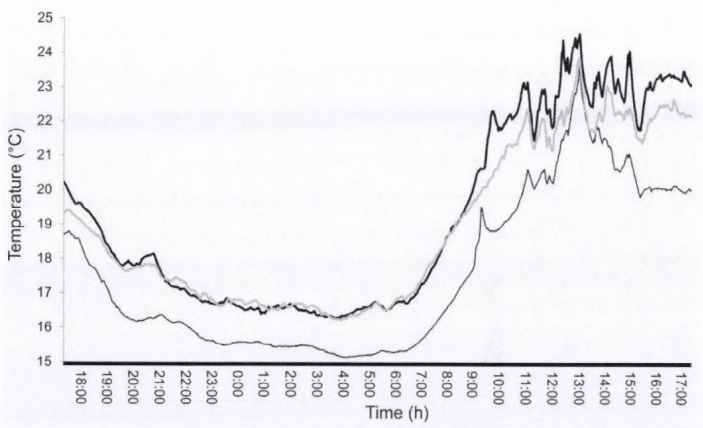

Fig. 3. Air temperature values in three plots along the transect (south-facing sinkhole slope: thick black line; sinkhole bottom: thin line; north-facing sinkhole slope: thick grey line) of the sinkhole of the Mecsek Mountains, measured over a 24-hour period (August 9–10, 2010).

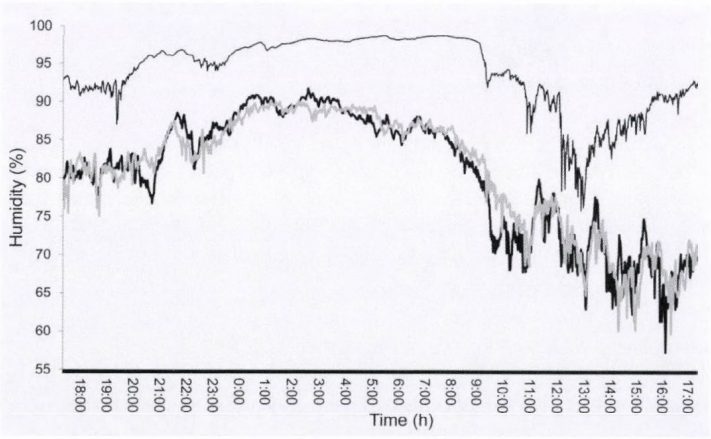

Fig. 4. Air humidity values in three plots along the transect (south-facing sinkhole slope: thick black line; sinkhole bottom: thin line; north-facing sinkhole slope: thick grey line) of the sinkhole of the Mecsek Mountains, measured over a 24-hour period (August 9–10, 2010).

The most frequent (>80%) species were *Fraxinus excelsior* L. on the upper sinkhole slopes and *F. excelsior* and *Galeobdolon luteum* s.l. on the sinkhole bottom. Species that occurred only in the sinkhole bottom include *Aconitum vulparia* Rchb., *Athyrium filix-femina* (L.) Roth, *Atropa belladonna* L., *Carex sylvatica* Huds., *Circaea lutetiana* L., *Dryopteris filix-mas* (L.) Schott, *Eupatorium cannabinum* L., *Paris quadrifolia* L., *Polystichum aculeatum* (L.) Roth, *P. setiferum* (Forssk.) Woyn., *Pyrus pyraster* (L.) Burgsd., *Rubus fruticosus* agg., *Solanum dulcamara* L., *Stachys sylvatica* L., *Urtica dioica* L., and *Veronica montana* L. According to the ANOVA, species number in the upper slopes and in the sinkhole bottom did not differ significantly (P=0.710). The proportions of the different species groups are shown in *Fig. 5*. Species of mesic oak forests (38%) and Central European beech forests (40%) had the highest proportions on the sinkhole slopes, but species of dry oak forests (9%) and Illyrian beech forests (9%) also had an important role in structuring the plant communities. The sinkhole bottom was covered mainly by beech forest species (54%), but the proportions of mesic oak forest species (14%) and indifferent species (12%) were also considerable. It is important to note that the sinkhole bottom held some species of deep ravines and gorges (e.g., *Aconitum vulparia* and *Polystichum aculeatum*) (2%), which were restricted to them.

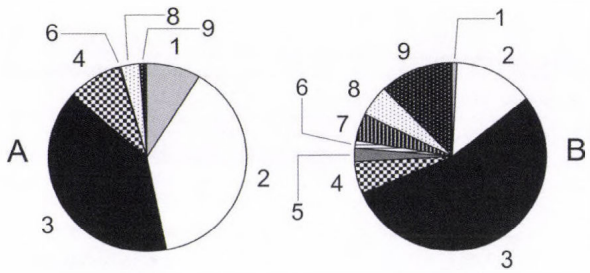

Fig. 5. Proportions of the different species groups of the sinkhole slopes (A) and of the sinkhole bottom (B). 1: species of dry oak forests; 2: species of mesic oak forests; 3: species of Central European beech forests; 4: species of Illyrian beech forests; 5: species of deep ravines and gorges; 6: species of wet forests; 7: species of marshes; 8: weed species; 9: indifferent species.

3.2. Microclimate and flora of the sand-dune slack

Air temperature and air humidity changed markedly along the transect of Bugac (*Fig. 6*). The lowest MDAT (15.8 °C) was recorded in the bottom of the dune slack where a remainder of the association *Molinio-Salicetum rosmarinifoliae* occurred. The highest MDAT (20.2 °C) was recorded in the open sandy

grassland of the upper slope. MDtAt and MNtAT values showed a marked decrease from the slopes to the bottom indicating a clear temperature gradient between them. Air humidity showed an opposite pattern with the highest values (MDAH: 79%; MNtAH: 96%; MDtAH: 62%) in the bottom of the dune slack and the lowest values (MDAH: 64%; MNtAH: 81%; MDtAH: 42%) on the upper slopes. The 24-hour pattern of air temperature and air humidity also differed markedly between the upper dune slopes and the bottom of the dune slack (*Figs. 7–8*).

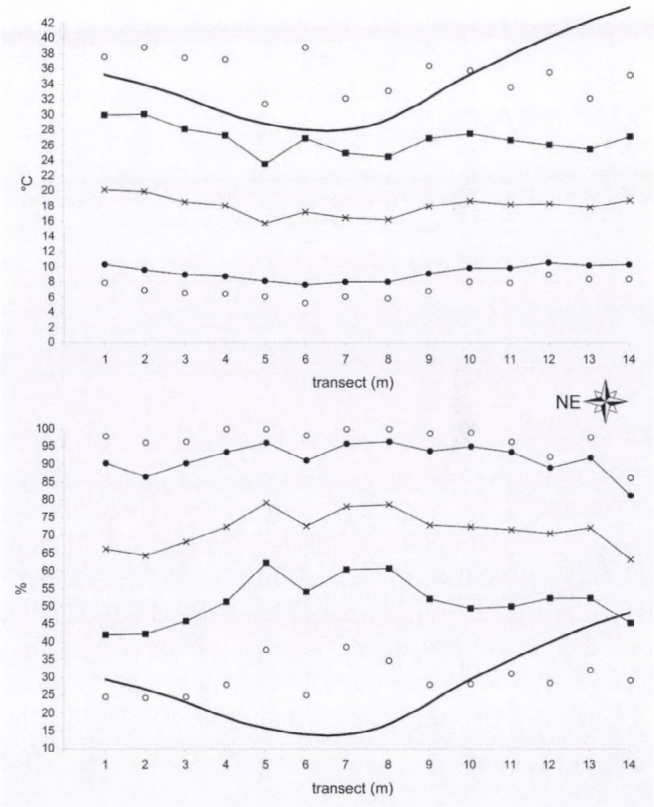

Fig. 6. Air temperature and air humidity values along the transect of the dune slack of Bugac (September 25–26, 2012). Notations: ○: minimum and maximum air temperature (DMinAT, DMaxAT) and air humidity (DMinAH, DmaxAH) values; ■: mean daytime air temperature (MDtAT) and air humidity (MDtAH) values; ×: mean daily air temperature (MDAT) and air humidity (MDAH) values; ●: mean nighttime air temperature (MNtAT) and air humidity (MNtAH) values.

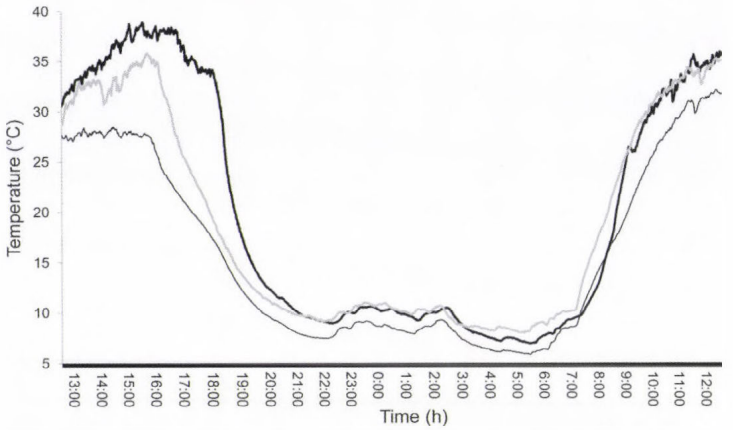

Fig. 7. Air temperature values in three plots along the transect (southwest-facing dune slope: thick black line; bottom of the dune slack: thin line; northeast-facing dune slope: thick grey line) of the dune slack of Bugac, measured over a 24-hour period (September 25–26, 2012).

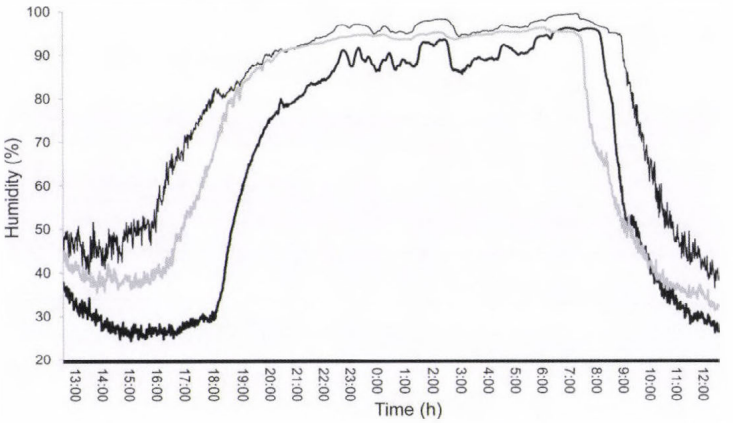

Fig. 8. Air humidity values in three plots along the transect (southwest-facing dune slope: thick black line; bottom of the dune slack: thin line; northeast-facing dune slope: thick grey line) of the dune slack of Bugac, measured over a 24-hour period (September 25–26, 2012).

Eryngium campestre L., *Festuca pseudovina* Hack., *Galium verum* L., *Stipa borysthenica* Klokov ex Prokudin, and *Thymus pannonicus* All. were the most frequent (>80%) species on the upper dune slopes, and *Carex liparicarpos* Gaudin, *Galium verum*, *Potentilla arenaria* Borkh., *Stipa borysthenica*, and

Thymus pannonicus in the bottom of the dune slack. Species that occurred only on the bottom of the dune slack include *Elymus repens* (L.) Gould, *Hieracium umbellatum* L., *Poa angustifolia* L., *Scirpoides holoschoenus* (L.) Soják, *Silene conica* L., *Salix rosmarinifolia* L. and *Trinia ramosissima* (Fisch.) W.D.J. Koch. According to the ANOVA, species number of the upper slopes and the dune slack did not differ significantly (P=0.245). Species of open sandy grasslands and closed sandy grasslands dominate all parts of the transect. However, fen species were only detected in the bottom of the dune slack with a proportion of 1.3% (*Fig. 9*).

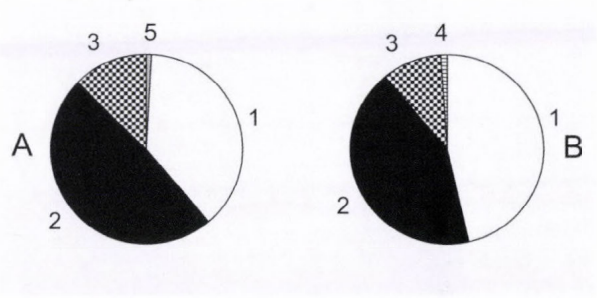

Fig. 9. Proportions of the different species groups of the dune slopes (A) and of the bottom of the dune slack (B). 1: species of closed sandy grasslands; 2: species of open sandy grasslands; 3: indifferent species; 4: fen species; 5: weed species.

3.3. Results of the multivariate analyses

The DCA-ordinations of the samples show a strong gradient along axis 1 with a very high species turnover in the sinkhole (eigenvalue: 0.63, gradient length: 4.4 S.D. units) and lower species turnover along the slopes of the dune slack (eigenvalue: 0.36, gradient length: 2.7 S.D. units).

The explanatory power of climatic variables in the 'one-predictor' db-RDA models is shown in *Table 1*. In Bugac, all of the 6 variables were significant, since they had P values under 0.001, 0.005, or 0.05, even though their F values varied considerably. In the Mecsek Mountains, there were minor differences among the variables in the explained variation, and all of them were found highly significant (<0.001). Both in Bugac and the Mecsek Mountains, MNtAT explained more variation of the vegetation than the daytime measurements, although the difference was negligible in the case of the Mecsek Mountains. MDAT had higher F values than MDtAT or MNtAT. Regarding air humidity, MDAH explained the most variation in both sites.

The 'two-predictor' models included MDAT and MDAH (*Figs. 10–11*). These models explained significant variation in both sites (*Table 2*).

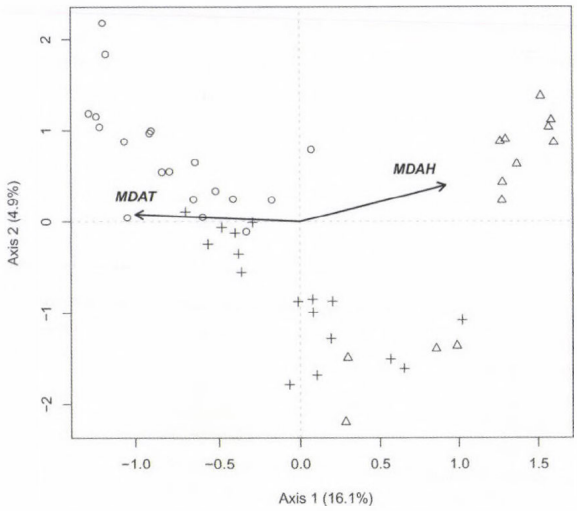

Fig. 10. Distance-based redundancy analysis diagram with 50 plots (○: plots of the south-facing sinkhole slope, +: plots of the north-facing sinkhole slope, △: plots of the sinkhole bottom) and environmental variables (MDAT: mean daily air temperature, MDAH: mean daily air humidity) of the Mecsek Mountains.

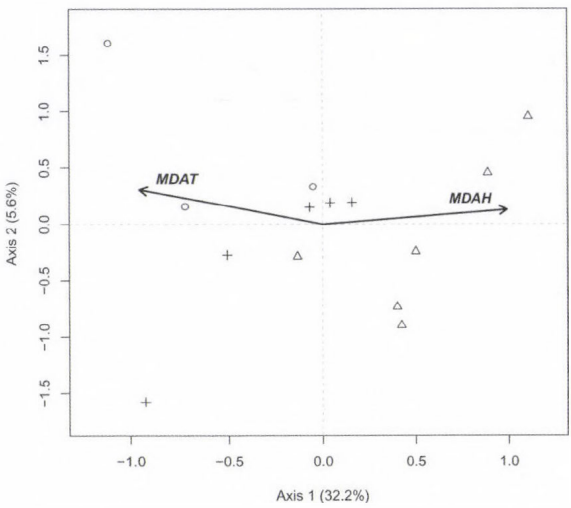

Fig. 11. Distance-based redundancy analysis diagram with 14 plots (○: plots of the southwest-facing dune slope, +: plots of the northeast-facing dune slope, △: plots of the bottom of the dune slack) and environmental variables (MDAT: mean daily air temperature, MDAH: mean daily air humidity) of Bugac.

4. Discussion

We studied the relationship between the spatial pattern of microclimatic parameters and the vegetation of natural habitat islands in Hungary. Our study yielded three main results. Firstly, the investigated habitat islands can be recognized as refugia for many species adapted to various climatic conditions. Secondly, the different elements of microclimate differently influenced the distribution of plant species. Thirdly, forest cover has a strong mitigating effect not only on air temperature but also on air humidity.

Previous studies showed that karst sinkholes may considerably affect the flora and vegetation of the karst surfaces (*Antonić et al.*, 2001; *Bátori et al.*, 2013; *Geiger*, 1950). As semi-isolated enclaves, lower sinkhole slopes and sinkhole bottoms are very important from a nature conservation point of view (*Bacsó* and *Zólyomi*, 1934; *Bátori et al.*, 2011; *Beck-Mannagetta*, 1906). Since they often harbor species that are very rare or missing from the surrounding habitats, they can be considered habitat islands (*Bátori et al.*, 2012b). We also found remarkable floristic differences between the bottom and the higher slopes of the investigated sinkhole. Many plants, in particular cool-adapted species, are restricted to the bottom of the sinkhole, where appropriate microclimatic conditions exist. The mean daily, daytime, and nighttime air temperature and air humidity values explained almost the same variation of species composition along the vegetation gradient. This is due to the mitigating effect of the forest, which reduces the differences between daytime and nighttime air temperatures and between daytime and nighttime air humidities at the same altitude (*Lehmann*, 1970; *Antonić et al.*, 1997). The extreme temperature value of the sinkhole bottom (DMaxAT: 32.1 °C) can be explained with the rate of canopy closure. Here, similarly to the ravine forests of deep valleys, frequent mass soil movements on the steep and wet slopes uproot trees allowing increased insolation through the sparse canopy. However, after this short high temperature period, the temperature of the sinkhole bottom decreased significantly, while the upper slopes remained warmer. Since karst surfaces are sensitive to climatic changes (*Loáiciga et al.*, 2000), sinkholes may play an essential role in reducing extinction rate of plant species, as they did in earlier geological times as well. The literature offers many excellent examples where sinkholes are mentioned as key habitats for cold-stage relicts and high mountain species (*Bátori et al.*, 2006; *Horvat*, 1953; *Lazarević et al.*, 2009). If we accept that the beech production optimum will shift in the future toward the pole and from lower elevation to higher elevation, and beech mortality risk will increase in its lower distribution range (*Hlásny et al.*, 2011; *Peñuelas et al.*, 2007; *Sykes* and *Prentice*, 1996), we can conclude that the beech forests of the Mecsek Mountains have a high chance of surviving in deep sinkholes for longer periods. In contrast, oak production and mortality seems almost insensitive to climate change in Central Europe, and in addition, the increasing oak production in elevations above 400 m a.s.l.

suggests a potential upward expansion of oak forests in the future (*Hlásny et al.*, 2011). This also means that the vegetation zones of sinkholes may shift toward the deeper sinkhole parts. This, in the worst scenario, would mean that vegetation types of the lowest parts (unable to shift even more downwards) may disappear from the sinkholes. A study by *Gargano et al.* (2010) on snow-bed vegetation of sinkholes has also showed that climate change would favor the replacement of snow-adapted species with the mesic ones occurring in surrounding habitats. In forest landscapes, climate-induced species replacement may be more striking if the forests are actively managed. Therefore, forest management should focus on maintaining forests not only in sinkholes but also in surrounding areas in order to moderate the potential impacts of climate change on karst surfaces.

Sand-dune slacks of the Kiskunság Sand Ridge play a similar role in preserving plant species as the karst sinkholes of mountain areas. Remnant patches of dune slacks have a high conservation value, since they support ancient steppe and fen vegetation with characteristic species such as *Carex flacca* Schreb., *Carex humilis* Leyss., *Chrysopogon gryllus* (L.) Trin., *Molinia caerulea* (L.) Moench, *Salix rosmarinifolia*, *Scirpoides holoschoenus*, *Schoenus nigricans* L., and *Thalictrum simplex* L. (*Borhidi*, 2012; *Molnár*, 2003). As our results revealed, microclimate is an important factor in structuring dune slack communities, although impacts of the nighttime and daytime air humidity and temperature values differ significantly (*Körmöczi et al.*, 1981). Although the investigated dune slack is much shallower than the karst sinkhole, its air humidity and temperature regimes are more extreme due to the large diurnal temperature variation, which can be explained by the different vegetation physiognomy. In the different parts of the world, several factors have been shown to contribute to the species composition changes of dune vegetation. The most important factors are the climate change- and human-induced drought (*Körmöczi*, 1991; *Muhs* and *Holliday*, 1995). Since the effect of precipitation and its spatial and temporal distribution are of great importance in xeric habitats (*Margóczi et al.*, 2007; *Thomas et al.*, 2005; *Yizhaq et al.*, 2009), the potential impact of precipitation decline on dune slack vegetation must be taken into consideration. For example, between 1981 and 1993, the average annual precipitation decreased by 16.7% on the Kiskunság Sand Ridge, causing a regional groundwater table decline (*Molnár et al.*, 2003). Apart from the climate change-induced drought, local human activities (e.g., afforestation, artesian and groundwater extraction, draining, hydrocarbon extraction, and intensive farming) also have had a strong negative influence on the groundwater table. A long-term vegetation study by *Tölgyesi* and *Körmöczi* (2012) revealed that both the wetter and drier sections of the dune fields of the Kiskunság are influenced by the water table decline, though most of the shifts were more prominent in the wet section (i.e., dune slack). The vegetation of the dune slack was getting more thermophilous, and its continental character was getting more pronounced. Since

climate change scenarios predict a significant temperature increase and a significant decrease in precipitation in summer for the Kiskunság Sand Ridge (*Bartholy et al.*, 2007), climate change could make the area even more vulnerable to drought and fire (*Blanka et al.*, 2013). Hence, conservation biologists must work on presenting arguments for policy makers and water management authorities in order to reduce the potential impact of drought on natural habitats of the Kiskunság.

As a summary, we have demonstrated the current and potential role of natural habitat islands in preserving different groups of plant species. According to our findings, the current vegetation of habitat islands is highly determined by the elements of microclimate, indicating the different importance of the daily, daytime, and nighttime humidity and temperature regimes. Presumably, these habitat islands will play an important role in mitigating species loss under future climate change. Probably the most important question in relation to the vegetation of natural habitat islands is how we can moderate and delay the impacts of climate change on species loss and vegetation replacement.

Acknowledgement—This research was supported by the TÁMOP-4.2.2/08/1/2008-0008 program of the Hungarian National Development Agency.

References

Allen, C.B., and *Burton, P.J.*, 1993: Distinction of soil thermal regimes under various experimental vegetation covers. *Can J Soil Sci 73*, 411–420.

Antonić, O., Hatic, D., and *Pernar, R.*, 2001: DEM-based depth in sink as an environmental estimator. *Ecol Model 138*, 247–254.

Antonić, O., Kušan, V., and *Hrašovec, B.*, 1997: Microclimatic and topoclimatic differences between the phytocoenoses in the Viljska Ponikva Sinkhole, Mt. Risnjak, Croatia. *Hrvatski Meteorološki Časopis 32*, 37–49.

Aude, E. and *Lawesson, J.E.*, 1998: Vegetation in Danish beech forests: the importance of soil, microclimate and management factors, evaluated by variation partitioning. *Plant Ecol 134*, 53–65.

Bacsó, N. and *Zólyomi, B.*, 1934: Mikroklíma és növényzet a Bükk-fennsíkon. *Időjárás 38*, 177–196. (in Hungarian)

Bartholy, J., Pongrácz, R., and *Gelybó, Gy.*, 2007: Regional climate change expected in Hungary for 2071-2100. *Appl Ecol Env Res 5*, 1–17.

Bátori, Z., Baráth, K., and *Csiky, J.*, 2006: *Dryopteris affinis* (Löwe) Fras.-Jenk. in the Mecsek Mountains. *Flora Pannonica 4*, 3–8. (in Hungarian)

Bátori, Z., Csiky, J., Erdős, L., Morschhauser, T., Török, P., and *Körmöczi, L.*, 2009: Vegetation of the dolines in Mecsek Mountains (South Hungary) in relation to the local plant communities. *Acta Carsologica 38*, 237–252.

Bátori, Z., Csiky, J., Farkas, T., Vojtkó, E. A., Erdős, L., Kovács, D., Wirth, T., Körmöczi, L., and *Vojtkó, A.*, 2013: The conservation value of karst dolines for vascular plants in woodland habitats of Hungary: refugia and climate change. *Int J Speleol 43*, 15–26.

Bátori, Z., Gallé, R., Erdős, L., and *Körmöczi, L.*, 2011: Ecological conditions, flora and vegetation of a large doline in the Mecsek Mountains (South Hungary). *Acta Bot Croat* 70, 147–155.

Bátori, Z., Erdős, L., and *Somlyay, L.*, 2012a: *Euphorbia prostrata* (*Euphorbiaceae*), a new alien in the Carpathian Basin. *Acta Bota Hung 54*, 235–243.

Bátori, Z., Körmöczi, L., Erdős, L., Zalatnai, M., and *Csiky, J.,* 2012b: Importance of karst sinkholes in preserving relict, mountain and wet woodland plant species under sub-Mediterranean climate: a case study from southern Hungary. *J Cave Karst Stud 74*, 127–144.

Beck-Mannagetta, G., 1906: Die Umkehrung der Pflanzenregionen in den Dolinen des Karstes. *Sitzungsberichte der Kaiserliche Akademie der Wissenschaften in Wien 65*, 3–4.

Begon, M., Townsend, C. R., and *Harper, J. L.,* 2006: Ecology: From Individuals to Ecosystems. Blackwell, Oxford.

Blanka, V., Mezősi, G., and *Meyer, B.,* 2013: Projected changes in the drought hazard in Hungary due to climate change. *Időjárás 117*, 219–237.

Borhidi. A., Kevey, B., and *Lendvai, G.,* 2012: Plant communities of Hungary. Akadémiai Kiadó, Budapest.

Dobrowski, S.Z., 2011: A climatic basis for microrefugia: the influence of terrain on climate. *Glob Change Biol 17*, 1022–1035.

Easterling, D.R., Meehl, G.A., Parmesan, C., Changnon, S.A., Karl, T.R., and *Mearns, L.O,* 2000: Climate extremes: Observations, modeling, and impacts. *Science 289*, 2068–2074.

Erdős, L., Gallé, R., Körmöczi, L., and *Bátori, Z.,* 2013: Species composition and diversity of natural forest edges: edge responses and local edge species. *Community Ecol 14*, 48–58.

Fetcher, N., Oberbauer, S.F., and *Strain, B.R.,* 1985: Vegetation effects on microclimate in lowland tropical forest in Costa Rica. *Int J Biometeor 29*, 145–155.

Forseth, I.N., and *Teramura, A.H.,* 1987: Field photosynthesis, microclimate and water relations of an exotic temperate liana, *Pueraria lobata*, kudzu. *Oecologia 71*, 262–267.

Gargano, D., Vecchio, G., and *Bernardo, L.,* 2010: Plant-soil relationships in fragments of Mediterranean snow-beds: ecological and conservation implications. *Plant Ecol 207*, 175–189.

Geiger, R., 1950: Das Klima der bodennahen Luftschicht: Ein Lehrbuch der Mikroklimatologie. Die Wissenschaft, 4. Verlag F. Vieweg and Sohn, Braunschweig. (in Deutsch)

Geiger, R. 1965: The climate near the ground. Harvard University Press, Cambridge.

Hammer, Ř., Harper, D. A. T., and *Ryan, P. D.,* 2001: PAST: Paleontological Statistics Software Package for Education and Data Analysis. Palaeontol Electron, http://palaeo-electronica.org/2001_1/past/issue1_01.htm.

Hampe, A. and *Jump, A.S.,* 2011: Climate relicts: Past, present, future. *Annu Rev Ecol Evol Syst 42*, 313–333.

Herrera, C.M., 1995: Microclimate and individual variation in pollinators: flowering plants are more than their flowers. *Ecology 76*, 1516–1524.

Hill, M. O., and *Gauch, H. G.,* 1980: Detrended correspondence analysis: an improved ordination technique. *Vegetatio 42*, 47–58.

Hlásny, T., Barcza, Z., Fabrika, M., Balázs, B., Churkina, G., Pajtík, J., Sedmák, R., and *Turčáni, M.,* 2011: Climate change impacts on growth and carbon balance of forests in Central Europe. *Clim Res 47*, 219–236.

Holl, K.D., 1999: Factors limiting tropical rain forest regeneration in abandoned pasture: seed rain, seed germination, microclimate, and soil. *Biotropica 31*, 229–242.

Horvat, I., 1953: Vegetacija ponikava. *Geografski Glasnik 14/15*, 1–25. (in Croatian)

Király., G., (Ed.) 2009: Új magyar füvészkönyv. Aggteleki Nemzeti Park Igazgatóság, Jósvafő. (in Hungarian)

Körmöczi, L., 1991: Drought-induced changes in a sandy grassland complex in the Great Hungarian Plain. *Acta Biol Szeged 37*, 63–74.

Körmöczi, L., and *Balogh, A.,* 1990: The analysis of pattern change in a Hungarian sandy grassland. In (*Krahulec, F., Agnew, A.D.Q., Agnew, S.,* and *Willems, H.J.* (Eds.)). Spatial processes in plant communities. Proceedings of the Workshop held in Liblice, 49–58.

Körmöczi, L., Bodrogközy, Gy., and *Horváth, I.,* 1981: Investigation of biological production and bioclimate of sandy grasslands in Bugac (Great Hungarian Plain between Danube and Tisza). *Acta Biol Szeged 27*, 55–69.

Lazarević, P., Lazarević, M., Krivošej, Z., and *Stevanović, V.,* 2009: On the distribution of *Dracocephalum ruyschiana* (Lamiaceae) in the Balkan Peninsula. *Phytologia Balcanica 15*, 175–179.

Legendre, P., and *Anderson, M.J.*, 1999: Distance-based redundancy analysis: testing multispecies responses in multifactorial ecological experiments. *Ecol Monogr 69*, 1–24.
Legendre, P., and *Legendre, L.*, 1998: Numerical Ecology. 2nd English edition. Elsevrier, Amsterdam.
Lehmann, A., 1970: Tarvágás által okozott ökológiai változások az abaligeti karszton. *Pécsi Műszaki Szemle 25*, 15–21. (in Hungarian)
Liu, X., Yin, Z.Y., Shao, X., and *Qin, N.*, 2006. Temporal trends and variability of daily maximum and minimum, extreme temperature events, and growing season length over the eastern and central Tibetan Plateau during 1961–2003. *J Geophys Res*: 111D19109.
Loáiciga, H.A., Maidment, D.R., and *Valdes, J.B.*, 2000: Climate-change impacts in a regional karst aquifer, Texas, USA. *Journal Hydrol 227*, 173–194.
Mantilla-Contreras, J., Schirmel, J., and *Zerbe, S.*, 2011: Influence of soil and microclimate on species composition and grass encroachment in heath succession. *J Plant Ecol-UK 5*, 249–259.
Margóczi, K., Szanyi, J., Aradi, E., and *Busa-Fekete, B.*, 2007: Hydrological background of the dune slack vegetation in the Kiskunság. *Ann Warsaw Univ of Life Sci – SGGW 38*, 105–113.
Marlatt, W. E., 1961: The interactions of microclimate, plant cover and soil moisture content affecting evapotranspiration rates. Atmospheric Science Technology Paper 23, Colorado State University, Fort Collins, Colorado.
Mohammed, A. R., and *Tarpley, L.*, 2009: High nighttime temperatures affect rice productivity through altered pollen germination and spikelet fertility. *Agr Forest Meteorol 149*, 999–1008.
Molnár, A., Tökölyi, J., Végvári, Zs., Sramkó, G., Sulyok, J., and *Barta, Z.*, 2012: Pollination mode predicts phenological response to climate change in terrestrial orchids: a case study from central Europe. *J Ecol 100*, 1141–1152.
Molnár, Zs., (Ed.) 2003: A Kiskunság száraz homoki növényzete. TermészetBÚVÁR Alapítvány Kiadó, Budapest. (in Hungarian)
Muhs, D. R., and *Holliday, V. T.*, 1995: Evidence of active dune sand on the Great Plains in the 19th century from accounts of early explorers. *Quaternary Res 43*, 198–208.
Müller, S.W., Rusterholz, H.P., and *Baur, B.*, 2006: Effects of forestry practices on relict plant species on limestone cliffs in the northern Swiss Jura mountains. *Forest Ecol Manag 237*, 227–236.
Oksanen, J., Kindt, R., Legendre, P., O'Hara, B., Simpson, G. L., Solymos, P., Stevens, M.H.M., and *Wagner, H.*, 2009: Stats Package and vegan: Community Ecology Package. R package version 2.10–1.
Oliver, S.A., Oliver, H.R., Wallace, J.S., Roberts, and *A.M.*, 1987: Soli heat flux and temperature variation with vegetation, soil type and climate. *Agr Forest Meteorol 39*, 257–269.
Parmesan, C., Root, T.L., and *Willig, M.R.*, 2000: Impacts of extreme weather and climate on terrestrial biota. *B Am Meteorol Soc 81*, 443–450.
Peñuelas, J., Ogaya, R., and *Boada, M.*, 2007: Migration, invasion and decline: changes in recruitment and forest structure in a warming-linked shift of European beech forest in Catalonia (NE Spain). *Ecography 30*, 830–838.
Pinke, Gy., Karácsony, P., Czúcz, B., Botta-Dukát, Z., and *Lengyel, A.*, 2012: The influence on environment, management and site context on species composition of summer arable weed vegetation in Hungary. *Appl Veg Sci 15*, 136–144.
R Development Core Team, 2009: R: A language and environment for statistical computing. R Foundation for Statistical Computing, Vienna, Austria. ISBN 3-900051-07-0, URL http://www.R-project.org.
Rasztovits, E., Móricz, N., Berki, I., Pötzelsberger, E., and *Mátyás, Cs.*, 2012: Evaluating the performance of stochastic distribution models for European beech at low-elevation xeric limits. *Időjárás 116*, 173–194.
Rich, P. M., and *Weiss, S. B.*, 1991: Spatial models of microclimate and habitat suitability: lessons from threatened species. Proceedings of the Eleventh Annual ESRI User Conference, Readlands: ESRI, 59–99.
Rijnsdorp, A.D., Peck, M.A., Engelhard, G. H., Möllmann, C., and *Pinnegar, J.K.*, 2009: Resolving the effect of climate change on fish populations. *ICES J Mar Sci 66*, 1570–1583.
Schwartz, M.W., Iverson, L.R., Prasad, A.M., Matthewa, S.N., and *O'Connorm, R.J.*, 2006: Predicting extinctions as a result of climate change. *Ecology 87*, 1611–1615.

Schimel, D.S., and *Parton, W.J.*, 1986: Microclimatic controls of nitrogen mineralization and nitrification in shortgrass steppe soils. *Plant Soil 93*, 347–357.

Shiu, C.J., Liu, S. C., and *Chen, J.P.*, 2009: Diurnally asymmetric trends of temperature, humidity, and precipitation in Taiwan. *J Climate 22*, 5635–5649.

Simon, T., (Ed.) 1991: Baktérium-, alga-, gomba-, zuzmó- és mohahatározó. Tankönyvkiadó, Budapest. (in Hungarian)

Simon, T., 2000. A magyarországi edényes flóra határozója. Nemzeti Tankönyvkiadó, Budapest. (in Hungarian)

Skyes, M.T., and *Prentice, I.C.*, 1996: Climate change, tree species distributions and forest dynamics: A case study in the mixed conifer/northern hardwoods zone of northern Europe. *Climatic Change 34*, 161–177.

Soó, R., 1980: A magyar flóra és vegetáció rendszertani-növényföldrajzi kézikönyve VI. Akadémiai Kiadó, Budapest. (in Hungarian)

Thomas, C.D., Cameron, A., Green, R.E., Bakkenes, M., Beaumont, L.J., Collingham, Y.C., Erasmus, B.F.N., de Siqueira, M.F., Grainger, A., Hannah, L., Hughes, L., Huntley, B., van Jaarsveld, A. S., Midgley, G.F., Miles, L., Ortega-Huerta, M.A., Peterson, A.T., Phillips, O.L., and *Williams, S.E.*, 2004: Extinction risk from climate change. *Nature 427*, 145–148.

Thomas, D.S.G., Knight, M., and *Wiggs, G.F.S.*, 2005: Remobilization of southern African desert dune systems ba twenty-first century global warming. *Nature 435*, 1218–1221.

Tichý, L., 2002: JUICE, software for vegetation classification. *J Veg Sci 13*, 451–453.

Tölgyesi, Cs. and *Körmöczi, L.*, 2012: Structural changes of a Pannonian grassland plant community in relation to the decrease of water availability. *Acta Bot Hung 54*, 413–431.

Turlure, C., Choutt, J., Baguette, M., and *van Dyck, H.*, 2010: Microclimatic buffering and resource-based habitat in a glacial relict butterfly: significance for conservation under climate change. *Glob Change Biol 16*, 1883–1893.

Unger, J., 1999: Comparisons of urban and rural bioclimatological conditions in the case of a Central-European city. *Int J Biometeorol 43*, 139–144.

Walther, G., Post, E., and *Convey, P.* 2002: Ecological responses to recent climate change. *Nature 416*, 389–437.

Whiteman, C.D., Haiden, T., Pospichal, B., Eisenbach, S., and *Steinacker, R.* 2004: Minimum temperatures, diurnal temperature ranges, and temperature inversion in limestone sinkholes of different sizes and shapes. *J Appl Meteorol 43*, 1224–1236.

Xu, M., Qi, Y., Chen, J., and *Song, B.*, 2004: Scale-dependent relationship between landscape structure and microclimate. *Plant Ecol 173*, 39–57.

Yizhaq, H., Ashkenazy, Y., and *Tsoar, H.*, 2009: Sand dune dynamics and climate change: A modeling approach. *J Geophys Res 114*: F01023.

Appendix

Table A1. Species composition (presence/absence data) of the plots along the sinkhole transect of the Mecsek Mountains

Part.1.

Plots	**1**	**2**	**3**	**4**	**5**	**6**	**7**	**8**	**9**	**10**	**11**	**12**	**13**	**14**	**15**	**16**	**17**	**18**	**19**
Species / Sinkhole	**South-facing rim and slope**																		
Acer campestre						1													
Acer platanoides											1								
Acer pseudoplatanus								1											1
Aconitum vulparia																			
Ajuga reptans							1											1	
Alliaria petiolata												1				1			
Arabis turrita																			
Asarum europaeum						1	1	1								1	1	1	1
Athyrium filix-femina																			
Atropa belladonna																			
Brachypodium sylvaticum		1	1																
Bromus ramosus agg.			1				1		1										
Campanula rapunculoides	1	1				1													
Cardamine impatiens																			
Carex pilosa	1	1	1	1	1	1	1	1	1	1	1	1	1			1	1	1	
Carex sylvatica																			
Carpinus betulus		1				1	1	1	1			1	1	1	1	1		1	1
Circaea lutetiana																			
Clematis vitalba																			1
Clinopodium vulgare							1												
Convallaria majalis			1																
Crataegus laevigata																			
Dactylis polygama	1	1	1	1	1	1	1	1	1			1							1
Dryopteris filix-mas																			
Eupatorium cannabinum																			
Euphorbia amygdaloides	1		1	1		1	1		1										
Fagus sylvatica														1	1			1	1
Fallopia dumetorum		1																	1
Festuca drymeja				1		1	1			1	1	1	1	1	1	1			
Fraxinus excelsior				1		1	1	1	1	1	1	1	1	1	1	1	1	1	1
Fraxinus ornus	1	1	1	1	1	1	1	1	1		1		1	1	1				
Galeobdolon luteum s.l.																		1	
Galium aparine					1										1	1			
Galium odoratum																		1	
Galium schultesii	1																		
Geranium robertianum																			
Geum urbanum																			
Glechoma hirsuta					1														
Hedera helix	1			1	1	1	1	1	1		1						1	1	
Helleborus odorus	1		1																1
Hepatica nobilis			1																
Lathyrus venetus											1						1	1	

Plots	1	2	3	4	5	6	7	8	9	10	11	12	13	14	15	16	17	18	19
Species / Sinkhole	**South-facing rim and slope**																		
Lathyrus vernus		1															1	1	
Ligustrum vulgare		1		1	1		1												
Luzula forsteri														1					
Melica uniflora	1	1	1	1	1	1	1	1	1	1	1	1	1		1	1	1	1	1
Mercurialis perennis																			1
Milium effusum																			
Moehringia trinervia																			
Mycelis muralis																			
Paris quadrifolia																			
Polygonatum multiflorum	1			1												1	1	1	
Polystichum aculeatum																			
Polystichum setiferum																			
Primula vulgaris																		1	
Pyrus pyraster																			
Quercus cerris				1		1													
Quercus petraea agg.					1	1				1	1	1							1
Rosa arvensis	1	1	1	1															
Rubus fruticosus agg.																			
Rubus hirtus																			
Rumex sanguineus																			1
Ruscus hypoglossum																			
Sambucus nigra																			1
Solanum dulcamara																			
Sorbus torminalis					1														
Stachys sylvatica																			
Stellaria holostea	1	1	1	1		1	1	1	1	1	1					1	1	1	1
Symphytum tuberosum	1																		
Tilia tomentosa						1	1	1	1	1	1	1	1	1	1	1	1		
Urtica dioica																			
Veronica montana																			
Viola alba							1												
Viola reichenbachiana							1												

Table A1. (cont.)

Part. 2.

Plots	20	21	22	23	24	25	26	27	28	29	30	31	32	33	34	35	36	37	38	39	40	41	42	43	44	45	46	47	48	49	50
Species / Sinkhole	**Bottom**													**North-facing rim and slope**																	
Acer campestre			1																										1		
Acer platanoides																										1	1	1			
Acer pseudoplatanus	1		1			1	1	1	1	1					1	1															
Aconitum vulparia		1																													
Ajuga reptans																															
Alliaria petiolata		1								1	1			1		1							1			1	1	1	1	1	1

Plots	20	21	22	23	24	25	26	27	28	29	30	31	32	33	34	35	36	37	38	39	40	41	42	43	44	45	46	47	48	49	50
Species / Sinkhole	**Bottom**													**North-facing rim and slope**																	
Arabis turrita																										1					
Asarum europaeum		1	1			1	1			1	1				1	1										1	1	1	1	1	
Athyrium filix-femina			1			1	1	1	1	1																					
Atropa belladonna	1					1	1	1																							
Brachypodium sylvaticum			1		1																										
Bromus ramosus agg.						1																						1	1		
Campanula rapunculoides																															
Cardamine impatiens			1																								1	1			1
Carex pilosa																										1	1	1	1	1	1
Carex sylvatica							1																								
Carpinus betulus			1			1	1																								
Circaea lutetiana	1			1	1		1	1		1																					
Clematis vitalba	1					1																									
Clinopodium vulgare																															
Convallaria majalis																															
Crataegus laevigata																															1
Dactylis polygama																											1				
Dryopteris filix-mas			1		1			1	1	1	1																				
Eupatorium cannabinum	1						1	1	1																						
Euphorbia amygdaloides																										1					
Fagus sylvatica																	1														
Fallopia dumetorum																										1					1
Festuca drymeja																															
Fraxinus excelsior	1	1	1	1	1	1	1	1	1		1	1		1	1	1	1		1	1	1		1	1	1	1	1	1	1	1	1
Fraxinus ornus														1					1	1	1	1	1	1	1	1	1	1	1	1	1
Galeobdolon luteum s.l.	1	1	1	1	1	1	1	1	1	1	1	1	1	1	1		1			1	1		1	1	1	1	1		1	1	1
Galium aparine	1			1																											
Galium odoratum										1					1																
Galium schultesii																												1			
Geranium robertianum										1																1		1			
Geum urbanum																															1
Glechoma hirsuta																															
Hedera helix											1	1	1				1						1				1	1	1		
Helleborus odorus		1	1										1			1									1						
Hepatica nobilis																															1
Lathyrus venetus																															
Lathyrus vernus																											1		1		
Ligustrum vulgare																										1			1	1	1
Luzula forsteri																															
Melica uniflora																										1	1	1	1	1	1
Mercurialis perennis	1		1	1	1	1									1	1	1	1				1				1	1	1	1	1	1
Milium effusum																													1		
Moehringia trinervia						1																						1	1		
Mycelis muralis																										1					
Paris quadrifolia				1																											
Polygonatum multiflorum																															
Polystichum aculeatum						1	1																								
Polystichum setiferum			1																												
Primula vulgaris																															

Plots	20	21	22	23	24	25	26	27	28	29	30	31	32	33	34	35	36	37	38	39	40	41	42	43	44	45	46	47	48	49	50
Species / Sinkhole	**Bottom**													**North-facing rim and slope**																	
Pyrus pyraster	1																														
Quercus cerris																															
Quercus petraea agg.																									1						
Rosa arvensis																										1					
Rubus fruticosus agg.	1							1																							
Rubus hirtus						1	1		1																	1					
Rumex sanguineus	1	1																													
Ruscus hypoglossum												1				1	1						1								
Sambucus nigra					1	1																									
Solanum dulcamara								1	1																						
Sorbus torminalis																															
Stachys sylvatica			1	1	1		1		1																						
Stellaria holostea																													1	1	1	1
Symphytum tuberosum																															
Tilia tomentosa	1											1				1										1					
Urtica dioica	1	1	1	1	1	1	1	1	1	1																					
Veronica montana			1			1																									
Viola alba																															
Viola reichenbachiana																1													1		

Table A2. Species composition (presence/absence data) of the plots along the dune slack transect of Bugac

Plots	1	2	3	4	5	6	7	8	9	10	11	12	13	14
Species / Dune slack	**Southwest-facing slope**			**Bottom**						**Northeast-facing slope**				
Achillea pannonica			1	1			1	1	1	1	1	1	1	
Calamagrostis epigeios							1	1		1	1			
Carex liparicarpos			1	1	1	1	1	1	1	1	1	1	1	
Cladonia convoluta	1	1												
Cladonia furcata	1	1	1	1						1	1	1	1	1
Cladonia magyarica		1	1	1					1	1	1	1	1	1
Crepis rhoeadifolia											1		1	
Crepis setosa													1	
Cynodon dactylon	1	1										1		1
Dianthus pontederae		1	1		1			1		1	1		1	
Elymus repens								1						
Eryngium campestre	1	1	1	1						1	1	1	1	1
Erysimum diffusum										1				
Euphorbia cyparissias						1	1	1	1	1	1		1	
Euphorbia seguieriana							1	1					1	
Falcaria vulgaris												1	1	1
Festuca pseudovina	1	1	1	1		1		1	1	1	1	1	1	1
Festuca vaginata										1		1	1	1
Galium verum		1	1	1	1	1	1	1	1	1	1	1	1	1
Hieracium umbellatum								1	1					

Plots	1	2	3	4	5	6	7	8	9	10	11	12	13	14
Species / Dune slack	**Southwest-facing slope**			**Bottom**						**Northeast-facing slope**				
Kochia laniflora	1													
Koeleria glauca		1				1				1	1	1	1	1
Odontites rubra						1					1			
Phleum phleoides												1		
Poa angustifolia						1	1							
Potentilla arenaria		1	1	1	1	1	1	1	1	1	1	1	1	
Salix rosmarinifolia						1								
Scabiosa ochroleuca						1						1		1
Scirpoides holoschoenus						1	1							
Silene conica						1								
Silene otites			1	1	1			1			1			1
Stipa borysthenica	1	1	1	1	1	1	1	1	1	1	1	1	1	1
Stipa capillata				1	1			1	1	1				1
Thymus pannonicus	1	1	1		1	1	1	1	1	1	1	1	1	
Tortula ruralis	1	1	1	1	1									
Tragopogon dubius			1				1	1			1			
Trinia ramosissima				1				1	1					
Verbascum lychnitis		1	1	1	1				1					1

IDŐJÁRÁS

Quarterly Journal of the Hungarian Meteorological Service
Vol. 118, No. 3, July – September, 2014, pp. 283–291

Impacts of extreme weather in supply chains

Zoltán Kovács and **Beáta Sz. G. Pató***

University of Pannonia, Department of Supply Chain Management
Veszprém, Egyetem u. 10, H-8200, Hungary

**Corresponding author E-mail: patog@vnet.hu*

(Manuscript received in final form March 10, 2014)

Abstract—There are many phenomena which confirm the fact of climate change. Two kinds of responses are mentioned often to this fact: 1. Actions by which this process can be interrupted or slowed down. 2. Accepting the fact of changes and finding adaptive strategies.

Authors present a research which aimed to increase the responsiveness of supply chains for the climate change – especially extreme weather. Secondary and primary investigation were carried out, and the nominal group technique was used to discover, group and assess the potential threats.

Results so far pointed out that both physical and control processes are involved in extreme whether consequences. Findings give good bases for a substantial risk analysis for any disaster coming from the climate change or other reasons.

The research is supported by the Government of Hungary.

Key-words: Climate change, disaster management in supply chains, extreme weather.

1. Introduction

Extreme weather event might cause wide range of problems in everyday life. While there is a debate on the fact of climate change (*Nordhaus*, 2013) and its possible source, there is no doubt that being ready for unexpected weather evens is not a bad decision. There are studies which deal with the source and implications of extreme weather.

Stott et al. (2004), in their pioneering study, concluded that human influence more than doubled the likelihood of the heat wave occurring. An

OECD study (*Agrawala et al.*, 2011) discovered that while companies are generally aware of the physical implications of climate change, few include it into their risk management system.

From this point of view, there are two possible strategies:

1. To reduce the climate change effects – mostly emission – in order to slow down or to turn back the negative trend. We have to be aware that outcomes of corrective and preventive actions will show up in middle or long time horizon.

2. To learn to live with climate change at least on middle range and to do our best to adapt to the situation.

Weather sensitive sectors such as agriculture, horticulture, food industries are involved mostly. *Thorpe* and *Fennel* (2012) present three case studies from coffee, cotton, and sesame oil business. Since supply is vital in wide area of society and life, it is important to examine the implications of climate change. The effects can have influence in direct and indirect ways.

Present youngsters are the most involved in the consequences of climate change. In the State of the Union speech, President Obama urged Congress "to get together, pursue a bipartisan, market-based solution to climate change, like the one John McCain and Joe Lieberman worked on together a few years ago." In his second inauguration speech (January, 2013), the president said: "We will respond to the threat of climate change, knowing that failure to do so would betray our children and future generations. Some may still deny the overwhelming judgment of science, but none can avoid the devastating impact of raging fires, and crippling drought, and more powerful storms."

The topic is especially relevant in Hungary, since we faced some extreme weather events recently, such as extreme temperature, excessive rainfall, flooding, and spring snowstorms.

Recognizing this and the fact that certain aspects of climate change issues are inevitable, University of Pannonia defined a project to carry out research on consequences of climate change, especially weather phenomena issues. Economics, agriculture, engineering, and social science researchers work in the project supported by the EU and the Hungarian government.

Inside economics, the main analyzed areas are: macroeconomics, regional development, tourism, health sector, and supply chains. Part of the research is a literature review, such as we introduced above. The other part is primary research, in first stage mostly forecast.

First we tried to discover a wide set of implications. The method we have used is the nominal group technique.

In our research we asked master level students – who are in supply chain related programs – about their judgments on the possible consequences of climate change, especially extreme weather.

2. *Literature review*

The main research question was to learn the opinion of next generation about weather change implications in supply chains.

According to *International Energy Agency* (2013), it is possible that global warming will be more than two degrees Celsius. Above this limit the climate could become unstable. This will affect production and transport processes as well. *Carey* (2011) suggests that extreme weather events have become more common in recent years.

Czifra, et al. (2013) argue that climate change affects competitiveness.

According to IPCC's annual report (*Trenberth*, 1999), Hungary is acutely vulnerable. Based on this forecast climate change will turn the weather towards extreme events. The temperature will be higher than it is now, and we can expect stormy winters with more fall (*Czifra, et al.*, 2013).

In Hungary one of the main supply related implications will be the deterioration of transport infrastructure. Extreme weather phenomena such as storm, flooding, high temperature, lots of fall will cause damages in transport infrastructure. *Hunyadi* (2010) gives examples for possible damages of road infrastructure. *Gáspár* (2003, 2004) has set up road durability requirements. He suggests that the requirement pyramid (*Fig. 1*) will change in the future as a respond to climate change.

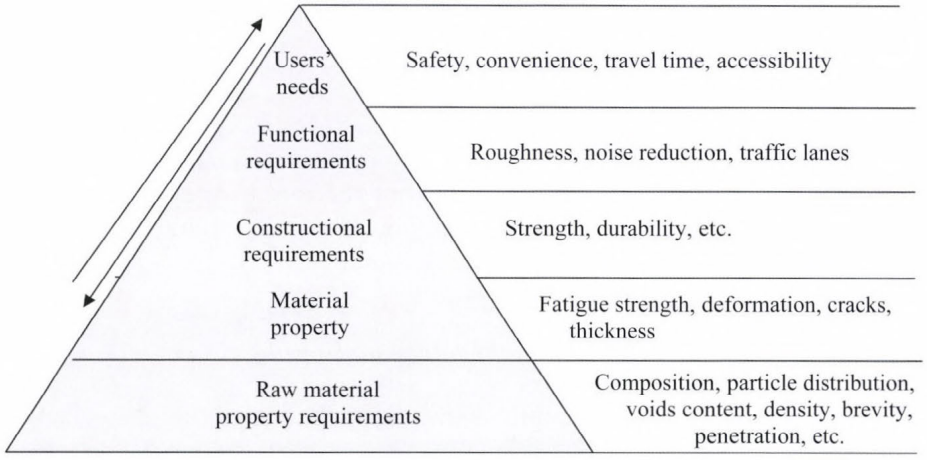

Fig. 1. Surface performance requirement related pyramid of requirements (*Gáspár*, 2003)

Hunyadi (2010) argues planting vegetation near the roads which have larger tolerance limits, in order to take consideration the effects of climate change in advance. *Gáspár* (2003) suggests life cycle design:"life cycle design includes both design methods and their phases which take into consideration economic issues, cultural integration and ecological aspects".

In addition to the environmental impacts on supply chains, there is an other important factor: restructuring of customer needs. Production infrastructure and distribution networks have to adjust to them (*Czifra et al*, 2013).

Caldwell et al. (2013) and others (*Thrope* and *Fennel*, 2012) examined the potential impacts of climate change to freight transport. *Table 1* summarizes the direct and indirect effects of meteorological factors on terrestial traffic safety.

Jüttner et al. (2003) give an overview of the potential research areas.

Table 1. Effects of weather on surface traffic safety (*Vissy* and *Bátyi*, 1998)

Surface conditions (road, rail)	**Direct effects**		**Indirect effects**	
	Visibility	**Loading**	**Biometeorological effects (front effects)**	
Snowing	Fog	Wind	Accident prevention	Health and safety
Snowdrift	Heavy rainfall	Heavy rainfall		
Temperature				

There are relatively small number of researches on the opinion of the future generation, however, *Revesz* and *Shahabian* (2010) evaluate opportunities for intergenerational discounting, which are often conflated in the literature. They have found that the existing justifications do not support the prevalent approach of discounting benefits to future generations at the rate of return in financial markets and, more generally, that discounting cannot substitute for a moral theory setting forth our obligations to future generations.

3. Research methodology and results

As previous studies from literature show, implications of climate changes include wide areas of supply chains. We can say that the whole society is involved in the climate change, partly due to the effects in supply chains. There are different ways to discover opinions on the topic.

Zaltman et al. (1982) and *Yin* (1994) used discovery oriented, practitioner-based approach, with semi-structured interviews.

The nominal group technique (NGT) is a group-based problem solving or decision making method (*Delbecq* and *VandeVen*, 1971, 1975; *VandeVen* and *Delbecq*, 1974). It combines the amenities of the un/low structured brainstorming and formal voting. We have followed the next steps:

1. Introduction and explanation: We welcomed the participants, who were master students in logistics, management, MBA and industrial engineering. We provided the question in written form on the top of an A4 format page: *What are the impacts of extreme weather to the operation of supply chains?* We have raised participants' attention to the importance of the question.

2. Silent generation of ideas: We asked participants to put down possible answers to the paper. Since any interaction is prohibited, in this phase we asked them not to consult or discuss their ideas with others. This stage lasted 10 minutes. In this stage, we repressed not only negative but useful positive interactions also. We allowed them in next steps.

3. Sharing ideas: We invited participants to read their ideas they have written on the paper. If they ran out of idea, they could 'pass'. If they have new idea – generated by others – they can join again. They can further develop others' ideas. We recorded each idea into a spreadsheet using the same words as participants formulated their ideas. (They were asked to use not more than 3 words to compose their idea.)

   The round robin process continued until all ideas have been presented. Since this phase supports only positive interaction, they could hear each other but were not allowed to comment others' ideas.

4. Discussion: Participants were invited to seek verbal explanation or further details about any of the ideas that others have produced that may not be clear to them. Anybody could ask, comment, interpret, explain any ideas on the screen. New ideas were generated, others were combined, extended or deleted (when they are proved to be equal with others: they called duplicates). There are two dangers in this stage (based on our more than 30 years NGT experiences):

   — Drawing together ideas might result so-called 'super idea' which will get lots of votes but is not concrete at all, thus, it can not be made real. Sometimes 'super idea' and some of its parts exist simultaneously.

   — There will be similar good ideas, which will compete again each other and share votes. In this way, each of them gets little weight and will drop out.

   It is important for the facilitator to keep good balance in the weight of ideas. Such aspects are complexity, extent, related hierarchy level of ideas. In this stage, we have received the list of possible effects in *Table 2*.

Table 2. List of potential effects after group discussion

1	Product damage
2	Communication problems in the EDI
3	Damage of factories
4	Routes are cancelled
5	Extreme work conditions
6	Other modal transport are forced
7	Cost, time, and resource losses
8	Low water-sailing ban
9	Increased preparations in the case of FMCG products
10	Huge storm - closed airports
11	Increased transport (supply) uncertainty
12	Additional storage costs
13	Appreciation of reliability models due to increased uncertainty
14	Increased number of risk factors
15	Increased costs of mining, excavating raw materials
16	Increased transport time requirement
17	Companies that fall out of the supply chains
18	Electric grid dropouts complicate storing
19	Necessity of work reorganization
20	Increased mental and physical load of labour
21	Higher vulnerability of electronic products, lower humidity during winter
22	Loss of goodwill due to delays and damages
23	Lack of agricultural products
24	Physical delivery becomes impossible
25	Difficult traffic conditions due to flooding
26	Development of resistant packaging
27	Railway comes to the fore
28	Coming out supply chain issues
29	Profile change is necessary (products)
30	Maintaining higher inventory
31	Accidents
32	Maintaining crisis staff
33	Alternative supply seeking
34	Further company social responsibilities
35	More pressure on co-operation, collaboration
36	Earthquake abyss engulfes the company
37	Daily 8-hour work period may be fragmented
38	Increasing number of non-forecasted transport errors
39	Closer relocation of supply chain players
40	Introduction of stricter limitations
41	Establishing specialized warehouses
42	Conflicts between partners
43	Consumer needs can not be satisfied
44	Material flow slows
45	More dense distribution points, necessity for warehouses
46	Shutdown due to state of emergency
47	Appreciation of taking out insurance
48	Good condition tires can not be calculated
49	Market rankings change
50	Development of vehicles
51	Needs assessment difficulties
52	IT equipment damage
53	Stress
54	Longer delivery lead times
55	Shipments over Arctic can not be solved
56	Decentralized inventory management
57	Necessity of rationalization
58	Increased energy consumption
59	Appreciation of meteorological information
60	Weakening of political stability
61	Growing importance of forecasts
62	Obstruction in mining
63	Rails freezing
64	Shifted seasonality
65	Appreciation of products with longer warranty period
66	Chain problems accumulate
67	Increasing weight of security/safety technology
68	Need for special storage conditions
69	Changes in priorities within the company
70	Co-operation with the army
71	Importance of loading and fastening technology
72	Rail deformation

5. Ranking: In this session there were little, spontaneous and informal interaction between participants. They were busy with their voting papers and selecting the most preferred ideas.
First they were asked to select the 5 most important effects from the list of 72. Then they ranked them. The ranking order was: 1 – 5 – 2 – 4 – 3 where 5 was the grade of the most important, 1 is the grade of least important one.
Finally, the grade points were summarized for all effects in the list of 72 ideas. *Table 3* shows the final ranks of the effects.
Then we summarized the grade points.

Table 3. The final ranks

Rank	Potential effects	Score
1.	Increased transport (supply) uncertainty	22
2.	Cost, time and resource losses	21
3.	Routes are cancelled	15
4.	Damage of factories	12
5.	Accidents	11
6-7.	Appreciation of reliability models due to increased uncertainty	10
6-7.	Maintaining crisis staff	10

4. Conclusions

Looking at the list we can conclude, that students have a realistic judgment on possible consequences of climate change, especially effects of extreme weather. It is especially important in Hungary where the frequency of extreme weather events is increasing, however, to put it cynically, they are tending to become not extreme ones.

We did not asked the participants about the 'to do's, it will be the part of further research. Based on their case studies *Thorpe* and *Fennel* (2012), using an EOCD study, suggest five possible actions:

1. Raise awareness and understanding of adaptation within the business: companies need to make more effort to understand and evaluate the potential physical impacts.

2. Ask producers about current climate trends and impacts: talking to producers directly, risks must be assessed.

3. Build longer-term and more stable relationships with suppliers: where markets are more stable, producers are empowered to invest for the future.

4. Support community development and environmental sustainability: climate resilient products, technologies, new forms of organizations and co-operations, managing social issues, new markets need to be supported.

5. Work through existing institutions, including governments.

Our other researches on modeling the implications (*Kovács et al.*, 2014) confirm this complex approach.

We are planning to get further information from the national disaster management system. This research will include the evaluation of extreme weather related cases such as snowstorm and flooding.

Acknowledgment–This paper presents the results of the projects TÁMOP-4.2.2/A-11/1-2012-0064.This project is supported by the European Union and co-financed by the European Social Fund.

References

Agrawala, S., Carraro, M., Kingsmill, N., Lanzi, E., Mullan, M., and *Prudent-Richard, G.* 2011: Private Sector Engagement in Adaptation to Climate Change: Approaches to Managing Climate Risks. *OECD Environment Working Papers 39,* http://dx.doi.org/10.1787/5kg221jkf1g7-en.

Caldwell, H., Quinn, H.K., Menuier, J., Subrier, J., and *Grenzeback, L.,* 2013: Potential Impacts of Climate Change on Freight Transport. http://climate.dot.gov/documents/workshop1002/caldwell.pdf.

Carey, J., 2011: Storm warnings: extreme weather is a product of climate change. Scientific American. http://www.scientificamerican.com/article/extreme-weather-caused-by-climate-change/

Czifra, T., Dobozi, E., Selmeczi, P., Kohán, Z., Rideg, A., and *Schneller, K.,* 2013: A területfejlesztés 4 éves szakmai programja a klímaváltozás hatásainak mérséklésére (2010–2013). http://www.vati.hu/files/sharedUploads/docs/ttei/A_teruletfejlesztes_klimaprogramja_2010-2013_1.pdf. In Hungarian)

Delbecq, A.L. and. *VandeVen, A.H.,* 1971: A Group Process Model for Problem Identification and Program Planning. *J. Appl. Behav. Sci. VII* (July/August, 1971), 466–491.

Delbecq, A.L., VandeVen, A.H., and *Gustafson, D.H.,* 1975: Group Techniques for Program Planners. Glenview, Illinois: Scott Foresman and Company.

Gáspár, L., 2003: Az élettartam mérnöki tudomány. *Közlekedéstudomány 53,* 81–129. (In Hungarian)

Gáspár, L., 2004: Az útburkolatok teljesítőképessége, *Közúti mélyépítési szemle 54 (11),* 7–12. (In Hungarian)

Hunyadi, D., 2010: A klímaváltozás hatása a közlekedési infrastruktúrára. *Közúti mélyépítési szemle 60 (3),* 35–40. (In Hungarian)

International Energy Agency, 2013: Redrawing the Energy Climate MapWorld Energy Outlook Special Report - released on 10 June 2013.

Jüttner, U., Peck, H. and *Christopher, M.,* 2003: Supply chain risk management: outlining an agenda for future research. *Int. J. Logistics: Res. Appl. 6,* 197–210.

Kovács Z., Pató Gáborné Szűcs B., and *Szabó L.,* 2014: Logisztika a klímaváltozás körülményei között. *Logisztikai Híradó. 2014/1,* 39–42. (In Hungarian)

Nordhaus, W.D., 2013: Why the Global Warming Skeptics Are Wrong? http://www.nybooks.com/articles/archives/2012/mar/22/why-global-warming-skeptics-are-wrong/?pagination=false.

Revesz, L.R. and *Shahabian, M.R.,* 2010: Climate Change and Future Generations. *Southern California Law Review 84,* 1099–1164.

Stott, P.A., Stone, D.A., and *Allen, M.R.,* 2004: Human contribution to the European heatwave of 2003. *Nature 432,* 610–614.

Thorpe, J. and *Fennel, S.,* 2012: Climate Change Risks and Supply Chain Responsibility: How should companies respond when extreme weather affects small-scale producers in their supply chain?" *Oxfam Discussion Papers, June 2012.*, www.oxfam.org.

Trenberth, K. E. 1999: Short-term Climate Variations. Recent accomplishments and issues for future progress. (Eds: *R. Pielke Sr* and *R. Pielke Jr*) Storms Vol 1. Routledge Press. London. 126–141.

United Nations Conference on Trade and Development (UNCTAD), 2011: Assuring Food Security in Developing Countries under the Challenges of Climate Change: Key Trade and Development Issues of a Fundamental Transformation of Agriculture. *Discussion Paper 2011(2).*

VandeVen, A.H. and *Delbecq, A.L.,* 1974: The effectiveness of nominal, Delphi, and interacting group decision making processes. *Acad. Manage J.* 605–621.

Vissy, K. and *Bátyi, F.,* 1998: A földfelszíni közlekedés meteorológiája. *Természet Világa, 129. I. különszám,* 75–78. (In Hungarian)

Yin, R. 1994: Case study research: design and methods. Thousand Oaks, CA, Sage.

Zaltman, G., Lemasters, K., and *Heffring, K.* 1982: Theory construction in marketing: some thoughts on thinking. New York, Wiley.

INSTRUCTIONS TO AUTHORS OF *IDŐJÁRÁS*

The purpose of the journal is to publish papers in any field of meteorology and atmosphere related scientific areas. These may be

- research papers on new results of scientific investigations,
- critical review articles summarizing the current state of art of a certain topic,
- short contributions dealing with a particular question.

Some issues contain "News" and "Book review", therefore, such contributions are also welcome. The papers must be in American English and should be checked by a native speaker if necessary.

Authors are requested to send their manuscripts to

Editor-in Chief of IDŐJÁRÁS
P.O. Box 38, H-1525 Budapest, Hungary
E-mail: journal.idojaras@met.hu

including all illustrations. MS Word format is preferred in electronic submission. Papers will then be reviewed normally by two independent referees, who remain unidentified for the author(s). The Editor-in-Chief will inform the author(s) whether or not the paper is acceptable for publication, and what modifications, if any, are necessary.

Please, follow the order given below when typing manuscripts.

Title page: should consist of the title, the name(s) of the author(s), their affiliation(s) including full postal and e-mail address(es). In case of more than one author, the corresponding author must be identified.

Abstract: should contain the purpose, the applied data and methods as well as the basic conclusion(s) of the paper.

Key-words: must be included (from 5 to 10) to help to classify the topic.

Text: has to be typed in single spacing on an A4 size paper using 14 pt Times New Roman font if possible. Use of S.I. units are expected, and the use of negative exponent is preferred to fractional sign. Mathematical formulae are expected to be as simple as possible and numbered in parentheses at the right margin.

All publications cited in the text should be presented in the *list of references*, arranged in alphabetical order. For an article: name(s) of author(s) in Italics, year, title of article, name of journal, volume, number (the latter two in Italics) and pages. E.g., *Nathan, K.K.,* 1986: A note on the relationship between photo-synthetically active radiation and cloud amount. *Időjárás 90,* 10-13. For a book: name(s) of author(s), year, title of the book (all in Italics except the year), publisher and place of publication. E.g., *Junge, C.E.,* 1963: *Air Chemistry and Radioactivity.* Academic Press, New York and London. Reference in the text should contain the name(s) of the author(s) in Italics and year of publication. E.g., in the case of one author: *Miller* (1989); in the case of two authors: *Gamov* and *Cleveland* (1973); and if there are more than two authors: *Smith et al.* (1990). If the name of the author cannot be fitted into the text: *(Miller,* 1989); etc. When referring papers published in the same year by the same author, letters a, b, c, etc. should follow the year of publication.

Tables should be marked by Arabic numbers and printed in separate sheets with their numbers and legends given below them. Avoid too lengthy or complicated tables, or tables duplicating results given in other form in the manuscript (e.g., graphs).

Figures should also be marked with Arabic numbers and printed in black and white or color (under special arrangement) in separate sheets with their numbers and captions given below them. JPG, TIF, GIF, BMP or PNG formats should be used for electronic artwork submission.

Reprints: authors receive 30 reprints free of charge. Additional reprints may be ordered at the authors' expense when sending back the proofs to the Editorial Office.

More information for authors is available: journal.idojaras@met.hu

Published by the Hungarian Meteorological Service

Budapest, Hungary

INDEX 26 361

HU ISSN 0324-6329

IDŐJÁRÁS

QUARTERLY JOURNAL
OF THE HUNGARIAN METEOROLOGICAL SERVICE

Special Issue: Application of information and communication technologies in environmental sciences: towards a sustainable future

Guest Editor: **Kálmán Kovács**

CONTENTS

****

http://www.met.hu/Journal-Idojaras.php

VOL. 118 * NO. 4 * OCTOBER – DECEMBER 2014

IDŐJÁRÁS

Quarterly Journal of the Hungarian Meteorological Service

Editorial Office: Kitaibel P.u. 1, H-1024 Budapest, Hungary
P.O. Box 38, H-1525 Budapest, Hungary
E-mail: journal.idojaras@met.hu
Fax: (36-1) 346-4669

Indexed and abstracted in Science Citation Index Expanded™ and Journal Citation Reports/Science Edition
Covered in the abstract and citation database SCOPUS®

Subscription by mail:
IDŐJÁRÁS, P.O. Box 38, H-1525 Budapest, Hungary
E-mail: journal.idojaras@met.hu

Editorial

Special Issue: Application of information and communication technologies in environmental sciences: towards a sustainable future

The Future Information and Communication Project (FuturICT) was launched by the European Union within the frame of Seventh Framework Programme. The ultimate goal of the FuturICT project is to understand and manage complex, global, socially interactive systems, with a focus on sustainability and resilience. Revealing the hidden laws and processes underlying societies probably constitutes the most pressing scientific grand challenge of our century and is equally important for the development of novel robust, trustworthy, and adaptive information and communication technologies, based on socially inspired paradigms. FuturICT is at heart of a revolutionary 21st century science, which will use and develop information and communication technologies to create a decision support system, combining data with models in order to solve the grand challenges humanity is facing. FuturICT is expected to lift our knowledge of social and economic systems to a new level of understanding, enabling us to discover promising paths towards a sustainable future.

In close connection to the goals above, the FuturICT.hu project was initiated and performed within the framework of TÁMOP-4.2.2.C-11/1/KONV-2012-0013 project involving cooperating partners from leading Hungarian universities as well as private research sector. Some results of the project relevant to the environmental aspects of application of ICT and their relation to social issues are presented in five papers in present thematic issue. The first paper discusses the assessements of greenhouse gas emissions and trends in Hungary related to the national policies and measures. In the second paper, the trends of precipitation and drought-related climate indices and the return period of the daily precipitation amount are analyzed based on the results of 11 regional climate models (RCMs) after applying a bias-correction procedure. The authors of the third paper deal with the trend analysis of a new MODIS satellite based drought severity index with emphasis on the Carpathian Basin. In the fourth paper, some important aspects of the impact of meteorological forecast uncertainties on environmental dispersion prediction are discussed. The final paper of this issue presents a statistical analysis of relationships between road accidents involving personal injury and meteorological variables in Hungary on the basis of a 20 years long database, and provides a qualitative outlook for the future expectations.

Kálmán Kovács
Guest Editor

IDŐJÁRÁS
Quarterly Journal of the Hungarian Meteorological Service
Vol. 118, No. 4, October – December, 2014, pp. 293–304

Progress towards emission targets through the development of climate change policies and measures in Hungary

Márk Molnár[1], **Sándor Molnár,**[2] and **Anita Csábrági**[2]

[1] *Szent István University, Faculty of Economics and Social Sciences*
H-2100 Gödöllő, Páter Károly u. 1.

[2] *Szent István University, Faculty of Mechanical Engeneering,*
H-2100 Gödöllő, Páter Károly u. 1.

**Corresponding author E-mail: Molnar.Sandor@gek.szie.hu;*

(Manuscript received in final form May 14, 2014)

Abstract—Parties included in Annex I to the UNFCCC are requested to regularly submit National Communications to the Secretariat. This report presents an overview of the results of the 6th National Communication (NC6) of Hungary with respect to the relevant provisions of the Convention and Article 8 of the Kyoto Protocol.

Key-words: mitigation scenarios, emission reduction, national reporting

1. Introduction

Hungary, as a Member State of the European Union and a Party to the Kyoto Protocol, considers efforts against climate change to be one of the most important challenges. Implementing, adopting, and planning measures and policies to tackle climate change related threats, designing mechanisms and plans to adapt to climate change, and pursuing scientific activities to assess, monitor, and decrease climate change vulnerability are in the focus of the Hungarian Government and the experts.

The recent findings outlined in the Fifth Assessment Report of the IPCC conclude that human activities are highly likely to be causing climate change and that actions against global warming are indispensable. In accordance with these results and responding to the 19th Conference of Parties in Warsaw in 2013, Hungary presents the future commitments, the progress made and other relevant topics in the 6th National Communication (*Ministry of National Development,* 2013), where Hungary provides information on greenhouse gas emissions and trends, quantified emission reduction targets, and progress towards their accomplishment, and gives an overview of emissions projections and financial and technical support provided to developing countries (*Molnár S. et al.*, 2012).

2. Information on GHG emissions and trends

In 2011, total emissions of greenhouse gases in Hungary were 66.1 million tons carbon dioxide equivalents (excluding the LULUCF – land use, land use change, and forestry – sector), which is the lowest value in the whole time series (1985–2011). Considering the carbon sinks in the LULUCF sector, the net emissions of Hungary were 62.4 million tons CO_2 equivalents in 2011. Being about 6–7 tons, the Hungarian per capita emissions are below the European average.

By far, the biggest emitting sector was the energy sector, contributing 71.6% to the total GHG emission in 2011. Agriculture was the second largest sector with 13.2%, while emissions from industrial processes (with solvent and other product use) accounted for 9.8%, and the waste sector contributed 5.3%. Compared to the base year, emissions were significantly reduced in the energy (–40.3%), agriculture (–54.0%), and industrial processes (–57.7%) sectors. In contrast, emissions in the waste sector have increased since 1985 (+14.5%). Solvent and other product use and land use, land use change and forestry (LULUCF) sectors show fluctuating behavior.

The most important greenhouse gas is carbon dioxide, accounting for 75.2% of the total GHG emissions. The main source of CO_2 emissions is burning of fossil fuels for energy purposes, including transport. CO_2 emissions have decreased by 41.8% since the middle of the 80's. Methane represents 12.8% in the GHG inventory. Methane is generated mainly at waste disposal sites and in animal farms, but the fugitive emissions of natural gas are also important sources. CH4 emissions are by 37.2% lower than in the base year. Nitrous oxide contributes 10.2% to the total GHG emissions. Its main sources are agricultural soils and manure management. N_2O emissions are 60.4% lower compared to the base year. The total emissions of fluorinated gases amount to 1.8%, but their steadily growing tendency seems to level off since 2008.

By ratifying the Kyoto Protocol, Hungary has committed to reduce its GHG emissions by 6%. Now, our emissions are 43.2% lower than in the base

year (average of 1985–87). For the most part, this significant reduction was a consequence of the economic transition in Hungary (1989–1990), which brought significant decline in the output of the national economy. The production decreased in almost every economic sector including also the GHG relevant sectors like energy, industry, and agriculture. Then, between 2005 and 2011, after a period of about 14 years of relatively stagnant emission levels (1992–2005), GHG emissions fell again quite significantly by 16.7 per cent.

The global financial and economic crises exerted a major impact on the output of the Hungarian economy, consequently on the level of GHG emissions as well. After a quite significant drop of 8.4% between 2008 and 2009, our emissions in the following three years (2009–2011) remained the lowest in the entire time series. Although the decline in economic output stopped in the first quarter of 2010 and Hungary had a moderate growth of 1.6%, emissions fell again by 2.6% in 2011, after a slight increase (+0,8%) in 2010.

Compared to the base year, emissions were significantly reduced in the energy (–40.3%), agriculture (–54.0%), and industrial processes (–57.7%) sectors. In contrast, emissions in the waste sector have increased since 1985 (+14.5%). Solvent and other product use and land use, land-use change and forestry (LULUCF) sectors show fluctuating behavior.

3. Assessment of the current situation

Under the EU's Climate and Energy Package, Hungary as an EU member is committed to a quantified economy-wide GHG emission reduction target of 20% by 2020, compared to the 1990 levels. This target is coupled with a renewable penetration rate of 14.65% for Hungary and an energy efficiency improvement of 20%; while the RED Directive (2009/28/EC) of the EU set the renewable target for Hungary as minimum 13% of the total gross final energy consumption, the objective defined by the NREAP is 14.65%.

This means that Hungary committed herself to a reduction of 20% of the 96 961,78 kt CO_2 equivalents emissions of 1990 (incl. LULUCF), the target to be achieved is 77 568,8 kt by 2020.

Sectors under the EU ETS are forecasted to provide a basis of GHG emissions savings until 2025. Beginning with 2013, from the third trading period onwards, a single EU-wide cap determines the amount of emissions allowed to be emitted by the EU ETS sectors. Furthermore, from 2013 onwards, a linear reduction factor of –1.74 % per annum applies to achieve a total of 21% of reduction in the ETS sectors. Under the joint Effort Sharing Decision (ESD) of the EU, Hungary took the commitment of a maximum 10% increase of the non-ETS sectors greenhouse gas emissions compared to their 2005 levels by 2020.

Hungary is also influenced by the Kyoto second period target of the EU. The EU has also committed to reduce its emissions by 20% under the Kyoto Protocol's second period, which runs from 2013 to 2020. Despite its identical nature, this commitment differs in several important respects from the EU's unilateral 2020 commitment:

- The Kyoto commitment is measured against base years, not 1990.
- LULUCF: the LULUCF sector in the EU is not included in the 20 % target under the Climate and Energy Package, but is accounted for under the KP according to the relevant decisions made in Durban.
- Inclusion of nitrogen trifluoride (NF3): NF3 is not included in the Climate and Energy Package, whereas the scope of the second commitment period has been extended to include the additional gas. The impact of NF3 on aggregate EU emissions is insignificant.
- It requires the EU to keep its emissions at an average of 20% below base-year levels over the whole period, not only in 2020.
- It differs in scope (for instance, it does not cover emissions from international aviation, since these are outside the scope of the Protocol, but it does cover emissions and their removals from land use, land use change and forestry, which is not covered by the unilateral commitment).
- The EU will meet its Kyoto commitment jointly with Iceland.

4. Policies and measures

Legislative and policymaking activities in climate change and the energy sector have been united under the auspices of the Ministry of National Development with the establishment of a sovereign State Secretariat of Climate Change and Energy Policy with two aides of the state secretary – a deputy state secretary for energy policy and another deputy for green economy development and climate change. The most important task of the Secretariat was the formation of the long-term energy strategy of Hungary, as well as submission of the National Action Plan for Renewable Energy to the European Commission. Recently, the administration was reformulated into a State Secretariat of Development, Climate Policy, and Key Public Services.

In the following section, the framework of climate change policies will be outlined. Details are provided in Chapter 4 of the 6th National Communication of Hungary.

The general context of policy development is the Programe of National Cooperation. Although in itself the Programe of National Cooperation is not focused on the GHG mitigation, the implementation of the Programe includes several similar elements, and the Programe itself has some priorities that serve this purpose. Some relevant key elements are:

- Promotion of the European initiative to employ "green" technologies and to research the energy efficiency of buildings and construction materials;
- Launching of a large scale energy efficiency program aiming at reconstruction of pre-fab buildings, thermal insulation projects of other building types, reconstruction of public buildings, etc.;
- Encouragement of renewable energy investments.

A cornerstone of climate change policy is the National Climate Change Strategy which was revised in 2013. Its key characteristics are as follows:

- Main areas of intervention are:
  - — Energy efficiency in buildings;
  - — Renewable energy utilization;
  - — Transport (road tolls, other economic incentives, modal split change);
  - — Afforestation.
- New element is increased emphasis on adaptation to climate change.
- The responsibility of the government is to create the necessary regulatory-legal framework; to review and adjust the subsidy systems; to raise the awareness of the society by giving priority to sustainability and providing good example.
- The residential sector is a key field of change: peoples' lifestyle needs to be changed; a large-scale reduction of demands for energy and materials must be achieved (by subsidized energy efficiency projects, among others);
- Industry and other enterprises also need to reduce their energy consumption, adopt emission reduction measures, "green" their profile, products, and services.
- NGOs, civil organizations shall have increased role in the dissemination of information, awareness raising, and civil control.

As the new EU Sustainable Development Strategy adopted by the European Council requires, Hungary prepares and regularly updates its National Sustainable Development Strategy (NSDS). The new NSDS has been adopted by the Hungarian Parliament in 2013.

Beginning from 1995, a regularly (every six year) revised and updated National Environmental Protection Programe (NEP) is prepared. The recent National Environmental Protection Programe 2009–2014 (NEP-III) was adopted by the Parliament in 2009. Similarly to the previous programes, the NEP-III identifies general objectives, which are then broken down to specific actions, the so-called thematic action programes or TAPs. The general objectives are the following:

- Improving the quality of the environment and life locally;

- Preservation of natural resources;
- Promotion of sustainable lifestyle, production, and consumption;
- Improvement of environmental safety.

The following TAPs are relevant from the aspect of GHG mitigation:

- Reinforcing environmental awareness:
  - — Education, training within the education system from the elementary school to the university;
  - — Environmentally conscious production and consumption;
  - — Access to environment-related information, information dissemination;
  - — Combating climate change;
  - — Reduction of GHG emissions (EU-ETS system, improvement of energy efficiency [NEEAP]);
  - — Reducing the environmental impact of transport (reducing demand, restructuring modal split, alternative fuels);
  - — Reducing emissions from the agriculture (improvement of production efficiency);
  - — Afforestation according to the National Afforestation Programe.
- Environment and health:
  - — Transport and environment (reversing the tendency of shifting to individual transport).
- Protection and sustainable utilization of waters:
  - — Utilization of the energy of geothermal waters.
- Waste management:
  - — Prevention (reduction of waste quantities);
  - — Utilization of wastes and recycling;
  - — Reduction of landfill waste.

The National Sustainable Development Strategy has recently been reformulated and accepted by the government, and it is an important element together with the National Environmental Programe. The New Széchenyi Plan (NSZP) is an economic development programe providing an operative background for the realization of strategic objectives.

The programes of the NSZP concerning GHG mitigation are as follows:

- Energy policy:
  - — Energy policy is to serve economic growth and job creation, together with security of supply, resource diversification, and the reduction of import dependence;

— Production and utilization of renewable energies are to be encouraged.

- Transport:
  - — Creating the financial resources necessary for a sustainable transport system;
  - — Encouraging intermodal transports;
  - — Enforcing environmental and climate policy considerations;
  - — Transformation of the primary energy mix – a greater proportion of renewable energy is necessary;
  - — Development of an adequate traffic and transport system, nodes as well as intermodal and multifunctional logistics centers and related industrial parks established in these nodes to reduce road transit.

The Green Investment Scheme (GIS) is considered to be a key source of funding GHG mitigation projects and efforts. Several of the policies described in this report have been or will be financed at least partly from GIS sources. The GIS is planned to be restructured with the following priorities in mind:

- Complex (deep) energy efficiency revamp of multi-flat and family houses, to increase the approximately 40% energy saving achieved by GIS programes so far to at least 60%;
- Support for the construction of new highly efficient buildings;
- Loan guarantee for the investors of the above projects, so that they could take loans at better conditions to provide their own share for the other supports from the GIS.

Maximum 5% of the GIS revenues can be used for covering the administrative costs of the GIS. It is also required by the regulation that the supported project should be additional (i.e., not implemented without the support).

The impact of policies and measures are summarized in *Table 1*.

Table 1 The impact of policies and measures in CO_2 equivalent

	Policy name	Status	2015 ($ktCO_2eq./yr$)	2020 ($ktCO_2$ eq./yr)	2025 ($ktCO_2$ eq./yr)	2030 ($ktCO_2$ eq./yr)
1	Promotion of renewables	implemented	5 600.2	8 821.2	11 299.1	13 061.0
2	Nuclear power	adopted	2 762.6	5 172.8	7 875.8	10 593.8
3	"Liveable panel buildings" sub-program	implemented	509.7	953.5	1 374.1	1 592.7
4	"Our home" reconstruction sub-program	implemented	402.9	844.4	1 324.6	1 861.8
5	"Power saving households" program	implemented	535.4	1 117.1	1 439.7	1 573.6
6	Renewable public institutions sub-program	implemented	366.6	722.1	1 058.1	1 360.4
7	Reduction of power demand of public institutions	implemented	495.3	972.8	1 451.6	1 866.4
8	District heating efficiency sub-program	implemented	135.1	242.0	312.7	347.2
9	Reducing the energy use of enterprises	implemented	655.9	1 477.6	2 182.0	2 737.5
10	Horizontal measures	implemented	126.3	336.7	547.2	757.7
11	Reducing the energy demand of cargo and passenger transport	implemented	38.7	98.2	111.8	122.4
12	Directing transport to railways	planned	51.3	80.6	89.7	89.7
13	Directing transport to public transport and developing public transport	planned	19.6	52.4	84.7	106.5
14	Reducing road transport emissions	adopted	727.5	1 549.7	2 578.0	3 622.7
15	Environmental awareness in agriculture	adopted	NA	NA		
16	Less nitrate get into water and N-cycle	implemented	NA	NA		
17	Draw attention to decrease GHG emission in agriculture	implemented	NA	NA		
18	National Forest Programe for increasing forest area	implemented	500.00	700.00	1 000.00	1 300.00
19	Frame for forestry management and forest protection	implemented	NA	NA		
20	Mitigation of agricultural emissions with partial change of nitrogen fertilizer utilization and cultivations change	implemented	200.00	NA		
21	Support for perennial herbaceous energy plantation by the European Agricultural Fund	implemented	NA	NA		
22	Complementary financing to support the plantation of energy crops by the European Agricultural Fund	implemented	NA	NA		
23	Rural development for sustainable and modern agriculture	implemented	NA	NA		
24	Climate protection by efficient manure management and biogas	implemented	135.00	NA		
25	New waste management instruments	adopted	2.14	4.62	12.70	16.96
26	Setting up regional waste management projects	implemented	17.14	20.77	34.29	51.83
27	Packaging waste governmental regulation	adopted	6.43	23.08	39.37	58.43
28	Budapest municipal door-to-door separate waste collection	adopted	12.86	20.77	31.75	45.24
29	Landfill recultivation, remediation	adopted	2.14	4.62	11.43	16.02
30	Prevention	adopted	0.00	9.23	25.40	29.22
31	Waste landfill tax	implemented	4.29	13.85	31.75	39.58

Source: *Ministry of National Development* (2013)

The total effect from policies and measures is summarized in *Table 2*.

Table 2. Total effects of policies and measures until 2030

Gg CO_2 equivalent per year	2015	2020	2025	2030
Estimated emission savings from PAMs	13 307.19	23 237.98	32 915.95	41 250.61

5. Projections and the total effect of policies, measures, and supplementarity relating to the Kyoto Protocol mechanisms

Average 2008–2011 emissions in Hungary were 40.8 % lower than the base-year level, well below the Kyoto target of -6 % for the period 2008–2012. In the sectors not covered by the EU ETS, emissions were significantly lower than their respective target, by an amount equivalent to 33.6 % of the base-year emissions. LULUCF activities are expected to reduce net emissions by an annual amount equivalent to 1.9 % of base-year level emissions. Hungary intends to use flexible mechanisms at governmental level by selling an amount of Kyoto units equivalent to 3.5% of base-year emissions per year. Taking all these effects into account, average emissions in the sectors not covered by the EU ETS in Hungary were standing below their target level, by a gap representing 31.1 % of the base-year emissions. Therefore Hungary was on track towards its Kyoto target by the end of 2011.

6. Progress towards EU 20/20/20 goals (ESD)

Total GHG emissions of Hungary decreased by 3.7% between 2011 and 2012, based on approximated GHG inventories for the year 2012 (see *Table 3*). When considering the scope of the EU's climate and energy package, which includes emissions from international aviation, Hungarian emissions in 2012 are approximately 55% lower compared to 1990 levels (98 980.69 Mt). Thus Hungary reaches its 20% reduction target, eight years ahead of 2020. This should not mean that the country has no dedicated tasks, as the reduction of emissions can be accounted to the decline in economic activity and economic growth beyond expectations.

Aggregated projections from Hungary indicate that the total emissions will further decrease between 2012 and 2020 (and 2025, see the Biennial Report for forecast figures). With the current set of national domestic measures in place, emissions are expected to reach a level in 2020 which is 65% below the 1990 level. Implementing the additional measures (at planning stage or realized at lower implementation levels) it is expected to achieve a reduction of 74% below the 1990 level in 2020.

Table 3. Hungary's emissions in the first commitment period

	Mt CO_2 equiv.	2008	2009	2010	2011	2012	Average of 2008-2012	Total of 2008-2012
1	Total GHG emissions	73.6	67.4	67.9	66.1	63.7	67.7	338.7
2	Verified emissions under the EU ETS	27.2	22.4	23.0	22.5	21.3	23.3	116.4
3	Non-ETS emissions	46.4	45.0	45.0	43.7	42.4	44.5	222.4
4	Initial Assigned Amounts (AAUs)	108.5	108.5	108.5	108.5	108.5	108.5	542.4
5	Allowances issued under the EU ETS	25.1	23.9	25.7	25.0	32.8	26.5	132.5
6	Non-ETS target	83.3	84.6	82.8	83.5	75.7	82.0	409.9
7	Difference between target and actual emissions (non-ETS domestic)	37.0	39.6	37.8	39.8	33.3	37.5	187.5
8	Expected carbon sequestration from LULUCF	2.2	2.2	2.2	2.2	2.2	2.2	11.1
9	Difference between target and actual emissions (non-ETS domestic) incl. carbon sequestration	39.2	41.8	40.0	42.0	35.5	39.7	198.6
10	Planned use of Kyoto mechanisms by government (net transfer of AAUs + purchase of CERs+ERUs)	–4.0	–4.0	–4.0	–4.0	–4.0	–4.0	–20.0
11	Emission reduction units (ERUs issued in JI projects)	0.0	1.2	1.4	1.6	3.1	1.5	7.3
12	Difference between target and actual emissions (non-ETS, domestic, incl. Kyoto mechanisms and carbon sinks)	35.2	36.6	34.7	36.4	28.4	34.3	171.3

Source: EEA Report (2013)

The projected reductions are to be achieved both in the sectors covered by the EU ETS (mostly energy supply and industry), where an emission cap is determined at EU level, and in the other sectors covered by national emission targets under the Effort Sharing Decision (ESD). Beyond the EU ETS itself, the largest reductions are expected via measures supporting renewable energy under the Renewable Energy Directive (RED) and implementation of efficiency and energy saving measures.

The average annual emissions and removals from LULUCF in the 2008–2011 are as follows: –1.15 Mt CO_2 equivalent for the average net carbon stock change (Art 3.3.), and –1.06 Mt from forest management (Art 3.4).

Concerning non-ETS emissions in Hungary, the absolute gap between the average non-ETS emissions in 2008–2012 and the Kyoto targets are 37.5 Mt CO_2 equivalents (excluding carbon sinks), which is 32.5% less than the targeted value.

Thus, the average 2008–2012 emissions in sectors not covered by the EU ETS, including the effect of carbon sinks, are less than the target for non-ETS sectors.

Despite these promising results, energy efficiency measures in the residential and services sectors are of key importance in the provision of further emission reductions by 2020.

Concerning the national GHG targets under the ESD: 2012 non-ETS emissions were below the 2013 ESD targets and 2020 non-ETS emissions are projected to be lower than the 2020 ESD target with the existing measures. Concerning the national targets for the RES share in the gross final energy consumption, the 2011 RES share was above the RED and NREAP 2011–2012 trajectories.

Concerning energy efficiency, some progress is made in reducing energy consumption, but further improvements are necessary to further develop policies or to better implement the existing ones.

Regarding the current progress towards 2013 ESD targets, the following conclusions can be drawn. Considering the proportional targets of 2020 by 2013 – the so-called 2013 ESD targets – then the reduction of -5% is the proportional goal until 2013 and +10% by 2020 for non-ETS sectors is allowed. The actual emissions from non-ETS sectors are 18% less in 2012 than the 2005 values and the 6.9 Mt (13%) below the 2013 ESD target.

Considering the projected emissions in 2020 in non-ETS sectors and comparing them with the targets for 2020, the With Existing Measures scenario forecasts a –8% aggregate emission reduction (a 11 Mt reduction) compared to the target, whilst the With Additional Measures scenario forecasts a 21 Mt reduction and a –16% relative gap.

Overall, the projections show that with the current measures, the non-ETS emissions in 2020 will be below the 2020 targets.

The projections presented herewith are developed for the years 2015, 2020, and 2025. The projections rely on energy demand forecasts, latest emission factors, and technological data, and use parametric assumptions. The detailed sectoral impact of measures is enumerated in Chapter 5 of the NC for the industry, energy, and power sector, transportation, public sector, agriculture, and forestry sectors.

Throughout the development of the projections, the impacts of EU level policy requirements and specific domestic policies were considered (e.g., Renewable Energy Directive, EU ETS). For the sake of a concise and methodologically sound forecast, the HUNMIT model was developed and adapted to the present forecast, which is a bottom up model enlisting all measures, their technical and economical characteristics. The model is capable of selecting an optimal set of measures allowing for a cost efficient emission reduction.

Table 4 summarizes total emissions for the two scenarios (with and without LULUCF).

Table 4. Total emissions in the WEM and WAM scenarios (Gg. CO_2 equivalent)

	2010	2015	2020	2025
Without measures scenario	67 679.0	63 568.7	65945.7	69473.6
WOM including LULUCF	63 694.3	66 193.0	68731.3	69473.6
With existing measures	67 679.0	63 475.5	59 840.2	58 598.0
WEM including LULUCF	63 694.3	60 680.0	58 046.5	56 391.1
With additional measures	67 679.0	61 515.1	56 774.2	55 400.2
WAM including LULUCF	63 694.3	58 719.6	54 980.5	53 193.4

It is visible that the two scenarios do not differ significantly at the end of the forecasting period. This indicates that the WEM scenario already incorporates a large share of potential abatament measures and mitigation options.

7. Conclusions and recommendations

Bringing together the results of the current progress towards the 2013 targets (based on 2012 proxy data) and projected progress to 2020 targets (based on Member States projections) allows for an overall assessment of the progress achieved so far by Hungary towards her objectives under the ESD. Thus, Hungary is presently considered to be on track towards her respective 2013 ESD targets, i.e., 2012 non-ETS emissions were below these targets.

If a modified base year (2005) would be set for the 2020 ESD targets (adjusted according to Art. 10) for Hungary it would mean a 16% reduction target or a 57 Mt CO_2 equivalent emission cap in the non-ETS sectors until 2020. This is expected to be reached already under the assumptions of the WEM scenario, which forecasts 43 Mt emission, while the WAM forecasts GHG emissions equivalent to 40 Mt of CO_2 by 2020. Thus Hungary is expected to reach her 2020 target with the current set of policies and measures through domestic emission reductions alone, even if a more demanding base year is chosen.

Overall, combining the above findings Hungary is well on track towards the ESD targets with 2012 emissions below 2013 ESD targets, and current policies and measures are sufficient to achieve 2020 targets through domestic emission limitations or reductions only.

References

Ministry of National Development, 2013: 6th National Communication of Hungary to the UNFCCC, Biennial Report of Hungary to the UNFCCC (as an Annex to the 6th National Communication).

Molnár, S. and *Molnár, M.*, 2012: Comprehensive assessment of climate change policies and measures in Hungary: concerns and tasks in an underestimated challenge. *Időjárás 116*, 297–321.

IDŐJÁRÁS

Quarterly Journal of the Hungarian Meteorological Service
Vol. 118, No. 4, October – December, 2014, pp. 305–321

Estimation of future precipitation conditions for Hungary with special focus on dry periods

Rita Pongrácz*, Judit Bartholy, and **Anna Kis**

Department of Meteorology, Eötvös Loránd University,
Pázmány Péter sétány 1/A, H-1117 Budapest, Hungary

E-mail: prita@nimbus.elte.hu, bartholy@caesar.elte.hu,
kisanna@nimbus.elte.hu

**Corresponding author*

(Manuscript received in final form August 25, 2014)

Abstract—In this paper, estimated trends of precipitation- and drought-related climate indices and the return period of the daily precipitation amount are analyzed. For this purpose 11 regional climate model (RCM) simulations from the ENSEMBLES project with 25 km horizontal resolution for the emission scenario A1B are used after applying a bias-correction procedure. According to the results, the summer 10- and 20-year return periods will increase by a factor of 1.2–2 by the late 21st century relative to the 1961–1990 reference period. The projected changes are considerably smaller for the other three seasons compared to future summer changes. Furthermore, drought-related climate indices in summer are projected to increase significantly in Hungary as well as in Central/Eastern Europe by the end of the 21st century. Additionally, precipitation-related indices are projected to decrease in summer by 2071–2100 compared to 1961–1990.

Key-words: precipitation index, dry period, return period, bias correction, regional climate model simulation

1. Introduction

Climate change is most often referred as higher temperature values and more frequent heat waves (e.g., *Pongrácz et al.*, 2013). However, it usually involves more intense and more frequent extreme events related to excess or lack of precipitation (e.g., severe dry spells, heavy precipitation, intense thunderstorms), too (*IPCC*, 2012). This highlights the importance of climate research in quantifying the detected past and the projected future changes from global to local scales. Frequent hot weather in summer and overall increasingly warm climatic conditions are quite straightforward consequences of global warming. Global and regional warming induced effects on precipitation are not as clear as on temperature, because the higher spatial and temporal variabilities might hide any robust changing signal. Nevertheless, precipitation is one of the most important meteorological variables, since it considerably affects natural ecosystems and cultivated vegetation as well as most of human activities. Extreme precipitation events – both excessive, intense rainfalls and severe droughts – may result in several environmental, agricultural, economical, and natural disasters. The lack of precipitation for extended period and coincidental intense heat wave often lead severe drought events. For instance, in 2003 a long-lasting, devastating heat wave occurred throughout Europe (*Stott et al.*, 2004), causing death of hundreds of people (*Bouchama*, 2004). In Hungary, the year 2003 was generally dry with 17% less annual precipitation than the 1971–2000 average (*Schirokné Kriston*, 2004). The Europe-wide heat wave in the summer superposed to these overall dry conditions, resulting in severe drought. The estimated monetary damage in the Hungarian agriculture reached 50–55 billion HUF by the end of the year (*Faragó et al.*, 2010). Another hot and dry summer from the past decades occurred in 2007, this drought resulted in reduced harvest of maize in Hungary and caused at least 80 billion HUF loss (*Faragó et al.*, 2010). On the contrary, in May 2010, the total rainfall in Hungary largely exceeded the average monthly precipitation of the 1971–2000 baseperiod for May, namely, almost three times more precipitation occurred than usual (*Móring*, 2011). The excessive precipitation led to inland inundation and floods on Sajó, Hernád, Bodrog, and Bódva rivers resulting in more than 10 billion HUF of defence and recovery costs (*KSH*, 2011). Overall, the year 2010 became the wettest year in Hungary since 1901 with 959 mm annual precipitation amount exceeding the annual mean of the 1971–2000 period by 65% (*Móring*, 2011). Besides Hungary, a large majority of the Central/Eastern European region was hit at the same time by severe floods (*Bissolli et al.*, 2011; *WMO*, 2011). After the year of excessive precipitation, Hungary experienced the driest year in 2011 since 1901 with only 407 mm annual total precipitation amount, being only 72% of the annual average in the 1971–2000 period (*Móring*, 2012), which affected the agricultural production quite negatively. The very

next year, 2012 was also dry in Hungary, the annual total precipitation was only 470 mm (*Horváth et al.*, 2012; *Rajhonáné Nagy*, 2013) resulting in more losses in agriculture than in 2011 (e.g., by 24% less harvested cereal and 20% less production of sunflower and grape) (*KSH*, 2013). Due to the large temporal variability of precipitation, after two consecutive very dry years, in late May and early June in 2013 large precipitation occurred again in Central Europe and resulted in extreme water levels, with record high peak levels on several Central European rivers, i.e., the Danube, the Elbe, and the Vltava (*BBC News*, 2013; *van der Schrier et al.*, 2013; *WMO*, 2014). Besides the great amount of precipitation, the large spatial extension and the strong intensity (exceeding 100 mm/24 hours) also contributed to this extreme event (*Horváth et al.*, 2013). Overall, this flood affected several countries in Central and Eastern Europe (e.g., Germany, Austria, Czech Republic, Hungary, Serbia) with 16 billion EUR losses and 22 deaths altogether (*Munich Re*, 2013).

In order to avoid or at least reduce the effects of these precipitation related hazards, national and local communities need to develop regional adaptation strategies (*IPCC*, 2012; *Motha*, 2009; *Sivakumar* and *Stefanski*, 2009; *Anwar et al.*, 2013), and then, act according to them. For this purpose, results of global climate model (GCM) simulations must be downscaled to regional and local scales, hence better serving end-users' needs. Downscaling of coarse resolution GCM simulation outputs is especially important in case of precipitation because of the large temporal and spatial variabilities, and consequently, since appropriate precipitation impact assessment studies require fine resolution information (e.g., *Marengo* and *Ambrizzi*, 2006; *Fowler et al.*, 2007; *Maurer et al.*, 2007; *Serinaldi* and *Kilsby*, 2014). From the agricultural point of view, especially potential dry conditions induce long-term planning, for which estimation of precipitation is evidently the key element.

Sheffield and *Wood* (2008) analyzed global and regional trends of drought using a moisture-based drought index for 1950–2000. According to their results, soil moisture has increased globally with regional differences. In Africa, a significant drying can be identified, whereas increasing trend is detected in North America. The annual precipitation sum in Hungary decreased in the 1901–2009 period; in Budapest the mean change is –20.5%, which is statistically significant (*Lakatos* and *Bihari*, 2011). Precipitation measurements in the Carpathian Basin suggest that both the overall intensity and frequency of extreme precipitation events – related to both excess and lack of precipitation – increased in the 20th century, whereas the mean climate became slightly drier (*Bartholy* and *Pongrácz*, 2005; *Lakatos et al.*, 2011). For the future, 50 km horizontal resolution regional climate model (RCM) experiments of the PRUDENCE project (*Christensen et al.*, 2007a) suggest that the annual distribution of precipitation will be totally restructured

in Hungary both in case of A2 and B2 emission scenarios (*Nakicenovic* and *Swart*, 2000), namely, the wettest season (currently summer) will become the driest, and the driest season (currently winter) is likely to be the wettest by the end of the 21st century (*Bartholy et al.*, 2008). The projected changes for Central/Eastern Europe involve large uncertainity, therefore, further analysis is necessary. In order to successfully adapt to the changing climatic and environmental conditions, appropriate assessment of possible changes is essential.

In the current study, fine (25 km) resolution RCM experiments of the ENSEMBLES project are analyzed taking into account the A1B intermediate emission scenario for the entire 21st century. First, the data and the bias correction method applied to the raw RCM outputs are presented. Then, the precipitation-related characteristics, return period of daily precipitation, and various climate indices are defined. Section 3 discusses projected changes in the seasonal return period of daily precipitation, and estimated seasonal changes of climate indices with special focus on dry conditions. Finally, Section 4 summarizes the main conclusions.

2. *Data and methods*

2.1. Data used in the analyses

In this paper, simulations of 25 km horizontal resolution RCMs nested in coarse resolution GCMs are used to estimate the future precipitation- and drought-related climatic conditions in Central/Eastern Europe covering the region 43.625°–50.625°N, 13.875°–26.375°E. The assessment focuses on analysis of daily precipitation outputs of 11 RCM simulations (listed in *Table 1*) from the ENSEMBLES project (*van der Linden* and *Mitchell*, 2009). This European Union funded project aimed and successfully completed to run several climate models between 2004 and 2009 in order to improve the reliability of climate projections, measure uncertainty, and help decision-makers with reliable information. All of the RCM simulations selected for this study cover the entire 1951–2100 period and apply the intermediate A1B emission scenario, according to which the estimated CO_2 concentration level will be 532 ppm and 717 ppm by 2050 and 2100, respectively (*Nakicenovic* and *Swart*, 2000). The necessary initial and boundary conditions are provided by three different GCMs: ECHAM (*Roeckner et al.*, 2006) developed at the Max Planck Institute, HadCM (*Gordon et al.*, 2000) developed at the UK MetOffice, and ARPEGE (*Déqué et al.*, 1998) developed at Météo-France.

Table 1. List of the selected RCMs, their main references, their driving GCMs, and the responsible institutes used in this analysis.

RCM (Reference)	Driving GCM	Institute
HadRM3Q0 (*Jones et al.*, 1995; 2004)	HadCM3Q	HC (Hadley Centre), United Kingdom
RCA3 (*Samuelsson et al.*, 2011)	HadCM3Q (high sensitivity version)	C4I (Community Climate Change Consortium for Ireland), Ireland
CLM (*Böhm et al.*, 2006)	HadCM3Q	ETHZ (Eidgenössische Technische Hochschule Zürich), Switzerland
RCA3 (*Samuelsson et al.*, 2011)	HadCM3Q (low sensitivity version) ECHAM5	SMHI (Swedish Meteorological and Hydrological Institute), Sweden
RACMO (*van Meijgaard et al.*, 2008)	ECHAM5	KNMI (Koninklijk Nederlands Meteorologisch Instituut), Netherlands
REMO (*Jacob* and *Podzun*, 1997)	ECHAM5	MPI (Max Planck Institut), Germany
RegCM (*Giorgi* and *Bi*, 2000)	ECHAM5	ICTP (International Centre for Theoretical Physics), Italy
HIRHAM (*Christensen et al.*, 2007b)	ECHAM5 ARPEGE	DMI (Danmarks Meteorologiske Institut), Denmark
ALADIN (*Radu et al.*, 2008)	ARPEGE	CNRM (Centre National de Recherches Météorologiques), France

2.2. Bias correction of RCM outputs

The evaluation of raw precipitation outputs of RCMs for 1961–1990 suggests that simulated values usually significantly overestimate the observations in Central/Eastern Europe, except in summer when mostly underestimations were found (*Pongrácz et al.*, 2011). In case of precipitation indices associated with specific thresholds, it is particularly important to use the most accurate simulations, as close to measurements as possible. For this purpose, before the analyses, a bias correction method should be applied to the raw simulated data. The biases of the raw RCM outputs are corrected using quantile matching technique. This is based on the assumption that two datasets are considered similar if their distributions are close to each other (and the closer is the more similar), therefore, the monthly empirical distribution functions of daily precipitation at each grid cell should be fitted (*Formayer* and *Haas*, 2010) to the observed distribution represented by the gridded E-OBS (*Haylock et al.*, 2008) data for a baseperiod, i.e., 1951–2000 in this study. These fitting procedures provide the multiplicative bias-correcting factors for each month, for each grid cell. Then, these calculated factors are applied to the raw daily outputs of RCM experiments both for the past (1951–2000) and the target (2000–2100) period.

Fig. 1 illustrates the successful fitting of the bias-correction for January for a selected grid cell, where the percentile values of the raw and bias-corrected simulations are compared to the percentiles of E-OBS data. The Q-Q plot clearly shows that after the correction, the distribution of the simulated precipitation fits perfectly to the distribution of the reference data (i.e., all the percentile value pairs are located along the y = x line).

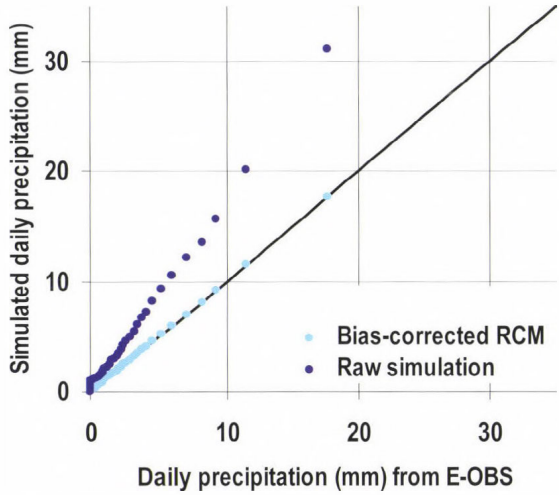

Fig. 1. Q-Q plot for raw and bias corrected simulation data, 1951–2000. Results for January daily data from the grid cell located at 47.625°N, 19.125°E using the ARPEGE-driven HIRHAM experiment are shown.

2.3. The return period and the selected climate indices

After the bias-correction, both the 10- and 20-year return periods of the daily precipitation amount are analyzed. The return period (τ) is defined as the inverse of the expected average number of occurrences (P) in a year (τ=1/P). *Fig. 2* shows an example for how to determine the change of the 10-year return period. First, the 90th percentile of the daily precipitation ($P_{0.9}$(1961–1990)) is calculated for the reference period (1961–1990) in each grid cell. Then, this daily precipitation amount should be compared to the future (2071–2100) percentile values, and that one (P_X(2071–2100)) is selected, which equals to this $P_{0.9}$(1961–1990) daily precipitation. In the example of *Fig. 2*, X = 0.94 since the 94th percentile value of the future period equals to $P_{0.9}$(1961–1990). So $\tau_{10\text{years, }1961\text{–}1990}$ = 100/(100–94) = 16.67 years, which implies a substantial increase of the return period, and hence, drier climatic conditions.

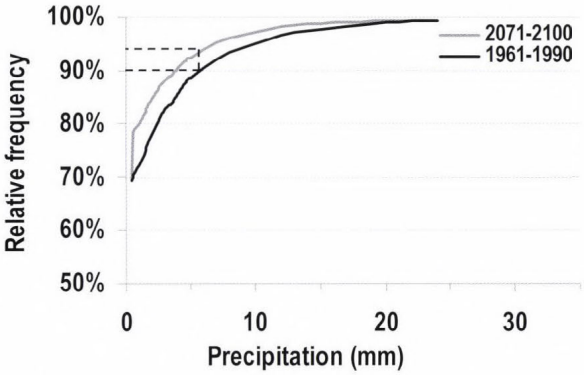

Fig. 2. Calculation of the projected value of the 10-year return period ($\tau_{10years,\ 1961-1990}$). Empirical distributions of summer daily data from the grid cell located at 47.625°N, 19.125°E using the ARPEGE-driven HIRHAM experiment are shown.

In order to assess future climate tendencies in the Central/Eastern European region, several precipitation-related indices are also analyzed on seasonal scales. *Table 2* lists the names, definitions, and units of the selected climate indices. Three indices are directly related to drought (DD, MDS, CDD), the other three indices refer to wet conditions using small precipitation thresholds (RR1, RR5, MWS). The grid cell values of all the six indices are calculated from the bias-corrected simulated precipitation data sets for the entire selected domain covering the latitude 43.625°–50.625°N and longitude 13.875°–26.375°E for the whole simulation period (1951–2100) using all the 11 RCM experiments. Overall projected seasonal changes by 2021–2050 and 2071–2100 periods relative to the 1961–1990 reference period are also calculated. Furthermore, spatial average changes for Hungary represented by the grid cells located within the country border are estimated for all the seasons both for mid to late 21st century.

Table 2. Drought- and precipitation-related climate indices used in the current analysis

Index	Definition	Unit
DD	Number of dry days ($R_{day} < 1$ mm)	day
MDS	Mean length of dry spell ($R_{day} < 1$ mm)	day
CDD	Maximum length of dry spell, i.e., maximum number of consecutive dry days ($R_{day} < 1$ mm)	day
RR1	Number of precipitation days exceeding 1 mm ($R_{day} \geq 1$ mm)	day
RR5	Number of precipitation days exceeding 5 mm ($R_{day} \geq 5$ mm)	day
MWS	Mean length of wet spell ($R_{day} \geq 1$ mm)	day

3. *Results and discussion*

First, we focus on the 10-year and 20-year return periods of the daily precipitation amount. The projected seasonal changes generally show similar patterns for the whole selected domain. According to our results, a slight decrease of the return period is likely to occur in winter, namely, the 10-year return period may change to 8–9 years by the end of the 21st century (*Fig. 3*). This implies wetter climatic conditions for winter. In spring and autumn, individual RCM experiments suggest slightly more diverse changes than in winter, which results in larger uncertainty but very small changes overall. In case of summer, the results for the 2071–2100 period clearly suggest that the return period of daily precipitation occurred once in a decade on average in the recent past is very likely to increase by a factor of 1.2–2, so drier climatic conditions are projected. Larger increase of the 10-year return period is estimated in the southern parts (exceeding 8 years) of the selected domain than in the northern subregions (less than 4 years).

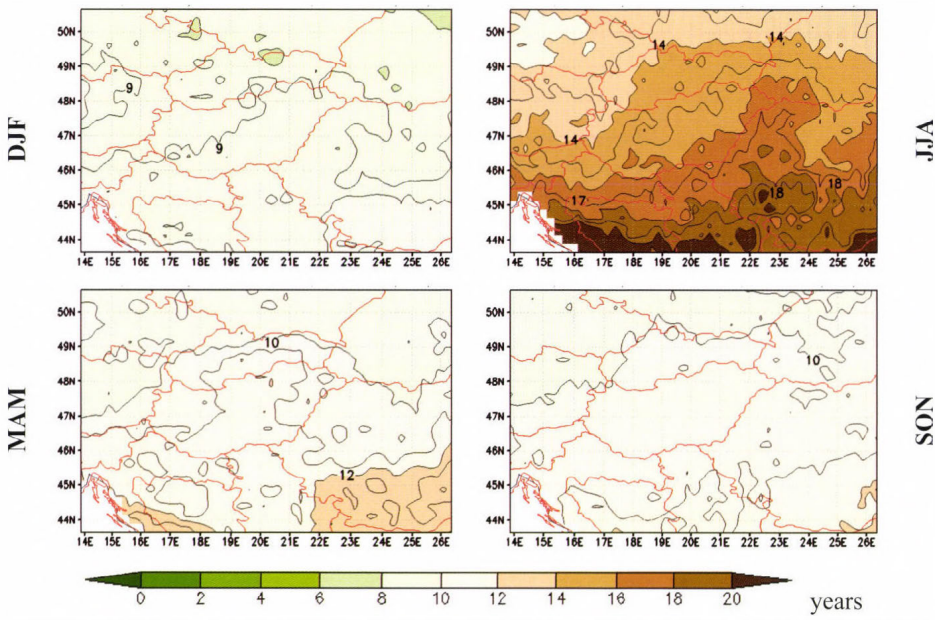

Fig. 3. Composite maps of 11 RCM simulations indicating the estimated seasonal mean changes of the 10-year return period by 2071–2100 relative to the reference period 1961–1990.

Besides the average return periods, the seasonal uncertainties for nine subregions are also determined (*Fig. 4*). Whisker-Box plot diagrams are used for

indicating the highest (maximum) and the lowest (minimum) values, and the lower and upper quartiles, i.e., the 25th and 75th percentiles of the 10-year return period of daily precipitation amount for each subregion based on the 11 individual RCM simulations. According to these results, the return period increases in summer, thus implying an overall future drying trend by almost all of the RCM simulations in every subregion (only a few RCM simulations project slight decrease in the northwestern subregions). Although the projected tendency is clear, the RCM-based projections cover a wide range of return periods, thus, the uncertainty of the estimation is quite large. The estimated changes are clearly larger as proceeding from the northwestern to the southeastern part of the domain. In Hungary and Slovenia, the doubling of the return period is estimated by only a couple of RCM simulations (using CLM for instance), whereas in the southern subregions (Romania, Croatia, and northern Serbia) 25% of the RCM simulations suggest larger increase than by a factor of 2. In the other three seasons, the overall uncertainties of the projections are smaller than in summer, however, even the signs of the estimated changes are not identical, especially in spring and autumn. In winter, most of RCM simulations suggest considerable decrease of the return period, thus implying wetter conditions in all subregions (only two RCM simulations project increase of winter return periods, namely, ALADIN and HIRHAM driven by ARPEGE).

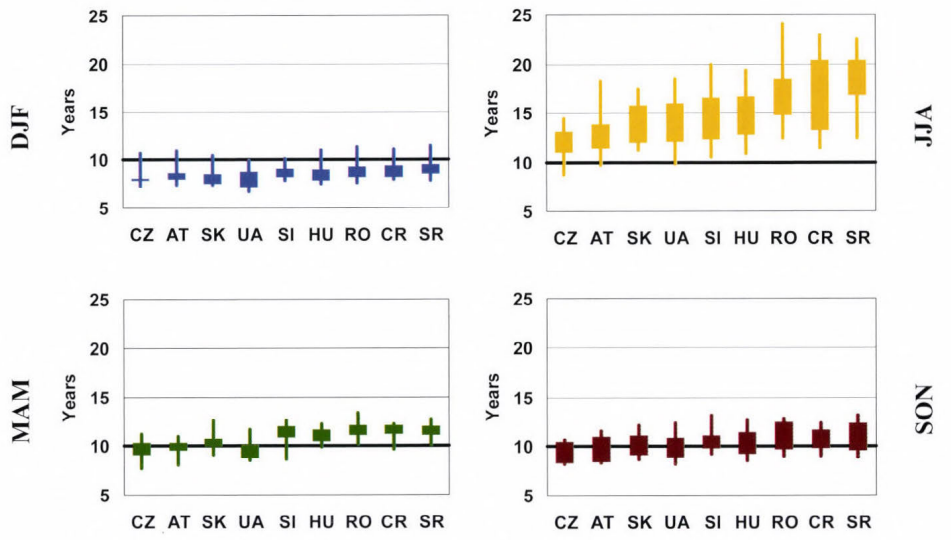

Fig. 4. The maximum, minimum, upper, and lower quartile values of the 10-year seasonal return period of the daily precipitation amount for nine subregions (CZ: southeastern Czech Republic, AT: eastern Austria, SK: Slovakia, UA: southwestern Ukraine, SI: Slovenia, HU: Hungary, RO: Romania, CR: Croatia and SR: northern Serbia).

The projected seasonal changes of 10- and 20-year return periods are compared for Hungary in *Fig. 5*. In general, the signs of the projected changes by one particular RCM simulation are identical for both return periods. It can be clearly seen that all the RCM simulations suggest clear increasing return period in summer. Most of the RCM simulations project similar rate of changes, except three RCM simulations (HIRHAM driven by ARPEGE, CLM driven by HadCM, and HadRM3Q driven by HadCM), when, when extremely large changes (larger than twofold increasing) is projected for Hungary in case of the 20-year return period of daily precipitation sum. The projected changes are considerably smaller for the other three seasons than for summer. Nevertheless, the estimated changes of the 10-year return period are slightly larger than the changes of the 20-year return period in winter and autumn.

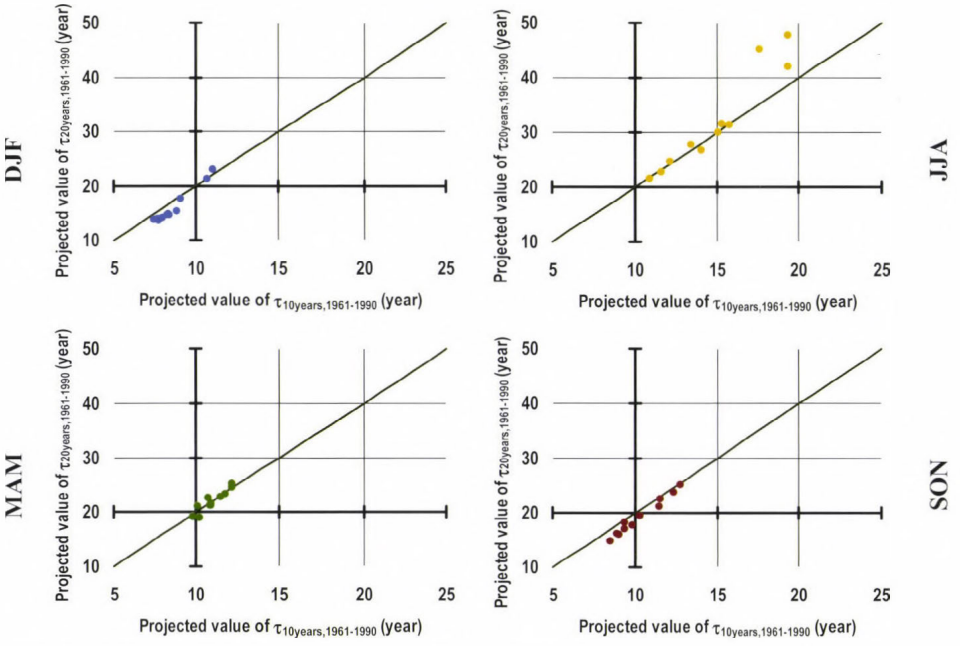

Fig. 5. Scatter-plot diagrams based on the 11 RCM simulations of the 10- and 20-year seasonal return periods for Hungary by 2071–2100 relative to the reference period, 1961–1990. Each dot represents the results of one RCM simulation.

In the second part of this section, we analyze the projected changes of the selected precipitation indices focusing on Hungary. According to the 11 bias-corrected RCM simulations in the 2021–2050 period, smaller changes are projected than in the 2071–2100 period (*Fig. 6*). By the mid-century, only a few

RCM simulations project statistically significant seasonal changes and the average estimated changes do not exceed 11%. In most of the indices, the signs of the projected changes are identical, which implies that the tendencies are likely to continue throughout the 21st century. In general, RR1 and RR5 (precipitation days exceeding 1 mm and 5 mm, respectively) are projected to decrease in summer and increase in winter. However, by the late century, almost all RCM simulations estimate significant decrease in summer (the average projected decrease is 27% relative to the reference period both for RR1 and RR5), and increase in winter for RR5 (the average projected increase is 25%). CDD and MDS in summer are projected to increase significantly in Hungary by the end of the 21st century (by 42% and 41% on average, respectively), clearly implying considerably drier future summers. Similar conclusions were found in *Bartholy et al.* (2013).

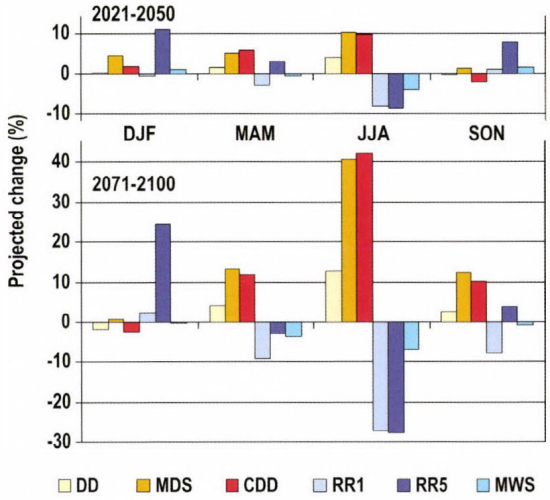

Fig. 6. Projected seasonal mean changes of climate indices for Hungary by 2021–2050 (upper panel) and 2071–2100 (lower panel) relative to the reference period, 1961–1990. Definitions of these indices are listed in *Table 2*.

The spatial pattern of the projected mean seasonal changes by the mid to late century are shown for CDD in *Fig. 7* (this index focuses on long dry periods when precipitation does not exceed 1 mm). The spatial averages of the estimated changes for the whole domain are –0.1%, +11%, +42%, and +10% in winter, spring, summer, and autumn, respectively (for Hungary the average projected changes are as follows: –2%, +12%, +42%, and +11%). In all the four seasons, larger increases are projected for the southern parts of the selected domain than

for the northern regions. For instance, the estimated mean increase of CDD in summer is about 50% in Serbia and Romania by 2071–2100, whereas it is less than 40% in southeastern Czech Republic. In Hungary, the average summer value of CDD is 14 days in 1961–1990, which is projected to increase by 42%, and thus, exceeding 20 days by the end of the 21st century.

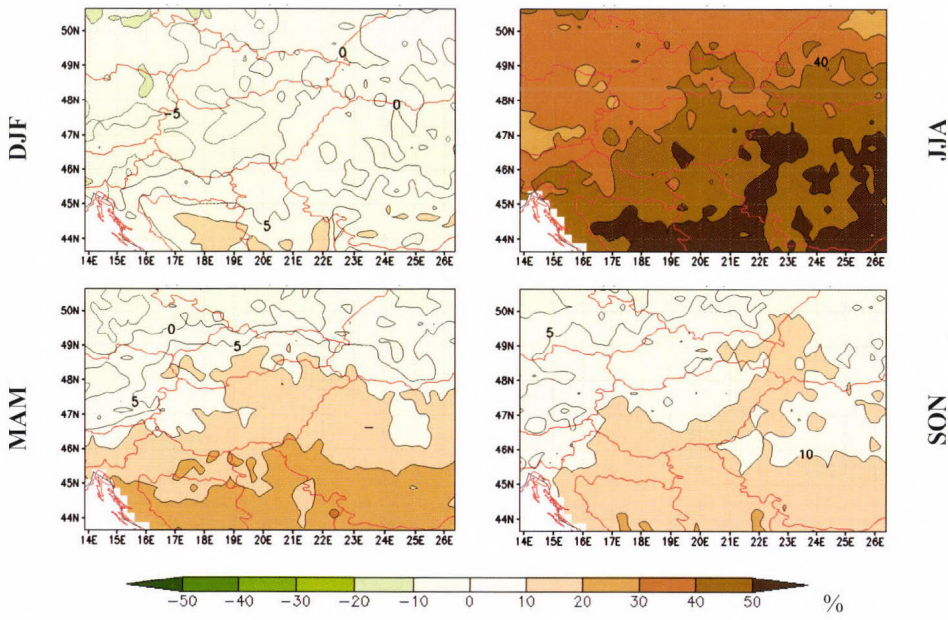

Fig. 7. Composite maps of 11 RCM simulations indicating the projected seasonal mean changes of CDD by 2071–2100 relative to the reference period 1961–1990.

Besides the multimodel seasonal averages, the standard deviations of estimated changes (characterizing the differences between the individual RCM projections) are also important, especially in terms of assessing the uncertainty of projections. The largest standard deviation values of the seasonal changes are found in summer, namely 15–30% depending on the location, with larger standard deviation in the northern regions and smaller in the southern regions of the domain. The smallest standard deviations of the late century changes are in spring (5–15%), however, winter and autumn standard deviation values are roughly in the same range. To present the inter-model uncertainty on decadal scale covering the whole 1951–2100 period, spatial average CDD values taking

into account all the gridcells within Hungary are shown in *Fig. 8* for winter and summer. According to the statistical analysis (t-test), the summer increasing trend is significant at 0.05 level, which implies future lengthening of consecutive dry days highly affecting agriculture in the region. The longest seasonal dry periods lasted 15 days on average in summer in the 1950s (only one individual RCM simulation resulted in CDD values for Hungary over 20 days). The RCM simulation ensemble projects dry periods lasting 22 days on average by the last decade of the 21st century, and one of the RCM simulations even resulted in 40-day-long summer dry periods in the 2090s.

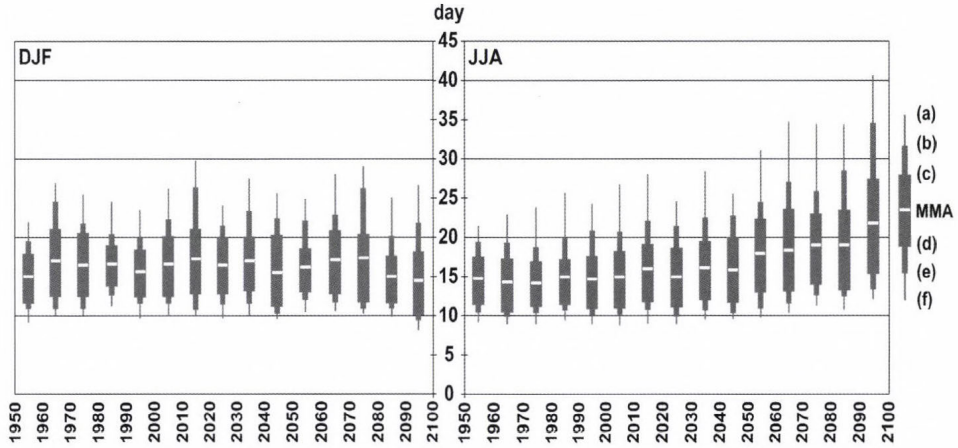

Fig. 8. Average decadal values of CDD in Hungary in winter (left panel) and summer (right panel), 1951–2100. MMA indicates the multi-model average. (a) and (f) indicate the maximum and minimum CDD values, respectively. (b) and (e) indicate the second largest and smallest CDD values, respectively. (c) and (d) indicate the third largest and smallest CDD values, respectively.

The mean length of dry spells is estimated to increase in Hungary in all seasons during the 21st century (*Fig. 9*). The largest change is projected for summer: MDS will increase by 41%, so the 5-day-long mean dry spells of the reference period are likely to lengthen by 3 days and last for 8 days on average by the end of the 21st century. The mean dry spells were the longest in autumn in the reference period (MDS average value is about 8 days), and the RCM simulations suggest that they will remain the longest in 2071–2100 when MDS is likely to exceed 9–10 days. Smaller and only slight changes are estimated in winter and spring.

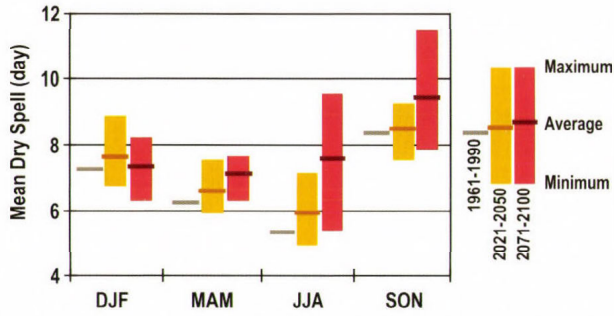

Fig. 9. Spatial average values of MDS in Hungary for three time slices: 1961–1990, 2021–2050, and 2071–2100. Columns represent the projections of the multi-model ensemble.

4. Conclusions

Projected changes of precipitation tendencies for Central/Eastern Europe have been analyzed for the 21st century using bias-corrected outputs of 11 RCM simulations available from the ENSEMBLES database. All the simulations applied 25 km horizontal resolution and took into account the intermediate SRES A1B emission scenario. In order to eliminate the systematic errors, we completed a bias-correction procedure using quantile matching technique. After the correction, we analyzed the return period of daily precipitation amount and different precipitation- and drought-related climate indices for nine subregions. In this paper we focused on the changes of the 10-year return period of daily precipitation amount, the maximum number of consecutive dry days, and the mean length of dry spells in Hungary. The main results can be summarized as follows:

(1) The RCM simulations suggest that the 10- and 20-year return periods will increase in summer by a factor of 1.2–2. Larger increases of the return periods are estimated in the southern parts of the domain than in the northern subregions. The projected changes are considerably smaller for the other three seasons compared to future summer changes. Nevertheless, the estimated changes of the 10-year return period are slightly larger than the changes of the 20-year return period in winter and autumn.

(2) Our results clearly suggest drier summers and wetter winters in the future, especially at the end of the 21st century. In summer, the maximum number of consecutive dry days, the mean length of dry spell, and the total number of dry days are all projected to increase significantly. Furthermore, the mean length of wet spell, the number of wet days, and the number of precipitation days exceeding 5 mm are projected to decrease in Hungary as well as in Central/Eastern Europe. In winter, opposite changes are very likely.

Acknowledgements: Research leading to this paper has been supported by the following sources: the Hungarian Scientific Research Fund under grant grants K-78125 and K109109, the European Union and the European Social Fund through project FuturICT.hu (TÁMOP-4.2.2.C-11/1/KONV-2012-0013). The ENSEMBLES data used in this work was funded by the EU FP6 Integrated Project ENSEMBLES (Contract number 505539) whose support is gratefully acknowledged. Furthermore, we acknowledge the E-OBS dataset from the EU-FP6 project ENSEMBLES (http://ensembles-eu.metoffice.com), and the data providers in the ECA&D project (http://eca.knmi.nl).

References

Anwar, M.R., Liu, D.L., Macadam, I., and *Kelly, G.*, 2013: Adapting agriculture to climate change: a review. *Theor. Appl. Climatol. 133*, 225–245.

Bartholy, J. and *Pongrácz, R.*, 2005: Tendencies of extreme climate indices based on daily precipitation in the Carpathian Basin for the 20th century. *Időjárás 109*, 1–20.

Bartholy, J., Pongrácz, R., Gelybó, Gy., and *Szabó, P.*, 2008: Analysis of expected climate change in the Carpathian Basin using the PRUDENCE results. *Időjárás 112*, 249–264.

Bartholy, J., Pongrácz, R., and *Hollósi, B.*, 2013: Analysis of projected drought hazards for Hungary. *Adv. Geosci. 35*, 61–66.

BBC News, 2013: Thousands flee flood-hit parts of Germany and Hungary. Available online at http://www.bbc.com/news/world-europe-22835154

Bissolli, P., Friedrich, K., Rapp, J., and *Ziese, M.*, 2011: Flooding in eastern central Europe in May 2010-reasons, evolution and climatological assessment. *Weather 66*, 147–153.

Böhm, U., Kücken, M., Ahrens, W., Block, A., Hauffe, D., Keuler, K., Rockel, B., and *Will, A.*, 2006: CLM - the Climate Version of LM: Brief Description and long-term Applications. *COSMO Newsletter 6*, 225–235.

Bouchama, A., 2004: The 2003 European heat wave. *Intens. Care Med. 30*, pp. 1–3.

Christensen, J.H., Carter, T.R., Rummukainen, M., and *Amanatidis, G.*, 2007a: Evaluating the performance and utility of regional climate models: The PRUDENCE project. *Climatic Change 81*, 1–6.

Christensen, O.B., Drews, M., Christensen, J.H., Dethloff, K., Ketelsen, K., Hebestadt, I., and *Rinke, A.*, 2007b: The HIRHAM Regional Climate Model Version 5 (beta). Techn. Report 06-17.

Déqué, M., Marquet, P., and *Jones, R.G.*, 1998: Simulation of climate change over Europe using a global variable resolution general circulation model. *Clim. Dynam. 14*, 173–189.

Faragó, T., Láng, I., and *Csete, L.*, 2010: Climate change and Hungary: mitigating the hazard and preparing for the impacts (the „VAHAVA Report"). MTA, Budapest.

Formayer, H. and *Haas, P.*, 2010: Correction of RegCM3 model output data using a rank matching approach applied on various meteorological parameters. Deliverable D3.2 RCM output localization methods (BOKU-contribution of the FP 6 CECILIA project). http://www.cecilia-eu.org/

Fowler, H.J., Blenkinsop, S., and *Tebaldi, C.*, 2007: Linking climate change modelling to impacts studies: recent advances in downscaling techniques for hydrological modelling. *Int. J. Climatol. 27*, 1547–1578.

Giorgi, F. and *Bi, X.Q.*, 2000: A study of internal variability of a regional climate model. *J. Geophys. Res. 105(D24)*, 29503–29521.

Gordon, C., Cooper, C., Senior, C.A., Banks, H., Gregory, J.M., Johns, T.C., Mitchell, J.F.B., and *Wood, R.A.*, 2000: The simulation of SST, sea ice extents and ocean heat transports in a version of the Hadley Centre coupled model without flux adjustments. *Clim. Dynam. 16*, 147–168.

Haylock, M.R., Hofstra, N., Klein Tank, A.M.G., Klok, E.J., Jones, P.D., New, M., 2008: A European daily high-resolution gridded dataset of surface temperature and precipitation. *J. Geophys. Res 113 (D20)*, 27.

Horváth, Á., Kerényi, J., Lakatos, M., Nagy, A., Németh, Á., and *Szenyán, I.*, 2012: Extreme drought in 2012 – weather circumstances. *Erdészeti Lapok CXLVII*, 347–348. (in Hungarian).

Horváth, Á., Nagy, A., and *Simon, A.*, 2013: Flooding on the Danube in June 2013 – weather circumstances. OMSZ, Budapest. Available online at http://met.hu/ismeret-tar/erdekessegek-_tanulmanyok/index.php?id=709&hir=A_2013._juniusi_dunai_arviz_idojarasi_hattere. (in Hungarian)

IPCC, 2012: Managing the Risks of Extreme Events and Disasters to Advance Climate Change Adaptation. A Special Report of Working Groups I and II of the Intergovernmental Panel on Climate Change. (Eds. *Field, C.B., Barros, V., Stocker, T.F., Dahe, Q., Dokken, D.J., Plattner, G-K., Ebi, K.L., Allen, S.K., Mastandrea, M.D., Tignor, M., Mach, K.J., Midgley, P.M.*), Cambridge University Press, Cambridge, UK and New York, NY, USA.

Jacob, D. and *Podzun, R.*, 1997: Sensitivity studies with the regional climate model REMO. *Meteorol. Atmos. Phys. 63*, 119–129.

Jones, R.G., Murphy J.M. and *Noguer, M.*, 1995: Simulation of climate change over Europe using a nested regional-climate model. I: Assessment of control climate, including sensitivity to location of lateral boundaries. *Q. J. Roy. Meteorol. Soc. 121*, 1413–1449.

Jones, R.G., Noguer, M., Hassell, D.C., Hudson, D., Wilson, S.S., Jenkins, G.J., and *Mitchell, J.F.B*, 2004: Generating high resolution climate change scenarios using PRECIS. Met Office Hadley Centre, Exeter, UK.

KSH, 2011: A 2010. évi árvíz Borsod-Abaúj-Zemplén megyében. (szerk. Szalainé H.A.) Központi Statisztikai Hivatal Miskolci Igazgatósága. ISBN 978-963-235-328-9 (in Hungarian)

KSH, 2013: Output of Hungary's agriculture in 2012 (Economic accounts for agriculture, 2012). *Statistical Reflections, 48 (7)*, 5.

Lakatos, M. and *Bihari, Z.*, 2011: A közelmúlt megfigyelt hőmérsékleti- és csapadéktendenciái. In (Eds: *Batholy, J., Bozó L., Haszpra, L.*): Klímaváltozás – 2011: Klímaszcenáriók a Kárpát-medence térségére. Magyar Tudományos Akadémia és Eötvös Loránd Tudományegyetem Meteorológiai Tanszék, Budapest, 146–169. (in Hungarian).

Lakatos, M., Szentimrey, T., and *Bihari, Z.*, 2011: Application of gridded daily data series for calculation of extreme temperature and precipitation indices in Hungary. *Időjárás 115*, 99–109.

van der Linden, P. and *Mitchell, J.F.B.*, (Eds)., 2009: ENSEMBLES: Climate Change and Its Impacts: Summary of research and results from the ENSEMBLES project. UK Met Office Hadley Centre, Exeter, UK.

Marengo, J.A. and *Ambrizzi, T.*, 2006: Use of regional climate models in impacts assessments and adaptations studies from continental to regional and local scales. Proceedings of 8 ICSHMO, Foz do Iguaçu, Brazil, April 24–28, 2006, INPE, 291–296.

Maurer, E.P., Brekke, L., Pruitt, T., and *Duffy, P.B.*, 2007: Fine-resolution climate projections enhance regional climate change impact studies. Eos, *Transactions American Geophysical Union 88* (47),. 504.

van Meijgaard, E., van Ulft, L.H., van de Berg, W.J., Bosveld, F.C., van den Hurk, B.J.J.M., Lenderink, G., and *Siebesma, A.P.*, 2008: The KNMI regional atmospheric climate model RACMO version 2.1. *Techincal Report*, 43p.

Móring, A., 2011: Weather of 2010 (in Hungarian). *Légkör 56*, 38–42. . (in Hungarian)

Móring, A., 2012: Weather of 2011 (in Hungarian). *Légkör, 57,* 38–42. (in Hungarian)

Motha, R.P., 2009: Developing an adaptation strategy for sustainable agriculture. *Időjárás 113*, 117–127.

Munich RE NatCatSERVICE, 2013: Natural catastrophes first half of 2013. 1p.
Available online at http://www.munichre.com/site/corporate/get/documents_E-2004907462/mr/assetpool.shared/Documents/0_Corporate%20Website/6_Media%20Relations/Press%20Releases/2013/2013_07_09_natcat_en.pdf

Nakicenovic, N. and *Swart, R.*, 2000: Emissions Scenarios. A special report of IPCC Working Group III. Cambridge University Press, UK, 570p.

Pongrácz, R., Bartholy, J. and *Miklós, E.*, 2011: Analysis of projected climate change for Hungary using ENSEMBLES simulations. *Appl. Ecol. Environ. Res. 9*, 387–398.

Pongrácz, R., Bartholy, J., and *Bartha, E.B.*, 2013: Analysis of projected changes in the occurrence of heat waves in Hungary. *Adv. Geosci. 35*, 115–122.

Radu, R., Somot, S. and *Déqué, M.*, 2008: Spectral nudging in a spectral regional climate model. *Tellus Ser. A - Dyn. Meteorol. Oceanol. 60*, 898–910.

Rajhonáné Nagy, A., 2013: Weather of 2012. *Légkör, 58*, 35–39. (in Hungarian)

Roeckner, E., Brokopf, R., Esch, M., Giorgetta, M., Hagemann, S., Kornblueh, L., Manzini, E., Schlese, U., and *Schulzweida, U.*, 2006: Sensitivity of simulated climate to horizontal and vertical resolution in the ECHAM5 atmosphere model. J. Climate, 19, pp. 3771–3791.

Samuelsson, P., Jones, C.G., Willén, U., Ullerstig, A., Gollvik, S., Hansson, U., Jansson, C., Kjellström, E., Nikulin, G., and *Wyser, K.*, 2011: The Rossby Centre Regional Climate model RCA3: model description and performance. *Tellus 63A*, 4–23.

Schirokné Kriston, I., 2004: Weather of 2003. *Légkör 49*, 36–39. (in Hungarian)

van der Schrier, G., van den Besselaar, E., Leander, R., Verver, G., Klein Tank, A., Beersma, J., van Oldenborgh, G.J., Plieger, M., Renshaw, R., and *Bissoli, P.*, 2013: Central European flooding 2013. EURO4M Climate Indicator Bulletin.
Available online at http://cib.knmi.nl/mediawiki/index.php-/Central_European_flooding_2013

Serinaldi, F. and *Kilsby, C.G.*, 2014: Simulating daily rainfall fields over large areas for collective risk estimation. *J. Hydrol. 512*, 285–302.

Sheffield, J. and *Wood, E.F.*, 2008: Global trends and variability in soil moisture and drought characteristics, 1950-2000, from observation-driven simulations of the terrestrial hydrologic cycle, *J. Climate 21*, 432–458.

Sivakumar, M.V.K. and *Stefanski, R.*, 2009: Climate change mitigation, adaptation, and sustainability in agriculture. *Időjárás 113*, 89–102.

Stott, P.A., Stone, D.A., and *Allen, M.R.*, 2004: Human contribution to the European heatwave of 2003. *Nature 432*, 610–614.

WMO, 2011: WMO statement on the status of the global climate in 2010. WMO-No. 1074. Geneva, Switzerland.
Available online at http://www.wmo.int/pages/publications/-showcase/documents/1074_en.pdf

WMO, 2014: WMO statement on the status of the global climate in 2013. WMO-No. 1130. Geneva, Switzerland. Available online at https://drive.google.com/file/d/0BwdvoC9AeW-jUeEV1cnZ6QURVaEE/edit?usp=sharing

IDŐJÁRÁS

Quarterly Journal of the Hungarian Meteorological Service
Vol. 118, No. 4, October – December, 2014, pp. 323–333

Trend analysis of a new MODIS drought severity index with emphasis on the Carpathian Basin

Péter I. Orvos[1,2], **Viktória Homonnai**[2], **Anita Várai**[3], **Zoltán Bozóki**[4], and **Imre M. Jánosi**[2,3]*

[1]*Department of Optics and Quantum Electronics, University of Szeged, Dóm tér 9, H-6720 Szeged, Hungary*

[2]*Regional Research Center, Eötvös Loránd University, Irányi Dániel u. 4, H-8000 Székesfehérvár, Hungary*

[3]*Department of Physics of Complex Systems, Eötvös Loránd University, Pázmány Péter sétány 1/A, H-1117 Budapest, Hungary*

[4]*MTA-SZTE Research Group on Photoacoustic Spectroscopy, University of Szeged, Dóm tér 9, H-6720 Szeged, Hungary*

**Corresponding author E-mail: imre.janosi@ttk.elte.hu*

(Manuscript received in final form July 15, 2014)

Abstract—Recently, *Mu et al.* (2013) have compiled an open access data base of a remotely sensed global drought severity index (DSI) based on MODIS satellite measurements. Observations cover a continuous period of 12 years between January 1, 2000 and December 31, 2011 with a temporal resolution of 8 days. The highest spatial resolution is around 5 km in the geographic band between 60°S and 80°N latitudes (more than 4.9 million locations over land). Here we extend the global trend analysis by *Orvos et al.* (2014) of these satellite based DSI time series in order to locate geographic areas where either positive or negative trends are statistically significant. Significance is established by a standard perturbation test, where each individual record is cut into annual pieces, and the statistics of 1000 randomly shuffled and glued time series is compared with the original record. We exhibit three regions of significant wetting and/or drying trends over extended geographic ranges and try to correlate them with recent reports of local climate shifts. We are fully aware of the fact that 12 years are too short for linking the findings to global climate change. Most probably, the identified significant trends can be considered as a component of natural climate variability on decadal time scales, however, a full explanation will require to identify a couple of explanatory variables.

We demonstrate that drying and wetting trends are weakly significant in the Carpathian Basin. Nevertheless, the observations can serve as benchmark for regional climate simulations, projections can be accepted when the test period is properly reproduced considering also high resolution DSI data.

Key-words: drought indices, linear trend analysis, high resolution mapping, statistical significance tests, remote sensing

1. Introduction

Severe droughts or floods are devastating events for both ecosystems and human society. There are several indices used widely for drought assessment integrating large amounts of data (precipitation, snowpack, stream-flow, etc.). Probably, the best known is the Palmer drought severity index (PDSI) (*Palmer*, 1968; *Alley*, 1984) determined by monthly water supply (precipitation), water outputs (evaporation and runoff), and preceding soil water status. New variants of the original approach have been emerged in order to overcome some limitations of the Palmer model (*Alley*, 1984; *Keyantas* and *Dracup*, 2002), such as the self-calibrating PDSI by *Wells et al.* (2004) or PDSI incorporating improved formulations for potential evapotranspiration (*Heim*, 2002). Remote sensing data from the Moderate Resolution Imaging Spectroradiometer (MODIS) combined with NCEP reanalysis records and statistical procedures together have supported to develop an evaporative drought index (EDI) by *Yao et al.* (2010, 2014) with 4 km spatial and 1 month temporal resolutions. Nevertheless, the development and improvement of drought indices are incomplete tasks, and numerous challenges remain for the future (*Vicente-Serrano et al.*, 2011).

In order to better exploit the strengths of continuous satellite observations, *Mu et al.* (2013) have recently developed a remotely sensed global drought severity index (DSI), and compiled an open access data base spanning 12 years between 2000 and 2011 at a temporal resolution of 8 days. The highest spatial resolution is around 5 km ($0.05° \times 0.05°$) with an almost global coverage. Permanently unvegetated locations such as deserts, high mountains, lakes, or large cities cannot provide input for DSI data, because the computation algorithm incorporates the following MODIS products (*Parkinson* and *Greenstone*, 2000):

1. The normalized difference vegetation index (MOD 13) determined as (NIR-VIS)/(NIR+VIS), where NIR and VIS denote the spectral reflectances in the near-infrared and visible (practically red) regions.
2. The surface resistance and evapotranspiration (MOD 16) calculated using land surface temperature data (MOD 11), the previously mentioned NDVI index (MOD 13) and incident radiation. For details, see *Mu et al.* (2011, 2013).

To our best knowledge, the most comprehensive and longest PDSI trend analysis has been provided by *Dai et al.* (2004). A monthly PDSI dataset from 1870 to 2002 has been derived using historical precipitation and temperature data for global land areas on a grid of $2.5° \times 2.5°$. An empirical orthogonal function (EOF) analysis resulted in a linear trend in the twentieth century, with drying over northern and southern Africa, the Middle East, Mongolia, and eastern Australia, and moistening over the United States, Argentina, and parts of Eurasia (*Dai et al.*, 2004). A follow-up study by *Dai* (2011) compared the

original and three other variants of PDSI records, but the main conclusion remained the same: warming in the second half of the last century is responsible for much of the drying trend over several land areas. Increased heating itself from global climate change may not cause droughts, but it is expected that when droughts occur they are likely to set in quicker and be more intense (*Trenberth et al.*, 2014). However, similarly to the open questions on an optimal definition of a drought index, debates on the trends are also not entirely closed (*Sheffield et al.*, 2012; *Damberg* and *AghaKouchak*, 2013; *Spinoni et al.*, 2013).

2. *Locations of significant DSI trends*

Here we extend the global trend analysis by *Orvos et al.* (2014) of the remotely sensed DSI data base by *Mu et al.* (2013). Records at 4 914 440 geographic locations are evaluated in order to identify linear trends. Each individual record consists of 552 points covering 12 years from January 1, 2000 to December 31, 2011. The basic time-step is 8 days, apart from the necessary cuts at the end of each year. Statistical significance of slopes is verified by the standard permutation test (*Manly*, 2007). Since most of the DSI signals exhibit marked seasonality, the basic unit of data shuffling was one whole calendar year. We cut a given record into 12 pieces, and built a test set from randomly shuffled and glued years. The mean slope and standard deviation were determined, and we accepted a fitted slope of a measured record to be significant when its distance from zero was larger than 2σ of its own test set. *Orvos et al.* (2014) demonstrated that a test set of 100 samples provides essentially the same statistics as 100 000 random samples, however, for the sake of minimizing errors, we fixed the size of test sets at 1000 samples. The larger the test sample size the closer the histogram of obtained slopes to a pure Gaussian, however, the mean and standard deviation do not show detectable sensitivity to the size of the test sets (*Orvos et al.* 2014). Statistically significant slopes are obtained for 852 373 data points (17.34%) at 2σ level, the numbers for 2.5σ and 3σ thresholds are 269 900 (5.49%) and 16 321 (0.33 %), respectively.

The main result of the global trend analysis is illustrated in *Fig. 1*. There are several geographically connected areas exhibiting drying (South America, Middle Asia, or Sub-Equatorial Africa) or wetting (Middle and North Africa, Indian Peninsula, or eastern Spain) tendencies. We emphasize that the remotely sensed DSI is a standardized variable (12-year mean value is removed and normalized by the standard deviation), thus values and trends provide local information: the same numerical value can be connected to very different local circumstances. In order to demonstrate the power of high resolution mapping, we illustrate zooms in three different regions where extended changes are clearly observable.

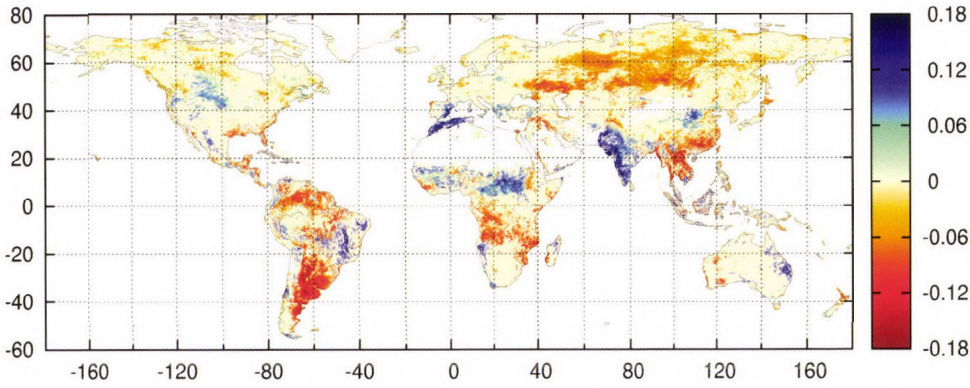

Fig. 1. Geographic locations of statistically significant drying (red) or wetting (blue) trends. Slopes are color coded in units of DSI/year. White color indicates missing data. (*Orvos et al.*, 2014)

Fig. 2 illustrates a detailed map of the southern part of the Asian subcontinent. As for climate shifts in India, *Kothyari* and *Singh* (1996) studied long-term time series of summer monsoon rainfall and identified decadal departures above and below the long-time average alternatively for three consecutive decades. *Singh* and *Sontakke* (2002) reported on an increase in extreme rainfall events over northwest India during the summer monsoon and a decline of the number of rainy days along east coastal stations in the past decades, resulting in a westward shift in rainfall activities. Similarly, *Murumkar* and *Arya* (2014) demonstrated by means of wavelet analysis that prominent annual rainfall periods exist ranging from 2 to 8 years at all the studied stations after 1960s. Large-scale spatial and temporal correlations between the trends of rainfall and temperature are found by *Subash* and *Sikka* (2013), without a direct relationship between increasing rainfall and increasing temperature of monthly or seasonal patterns over meteorological subdivisions of India. As for the particular area, even glaciers can be listed as candidate explanatory factors, since they influence runoff into lowland rivers, and recharge river-fed aquifers (*Bolch et al.*, 2012). In order to illustrate the difficulties of interpreting DSI trends, *Panda* and *Kumar* (2014) also found increasing trends of extreme rainfall indices based on the percentile and absolute values, simultaneously with a significantly increased length of dry spells over northern and central regions of India, suggesting a serious threat to the Indian agriculture.

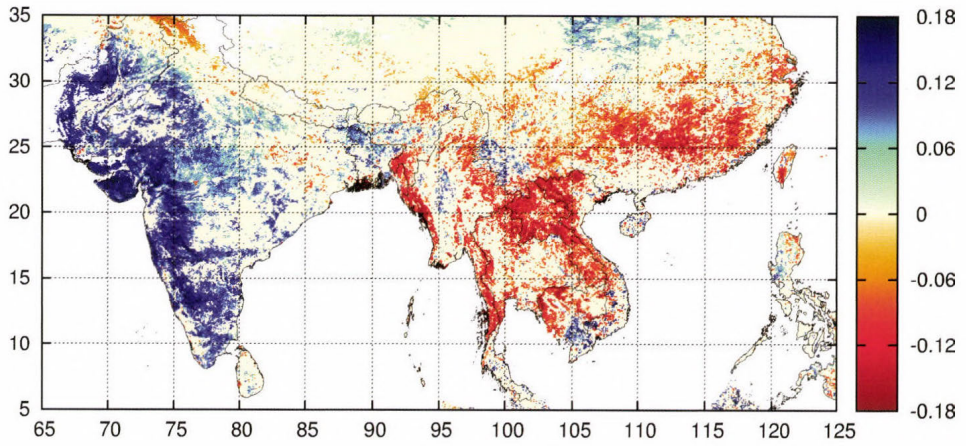

Fig. 2. Geographic locations of statistically significant drying (red) or wetting (blue) trends in Southern Asia. Slopes are color coded in units of DSI/year.

At the other side of the Bay of Bengal, the largest part of Laos, Northern Vietnam, and extended territories in South China are affected by an opposite, drying trend. *Nguyen et al.* (2014) studied a total of 40 years of data from 60 stations around Vietnam. They concluded that dominant trends for annual rainfall are declines, but not in a statistically significant way (they used the Mann-Kendall test). Among the eight climate regions, five of them in Northern Vietnam show decreasing trends, but only the sub-region around Ha Noi has statistically significant decreases. Note that DSI is not a direct measure of precipitation, however, the spatial and temporal coincidences indicate a strong relationship between them. *Hsu et al.* (2014) reviewed the variability of East Asian, Indochina, and Western North Pacific Summer Monsoon on time scales ranging from diurnal to interannual and interdecadal. They concluded that one of the largest challenges is to understand the observed long-term changes and regime shifts in terms of global monsoon. Regional climate model runs by *Zhou et al.* (2013) suggest that the high-speed emission of SO_2 and its uneven distribution over eastern China can contribute to the change in the May-August rainfall over eastern China between the two decades of 1999–2008 and 1989–1998, especially to the decrease of rainfall in the Yangtze River valley.

As a next example, *Fig. 3* demonstrates also an interesting large-scale pattern in DSI trends at the opposite sides of the equator. Large regions in Sudan and in the Central African Republic exhibit positive (wetting), while Eastern Congo, Angola, and Mozambique suffer from negative (drying) tendencies. Various regions in Africa are commonly accepted to be among the most vulnerable territories considering global climate change, the climatological literature is quite controversial and uneven. One reason is that Africa has the

lowest density and quality observational network, therefore, most of the studies are based on reanalysis data or numerical modeling. Since the DSI strongly depends on NDVI data, a proper interpretation would require reliable information on local circumstances such as land use changes, shepherding, large-scale migrations, etc.

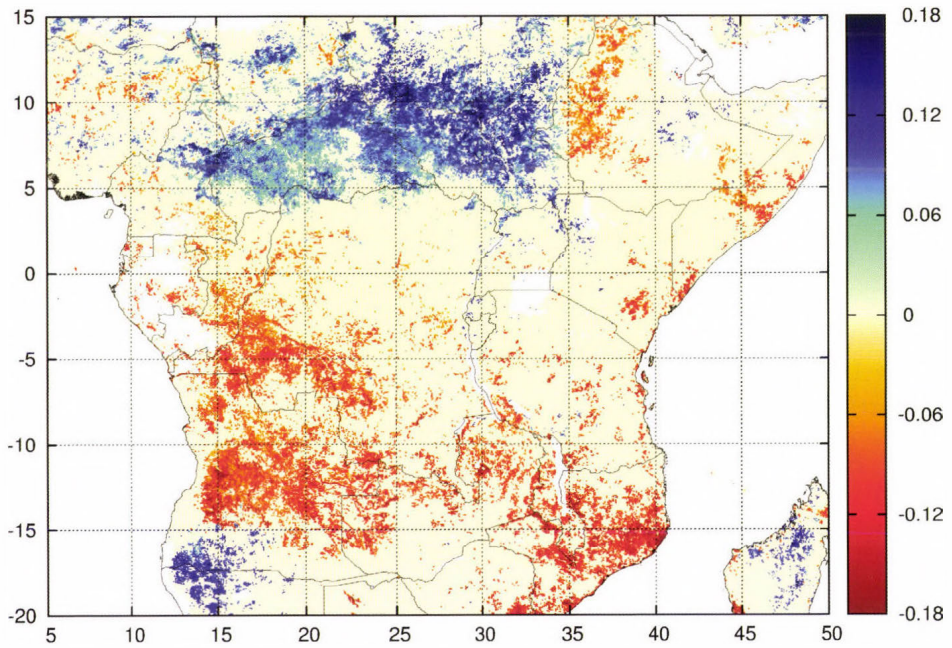

Fig. 3. Geographic locations of statistically significant drying (red) or wetting (blue) trends in Middle Africa. Slopes are color coded in units of DSI/year.

Fig. 4 demonstrates remarkable tendencies around the western Mediterranean basin: northern Morocco, Algeria, and Eastern Spain exhibit strong and significant wetting trends. The main characteristic of the region is the strong gradient between two large-scale systems, namely the North Atlantic (Azores) anticyclone and the low pressure monsoon system over the Indian Ocean and Middle East. This strong gradient establishes a flow from north to south during all seasons that is enhanced by the differential heating between the land of North Africa and South Europe with the Mediterranean waters. It is interesting to note that a recent collaborative assessment on regional climate change (see: *Navarra* and *Tubiana*, 2013) concluded that no basin-wide trends in precipitation and droughts are detectable for the second half of the twentieth century.

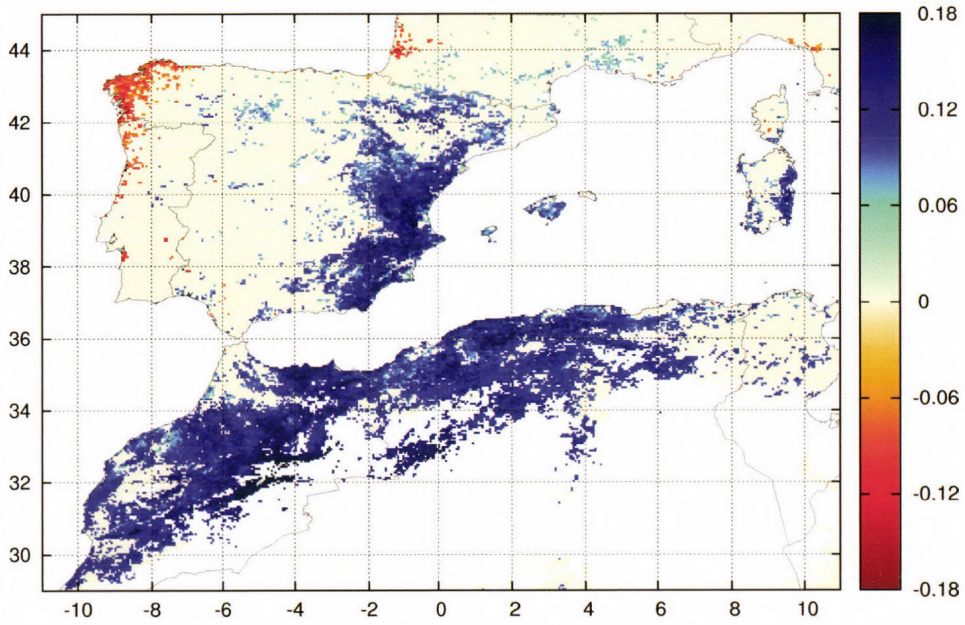

Fig. 4. Geographic locations of statistically significant drying (red) or wetting (blue) trends around the western Mediterranean region. Slopes are color coded in units of DSI/year.

3. Weak DSI trends in the Carpathian basin

Since the drought severity index basically conveys local information, it is worth to check regions where trends are not such significant as in the examples in the previous Section. As a case study, *Fig. 5* shows the geographic distribution of DSI trends in the Carpathian Basin, Central Europe. Locations are plotted where measured slopes passed the significance test by at least 1σ level (the number of sites obeying 2σ significance is not more than 1.1%). While an isolated point of weak DSI trend can easily be a consequence of statistical uncertainties, larger connected regions of similar tendencies support the existence of real effects in the background.

Representative locations are indicated in *Fig. 5*. Sites around České Budějovice (Czech Republik), Szombathely (Hungary), or Pula (Croatia) obey weak wetting, while weak drying is characteristic in the surroundings of Doboj (Bosnia and Herzegovina) or the diagonal band between 49°N–23.5°E and 48°N–25°E (see *Fig. 5*). The latter band coincides with a by and large unpopulated region of Carpathian Mountains in Ukraine, where the observed tendencies are probably consequences of forest cover loss (*Dezső et al.*, 2005).

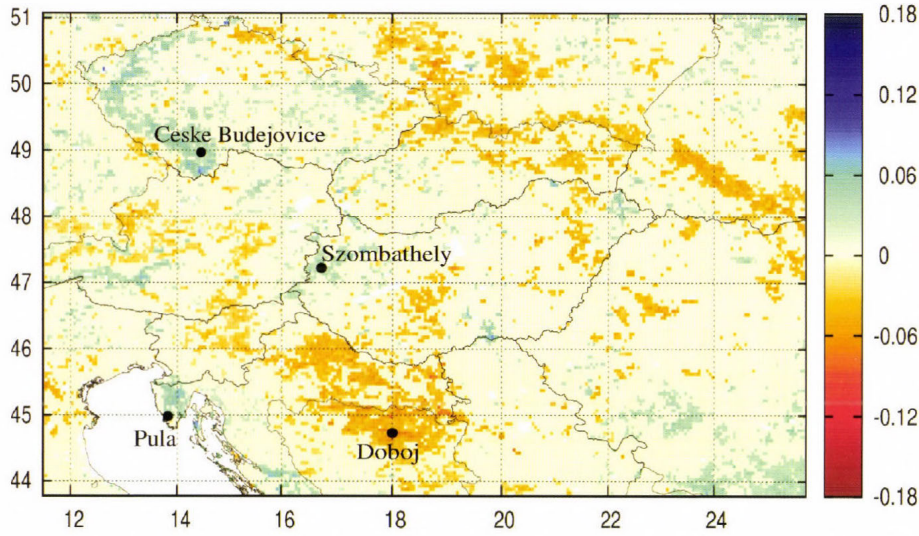

Fig. 5. Geographic locations of weakly significant drying (red) or wetting (blue) trends at 1σ level in the Carpathian Basin. Slopes are color coded in units of DSI/year (note that the range of the color scales is identical for all maps). Locations of a few cities are indicated for an easier orientation.

Repeated analyses and projections of regional climate change are in focus of several research projects also in the Carpathian Basin (*Gálos* and *Jacob*, 2007; *Szépszó* and *Horányi*, 2008; *Krüzselyi et al.*, 2011; *Torma et al.*, 2011; *Bartholy et al.*, 2012; *Bartholy et al.*, 2013; *Mezősi et al.,* 2013). The results are somewhat controversial similarly to other efforts in regional climate modeling: warming and drying tendencies are often identified with various intensities for different geographic sub-regions. However, it should be emphasized that a direct comparison of numerical simulation with empirical results such as illustrated in *Fig. 5* is not really possible, simply because the models cannot determine the very drought severity index analyzed in this work (*Rummukainen,* 2010).

4. Discussion

We have shortly described the way of obtaining DSI records in Section 1. Clearly, any drought severity index is related to precipitation in some way, however, we have illustrated in *Orvos et al.* (2014) that several other local factors, most importantly changing land-use, contribute to a given index value. As a further illustration we show in *Fig. 6* that precipitation trends are not directly related to local DSI trends. Two locations from the map of *Fig. 5* are chosen, where the weakly significant DSI trends of opposite signs are not related to daily precipitation time series at all.

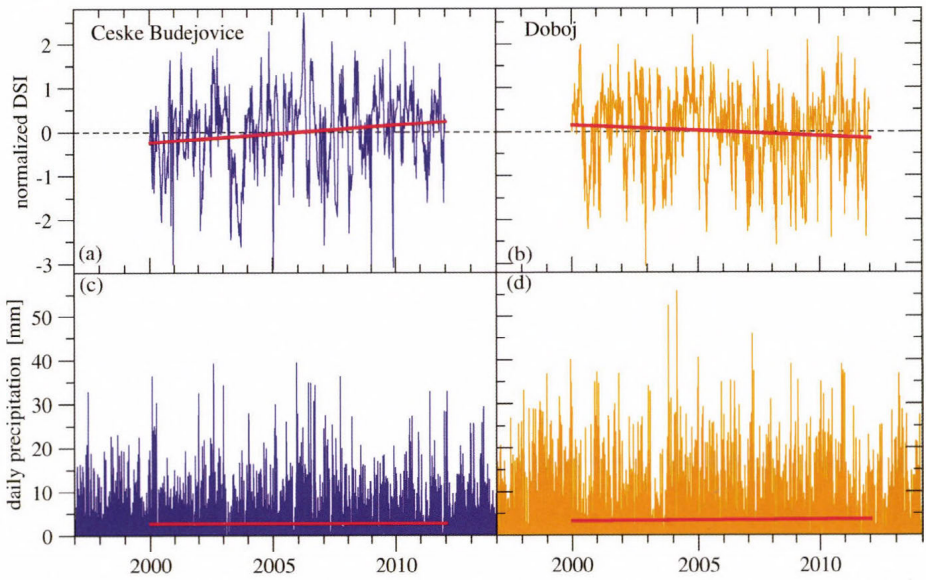

Fig. 6. Weakly significant wetting/drying trends at 1σ level at (a) České Budějovice (49.5°N, 14.5°E) and (b) Doboj (44.5°N, 18.5°E). Red lines indicate slopes of +0.0394 and -0.0243 DSI/year, respectively. (c) and (d) show daily precipitation time series in units of mm for the same geographic locations. Note that fitted trends for the same 12-year period (red lines) are statistically not significant, however the slopes are opposite: –0.0042 mm/year for České Budějovice (c) and +0.0317 mm/year for Doboj (d).

As for the Carpathian Basin, our findings are in agreement with a high spatial resolution trend analysis of monthly self-calibrating PDSI records by *van der Schrier et al.* (2005). Trends in summer moisture availability over Europe for the 1901–2002 period failed to be statistically significant, both in terms of spatial means of the drought index and the area affected by drought. While the time interval of our analysis has a negligible overlap with the cited study (*van der Schrier et al.,* 2005), we also found that the MODIS DSI time series have non-significant local trends in the middle of the European continent.

Nevertheless, we think that the DSI defined by *Mu et al.* (2013) can be implemented in numerical models. Considering the high temporal and spatial resolutions of the data set, it can serve as an exceptional tool for model parameterization and benchmarking.

Acknowledgements: This work was partially supported by the European Union and the European Social Fund through the project FuturICT.hu (grant no. TAMOP-4.2.2.C-11/1/KONV-2012-0013), furthermore the project StratoClim (grant no. 603557-FP7-ENV.2013.6.1-2), and the Hungarian Science Foundation (grant no. OTKA NK100296).

References

Alley, W. M., 1984: The Palmer drought severity index: Limitations and assumptions. *J. Climate Appl. Meteor. 23*, 1100–1109.

Bartholy, J, Pongrácz R, Nagy, J., Pieczka, I., and *Hufnagel, L.*, 2012: Regional climate change impacts on wild animals' living territory in Central Europe. *Appl. Ecol. Environ. Res. 10*, 107–120.

Bartholy, J., Pongrácz, R., and *Hollósi, B.*, 2013: Analysis of projected drought hazards for Hungary. *Adv. Geosci. 35*, 61–66.

Bolch, T., Kulkarni, A., Kääb, A., Huggel, C., Paul, F., Cogley, J.G., Frey, H., Kargel, J.S., Fujita, K., Scheel, M., Bajracharya, S., and *Stoffel, M.*, 2012: The state and fate of Himalayan glaciers. *Science 336*, 310–314.

Dai, A., 2011: Characteristics and trends in various forms of the Palmer Drought Severity Index during 1900–2008. *J. Geophys. Res. 116*, D12115.

Dai, A., Trenberth, K.E., and *Qian, T.*, 2004: A global dataset of Palmer drought severity index for 1870–2002: Relationship with soil moisture and effects of surface warming, *J. Hydrometeor. 5*, 1117–1130.

Damberg, L. and *AghaKouchak, A.*, 2013: Global trends and patterns of drought from space. *Theor. Appl. Climatol.*, early view, doi: 10.1007/s00704-013-1019-5.

Dezső, Z., Bartholy, J., Pongrácz, R., and *Barcza, Z.*, 2005: Analysis of land-use/land-cover change in the Carpathian region based on remote sensing techniques. *Phys. Chem. Earth. 30*, 109–115.

Gálos, B., Lorenz, Ph., and *Jacob, D.*, 2007: Will dry events occur more often in Hungary in the future? *Environ. Res. Lett. 2*, 034006.

Heim, R.R. Jr., 2002: A review of twentieth-century drought indices used in the United States. *Bull. Amer. Meteor. Soc. 83*, 1149–1165.

Hsu, H-H., Zhou, T., and *Matsumoto, J.*, 2014: East Asian, Indochina and Western North Pacific Summer Monsoon - An Update. *Asia-Pac. J. Atmos. Sci. 50*, 45–68.

Keyantash, J., and Dracup, J.A., 2002: The quantification of drought: An evaluation of drought indices. *Bull. Amer. Meteor. Soc. 83*, 1167–1180.

Kothyari, U.C. and *Singh, V.P.*, 1996: Rainfall and temperature trends in India. *Hydrol. Process. 10*, 357–372.

Krüzselyi, I., Bartholy, J., Horányi, A., Pieczka, I., Pongrácz, R., Szabó, P., Szépszó, G., and *Torma, Cs.*, 2011: The future climate characteristics of the Carpathian Basin based on a regional climate model mini-ensemble. *Adv. Sci. Res. 6*, 69–73.

Manly, B.F.J., 2007: Randomization, Bootstrap and Monte Carlo Methods in Biology. 3rd Ed., Chapman and Hall/CRC, Boca Raton.

Mezősi, G., Meyer, B.C., Loib, W., Aubrecht, l Ch., Csorba, P., and *Bata, T.*, 2013: Assessment of regional climate change impacts on Hungarian landscapes. *Reg. Environ. Change 13*, 797–811.

Mu, Q., Zhao, M., and *Running, S.W.*, 2011: Improvements to a MODIS Global Terrestrial Evapotranspiration Algorithm. *Remote Sens. Environ. 115*, 1781–1800.

Mu, Q., Zhao, M., Kimball, J.S., McDowell, N.G., and *Running, S.W.*, 2013: A remotely sensed global terrestrial drought severity index. *B. Am. Meteorol. Soc. 94*, 83–98.

Murumkar, A. R. and *Arya, D.S.*, 2014: Trend and periodicity analysis in rainfall pattern of Nira basin, Central India. *Am. J. Clim. Change 3*, 60–70.

Navarra, A. and *Tubiana L. (Eds.)*, 2013: Regional Assessment of Climate Change in the Mediterranean. Volume 1: Air, Sea and Precipitation and Water. Springer Science+Business Media, Dordrecht.

Nguyen, D-Q., Renwick, J., and *McGregor, J.*, 2014: Variations of surface temperature and rainfall in Vietnam from 1971 to 2010. *Int. J. Climatol. 34*, 249–264.

Orvos, P.I., Homonnai, V., Várai, A., Bozóki, Z., and *Jánosi, I.M.*, 2014: Global trend analysis of the MODIS drought severity index with local statistical significance tests. Submitted to *Geosci. Instr. Methods Data Syst.*

Palmer, W.C., 1968: Keeping track of crop moisture conditions, nationwide: The new crop moisture index. *Weatherwise 21*, 156–161.

Panda, D.K. and *Kumar, A.*, 2014: The changing characteristics of monsoon rainfall in India during 1971–2005 and links with large scale circulation. *Int. J. Climatol.*, early view, doi: 10.1002/joc.3948

Parkinson, C.L. and Greenstone, R. (Eds.), 2000: EOS Data Product Handbook (Vol. 2), NASA Goddard Space Flight Center, Greenbelt, Maryland.

Rummukainen, M., 2010: State-of-the-art with regional climate models. *Wiley Interdisciplinary Reviews: Climate Change, 1,* 82–96.

Sheffield, J., Wood, E.F., and *Roderick, M.L.*, 2012: Little change in global drought over the past 60 years. *Nature 491*, 435–438.

Singh, N. and *Sontakke, N.A.*, 2002: On climatic fluctuations and environmental changes of the Indo-Gangetic Plains, India. *Climatic Change 52*, 287–313.

Spinoni, J., Naumann, G., Carrao, H., Barbosa, P., and *Vogt, J.*, 2013: World drought frequency, duration, and severity for 1951-2010. *Int. J. Climatol.*, early view, doi: 10.1002/joc.3875

Subash, N. and *Sikka, A.K.*, 2013: Trend analysis of rainfall and temperature and its relationship over India. *Theor. Appl. Climatol.*, early view, doi: 10.1007/s00704-013-1015-9

Szépszó, G. and *Horányi, A.,* 2008: Transient simulation of the REMO regional climate model and its evaluation over Hungary. *Időjárás 112*, 203–231.

Torma, Cs., Coppola, E., Giorgi, F., Bartholy, J., and *Pongrácz, R.*,2011: Validation of a high-resolution version of the regional climate model RegCM3 over the Carpathian Basin. *J. Hydrometeorol. 12*, 84–100.

Trenberth, K. E., Dai, A., van der Schrier, G., Jones, P.D., Barichivich, J., Briffa, K.R., and *Sheffield, J.*, 2014: Global warming and changes in drought. *Nature Clim. Change 4*, 17–22.

van der Schrier, G., Briffa, K.R., Jones, P.D., and *Osborn, T.J.,* 2006: Summer moisture variability across Europe, *J. Climate 19*, 2828–2834.

Vicente-Serrano, S.M., Beguería, S., and *López-Moreno, J.I.*, 2011: Comment on "Characteristics and trends in various forms of the Palmer Drought Severity Index PDSI) during 1900–2008"' by Aiguo Dai, *J. Geophys. Res. 116*, D19112

Wells, N., Goddard, S., and *Hayes, M.J.*, 2004: A self-calibrating Palmer drought severity index. *J. Climate 17*, 2335–2351.

Yao, Y., Liang, S., Qin, Q., and *Wang, K.*, 2010: Monitoring drought over the conterminous United States using MODIS and NCEP Reanalysis-2 data. *J. Appl. Meteorol. Climatol. 49*, 1665–1680.

Yao Y., Liang, S., Zhao, S., Zhang, Y., Qin, Q., Cheng, J., Jia, K., Xie, X., Zhang, N., and *Liu, M.*, 2014: Validation and application of the modified satellite-based Priestley-Taylor algorithm for mapping terrestrial evapotranspiration. *Remote Sens. 6*, 880–904.

Zhou, Y., Jiang, J., Huang, A., La, M., Zhao, Y., and *Zhang, L.,* 2013: Possible contribution of heavy pollution to the decadal change of rainfall over eastern China during the summer monsoon season. *Environ. Res. Lett. 8*, 044024.

IDŐJÁRÁS

Quarterly Journal of the Hungarian Meteorological Service
Vol. 118, No. 4, October – December, 2014, pp. 335–347

Some aspects of the impact of meteorological forecast uncertainties on environmental dispersion prediction

Tímea Haszpra[1*] and **András Horányi**[2]

[1]*MTA–ELTE Theoretical Physics Research Group,*
Pázmány Péter sétány 1/A, H-1117 Budapest, Hungary,
hatimi@caesar.elte.hu

[2]*Hungarian Meteorological Service,*
Kitaibel Pál u. 1., H-1024 Budapest, Hungary,
Currently on leave at the European Centre for Medium-Range Weather Forecasts,
Shinfield Park, Reading, RG2 9AX, United Kingdom
Andras.Horanyi@ecmwf.int

**Corresponding author*

(Manuscript received in final form August 25, 2014)

Abstract—There are several types of uncertainties related to the simulation of the dispersion of pollutants in the atmosphere. For a dispersion forecast, one of the most important error sources is the meteorological data produced by a numerical weather prediction model and utilized by the dispersion model. In this paper, we will present the results of an ensemble dispersion forecast created by using an ensemble meteorological forecast and the high-resolution forecast for 2.5 days. The dispersion simulations are carried out by the RePLaT Lagrangian dispersion model for particles of different radii. Significant deviations appear both in the extension and location of the ensemble of pollutant clouds consisting of particles of the same size. Differences appear also between the dispersion scenarios which use the unperturbed meteorological forecasts with different resolutions. The difference among the ensemble members increases for small particles. The area where at least one ensemble member predicts pollutant is much larger than the area covered by the pollutant cloud of the high-resolution forecast.

Key-words: dispersion, realistic particles, ensemble forecast, RePLaT model

1. Introduction

Pollutants from different sources may be advected far away from their initial position and cause pollution episodes at distant locations. The effects of ash clouds from volcano eruptions and of gases and aerosol particles from industrial accidents underline the need for investigating dispersion in the atmosphere as the emitted material can be hazardous. Volcanic ash can be dangerous, e.g., for air transport, and hence, may imply an economic hazard even if the eruption itself is not a strong one (for instance as it was the case for the Eyjafjallajökull's eruptions in 2010). The disaster of Chernobyl in 1986 and Fukushima in 2011 drew attention to the significance of the fact that radioactive materials from nuclear power plant accidents or air pollutants from other sources can also be a risk for health both in the atmosphere and as deposited material, therefore, the accurate prediction of their dispersion is essential.

As a consequence, the demand for more and more accurate tracking and forecasting of atmospheric pollutants has increased due to the growing interest in environmental problems.

However, dispersion simulations are subject to numerous uncertainties. There might be inaccuracies in the emission data for the dispersion model as the source term (the emitted amount, physical and chemical properties, emission height and period, initial extension and size distribution of the pollutant cloud) is only estimated. Obviously, in particular cases, e.g., for sudden and intense volcano eruptions, the 3-dimensional extent of the ash cloud and the size distribution of the aerosol particles can be estimated only with much more uncertainty than in other cases, like e.g., for a weak leaking from a plant close to the ground.

The other set of the input data on which the dispersion calculation is based, that is, the meteorological forecast data produced by the numerical solution of the atmospheric hydro-thermodynamic equations also include uncertainty. This is, on the one hand, the consequence of the inaccurate initial conditions of the forecasts that cannot be precisely determined due to the inaccuracies in the measurements and the approximations in the data assimilation procedures. On the other hand, the reason for the uncertainties in the meteorological data is also the fact that the meteorological weather prediction model is not fully precise as for instance it uses parameterizations for certain processes and applies numerical schemes. The uncertainty in the meteorological forecasts can be quantified by the ensemble technique including the execution of multiple meteorological forecasts (*Leutbecher* and *Palmer*, 2008). This meteorological uncertainty estimate can be carried forward to the dispersion models for assessing the implied uncertainties in the air pollution prediction.

The dispersion model itself also contains uncertainties. Its reliability depends on the processes taken into account (like advection, turbulent diffusion, dry and wet deposition, chemical reactions, etc.), their parameterizations, numerical approximations, and interpolations applied in the model. The importance of all the above-mentioned uncertainty sources is summarized in *Galmarini et al.* (2004).

Furthermore, it is important to emphasize that in 2D time-dependent flows or in 3D flows, as it is the case of the atmosphere, the advection of pollutants is chaotic. The typical characteristics of chaotic behavior are the sensitivity to the initial conditions, irregular motion, and complex but regular (fractal-like) structures (*Aref*, 1984). Thus, chaotic advection of pollutants amplifies the inaccuracies mentioned before.

It is a relevant question to understand the relative merits of the various uncertainty sources during the entire dispersion modeling process. The uncertainties related to the meteorological inputs can be minimized when such observation-related analysis meteorological fields are used as re-analysis (*Dee et al.*, 2011). With the use of re-analysis information, the meteorological inputs are considered to be perfect, therefore, only the other uncertainty sources play role in the overall uncertainty pattern of the dispersion model.

As an example, *Fig. 1* illustrates the dispersion of volcanic ash from the Eyjafjallajökull's eruption in the spring of 2010. In the beginning of the eruption period, northern flows were dominating south to Iceland, and a high pressure area was located in the Atlantic region. *Fig. 1* shows that, first, the volcanic ash becomes transported to south in the anticyclonic circulation. It is due to the northerly winds that the volcanic ash can reach even the Iberian Peninsula located about 2000 km away from Iceland. Some days later (not shown here) the volcanic ash is dispersed all over Europe. We compared the results of the simulation with satellite observation on May 10 (see right panel of *Fig. 1*). The shape of the ash cloud was found to be remarkably similar in the simulation and in the satellite image. Even the fat patch at the southwest "edge" of the ash cloud found in the simulation appears in the satellite image. Therefore, according to this comparison, there seems to be a satisfying agreement between the simulation and the measurement. This means that in this particular case, the dispersion simulation uncertainties are low, consequently, the non-meteorological related uncertainties have only a small impact. Based on this result, we consider that the uncertainties related to the meteorological inputs are presumably more important than the other ones.

Therefore, in this paper we focus on the impact of uncertainty of the meteorological forecasts on the dispersion calculation. This kind of variability was studied in different ways for gases (see, e.g., *Holt et al.*, 2009; *Lee et al.*, 2009; *Scheele* and *Sigmund*, 2001; *Straume et al.*, 1998; *Straume*, 2001). To our knowledge, no systematic investigation has been carried out for aerosol particles before the study of *Haszpra et al.* (2013). In order to study this problem we

carried out multiple dispersion simulations using 50+1 members of an ensemble forecast and the corresponding high-resolution forecast (HRES, referred as deterministic forecast in earlier references). The dispersion simulations were performed with particles of different sizes composing the pollutant clouds in order to investigate the dependence of the impact on the particle radius. This work serves as a complement to *Haszpra et al.* (2013) as the results are based on the same meteorological and emission data and, therefore, on the same dispersion simulations. Although, in contrast to that, this paper mostly concentrates on the properties of the individual pollutant clouds in the ensemble dispersion forecast rather than looking them altogether to characterize them with various statistical properties.

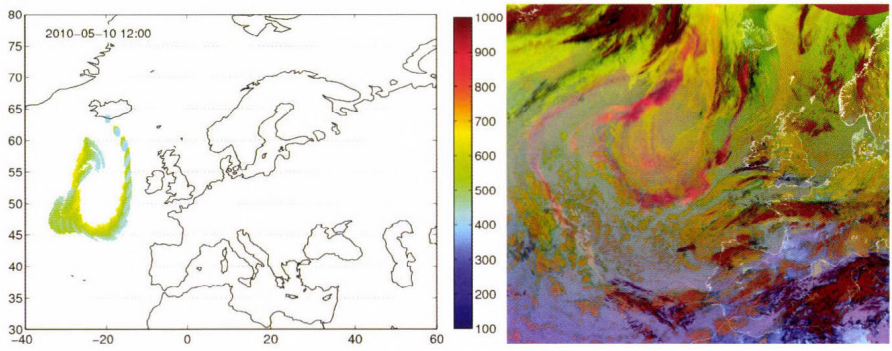

Fig. 1. Left: The dispersion of a sequence of volcanic ash puffs from the Eyjafjallajökull's eruption in RePLaT simulation (see Section 2). Each volcanic ash puff consists of 10^3 particles with radius $r = 1$ μm. The initial altitude of the centre of puffs is $p = 500$ hPa, the initial extension is 1°×1°×200 hPa. The puffs are emitted in every 6 hours from May 8, 00 UTC on. The color bar indicates the altitude of the particles in hPa. Right: Satellite image at 12 UTC, May 10, 2010. Volcanic ash is indicated by pink. [http://oiswww.eumetsat.org/WEBOPS/medialib/medialib/images/2010_05_10_1200_m8_rgb_24hmicro.jpg]

Section 2 gives a brief overview of the RePLaT dispersion model by which the dispersion simulations were carried out (it was also used for the computations shown in *Fig. 1*). In Section 3, the meteorological data utilized for the dispersion calculation is presented. Section 4 provides the results of the ensemble dispersion simulation, and Section 5 summarizes the main conclusions of the work.

2. *The RePLaT dispersion model*

The RePLaT (Real Particle Lagrangian Trajectory) dispersion model – as its name also suggests – is a Lagrangian trajectory model that tracks individual spherical aerosol particles with fixed, realistic radius r and density ρ_p. The velocity of a particle is equal to the velocity of the ambient air in horizontal, and in the vertical direction (owing to the impact of gravity), deposition has to be taken into account with the terminal velocity w_{term}. The effect of turbulent diffusion is built into the equations as a stochastic term. Thus, the equation of motion of a particle is the following:

$$\frac{d\mathbf{r}_p}{dt} = \mathbf{v} + w_{term}\mathbf{n} + \boldsymbol{\xi} \cdot \mathbf{K}, \tag{1}$$

where

$$w_{term} = -\frac{2}{9}\frac{\rho_p r^2 g}{\rho \nu}. \tag{2}$$

This follows from Stokes's law which is valid for small and heavy particles (ρ_p is in the order of 2000 kg m^{-3}, $r \leq 10$ μm). In Eq. (1) and (2), $\mathbf{r}_p(t)$ denotes the particle trajectory, $\mathbf{v} = (u, v, w)$ is the velocity of air, $\mathbf{n}$ is the vertical unit vector pointing upwards, g is gravitational acceleration, ρ and ν indicate the density and viscosity of the air, $\boldsymbol{\xi}$ is a random walk process and $\mathbf{K}$ represents the turbulent diffusivity in the different directions which might be location- and time-dependent.

RePLaT also takes into account the impact of scavenging of particles by precipitation. It is built into the model as a random process that results in a particle that is captured by a raindrop with a certain probability. The probability of the transformation from an aerosol particle to a raindrop depends on the precipitation intensity. The trajectory of the "new" particle (the particle that turned into a raindrop) is computed using the terminal velocity based on the new properties of the particle, typically using a terminal velocity w_{term} derived from the quadratic drag law for large particles:

$$w_{term} = -\frac{8}{3}\frac{\rho_{rain} r_{rain} g}{\rho C_d}, \tag{3}$$

where $C_d = 0.4$ is the drag coefficient for spheres. The transformed particle does not leave the atmosphere instantaneously, but as a raindrop falling through the air according to Eq. (1).

The meteorological data given on a grid are interpolated to the location of the particles using bicubic spline interpolation in horizontal and linear interpolation in vertical and in time. The equation of motion is solved by Euler's method. For more details about RePLaT, see *Haszpra* and *Tél* (2013).

3. Data and methods

In order to demonstrate the variability of an ensemble dispersion forecast, the RePLaT model was run with an ensemble meteorological forecast of the European Centre for Medium-Range Weather Forecasts (ECMWF) (*Molteni et al.*, 1996; *Leutbecher* and *Palmer*, 2008) including 50 perturbed members and the unperturbed control forecast (CF). Additionally, simulations were also carried out with the unperturbed high-resolution forecast (HRES). The horizontal resolution of the former ones is 0.25°×0.25°, while that of the latter is 0.125°×0.125°; the time resolution is 3 hours in both datasets. In vertical direction, the meteorological data utilized in the simulations are given on pressure levels (1000, 925, 850, 700, 500, 400, 300, 250, 200, 100, 50, 10 hPa). The dispersion calculation covers a 2.5-day period and starts at 00 UTC on March 12, 2011.

As a first approach, we are interested in the simplest case when the motion of the pollutants is determined only by advection and their terminal velocity, and the effects of turbulent diffusion and precipitation are neglected. These conditions are fulfilled in the free atmosphere with good approximation. Therefore, the simulations are carried out above the 850 hPa level (considered as the bottom of the free atmosphere), and particles sunk below this region are considered to "be deposited" and are no longer tracked.

4. Results

4.1. Ensemble evaluation of meteorological uncertainties

4.1.1. Evaluation of ensemble members

In order to study the impact of the uncertainty of the meteorological fields on the dispersion calculation, a hypothetical emission is considered centered at $\lambda = 141°$, $\varphi = 37.5°$, $p = 500$ hPa (above Japan). Initially, 9×10^4 particles of density $\rho_p = 2000$ kg m^{-3} are distributed uniformly in a horizontal square of size 1°×1°. The simulations are performed for particles of radius $r = 0, 1, 2, \ldots,$ 10 μm so that one can follow the size-dependence of the variability in the ensemble of dispersion forecast.

Particle dispersion patterns were determined in all the 50 ensemble members along with the HRES and CF members 2.5 days after the emission. However, for an easier overview, only some representative members of the whole ensemble dispersion simulation are presented here. *Fig. 2* illustrates the distribution of $r = 1$ μm aerosol particles, while *Fig. 3* is the same for $r = 4$ μm particles. The mean sea level pressure characteristics of each ensemble member are also displayed in the figures. The colors indicate the altitude of the particles

in hPa. In all dispersion simulations, the pollutant cloud of the particles is advected to east, over the Pacific Ocean. In most of them, the cloud stretches more or less in the west–east or southwest–northeast direction. This deformation is the consequence of a jet located east to Japan and some cyclones above the Pacific Ocean during these days: the strong wind shear and mixing effects related to them elongates most of the clouds (*Haszpra et al.*, 2013). The particles happen to sink in the first day. In some members, significant fraction of the $r = 1$ μm particles (having terminal velocity smaller than or of the same order as the vertical velocity component of the air) is captured by a cyclone passing towards the Californian coast. In the upwelling zone, particles lift higher in the atmosphere (green and light blue region), e.g., in members no. 6, 13, etc.

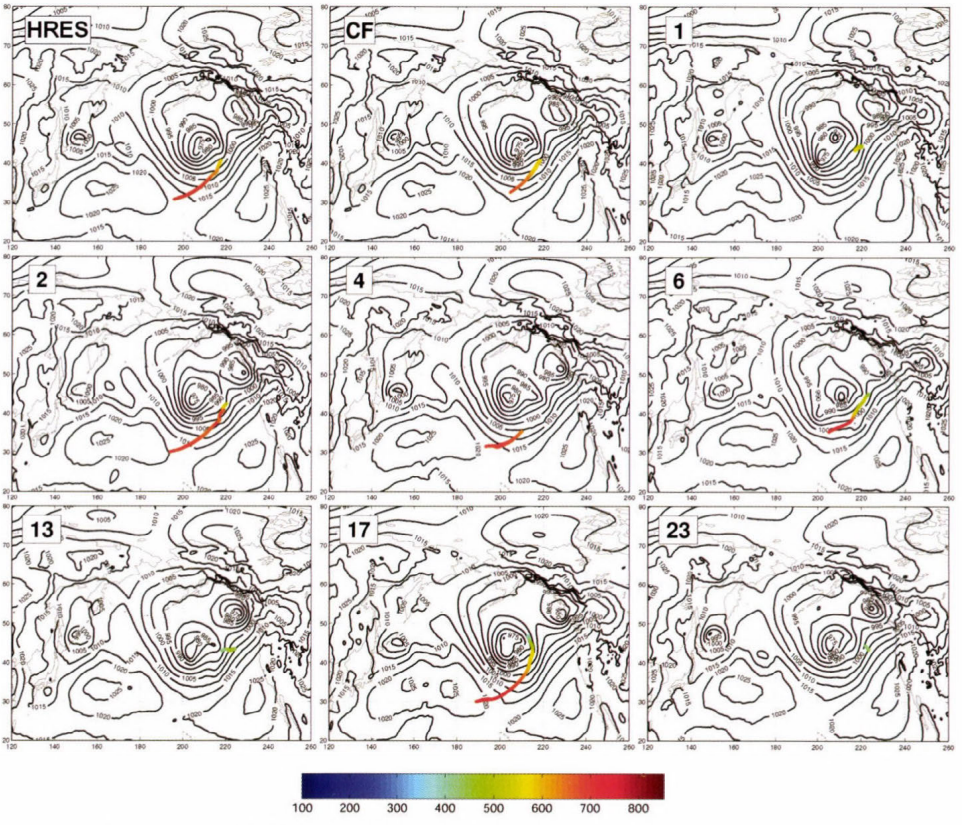

Fig. 2. The distribution of $r = 1$ μm aerosol particles 2.5 day after the emission using the high-resolution forecast (HRES), the control forecast (CF), and the perturbed ensemble members, respectively. Only some representative members of the whole ensemble dispersion simulation are presented. Color bar indicates the height of the particles in hPa. Black contours denote the mean sea level pressure in hPa.

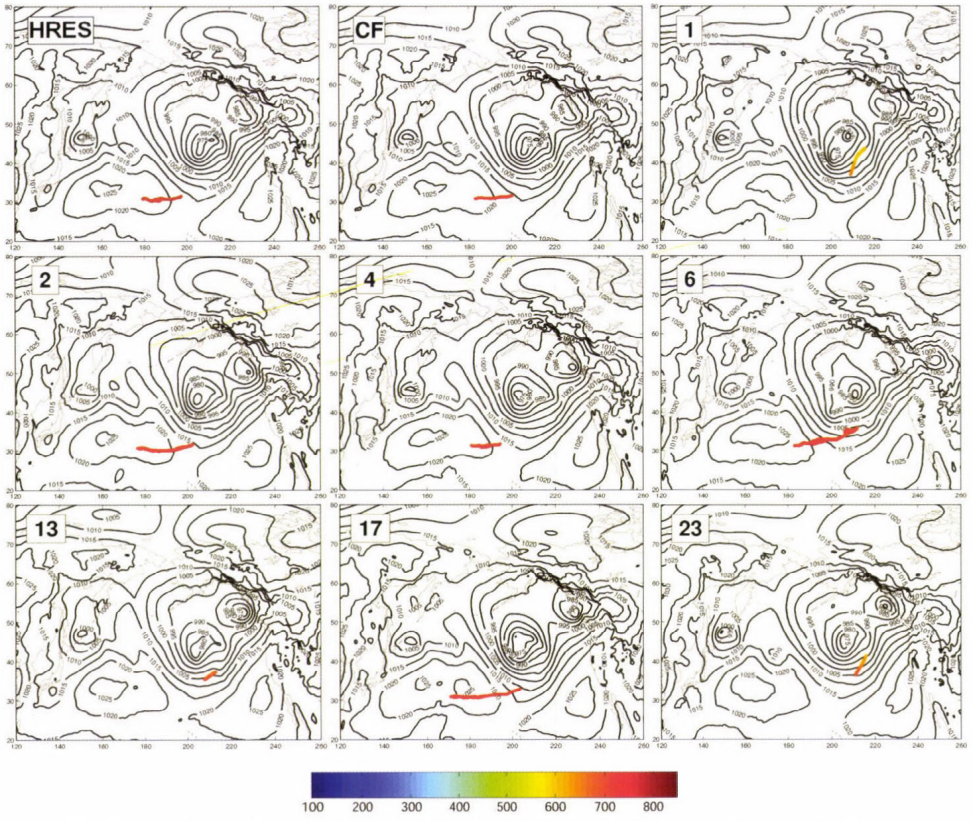

Fig. 3. The distribution of $r = 4$ μm aerosol particles 2.5 day after the emission using the high-resolution forecast (HRES), the control forecast (CF), and the perturbed ensemble members, respectively. Only some representative members of the whole ensemble dispersion simulation are presented. Color bar indicates the height of the particles in hPa. Black contours denote the mean sea level pressure in hPa.

Without any quantitative characterization of the location or extension of the pollutant clouds, just by visual inspection, different types of dispersion events can be distinguished. In *Fig. 2* for the $r = 1$ μm particles in some of the ensemble members, the pollutant cloud is hardly lengthened during the 2.5 days and remains located in the 600–350 hPa layer of the atmosphere (like no. 1, 13, 23, 43, 46[1]). Another class may be formed by dispersion members HRES and no. 2, 5, 10, 11, 14, 27, 29, etc.[1] characterized principally by orange color (750–600 hPa) and strong stretching. A similar, but distinct group can be detected e.g., from members no. 4, 20, 24, 34, 44[1] with a stretched, but less expanded shape (compared to the previous group). As mentioned before, there are

[1] Only some of the listed ensemble members are shown in *Figs. 2* and *3*.

dispersion members (e.g., no. 17, 28, 48[1]) in which the pollutant cloud is strongly influenced by the cyclonic flow, and thus, particles form a spiral towards the center of the cyclone, and the vertical extent of the pollutant cloud covers a wide region from 800 to 300 hPa (red to light blue colors). Finally, there is a similar class of members with particles lifted high in the atmosphere, where the pollutant cloud starts to turn away from the center of the western low pressure system near the North American coast due to the flow of the eastern cyclone (e.g., member no. 6, 16, 33[1]).

An analogous "visual" clustering can be carried out for the $r = 4$ μm particles based on *Fig. 3*. However, in this case fewer groups can be identified. Especially, the vertical distribution of the particles is much narrower, since these particles have 16 times greater terminal velocity than that of the $r = 1$ μm ones (based on Eq. (2)), and therefore, most of them reach the bottom level of the simulation, on which they are formally deposited, within 2.5 days. Almost all of the dispersion members can be classified into two groups: one characterized by slightly or moderately stretched shape in the west–east direction (e.g., HRES, CF, no. 2, 3, etc.[1]), and one including clouds with shorter extension and southwest–northeast direction close to the second low pressure area from North America (member no. 13, 21, 28, 46[1]). It is interesting to note that there are two "outlier" pollutant clouds in *Fig. 3* (member no. 1 and 23). Member 1 has almost all of its particles in the 750–700 hPa layer, while member 23 has half of its particles in the 800–750 hPa and 750–700 hPa layers, respectively. For both members, particles get much higher than those of the other dispersion clouds.

4.1.2. "Outlier" dispersion forecast – "outlier" meteorological forecast?

In connection with the above-mentioned "outlier" predictions for the $r = 4$ μm particles, the question arises whether dispersion member no. 1 and/or 23 is related to a strongly atypical meteorological event. The mean sea level pressure contour lines of the postage stamps charts in *Fig. 2* and *3* do not seem to confirm the idea of a likewise "outlier" meteorological forecast: the general circulation patterns of member 1 and 23 do not appear to differ much more from that of the others than the other members from each other.

Even without computing any statistical quantity, the question may be answered by comparing the $r = 1$ μm and $r = 4$ μm pollutant clouds. In the case of $r = 1$ μm particles in *Fig. 2,* both member no. 1 and no. 23 are characterized by short clouds. However, in contrast to the $r = 4$ μm particles in *Fig. 3*, they are not the only members with these properties; members no. 12, 13, 43, 46 show the same features (and possibly member 3 and 35 also can be included into the group). In the case of $r = 4$ μm particles, these members differ significantly from the two "outlier" predictions with lower and, in certain cases, longer clouds.

Based on these arguments, we cannot claim that the "outlier" members for $r = 4$ μm particles would be the consequence of considerably different meteorological forecasts. In fact, the phenomenon can be attributed to the result of the chaotic advection due to which small differences can produce significantly different dispersion patterns.

It is noted here that it would be a natural idea to run the dispersion calculations only with the representative members of the meteorological ensemble clusters in order to reduce the computational cost of the dispersion prediction. However, some studies suggest that there is not a one-to-one correspondence between the meteorological ensemble clustering and the dispersion clustering (see, e.g., *Straume*, 2001). Therefore, using only the meteorological representatives for a dispersion forecast may not necessarily give a general overview of the possible dispersion scenarios.

4.1.3. Probabilistic evaluation

It is illustrated in Section 4.1.1, that a dispersion calculation run by an ensemble meteorological forecast may result in pollutant clouds which deviate both in location and extension from each other even within 2.5 days. The difference among the pollutant clouds can be quantified by various statistical measures and probability information, see e.g. *Haszpra et al.* (2013), *Scheele* and *Sigmund* (2001), *Straume et al.* (1998), *Straume* (2001). One of the most elegant probability information is demonstrated in *Fig. 4.*

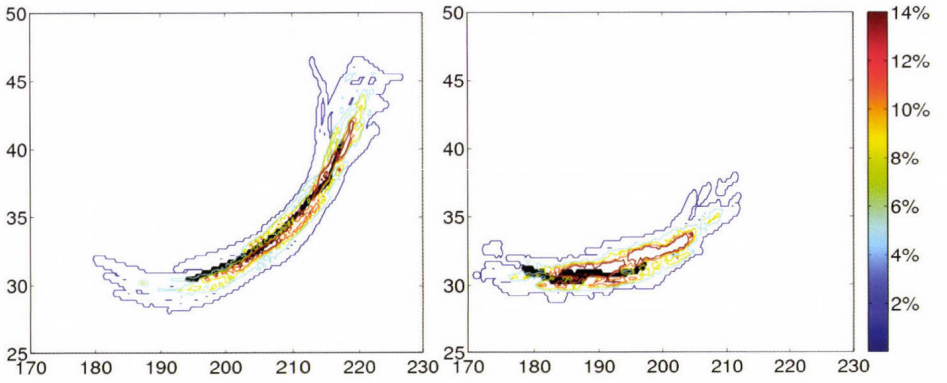

Fig. 4. Horizontal distribution of the ensemble of pollutant clouds after 2.5 days. Contours (at 2, 5, 8, 11 and 14%) indicate the percentage of the dispersion calculations predicting at least one particle in 0.25°×0.25° air columns for particles of $r = 1$ μm remained in the free atmosphere (left) and in 0.25°×0.25° cells for deposited particles of $r = 4$ μm (right). Black color denotes the pollutant cloud obtained by using the high-resolution forecast.

The particle number in 0.25°×0.25° air columns is determined for particles remained above 850 hPa, and this quantity is also calculated in 0.25°×0.25° cells in the "deposition field" for particles which subside below this level, respectively, in each member of the ensemble of pollutant clouds. The left panel of *Fig. 4* demonstrates the horizontal distribution of the ensemble of pollutant clouds in the case of $r = 1$ μm for particles remaining in the simulation range, and the right panel is the same for $r = 4$ μm for particles "deposited" within 2.5 days. Contour lines indicate areas where certain proportion of the ensemble dispersion members predicts at least one particle. Black cells demonstrate the location of the pollutant cloud given by the high-resolution forecast. Both panels of *Fig. 4* point to the fact (as expected) that the area covered by the cloud of the high-resolution forecast is much smaller than the region where at least one ensemble member predicts any particles.

This kind of information is rather useful in risk assessment when one would like to estimate the potential area in the deposition field or the region in air where the concentration of the pollutant exceeds a certain threshold.

4.2. The impact of the resolution of the meteorological data

Comparing the results of the simulations which use the unperturbed high-resolution forecast (HRES) and control forecast (CF), it is possible to study the impact of the resolution of the meteorological forecasts on the dispersion calculation. *Fig. 5* illustrates the horizontal location of the center of mass of the HRES and CF clouds for different particle radii (denoted by the numbers in μm) both for particles in the air (left) and in the deposition field (right). Neither the HRES cloud nor the CF cloud with particles of $r \geq 5$ μm have any particles in the air after 2.5 days, and similarly, clouds consisting of small particles (HRES: $r \leq 1$ μm, CF: $r \leq 2$ μm) have no particles in the deposition field.

As a general rule, it can be concluded that for all particle sizes, differences can be observed between the HRES and CF cloud centers. For those particles of the pollutant clouds that remain in the free atmosphere during the observation period (left panel), the distance between the centers of mass varies between 500 and 1400 km. In the deposition field, the distances range from about 300 km (small particles) down to the order of 10 km (large particles). This is due to the fact that larger particles have larger terminal velocities, hence they deposit sooner and the clouds have less time to separate in the different meteorological fields. *Fig. 5* reveals that also the extension of the HRES and CF pollutant cloud differs somewhat. The rate of the standard deviation values of the HRES and CF clouds in most of the cases is found to be greater than 1 (between 1.1 and 2.5). This implies that the dependence of the dispersion calculation on the resolution of the meteorological data used in the simulation is still significant, especially for pollutants consisting of small particles.

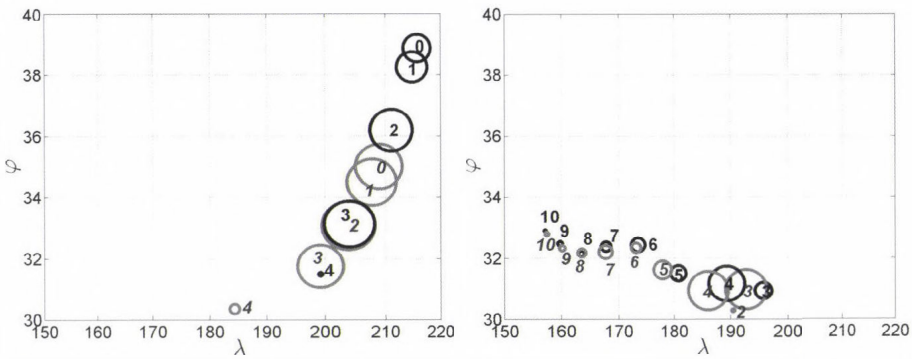

Fig. 5. The horizontal location of the center of the pollutant clouds using the high-resolution forecast (grey, italic font) and the control forecast (black, normal font). Left: center of the pollutant clouds consisting only particles remained in the air for 2.5 days. Right: the same for particles deposited during the 2.5 days. Numbers indicate the particle radius r of the clouds. The radii of the circles are proportional to the standard deviation of the particles within the cloud.

5. Final remarks

In this paper, the case study of a hypothetical emission illustrates that significant deviations may appear among the pollutant clouds of an ensemble of dispersion forecast, and also between the simulations using unperturbed forecasts with different resolutions, even in the simplest case when only advection influences the dispersion of the pollutants. Presumably, in simulations that take into account the impact of turbulent diffusion and precipitation on the particles, even more remarkable differences could be found, since in that case the uncertainties in the dispersion model would be enhanced.

In practice, dispersion models are usually run by a single forecast which is considered to be the best one (i.e., the high-resolution forecast). However, as the paper demonstrates, it can be useful to perform simulations using a whole ensemble of forecasts, i.e., producing an ensemble dispersion prediction in order to get a detailed and more reliable overview of the uncertainties and possible hazards related to the dispersion event.

Acknowledgements: The authors thank *T. Tél* for useful suggestions. This work was partially supported by the European Union and the European Social Fund through the project FuturICT.hu (grant no. TAMOP-4.2.2.C-11/1/KONV-2012-0013), and by the Hungarian Science Foundation (grant no. OTKA NK100296).

References

Aref, H., 1984: Stirring by chaotic advection. *J. Fluid. Mech. 143*, 1–21.

Dee, D.P., Uppala, S.M., Simmons, A.J., Berrisford, P., Poli, P., Kobayashi, S., Andrae, U., Balmaseda M. A., Balsamo, G., Bauer, P., Bechtold, P., Beljaars, A.C.M., van de Berg, L., Bidlot, J., Bormann N., Delsol, C., Dragani, R., Fuentes, M., Geer, A. J., Haimberger, L., Healy, S.B., Hersbach, H., Hólm, E.V., Isaksen, L., Kållberg, P., Köhler, M., Matricardi, M., McNally, A.P., Monge-Sanz, B.M., Morcrette, J.-J., Park, B.-K., Peubey, C., de Rosnay, P., Tavolato, C., Thépaut, J.-N., Vitart, F., 2011: The ERA-Interim reanalysis: Configuration and performance of the data assimilation system. *Q. J. Roy. Meteor. Soc. 137(656)*, 553–597.

Galmarini, S., Bianconi, R., Klug, W., Mikkelsen, T., Addis, R., Andronopoulos, S., Astrup, P., Baklanov, A., *Bartniki, J., Bartzis, J., Bellasio, R., Bompay, F., Buckley, R., Bouzom, M., Champion, H., D'Amours, R., Davakis, E., Eleveld, H., Geertsema, G., Glaab, H., Kollax, M., Ilvonen, M., Manning, A., Pechinger, U., Persson, C., Polreich, E., Potemski, S., Prodanova, M., Saltbones, J., Slaper, H., Sofiev, M., Syrakov, D., Sørensen, J., der Auwera, L., Valkama, I., Zelazny, R.*, 2004: Ensemble dispersion forecasting – Part I: concept, approach and indicators. *Atmos. Env. 38(28)*, 4607-4617.

Haszpra, T., Lagzi, I., and *Tél, T.*, 2013: Dispersion of aerosol particles in the free atmosphere using ensemble forecasts. *Nonlinear Proc. Geoph. 20*, 759–770.

Haszpra, T. and *Tél, T.*, 2013: Escape rate: a Lagrangian measure of particle deposition from the atmosphere. *Nonlinear Proc. Geoph. 20*, 867–881.

Holt, T., Pullen, J. and *Bishop, C.H.*, 2009: Urban and ocean ensembles for improved meteorological and dispersion modelling of the coastal zone. *Tellus A 61*, 232–249.

Lee, J.A., Peltier, L.J., Haupt, S.E., Wyngaard, J.C., Stauffner, D.R., and Deng, A., 2009: Improving SCIPUFF dispersion forecasts with NWP ensembles. *J. Appl. Meteorol. Climatol. 48*, 2305–2319.

Leutbecher, M. and *Palmer, T.N.*, 2008: Ensemble forecasting. *J. Comput. Phys. 227*, 3515–3539.

Molteni, F., Buizza, R., Palmer, T.N., and *Petroliagis, T.*, 1996: The ECMWF ensemble prediction system: Methodology and validation. *Q. J. Roy. Meteor. Soc. 122*, 73–119.

Scheele, M.P. and *Siegmund, P.C.*, 2001: Estimating errors in trajectory forecasts using ensemble predictions. *J. Appl. Meteorol. 40*, 1223–1232.

Straume, A.G., 2001: A more extensive investigation of the use of ensemble forecasts for dispersion model evaluation *J. Appl. Meteorol. 40*, 425–445.

Straume, A.G., Koffi, E.N.D. and *Nodop, K.*, 1998: Dispersion modeling using ensemble forecasts compared to ETEX measurements. *J. Appl. Meteorol. 37*, 1444–1456.

IDŐJÁRÁS

Quarterly Journal of the Hungarian Meteorological Service
Vol. 118, No. 4, October – December, 2014, pp. 349–378

Statistical analysis of relationships between road accidents involving personal injury and meteorological variables in Hungary

Pál Vécsei[*1] and **Kálmán Kovács**[2]

[1] *Senior research adviser,*
Denevér köz 2, H-1121 Budapest, Hungary
pvecsei@t-online.hu

[2] *Director, Federated Innovation and Knowledge Centre of Budapest*
University of Technology and Economics,
Egry József utca 18, V1 C201, H-1111 Budapest, Hungary
kovacsk@mail.bme.hu

**Corresponding author*

(Manuscript received in final form September 10, 2014)

Abstract— Public opinion and certain human meteorological communications assume close relationship between meteorological variations and human conditions, especially the development of traffic accidents. This paper presents a detailed statistical analysis between domestic road accidents involving personal injury and relevant meteorological conditions for the period of 1990–2010 in Hungary. Approximately 431 thousand accidents were analyzed based on official statistical data. In general, a significant but weak interrelation was found between the absolute change – calculated from the previous day – of road traffic accidents involving personal injury and meteorological conditions. The results of multivariate linear regression analysis show that meteorological variations affected only nearly four percent of the variation of accidents relative to traffic. We demonstrated, however, that together with the significant variation of certain meteorological parameters, the number of accidents also significantly varies. Days with extreme meteorological variations explain the development of accidents in 9.8 percent, while in the case of days with non-extreme variations, this value was only 2.6 percent.

Key-words: road accidents with personal injury, multivariate regression, main component analysis, discriminant analysis, climate variation

1. Introduction

There is little scientifically grounded understanding of the effect of climatic variations on everyday living conditions, notwithstanding the numerous studies based on rather limited evidence – looking mainly at the relationship of accident rescue and weather (*Andersson* and *Chapman,* 2011; *Edwards*, 1999; *Jaroszweski et al.*, 2010; *Suarez et al.*, 2005). In spite of this, public opinion and certain human meteorological communications assume close relationship between meteorological variations and human conditions, especially the development of traffic accidents. During the past fifty years, significant results were achieved in the field of the investigation of relationship between road traffic conditions and meteorological parameters. The research activity carried out so far focused only on selected meteorological variables (*Sándor*, 2013). Present paper is aimed at exploring, as far as possible, complex statistical interrelations between road accidents involving personal injury and related meteorological parameters in Hungary.

Due to relatively advantageous circumstances, an opportunity presented itself to perform the joint statistical analysis of all domestic road traffic accidents involving personal injury between 1990 and 2010 (source: KSH data collection, data provider: police OSAP1009) and the relatively detailed data of selected meteorological observatory sites of the Hungarian Meteorological Service (Budapest, Pécs, Szeged, Debrecen, Szombathely, Győr, Nagykanizsa, and Siófok) for the same period. Nearly 13 million data of the approximately 431 thousand accidents were analyzed in details. The statistical analyses were done mostly on the basis of daily averages of the originally hourly data and absolute changes calculated from the previous day.

The key studies were completed with the temperature data of the eight meteorological observatory stations, the measured values of precipitation, wind speed, air pressure, relative humidity of the first five stations, and the average values of cloud cover data, as well as the daily average values of road traffic accidents involving personal injury and partially determined by estimation values for traffic on account of absent factual data. Beyond the interrelations between variations in meteorological conditions and the totality of accidents, the analysis touched upon the study of relations among key accident situations and locations.

2. Relationship between traffic accidents and complex variations of meteorological conditions

In general, it can be concluded, that there is significant but weak interrelation between the absolute change – calculated from the previous day – of road traffic accidents involving personal injury and meteorological conditions. The completed multivariate linear regression analysis shows that climatic variations affected only nearly four percent the variation of accidents relative to traffic as summarized in *Table 1* and *Fig. 1.*

Among the analyzed meteorological variations, the variation of precipitation patterns (1.9% points, nearly half of the total impact) had the most significant impact on the development of accidents, followed by temperature variation (0.7% points). Besides the aforementioned components, the variation of cloud cover and relative humidity influenced the development of accidents to 0.5 percentage points, while air pressure variation to 0.4 percentage points. The impact of wind speed was not statistically significant.

*Table 1.*Multivariate regression interrelations of daily variation of accidents (dependent variable) for estimated traffic between 1990 and 2010 with daily meteorological variation indicators (independent variables), (Stepwise method)

Model summary*									
Model	R	R-squared	Adjusted R-squared	Std. error of the estimate	Change statistics				
					R-squared Change	F change	df1	df2	Sig. F change
1	0.137[a]	0.019	0.019	0.59959	0.019	147.540	1	7668	0.000
2	0.162[b]	0.026	0.026	0.59738	0.007	57.832	1	7667	0.000
3	0.177[c]	0.031	0.031	0.59585	0.005	40.217	1	7666	0.000
4	0.191[d]	0.036	0.036	0.59434	0.005	40.071	1	7665	0.000
5	0.199[e]	0.040	0.039	0.59337	0.003	25.996	1	7664	0.000

* Dependent variable: Daily variation of the number of accidents per estimated traffic

[a] Predictors: (constant), variation of daily mean precipitation amount

[b] Predictors: (constant), variation of daily precipitation amount, variation of daily mean temperature

[c] Predictors: (constant), variation of daily mean precipitation amount, variation of daily mean temperature, variation of daily mean cloud cover

[d] Predictors: (constant), variation of daily mean precipitation amount, variation of daily mean temperature, variation of daily mean cloud cover, variation of daily mean relative humidity

[e] Predictors: (constant), variation of daily mean precipitation amount, variation of daily mean temperature, variation of daily mean cloud cover, variation of daily mean relative humidity, variation of daily mean air pressure

Besides the diverse significance of climatic component variations, their direction of effect was also differentiated (*Fig. 1*).

In general – regarding the measured interrelations, the increase of the amount of precipitation, temperature, and relative humidity, the thinning of the cloud cover and the decrease of the air pressure resulted in an increasing number of accidents. Resulting from the foregoing, opposite meteorological processes impacted on or became characteristic of the moderation of accidents. Therefore, nearly parallel with the decrease of precipitation, temperature, and relative humidity, and with the increase of cloud cover and the rise of air pressure, the number of traffic accidents involving personal injury decreased.

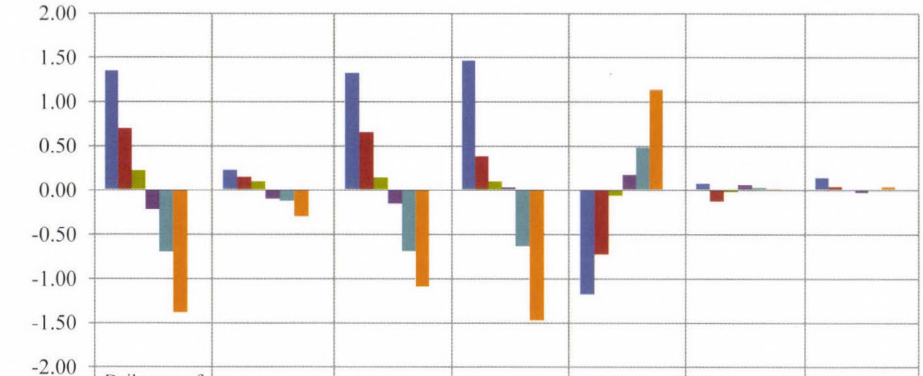

	Daily var. of the number of accidents for estimated traffic [accident / hundred thousand vehicles]	Var. of daily mean temperature [°C]	Var. of daily mean precipitation amount [mm]	Var. of daily mean relative humidity [% points]	Var. of daily mean air pressure [hPa]	Var. of daily mean cloud cover [okta]	Var. of daily mean wind speed [m/s]
1.0 – X increase	1.35	0.23	1.32	1.46	-1.19	0.07	0.14
0.5 – 1.0 increase	0.70	0.15	0.65	0.38	-0.73	-0.13	0.04
0.0 – 0.5 increase	0.22	0.10	0.14	0.10	-0.07	-0.03	0.00
0.0 – 0.5 decrease	-0.23	-0.10	-0.16	0.03	0.17	0.06	-0.04
0.5 – 1.0 decrease	-0.70	-0.13	-0.70	-0.63	0.48	0.03	-0.01
1.0 – X decrease	-1.39	-0.30	-1.10	-1.48	1.14	0.01	0.04
Total	0.00	0.00	0.00	0.00	0.00	0.00	0.00

Fig 1. Daily variation of average values of key meteorological features and of accidents involving personal injury per estimated traffic, calculated from the previous day by categorized values of daily variation of accidents between 1990 and 2010.

Analyses concluded with indicators expressing the daily variation of accidents (not standardized with traffic) and with variants (estimated factor and discriminant function values) obtained from multivariate statistical (factor and discriminant) analysis of the original meteorological indicators led to results almost perfectly identical with the above-mentioned findings.

In contrast with this interrelation, that can be considered generally weak, there are significant differences in the relationship of significantly differing components, types, and categories according to the content and factors, direction and intensity of meteorological variations – separated with multivariate statistical procedures (factor, cluster, and discriminant analysis) – with traffic accidents involving personal injury.

The score of factor analysis of daily meteorological variations represents 87.5% of the variance of the original variants with four relatively well identifiable components (variation of cloud cover, temperature, precipitation, and wind force), and these components well reflect the variation of relative humidity and air pressure, as well (*Table 2*).

Table 2. Scores of key components and factor analysis of indicators representing the absolute variation of meteorological features calculated from the previous day, for days between 1990 and 2010

Component Matrix					
	Component 1	**Component 2**	**Component 3**	**Component 4**	**Communalities**
Variation of daily mean temperature	–0.001	0.787	–0.492	–0.110	0.874
Variation of daily mean precipitation amount	0.714	–0.145	0.246	–0.588	0.936
Variation of daily mean wind speed	0.279	0.557	0.738	0.149	0.956
Variation of daily mean air pressure	–0.671	–0.498	0.22	0.082	0.753
Variation of daily mean humidity	0.746	–0.468	–0.254	0.037	0.842
Variation of daily mean cloud cover	0.787	–0.046	–0.056	0.515	0.889
Extraction sums of squared Loadings in % of variance	36.87	23.68	16.07	10.88	
Extraction sums of squared Loadings in cumulative %	36.87	60.55	76.62	87.50	
Rotated Component Matrix					
	Component 1	**Component 2**	**Component 3**	**Component 4**	**Communalities**
Variation of daily mean temperature	–0.131	**0.914**	–0.150	0.007	0.874
Variation of daily mean precipitation amount	0.181	–0.008	**0.943**	0.118	0.936
Variation of daily mean wind speed	0.041	0.079	0.096	**0.969**	0.956
Variation of daily mean air pressure	–0.403	–0.667	–0.328	–0.195	0.753
Variation of daily mean humidity	0.735	–0.091	0.445	–0.310	0.842
Variation of daily mean cloud cover	**0.919**	0.069	0.068	0.186	0.889
Extraction sums of squared Loadings in % of variance	26.64	21.66	20.51	18.69	
Extraction sums of squared Loadings in cumulative %	36.87	60.55	76.62	87.50	

Extraction method: principal component analysis.
Rotation Method: varimax with Kaiser normalization.

The separation of types, essentially different in the content, structure, and direction of climatic variations, was completed with the so-called K-mean cluster analysis of rotated components obtained from factor analysis, in five variations, incrementally expanding the number of possible types (clusters). The applied procedure resulted in typologies of 7, 10, 15, 20, and 25 numbers of element, the reliability and final content of which were tested partially with four climate change components from factor analysis, and partially with discriminant analyses run on the original variants (*Table 3*).

Table 3. Tests of equality of group means

	Wilks' lambda	F	df1	df2	Sig.
Daily meteorological variations, 25 clusters					
Variation of daily mean precipitation amount	0.208	1215	24	7645	0.00
Variation of daily mean cloud cover	0.313	698	24	7645	0.00
Variation of daily mean wind speed	0.317	688	24	7645	0.00
Variation of daily mean temperature	0.394	491	24	7645	0.00
Variation of daily mean humidity	0.413	452	24	7645	0.00
Variation of daily mean air pressure	0.487	336	24	7645	0.00

Although both approaches hold statistically significant classifications, corresponding to approaches searching less types, the 25-cluster solution represents more reliable and detailed diversity of day-to-day climatic variations of the period, both in total and in the various components. The above is confirmed furthermore by the fact, that the discriminant analyses qualified the distribution of daily variations by 25 types to be rather good – namely, cross classification with four components was matched in 96.5%, and with six original meteorological variations it matched 92.8% of the original classification, therefore, it qualified the classification as correct. The minor difference between the scores of cluster analysis and the discriminant analyses is partially due to that factor analysis and discriminant analysis which defined the significance hierarchy of meteorological variation components somewhat differently.

According to discriminant analyses, in the period between 1990 and 2010, the key determinant, the component of day-to-day climatic variations was the development of precipitation patterns (34.3% variance explained), followed by – with nearly identical weight – cloud cover (24.1%), wind force (21.2%), and temperature change (19.7%).

The rather detailed classification offered empirical opportunity to a more aggregate categorization by intensity and directions of multidimensional variations, to the separation of extreme or non-extreme variations considering the general trend, furthermore, to differentiate extremities according to their direction – appearing, rising or moderating, disappearing. The categorization of the 25 clusters was mainly based on the automatic classification (K-mean clustering) of the group average of estimated values of discriminant functions obtained from the discriminant analysis, but the result from the former ones was supplemented by the content analysis of factor values calculated for the clusters and of the original variants. Finally, 5 groups (9 percent of days) of the 25 cluster solution fell in the appearing-rising extremes category, 6 groups (9.7 percent of days) fell in the disappearing-moderating extremes category, and the remaining 14 groups with 81.3 percent of the days of the 20 years form the group of changes not classified as extreme (*Table 4*). The category of extreme changes is, naturally, the result of the pooling of rising and moderating extremes.

Table 4. Group means of rotated components and discriminant functions of groups separated by the direction and intensity of day-to-day meteorological variations

	Rotated factors from factor analysis of day-to-day meteorological variations				**Value of discriminant functions from the discriminant analysis based on rotated factors of the 25-cluster solution of meteorological variations**				**Days**	
	Meteorological variation component				**Discriminant function**					
	3. Var. of precipitation amount	**1. Var. of cloud cover**	**4. Var. of wind speed**	**2. Var. of temperature**	**1. Var. of daily precipitation amount**	**2. Var. of daily cloud cover**	**3. Var. of daily wind speed**	**4. Var. of daily temperature**	**Number of**	**Distribution of (%)**
	Factor score				**Discriminant scores**					
	Group means									
Rising extreme	1.67	0.00	0.72	–0.70	3.71	–0.35	1.16	–0.87	694	9.0
Decreasing extreme	–1.18	–0.61	–0.68	–1.02	–2.60	–1.50	–0.52	–1.83	741	9.7
Extreme variation	0.20	–0.31	0.00	–0.86	0.45	–0.94	0.29	–1.37	1435	18.7
Non-extreme variation	–0.05	0.07	0.00	0.20	–0.10	0.22	–0.07	0.31	6235	81.3
Days total in 1990–2010	0.00	0.00	0.00	0.00	0.00	0.00	0.00	0.00	7670	100.0

(The plus and minus 0.5, and especially, the above and below (plus and minus) 1.0 group means resulting from the standardizing and normalizing procedure applied in the construction of factor values resulting from factor analyses can be clearly regarded as extremes.) Daily variation of the average values of key meteorological features, and of accidents involving personal injury per estimated traffic, calculated from the previous day by extremity of meteorological variation are shown in *Figs. 2, 3.* and *4.*

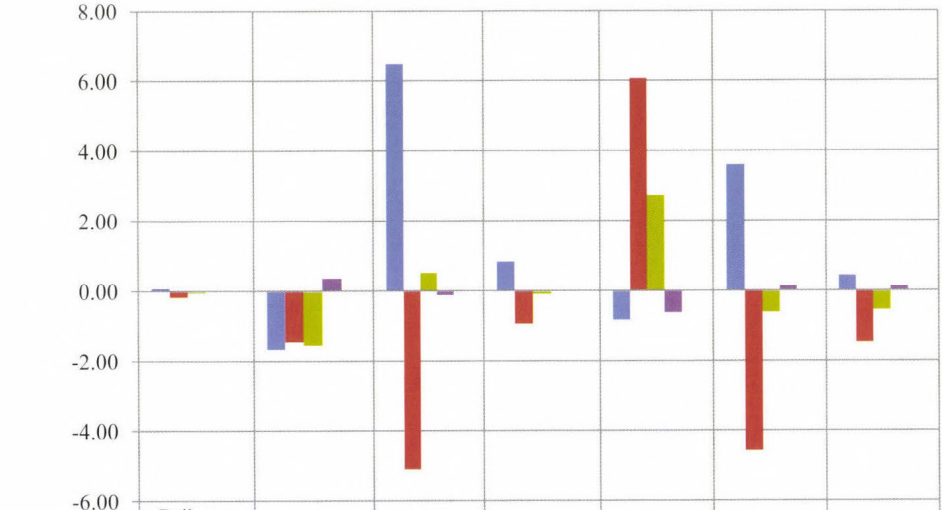

	Daily var. of accidents for estimated traffic	Var. of daily mean temperature [°C]	Var. of daily mean precipitation amount [mm]	Var. of daily mean wind speed [m/s]	Var. of daily mean air pressure [hPa]	Var. of daily mean relative humidity [% points]	Var. of daily mean cloud cover [okta]
Rising extremes	0.08	-1.67	6.49	0.84	-0.83	3.61	0.43
Moderating extremes	-0.17	-1.45	-5.09	-0.95	6.06	-4.57	-1.46
Extreme variations total	-0.05	-1.56	0.51	-0.08	2.73	-0.61	-0.55
Non-extreme variations total	0.01	0.36	-0.12	0.02	-0.63	0.14	0.13
1990 – 2010 total	0.00	0.00	0.00	0.00	0.00	0.00	0.00

Fig 2. Daily variation of the average values of key meteorological features, and of accidents involving personal injury per estimated traffic, from the previous day calculated by extremity of meteorological variation between 1990 and 2010.

The aggregate categorization of meteorological variations by the intensity and direction of the extremes, according to the prepared statistics, is significant for all meteorological indicators especially for the variation of precipitation, then air pressure, wind speed and temperature, however, not nearly to the extent as in the case of the 25 categories.

Because of the complexity and type richness of climatic variations, it may seem a problematic endeavor to condense in three categories the result of a classification based on four independent components of different significances, because even allowing 25 types will leave significant heterogeneities within the different types (clusters). Despite the above reservations, statistical control examinations qualified the classification as satisfactorily reliable. For example, the discriminant analyses - based on the original variables as well as on the factors formed from these - qualified the conformity of the three-category classification to be correct in 89 percent – pertaining to the same category as the initial classification. In terms of content, the only difference is that reclassifications drew somewhat broader borders for the extremes, and this directly resulted in a lower (down to 72 percent of days) proportion of non-extreme days (*Table 5*).

Table 5. Results of classification

Classification results[b,c]						
Meteorological extremes 1990–2010			Predicted group membership			Total
			Rising extremes	Moderating extremes	Non-extreme days	
Original	Count	Rising extremes	602	19	73	694
		Moderating extremes	10	675	56	741
		Non-extreme days	250	460	5525	6235
	%	Rising extremes	86.7	2.7	10.5	100.0
		Moderating extremes	1.3	91.1	7.6	100.0
		Non-extreme days	4.0	7.4	88.6	100.0
Cross-validated[a]	Count	Rising extremes	601	19	74	694
		Moderating extremes	10	674	57	741
		Non-extreme days	252	460	5523	6235
	%	Rising extremes	86.6	2.7	10.7	100.0
		Moderating extremes	1.3	91.0	7.7	100.0
		Non-extreme days	4.0	7.4	88.6	100.0

[a] Cross validation is done only for the cases in the analysis. In cross validation, each case is classified by the functions derived from all cases other than that case.
[b] 88.7% of original grouped cases correctly classified.
[c] 88.6% of cross-validated grouped cases correctly classified.

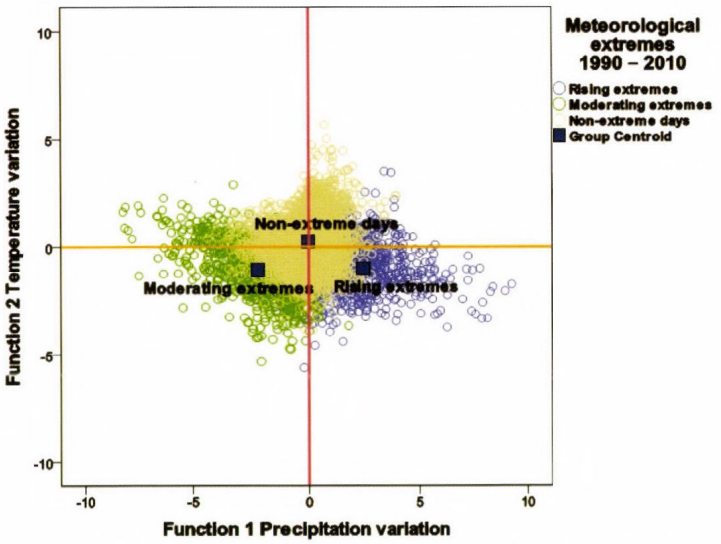

Fig 3. Meteorological extremes for the period 1990–2010 (canonical discriminant functions).

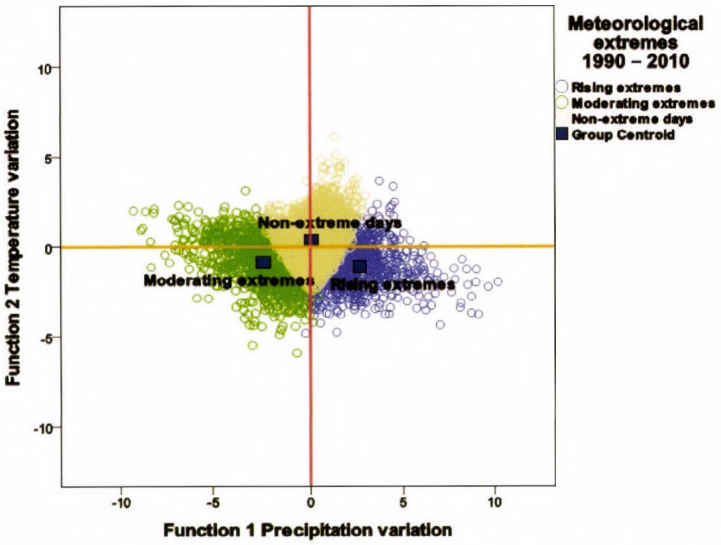

Fig 4. Meteorological extremes for the period 1990–2010 (canonical discriminant functions reclassified).

The grouping of day-to-day meteorological variations by intensity and direction created the opportunity of in-detail analysis of accidents involving personal injury by the indicated categories. The development of multivariate linear regression analysis relation (R-squared) calculated between traffic accidents involving personal injury per estimated traffic and day-to-day variation of meteorological features by meteorological change extremes can be seen in *Fig. 5*.

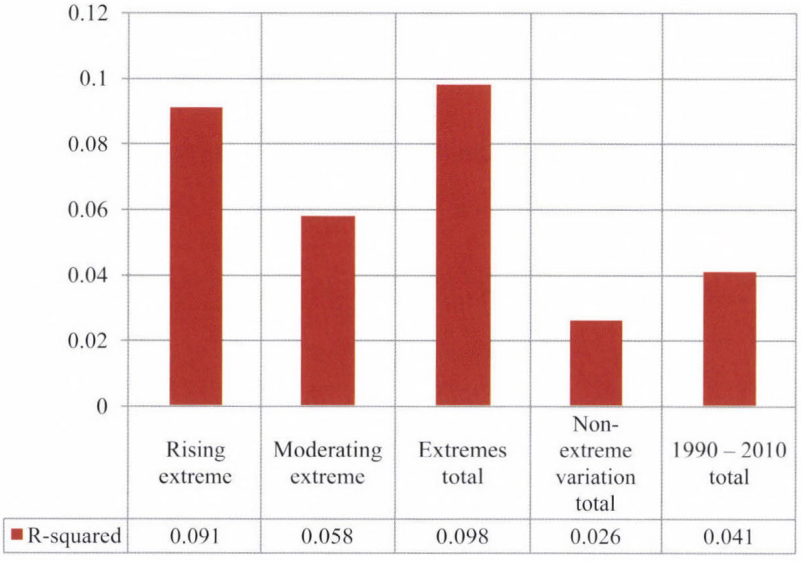

	Rising extreme	Moderating extreme	Extremes total	Non-extreme variation total	1990 – 2010 total
R-squared	0.091	0.058	0.098	0.026	0.041

Fig. 5. The development of multivariate linear regression analysis relation (R-squared) calculated between traffic accidents involving personal injury per estimated traffic and day-to-day variation of meteorological features by meteorological change extremes.

Analyses and classifications in the case of days qualified as extreme in meteorological change show marked interrelations between accidents and climatic variations. Moreover, the more intense the variation, the more powerful the correlation formed with the variation (rise or modification) of accidents.

In accordance with the multivariate linear regression calculated between the extreme meteorological change and accident variation, meteorological variations explained already 9.8 percent of accident variation. In contrast, road traffic accidents involving personal injury under non-extreme meteorological variation conditions can only be attributed in 2.6 percent – more than three and half times smaller proportion than in case of extreme variations – to climatic changes from the previous day. Results of stepwise method applied are summarized in *Table 6*.

Among the components of extreme meteorological variation conditions, the variation of accidents (increase or decrease) was most fundamentally affected by the combination of relative humidity and precipitation (nearly 8.4 percentage point), followed by, together with the previous factors, or independently from them, the nearly 1.0 percentage point effect of temperature variation. The moderated decrease of cloud cover only slightly modified the combined effect of the former factors, and the variation of wind force did not have significant effect. The significance and direction of the partial effect of the various climatic factors were also varied. The decrease of relative humidity and especially of temperature moderated, while the increase of precipitation and the decrease of cloud cover increased the probability of accidents.

Table 6. Multivariate regression interrelations of daily variation of accidents (dependent variable) for estimated traffic with daily meteorological variation indicators (independent variables) (Stepwise method), between 1990 and 2010

Model summary*									
					Change statistics				
Model	R	R-squared	Adjusted R-squared	Std. error of the Estimate	R-squared change	F change	df1	df2	Sig. F change
1	0.262[a]	0.069	0.068	0.64266	0.069	106.043	1	1433	0.000
2	0.290[b]	0.084	0.083	0.63761	0.015	23.830	1	1432	0.000
3	0.307[c]	0.094	0.093	0.63424	0.010	16.235	1	1431	0.000
4	0.313[d]	0.098	0.095	0.63327	0.003	5.384	1	1430	0.020

* Dependent variable: daily variation of the number of accidents for estimated traffic

[a] Predictors: (constant), variation of daily mean relative humidity

[b] Predictors: (constant), variation of daily mean relative humidity, variation of daily mean precipitation amount

[c] Predictors: (constant), variation of daily mean relative humidity, variation of daily mean precipitation amount, variation of daily mean temperature

[d] Predictors: (constant), variation of daily mean relative humidity, variation of daily mean precipitation amount, variation of daily mean temperature, variation of daily mean cloud cover

In the case of non-extreme – slightly deviating from the mean – meteorological changes, only very weak partial relation prevailed among accident variations and the variations in precipitation, cloud cover, air pressure, and temperature, and there was no significant relation with the variation of relative humidity and wind force.

The mutually neutralizing character of the various meteorological factors played significant role in the weakness of the effect on accident variations, because the accident increasing effect of the rise of temperature and the decrease

of air pressure was largely compensated by the accident risk moderating effect of the decrease of precipitation and the growth of cloud cover.

The extreme and non-extreme categories only expressed deviations from the general trend of climatic processes – and not with equal accuracy –, however, they did not reflect the direction of the changes. Consequently, these are not appropriate for the separate examination of interrelations between the development of accidents and the appearance and rising or moderation and disappearance of extremes. Furthermore, they do not offer opportunity to consider and prognosticate the possible consequences on the development of accidents, and in general, on the human and social relations if, in the future, the frequency of appearance and rise, or temporal durability of extreme meteorological conditions should increase compared to non-extreme days and periods. Variation of the daily mean values of the meteorological features by the rate and direction of extremes between 1990 and 2010 is presented in *Fig. 6*.

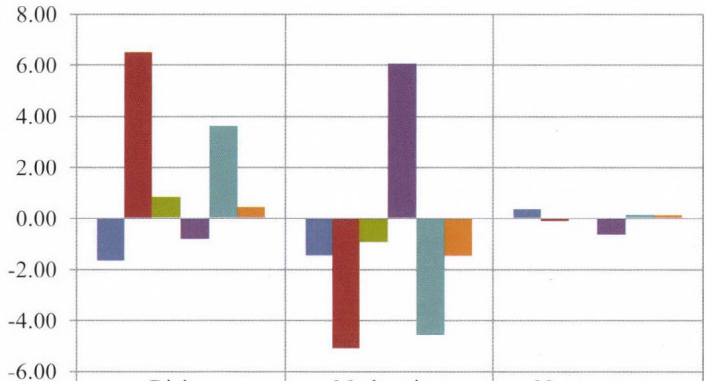

	Rising extreme	Moderating extreme	Non-extreme variation total
Var. of daily mean temperature [°C]	-1.67	-1.45	0.36
Var. of daily mean precipitation amount [mm]	6.49	-5.09	-0.12
Vari. of daily mean wind speed [m/s]	0.84	-0.95	0.02
Var. of daily mean air pressure [hPa]	-0.83	6.06	-0.63
Var. of daily mean relative humidity [% points]	3.61	-4.57	0.14
Var. of daily mean cloud cover [okta]	0.43	-1.46	0.13

Fig. 6. Variation of the daily mean values of the meteorological features by the rate and direction of extremes between 1990 and 2010.

Regarding the direction of extremes in the various categories among the mean values of examined meteorological indicators – excluding temperature variation –, usually significant and partially symmetric differences were developed. For example, while on days with rising extremes, precipitation increased by a mean of 6.5 mm, relative humidity by 3.6% points, wind force by 0.84 m/s, compared to the previous day, then on days with moderating extremes, precipitation decreased by 5.1 mm, relative humidity by 4.6% points, and wind force by 0.95 m/s. However, the variation of air pressure and cloud cover significantly deviated from the generic trend only in the case of moderating extremes. The air pressure increased rather significantly, and cloud cover decreased. However, temperature usually fell in the course of both rising and moderating extremes.

Applied statistical tests have shown that the most significant difference among the various categories by the direction of the extremes appeared in the precipitation amount variation, but the deviations of air pressure, cloud cover and wind force are also rather characteristic. The differences in the variations of relative humidity, and especially that of temperature, are less relevant than the above-mentioned components.

The appearing and rising meteorological extremes already impacted the increase of accidents by nearly 9.1 percentage. The rise of humidity (in nearly 80 percent), the decrease of temperature, and the strengthening of wind had the most significant impact. The effect of the various meteorological components was not restricted to one-way only. The rise of relative humidity (and of the mostly well correlated precipitation amount) and the increase of wind force impacted the increase of accidents, while the moderation of temperature impacted the decrease of accidents. According to the results of regressive analysis, the effect of temperature decrease slowed the increase of the number of accidents by nearly one third.

In the moderating and disappearing extreme periods the relation between the climatic variations and the variation of accidents is significantly weaker (5.8% R-Square) than in the period of rising extremes, yet still more than twice stronger than in the case of non-extreme variations. It may lay behind the relative weakness of the interrelation that the temporal processes of appearing, rising, and moderating, disappearing are not necessarily of the same length. In moderating extreme periods, the moderation of precipitation amount, closely followed by the moderation of temperature and relative humidity had the most significant impact on the characteristic decrease of accidents. At the same time, the decrease of cloud cover affected the increase of accidents, and as a result, the one-third slower moderation of the number of accidents.

3. Relationship between traffic accidents and key meteorological components

More detailed analyses uncovered significantly stronger relations than in case of categories containing the direction and intensity of meteorological variations rather aggregated regarding the extremes. Especially in the case of the most extreme variation of meteorological conditions, and in the autumn and winter periods, strong correlation was formed with the variation of accidents.

Among the meteorological types of variations came from the 25-element solution, in the case of the group carrying the unfolding of the most extreme variation, the number of accidents increased already in nearly one fifth as the effect of the climatic variations (especially the excessively significant increase of precipitation amount and relative humidity, and decrease of air pressure and temperature) to an outstanding level exceeding the mean value of rising extremity nearly two and a half times. The type is particularly characterized by above the average proportion of summer days with rain, rain shower, and thunderstorm. The number of rainy days is six times, and those with rain shower, and thunderstorm is nearly three times higher than the national average. The climatic determination of accident locations and situations also shows characteristic features. Meteorological variation had particularly significant effect on the development of the frequency of accidents involving slight injuries, hitting pedestrians, oncoming traffic, road bends, and residential area. The effects on accidents involving slight injury nearly ten times, and on accidents involving hitting pedestrians and occurring in road bends over eight times exceeded the general impact.

The strengthening of the interrelation between the intensity of meteorological extremes and the increase of the frequency of accidents can be typically explained by the grouping by direction and intensity of the variation of the analyzed primary meteorological features. In a method identical with multidimensional classifications, the categorization of the various meteorological indicators was also performed with automatic classification technique (K-mean clustering) – in order that the result of classification factually express the spatial distance among the groups as regards their content.

Seven search groups were conventionally determined, therefore because of the differences among the distributions, the number of days significantly differs in the various categories. For example, barely one percent of the days of the examined 21 years was classified into the category of the most intensive precipitation increase, and nearly identically with this proportion, the element number of the most extreme temperature variation (increase and decrease) categories increasing (*Figs. 7* and *8*).

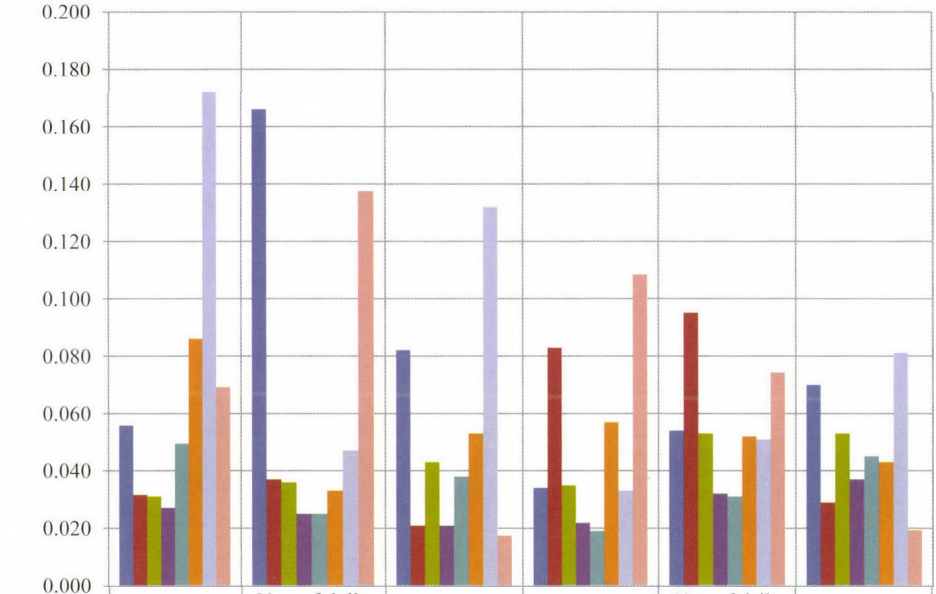

	Var. of daily mean temperature [°C]	Var. of daily mean precipitation amount [mm]	Var. of daily mean wind speed [m/s]	Var. of daily mean air pressure [hPa]	Var. of daily mean relative humidity [% points]	Var. of daily mean cloud cover [okta]
Cluster 1	0.056	0.166	0.082	0.034	0.054	0.070
Cluster 2	0.032	0.037	0.021	0.083	0.095	0.029
Cluster 3	0.031	0.036	0.043	0.035	0.053	0.053
Cluster 4	0.027	0.025	0.021	0.022	0.032	0.037
Cluster 5	0.050	0.025	0.038	0.019	0.031	0.045
Cluster 6	0.086	0.033	0.053	0.057	0.052	0.043
Cluster 7	0.172	0.047	0.132	0.033	0.051	0.081
Total	0.069	0.137	0.017	0.108	0.074	0.019

Fig. 7. Multivariate linear interrelation of daily variation of accidents for traffic with the totality of daily meteorological variations (R-squared) calculated by clusters obtained by automatic classification of certain meteorological variation components.

The offered charts clearly indicate that progressing from the general trend of variations towards the intensification of extremities by an approximately U-shaped curve the effect of the various meteorological factors is increasingly stronger on the development of accidents, and depending on the direction of the variation, increasingly more significant scale variation (rise or decrease) occurred in the number of accidents, as well.

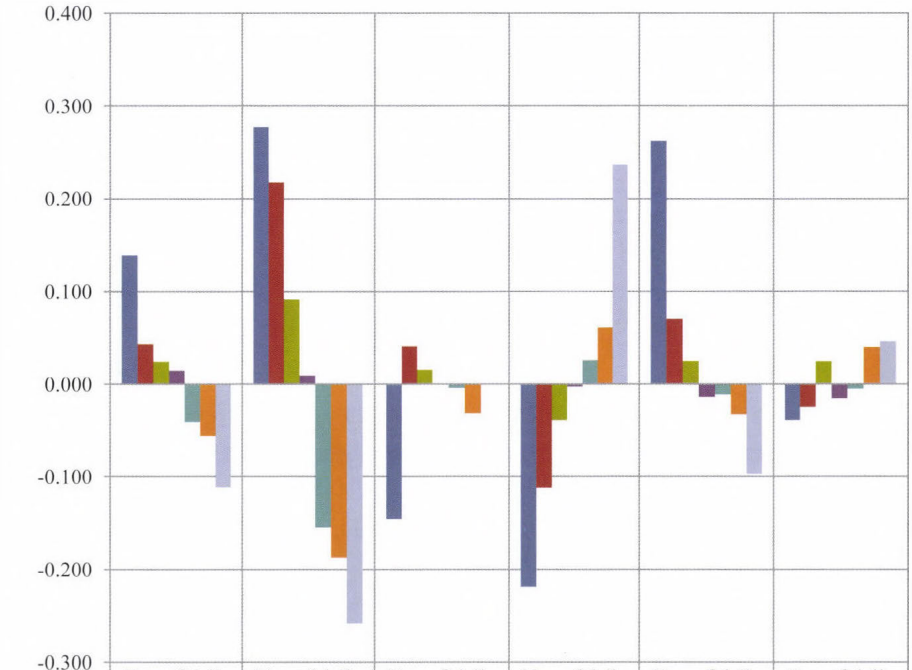

	Var. of daily mean temperature [°C]	Var. of daily mean precipitation amount [mm]	Var. of daily mean wind speed [m/s]	Var. of daily mean air pressure [hPa]	Var. of daily mean relative humidity [% points]	Var. of daily mean cloud cover [okta]
Cluster 1	0.139	0.277	-0.146	-0.219	0.263	-0.039
Cluster 2	0.043	0.217	0.041	-0.112	0.070	-0.025
Cluster 3	0.024	0.091	0.015	-0.039	0.024	0.024
Cluster 4	0.015	0.009	0.000	-0.003	-0.014	-0.016
Cluster 5	-0.041	-0.155	-0.004	0.025	-0.011	-0.005
Cluster 6	-0.056	-0.187	-0.031	0.061	-0.033	0.040
Cluster 7	-0.111	-0.258	-0.001	0.236	-0.097	0.046

Fig. 8. Mean of daily variation of accidents for traffic calculated by clusters obtained by automatic classification of certain meteorological variation components.

In the case of the most extreme categories according to the increase of precipitation amount and the decrease of temperature, the combined effect of all the meteorological factors exceeds four times the average, and more than six times the average of non-extreme days. It can be said of all the above-mentioned categories, that the significant scale variation of accidents (increase in the case of precipitation variation and decrease in the case of temperature variation) was already induced in a proportion of one-sixth by meteorological change or inappropriate accommodation to these.

Besides the above mentioned facts, the combined effect of meteorological variation factors was very significant in the most extreme categories as regards wind force strengthening (8.2 and 13.2 percent) but in the frames of both extremes the accident moderating effect became dominant. Furthermore, this effect was significant on the opposing poles of the variation of cloud cover (7, and 8.1 percent determination). The relationship between the variation of accidents and cloud cover – jus as that of air pressure variation – essentially developed inversely as temperature and precipitation variation, because the increase of cloud cover and air pressure amount correlates with the moderation of accidents, while the decrease of these factors correlates with the increase of accidents.

In contrast to the most extreme – mostly containing the rise – categories of air pressure and relative humidity variation, the relationship of one degree less extreme categories was the strongest with the variation of accidents, while accident variation was the most intensive in the most extreme categories. It cannot be excluded, that the use of multidimensional, nonlinear methods or the proper transformation of variants should lead to different results.

4. Relationship between traffic accidents and extreme meteorological variations

The determination by meteorological variations of accident development changed extraordinarily differently by the seasons. The spring and summer period determination does not reach even half of the average, and only in the period of the moderation of extremes does remarkable relationship manifest itself. In contrast, in the second half-year, meteorological extremes had significant – 17.4 percent in autumn, 13.4 percent in winter – effect on the development of accidents. The linear regressive interrelations (R-squared) between the daily variations by seasons of road traffic accidents involving personal injury and meteorological conditions are shown in *Fig. 9.*

The differences can be partially explained by the unequal distribution of extreme meteorological conditions, according to which, in the second half-year, the frequency of extreme variations characteristically exceeded the average in winter, typically because of the excessive proportion of moderating extremes, while in spring, it significantly fell short of it. The proportion of rising extreme days, on the other hand, exceeded the prorated distribution, especially in summer and autumn. Distribution of daily variations categorized by the type of meteorological extremity across the seasons is presented in *Fig. 10*, while seasonal averages of road accidents involving personal injury for estimated traffic, between 1990 and 2010 can be found in *Fig. 11.*

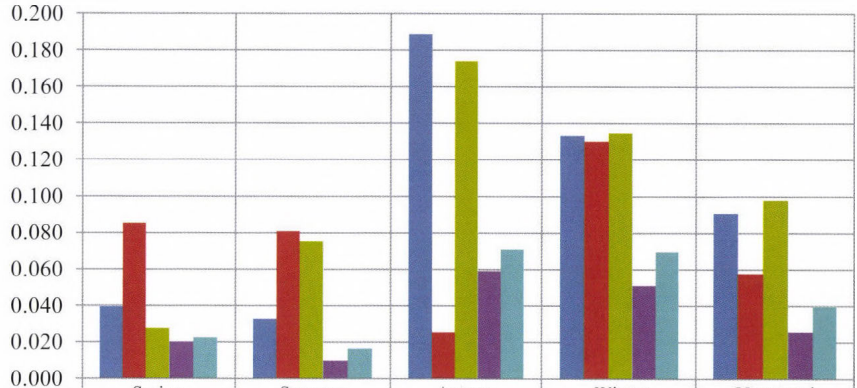

	Spring	Summer	Autumn	Winter	Year total
Rising extreme	0.040	0.033	0.189	0.134	0.091
Moderating extreme	0.085	0.081	0.026	0.130	0.058
Extreme days total	0.028	0.075	0.174	0.135	0.098
Non-extreme days total	0.020	0.010	0.059	0.051	0.026
1990 – 2010 days total	0.023	0.017	0.071	0.070	0.040

Fig. 9. Linear regressive interrelations (R-squared) between the daily variations by seasons of road traffic accidents involving personal injury and meteorological conditions, between 1990 and 2010.

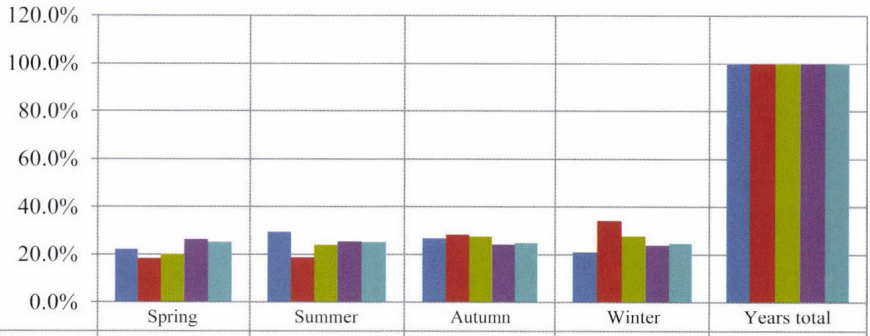

	Spring	Summer	Autumn	Winter	Years total
Rising extreme	22.3%	29.7%	26.8%	21.2%	100.0%
Moderating extreme	18.4%	18.8%	28.6%	34.3%	100.0%
Extreme days total	20.3%	24.0%	27.7%	27.9%	100.0%
Non-extreme days total	26.3%	25.5%	24.3%	24.0%	100.0%
1990 – 2010 days total	25.2%	25.2%	24.9%	24.7%	100.0%

Fig. 10. Distribution of daily variations categorized by the type of meteorological extremes across the seasons.

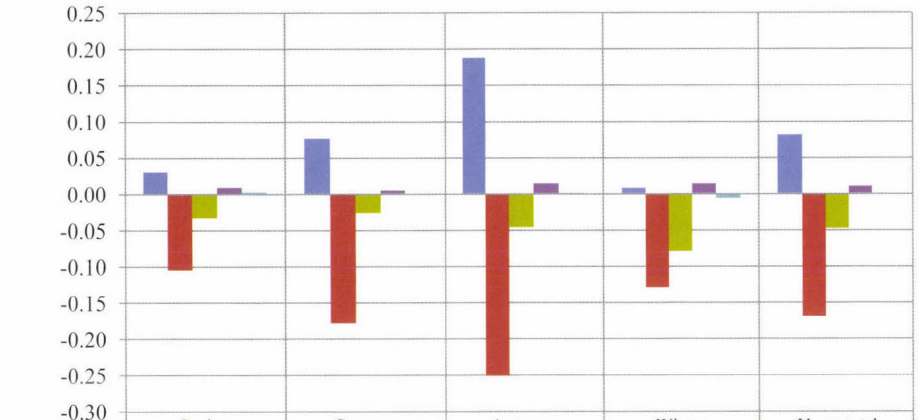

	Spring	Summer	Autumn	Winter	Years total
Rising extreme	0.03	0.08	0.19	0.01	0.08
Moderating extreme	-0.10	-0.18	-0.25	-0.13	-0.17
Extreme days total	-0.03	-0.03	-0.05	-0.08	-0.05
Non-extreme days total	0.01	0.01	0.01	0.01	0.01
1990 – 2010 days total	0.00	0.00	0.00	-0.01	0.00

Fig. 11. Seasonal averages of road accidents involving personal injury for estimated traffic between 1990 and 2010.

The variation in the number of accidents under unfolding and rising extreme conditions increased in autumn – more than twofold – above the average, and the relationship between accidents and climate variations was the strongest in this season, as well. To an extent nearly one-fifth, the complex impact of climate variation, but especially, the variation of relative humidity (and behind this, the mostly well correlated cloud cover and precipitation amount variation) and the variation of temperature and wind force impacted the development of accidents. The increase of relative humidity and strengthening of wind force impacted the increase of accidents, while the decrease of temperature impacted the decrease of accidents, however, it could only partially slow the increase of accidents. Variation of daily average value of the main meteorological features and the traffic accidents related to estimated traffic density due to previous day in case of rising extremes by seasons is shown in *Fig. 12,* while the development of the calculated standardized Beta coefficient between the daily variations of the traffic accidents with personal injury related to estimated traffic density and the daily variations of the meteorological features in case of rising extremes by seasons is presented in *Fig. 13.*

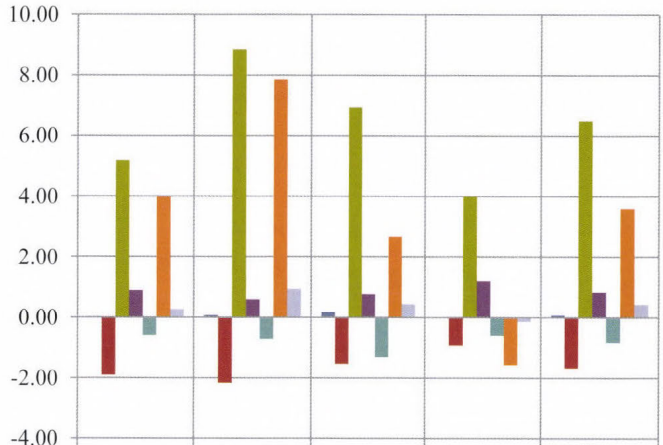

	Spring	Summer	Autumn	Winter	Rising extremes total
Daily var. of the number of accidents for estimated traffic [accident / hundred thousand vehicles]	0.03	0.08	0.19	0.01	0.08
Var. of daily mean temperature [°C]	-1.90	-2.16	-1.53	-0.92	-1.67
Var. of daily mean precipitation amount [mm]	5.18	8.85	6.94	4.00	6.49
Var. of daily mean wind speed [m/s]	0.90	0.59	0.76	1.21	0.84
Var. of daily mean air pressure [hPa]	-0.60	-0.72	-1.31	-0.60	-0.83
Var. of daily mean relative humidity [% points]	3.99	7.87	2.66	-1.56	3.61
Var.of daily mean cloud cover [okta]	0.27	0.94	0.44	-0.14	0.43

Fig. 12. Variation of daily average value of the main meteorological features and the traffic accidents related to estimated traffic density due to previous day in case of rising extremes by seasons between 1990 and 2010.

Opposed to the autumn periods of rising extremes, the increase of accident numbers in winter reached only one tenth of the average of this type; despite that the totality of meteorological effects directed toward it was relatively significant (13.4 percent). The increase of precipitation amount and the strengthening of wind were especially impacting the increase of accidents, while its decrease was affected characteristically by decreasing relative humidity and decrease of temperature (unlike the rest of the seasons). The moderate increase in the number of accidents is primarily explained by that, in total, in the winter, the intensity of the variation of components of climatic conditions – with the exception of wind force, which increased in a rate exceeding that of the other seasons – was far below the 1990–2010 average of rising extreme variation.

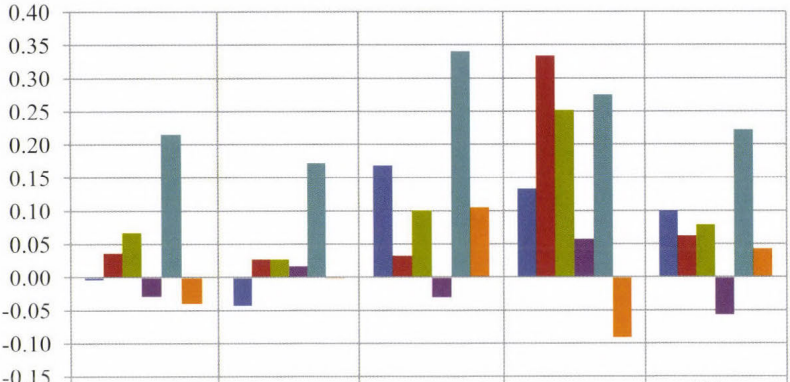

	Spring	Summer	Autumn	Winter	Rising extreme total
Var. of daily mean temperature [°C]	0.00	-0.04	0.17	0.13	0.10
Var. of daily mean precipitation amount [mm]	0.04	0.03	0.03	0.33	0.06
Var. of daily mean wind speed [m/s]	0.07	0.03	0.10	0.25	0.08
Var. of daily mean air pressure [hPa]	-0.03	0.02	-0.03	0.06	-0.06
Var. of daily mean relative humidity [% points]	0.22	0.17	0.34	0.28	0.22
Var. of daily mean cloud cover [okta]	-0.04	0.00	0.11	-0.09	0.04

Fig. 13. Development of the calculated standardized Beta coefficient between the daily variations of the traffic accidents with personal injury related to estimated traffic density and the daily of the meteorological features in case of rising extremes by seasons.

In the spring and summer periods of appearing, rising extremes, only relatively weak (4 and 3.3%, respectively) multivariate linear relationship prevailed between the variation of accidents and climatic conditions; and the change in the number of accidents developed below the average of the category averages, especially in spring, however, still exceeding nearly three times the extent of winter variation. In both seasons, only the increase of relative humidity (or, behind that, the increase of cloud cover and precipitation) had substantial effect on the increase of accidents, yet this effect was much weaker than in autumn or – with different sign – in winter. The different extent increase of accidents was basically brought about by the significantly different intensity of meteorological variations. While springtime variations developed in an extent nearly identical with the annual average of the category, then the relative humidity and cloud cover increased with more than double, and precipitation amount more than one third above the average in the summer period of rising extremes. Only the extent of the increase of wind force fell below the average.

5. *Relationship between traffic accidents and extreme meteorological variations by accident severity, and situation*

Looking at the whole of the 1990–2010 period, the relationship of climatic variations with a more detailed breakdown of accidents – with the development by outcomes involving persons, gravity, accident locations and situations – is rather weak, falling behind the already described overall effect (*Table 7*).

Table 7. Development of multivariate linear regression relationships of the daily variation of meteorological variations and accidents involving personal injury per accident consequences, locations, and situations, and the extremity of meteorological change

Absolute variation from the previous day	Rising extreme days	Moderating extreme days	Extreme days total	Non-extreme days total	Days total in 1990–2010
	R-squared				
Variation of number of accidents	0.104	0.063	0.097	0.027	0.041
Variation of number of fatal accidents	0.026	0.021	0.015	0.005	0.006
Variation of number of serious accidents	0.062	0.036	0.052	0.013	0.020
Variation of number of slight accidents	0.076	0.045	0.079	0.022	0.032
Variation of number of accidents in residential areas	0.061	0.049	0.049	0.025	0.029
Variation of number of accidents outside residential areas	0.121	0.035	0.111	0.016	0.036
Variation of number of accidents on straight paths	0.074	0.038	0.063	0.014	0.023
Variation of number of accidents in road bends	0.117	0.056	0.120	0.014	0.035
Variation of number of accidents in road crossings	0.040	0.046	0.037	0.028	0.027
Variation of number of accidents in other road sections	0.022		0.010		0.003
Variation of number of accidents due to head-on collision of vehicles	0.160	0.053	0.150	0.027	0.055
Variation of number of accidents due to collision of vehicles travelling in the same direction	0.008	0.050	0.023	0.010	0.012
Variation of number of accidents due to collision of vehicles crossing paths	0.006	0.033	0.013	0.022	0.018
Variation of number of accidents due to slipping, skidding, tipping on road	0.015	0.017	0.012	0.003	0.004
Variation of number of accidents involving hitting pedestrian	0.077	0.013	0.049	0.012	0.021

(Note: The table contains only significant statistics.)

Interrelation stronger than the average can we observed only in the case of accidents due to collision of vehicles travelling towards each other ; however, this is not explained by the effects characterized days without meteorological extremes, but by the extremely strong consequences of the appearance and rise of extremes affecting the whole category. The increase in the number of accidents due to the collision of vehicles travelling towards each other in the period of appearing and rising extreme meteorological conditions – beyond all other categories shown in the table – was determined by climatic variations in a proportion of nearly one sixth, or at least developed synchronously with those in this degree. The formation of the interrelation and the significant increase of accidents in scale were primarily (in nearly 90 percent) impacted by the increase of relative humidity of air, and, in the remaining proportion, by the decrease of air pressure.

Besides the above category, meteorological change had particularly significant impact on the increase of accidents outside residential areas and in road bends in an extent exceeding the average of the category of the total appearing and rising extremes (nearly 12 percent). The overall effect was, however, less significant; but in the case of accidents involving hitting pedestrians – in general slight and serious accidents –, on straight paths and in residential areas, the effect of climatic variations in the period of rising extremes exceeds multiple times those prevailing in non-extreme periods. (For example: in the case of hitting pedestrians, nearly six times, and three-four times in the case of accidents involving slight and serious injuries and on straight path, and over twice in case of accidents in residential areas.) Although, in total, the determination of the variation of fatal accidents by climatic variations can be regarded to be modest, it was nearly five times stronger among extreme meteorological conditions than in other periods.

6. Future expected tendencies between traffic accidents and key meteorological variations

The time series data of the endeavor to differentiate extreme and non-extreme meteorological changes show, that between 1990 and 2010 the climatic variations became somewhat more extreme. This is supported by the data expressing the annual proportions of extreme, and appearing and rising extreme days, and the linear trends calculated on their basis. The relatively detailed classification and the reclassified – giving a broader sense to extremity – categorization essentially led to the same result. According to both approaches, the linear trend of extremity and rising extremes – in spite of fluctuations – took a decidedly upward direction. Proportion of extreme days as well as that of rising extreme days is shown in *Figs. 14* and *15*.

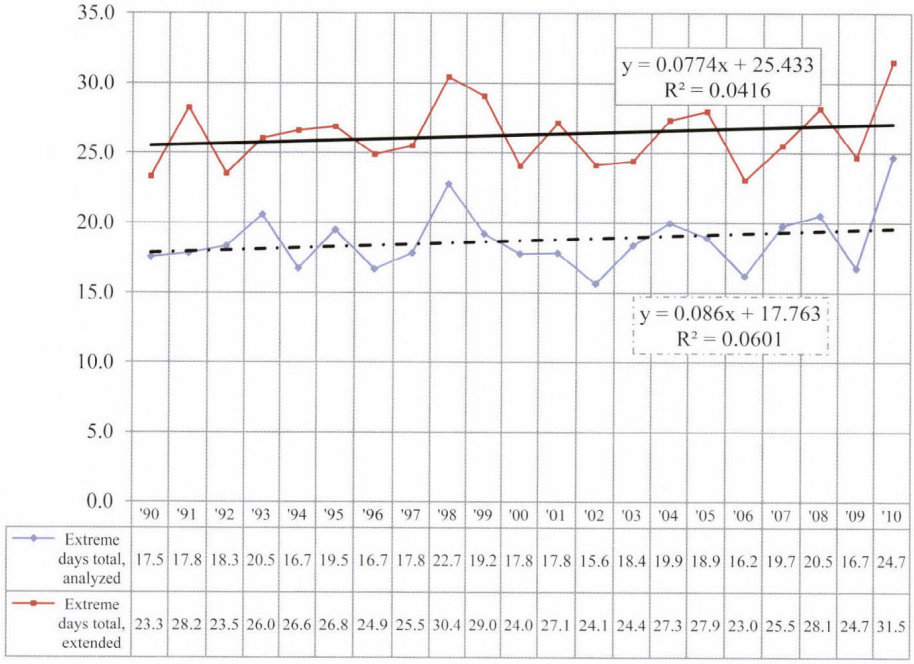

	'90	'91	'92	'93	'94	'95	'96	'97	'98	'99	'00	'01	'02	'03	'04	'05	'06	'07	'08	'09	'10
Extreme days total, analyzed	17.5	17.8	18.3	20.5	16.7	19.5	16.7	17.8	22.7	19.2	17.8	17.8	15.6	18.4	19.9	18.9	16.2	19.7	20.5	16.7	24.7
Extreme days total, extended	23.3	28.2	23.5	26.0	26.6	26.8	24.9	25.5	30.4	29.0	24.0	27.1	24.1	24.4	27.3	27.9	23.0	25.5	28.1	24.7	31.5

Fig. 14. Proportion of extreme days between 1990 and 2010 (%).

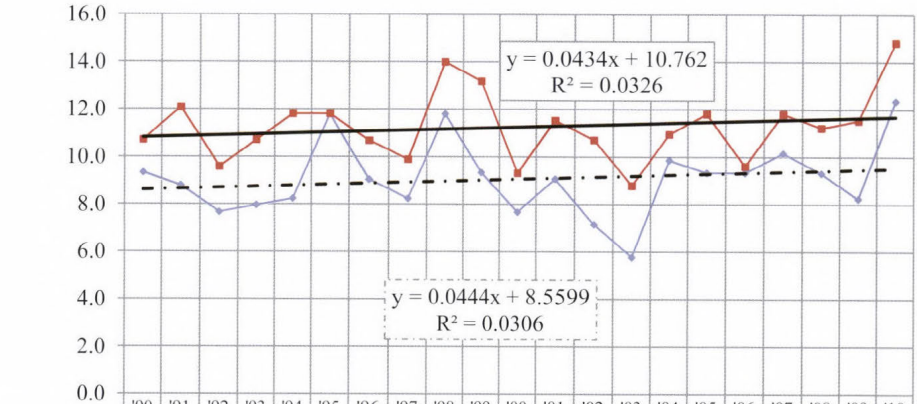

	'90	'91	'92	'93	'94	'95	'96	'97	'98	'99	'00	'01	'02	'03	'04	'05	'06	'07	'08	'09	'10
Rising extreme, analyzed	9.3	8.8	7.7	7.9	8.2	11.8	9.0	8.2	11.8	9.3	7.7	9.0	7.1	5.8	9.8	9.3	9.3	10.1	9.3	8.2	12.3
Rising extreme, extended	10.7	12.1	9.6	10.7	11.8	11.8	10.7	9.9	14.0	13.2	9.3	11.5	10.7	8.8	10.9	11.8	9.6	11.8	11.2	11.5	14.8

Fig. 15. Proportion of rising extreme days between 1990 and 2010 (%).

The variability trends of the various meteorological features mostly support the picture painted by the typologies. The linear trends of temperature, precipitation, air pressure, and relative humidity – although to varying extent – refer to the rising of extremes, while that of wind force and cloud cover to moderating extremes. Absolute deviation (range) by the year of the daily variation of the meteorological indicators between 1990 and 2010 is presented in *Fig. 16.*

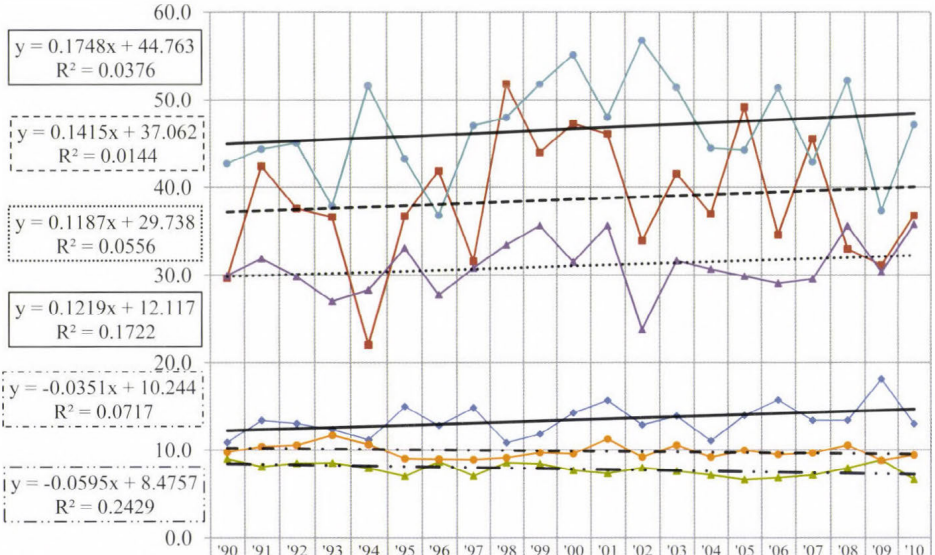

	'90	'91	'92	'93	'94	'95	'96	'97	'98	'99	'00	'01	'02	'03	'04	'05	'06	'07	'08	'09	'10
Var. of daily mean temperature [°C]	10.9	13.5	13.1	12.4	11.2	15.0	12.9	14.9	10.9	11.9	14.3	15.7	12.9	13.9	11.1	14.0	15.8	13.4	13.5	18.2	13.1
Var. of daily mean precipitation amount [mm]	29.7	42.4	37.6	36.7	22.1	36.8	41.9	31.6	51.9	44.0	47.3	46.1	33.9	41.6	37.0	49.2	34.6	45.6	33.0	31.2	36.8
Var. of daily mean wind speed [m/s]	9.0	8.1	8.5	8.6	8.0	7.1	8.7	7.1	8.6	8.5	7.7	7.4	8.0	7.6	7.2	6.7	6.9	7.2	8.0	8.9	6.7
Var. of daily mean air pressure [hPa]	30.0	31.9	29.9	27.0	28.3	33.1	27.8	30.9	33.5	35.7	31.5	35.7	23.8	31.7	30.7	29.9	29.1	29.6	35.6	30.4	35.8
Var. of daily mean relative humidity [% points]	42.8	44.4	45.1	37.9	51.7	43.3	36.9	47.1	48.0	51.8	55.2	48.1	56.8	51.5	44.5	44.3	51.4	42.9	52.3	37.4	47.2
Var. of daily mean cloud cover [okta]	9.8	10.4	10.6	11.7	10.7	9.1	9.0	8.9	9.2	9.7	9.6	11.3	9.2	10.6	9.2	10.0	9.5	9.7	10.6	8.8	9.4

Fig. 16. Absolute deviation (range) by the year of the daily variation of the meteorological indicators between 1990 and 2010.

On the basis of interrelationships seen between the slight extremization of meteorological variations, furthermore the extreme climatic variations and the variation of traffic accidents involving personal injury, it could be assumed that approaching our days, the connection would be further strengthened. This

hypothesis, however, was supported neither by the totality of meteorological variations, nor the statistical analyses of the various extremity categories.

According to the linear regression analysis of the annual (and three-year period) relationships of accident and meteorological variations, the correlation essentially did not change between 1990 and 2010, however, compared to 1993, the correlation weakened, and there were significant fluctuations within the period. (Note, that statistically not significant relations are not shown in the diagrams.) Results are shown in *Figs. 17, 18,* and *19.*

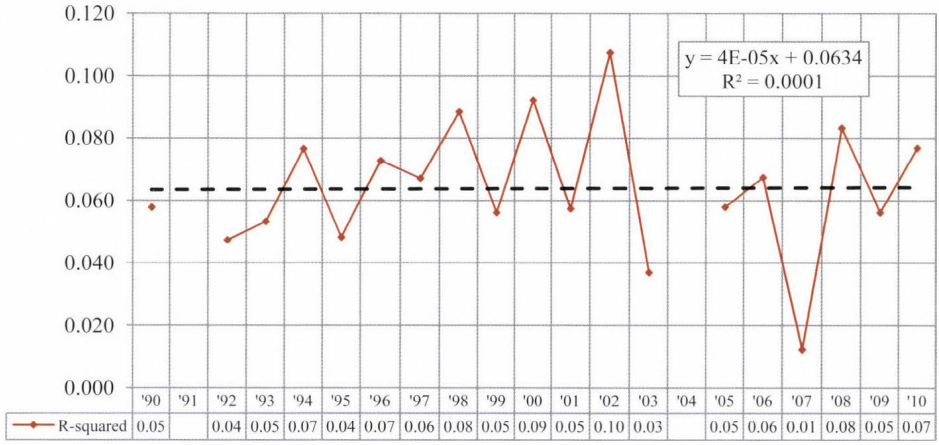

	'90	'91	'92	'93	'94	'95	'96	'97	'98	'99	'00	'01	'02	'03	'04	'05	'06	'07	'08	'09	'10
R-squared	0.05		0.04	0.05	0.07	0.04	0.07	0.06	0.08	0.05	0.09	0.05	0.10	0.03		0.05	0.06	0.01	0.08	0.05	0.07

Fig. 17. The multivariate linear regression analysis interrelation (R-squared) calculated among the daily variation of traffic accidents involving personal injury with the daily variation of analyzed meteorological characteristics between years 1990 and 2010.

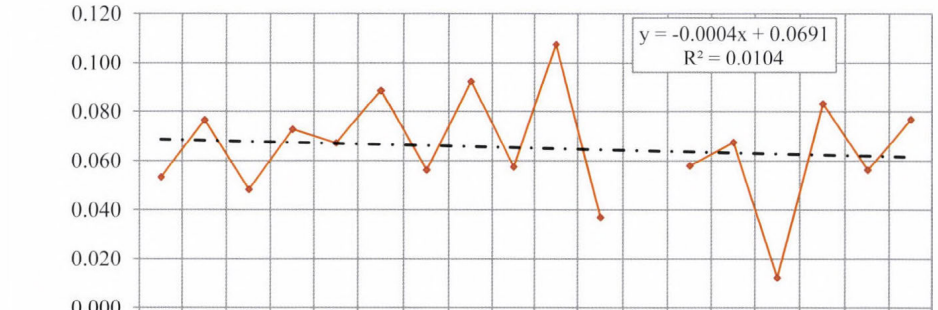

	'93	'94	'95	'96	'97	'98	'99	'00	'01	'02	'03	'04	'05	'06	'07	'08	'09	'10
R-squared	0.053	0.076	0.048	0.073	0.067	0.088	0.056	0.092	0.057	0.107	0.037		0.058	0.067	0.012	0.083	0.056	0.077

Fig. 18. The multivariate linear regression analysis interrelation (R-squared) calculated among the daily variation of traffic accidents involving personal injury with the daily variation of analyzed meteorological characteristics between years 1993 and 2010.

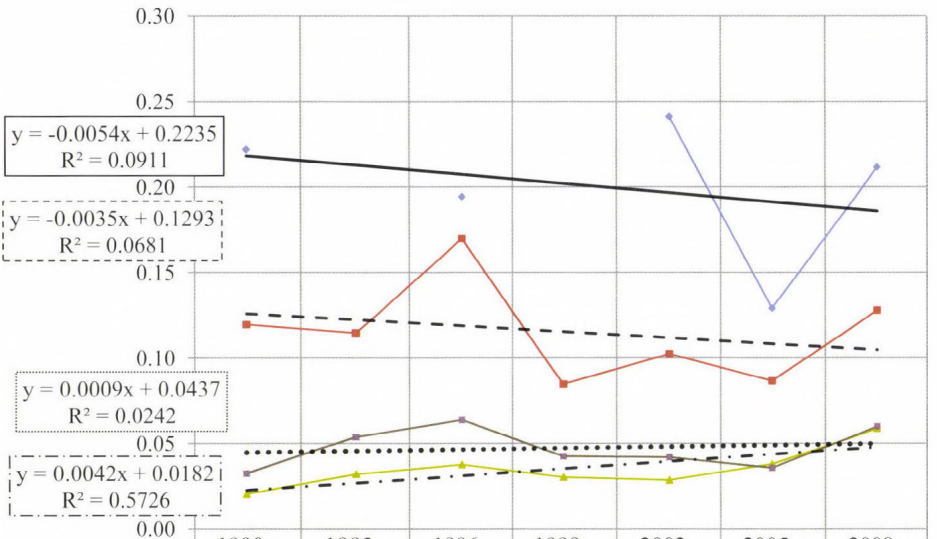

	1990 - 1992	1993 - 1995	1996 - 1998	1999 - 2001	2002 - 2004	2005 - 2007	2008 - 2010
Rising extremes	0.22		0.19		0.24	0.13	0.21
Extreme days total	0.12	0.11	0.17	0.08	0.10	0.09	0.13
Non-extreme days	0.02	0.03	0.04	0.03	0.03	0.04	0.06
Days total	0.03	0.05	0.06	0.04	0.04	0.04	0.06

Fig. 19. The multivariate linear regression interrelations (R-squared) calculated among the daily variation of traffic accidents involving personal injury with the daily variation of analyzed meteorological features, between 1990 and 2010, in three years breakdown.

Presumably, the weakness and weakening of relationships can primarily be explained by the rather significant moderation of total traffic accidents involving personal injury, by their relatively hectic development, and by economic processes and regulatory environment affecting the above. In 2010, the number of accidents was nearly forty percent lower than in 1990, primarily on account of the decrease of fatal and serious accidents. At the same time, the number of slight accidents fell only by 21.8% compared to 1990; what's more, between 1993 and 2010, it moreover even increased. On account of the above circumstances, it seemed appropriate to extend the analysis to slight accident data between 1993 and 2010. The result of this shows that interrelation between extreme climatic variations and the variation of traffic accidents involving slight personal injury strengthened in the analyzed epoch (*Figs. 20* and *21*).

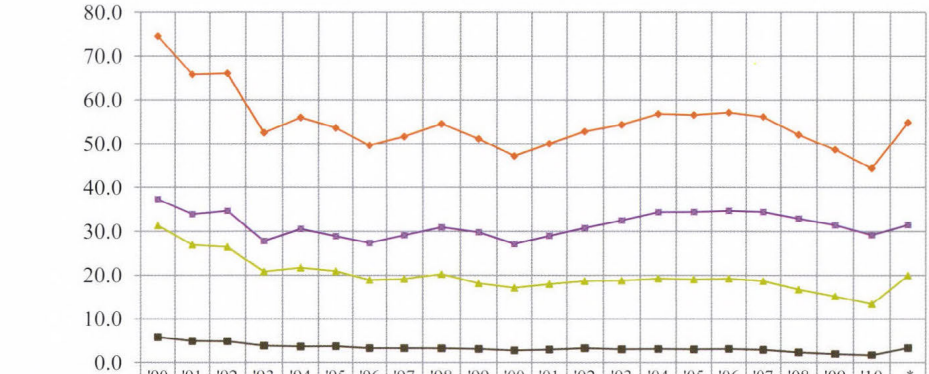

	'90	'91	'92	'93	'94	'95	'96	'97	'98	'99	'00	'01	'02	'03	'04	'05	'06	'07	'08	'09	'10	*
Number of accidents	74.6	65.9	66.1	52.6	56.0	53.7	49.7	51.7	54.6	51.2	47.2	50.1	52.9	54.4	56.8	56.6	57.2	56.2	52.1	48.7	44.4	54.9
Number of fatal accidents	5.8	5.0	4.9	3.9	3.7	3.8	3.4	3.4	3.3	3.2	2.8	3.0	3.3	3.1	3.2	3.1	3.2	3.0	2.4	2.0	1.8	3.4
Number of serious injury accidents	31.4	27.0	26.5	20.8	21.7	20.9	18.9	19.2	20.3	18.2	17.2	18.0	18.7	18.8	19.3	19.1	19.2	18.7	16.8	15.2	13.4	20.0
Number of slight injury accidents	37.4	34.0	34.7	27.9	30.6	29.0	27.4	29.2	31.0	29.9	27.2	29.0	30.8	32.5	34.4	34.5	34.7	34.5	33.0	31.5	29.2	31.5

*1991–2010 annual average

Fig. 20. Road traffic accidents involving personal injury between 1900 and 2010.

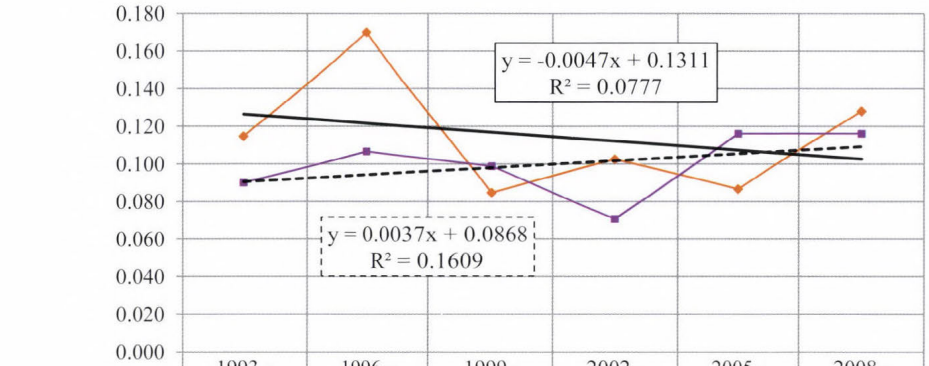

	1993 - 1995	1996 - 1998	1999 - 2001	2002 - 2004	2005 - 2007	2008 - 2010
Daily var. of accident numbers	0.115	0.170	0.085	0.103	0.087	0.128
Daily var.of slight accident numbers	0.090	0.107	0.099	0.071	0.116	0.116

Fig. 21. Three-year multivariate linear interrelations of day-to-day variation of accidents and meteorological conditions between 1993 and 2010 (R-squared) in case of extreme variation.

Naturally, the above described results will provide little guidance to the prognosticability of future developments; however, on the basis of the analysis results, it can be said that the significant future rise of extreme meteorological conditions, and, possibly as a result, the appearing and rising climate change will have significant effect on the development, on the number of accidents, or on the deceleration of the rate of moderation, and, in general, on the development of social relations, which are generally relatively well represented by accident conditions.

7. Conclusions

Compared to other economically and socially important sectors such as energy, water resources, agriculture, and human health (*Törő et al.*, 2010), the assessment of the potential impacts of climate change on transport and road accidents is an area with very limited investigations so far. The increased demand for personal mobility, the dependence on reliable movement of goods and components in the supply chain, and the observed disruption effect of the weather (*Koetse* and *Rietveld*, 2009) make the study of current and future transport resilience essential.

The investigations presented above might provide a potential guidance to the expectation of future developments in the forthcoming decades. On the basis of the results, it can probably be said that the expected increase in the number and intensity of extreme meteorological conditions can have a visible effect on the increase of the number of road accidents. The problem is rather complex, since the future climate change is expected to influence several layers of the social conditions as well, which is also going to be reflected in the road accident conditions.

Acknowledgements: This work is connected to the scientific project „Infocommunication technologies and the society of the future – Project ID: TÁMOP-4.2.2.C-11/1/KONV-2012-0013" of BME VIKING Zrt. (Budapest, Magyar tudósok körútja 2. H-1117) supported by European Social Fund. The assisstance of the Hungarian Meteorological Service in providing surface meteorological data for this research is also highly acknowledged.

References:

Andersson, A. and *Chapman, L.*, 2011: The impact of climate change on winter road maintenance and traffic accidents in West Midlands, UK. *Accident Anal. Prev. 43*, 284–289.

Edwards, J.B., 1999: The temporal distribution of road accidents in adverse weather. *Meteorol. Appl. 6*, 59–68.

Jaroszweski, D., Chapman, L. and *Petts, J.*, 2010: Assessing the potential impact of climate change on transportation: the need for an interdisciplinary research. *J. Transp. Geogr. 18*, 331–335.

Koetse, M.J. and *Rietveld, P.*, 2009: The Impact of climate change and weather on transport: an overview of empirical findings. *Transport. Res. Part D, 14*, 205–221.

Sándor, Zs.P., 2013: Az esőzés hatása a hazai autópályák forgalmi jellemzőire. *Közlekedéstudományi Szemle 63*, 25–35. (In Hungarian)

Suarez, P., Anderson, W., Mahal, V. and *Lakshmanan, T.R.*, 2005. Impacts of flooding and climate change on urban transportation: A systemwide performance assessment of the Boston Metro Area. *Transport. Res. Part D 10*, 231–244.

Törő. K., Bartholy. J., Pongrácz. R., Kiss. Zs., Keller. É. and *Dunay. Gy.*, 2010: Evaluation of meteorological factors on sudden cardiovascular death. *J. Forensic Legal Med. 17*, 236–242.

IDŐJÁRÁS

VOLUME 118 * 2014

BUDAPEST, HUNGARY

AUTHOR INDEX

TABLE OF CONTENTS

SUBJECT INDEX

A

V

W

INSTRUCTIONS TO AUTHORS OF *IDŐJÁRÁS*

The purpose of the journal is to publish papers in any field of meteorology and atmosphere related scientific areas. These may be

- research papers on new results of scientific investigations,
- critical review articles summarizing the current state of art of a certain topic,
- short contributions dealing with a particular question.

Some issues contain "News" and "Book review", therefore, such contributions are also welcome. The papers must be in American English and should be checked by a native speaker if necessary.

Authors are requested to send their manuscripts to

Editor-in Chief of IDŐJÁRÁS
P.O. Box 38, H-1525 Budapest, Hungary
E-mail: journal.idojaras@met.hu

including all illustrations. MS Word format is preferred in electronic submission. Papers will then be reviewed normally by two independent referees, who remain unidentified for the author(s). The Editor-in-Chief will inform the author(s) whether or not the paper is acceptable for publication, and what modifications, if any, are necessary.

Please, follow the order given below when typing manuscripts.

Title page: should consist of the title, the name(s) of the author(s), their affiliation(s) including full postal and e-mail address(es). In case of more than one author, the corresponding author must be identified.

Abstract: should contain the purpose, the applied data and methods as well as the basic conclusion(s) of the paper.

Key-words: must be included (from 5 to 10) to help to classify the topic.

Text: has to be typed in single spacing on an A4 size paper using 14 pt Times New Roman font if possible. Use of S.I. units are expected, and the use of negative exponent is preferred to fractional sign. Mathematical formulae are expected to be as simple as possible and numbered in parentheses at the right margin.

All publications cited in the text should be presented in the *list of references*, arranged in alphabetical order. For an article: name(s) of author(s) in Italics, year, title of article, name of journal, volume, number (the latter two in Italics) and pages. E.g., *Nathan, K.K.,* 1986: A note on the relationship between photo-synthetically active radiation and cloud amount. *Időjárás 90,* 10-13. For a book: name(s) of author(s), year, title of the book (all in Italics except the year), publisher and place of publication. E.g., *Junge, C.E.,* 1963: *Air Chemistry and Radioactivity.* Academic Press, New York and London. Reference in the text should contain the name(s) of the author(s) in Italics and year of publication. E.g., in the case of one author: *Miller* (1989); in the case of two authors: *Gamov* and *Cleveland* (1973); and if there are more than two authors: *Smith et al.* (1990). If the name of the author cannot be fitted into the text: *(Miller,* 1989); etc. When referring papers published in the same year by the same author, letters a, b, c, etc. should follow the year of publication.

Tables should be marked by Arabic numbers and printed in separate sheets with their numbers and legends given below them. Avoid too lengthy or complicated tables, or tables duplicating results given in other form in the manuscript (e.g., graphs).

Figures should also be marked with Arabic numbers and printed in black and white or color (under special arrangement) in separate sheets with their numbers and captions given below them. JPG, TIF, GIF, BMP or PNG formats should be used for electronic artwork submission.

Reprints: authors receive 30 reprints free of charge. Additional reprints may be ordered at the authors' expense when sending back the proofs to the Editorial Office.

More information for authors is available: journal.idojaras@met.hu

Published by the Hungarian Meteorological Service

Budapest, Hungary

INDEX 26 361

HU ISSN 0324-6329